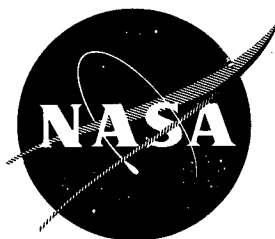


N73-18800
NASA CR-120895



CASE FILE COPY

HYDROGEN - OXYGEN AUXILIARY PROPULSION FOR THE SPACE SHUTTLE

VOLUME I: HIGH PRESSURE THRUSTERS

by

Aerojet Liquid Rocket Company
Sacramento, California 95812

prepared for

NATIONAL AERONAUTICS AND SPACE ADMINISTRATION

NASA Lewis Research Center

Contract NAS 3-14354

John W. Gregory, Technical Management

NOTICE

This report was prepared as an account of Government-sponsored work. Neither the United States, nor the National Aeronautics and Space Administration (NASA), nor any person acting on behalf of NASA:

- A. Makes any warranty or representation, expressed or implied, with respect to the accuracy, completeness, or usefulness of the information contained in this report, or that the use of any information, apparatus, method, or process disclosed in this report may not infringe privately-owned rights; or
- B. Assumes any liabilities with respect to the use of, or for damages resulting from the use of, any information, apparatus, method or process disclosed in this report.

As used above, "person acting on behalf of NASA" includes any employee or contractor of NASA, or employee of such contractor, to the extent that such employee or contractor of NASA or employee of such contractor prepares, disseminates, or provides access to any information pursuant to his employment or contract with NASA, or his employment with such contractor.

Requests for copies of this report should be referred to

National Aeronautics and Space Administration
Scientific and Technical Information Facility
P.O. Box 33
College Park, Md. 20740

Final Report

HYDROGEN-OXYGEN AUXILIARY PROPULSION
FOR THE SPACE SHUTTLE

Volume I: High Pressure Thrusters

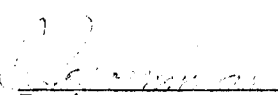
Prepared for

National Aeronautics and Space Administration
Contract NAS 3-14354

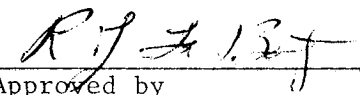
30 January 1973

by

Aerojet Liquid Rocket Company



Project Manager
L. Schoenman



Approved by
R. J. LaBotz
Program Manager

Technical Management: John W. Gregory
Liquid Rocket Technology Branch
NASA Lewis Research Center
Cleveland, Ohio 44135

ABSTRACT

Technology for long life, high performing, gaseous hydrogen-gaseous oxygen rocket engines suitable for auxiliary propulsion was provided by a combined analytical and experimental program. Propellant injectors, fast response valves, igniters, and regeneratively and film-cooled thrust chambers were tested over a wide range of operating conditions. Data generated include performance, combustion efficiency, thermal characteristics film cooling effectiveness, dynamic response in pulsing, and cycle life limitations.

FOREWORD

This report was prepared by the Aerojet Liquid Rocket Company, a division of the Aerojet-General Corporation, under Contract NAS 3-14354, which is sponsored by the NASA Lewis Research Center. The NASA project manager is J. W. Gregory.

The purpose of this contract was to develop a comprehensive technology base for high performance, long life, gaseous hydrogen-gaseous oxygen rocket engines suitable for the Space Shuttle Auxiliary Propulsion System (APS). Durability requirements include injector and thrust chamber designs capable of a 50-hour firing life over a 10-year period, with up to 10^6 restarts including 10^5 full thermal cycles and single firings up to 1000 sec.

The program Phase I was initially structured as two parallel efforts: one directed toward high pressure (100 to 500 psia [6.9 to 34.5 N/cm²]) systems and the other toward low pressure (10 to 20 psia [6.9 to 13.8 N/cm²]) systems. Nominal engine thrust in each case was 1500 lb (6680 N). Initial program tasks were devoted to the analytical evaluation and screening of injector and cooled thrust chamber concepts for both pressure levels. This was followed by parallel experimental evaluations of low and high pressure injectors and ignition devices. Recommendations of specific injector and igniter designs were made for both pressure levels as a result of these tests.

The program was redirected at midpoint to apply additional emphasis on the high P_c technology with a revised schedule on propellant inlet temperatures. The program's resources originally planned for the low pressure activities were reallocated to provide a Phase II high P_c expanded design, fabrication, and test effort related to the lower temperature gaseous propellants. Volume I of this final report covers Phase I and II high pressure thrusters; the low pressure activities are presented in Volume II, which is published separately as NASA CR-120896.

FOREWORD (cont.)

Volume I contains a large amount of information and data which was generated in parallel activities and is, to a large extent, interrelated. The following comments to the user concerning the preparation of this document are therefore offered:

Section IV follows the introductory and summation material (Sections I through III) and is the first in-depth section of the volume. This section provides a description of the injectors, thrust chambers, igniters, and valves employed in the program. It also includes the igniter and valve testing that was completed in separate tasks prior to initiation of complete thruster testing.

Section V provides a description of the test facilities used in the sea level, altitude, and pulse testing; a chronological record of the testing and conditions; some of the test records; and a tabulation of the measured data.

Section VI provides a discussion of the test results, and presents experimental performance and thermal characteristics of each design tested as related to the end product.

Section VII contains supporting analysis and data correlation which may be useful in future programs of this type.

Section VIII is devoted to the fatigue life analyses and predictions based on the experimental test data. Data are presented as curves of life vs pulse width and life vs film cooling.

TABLE OF CONTENTS

	<u>Page</u>
Standardized Graphical Data Presentation	xii
Nomenclature List	xiii
Table List	xv
Figure List	xvi
I. Introduction	I-1
II. Summary	II-1
III. Conclusions and Recommendations	III-1
IV. Thruster Component Design and Fabrication	
A. Injectors	IV-1
1. Concept Screening	IV-2
2. Comparison of Recommended Approaches	IV-5
3. Detailed Description of Selected Designs and Injector Fabrication	IV-6
B. Thrust Chambers	IV-16
1. Summary of Activities	IV-16
2. Design Requirements	IV-17
3. Cooling Concept Selection	IV-18
4. Design and Fabrication Descriptions	IV-21
C. Igniters	IV-37
1. Requirements	IV-37
2. Design Selection	IV-37
3. Spark Igniter Design	IV-38
4. Catalytic Ignition	IV-48
D. Valve Design and Operating Characteristics	IV-59
1. Requirements	IV-59
2. Valve Description	IV-59
3. Valve Dynamic Characteristics	IV-60
4. Hydraulic Characteristics	IV-62
5. Service History	IV-63
6. Igniter Valves	IV-68

TABLE OF CONTENTS (cont.)

	<u>Page</u>
V. Thrust Chamber Testing Conditions and Data	
A. Sea Level Tests	V-1
1. Test Hardware	V-1
2. Measurements and Calibration	V-3
3. Vacuum Start Conditions	V-6
4. Summary of Test Conditions and Results	V-6
5. Injector Performance Summary	V-7
6. Stability Testing	V-8
B. Cooled Chamber Altitude Testing	V-10
1. Introduction	V-10
2. APS Altitude Test Facility Description	V-10
3. Summary of Altitude Testing	V-15
C. Regeneratively Cooled Chamber Testing	V-24
1. Testing Summary	V-24
D. Phase II - Film Cooled Chamber Test Conditions - Series 1680-006	V-31
E. Phase II - Regeneratively Cooled Chamber Tests - Series 1680-006	V-33
F. Pulse Testing	V-35
1. Test Objectives	V-35
2. System Description	V-35
3. Data Acquisition and Analysis	V-37
4. Summary of Pulse Testing Events - Ambient Temperature Propellants	V-40
5. Pulse Repeatability Tests with Low Temperature Propellants	V-46
VI. 40:1 Thruster Test Results	
A. Steady State Tests	VI-1
1. Cold Flow Acceptance Tests	VI-1
2. Altitude Performance Testing	VI-2
3. Steady State Firing Temperature Measurements	VI-10

TABLE OF CONTENTS (cont.)

	<u>Page</u>
B. Pulse Testing	VI-28
1. Valve Response	VI-28
2. Minimum Impulse (Thrust Time Integral)	VI-29
3. Pulsing Performance	VI-33
4. Ignition Repeatability	VI-33
5. Thermal Characteristics	VI-34
VII. Supporting Analyses and Data Correlation	
A. Injector Performance and Compatibility	VII-1
1. Injector Element Cold Flow Testing	VII-1
2. Manifold Design and Flow Studies	VII-16
3. Injector Face Cooling and Cycle Life	VII-19
4. Phase II Premix Injectors Structural Analysis	VII-34
5. Hot Test Performance Evaluation Methodology	VII-37
B. Thrust Chamber Cooling	VII-51
1. Analytical Approach	VII-51
2. Experimental Results of Sea Level Testing	VII-56
3. Experimental Heat Transfer Coefficients with Film Cooling	VII-68
4. Film Cooling Effectiveness (Data Correlation)	VII-69
5. Subsonic Cooling Injection	VII-70
6. Film Cooling Effectiveness with Supersonic Coolant Injection	VII-73
C. Nozzle Contour Selection	VII-78
D. Materials Evaluation	VII-83
E. Structural and Life Analyses	VII-88
1. Design Loads	VII-88
2. Thermal Environment	VII-88
3. Life Goal	VII-89
4. Methods of Analysis	VII-89
5. Material Properties	VII-93

TABLE OF CONTENTS (cont.)

	<u>Page</u>
VIII. Life Analysis and Predictions for 40:1 Cooled Thrust Chamber	
A. Film Cooled Chambers	VIII-1
1. Phase I Designs	VIII-1
2. Life Expectations of Phase II Film-Cooled Chamber Design in Pulse Mode and Off-Nominal Operation	VIII-3
B. Regeneratively Cooled Chambers	VIII-15
1. Phase I Designs	VIII-15
2. Phase II Regeneratively Cooled Chambers	VIII-17

References*

*References called out in text are located at the end of report.

STANDARDIZED GRAPHICAL DATA PRESENTATION*

Shapes designate chamber pressure

- △ 100 psia data
- ◻ 300 psia data
- 500 psia data

Shades designate mixture ratio

- ▲ ◐ Right shade MR = 3
- △ ◑ Open MR = 4
- ▲ ◑ Solid MR = 5
- ▲ ◐ Left Shade MR = 6

Orientation designates propellant temperature

- △ ◑ Ambient = up
- ◊ ◄ ◑ Cold = left
- ▷ ◑ Heated = right

Slash marks designate injectors

- | | | |
|---|------|-------------------|
| ⌈ | SN-7 | } "I" pattern |
| ⌋ | SN-6 | |
| ⌋ | SN-5 | |
| ⌋ | SN-4 | } Triplet pattern |
| ⌋ | SN-3 | |

*unless otherwise noted on Figure.

NOMENCLATURE LIST

<u>Parameter</u>	<u>Definition</u>
BLL	Boundary layer loss
CSTAR	Measure characteristic exhaust velocity
c^*	Characteristic exhaust velocity
Date	Test date
DL	Curvature - Divergence loss
DP	Data period
DT1	Data time start
DT2	Data time end
ERE	Energy release efficiency
ERL	Energy release loss
FCL	Film cooling loss
F_{vac}	Vacuum thrust
I_{st}	Theoretical vacuum specific impulse
I_{sv}	Measured vacuum specific impulse
KL	Kinetics loss
MR	Overall mixture ratio
MR_c	Core mixture ratio
MR_D	Igniter mixture ratio distribution loss
P_A	Altitude pressure
P_c	Chamber pressure
Test Number	Reference test series and number
T_{H_2}	Hydrogen temperature
T_{H_2C}	Film coolant inlet temperature
T_{H_2I}	Regen coolant inlet temperature
T_{H_2OT}	Regen coolant outlet temperature
T_{O_2}	Oxygen temperature
\dot{w}_f	Hydrogen mass flow rate
\dot{w}_{FC}	Fuel coolant mass flow rate
\dot{w}_{FI}	Igniter hydrogen mass flow rate
\dot{w}_o	Oxygen mass flow rate
\dot{w}_{oI}	Igniter oxygen mass flow rate

NOMENCLATURE LIST (cont.)

<u>Parameter</u>	<u>Definition</u>
\dot{w}_T	Total thrust mass flow rate
% c^*	Percent characteristic exhaust velocity
% FC and % FCC	Percent of total fuel as coolant
% IG	Percent of total flow through igniter
% I_s	Percent vacuum specific impulse
L'	Chamber length, injector face to throat
L^*	Chamber characteristic length
EPW	Electrical pulse width
EPWV	Electrical pulse width based on valve timing

TABLE LIST

Table*

IV-1	Thruster Design Requirements
IV-2	Cycle Life Performance Matrix
IV-3	Phase I Film-Cooled Chamber Projected Life
IV-4	Comparison of Phase I and II Film-Cooled Chambers
IV-5	Igniter Design Criteria
IV-6	Spark Igniter-Only Mode Thermal Tests
IV-7	Igniter Power Supply
IV-8	Short Summary of Spark Igniter Test Conditions and Results
IV-9	Catalytic Igniter Test Summary (Igniter-Only Mode)
IV-10	Catalytic Igniter Test Summary (Complete Thruster Mode)
V-1	Sea Level Performance Summary
V-2	Summary of 40:1 Test Conditions and Hardware
V-3	Summary of Film-Cooled Chamber Test Conditions and Performance
V-4	Summary of Film-Cooled Chamber Thermal Profiles
V-5	Summary of Regeneratively Cooled Chamber Test Conditions and Performance
V-6	Summary of Regeneratively Cooled Chamber Thermal Profiles
V-7	Pulse Test Summary
V-8	System Sequencing and Resulting Events
VI-1	Delivered Vacuum Specific Impulse
VI-2	40:1 Altitude Performance Summary
VI-3	Bit Impulse Test Conditions and Repeatability
VI-4	Cold Propellant Bit Impulse Data, Tests D06-OA-009, -010
VII-1	Coaxial Element Cold Flow Tests
VII-2	Equations for Estimating Maximum and Allowable Face Temperature Gradients
VII-3	Summary of No Film Cooling Heat Flux Data
VII-4	Summary of Heat Flux Data with Film Cooling
VIII-1	Summary of Film-Cooled Chamber Design Analyses

*Tables are located prior to figures at the end of each respective section.

FIGURE LIST

Figure *

IV-1	Coaxial Element Injector Components and Assembly
IV-2	Phase I Premix Injector Components and Assembly
IV-3	Phase II Premix Injector Components and Assembly
IV-4	Phase I Premix Element Injector Manifolding and Flow Schematic
IV-5	Premix Injector Element Configurations
IV-6	Injector Assembly Schematic
IV-7	72-Element Premix Injector Manifolding
IV-8	Thrust Chamber Cooling Evaluation
IV-9	Assembly Drawing Film-Cooled Thrust Chamber
IV-10	Thrust Chamber Assembly Schematic
IV-11	Film-Cooled Thrust Chamber Components and Assembly
IV-12	Phase II Film-Cooled Chamber
IV-13	Assembly Drawing, Phase I Regeneratively Cooled Chamber
IV-14	Phase I Regeneratively Cooled Chamber Components
IV-15	Phase I Regeneratively Cooled Chamber Prior to Electroforming
IV-16	Phase II Regeneratively Cooled Chamber Section
IV-17	Phase II Regeneratively Cooled Chamber Components
IV-18	Phase II Regeneratively Cooled Chamber Assembly
IV-19	Comparison of Phase I and II Nozzle Contours and Coolant Channel Configurations
IV-20	Effect of Mixture Ratio on Flame Quenching Parameter
IV-21	Igniter Isometric Drawings and Photographs
IV-22	Thermal Characteristics of Electrical Igniter
IV-23	Paschen's Law Curves
IV-24	Electrical Igniter Maximum Ignition Pressure Limits
IV-25	Schematic Drawing of Catalytic Igniter
IV-26	Oscillograph Trace, Catalytic Igniter-Only Test No. 110
IV-27	Oscillograph Trace, Catalytic Igniter-Only Pulse Test No. 115
IV-28	Valve and Valve Actuator Cross Section

*Figures are located at the end of each respective section.

FIGURE LIST (cont.)

Figure

IV-29	Fast Response Poppet Valves Before and After Assembly
IV-30	Physics Lab Bay 7 Test Stand
V-1	25 L* Heat Sink Chamber
V-2	15 L* Ablative Chamber
V-3	Film Cooling Injection Rings
V-4	Limits of Flow Rate Calculations for Real Gases
V-5	Injector Energy Release Efficiency Comparison
V-6	Effect of L* Propellant Temperature and Chamber Pressure on Injector Energy Release Efficiency
V-7	Combustion Stability Bomb Test Results
V-8	Spectral Analysis of Bomb Test Data
V-9	Film-Cooled Thruster Mounted in J-3 Altitude Test Facility
V-10	Test Zone J Altitude System Capabilities
V-11	Film-Cooled Chamber Flow and Instrumentation Schematic
V-12	Postfire Photograph, Test 015
V-13	Computer Controlled Flow Rates
V-14	Thruster Wall Temperatures, Chamber Region
V-15	Thruster Wall Temperatures, Throat Region
V-16	Thruster Wall Temperatures, Skirt Region
V-17	SN 4 Triplet Injector after 2600 Restarts and 700 sec of Firing
V-18	Postfire Photograph, SN 6 Injector - SN 2 Film-Cooled Chamber
V-19	Regeneratively Cooled Chamber Instrumentation
V-20	Regeneratively Cooled Chamber Test with Variable Propellant Inlet Temperatures
V-21	Regeneratively Cooled Chamber Postfire Run 03-035
V-22	SN 3 Film-Cooled Chamber Flow and Instrumentation
V-23	SN 3 Regeneratively Cooled Chamber Instrumentation
V-24	Flow Schematic for Pulse Tests
V-25	Digitized Measurements and Integrals in Pulse Testing
V-26	Anemometer Response and Calibration for Pulse Testing

FIGURE LIST (cont.)

Figure

V-27	Igniter Propellant Sequencing Tests
V-28	Igniter Lead - Mainstage Sequencing Tests
V-29	Ignition Delay with Mainstage Fuel Leading Igniter Ignition
V-30	Ignition and Pulse Characteristics with Simultaneous Fuel and Oxidizer Flow
V-31	Pulsing Characteristics for Nominal Pulse Width of 0.2 sec
V-32	Pulsing Characteristics for Nominal Pulse Width of 0.1 sec
V-33	Pulsing Characteristics for Nominal Pulse Width of 0.035 sec
V-34	Pulse Train for Nominal Pulse Series, 0.035 sec
V-35	Pulse Series with Cold Propellants
V-36	Photograph of SN 7, Modified "I" Premix Following the 2500 Pulse Test Series
VI-1	Coolant Channel Flow Distribution
VI-2	Vacuum Specific Impulse, SN 6 and 7 Modified "I" Premix Injector, Ambient Temperature Propellants, 40:1 Regenerative and Film Cooled Chambers
VI-3	Vacuum Specific Impulse, SN 6 and 7 Modified "I" Premix Injector, Cold Propellants, 40:1 Regenerative and Film Cooled Chambers
VI-4	Vacuum Specific Impulse, SN 6 and 7 Modified "I" Premix Injector, Regeneratively Cooled Chambers, 10% Supersonic Film Cooling
VI-5	Influence of Hydrogen Supply Temperature on Measured Vacuum Specific Impulse, SN 6 Modified "I" Premix Injector, Regeneratively Cooled Chamber, 10% FFC
VI-6	Vacuum Specific Impulse, SN 5 "I" Injector, Film Cooled Chamber, Ambient Temperature Propellants
VI-7	Vacuum Specific Impulse, SN 4 Premix Triplet Injector, All Test Conditions
VI-8	Energy Release Efficiency, SN 4 Premix Triplet Injector
VI-9	Influence of Velocity Ratio on Injector ERE
VI-10	Experimental and Predicted Specific Impulse Loss vs % Film Cooling
VI-11	Film Cooled Chamber Measured Steady State Wall Temperatures vs Injector Mixture Ratio and % Film Cooling
VI-12	Film Cooled Chamber Measured Steady State Wall Temperatures vs Pressure, Mixture Ratio, and Propellant Temperature

FIGURE LIST (cont.)

Figure

- VI-13 Film Cooled Chamber Transient Thermal Characteristics with Ambient Temperature Propellants, Tests 03-012 and 015
- VI-14 Experimental Wall Temperatures, Phase I Regeneratively Cooled Chamber, Pressure Effects
- VI-15 Experimental Wall Temperature, Phase I Regeneratively Cooled Chambers vs % Film Cooling, Coolant Supply Temperatures and Mixture Ratio
- VI-16 Comparison of Predicted and Measured Gas and Backside Wall Temperatures, Phase I Regeneratively Cooled Chambers
- VI-17 Skirt Temperature Profile, Phase I Regeneratively Cooled Chamber vs MR and % Film Cooling
- VI-18 Phase II Regeneratively Cooled Chamber Wall Temperatures vs Chamber Pressure, Ambient Temperature Propellants
- VI-19 Comparison of Measured and Predicted Wall Temperature Profiles, Phase II Regeneratively Cooled Chamber
- VI-20 Phase II Regeneratively Cooled Chamber Wall Temperature Profiles vs Chamber Pressure, Cold Propellants
- VI-21 Summary of Upper Limit Experimental Gas-Side Wall Temperatures for Phase II Regeneratively Cooled Chamber vs Pressure and Propellant Temperature
- VI-22 Summary of Steady State Gas-Side Thermal Data for Phase II Regeneratively Cooled Chamber
- VI-23 Summary of Steady State Skirt Temperatures and Chamber Thermal Gradients for Phase II Regeneratively Cooled Chamber
- VI-24 Transient Thermal Data for Phase II Regeneratively Cooled Chamber
- VI-25 Film Cooled Chamber Bit Impulse
- VI-26 Film Cooled Chamber Bit Impulse Repeatability, Ambient Temperature Propellants (Constant Pressure Supply)
- VI-27 Film Cooled Chamber Bit Impulse Repeatability with Cold Propellants (Mass Flow Controlled System)
- VI-28 Bit Specific Impulse vs Pulse Width, Film Cooled Chamber, Ambient Temperature Propellants
- VI-29 Film Cooled Chamber Temperatures in Pulse Mode Operation, Test 05-021, 266 Pulses, 0.2 sec On - 0.3 sec Off
- VI-30 Film Cooled Chamber Temperatures in Pulse Mode Operation, 1220 Pulses, Pulse Width = 0.035 and 0.100 sec

FIGURE LIST (cont.)

Figure

VII-1	Typical Uni-Element Cold Flow Test Setup
VII-2	Schematic Drawing of Coaxial Element Cold Flow Test Apparatus
VII-3	Coaxial Elements Employed in Cold Flow Testing
VII-4	Cold Flow Profiles, Oxidizer Only
VII-5	Coaxial Jet Element, Mass and Mixture Ratio Profiles
VII-6	Coaxial Jet Element Mixing Efficiency
VII-7	Mixture Ratio Profiles for Scarfed and Nonscarfed Swirler Elements
VII-8	Orifice Wall Mixture Ratio vs Oxidizer Tube Recess
VII-9	Premix Element Cold Flow Mixing Efficiency
VII-10	Premix Element Schlieren Photographs
VII-11	Premix Element Mass and Mixture Ratio Profiles
VII-12	Flow Schematic of Selected Manifold Designs
VII-13	Phase II Premix Injector Manifold and Cold Flow Results
VII-14	Coaxial Injector Face Cooling Optimization Analysis
VII-15	Coaxial Injector Experimental Face Temperatures
VII-16	Premix Injector Experimental Gas-Side Face Temperatures (Transient)
VII-17	Premix Injector Steady-State Face Temperatures
VII-18	Modified "I" Premix, Face Thermal Profiles and Heat Flux
VII-19	Premix Injector Thermal Strain vs Fatigue Life
VII-20	Predicted Life of Modified Premix "I" Injector
VII-21	Premix Injector Structural Analysis
VII-22	Effect of Element Mixing Efficiency on ERE
VII-23	Streak Chamber Compatibility
VII-24	Cooled Chamber Compatibility
VII-25	Combustion Temperature and Enthalpy Heat Transfer Coefficient Correction for Oxygen/Hydrogen
VII-26	Film Cooling Mixing Model
VII-27	Throat Heat Flux vs Wall Temperature
VII-28	Heat Transfer Coefficients Without Film Cooling

FIGURE LIST (cont.)

Figure

- VII-29 Throat Heat Transfer Coefficients with Chamber Pressure as a Parameter
- VII-30 Throat Region Heat Flux Profiles for Coaxial Element Injectors
- VII-31 Chamber Heat Flux Profiles with Coaxial Element Injector
- VII-32 Chamber Heat Flux Profiles Injector Design Dependency
- VII-33 Chamber Heat Flux Profiles with Premix "I" Triplet Injector
- VII-34 Chamber Heat Flux Profiles with Premix Triplet Injector
- VII-35 Heat Sink Chamber Thermal Instrumentation
- VII-36 Error Analysis and Comparison of Various Experimental Techniques
- VII-37 Comparison of Throat Flux vs Wall Temperature With and Without Film Cooling
- VII-38 Experimental Thermal Data at 25 L* with Film Cooling
- VII-39 Effect of Film Cooling Ring Length on Heat Flux
- VII-40 Throat Region Heat Flux Dependency on Injector Coolant Ring Length and Coolant Flow
- VII-41 Influence of Film Cooling on Gas-Side Heat Transfer Coefficient (Sea Level Tests)
- VII-42 Influence of Film Cooling on Gas-Side Heat Transfer Coefficients (Altitude Tests, 40:1 Nozzle)
- VII-43 Film Cooling Entrainment Multiplying Factor and Effectiveness
- VII-44 Film Cooling Characteristics, Premix "I" Injector, Ambient Temperature Propellants
- VII-45 Film Cooling Characteristics, Modified "I" Premix Injector, Ambient Temperature Propellants
- VII-46 Film Cooling Characteristics, Modified "I" Premix Injector, Cold Propellants
- VII-47 Maximum Skirt and Throat Temperatures vs Coolant Flow (All 40:1 Film Cooled Chamber Tests)
- VII-48 Supersonic Film Cooling Injector Design Details
- VII-49 Measured Skirt Temperatures for Supersonic Film Cooling Injection
- VII-50 Supersonic Injection, Film Cooling Effectiveness Correlation

FIGURE LIST (cont.)

Figure

- VII-51 Mixing Parameters for Supersonic Film Cooling Injection
- VII-52 Supersonic Film Cooling Injection Enthalpy Effectiveness and Correlating Factors
- VII-53 Optimization of the Rao Nozzle Contour
- VII-54 Aero- and Thermodynamic Flow Characteristics of Selected Nozzle Contour
- VII-55 Nozzle Throat Heat Transfer Characteristics
- VII-56 Criteria for Laminarization of the Regeneratively Cooled Chamber
- VII-57 Predicted Laminar and Turbulent Heat Transfer Coefficients for Phase II Regeneratively Cooled Chamber
- VII-58 Stress vs Fatigue Life (N_f), Haynes Alloy 188
- VII-59 Total Strain vs Fatigue Life (N_f), ARMCO 22-13-5
- VII-60 Total Strain vs Fatigue Life (N_f), Copper and Copper Alloys
- VII-61 Attachment Methods for Removable or Refractory Skirts
- VII-62 Secant Modulus Stress-Strain for Zirconium Copper
- VII-63 Haynes Alloy 188 Sheet Stress Rupture Strength (Larsen Miller)
- VIII-1 Film Cooled Chamber, Haynes 188, Maximum Combined Stress Profile at Throat Station During Thermal Transient (300 psia [207 N/cm²])
- VIII-2 Film Cooled Chamber Steady State Nozzle Stress Profiles (300 psia [207 N/cm²])
- VIII-3 Bit Impulse and Cycle Life of Phase I Film Cooled Chamber at Nominal Operating Conditions
- VIII-4 Bit Impulse and Cycle Life for Phase II Film Cooled Chamber at Nominal Operating Conditions
- VIII-5 Phase II Film Cooled Chamber Steady State Throat and Skirt Temperatures vs Engine MR, % Film Coolant and Propellant Supply Temperature
- VIII-6 Film Cooled Chamber Throat Region Fatigue Life
- VIII-7 Film Cooled Chamber Copper Lined Region Thermal Transient at Nominal Phase II Operating Conditions
- VIII-8 Film Cooled Chamber with Monowall Manifold, Steady State Temperatures
- VIII-9 Film Cooled Chamber Noncontacting Manifold and Liner
- VIII-10 Film Cooled Chamber with Dual Wall Manifold, Steady State Temperature

FIGURE LIST (cont.)

Figure

- VIII-11 Film Cooled Chamber Structural Analysis, Steady State Nominal Phase II Conditions
- VIII-12 Phase I Regeneratively Cooled Chamber Experimental Temperatures and Predicted Life at Steady State
- VIII-13 Phase I Regeneratively Cooled Chamber Experimental Temperatures and Life Predictions in Pulse Mode Operation

I. INTRODUCTION

Considerable work has been done in the application of hydrogen and oxygen as rocket propellants. The main interest in this propellant combination stems from the high specific impulse potential, the excellent cooling characteristics of hydrogen, and, more recently, the fact that the products of combustion are pollution free. Past investigations for the most part lacked two important parameters: the hardware reusability aspect which, for the Space Shuttle, projects to 100 flights per vehicle with up to 10^4 pulses per flight as a design criterion and the mixing and combustion characteristics with the injection of both propellants in the gas phase.

The selection of gas phase injection for the APS thrusters application was made mainly to ensure good pulsing characteristics and avoid the need for liquid recirculation pumps, hardware chill-in, the possibility of vapor lock, and potential ignition difficulties associated with nonhypergolic cryogenic liquids. Extensive laboratory work, feasibility demonstrations, R&D work, and production hardware such as the RL-10 and J-2 engines are available for reference; however, these employ liquid phase oxidizer injection and require a limited number of restarts.

This program was directed toward: (1) investigating potential problems associated with gas phase propellant injection, mixing, ignition, and combustion; (2) determining if the cyclic life goals could be achieved using state-of-the-art designs and materials and identifying the relationship between performance and component life for various design approaches; (3) demonstrating the durability and pulsing characteristics of selected designs; and (4) creating a broad technology base suitable for prototype designs.

Table IV-1 provides a summation of the design requirements at the nominal operating point and a test range over which the hardware should be capable of steady-state operation. Additional durability requirements for the Space

I, Introduction (cont.)

Shuttle application include the ability to withstand: (1) pressure and thrust induced loads corresponding to 10^6 engine pulses, (2) transient thermal strains induced by the temperature gradients resulting from 10^5 heating and cooling cycles, (3) creep damage resulting from 50 hours of operation at steady-state temperatures, and (4) some level of reentry heating (possibly up to 1700°F [1143°K]) and associated oxidation, plus (5) normal sea level salt air and environmental chemical attack.

II. SUMMARY

The objectives of the high pressure portion of this program were to establish a technology base for subsequent development of high cycle life thrusters in the 100 to 500 psia (69 to 345 N/cm²) range using gaseous hydrogen-gaseous oxygen as propellants. Primary emphasis was placed on developing igniter, injector, and cooled chamber technology, suitable for both long duration firings and pulse mode operation with no duty cycle limitations at a nominal design pressure of 300 psia (207 N/cm²).

Initial hardware analysis, design, fabrication, and testing were based on propellants at ambient temperatures. A Phase II effort initiated about midpoint in the contract required modified injector and thrust chamber designs and test hardware more suitable for operation with lower temperature propellants [250°R (139°K) H₂, 375°R (208°K) O₂].

Igniters

Catalytic and spark igniters were tested over a wide range of operating conditions which include both propellant temperature and pressure variations. Both igniters were center mounted in the injector and generated a torch having a mixture ratio (O/F) of 5.0 for main chamber ignition using 1.6% of the total propellant flow. The catalytic igniter employed a four-stage ignition sequence. A very small Shell 405 catalyst bed, which reacted 5% of the igniter flow at a mixture ratio of 1.0, provided the energy source. Subsequent staging, by adding oxygen immediately downstream of the bed to provide a mixture ratio of 40 and then addition of hydrogen to bring the torch to a MR of 5.0, resulted in very rapid response (≈ 0.02 sec). The main limitations of the catalytic igniter were an increase in ignition delay time with the use of very cold propellants and the tendency for the thruster to ignite without using the igniter during mainstage cold flow and propellant bleed-in.

II, Summary (cont.)

Selection of the spark ignition approach was based on the ability to achieve response times of 0.010 sec with very cold hydrogen and either cold gaseous or two-phase oxygen as demonstrated in Contract NAS 3-14348. More than 6000 igniter firings had been completed with satisfactory results prior to supplying the hardware to the Lewis Research Center for additional testing. The main difficulties encountered with the spark igniter were associated with the high voltage electrical system which resulted from the use of laboratory equipment in a nonlaboratory environment.

Injectors

Coaxial jet and premix elements were evaluated in cold flow testing to determine the configurations which maximize mixing efficiency. Full-scale injectors of each element type were designed and fabricated following manifolding cold flow studies. Approximately 100 hot fire performance, compatibility, and heat transfer tests were conducted in highly instrumented sea level chambers of varying length. The premix approach was selected for use in 40:1 cooled thruster testing based on its somewhat higher performance, superior compatibility, and lower fabrication costs. Combustion stability testing of the selected pattern with low temperature propellants showed a 0.006-sec recovery in three successive tests from a 200% overpressure initiated by a thermally detonated 2-grain RDX charge.

The Phase II injectors were of the premix element type with manifolding similar to the Phase I coaxial element design, which provided more uniform flow distribution.

II, Summary (cont.)

40:1 Cooled Chambers

Two cooled chambers were evaluated in Phase I testing. One was a single-pass - counterflow, regeneratively cooled copper chamber and nozzle with a film-cooled, thin wall steel skirt extending from an area ratio of 8.3. The second design contained a short single-pass - counterflow, regeneratively cooled copper chamber section and a film-cooled, thin wall steel throat and skirt. The Phase II designs were similar to the Phase I except that the nozzle contour was modified to favor relaminarization of the hot gas boundary layer in the regeneratively cooled design and thus improve cycle life. The change in the film-cooled thruster design consisted of decreasing the coolant injection area to compensate for the higher density of the colder hydrogen.

Test Results

The range of altitude test variables were as follows:

P_c	100 to 500 psia (69 to 345 N/cm ²)
Mixture ratio	3 through 6
Fuel temperature	190°R through 780°R (106°K - 434°K)
Oxidizer temperature	Saturated vapor through 685°R (380°K)
Total chamber pulses	2800
Maximum duration	~2000 sec
Minimum duration	0.025 sec

Testing demonstrated 5:1 throttling and changes in mixture ratio and propellant temperatures during firing.

Both Phase I cooled thrusters exceeded the contract performance goal of 435 sec I_s at the nominal design point as follows:

II, Summary (cont.)

	<u>I_s, sec</u>	<u>% FFC</u>	<u>Thruster ΔP Injector & Chamber, psia (N/cm²)</u>
Regeneratively cooled chamber	452	10	124 (85.5)
Film-cooled chamber	443	18	125 (86.0)

Cycle life was found to be a function of pulse width and the thermal state of the hardware. Cold starts were more severe with ambient temperature propellants than hot starts.

The cycle life analysis using minimum fatigue life properties and based on thermal data obtained for cold starts indicated the Phase I regenerative chamber to be capable of providing 10^6 pulses of 0.09 sec duration or less and 2000 full thermal cycles, where a full thermal cycle consisted of a firing greater than ≈ 0.5 sec. The film-cooled design is capable of providing 10^6 pulses of 0.15 sec duration or less and 6000 long burns of 1.0 sec or greater. The Phase I film-cooled chamber is life limited by the workhorse manifolding. The redesigned manifolding recommended but not fabricated for the Phase II design will allow 100,000 full thermal cycles and 10^6 pulses of 0.12 sec or less. Curves were generated to define life vs pulse width for the range between steady state and minimum pulse width for each design. These results also define operating modes which maximize thruster life by identifying the regimes where several short pulses are less damaging than a longer burn of equivalent total impulse.

The performance and pressure drop for the two Phase I designs with low temperature propellants [200°R (111°K) H₂, 375°R (208°K) O₂] was:

	<u>I_s, sec</u>	<u>% FFC</u>	<u>Thruster ΔP Injector & Chamber, psia (N/cm²)</u>
Regeneratively cooled chamber	442	8	77 (53)
Film-cooled chamber	436	17	61 (42)

II, Summary (cont.)

Testing with the Phase II hardware with cold propellants gave essentially the same performance. Data obtained on the regeneratively cooled design showed the maximum measured throat region temperature to be significantly reduced from the Phase I design with an accompanying improvement in cycle life. The thruster pressure drop also decreased to 56 psia (38.6 N/cm^2). The extent to which relaminarization was achieved was not firmly established because of ambiguities in the measured data.

Extensive pulse testing was conducted with and without the use of a mass flow controlled feed system. Approximately 2700 pulses were conducted with ambient temperature propellants and ~90 pulses with cold propellants. The minimum demonstrated pulse width was 27.5 lb-sec (122.5 N-sec). Minimum impulses were primarily determined by valve sequencing and response.

The longest single firing was 1976 sec on the Phase II regeneratively cooled chamber and was terminated by the limits of the altitude facility. This thruster assembly was delivered to the NASA Lewis Research Center in the as-tested condition for further testing.

III. CONCLUSIONS AND RECOMMENDATIONS

A. CONCLUSIONS

(1) The premix injector and film-cooled chamber provide a low cost, easily fabricated assembly which appears capable of meeting the 50-hr firing life, 10^6 restarts, 10^5 full thermal cycle requirements while providing a delivered specific impulse in excess of the program goals.

(2) The regeneratively cooled chamber will provide higher performance but is extremely limited in cycle life; however, relaminarization of the hot gas boundary layer in the throat can result in an improved cycle life which is capable of meeting the APS requirements.

(3) The film-cooled chamber approach is inherently lighter and less expensive than the regeneratively cooled design.

(4) The internal surface of the chamber and skirt can be kept sufficiently cool to allow the use of conventional, nonrefractory, noncoated materials. The use of 0.5-in. (1.2 cm) thick, low cost, lightweight, commercially available blanket insulations will keep external skirt temperatures below 800°F (700°K).

(5) Either design can be cooled within the 75 psi (52 N/cm^2) pressure drop budget using the Phase II propellant temperature schedule.

(6) The minimum impulse goal of 50 lb-sec (223 N-sec) was demonstrated for the film-cooled design and can be attained with the regeneratively cooled chamber since pulsing performance is primarily determined by valve response.

III, A, Conclusions (cont.)

(7) The oxidizer torch spark igniter provided reliable operation over the complete range of test conditions except where electrical problems with the power supply were encountered.

B. RECOMMENDATIONS

(1) Additional igniter, injector and chamber testing is required to explore the cycle life limits.

(2) Additional igniter testing is required to explore the limits of off-design operation on igniter cooling and cycle life. These tests should be conducted with a prototype power supply.

(3) Laboratory fatigue testing of various types of copper alloys, by a single investigator, under strain, temperature, and a chemical environment which simulate APS conditions, will help resolve a significant disparity in published fatigue life data.

(4) Further exploration of the laminarization process in the presence of combustion turbulence and highly cooled walls will help resolve some of the uncertainties encountered in testing. Injector element design and chamber length should be evaluated in future testing.

IV. THRUSTER COMPONENT DESIGN AND FABRICATION

A. INJECTORS

The injector technology portion of the program progressed through the following sequence of activities. The design task began with the screening of five candidate propellant injection techniques which appeared to have potential for providing high mixing efficiency with gaseous propellants and good chemical and thermal compatibility with the chamber wall. Two of these five (a coaxial design and a premix triplet) were selected for more detailed design studies. These studies consisted of (1) element optimization through empirical cold flow mixing studies, (2) manifolding design studies, (3) face cooling and structural analyses, and (4) fabrication studies to provide designs capable of being reproducibly fabricated in quantity at low cost. Following the design task, injectors of each design were fabricated and subjected to injector characterization testing using streak chambers and uncooled heat sink chambers. Based on the results of these tests, the premix triplet was selected for the cooled chamber testing. At this point, the contract redirection toward lower temperature propellants (Phase II) occurred and a modified premix triplet injector for use with cold propellants was designed and fabricated. The modified design also incorporated a manifolding redesign which gave it a manifold similar to that which was successful on the coaxial injector. Injectors of both the original and modified designs were employed in the altitude testing of the cooled chambers.

An injector of the modified configuration was subjected to a matrix of long duration firings encompassing thruster mixture ratios from 2 to 6, pressures of 100 to 500 psia (69 to 345 N/cm²), and propellant temperatures from 200 to 550°R (111 to 305°K). Durability was further demonstrated in a pulsing series involving 2600 restarts with propellant temperatures ranging from 200 to 550°R (111 to 305°K) and a single burn of over 33 minutes duration. Analyses and test data show the developed design to provide

IV, A, Injectors (cont.)

delivered specific impulse ranging from 10 to 16 sec greater than the performance goals (depending on cooled chamber selection) and cyclic life in excess of 10^6 full thermal cycles at nominal operating conditions.

The following sections provide a detailed discussion of the injector development activities outlined above.

1. Concept Screening

Candidate injector concepts considered for this program included the following types:

- Coaxial jet element
- Externally impinging like and unlike circular orifices
- Concentric vane (fine pattern noncircular orifice)
- Premix element (noncircular orifice)
- HIPERTHIN (ultrafine pattern)

A brief description of each concept and the reason for its selection or rejection is given below.

a. Coaxial Jet Element

The coaxial jet element design shown in Figure IV-1 was selected primarily because of a favorable history of providing high performance and compatibility with the gaseous hydrogen/liquid oxygen propellant combination. The goal of this program with respect to the coaxial element injector design was to:

IV, A, Injectors (cont.)

(1) Develop a further understanding of shear mixing and element optimization for gas-gas phase H_2/O_2 via a series of element cold flow tests and computer models.

(2) Study the face thermal environment and cooling capabilities.

(3) Design and evaluate via cold flow model tests a propellant manifolding system which feeds each of the optimized elements uniformly.

(4) Develop the technology to produce a low cost, high performance injector that can provide the required 50-hr, 10-year, 10^6 restart life cycle capabilities.

b. Premix Element

The second concept selected for evaluation on this contract was the premix element design shown in Figure IV-2. This injection concept provides a significant theoretical mixing advantage and had a brief but highly successful test history with gaseous hydrogen-oxygen propellants prior to the start of this program. The main advantages of this design are: (1) the ability to achieve intimate propellant contact and mixing via a geometrically optimized mixing cup, (2) complete freedom to shape the fuel injection orifices, and (3) demonstrated fabrication techniques which allow a high degree of precision to be attained in either small or large quantity production at low cost and to allow the use of a larger quantity of orifices without a significant cost impact. The technology and life goals regarding element and manifold optimization parallel goals (1) through (4) cited above for the coaxial element design.

IV, A, Injectors (cont.)

c. Externally Impinging Circular Orifices

The impinging drilled orifice approach was predicted to be more difficult to cool with unlike impinging jets and the resulting flow streams to be less compatible with the chamber wall than in the selected designs. Like propellant impinging jets were expected to provide a milder thermal environment at the injector face at the expense of efficient mixing.

d. HIPERTHIN

The HIPERTHIN concept was discarded primarily as a result of the weight penalty associated with manifolding the very low density gaseous propellants in a platelet structure.

e. Concentric Vane Concept

The concentric vane concept proposed for study was the extension of a gas/liquid propellant injection approach developed and successfully demonstrated at ALRC during the period from 1966 through 1969. The use of alternating concentric raised and recessed oxidizer and fuel vanes was predicted to provide the high performance capabilities of unlike externally impinging elements while simultaneously overcoming the cooling limitations which exist in a conventional flat face drilled orifice injector.

This concept, although considered to have great performance potential, was rejected for this application on the basis that fabrication costs, even in large quantities, would be considerably higher than the premix design approach which could have equally high performance potential.

IV, A, Injectors (cont.)

2. Comparison of Recommended Approaches

The injectors shown in Figures IV-1 and IV-2 were designed to be interchangeable with test stand and thrust chamber interfaces and are adaptable to either film, dump, or regeneratively cooled thrust chambers. Essential features of these injectors are compared in the following table:

	<u>Phase I</u>		<u>Phase II</u>
	<u>Coaxial Element</u>	<u>Premix Element</u>	<u>Modified "I" Premix</u>
No. of elements	42	72	72
Fuel manifold type	Radial inflow	Pie and concentric ring	Radial inflow
Oxid. manifold type	Flooded back	Pie and concentric ring	Flooded back - radial inflow
Igniter location	Center	Center	Center
Face cooling	Conduction/ convection	Convection/ transpiration	Convection/ transpiration

The Phase II design shown in Figure IV-2 incorporated the results and best features of Phase I designs and is discussed in a later section.

Both injector designs contain ports for recording pressures in the fuel and oxidizer manifolds and inlet lines, fast response thermocouples for recording injector face temperatures on the combustion side surface, and manifold thermocouples for recording propellant temperatures. Both injector designs accept either a spark or catalytic type igniter through a centrally located port. The following section provides a more detailed description of the design and fabrication of the selected approaches. The supporting analyses and test results are presented in Section VII,A.

IV, A, Injectors (cont.)

3. Detailed Description of Selected Designs and Injector Fabrication

a. Premix Injector

The postfiring photograph shown in Figure IV-2 is of the 72-313m3n5 F-O-F premix type injector which features a stack of seven orifice pattern bonded to a CRES 347 body. The pie and concentric ring manifolding contained within this body is shown in Figures IV-3 and IV-4. Also, in Figure IV-4, a schematic insert is provided, which shows how the bonded plates turn the fuel 90° to flow parallel with the face, giving a triplet pattern with two fuel streams impinging at right angles on the axial oxidizer stream. The flow pattern in the bonded plates determines the cross section of the fuel stream as it impinges on the oxygen and, in so doing, controls the momentum mixing characteristics of the basic element, the face temperature, and compatibility with the thrust chamber wall. The use of the photoetched plate allows complete freedom in selection of the fuel channel cross section and, therefore, a high degree of design optimization. The mixing characteristics of these elements, investigated in cold flow testing, resulted in selection of two fuel channel configurations which were evaluated in hot fire tests. A channel cross section having an "I" shape with particular proportions between the vertical and horizontal legs has been found to provide excellent mixing and thus high performance with reasonable compatibility, while a rectangular cross section provides a more favorable thermal environment at the injector face and forward chamber wall in exchange for a slight loss in performance

In Phase II of the program, the "I" pattern was modified based on "Phase I" hot fire test data to provide a very mild thermal environment at the injector face, good compatibility with the chamber wall, and a

IV, A, Injectors (cont.)

slight improvement in performance. In following discussions, these injector patterns will be referred to as the "I" triplet and triplet patterns and modified "I", respectively. Figure IV-5 shows the orifice geometry and relative operating characteristics of these three configurations. The procedure by which these particular element configurations were established are discussed in the sections covering element cold flow tests and face cooling analyses.

The Nickel 200 face material, selected for its high thermal conductivity and oxygen compatibility, is convectively cooled by the flow of fuel at high velocity through the noncircular injection channels oriented parallel to the injector face and 0.030 in. (0.076 cm) below the surface. Additional convective and face bleed cooling is provided by diverting approximately 5% of the fuel to the auxiliary network of smaller high velocity channels located 0.010 in. (0.025 cm) below the flame surface plate. These discharge through a system of 300 0.013-in. (0.033 cm) dia. orifices selectively located in the normally high heat flux zone between elements. These components are shown in Figure IV-3.

b. Phase I Premix Injector Fabrication - Pie and Concentric Ring Manifolding

The injectors built for the APS thruster program were based on fabrication techniques which were state-of-the-art within the Aerojet Liquid Rocket Company. The fabrication and assembly procedures that were employed are discussed only briefly since most of the procedures are standard shop practices.

The fabrication and assembly of each of the injectors can be best understood by examining the exploded schematic assembly drawing shown in Figure IV-6 and then the appropriate photographs of the hardware during the fabrication phase.

IV, A, Injectors (cont.)

This injector consists of four major components:

- (1) The photoetched nickel face plates containing the fuel pattern and face coolant bleed channels.
- (2) A 304 stainless steel basic injector body containing the drilled orifices which mate with the photoetched plates; seven concentric alternating fuel and oxidizer channels, 0.150 in. (0.38 cm) wide by 1.312 in. (3.3 cm) deep with a 0.050 in. (0.127 cm) separating wall; and a portion of the fuel manifold.
- (3) The manifold body, providing the remainder of the fuel and oxidizer pie manifolds which, when brazed to Item (2), forms an assembly with only one interpropellant joint. With appropriate fixturing, the joint is capable of being pressurized and inspected for interpropellant leaks.
- (4) Components forming the oxidizer and fuel manifold cover and inlet lines which are welded on.

The deep channels in the injector body are formed by eloxing techniques because the relative depth to width was found to exceed the capabilities of conventional cutters. Joining of the manifold and body was accomplished by brazing.

The entrance slots from the pie manifold to the concentric propellant channels were eloxed through after brazing and leak check inspection as shown in Figure IV-3. All corners were radiused to provide low pressure drop and improve propellant flow distribution. The next operation consisted of welding on the sheet metal manifold covers.

IV, A, Injectors (cont.)

The face plates were joined to each other and the body in a second bonding operation using a process developed by the Aerojet Liquid Rocket Company. The final operation includes welding on the inlet lines and final machining of the seal surfaces. The 24 holes radially inboard of the bolt circle (Figure IV-3) were drilled following heat soak testing to allow the injector fuel to be supplied directly from the cooled chamber.

(1) Quality Control

Critical parameters in the design are the diameter of the drilled oxidizer orifices and the fuel pattern in the photoetched plates. The oxidizer pattern is generated by a tape controlled drilling process to ensure pattern repeatability between successive components. Drilling is a simple operation since the holes are large, 0.1220 in. (0.310 cm), and drilled normal to the surface. The final orifice sizing is accomplished by a reaming operation to provide dimensional tolerances within ± 0.0005 in. (0.0013 cm). Fabrication of the face plates is also a low cost precision operation. Patterns are produced ten times actual size to within 0.005 in. These are then photographically reduced by precision optical equipment to full size which also reduces the error by a factor of 10, to 0.0005 in. (0.0013 cm). The patterns are etched in commercially available 0.010 in. (0.025 cm) stock which is normally accurate to within 0.0002 to 0.0005 in. (0.0005 to 0.0013 cm).

(2) Instrumentation

To better determine the injector face temperatures during operation, the injector face was instrumented with three thermocouples. This was accomplished by brazing three 0.062 in. OD by 0.020 in. (0.157 cm by .051 cm) wall tubes to the body which passed through both the manifold and manifold cover. A 0.010-in.-dia (.025 cm) hole was also through-etched in the face plates at the

IV, A, Injectors (cont.)

desired thermocouple locations. After final assembly, 0.010-in. (0.025 cm) thermocouples were passed through the tubes, swaged to the face, and torch-brazed on the backside to form a gas seal.

c. Coaxial Tube Design

The second injector design evaluated in this program was the more conventional coaxial tube type element shown in Figure IV-1. This design featured: (1) a hydrogen convectively cooled face plate (copper and aluminum were tested) which can be either bolted or brazed to the 304L stainless steel body; (2) 42 Nickel 200 oxidizer elements of the type shown in the assembly foreground of Figure IV-1 which are brazed to the 304L body; and (3) for technology purposes, interchangeable oxidizer flow control discs (first unit only) which facilitate the introduction of various levels of swirl into the oxidizer flow or the regulation of propellant pressure drop for the straight-flow element configuration. The two types of oxidizer flow control plates shown in Figure IV-1 are a single photoetched stainless steel plate (left) containing 42 sharp-edged orifices and a bonded stack of swirler plates (right). Swirl velocity is controlled by stack height. The flow control single plate or bonded stack is held in position, aligned with the inlet side of the oxidizer tubes, by ten small screws. Access to the plate is via a removable back cover plate. Serial No. 1 coaxial tube injector was tested with both types of flow control plates. Data from the swirl flow configuration with zero and 0.080 in. (0.203 cm) tip recess is reported under the designation CA-SN-1 and from the straight flow with zero tip recess as CA-SN-1A.

The design flexibility was incorporated in the injector body since most of the fabrication was being accomplished in parallel with element cold flow optimization studies.

IV, A, Injectors (cont.)

The procedures by which the injection orifices were configured and face cooling analysis conducted are covered in Section VII,A.

A critical design item in this injector is the method by which the concentric oxidizer tube or post is manufactured and held concentric with the fuel annulus. Since the range of fuel annuli of interest for this application are from 0.015 to 0.025 in. (0.038 to 0.63 mm), manufacturing tolerances as small as 0.001 in. (0.025 mm) will have measurable influence on flow distribution and performance. The second critical item is face cooling and cooling at the tip of the oxidizer tube when both propellants are injected in a gaseous state.

d. Coaxial Element Injector Fabrication

The components of the coaxial injector are shown schematically in Figure IV-6; photographs of this injector are shown in Figure IV-1. The major components include: the face plate, oxidizer tubes, injector body, oxidizer manifold, inlet lines, and igniter adapter.

The face plate contains 42 drilled and reamed fuel orifices of 0.3080 ± 0.0005 in. dia. Face plates of OFHC copper and T-6061 T-6 aluminum were fabricated using a computer-controlled machine.

The forty-two Nickel 200 oxidizer tubes were 1.47 in. (3.73 cm) long and had inlet and discharge diameters of 0.1650 in. (0.419 cm) and 0.2640 in. (0.670 cm), respectively, with a 3° half-angle diffuser to reduce the oxidizer injection velocity. These tubes were drilled from bar stock. The conical diffuser section was reamed to final dimensions. This was followed by an annealing operation and turning of the outside contour on a contour tracing lathe. Outside dimensions were held to ± 0.0005 in. (0.0013 cm). The final operation on the oxidizer tubes involved diametrical removal of 0.017 in. (0.0432 cm) in four arcs from the injection end, leaving four axial ribs between the arcs for centering the tube within the fuel orifice. This was accomplished by

IV, A, Injectors (cont.)

electrical discharge machining using a four-arc graphite electrode. The maximum precision which could be economically maintained on the 0.017 in. (0.043 cm) dimension was ± 0.001 in. (0.0025 cm). The injection tip wall ranged from 0.005 to 0.007 in. (0.0127 to 0.0178 cm). With the maximum stackup of tolerances on tube and fuel orifice, the fuel gap could vary from 0.0157 to 0.0172 in. (0.040 to 0.0436 cm). One of the main limitations of this design is considered to be the cost involved in producing a precision fuel injection annulus.

The third major component is the body which contains the fuel and oxidizer manifold and into which the 42 nickel elements are brazed. The manifold machining is a simple lathe turning operation with the exception of the side cover which is rolled from sheet metal and welded on. The hole pattern into which the nickel tubes were brazed was drilled by the same tape-controlled machine as the face plate. The elements were furnace brazed into the body in a hydrogen atmosphere using Nicro braze alloy prior to final machining of critical sealing surfaces on the body.

Fabrication of the platelet stack which controls the flow (swirl or shower) through the oxidizer orifices was accomplished by the same precision processes as those discussed earlier. This includes a tenfold optical reduction of the pattern layout, through-etching of the pattern in 0.010 in. (0.025 cm) plate stock, and bonding of the stacks in three heights corresponding to three levels of swirl component.

IV, A, Injectors (cont.)

Six 0.020-in.-dia stainless steel sheathed, chromel/alumel thermocouples were installed at the flame surface of the injector face after all machining was completed. These thermocouples were fed through close tolerance holes drilled through the thick copper face plate and staked into position on both the internal and external surfaces. The thermocouple lead wires passed through the adapter which provided a gas seal.

e. Phase II Premix Injector Design

Phase II injector designs incorporate the best features of the two different Phase I injectors. The Phase I and II premix designs are similar in that they provide the same premix cup configuration with only slight modification to the fuel and oxidizer orifices to reflect the changes in propellant temperatures and incorporate modifications based on the experimental results obtained in Phase I testing. This resulted in the modified "I" pattern shown in Figure IV-5.

Substantial changes were made in the manifolding to reduce both weight and volume and to improve the propellant flow distribution. The new manifolding adapted (shown in Figure IV-7) provides radial inflow on both the fuel and oxidizer circuits. The fuel circuit is fed directly from the discharge manifold of the chamber cooling circuit with a stainless steel piston ring providing the injector-chamber gas seal as noted in Figure IV-7. The oxidizer is fed from a central plenum containing a diffuser plate which distributes the oxidizer radially outward to provide a uniform flow condition prior to the final inflow pass which feeds the injection elements. This design also incorporated long L/D oxidizer injection tubes with the flow control arising from an orifice section halfway down the length of the tube. The benefit of this design feature was that it allowed the pressure drop and injection velocity to be independently optimized. Drawings for two versions of this design were prepared; one containing axial tubes for a cylindrical chamber, the other containing tubes canted 7° which makes it suitable for use in a conical chamber

IV, A, Injectors (cont.)

such that the oxidizer flow is always oriented parallel to the chamber wall. The long L/D oxidizer tube design also allows each oxidizer orifice to be fabricated as a high recovery, critical flow nozzle if it should become necessary to employ this technique to improve mixture ratio control. A complete description of the manifolding and element design is provided in Section VII,A.

f. Phase II Premix Injection Fabrication

Schematic drawings and components are shown in Figures IV-2, IV-6, and IV-7. The design consists of a minimum of parts and features designs which are easily fabricated by lathe turning and conventional drilling operations. Component fabrication is as follows:

The body and face plate are turned from 304L plate stock. All turning operations are concentric with the central axis. The body and face plate are then clamped together and match drilled in a single operation to reduce costs and assure good alignment of the holes, which is very important.

The oxidizer tubes are fabricated from commercially available stainless steel tubing. The tubes are cut to length, step drilled, and reamed on the ID from two ends (with a dimensional accuracy of ± 0.0005 in. [0.00127 cm]). The diametrical accuracy of the oxidizer flow controlling orifices is within $\pm 0.44\%$. The tubes are then centerless ground to a uniform OD of ± 0.0005 in. (± 0.00127 cm).

The two diffuser plates are turned from 0.060 in. (.153 cm) sheet stock and milled to form the support tabs as can be seen in Figure IV-2. The cover body and adapter which provide the igniter port are also turned to final dimensions, with the exception that the igniter port ID is not drilled at this time.

IV, A, Injectors (cont.)

The assembly sequence was as follows:

(1) The machined face plate, igniter spud, oxidizer tubes, and flange were furnace brazed using Palniro 7 preforms. The spud, face, flange plates were then assembled and the oxidizer tubes were pushed through both plates. Brazing was done at 1950°F (134°K) for 15 minutes.

(2) The internal baffles and finish machined cover were electron beam welded and then stress relieved at 1800°F (1255°K) for 30 minutes.

(3) The assembly was then finish machined on the back-side, the igniter port drilled, and the face was ground flat to 0.0005 in. (0.0013 cm) with a surface finish about 16 RMS.

(4) The face pattern and cooling platelets were then bonded in a single operation.

(5) The oxidizer inlet was welded on and all surfaces final machined, including tabs on injector face left from the plates and the piston ring retainer groove.

(6) The final assembly was instrumented with six gas-side thermocouples. A photograph of the two 0.020-in.-dia and four 0.010-in.-dia (0.051 cm and 0.025 cm) thermocouples being installed is shown in the lower right of Figure IV-2.

IV, High P_c Technology Program (cont.)

B. THRUST CHAMBERS

1. Summary of Activities

The thrust chamber analysis and design task of this program involved the preliminary screening of five candidate cooling techniques for 40:1 area ratio nozzles. Two of the five were then selected for detailed analyses and design optimization studies. One selected design was regeneratively cooled, the other was film cooled. The final selected designs were based upon experimental performance vs. L^* and film cooling vs. heat flux data generated in a parallel activity which involved firing the injectors described in the previous section, in heat sink, film cooled, and ablative streak chambers at sea level conditions.

A set of engineering drawings was prepared for each of the selected designs and submitted for NASA program manager approval prior to the initiation of fabrication. The designs represented by the fabrication drawings were backed by appropriate thermal and structural analyses assuring the ability of the components to operate throughout the specified MR, P_c and propellant inlet temperature range indicated in Table IV-1.

Each of the designs were successfully tested over the range of variables in a highly instrumented condition. These test results were then employed to uprate the analytical models. Boundary conditions to the thermal models were further refined such that the computer model was able to analytically reproduce the transient and steady state temperatures observed in actual testing. These validated models were then used to generate two and three dimensional transient and steady state thermal maps necessary for thermal fatigue life predictions of the test articles.

IV,B, Thrust Chambers (cont.)

As in the case of the injectors, a Phase II chamber design activity which called for lower temperature propellants, was initiated. One modified design for each of the selected cooling approaches was prepared and one completely new concept was investigated. Analyses of these designs incorporated the Phase I 40:1 area ratio, cooled chamber experimental results. Additional test data were obtained for Phase II design conditions using a newly fabricated regeneratively cooled chamber and a modified Phase I film cooled chamber. Parametric performance and thermal fatigue life analyses for prototype hardware configurations were generated for the anticipated operating envelope. The cyclic life-performance matrix resulting from these activities is provided in Table IV-2. The conclusion reached is that a tradeoff exists between life and performance. The Phase I regeneratively cooled chamber is capable of operating with as little as 10% film cooling at which point the delivered specific impulse is 452 sec and the cyclic life is 2000 thermal cycles. The life can be increased by using additional film coolant. Approximately 30% film cooling will increase the life of this chamber to 30,000 thermal cycles, and reduce the performance to 428 sec.

The film cooled chamber requires 18% film coolant as a minimum for safe operation at which point the performance is 442 sec. The life of the film cooled design is significantly above that of the regenerative design and is discussed in detail later in this section.

2. Design Requirements

The five thrust chamber cooling concepts shown in Figure IV-8 were evaluated on the basis of their ability to:

(1) Provide high cycle life durability with a minimum of performance loss due to film cooling requirements.

(2) Minimize coolant circuit pressure drop.

IV,B, Thrust Chambers (cont.)

- (3) Minimize manifold and coolant channel volumes to allow good pulsing characteristics.
- (4) Be light in weight and low in cost for a flight configuration.
- (5) Allow for either nozzle scarfing or extension to larger area ratios with a minimum of design changes.
- (6) Withstand some re-entry heating.

3. Cooling Concept Selection

The designs considered were:

- (a) Regeneratively cooled throat and combustion chamber with either a film cooled, partial dump, or full length dump cooled skirt.
- (b) A short regeneratively cooled combustion chamber and monowall film cooled throat and skirt.
- (c) A short regeneratively cooled combustion chamber with a combined up pass dump and full length dump cooled skirt.
- (d) A convectively cooled section fed from the injector, wherein the coolant is dumped a short distance upstream of the throat to film cool the throat and exit nozzle to a 40:1 area ratio. (This design is sometimes called the ducted chamber.)
- (e) A full 40:1 area ratio regeneratively cooled chamber.

The relative ranking of the five concepts are summarized in Figure IV-8 in which concepts shown as a and b (top two) were recommended to the NASA program manager for final evaluation.

Certain approaches were ruled out on the basis that they could not satisfy the basic design requirements or were expected to be difficult and expensive to fabricate. Concepts c and e fell into this class. Concept e, a

IV,B, Thrust Chambers (cont.)

full 40:1 regeneratively cooled chamber, appeared to have the highest performance potential based on the preliminary thermal analyses which indicated the design life to be satisfactory with 15% film cooling. This design was rejected mainly because it was not easily adaptable to nozzle scarfing. It is also the heaviest of all the approaches considered.

Concept c is lighter in weight mainly because the coolant passages are sized to handle only a small percentage of the total fuel flow and therefore the wall is much thinner. This design is also high performing because it requires a minimal amount of film cooling and the performance loss associated with the dump cooled skirt is small. This approach was rejected because it did not lend itself to scarfing. The fabrication was also expected to be difficult and expensive because of the very small coolant channel sizes in the skirt [.01 in. (.025 cm) deep] and the need for three separate manifolds.

The partial dump and full dump skirt options on Concept a were also rejected as not being easily fabricated and not amenable to skirt scarfing. The remaining concepts were considered equally attractive.

Concept d, employing ducted hydrogen flow, although simple to fabricate and light in weight, was considered a higher risk approach than Concept b because it is more sensitive to injector streaking and could result in considerable performance losses if a long chamber L^* were required. The potential problem with this concept, assuming the liner or duct is free standing, center on: (1) the cooling required to protect the ducted section, (2) dimensional changes in the duct-wall gap due to thermal growth of the inner liner, (3) duct collapse with an oxidizer lead due to flash-back into the coolant channels, (4) centering the duct, and (5) thermal choking of the film coolant due to potential injector hot streaks. Although not considered in Phase I, for the above reasons, the approach was reinvestigated in detail in Phase II, once

IV, B, Thrust Chambers (cont.)

it became apparent that a streak-free injector was available and that high performance could be achieved in a small chamber length. In the recommended Phase II design, the duct was bonded to the chamber wall, thus overcoming the potential difficulties of thermal growth, centering, and collapse due to flashback.

The selected designs offer, in one case (Concept a), a conservative approach employing proven state-of-the-art regenerative cooling in the higher heat flux chamber in conjunction with an easily scarfed film-cooled skirt. The second selection (Concept b), the film-cooled monowall throat, offered considerable potential for reductions in weight and fabrication costs, while providing performance in excess of the program goals, but was undemonstrated and of obviously higher risk.

An additional reason for the recommendation of this combination of chambers for the technology oriented program was the major role that fuel film cooling plays in meeting the required cyclic life of the thrust chambers. With these two designs, it was possible to obtain data relating performance loss at altitude to film cooling effectiveness for the following conditions: (1) film cooling introduced from the plane of the injector, (2) film cooling introduced a short distance upstream of the throat, and (3) film cooling injected supersonically into the supersonic flow downstream of the throat.

All of the above technology goals were achieved in the test program and are discussed later in this section.

The two chambers were designed for the operating conditions presented in Table IV-1.

IV, B, Thrust Chambers (cont.)

4. Design and Fabrication Descriptions

a. Phase I - Film Cooled Chamber Design

Engineering drawings, a schematic assembly drawing and component photographs of this design at various phases of fabrication are shown in Figures IV-9 through IV-11. This design consists of a short cylindrical regeneratively cooled copper chamber section from which the coolant fuel discharges into the injector and a convectively cooled conical copper section which dumps film coolant 1.3 in. (3.3 cm) upstream of the throat to cool the throat and exit nozzle. Hydrogen enters a constant area inlet manifold located at the downstream end of the regenerative section via two 1-in. dia (2.54 cm) feed lines and flows through 80, 0.180 in.-deep (.458 cm) by 0.050-in.-wide (.127 cm) slots in a copper liner at approximately 1000 fps. The fuel discharges directly into the injector manifold. The wall thickness of the copper inboard of the slot is a nominal 0.060 in. (.153 cm) in the design tested. Several types of copper -- including OFHC, zirconium copper and beryllium copper -- were analytically investigated, one zirconium copper and one OFHC copper unit were fabricated.

The throat film coolant is introduced through a separate manifold which allows flow regulation and thus optimization of the film coolant while the engine is firing. This coolant flows through 120, 1.5 in.-long slots, .040 in.-wide by .040 in.-deep (\pm .001 in.) (3.8 x .102 x .102 cm) convectively cooling the convergent nozzle before being dumped to film cool the downstream region.

The sequence of fabrication and assembly events is described with the aid of the photograph on Figure IV-11 as follows:

(1) The Haynes 188 throat is spun from a conical perform made from rolled and welded .050 in. (.127 cm) thick sheet material. Haynes 188 rod is employed in all welding operations, spinning is accomplished on a

IV,B, Thrust Chambers (cont.)

contoured male mandrel with periodic stress relief per the manufacturer's specification for this material. The final spun section shown in the upper left includes a portion of the manifolding required to feed the coolant channels. The spun part is dye penetrant inspected to insure the product is free of surface cracks.

(2) The ID of the above nozzle and the OD of the conical coolant distribution and injection ring are matched machined after which the coolant channels are milled.

(3) The above components are bonded and inspected. Inspection includes ultra sonic scanning of the bond joint to insure complete attachment and visual water flow checking of the coolant channels to insure that all are open and flowing properly. A sample of the ultrasonic inspection results showing 100% attachment is provided in the lower left. This process was repeated for three chamber assemblies and all were successful. The appearance of the discharge end of the bonded coolant ring can be observed in Figure IV-11.

(4) The next operation involves completion of the chamber jacket subassembly. The jacket has a 0.060-in. (0.152 cm) thick 304L stainless steel wall which seals the slots, mounts the chamber to the injector, serves as a pressure vessel, and transfers the thrust loads. The jacket also serves as the attachment point for the 304L aft closure which supports the throat and skirt. The jacket and aft flange, when later assembled, form a second manifold which receives the throat coolant via three 1/2-in. (1.27 cm) OD tubes.

(5) Assembly of the above subassembly with the turned and slotted copper chamber body and the throat section is accomplished by inserting the throat section from the aft end and the copper body from the forward end. The bonding is accomplished in a single furnace braze. A second braze is

IV,B, Thrust Chambers (cont.)

required to install the six gas side thermocouples.

(6) The bonding operations are followed by final machining of the ID of the copper body and coolant distribution ring.

(7) The spun 40:1 304L skirt, which is fabricated from rolled and welded .050 in. (.127 cm) thick sheet is then welded to the Haynes 188 throat section. The weld is then ground and polished inside and out and the complete throat and skirt assembly subjected to a final spin-to-size and polishing operation. The end product is shown being instrumented with backside thermocouples on the right side of Figure IV-11.

Instrumentation consists of six 0.020-in. (.051 cm) dia. chromel/alumel thermocouples inserted through the ribs in the regenerative section and brazed at the gas side surface. An additional 30 thermocouples are spot welded to the back of the sheet metal components. Inlet and outlet coolant pressures and coolant temperature monitoring ports are provided and a through-the-rib chamber pressure tap is located 1 in. (2.54 cm) downstream of the injector face.

The skirt insulation is 1/2-in. (1.27 cm) thick Fiberfrax Lo-con Blanket with a .002-in. (.005 cm) aluminum backing. This material is suitable for continuous service to temperatures of 2300°F (1530°K). Two thermocouples are epoxied to the exterior of the insulation.

Projected Life Analysis

The manifold region of the Phase I designs were not considered in the life analysis because they were low-cost, easy-to-fabricate workhorse components and incorporated a separate circuit for the film coolant which would

IV,B, Thrust Chambers (cont.)

not be part of the end product. The restraining influence that the manifolding has on the coolant jacket wall, however, is considered in the life analysis.

Table IV-3 provides a summary of the predicted life for this design at nominal operating conditions.

The life of the Phase I chamber designs is limited by the restraint that the propellant inlet manifold places on the copper liner. The expected life for full thermal cycles (burn time > 1.0 sec) ranges between 5000 and 10,000 cycles, the variance being due to the differences in published fatigue life data. Increasing the film cooling flow does not significantly increase chamber life. The use of a higher strength copper can increase the minimum life slightly and maximum possible life significantly. (The Phase II chamber design eliminates the low cycle life in this region by employing a flightweight, flexible manifold. The life capabilities of this design as a function of pulse width are covered in Section VII-B.) The long burn potential of the Phase I design, exclusive of the manifold region, ranges from 10,000 to 35,000 for the SN 1 OFHC unit to 23,000 to 80,000 for the SN 2 ZrCu unit. These limits are also increased in the Phase II design by reducing the thickness of the copper wall and steel jacket. The monowall Haynes 188 and 304 skirt can provide a cyclic life capability in excess of 10^6 cycles when the appropriate wall thickness is selected. The selection of wall thickness is covered in Section VII.

b. Phase II - Film Cooled Chamber Design

A redesigned prototype film-cooled chamber for Phase II propellant conditions was initiated using Phase I experimental data. The Phase II design goals were to make the design more optimum for cold propellants, to eliminate the life restrictions resulting from the use of a dual fuel feed

IV, B, Thrust Chambers (cont.)

manifold of workhorse construction, and to upgrade the life characteristics throughout the entire assembly. The Phase II film-cooled chamber design is shown in Figure IV-12.

Phase II activities included the analysis of a slightly modified regeneratively cooled chamber region, a slightly modified film coolant injection channel in the convergent nozzle to allow the entire copper liner to be machined and bonded as a single component, and a major redesign of the fuel supply manifold so that it would not be a limiting factor in chamber life. Table IV-4 provides a comparison of Phase I and Phase II design detail.

The major design changes outlined in Table IV-4 are:

(1) A reduction in both wall thickness of all components and in channel depths. This increases life and reduces weight approximately 30%. New weight (no flange) is 11 lb (4.5 kg).

(2) A change in the structural jacket material from CRES 304 to the higher strength 22-13-5.

(3) The copper section containing coolant channels is manufactured as a single component and the number of cooling channels in the dump section made an even multiple of the number of chamber channels (80/160).

Phase II - Chamber Life Predictions

The results of the changes outlined in Table IV-4 are highlighted as follows for nominal Phase II operating conditions:

IV,B, Thrust Chambers (cont.)

(1) The life in the manifold region now exceeds 100,000 full thermal cycles based on minimum value material properties and 10^6 pressure cycles.

(2) The new life limiting location is the copper at tip of the film cooling ring; however, material failure (a crack of engineering significance) at this location will not impact thruster operation. The N_f (full thermal cycles) of 50,000 is based on minimum values for material properties. A thermal cycle at this location corresponds to a bit impulse in excess of 275 lbf-sec (1110 N-sec).

(3) A failure condition of operational significance could occur in the regenerative chamber as early as 100,000 full thermal cycles. A thermal cycle at this location corresponds to a bit impulse greater than ≈ 750 lbf-sec (3330 N-sec). Life expectations at off design operating conditions are provided in Section VII.

c. Phase I - Regeneratively Cooled Chambers

(1) Design and Fabrication Description

Engineering drawings of the Phase I regeneratively cooled chambers, a schematic assembly, and photographs taken at various phases of fabrication and assembly are shown in Figures IV-10, IV-13, IV-14 and IV-15, respectively. This design consists of a single pass counterflow fuel regeneratively cooled copper chamber which extends from the injector to an area ratio of 8.3. At that point a bolt-on film-cooled skirt is attached which extends to an area ratio of 40:1. This bolt-on skirt contains its own manifolding and coolant injection nozzles as shown in Figure IV-14.

IV,B, Thrust Chambers (cont.)

The principle components of the chamber can be identified in the schematic drawing (Figure IV-10). These are:

(1) The copper chamber body containing 60 milled slots, 0.050 ± 0.001 in. wide (0.127 cm). The channels are of varying depth, starting at 0.4 in. (1.02 cm) deep at the aft inlet, decreasing to 0.2 in. (.51 cm) at the throat, and then increasing to 0.4 in. (1.02 cm) at the injector end.

(2) The CRES 304L manifold jacket which supplies the fuel through dual 1-in.-dia (2.54 cm) inlets to the 60 coolant slots and to which the skirt is bolted.

(3) The forward flange of CRES 304L which allows the chamber to be bolted to the injector and contains instrumentation bosses for coolant temperature and pressure and for a through-the-wall chamber pressure measurement.

(4) The skirt subassembly consists of a spun 304L skirt of 0.050 in. (.127 cm) wall thickness, a distribution ring for the film coolant consisting of 100 convergent-divergent nozzles photoetched in a 0.015-in.-thick (.038 cm) copper sheet and additional machined components required to contain these nozzles and bolt the skirt to the forward assembly.

The chamber-skirt interface is at an area ratio of 8.3. The selection of this attachment point was based on: (1) fabrication considerations (this was the smallest diameter aft manifold that could be installed from the forward end), (2) allowance for nozzle scarfing up to 48° , and (3) the desire to have sufficient length (10.5-in. (26.7 cm)) over which to obtain thermal data related to the injection of supersonic film cooling.

IV,B, Thrust Chambers (cont.)

Nozzle attachment at larger area ratios would increase weight while attachment at smaller area ratios was expected to result in significant increases in the film cooling requirements.

Skirt film coolant injection is accomplished via the 100 two-dimensional converging-diverging nozzles shown in Figure IV-14, which have the following characteristics:

Contraction ratio	2.07
Expansion ratio	2.8:1
Throat width	0.058 in. (1.47 mm)
Height	0.015 in. (0.381 mm)

The injector end of the chamber is designed to accommodate a film cooling ring which can be fed either from the discharge of the regenerative chamber through the four 1/2-in. (1.27 cm) bosses located in the forward flange or via a separate flow-controlled coolant supply circuit. The chamber can be fired without film coolant at the injector end by replacing the cooling ring by a blank adapter.

The fabrication sequence which was employed is illustrated in Figure IV-14. After ultrasonic inspection for voids, the copper forging was rough bored on the ID and finish machined to contour on the OD using a tracer lathe and template. Although the ID was not finish machined, the dimensions were controlled very accurately and sized to accommodate the tooling required to center the work and locate critical dimensions in subsequent operations. The copper was stress relieved at appropriate stages in the fabrication process.

The channel slotting operations were accomplished in two steps. First, a constant depth, constant width (0.060 x 0.060 in.)

IV,B, Thrust Chambers (cont.)

(0.15 x 0.15 cm) cut was made. This slot eventually received the 0.060 x 0.060 in. (0.15 x 0.15 cm) copper wires which provided the coolant channel closeout. A second variable depth, 0.050-in.-wide (0.127 cm) contour cut formed the coolant channels of variable cross-sectional flow area. Channel closeout was accomplished by press fitting precontoured 0.060-in. (0.15 cm) square copper wires into the slots with the 0.005-in. (0.0127 cm) ledge formed by the stepped machining providing a positive channel depth control. The wires were then brazed in position by running the unit through a braze cycle, the wires having been plated with braze alloy prior to their insertion in the slots. Following bonding the ID was machined to the final contour and the OD of the chamber at the forward and aft ends remachined to receive the forward flange and aft manifold jacket subassemblies. The ID of the two flanges were match machined to the OD of the chamber to ensure a true fit for brazing. The forward flange was finished with a slight interference fit and had to be heated to allow final assembly. These components also employed the plated braze technique to obtain proper braze alloy control. Fifteen 0.022-in.-dia (0.056 cm) thermocouple holes and a 0.040-in.-dia (0.102 cm) pressure port were also drilled through the ribs to the gas side at this time.

A second braze operation was employed to join the flanges and thermocouples to the body. Additional braze alloy was applied to the wire closeouts as required to correct those areas which did not properly seal. Figure IV-15 shows the chamber following this operation.

Braze assembly of components was conducted on a one-chamber-at-a-time schedule. In some instances, it was necessary to repeat a braze run to obtain proper flow of braze material and to install gas-side thermocouples or flanges. The ability to recycle components at or after the final assembly stage is a desirable feature.

IV,B, Thrust Chambers (cont.)

The pressure vessel structure in the regeneratively cooled design (the hoop loading cannot be carried by copper wires at 500 psia (345 N/cm^2) chamber pressure) is provided by electroforming a thin nickel jacket (0.050 in. (0.127 cm)) over the chamber following the wire braze. The electroformed nickel is isolated from the hydrogen by the wire closeout and therefore not subject to the embrittlement phenomena associated with the electroformed material. The condition following the electroforming operation is shown in the lower midportion of Figure IV-14. The electroforming operation was conducted after the thermocouples were in position because electroformed materials were previously found to blister when brazed. This sequence, however, precluded a final machining operation following electroforming since there was a high risk of damaging the thermocouple wires projecting from the chamber wall. The final operation on the instrumented version of the chamber involved machining the forward and aft seal surfaces to final dimensions.

Fabrication of the bolt-on skirt was initiated by turning the stainless steel manifold and copper ring. The OD of the ring and ID of the manifold were match machined to a conical surface which closely approximates the expansion angle of the Rao nozzle contour at the coolant injection station. The copper strip containing the 100 coolant injection nozzles was rolled to the identical conical form, sandwiched between these heavier structures, and bonded into position. As shown in Figure IV-14, this subassembly contained a manifold complete with inlet fittings and was flow checked with GN_2 to ensure that all nozzles were flowing properly and that the distribution was uniform.

The next operations involved: (1) turning the ID of the copper to the Rao nozzle contour, (2) welding the spun skirt to the flange (approximately 1 in. (2.54 cm) downstream of the copper), and (3) blending the weld and respining the assembly on the male mandrel to assure the accuracy of contour and roundness. The final operation involved assembly of the chamber and skirt.

IV,B, Thrust Chambers (cont.)

(2) Fabrication Summary

Initial difficulties were encountered in cutting deep, narrow slots in the regeneratively cooled copper chamber. These were a result of using nonoptimum tooling and cutting rates. Slotting operations proceeded smoothly once proper cutters were obtained and feed rates established. All designs employed constant-width cooling channels and were free of splits or bifurcations requiring milling operations, thereby lending themselves to low-cost quantity production.

The first electroformed chamber assembly resulted in nonuniform material deposition in both the circumferential as well as axial directions and some minor chamber warpage. A modification to the electroforming procedure for the second chamber assembly overcame these shortcomings. This is significant since an electroformed case would be required if it became necessary to employ a grade of alloy copper whose properties are adversely affected by brazing.

The 100 nozzles in the supersonic film cooling injection ring were fabricated by photoetching a single 0.015-in.-thick (0.038 cm) strip which was laid out to form the surface of a cone. The as-fabricated throat width and height were within 0.0005 in. (.0012 cm) of the design dimensions for all 100 nozzles.

The first chamber fabricated (SN 1) was of OFHC copper and the second (SN 2) was of ZrCu. No significant differences were reported in the fabricability and both units were satisfactorily completed and available for testing.

The projected life of this design is limited by a station 0.6 in (1.52 cm) upstream of the throat at nearly all operating

IV,B, Thrust Chambers (cont.)

conditions. The projected life capabilities are summarized in Table II and discussed in detail in Section VII-B along with the chamber thermal characteristics.

d. Phase II Regeneratively Cooled Chamber Design

The regeneratively cooled chamber designed for the Phase II low temperature propellant conditions is shown in Figures IV-16, IV-17, and IV-18. The major differences between this design and the Phase I design are as follows:

(1) The coolant inlet manifold was moved from area ratio 8 to area ratio 3, while the skirt film coolant injection plane was held fixed. This resulted in a short dump-cooled section between area ratios 3.5 and 8 which served to preheat the cold fuel used for skirt film cooling. The preheating allowed more favorable, higher supersonic coolant injection velocities to be achieved than would be possible by direct injection of cold fuel. Movement of the inlet manifold forward reduced the diameter of the manifold, volume of the coolant channels, the weight of the chamber, and helped reduce the pressure drop for the regenerative circuit.

(2) The chamber contour was modified to produce higher pressure gradients in the combustion gases in the throat. The laminarization analysis indicated this could result in a significant heat flux reduction in the throat.

(3) The coolant channels were modified to reduce chamber weight and coolant volume to take advantage of the higher density low temperature coolant. The channel width was increased from 0.050 to 0.062 in. (127-158 cm). A comparison of the depths is provided in Figure IV-19.

IV,B, Thrust Chambers (cont.)

(4) The channel closeout approach was modified to;

(a) eliminate the need for machining stepped coolant channels; (b) allow use of a photoetched, precontoured stainless steel truss in place of the hand-formed square copper wires; and (c) employ a shrunk-fit and brazed steel jacket rather than the electroformed nickel pressure vessel. The use of the etched steel channel closure allowed greater optimization of coolant channel flow configuration than could be achieved by conventional machining.

In this design, the chamber coolant entered the cylindrical coolant jacket via a single 1.5-in. (3.8 cm) diameter line located behind the throat (actual ID = 1.342 in. (3.4 cm)). The coolant then flowed around the periphery of the chamber in the manifold cavity formed by the outer steel jacket and the nozzle portion of the liner. The coolant entered each of the 60 0.062-in. (.152 cm)-wide coolant channels through aerodynamically contoured inlets as shown in Figure IV-17. The channel depth at this position is 0.28 in. (0.71 cm). The coolant flowed forward, accelerating slightly to a point immediately downstream of the throat. At this location, the flow was rapidly accelerated by a small nozzle formed in the etched channel closeout. The nozzle was oriented in such a fashion as to direct the flow towards the heated wall. The channel depth at the throat was 0.13 in. (0.33 cm). The region forward of the throat provided a diffuser section to recover as much of the kinetic energy of the coolant as possible. The channel depth continued to increase until the flow reached the cylindrical section where the depth remained constant at 0.28 in. (0.71 cm). The coolant discharging from the channels entered directly into the injector fuel manifold as shown in Figure IV-7.

The dump-cooled section downstream of the throat consisted of a 60-channel pass-and-a-half design. The coolant entered through a midpoint manifold, flowed forward, and then aft through a constant-area channel. The etched channel closeouts and the aerodynamically shaped turn-around manifold

IV,B, Thrust Chambers (cont.)

created the pass-and-a-half channel configuration when inserted in the slotted channel. The dump coolant discharged into a common peripheral collection manifold prior to entering the 100 nozzles for injection into the supersonic flow stream.

(1) Design Description and Fabrication

The Phase II regeneratively cooled chamber consisted of four major components:

(1) The copper liner(machined from a forging similar to the Phase I design) which contained 60 coolant channels of constant width and variable depth.

(2) A 0.015-in.-thick (.038 cm) photoetched copper strip containing 100 nozzles for distribution and injection of the skirt film cooling.

(3) A set of 60 photoetched channel closeouts which also provided the necessary channel contouring, structural supports, and manifold for the downstream dump section. The truss section was designed to restrain the thin-wall copper liner from collapse inward due to possible manifold overpressure to 850 psia (587 N/cm^2) by giving it a greater section modulus and fixing it to the outer jacket. The truss is less restrictive than the contoured electroformed case because it does not provide hoop restraint and is not efficient in compression due to the long L/D which allows the hot copper liner to grow. The channel closeouts also divide the axial slots into the upstream regenerative portion and downstream dump section. This separation can be observed to occur a short distance downstream of the throat and allowed the dump cooling flow to be varied independently on the experimental designs. In the prototype configuration, these dividers would be eliminated and flow

IV,B, Thrust Chambers (cont.)

controlled by sizing the throats in the coolant injection nozzles. The etched approach to fabrication allows the inlet region to the coolant channel and the channel area reduction approaching the throat to be manufactured to an aerodynamically optimum configuration without concern for fabrication difficulties. This results in lower pressure drops.

(4) The external structure consisted of a spun thin-wall stainless 40:1 skirt, several match machined conical sections for closing out the channel section in the divergent nozzle, and a tubular steel jacket which closed out the coolant channels in the chamber region and provided the necessary hoop restraint, transferred thrust loads, etc. The design thickness requirements for this case are 0.060 in. (.160 cm) for 304 stainless steel and 0.040 in. (0.101 cm) for the higher strength 22-13-5 material.

(2) Fabrication and Assembly

The fabrication and assembly sequence can best be understood with reference to Figure IV-17. The copper chamber was turned, contoured, and slotted similar to the Phase I design. The etched rib and channel closeouts were then press fit into the slots with the depth of insertion being controlled by three positive stops. This operation and the following one in which the coolant nozzles were applied are shown in the lower left of Figure IV-17. The position of the nozzle relative to the slots is shown by six nozzles for descriptive purposes only; in actual assembly, the 100 nozzles were installed as a single strip which was held in position by a match machined conical steel ring. The insert in the upper right shows the chamber following the first braze operation which unitizes the structure. The next operation involved remachining of the OD of the chamber body to provide smooth cylindrical and conical surfaces to receive the next closure assemblies (shown in the upper left and midsection of the figure). The thermocouple holes were also drilled through the ribs to the gas-side surface at this time.

IV,B, Thrust Chambers (cont.)

All pressure tap and inlet fittings were welded to the steel jacket prior to final assembly in order to eliminate the need for welding in close proximity to braze joints. The conical aft closure and cylindrical section closure were then brazed into position and the assembly leak and pressure checked.

The final operation was to weld the spun skirt to the aft end of the steel jacket and clean and polish the weld joint. An electron beam welding process was employed to minimize the heat input to the adjacent structure. The final assembly is shown in Figure IV-18.

The performance vs. life summary for the design is presented in Table IV-2 and supporting analysis and test results are presented in Sections V, VI, and VII.

IV, High P_c Technology Program (cont.)

C. IGNITERS

This section describes the igniter design criteria and checkout testing in the igniter-only mode which was conducted in advance of the full thruster testing.

1. Requirements

The requirements for the ignition system were to provide an energy source which would reliably and rapidly ignite a 1500-lbf (6670-N) thruster over a very wide range of operating conditions. Thruster systems showed that the ignition device would be called upon to ignite the mainstage propellants (oxygen and hydrogen) over a wide range of mixture ratios (3 to 5); propellant temperatures from saturated vapor to many hundreds of degrees of superheat; and propellant mass flows which could range from 30 to 170% of the nominal design value.

Further analysis of the system revealed that the same variations in propellant flows, temperatures, pressures, etc., predicted for the inlet to the mainstage should be expected within the igniter. The ignition device itself therefore was required to ignite gaseous hydrogen and oxygen in all concentrations, pressures, and supply temperatures which could be projected for the extremes of the operating conditions.

2. Design Selection

Two ignition concepts were selected for evaluation in this program. One was an electrically energized device (spark), the other a catalytic ignition system. On the basis of the ignitability analysis shown in Figure IV-20, an oxidizer-rich torch igniter approach was selected to

IV, C, Igniters (cont.)

amplify the energizing source. This analysis, described in Reference 1, indicated that ignition could most readily be achieved in the 5 to 100 O/F range. A design mixture ratio range of 35 to 40 was selected as optimum in that it provided sufficient latitude in ignitability to accommodate the projected off-design mixture ratio range which, under the most adverse combinations of propellant temperatures and pressures, could vary from 15 to 70.

After extensive testing, the spark ignition system was selected over the catalytic system on the basis of its (1) faster response, (2) greater reliability, (3) ability to safely cold flow the igniter without having an automatic ignition, and (4) demonstrated capability of maintaining rapid and repeatable restarts with very cold propellants over a wide range of mixture ratios. As part of the igniter evaluation, cold propellant tests were conducted which covered igniter chamber mixture ratios ranging from 30 to 120 with fuel temperatures down to 175°R (97°K) and oxygen temperatures as low as 250°R (139°K). Ignition with the spark igniter was successfully accomplished within about 0.010 sec under all test conditions. A complete presentation of the spark igniter design and ignition characteristics can be found in the final report to Contract NAS 3-14348.

3. Spark Igniter Design

An isometric cutaway view of the spark igniter assembly is shown in Figure IV-21. This design is capable of dual mode operation; i.e., either as an ignition source or as a 25-lbf (111-N) thruster for minimum impulse when supplied with separate valves. The igniter consists of two major components: (1) a body which contains the manifolding, a platform for retaining the spark plug and two valves, and the flange for mounting to the injector; and (2) a nickel chamber which transports the igniter flow safely through the injector body. The separate coolant jacket shown is not employed for normal operation but was fabricated to simulate the internal cavity of

IV, C, Igniters (cont.)

the injector into which the chamber would normally be installed. This allowed the igniter to be fired for long durations in a separate test facility.

In this design, all of the igniter oxygen flows through the gap between the electrodes. Mixing of the oxygen and hydrogen does not occur until downstream of the electrodes. When spark discharge occurs, it passes through the oxygen stream, exciting some of the oxygen to a highly energetic state. Ignition takes place when this high energy oxygen mixes with the hydrogen downstream of the electrodes. The stream of oxygen passing over the electrodes both shields them from the combustion gases and also cools them.

The fuel flows from an annular manifold into parallel coolant and injection flow passages. Only a small portion of the hydrogen is injected into the igniter chamber through six small holes. It impinges on the spark-excited oxygen, producing ignition within the igniter at a high mixture ratio. The bulk of the fuel bypasses the reaction zone and is used as igniter coolant. It is ducted along an annular passage formed by the nickel chamber and the internal cavity of the injector into which the igniter is inserted. The annular passage dimensions and flow are selected to provide the necessary cooling of the nickel chamber which contains the high mixture ratio hot gas. The MR = 40 gas within the cooled chamber ejects through the igniter chamber throat coaxially with the fuel discharging from the coolant annulus. These coaxial streams mix to produce the MR = 5.0 torch which ignites the mainstage.

a. Stress and Heat Transfer Analyses

Hydraulic, heat transfer, stress, and ignition characteristics of the high P_c igniter were analyzed to verify igniter design. The results of these analyses are discussed below.

IV, C, Igniters (cont.)

(1) Hydraulic Analysis

The hydraulic analysis employed the design parameters listed in Table IV-5 (such as valve inlet pressure and fuel oxidizer flow rates) to size critical dimensions of the basic igniter design, i.e., coolant and igniter hot gas throat diameter. The throat diameters required to satisfy design flow rates were calculated by evaluating feed line pressure drops and heat transfer and friction losses within both the coolant and hot gas circuits. The stagnation pressures at certain system key points were iterated by varying geometry until initial design flow rate requirements were met.

Two igniters were analyzed, one designed for a nominal thrust of 25 lbf (111 N) and one designed for 50 lbf (222 N). The igniter design P_c was 300 psia (207 N/cm^2) in the zero back pressure case. The system was evaluated at a core mixture ratio of 35:1 and an overall mixture ratio of 5.0. The two igniters analyzed only differed in the chamber throat area and fuel injector spacer size.

An important objective of the analysis was to evaluate the effect of varying back pressure on igniter flow rates and mixture ratio as the back pressure at the main engine injector face varies from 0 to 300 psia (0 to 207 N/cm^2). The technique used was to assume throat inlet stagnation pressures and to determine whether the resulting flow rate satisfied the initial valve inlet pressure of 375 psia (259 N/cm^2). Another important consideration was the effect of nozzle thermal expansion on the annular coolant flow passage. All sizing was based upon the use of Nickel 200 as the igniter material with a thermal expansion coefficient of $9.1 \times 10^{-6} \text{ in./in./}^\circ\text{F}$.

IV, C, Igniters (cont.)

In the case of zero back pressure, a normal sonic compressible flow equation was used to check flow rates through the fuel coolant orifice and the hot gas and coolant throats. Appropriate Rayleigh and Fanno line relations were employed where pressure losses were significantly influenced by heat addition and frictional losses.

The case in which the injector face is at 300 psia (207 N/cm^2) required a more complex analysis which employed a subsonic compressible equation in a process of iteration. The results of this analysis, in addition to providing the data required to size the fuel coolant circuit and the hot gas circuit, indicated that the presence of the 300 psia (207 N/cm^2) back pressure caused a reduction in overall mixture ratio for the 25-lbf (111-N) igniter, i.e., from 5.0 to 4.37. Similarly, the 300 psia (207 N/cm^2) back pressure caused a reduction in the core mixture ratio from 35 to 33.5. Both mixture ratio shifts are modest and did not limit igniter operation.

Further investigation showed the influence of propellant supply temperatures to be of greater significance in shifting the igniter mixture ratio than variation in chamber pressure during mainstage ignition. The extreme situations of warm fuel and cold oxidizer and cold fuel and warm oxidizer could shift the mixture ratio from approximately 52 to 20. This condition is further aggravated if the supply pressures also shift. Although this mixture ratio range was not of concern from the standpoint of providing reliable ignition, the lower values do result in a more severe thermal environment and lower coolant flow rates.

(2) Heat Transfer Analysis

The steady-state heat transfer characteristics of the igniter were calculated using the Aerojet HEAT computer program. This program is used for the analysis of convective cooling. The temperature and

IV, C, Igniters (cont.)

pressure, as well as transport properties, Mach number, etc., of the coolant are determined at each station along the contour by a "marching" calculation that proceeds in the direction of the coolant flow. The heat flux and wall temperatures are also calculated at each station.

The hot gas-side thermal boundary conditions were based on heat flux data obtained from a series of short (0.1 sec) heat sink chamber (no coolant jacket) tests using a 0.05-in.-thick (0.127 cm) Hastelloy X chamber which had seven backside thermocouples located along the axis and around the periphery. The experimental data indicated that the heat flux calculated from the theoretical combustion temperature at nominal mixture ratio and the simplified Bartz correlation for local heat transfer coefficient in the chamber region was adequate for design. The experimental heat flux data for mixture ratios 35 and 50 were employed to design a cooled nickel igniter chamber having a combination of coolant velocities, core mixture ratios, and hot gas flow rates which resulted in a predicted maximum wall temperature as follows:

Thrust Level	Igniter Core MR	Overall MR	Wall Material	Throat Gas-Side Temp, °F(°K)	Throat Coolant Side Temp, °F(°K)	Wall ΔT, °F(°K)	Coolant Velocity, ft/sec (m/sec)	Heat Flux, Btu/in ² -sec (W/cm ²)
25	35	5	Nickel*	2015 (1375)	1661 (1178)	354 (197)	1800 (548)	5.41 (886)
25	35	5	Hastelloy X (original igniter)	2630 (1720)	1996 (1365)	639 (355)	389 (118)	2.57 (421)
25	50	4	Nickel*	1436 (1052)	1142 (890)	294 (163)	930 (283)	3.92 (642)
25	35	5	Nickel**	680 (633)	400 (477)	280 (155)	1800 (545)	3.20 (525)

*New design, original boundary conditions.

**New design, estimated new boundary conditions (contour change).

IV, C, Igniters (cont.)

The analysis of the initial design using the experimental data shows higher than desirable wall temperatures. The following design and operating modifications were made to the original design to improve the thermal safety factor:

- (1) The chamber tube material was changed from Hastelloy X to Nickel 200, which has a higher thermal conductivity.
- (2) The coolant velocity was increased by reducing the coolant annulus gap and the flow control moved from the gap to a series of drilled orifices at the inlet to the cooling jacket. This latter change was made to prevent a reduction in coolant flow as the chamber heated and the gap closed down.
- (3) The igniter throat approach contour was changed to eliminate the sharp edge entrance resulting from the step drill manufacturing approach. A smooth contour was recommended, which should result in laminarization of the throat boundary and a substantial reduction in throat heat flux.
- (4) The nominal core operating mixture ratio was increased from 35 to 45.
- (5) The fuel injection downstream of the spark plug was changed from injection through a 0.001-in. (0.0254 mm) slot to injection through six drilled orifices of equivalent area. This modification produced greater penetration of the fuel into the oxidizer. Moving the fuel away from the wall in effect produced a more oxidizer-rich boundary which lowered both the film temperature and heat transfer coefficients and thus heat flux.

This program was not afforded the opportunity to repeat the experimental identification of the igniter chamber gas-side boundary conditions with the final hardware configuration using instrumented type heat sink chambers. Additional testing, however, was accomplished with an intermediate hardware design, using the cooled chamber in the igniter-only

IV, C, Igniters (cont.)

setup. The hardware at this point contained all the recommended design modifications with the exception that the single fuel injection slot, rather than the six holes, was still being employed. In this series, several thermocouples were installed on the backside of the hydrogen-cooled chamber internal to the coolant jacket. The results of these tests are summarized in Table IV-6. Maximum recorded external temperatures during these tests at a core MR of 40 were 738°F (666°K) following soakout from a 0.6-sec burn. From these data, the inferred maximum gas-side temperature was 850°F (728°K) and the wall gradient 220°F (122°K). Steady conditions were approached but not achieved in these tests. An additional series of 24 and 48 0.120-sec pulse tests was conducted as shown in Figure IV-22. Maximum steady temperatures of 840°F (722°K) were recorded after approximately 20 pulses. The testing demonstrated the igniter's ability to pulse continuously. Since the major emphasis in this program was on injector and thruster testing, igniter burns were conservatively limited to 0.1 sec for full thruster firings in which the possibility of extensive mixture ratio shifts could exist; i.e., igniter oxidizer flow was shut off after mainstage ignition and fuel left on to cool the chamber. In this mode, the heat sink capabilities of the nickel igniter chamber provided a considerable safety margin.

These design and operating recommendations were found completely adequate for the program. No igniter thermal failures were experienced with the modified design in the approximately 7000 igniter firings conducted on this and the concurrent ignition study contract, NAS 3-14348. Long duration burns (150 sec) were accomplished at design mixture ratio, thus substantiating the analytical prediction of steady-state operation under nominal conditions.

IV, C, Igniters (cont.)

(3) Ignition Characteristics

The maximum and minimum ignition pressure limits for the igniter designs were predicted on the basis of existing Aerojet ignition data. The maximum cold flow pressure at which ignition can occur in the spark igniter is controlled by the output voltage of the power supply and the electrode spacing. The relationship between the breakdown voltage and the pressure and electrode spacing are defined by Paschen's Law as indicated in Figure IV-23. The power supplies can deliver 30,000 volts. Therefore, the upper limiting value of pressure times the electrode space ($P \cdot D$) is about 5.5 lbf in. if air and oxygen are assumed similar. The curve of pressure versus electrode spacing shown in Figure IV-24 was drawn using this value of ($P \cdot D$).

The design values on the spark electrode spacing and the corresponding cold flow pressures are indicated on Figure IV-24. The steady-state cold flow chamber pressure for these igniters is 100 psia (68.9 N/cm^2). The spark igniter design point occurs at the 100 psia (68.9 N/cm^2) level, placing it 10 psi (6.9 N/cm^2) below the ignition limit. This may appear to give only a small margin of safety. However, the unit ignites during the initial flow transient when pressures in the chamber are well below the 100 psia (68.9 N/cm^2) steady-state level indicated on Figure IV-23. The actual location of the pressure limit line and the desired margin of safety was investigated during the test program of Reference 1. The steady-state cold flow pressure limitation did not prevent ignition.

The minimum ignition pressure limit is determined by the flame quenching phenomena. Therefore, it is independent of the ignition technique. Rather, it depends on the mixture ratio, the igniter chamber diameter and, to a lesser extent, the propellant temperature. The critical value of the flame quenching parameter ($P \cdot D$) is about 5.0 lbf in. at a mixture ratio of 35 while the igniter design cold flow pressure is a factor of 6 higher than the quenching pressure; therefore, ignition failures due to flame quenching did not constitute a problem.

IV, C, Igniters (cont.)

An analysis of the effect of varying the propellant inlet temperature on igniter mixture ratio was made to determine its effect on engine ignition. This was done by holding both the oxidizer and fuel inlet pressures constant at 375 psia (259 N/cm^2) and letting first the fuel temperature vary and then letting the oxidizer temperature vary. The results of this calculation are included in Figure IV-20. The core MR is seen to vary from MR = 20 to MR = 52. The igniter exhaust temperature will be adequate for reliable engine ignition over this range of mixture ratios. Previous work has indicated ignition should occur up to an igniter mixture ratio of about 75. However, the MR = 20 condition will result in a high igniter chamber temperature which will reduce igniter life.

(4) Spark Plug and Power Supply

The spark plug used for the spark ignition system evaluation was a modified version of General Laboratory Associates (GLA) Spark Plug, PN 48036. Table VI-7 summarizes the power supply characteristics.

b. Test Results

A total of 258 High P_c igniter-only and full thruster ignition tests were conducted on the final igniter configuration for the exclusive purpose of studying ignition characteristics. These included a wide range of mixture ratios, propellant temperatures, power levels, pressures, and other design and operating variables. A full description of the testing and test results are published in Reference 1, which states that no limiting ignitability conditions were encountered and ignition delays (lagging propellant to 90% P_c) were on the order of 0.01 sec or less for all test conditions. Table IV-8 provides a short summary of these test conditions and results.

IV, C, Igniters (cont.)

A series of igniter no-ignitions were experienced in the latter phases of the 40:1 nozzle altitude testing on this program which are not covered in Reference 1. These generally involve the inability to get the igniter operational after an extended period of disuse and, in one case, repeated failure of the igniter to ignite with cold propellants when operating in an off-design condition. In all but the last case, the problems were resolved by disassembly of the spark plug and cabling, drying and cleaning electrical contacts, and then reassembly. During this period, it was found that reducing the spark gap from 0.050 to 0.025 in. (0.127 to 0.063 cm) minimized these apparent electrical problems. Also, it was noted that employing a fuel lead on the igniter could correct an erratic igniter ignition situation, probably because it provided an ignitable mixture in the igniter at a lower pressure than occurs with an oxidizer lead.

Unfortunately, it was impractical for these ignition failures to be researched since they occurred very late in the program and in a large, highly automated altitude facility which was ideally suited for full-scale engine testing and not for researching ignition problems. Similar events reported in Reference 1 were without exception traced to electrical problems and associated with the fact that the igniter design and power system employed was developed as a research tool to investigate ignition phenomenon and was not meant to be a rugged, all-weather, all-environment type hardware.

c. Recommendations for Future Spark Igniter Work

Several areas of design and operation warrant further investigation. One is to better characterize the electrical characteristics of the current power source, cables and electrical insulation to determine their limitations. New all-weather, rugged electrical package designs should then be immediately subjected to all environments which cause failure of existing designs and all conditions which are anticipated for actual service.

IV, C, Igniters (cont.)

The second area involves igniter cooling at off-design conditions, especially at low mixture ratios associated with a propellant supply of warm oxidizer and cold fuel. Two parallel activities are recommended in this area. One is to obtain thermal data from heat sink igniter chambers (laboratory hardware) to better understand the combustion side internal environment as a function of propellant supply conditions. The other is to conduct extensive durability tests and off-design limit testing on prototype igniter configurations and explore those operating points not demonstrated in Reference 1.

4. Catalytic Ignition

a. Introduction

The primary deficiency of catalytic ignition systems for O_2/H_2 has historically been poor thermal response. If the propellants and/or the catalyst are very cold, the propellants may fail to react at all or only with long delays, even in the presence of the most active catalysts. Lower temperature is, however, only part of the thermal response problem. Another part stems from the fact that the catalyst and its associated hardware present a relatively large heat sink and a good heat transfer media. Thus, the exit gases and catalyst currently take a relatively long period of time to come to a high enough temperature to ignite a primary engine.

Aerojet Liquid Rocket Company in July 1970 found, as a result of company-funded research, that the standard two-step catalytic igniter would not provide fast response even under benign conditions. It was found, however, that the thermal response problem could be overcome by proper catalytic igniter design without heating the catalyst bed within the igniter by using a four-step ignition approach which featured downstream oxygen injection. Most catalytic igniters for O_2/H_2 engines have been based on a two-step ignition process, i.e., (1) the catalytic ignition of O_2/H_2 within

IV, C, Igniters (cont.)

the catalyst bed ($MR = 1$), and (2) the thermal ignition of the main engine O_2/H_2 by the catalyst bed exhaust. The ignition of the main engine is directly related to the temperature of the catalyst bed exhaust, i.e., $1850^\circ F$ ($1285^\circ K$) (theoretical) at steady state. In contrast, the ALRC catalytic igniter was based on a four-step ignition process; i.e., (1) the catalytic ignition of O_2/H_2 within the catalyst bed ($MR = 1$), (2) the thermal ignition of the catalyst bed exhaust with secondary oxygen ($MR = 40$), (3) the thermal ignition of the cooling jacket hydrogen with igniter chamber exhaust ($MR = 5$), and (4) the thermal ignition of the main engine O_2/H_2 by the igniter torch. The steady-state temperature of the igniter torch is $5600^\circ F$ ($3390^\circ K$) (theoretical). Thus, by a series of bootstrap ignitions, the igniter torch exhaust temperature is increased threefold while the inherent limitations of the catalyst bed are not exceeded. In addition, an order-of-magnitude increase in igniter response, as demonstrated by faster temperature and pressure rise rates, was achieved by the ALRC catalytic igniter.

b. Background for Design Selection

The limitations of the two-step igniter appeared to rest with the inherent characteristics of the catalyst, e.g., Shell 405, and the catalyst bed, e.g., a packed bed of catalyst pellets (14-18 mesh). The thermal stability of the catalyst limits the "hot-fire" thermal environment to $1800-1900^\circ F$ ($1255-1310^\circ K$) to avoid sintering the pellets with a resultant loss of catalytic activity. This limitation fixes the O_2/H_2 mixture ratio to approximately 1.0. The result is that the relatively low level of energy release within the bed, when coupled with the low flow rates through the bed, makes thermal response a problem. The catalyst bed and its attendant hardware act as a heat sink in the reaction environment, generally resulting in slow response.

IV, C, Igniters (cont.)

In considering these limitations, it became apparent that the inherent thermal limitation of the catalyst could not be improved but that the other limitations could be circumvented by minimizing the size of the catalyst bed and by adding additional steps to the ignition process. It was hypothesized that a small catalyst bed operated at a mixture ratio of 1.0 would provide a "warm" gas which could be "instantaneously" changed into a "hot" gas by secondary oxygen injection in a well-defined plenum. The plenum, in turn, could be regeneratively cooled with hydrogen and the cooling hydrogen could be burned with the secondary oxygen combustion exhaust to provide a very hot torch to ignite the main engine propellants. Thus, the limitations associated with response time and low igniter effluent temperature could be solved without changing the mixture ratio of the O_2/H_2 flowing through the catalyst bed.

c. Design Description

The design provided by ALRC is described with reference to Figures IV-21 and IV-25. Figure IV-21 is a cutaway isometric view of the igniter used in obtaining the test results presented in a later discussion, while Figure IV-25 is a schematic drawing of this igniter.

As noted previously, only a small portion of the total igniter propellant flow actually passes through the catalyst bed, the majority of the propellant being mixed with the bed effluent downstream of the bed. The manner in which this is accomplished is illustrated in Figure IV-25. Both the oxygen and hydrogen enter small plenums at the back of the igniter. At that point, the oxygen is divided into two streams; 2.5% of the oxygen is bled off through the oxygen core flow control orifice for injection through the catalyst bed, while the remainder flows into the annulus surrounding the catalyst bed housing. From there, it is injected through the O_2 secondary flow control orifices into the $MR = 1.0$ catalyst bed exhaust, raising the mixed gases to an MR of 40.

IV, C, Igniters (cont.)

The path followed by the hydrogen can also be seen in Figure IV-25. As the hydrogen leaves the inlet plenum, 12.5% of the flow passes through the H_2 core flow control orifices. This hydrogen is mixed with the O_2 core flow gas to give the $MR = 1.0$ gas, which is injected into the catalyst bed. The remainder of the hydrogen flows forward through the H_2 coolant channel surrounding the igniter chamber. This hydrogen convectively cools the igniter chamber in which the $MR = 40$ combustion is taking place. At the igniter discharge, the cooling hydrogen is injected coaxially with the $MR = 40$ gas, bringing the overall MR of the injected torch to 5.0.

There are several features of the mechanical design which are worthy of specific mention. The small catalyst bed, which contains Shell 405 catalyst, is contained in a thin-walled stainless steel housing. As a result, it not only has a low thermal capacitance but is also in poor thermal communication with the remainder of the igniter. This largely reduces heat soak as a problem in pulse mode firing and gives slightly improved bed thermal response. More important, however, is what the bed location produces in the igniter chamber. By placing the catalyst bed in the center and allowing the secondary oxygen to be injected coaxially around the bed effluent, the igniter chamber wall approaches the $MR = 40$ condition from the oxygen-rich side. This allows going from the $MR = 1.0$ gas exhaust to the $MR = 40$ gas exhaust in the igniter chamber without the chamber wall being exposed even locally to stoichiometric combustion products. This substantially reduces the thermal load to the chamber wall.

A final feature of the design is that the use of cooling H_2 makes the igniter capable of extended duration operation, either by itself or with the engine firing, without significant heating of either the igniter or injector. This makes it possible to use the igniter in an igniter-only pulsing mode for minimum impulse bit generation independent of injector operation.

IV, C, Igniters (cont.)

d. Test Results

(1) Igniter-Only Mode, Ambient Temperature Propellants

Ambient and low temperature propellant checkout tests of the catalytic igniter were accomplished in three series, which are summarized in Table IV-9. In Series I, steady igniter P_c was achieved 0.018 sec after the initiation of propellant flow. Evaluation of the temperature measurements from thermocouples located within the catalyst bed indicated the bed mixture ratio to be slightly higher than nominal. Inspection of the hardware revealed the bed to be undamaged, the screen retaining the bed to show signs of overheating, and the fuel valve to have a potential leak because of contamination of the valve seat.

These tests were repeated in Test Series II in which the bed mixture ratio was reduced slightly and a 0.010- to 0.015-sec fuel lead added to the start sequence. The igniter P_c rise characteristics were similar to Test Series I, with the exception of the extension of the period from first fuel flow to full P_c by a time period equal to the fuel lead.

The results of Test No. 110 are shown in Figure IV-26 for nominal pressures and ambient temperature propellants. The response time in this test is 0.017 sec. Note that, while the catalyst bed temperature rises comparatively slowly as indicated by T_2 (which is buried in the catalyst bed), the chamber temperature rises comparatively rapidly as indicated by T_c (which is buried in the chamber wall). It is apparent that the combustion of the catalyst bed exhaust with the secondary oxygen is fully established within 10 millisecon of the ignition of O_2/H_2 within the catalyst bed, as indicated by the chamber pressure rise.

IV, C, Igniters (cont.)

The 100-pulse test (Test No. 115) demonstrated the durability of the igniter and the reproducibility of its performance. The last three pulses of this test, which are representative of the entire test, are displayed in Figure IV-27. Note the rapid pressure rise (17 millisec), very short ignition delay (4 millisec), and precise pulse-to-pulse reproducibility obtained in this operational mode.

Tests 113 and 114 provide additional insight to the operation of the igniter. Test 113 was conducted, in part, to determine the effect on response time of lowering the O_2/H_2 mixture ratio within the catalyst bed. This was accomplished by reducing the total O_2 flow rate. A 5-millisec increase in response time was obtained. In addition, an accompanying $554^\circ F$ ($308^\circ K$) increase in secondary chamber wall temperature was obtained as compared with Test 114. The reduction in the total O_2 flow rate resulted in a reduction of the mixture ratio in the igniter chamber. This, in turn, results in a higher combustion temperature in the chamber. The bed mixture ratio appears to have an effect on response time; i.e., the lower the bed mixture ratio, the longer the response time. The chamber mixture ratio can be controlled independently in an improved design. Proper control of flow rates and flow distribution will result in a high degree of operational flexibility while maintaining the fast response characteristics of the basic design.

(2) Igniter Testing with Cold Propellants

Tests with reduced temperature propellants were conducted in Bay 1 of the Physics Laboratory, where a vacuum firing position and equipment for conditioning propellants to low temperatures were located. The propellant conditioning equipment consisted of two storage vessels, one for oxygen and one for hydrogen, located within refrigerators connected to a liquid nitrogen supply. The facility also included the necessary instrumentation and propellant control equipment.

IV, C, Igniters (cont.)

This third test series consisted of 16 tests. Testing was started with two facility cold flow tests to verify that all equipment was functioning properly. The next six tests were performed at ambient temperature to achieve the correct start sequence, i.e., valve timing, and to provide data that could be used for baseline purposes.

The procedure for the cold temperature tests consisted of the following steps: (1) reducing the propellant temperatures in increments of approximately 50°R (28°K); (2) prepurging the igniter with fuel to chill the bed; and (3) conducting the test. The tests were performed at successively lower temperatures in an attempt to find the point where either the response time would increase or ignition would not be achieved.

As the testing proceeded and the temperature was lowered, it was found that the igniter could not be chilled sufficiently with cold propellants and prepurges alone. Therefore, prior to Test 129, the igniter, valves, and attendant hardware were conditioned with liquid nitrogen. At the same time, the propellants were refrigerated to the lowest temperature possible with this setup. Critical flow (sonic) control venturis were used to set propellant flow rates. At a tank pressure of approximately 350 psia (241 N/cm^2) (the lowest level), an isentropic expansion on the Mollier diagram for oxygen limits the minimum temperature to approximately 300°R (167°K) to prevent liquefaction in the throat of the venturi. No such restriction exists for hydrogen when chilling only to LN_2 temperature.

When Test 129 was attempted, the "oxidizer-valve pilot valve" would not open. The tank safety valve was then closed to prevent loss of the oxidizer and current was allowed to flow through the solenoid valve until it was heated enough to function properly. The safety valve was opened, allowing oxygen to flow back to the igniter valve; the igniter was purged with cold fuel; and Test 130 was performed. A long ignition delay was observed,

IV, C, Igniters (cont.)

0.109 sec, as compared with approximately 0.033 sec at other conditions. As shown by the data, the last test (131) was conducted with incoming propellant temperatures just 20 to 30°R (11 to 16°K) higher to determine whether a limiting condition had been found. Testing was terminated with Test 131 which functioned normally with a 0.023-sec response.

The data contained in Table IV-9, Series II, are divided into two sections. The first eight columns represent the test conditions and results, and the remaining six columns contain the propellant and hardware temperature achieved during the tests. T_{oT} and T_{fT} are the temperatures of oxygen and hydrogen, respectively, as measured in the storage vessels; T_{oTCV} and T_{fTCV} are the propellant temperatures measured at the inlets to the oxygen valve and hydrogen valve, respectively. T_{Body} , divided into columns labeled T_{fj} and T_{oj} , represents measurements of igniter body temperature taken just before each test. The T_{oj} and T_{fj} thermocouples were positioned in contact with the metal surrounding the propellant manifolds. As such, they do not provide a measure of propellant temperature for tests of this short duration. Rather, they provide a measure of igniter hardware temperature just prior to test initiation.

The results of these tests show that the fast response of the catalyst igniter is retained with ~350°R (194°K) temperature propellants flowing into the igniter but that significant delays may be expected when temperatures drop below this level.

The final column in this table provides an ignition delay parameter which is defined as first oxidizer flow to 90% igniter P_c .

IV, C, Igniters (cont.)

(3) Igniter-Complete Thruster Testing

The results of two tests conducted with the catalytic igniter in the igniter-complete thruster mode are summarized in Table IV-10. The major difference between Tests 120 and 136 is the former was conducted at a nominal overall mixture ratio of 4.0, while the latter was conducted at 5.0. Once again, the four-step igniter demonstrated extremely rapid response, i.e., 25 to 28 millisecc. The complete engine start transient, from the first pressure response in the igniter hydrogen manifold to the establishment of full engine chamber pressure, was 80 millisecc in Test 120 and 67 millisecc in Test 136.

These tests were conducted such that the hydrogen lead in the igniter was 10 msec, the hydrogen lead in the main chamber was 2 msec, and the igniter was at steady state for 10 msec before propellants were admitted to the main chamber. Examination of the oscillograph traces indicates that the complete engine start transient can be reduced by 40 msec in each of these tests by improved valve sequencing.

Comparison of the igniter response times reported for the igniter-only tests with those of the igniter-complete thruster tests indicates an increase of approximately 7 msec. Different pairs of igniter valves were used on these test series, i.e., Futurecraft for igniter-only and Marotta for igniter-complete thruster. The Futurecraft valves have faster opening times. This effect is particularly noticeable in the oxygen flow transient as determined by the oscillograph traces.

A normal procedure, in the course of complete thruster firings, is to pressurize the propellant feed system and to cycle each main valve independently prior to a firing. These cold flow tests with

IV, C, Igniters (cont.)

the catalytic igniter in position frequently resulted in ignition of the fuel and air within and external to the thrust chamber, even though the igniter was not operating. This phenomenon represented a substantial hazard in testing and the number of full thruster tests were therefore kept to a minimum.

(4) Discussion of Test Results

It is apparent from the test results that the ALRC four-step catalytic igniter demonstrated very fast response time and the ability to ignite a main thruster smoothly and very rapidly under ambient conditions. The establishment of full igniter chamber pressure was obtained within 17 millisec. The establishment of full thruster chamber pressure was obtained within 63 msec and, in all probability, can be obtained within 50 to 55 millisec. These results are highly encouraging at the current state of the development of this catalytic igniter.

A single catalyst charge was used for all of the tests reported in Series II of Table IV-9. Posttest examination showed the catalyst to be in excellent condition with the exception of a small area at the center of the inlet to the bed where some of the pellets were sintered together. A new catalyst charge was used in each of the tests reported in Table IV-10. Posttest examination showed the catalyst to be in excellent condition in each case; no catalyst sintering was evident. Proper mixture ratio control of the propellant entering the catalyst bed should eliminate pellet sintering and long catalyst life should be attainable.

While the control of the total oxygen and hydrogen flow to the igniter is precise and the total flow rates are accurately measured, the flow split of each propellant within the igniter is not measured. The flow splits are fixed by the size of flow control orifices. These splits have not been verified experimentally. The propellant flow to the bed is nominally fixed at MR = 1.0, giving a bed temperature of 1850°F (1285°K). Note,

IV, C, Igniters (cont.)

however, that in Test 110 the aft bed thermocouple reached a temperature of 2247°F (1500°K), indicating the bed mixture ratio approached 1.25 (theoretical). Whether this mixture ratio shift was caused by increased oxygen flow to the bed, decreased hydrogen flow to the bed, or both cannot be determined from the available data. It is apparent that precise control of each propellant flow circuit is required to learn more about the operating characteristics of this igniter.

The hypothesis that a small catalyst bed operated at a mixture ratio of 1.0 would provide a "warm" gas which could be "instantaneously" changed into a "hot" gas by secondary oxygen injection in a well-defined plenum appears to have been validated. This mechanism appears to provide the basis for the extremely rapid igniter response time. In addition, the combustion of the cooling hydrogen with the secondary oxygen combustion exhaust appears to provide a very hot torch which results in extremely rapid thruster response time. However, the catalytic ignition approach was not recommended for further use in this program because of possible ignition problems at low temperatures, the hazards of ignition during cold flow, and the generally superior starting characteristics demonstrated by the spark igniter.

IV, High P_c Technology Program (cont.)

D. VALVE DESIGN AND OPERATING CHARACTERISTICS

1. Requirements

The valve requirements for this program were to provide a highly reliable, fast response, low pressure drop design which closely simulated the operating characteristics specified for APS prototype valves. The valve employed in thruster testing was to be of a proven design but was not required to provide the 10^6 cycle capabilities or the very low internal leakage. Separate valves were selected rather than a single bipropellant valve because this offered the capability of easily varying the propellant lead/lag relationship.

2. Valve Description

Two independent, pneumatically (helium) actuated poppet valves (one fuel and one oxidizer) of the side entry angle type with a port diameter of 1.125 in. (2.85 cm) were supplied for program use by the Aerojet Liquid Rocket Company. The two valve bodies and poppets were manufactured by Controls Components Inc. and incorporated a soft seat (Teflon) seal in a standard encapsulated configuration. The aerodynamic configuration of the valve gallery, port approach, and post-port pressure recovery area were supplied by ALRC to ensure that the pressure drop was less than the 25 psid (17.3 N/cm^2) design goal. A cross-section drawing of the valve and valve actuator is shown in Figure IV-28.

Figure IV-29 shows the fuel valve body, poppet, seals, pneumatic actuator, and linear potentiometer prior to and following assembly. The valve body was stainless steel; the poppet was of tubular stainless steel construction and the actuator was fabricated from aluminum. Although this

IV, D, Valve Design and Operating Characteristics (cont.)

valve was of workhorse construction and designed for a 2000 psia (1380 N/cm^2) inlet pressure, the weight of all moving parts was less than 2 lb (0.9 kg) to produce fast dynamic characteristics. The oxidizer valve was identical to the fuel valve except the large inlet flange was on the opposite side. Figure IV-30 shows the valves mounted on the test stand in Bay 7 of the Research Physics Laboratory. The long approach section and side entry to the valves provide both feed line flexure and a straight section for close-coupled flow measurements. This same feed line approach configuration was employed in all altitude testing.

The mainstage valves employed pneumatic actuation. The valve actuation system consisted of two 1/2-in. (1.27 cm) Marotta Model No. MV583 (PN 803664-1) pilot valves for each main valve. One pilot valve supplied helium to or vented the lower portion of the actuating piston, the other the upper portion of the piston. The supply and vent port areas and electrical characteristics of the pilot valves controlled the dynamics of the valve system.

The valve actuator shown in Figure IV-29 is a simple aluminum piston 3.23 in. (8.2 cm) in diameter that provides a 0.4-in. (1.02 -cm) stroke. The piston was driven by helium at a supply pressure of 150 psia (103.5 N/cm^2). It can also be actuated by the gaseous fuel.

3. Valve Dynamic Characteristics

Typical valve dynamic characteristics measured in the initial series of checkout and firing tests are summarized in the following table.

IV, D, Valve Design and Operating Characteristics (cont.)

Helium pressure	150 psia (103.5 N/cm ²)
Thrust chamber valve travel time	
300 psia (207 N/cm ²)	0.006 sec full closed to full open
500 psia (345 N/cm ²)	0.008 sec full closed to full open
Electrical signal to TC valve full open	0.085 sec (fuel) 0.100 sec (oxidizer)
Pilot valve travel time	0.010 sec (estimated)

The thrust chamber valve travel time (0.006 to 0.008 sec, full closed to full open) was sufficiently fast for the program requirements for rapid start transients. The valve travel time was found to be insensitive to substantial variations in helium supply pressure and to propellant temperatures.

The actuation times for the 1/2-in. (1.27 cm) Marotta pilot valve were unacceptable for pulse mode operation because of the delay between electrical signal and the start of pilot valve travel. This condition was corrected by improving the quality of the electrical signal to the pilot valves. The initial voltage was increased and inductance and capacitance characteristics of the circuitry optimized to maximize the rate of current buildup in the pilot valve coils. Valve dynamic characteristics following this modification are summarized in the following table:

		<u>Oxidizer Valve</u>		<u>Fuel Valve</u>	
		<u>Open</u>	<u>Close</u>	<u>Open</u>	<u>Close</u>
Travel time, sec	Initial	0.008	0.010	0.010	0.0074
	Intermediate	0.008	0.010	0.008	0.009
	Final	0.010	0.010	0.012	0.012
Electric signal to full travel, sec	Initial	0.042	0.043	0.045	0.039
	Intermediate	0.036	0.032	0.035	0.042
	Final	0.040	0.030	0.045	0.048

IV, D, Valve Design and Operating Characteristics (cont.)

The initial valve dynamic characteristics data were taken from one of a series of 25 engine pulse tests conducted in the injector checkout test series. The intermediate data were taken following stem and seat/seal replacements on the main valves after approximately 5500 cycles. The final dynamic characteristics were those recorded after approximately 8500 valve actuations of which about 6000 were actual engine firings.

Valve travel time was reproducible within 0.004 sec for all test conditions. Valve actuation time was reproducible within 0.013 sec with the largest variations occurring immediately following a servicing, i.e., during the wear-in period.

4. Hydraulic Characteristics

Valve weight flow vs pressure for high speed compressible flow is predicted by the following equation:

$$\dot{w} = \frac{C_d A P_{in} (8.02)}{\sqrt{T_1} \frac{1545}{Mw}} \left[\frac{K}{K-1} \left[\left(\frac{P_{out}}{P_{in}} \right)^{2/K} - \left(\frac{P_{out}}{P_{in}} \right)^{\frac{K+1}{K}} \right] \right]^{1/2}$$

where: A is the valve port area (1.00 in.²) (6.35 cm²).

The experimental value of C_d was obtained for each valve from bench tests using GN₂. Experimental C_d values are 0.735 for the oxidizer valve and 0.736 for the fuel valve.

The relation which best approximates the flow vs pressure drop characteristics for the valves in actual engine tests are:

$$\Delta P = 34 \frac{\dot{w}^2 T_{in}}{Mw P_{in}}$$

IV, D, Valve Design and Operating Characteristics (cont.)

Data from a typical test at nominal conditions are as follows:

	<u>Flow,</u> <u>lb/sec (kg/sec)</u>	<u>Propellant</u> <u>Temp, °R (°K)</u>	<u>P_{out},</u> <u>psia (N/cm²)</u>	<u>ΔP,</u> <u>psid (N/cm²)</u>
Fuel valve (H ₂)	0.69(0.31)	522(290)	354(244)	10.9(7.52)
Oxid valve (O ₂)	2.76(1.25)	522(290)	356(246)	10.5(7.25)

5. Service History

Main valve actuators were disassembled three times during the course of the program for inspection and preventive maintenance. The first disassembly was for inspection purposes only following bench testing, during which each valve was leak checked, cold flowed, and actuated 500 times at rated back pressure. No wear or leakage was recorded, and the valves were reassembled.

The valves were installed in Bay 7 of the Research Physics Laboratory as shown in Figure IV-30 and were used concurrently on two contracts, this and the ignition contract NAS 3-14348. During the period, the valves were cycled an additional 4500 times (approximately), of which 3000 were actual engine firings; 2500 of these were accomplished within a four-hour period. The performance history during the 2500 firings is described below.

a. Performance of APS Thrust Chamber Valves During 2500-Pulse Series 2K7-115

The performance of the valves was evaluated in two categories: motion repeatability and leakage. Leakage of both poppet and stem seals was checked periodically during the series of 2500 engine pulses.

IV, D, Valve Design and Operating Characteristics (cont.)

Prior to initiating the pulse series, both oxidizer and fuel valves indicated a very slight stem seal leak; no poppet leakage was detected. Stem seal leaks were tested for with a standard leak check fluid. Poppet leakage was tested for with a standard bubble indicator. Leak check pressure on both valves was 100 psi (69 N/cm^2). The bubble indicator was left attached to each valve for 5 min. Pressurant was the effluent, i.e., GH_2 , fuel valve; GO_2 , oxidizer valve.

Valve motion during the pulse series was measured by linear potentiometers attached to the valve stem. Output signals from the potentiometers were recorded on an oscillograph. Valve data were collected at the 100th, 500th, 900th, 1200th, 1400th, and 2500th pulse. The following data resulted:

<u>Pulse No.</u>	<u>Valve</u>	<u>External Leakage</u>	<u>Internal Leakage</u>
100	Oxidizer	None	None
100	Fuel	None	None
500	Oxidizer	Stem - Moderate	None
500	Fuel	Stem - Slight	None
900	Oxidizer	Stem - Moderate	None
900	Fuel	Stem - Slight	None
1200	Oxidizer	None	None
1200	Fuel	Stem - Slight	None
1400	Oxidizer	Stem and Nut - Moderate	None
1400	Fuel	Stem and Nut - Slight	None
2500	Oxidizer	Stem and Nut - Heavy	None
2500	Fuel	Stem and Nut - Heavy	None

After each leak check, the packing nut on the oxidizer valve was tightened with the exception of Pulse No. 100 at which time no leakage was noted. Tightening of the packing nut reduced each measured leak to a negligible value. During the course of 2500 pulses, the oxidizer valve pack nut was advanced approximately $1/8$ turn. The packing nut on the fuel valve was not tightened as its position was inaccessible.

IV, D, Valve Design and Operating Characteristics (cont.)

Fuel valve motion appeared to be regular, approximately 10 ms opening and closing. Oxidizer valve motion appeared somewhat irregular, shifting on closing from approximately 10 ms to 20 ms after some 200 pulses.

b. Posttest Series Valve Inspection

Following this test series, the valves were removed from the test stand, disassembled, and inspected for wear.

The Teflon stem seal on the fuel valve was badly worn and showed evidence of cold flowing away from the seal area. The valve stem was lightly scratched, indicating metal-to-metal contact in the seal area. The valve poppet seal and internal seat showed no sign of wear.

The oxidizer valve Teflon stem seal, much the same as the fuel valve, was badly worn. The valve stem was moderately scratched, as was one side of the large diameter of the poppet. The valve poppet seal and internal seat showed no sign of wear. However, more Teflon was extruded from the oxidizer valve poppet seal than could be considered normal; therefore, the poppet seal assembly was disassembled for inspection. All seal parts appeared normal and a new Teflon seat seal was installed upon reassembly. No further evaluation on this part was performed.

Both fuel and oxidizer valve actuation assemblies were inspected for wear. Internal surfaces showed slight wear and some scratches. Wear of these aluminum components was considered normal.

IV, D, Valve Design and Operating Characteristics (cont.)

c. Corrective Action

The stem seal areas of the oxidizer and fuel valve poppets were polished. Nearly all scratches were removed from the seal area. The virgin Teflon stem seals were replaced with glass-filled Teflon seals. The glass-filled Teflon seals were expected to reduce the tendency of the seals to cold flow.

The valves were reassembled, operated, and leak checked and delivered to the altitude test facility for the next phase of the test program.

Several hundreds of additional cycles were added to the valves in the altitude test facility. This included a wide range of propellant temperatures, ranging from 200°R (111°K) to 800°R (445°K). The environment in the altitude facility was considerably more severe than the previous sea level tests. During the rapid evacuation of the altitude cell and in long tests with cold propellants, the valves and actuators were coated with ice. The environment in the cell following shutdown from an altitude test was estimated to be 100% humidity with temperatures ranging from 100 to 200°F (310 to 370°K). This condition is a result of blowback from the steam ejection system following facility shutdown. The post-shutdown blowback also deposited substantial quantities of scale from the duct and sand around the hardware, some of which eventually worked its way through the stem seals and into the valves.

In spite of the adverse conditions, the mainstage valves performed satisfactorily during this period and no internal leaks were reported. Slight stem seal leaks were periodically corrected by tightening the packing nut. A separate film cooling valve of a different design did fail

IV, D, Valve Design and Operating Characteristics (cont.)

to open in one test; however, that valve is not required for the final system. The mainstage valves and valve actuators were disassembled for inspection prior to executing the second 2500-pulse series. The condition of the valves at this stage was comparable to that following the previous inspection; namely, the valve stems and body were scratched and the Teflon seat seals showed excessive wear. In this case, however, wear could be traced to the sand which was observed in the Teflon stem seal. The hardened valve seats and aluminum actuators were in good condition. The valve poppets were polished again and all Teflon seals replaced. This time an extra thick stem seal was employed. The actuator seals were also replaced even though they were in good condition. A sheet metal shield was also formed at this time to close off the area between the valve body and valve actuator where the sand was depositing.

The valves were returned to the test stand and an additional 3500 valve actuations accomplished, of which about 3000 were actual engine firings. During this period, no internal leakage was recorded. The slight stem seal leakage was corrected periodically by tightening the packing nut. The valves were not inspected following this test series.

d. Mainstage Valve Limitations

The valves employed were completely reliable in that no test was ever terminated because of a failure of either valve to operate properly, with one exception. The exception was a result of a human error in which a pilot valve was not connected. No limitations were found due to propellant temperatures or supply pressures. Linear potentiometers periodically malfunctioned and had to be rebuilt or replaced. The Model MV583 Marotta pilot valve was found to be erratic after functioning over a long period at 10 cycles per second because of overheating of the electrical coil.

IV, D, Valve Design and Operating Characteristics (cont.)

It is difficult to estimate the life potential of the soft seat seal design in actual service since failure or leakage was avoided by preventive maintenance. Five thousand cycles were demonstrated without leakage, and it is not unreasonable to project that an additional 5000 could have been accomplished under favorable operating conditions.

The frictional type sliding stem seal is obviously unsuitable for a zero leakage, maintenance-free valve.

6. Igniter Valves

Two sets of igniter valves were employed in this program. One set consisted of a 3/8-in. Marotta Model 563 which was electrically actuated. The other set was a Futurecraft solenoid valve (PN 20714) which was a combined electrical-nitrogen-actuated design. The Futurecraft valves were found to be unsuitable for the severe environment of the altitude facility and repeatedly developed internal leaks. A single set of the Marotta Model 563 valves was employed throughout the program and was found to be exceptionally reliable and fast responding. The Marotta valves were employed for cryogenic service even though this was beyond the recommended range of operation. To protect against freezing in the open position, 28-volt electrical blanket heaters were wrapped around the valves and the temperatures monitored to ensure they were not getting too cold. This procedure worked very well.

TABLE IV-1
THRUSTER DESIGN REQUIREMENTS

	<u>Phase I</u>		<u>Phase II</u>	
	<u>Nominal</u>	<u>Test Range</u>	<u>Nominal</u>	<u>Test Range</u>
Thrust				
lbf	1500	500-2500	1500	500-250
Newtons	6680	2225-8900	6680	2225-8900
Chamber Pressure				
psia ₂	300	100-500	300	100-500
N/cm ²	207	69-345	207	69 -345
Mixture Ratio	4.0	3-5.0	4.0	3-5.0
Propellant Temperature				
Fuel: °R	540	200-800	250	150-600
°K	300	111-445	139	83-333
Oxid: °R	540	Sat-800	375	Sat-600
°K	300	Sat-445	208	Sat-333
Supply Pressure to Valves				
psi ₂	375	--	375	--
N/cm ²	259	--	259	--
c* Efficiency Goal	97%	--	97%	--
Specific Impulse Goal, sec	435	--	425	--

ENGINE DESIGN REQUIREMENTS

Fuel: Gaseous hydrogen derived from the vaporization of liquid hydroger per MIL-P-27201.

Oxidizer: Gaseous oxygen derived from the vaporization of liquid oxygen per MIL-P-25508A.

Installation: Buried within vehicle mold line.

Maximum External Temperature: 700°K (800°F)

Total Life Capability: Estimated 50 hours, with maintenance, based on 30 minutes life required per mission for 100 missions during a 10 year period.

Total Number of Pulses: Estimated 1,000,000 pulses, with maintenance, based on 10,000 pulses per mission for 100 missions during a 10 year period.

Maximum Single Firing Duration: 1000 seconds

Duty Cycle Limitations: None

TABLE IV-1 (cont.)

Engine Design Requirements (cont.)

Compatibility: Compatible with propellants, test fluids, and cleaning fluids for 10 year life requirement.

Reusability: To be reusable with minimum servicing and refurbishment.

Service and Maintainability: Designed for ease of service and maintenance when required.

Minimum Impulse Bit (goal): 223 N sec (50 lb sec)

Response: 50 milliseconds (Time from electrical signal to 90% thrust).

TABLE IV-2
CYCLE LIFE PERFORMANCE MATRIX

PHASE I CHAMBER DESIGNS AND CONDITIONS AMBIENT TEMPERATURE PROPELLANTS					
P_c , psia (N/cm^2)	100 (69)	300 (207)			500 (345)
MR	4	3	4	5	4
Regen Chamber, 10% FFC					
I_s , lbf-sec/lbm (N-s/kg)	449 (4400)	455 (4459)	452 (4429)	440 (3952)	455 (4459)
N_f	3.5×10^4	3×10^4	3×10^4	3×10^4	1.2×10^3
N_{fT}	3.5×10^4	2×10^3	2×10^3	2×10^3	
Film Cooled Chamber, 20% FFC					
I_s , lbf-sec/lbm (N-s/kg)		448 (4390)	443 (4341)	430 (4214)	447 (4380)
N_f		--	10^6	--	
N_{fT}		9×10^3	9×10^3	9×10^3	

PHASE II CHAMBER DESIGNS AND CONDITIONS
COLD PROPELLANTS

Regen Chamber, 9% FFC					
I_s , lbf-sec/lbm (N-s/kg)	--	444 (4351)	442 (4332)	431 (4224)	442 (4332)
N_f	10^6	10^6	10^6	10^6	--
N_{fT}	2×10^5	1.5×10^4	1.5×10^4	1.5×10^4	7.5×10^3
Film Cooled Chamber					
15% FFC					
I_s , lbf-sec/lbm (N-s/kg)		441 (4322)	438 (4292)	428 (4194)	
N_f	10^6	10^6	4×10^5	10^5	4×10^4
N_{fT}	$> 10^5$	10^5	10^5	10^5	4×10^4
20% FFC					
I_s , lbf-sec/lbm (N-s/kg)		438 (4292)	435 (4263)	425 (4165)	
N_f	10^6	10^6	10^6	8×10^5	2×10^5
N_{fT}	$> 10^5$	10^5	10^5	10^5	--

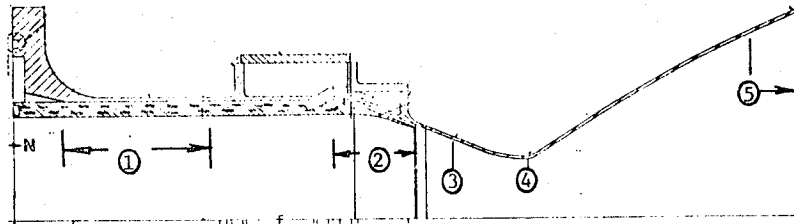
N_f = Thermal cyclic life for pulses of 200 lbf-sec or less.

N_{fT} = Thermal cyclic life for full thermal cycles. Firings $> \sim 750$ lb-sec total impulse.

All designs provide 10^6 pulse capability for 50 lb-sec bit impulse.

TABLE IV-3

PHASE I FILM-COOLED CHAMBER PROJECTED LIFE



Location/Time	T_{wg} , °F(°K)	ΔT , °F(°K)	ϵ_T	% FFC	Material	$\eta_f^* \times 10^{-3}$	
						Min	Max
① Trans @ 0.35 sec	420 (490)	260 (144)	0.47 "	20-30	ZrCu & B-D OFHC AgZrCu	23 10 23	80 35 250
① S.S.	600 (590)	210 (112)	0.34	20-30	ZrCu & B-D OFHC AgZrCu	40 18 40	400 80 1000
②** Trans 1.0 sec	510/455 (540)/(510)	370/315 (205)/(175)	0.74/0.61	20/25	ZrCu & B-D OFHC AgZrCu	6/9 5/6 6/9	25/40 10/17 80/100
③ Trans @	450 (505)	300 (166)	0.47	20	ZrCu & B-D OFHC AgZrCu	23 10 23	80 35 250
③ S.S.	834/704 (715)/(650)	184 (102)	0.29	20/25	ZrCu & B-D OFHC AgZrCu	55 25 55	500 100 >1000
④ Trans @ 0.05-0.10 sec	500 (530)	340 (188)	0.27 0.21	20 20	Haynes 188 0.04 wall 0.03 wall		460 1000
④ S.S.	1250 (960)	0		20	Haynes 188	>>50 hr creep rupture	
⑤ Trans	--	--	--	20	CRES 304	>>1000	
⑤ S.S.	1800 (1260)	0	--	20	CRES 304	>50 hr creep rupture	

**Life in this region is limited by restraint of workhorse manifolds.

*Full thermal cycles based on available published data for specified materials.

TABLE IV-4

COMPARISON OF PHASE I AND II FILM-COOLED CHAMBERS

<u>Design Parameter</u>	<u>Phase I, in. (cm)</u>	<u>Phase II, in. (cm)</u>
Chamber Region		
No. channels	80	80
Material (liner)	ZrCu and OFHC	ZrCu
Liner wall thickness	0.060 (0.153)	0.035 (0.089)
Jacket material	CRES 304L	22-13-5
Jacket wall thickness	0.060 (0.153)	0.040 (0.101)
Channel depth	0.180 (0.458)	0.150 (0.382)
Channel width	0.050 (0.127)	0.050 (0.127)
Coolant Injection Region		
No. channels	120	160
Material (liner)	OFHC	ZrCu
Liner wall thickness	0.060 (0.153)	0.035 (0.089)
Jacket material	CRES 304	22-13-5
Jacket thickness	0.050 (0.127)	0.040 (0.101)
Channel width	0.040 (0.101)	0.030 (0.076)
Channel depth	0.040 (0.101)	Variable tip 0.030 (0.076)
Throat		
Material	Haynes 188	Haynes 188
Thickness	0.050 (0.127)	0.040 (0.104)
Skirt		
Material	CRES 304L	CRES 304 or Haynes 188
Thickness	0.050 (0.127)	0.040 (0.104)
Manifold		
	Rigid 304	Flexible 22-13-5
Regen section ΔP , psi (N/cm^2)	38 (27)	35 (24)

TABLE IV-5

DESIGN CRITERIA - HIGH P_c O_2/H_2 SPARK IGNITER

	Nominal Thrust Level Igniter-Only Mode			
	50 lb		25 lb	
Oxygen Inlet Pressure, psia (N/cm^2)	375	(259)	375	(259)
Oxygen Inlet Temperature, °R (°K)	540	(300)	540	(300)
Hydrogen Inlet Pressure, psia (N/cm^2)	375	(259)	375	(259)
Hydrogen Inlet Temperature, °R (°K)	540	(300)	540	(300)
Oxygen Flow Rate lb/sec, (Kg/S)	0.125		0.0623	(.0283)
Hydrogen Flow Rate				
Igniter Core lb/sec, (Kg/S)	0.00357	(.00162)	0.00179	(.00813)
Coolant, lb/sec, (Kg/S)	0.0124	(.00564)	0.0107	(.00487)
Total, lb/sec (Kg/S)	0.025	(.0112)	0.0125	(.00564)
Mixture Ratio				
Overall	5		5	
Igniter Core	35		35	
Exhaust Temperature °R, (°I)	5000	(2770)	5000	(2770)
Spark Gap in., (cm)	0.050	(.127)	0.050	(.127)
Spark Rate, sps	500		500	
Spark Energy, millijoules/spark	10		10	
Minimum Ignition Pressure, psia, (N/cm^2)	17	(11.7)	17	(11.7)
Maximum Ignition Pressure, psia, (N/cm^2)	110	(76)	110	(76)

TABLE IV-6

SPARK IGNITER-ONLY MODE THERMAL TESTS

Test No.	P _c , psia	\dot{w}_{O_2} lb/sec	\dot{w}_{H_2} lb/sec	MR	\dot{w}_{H_2} lb/sec	MR	Core	\dot{w}_{H_2} lb/sec	(gm/sec)	Ignition	Burn Duration, sec	Max Temp Run/Soak, °F	(°K)
Vacuum Start													
242-244	356 (246)	0.082 (37.15)	0.016 (7.25)	5.12	0.002	(.906)	40.7	0.0139	(6.297)	Yes	0.1	322/467	(439/514)
243	133.5 (92.1)	0.031 (14.04)	0.006 (2.72)	5.16	0.00076	(.3443)	40.8	0.0052	(2.374)	Yes	0.1	266/356	(403/453)
246-247	111.2 (76.7)	0.025 (11.33)	0.005 (2.27)	5.00	0.00066	(.2990)	37.9	0.00434	(1.966)	Yes	0.1	286/342	(414/445)
228	122 (84)	0.024 (10.87)	0.005 (2.27)	4.8	0.00061	(.2763)	39.4	0.00439	(1.989)	Yes	0.1	397/372	(475/461)
Ambient Start													
249	582 (402)	0.135 (61.16)	0.027 (12.23)	5.0	0.00332	(1.504)	40.6	0.0236	(10.69)	Yes	0.1	407/522	(481/545)
250	527 (364)	0.127 (57.53)	0.025 (11.33)	5.0	0.00304	(1.377)	41.7	0.0219	(9.92)	Yes	0.1	407/506	(481/536)
251	523 (361)	0.126 (57.08)	0.025 (11.33)	5.0	0.00299	(1.354)	42.2	0.0220	(9.97)	Yes	0.1	482/490	(523/527)
252	527 (364)	0.128 (57.98)	0.024 (10.87)	5.3	0.00299	(1.354)	42.8	0.0210	(9.51)	Yes	0.1	391/506	(472/536)
Ambient Start													
253	345 (238)	0.081 (36.69)	0.016 (7.25)	5.1	0.00199	(.9015)	40.7	0.0140	(6.34)	Yes	0.16	422/496	(489/530)
254	330 (228)	0.078 (35.33)	0.015 (6.80)	5.1	0.00186	(.8426)	41.9	0.0131	(5.93)	Yes	0.20	473/544	(518/557)
255	304 (210)	0.071 (32.16)	0.014 (6.34)	5.1	0.00176	(.7923)	40.4	0.0122	(5.53)	Yes	0.25	487/549	(525/560)
256	304 (210)	0.071 (32.16)	0.014 (6.34)	5.1	0.00179	(.8109)	39.6	0.0122	(5.53)	Yes	0.30	556/643	(564/612)
257	304 (210)	0.071 (32.16)	0.014 (6.34)	5.1	0.00176	(.7923)	40.3	0.0122	(5.53)	Yes	0.35	396/694	(475/640)
258	304 (210)	0.071 (32.16)	0.014 (6.34)	5.0	0.0017	(.7882)	39.6	0.0122	(5.53)	Yes	0.40	625/738	(602/665)
259	289 (199)	0.070 (31.71)	0.014 (6.34)	4.9	0.00176	(.7923)	39.8	0.0122	(5.53)	Yes	0.45	638/688	(609/637)
260	285 (197)	0.069 (31.26)	0.014 (6.34)	4.9	0.00176	(.7923)	39.2	0.0122	(5.53)	*	0.50	642/642	(611/611)
261	285 (197)	0.069 (31.26)	0.014 (6.34)	5.1	0.00176	(.7923)	39.2	0.0122	(5.53)	*	0.60	638/408	(609/481)
Pulse Tests - 0.120 sec on, 0.300 sec off													
263	304 (210)	0.071 (32.16)	0.014 (6.34)	5.1	0.00176	(.7923)	40.3	0.0122	(5.53)	Yes	24 pulses	See Fig.	
264	304 (213)	0.071 (32.16)	0.014 (6.34)	5.1	0.00176	(.7923)	40.1	0.0122	(5.53)	Yes	48 pulses	See Fig.	

*Thermal expansion causes igniter P_c to decay at 0.48 sec.

TABLE IV-7

IGNITER POWER SUPPLY

SPECIFICATION FOR VARIABLE ENERGY SYSTEM 30342
GENERAL LABORATORY ASSOCIATES

<u>Parameter</u>	<u>Specification</u>
Input Voltage	120 volts, 60 Hz
Spark Rate	500 sparks per sec (fixed)
Spark Energy Level	0.01, 0.02 and 0.03 joule
Storage Capacitor Voltage	3500 volts DC (adjustable)
Output Voltage	25 to 30 KV (will fire 0.100 in. ² (0.25 cm) gap at 35 psia (24 N/cm ²))
Delay Time from Control Input to First Spark	Ca. 0.010 sec
Unidirectional Output Pulse	N/A
Spark Igniter	Air Gap Type
Remote Control Capability	(28 VDC)
Peak Reading Voltmeter	N/A

TABLE IV-8

SHORT SUMMARY OF SPARK IGNITER TEST CONDITIONS AND RESULTS

IGNITER-ONLY TESTS

TEST SERIES	TEST VARIANCES				NO. OF TESTS PERFORMED	TEST RESULTS
	P RANGE psia (N/cm ²)	ENERGY RANGE (mj)	GAP RANGE in. (cm)	TEMP RANGE °R (°K)	BACK PRESSURE RANGE	
High P _c Spark Igniter-Only with Ambient Temperature Propellants	100,300,500 (69,207,345)	1 to 30	0.025 to (.064 to .254)	Ambient	1 atm to 10 ⁻⁴ mmHg*	99 1. 10 msec response to 90% P _c 2. No limiting variables encountered 3. Durability demonstrated, 10 sec at steady state 4. Pulse capability demonstrated, 1000 pulses - 100 msec "on"/200 msec "off"
High P _c Spark Igniter-Only, Special Tests	See Results	1	0.100 (.064)	Ambient	Ambient	9 1. Ignition at 220 psia (152 N/cm ²) 2. 150 sec at steady state
High P _c Spark Igniter-Only with Low Temperature Propellants	100,300,500 (69,207,345)	1,5,10	0.025 to 0.100 (.064 to .254)	O ₂ : 423 to 297 (234 to 165) H ₂ : 313 to 255 (174 to 142)	0.5 psia	30 1. 10 msec response to 90% P _c 2. No limiting variables encountered
High P _c Spark Igniter-Only with Very Low Temperature Propellants	100,300 (69,207)	1	0.100 (.064)	O ₂ : 200 (111) H ₂ : 150 (83)	Ambient	13 1. Ignitions demonstrated at very low temperatures 2. Ignitions demonstrated with 2-phase oxidizer
High P _c Spark Igniter, Wide Range MR Survey (Tests Conducted with Above Series)	--	--	--	--	--	Core MR range of 40 to 122 demonstrated
High P _c Spark Igniter-Only EMI Tests		10	0.050 (.012)	--	Ambient	-- Meets MIL-STD-461

*Igniter response was found to be independent of back pressure.

IGNITER-COMPLETE THRUSTER TESTS

TEST SERIES	THRUSTER P RANGE psia (N/cm ²)	IGNITER ENERGY (mj)	IGNITER GAP in. (cm)	THRUSTER THRUST LEVEL lbf, nom (N)	BACK PRESSURE RANGE	NO. OF TESTS PERFORMED	TEST RESULTS
High P _c Spark Igniter-Complete Thruster with Ambient Temperature Propellants	100,300,500 (69,207,345)	10	0.050 (.012)	1000,1500,2000 (4450,6675,8900)	1 atm to 10 ⁻⁴ mmHg*	61	1. 10 msec igniter response to 90% igniter P _c 2. 15 msec thruster response to 90% thruster P _c 3. Main propellant fuel lead best 4. Pulse capability demonstrated, 25 pulses - 90 msec "on"/160 msec "off"
High P _c Spark Igniter-Complete Thruster with Low Temperature Propellants	100,300,500 (69,207,345)	1	0.050 (.012)	1000,1500,2000 (4450,6675,8900)	Ambient	34	1. Temperatures tested--O ₂ : 306°R (170°K) --H ₂ : 193°R (107°K) 2. No effect on ignition was encountered
High P _c Spark Igniter-Complete Thruster, Durability Test	300 (207)	10	0.050 (.012)	1500 (6675)	Ambient	--	1. 2500 engine ignitions 2. Hardware condition: Excellent 3. APS requirements demonstrated

*Propellant use found to be independent of back pressure.

TABLE IV-9

CATALYTIC IGNITER TEST SUMMARY (IGNITER-ONLY MODE)

SERIES I - AMBIENT PROPELLANTS

Test No.	Test Objectives	Duration, sec	P _c , psia (N/cm ²)	$\dot{W}_{O_2}^{-\epsilon}$, lb/sec (gm/sec)	$\dot{W}_{O_2}^{-\text{Bed}}$, lb/sec (gm/sec)	$\dot{W}_{H_2}^{-\epsilon}$, lb/sec (gm/sec)	$\dot{W}_{H_2}^{-\text{Bed}}$, lb/sec (gm/sec)	MR, ϵ	MR, Bed	Bed Temperatures (Max)	
										T ₁ , °F(°K)	T ₂ , °F(°K)
101	Explore operation @ nom. design cond.	0.140	243 (168)	0.067 (30.35)	0.0019 (0.861)	0.013 (5.89)	0.00188 (0.852)	5.1	1.03	1460 (1065)	2310 (1537)
102	Adjust flow rates	0.150	240 (166)	0.063 (28.54)	0.0018 (0.861)	0.013 (5.89)	0.00182 (0.824)	4.9	0.99	1605 (1146)	2155 (1451)
103	Extend time	0.290	240 (166)	0.063 (28.54)	0.0018 (0.861)	0.014 (6.34)	0.00195 (0.883)	4.5	0.92	1820 (1265)	2310 (1537)
104	Achieve full P _c	0.295	303 (209)	0.080 (36.24)	0.00232 (1.051)	0.016 (7.25)	0.00228 (1.032)	5.0	1.02	1940 (1332)	2385 (1579)
105	Repeat @ P _a = 0.3 psia (0.21 N/cm ²)	0.295	300	0.080	0.00232	0.0165	0.00234	4.9	0.99	1880* (1298)	2250* (1504)

*Temperatures taken at 0.234 sec into test when both thermocouples opened up.

TABLE IV-9 (cont.)

SERIES II - AMBIENT PROPELLANTS

Test No.	Test Objectives	Response, ^a sec	Duration, ^b sec	P _c , psia (N/cm ²)	\dot{w}_{O_2} , lb/sec (gm/sec)	\dot{w}_{H_2} , lb/sec (gm/sec)	MR _T	T ₁ , °F(°K)	T ₂ , °F(°K)	T _c , °F(°K)	Ignition Delay Time, sec ^f
106	Initial test to determine operating characteristics ^c	0.044	0.070	215 (148)	0.063 (28.54)	0.013 (5.89)	4.84	797 (697)	947 (781)		0.032
107	First test to explore new design conditions	0.028	0.065	253 (175)	0.063 (28.54)	0.013 (5.89)	4.84	817 (708)	1057 (842)	900 (755)	0.016
108	Extend test duration	0.035	0.117	265 (183)	0.064 (28.99)	0.013 (5.89)	4.92	1076 (852)	1726 (1213)	968 (792)	0.023
109	Increase flow rates	0.034	0.116	303 (209)	0.072 (32.62)	0.015 (6.80)	4.80	1888 (1303)	2188 (1469)	1329 (993)	0.022
110	Extend test duration	0.028	0.207	295 (204)	0.072 (32.62)	0.015 (6.80)	4.80	1930 (1326)	2247 (1502)	1201 (922)	0.016
111	Test at low P _c	0.035	0.195	104 (72)	0.024 (10.87)	0.005 (2.27)	4.80	1425 (1046)	1750 (1226)	1450 (1060)	0.023
112	Test at high P _c	0.029	0.126	465 (321)	0.106 (48.02)	0.025 (11.33)	4.24 4.24	d	d	1057 (842)	0.017
113	Pulse test at low MR (6 pulses)	0.034	e	265 (183)	0.052 (23.57)	0.013 (5.89)	4.00			1864 (1290)	0.022
114	Pulse test at nominal MR (6 pulses)	0.029	e	294 (203)	0.064 (28.99)	0.013 (5.89)	4.92			1310 (982)	0.017
115	100-pulse test	0.028	e	301 (208)	0.064 (28.99)	0.013 (5.89)	4.92			1450 (1060)	0.016

(a) Response: First pressure response in fuel manifold to establishment of full P_c.(b) Duration: Time of full P_c.

(c) First test was preceded by a fuel purge to activate the Shell 405 catalyst bed.

(d) Thermocouples in bed (T₁ and T₂) were lost during the high P_c test.

(e) Pulse cycle: 0.120 sec "on"/0.380 sec "off".

(f) Thermocouples in bed (T₁ and T₂) lost during high P_c test.

TABLE IV-9 (cont.)

SERIES III - LOW TEMPERATURE PROPELLANTS

Test No.	Test Objectives	Response, sec(1)	Duration, sec(2)	H ₂ Lead, sec	P _c , psia (N/cm ²)	\dot{w}_{O_2} , lb/sec (gm/sec)	\dot{w}_{H_2} , lb/sec (gm/sec)	MR	P _A , psia (N/cm ²)	T _{OT} , °R(°K)	(3)	T _{OTCV} , °R(°K)	(4)	T _{FTCV} , °R(°K)	(4)	T _{Body} , °R(°K)	T _{fj} , °R(°K)	Ignition Delay Time, sec(7)
116	Facility cold flow	--	--	--	--	--	--	--	--	--	--	--	--	--	--	--	--	--
117	Facility cold flow	--	--	--	--	--	--	--	--	--	--	--	--	--	--	--	--	--
118	Initial test	0.033	0.197	0.010	255 (176)	0.063 (28.54)	0.013 (5.89)	4.84	0.35 (0.242)	499 (277)	499 (277)	501 (278)	500 (278)	512 (284)	511 (284)	512 (284)	511 (284)	0.019
119	Adjust valve sequence	0.032	0.193	0.010	230 (159)	0.063 (28.54)	0.013 (5.89)	4.84	0.35 (0.242)	499 (277)	499 (277)	501 (278)	500 (278)	512 (284)	511 (284)	512 (284)	511 (284)	0.017
120	Adjust valve sequence	0.031	0.192	0.010	230 (159)	0.063 (28.54)	0.013 (5.89)	4.84	0.35 (0.242)	499 (277)	499 (277)	501 (278)	500 (278)	512 (284)	511 (284)	512 (284)	511 (284)	0.018
121	Increase flow rates	0.032	0.201	0.010	239 (165)	0.068 (30.80)	0.014 (6.34)	4.85	0.35 (0.242)	499 (277)	499 (277)	501 (278)	500 (278)	512 (284)	511 (284)	512 (284)	511 (284)	0.017
122	Increase flow rates	0.029	0.220	0.008	250 (173)	0.072 (32.62)	0.015 (6.80)	4.80	0.36 (0.248)	499 (277)	499 (277)	501 (278)	500 (278)	512 (284)	511 (284)	512 (284)	511 (284)	0.016
123	Validate last test	0.032	0.217	0.012	250 (173)	0.072 (32.62)	0.015 (6.80)	4.80	0.36 (0.248)	499 (277)	499 (277)	501 (278)	500 (278)	512 (284)	511 (284)	512 (284)	511 (284)	0.017
124	Test with cold prop.	0.033	0.199	0.010	250 (173)	0.072 (32.62)	0.015 (6.80)	4.80	0.36 (0.248)	452 (251)	443 (246)	460 (255)	460 (255)	506 (281)	508 (282)	506 (281)	508 (282)	0.019
125	Test with cold prop.	0.033	0.189	0.012	258 (178)	0.072 (32.62)	0.016 (7.25)	4.80	0.36 (0.248)	423 (235)	386 (214)	425 (236)	410 (228)	439 (244)	491 (273)	439 (244)	491 (273)	0.018
126	Test with cold prop.	0.033	0.202	0.009	261 (180)	0.084 (38.05)	0.017 (7.70)	4.95	0.35 (0.242)	360 (200)	355 (197)	418 (232)	360 (200)	493 (274)	498 (276)	493 (274)	498 (276)	0.020
127	Test with cold prop.	0.032	0.208	0.011	262 (181)	0.095 (43.04)	0.024 (10.87)	4.00	0.34 (0.235)	342 (190)	326 (181)	391 (217)	330 (183)	439 (244)	491 (273)	439 (244)	491 (273)	0.016
128	Test with cold prop.	0.039	0.209	0.010	250 (173)	0.095 (43.04)	0.031 (14.04)	3.06	0.34 (0.235)	307 (170)	239 (133)	392 (218)	261 (145)	438 (243)	490 (272)	438 (243)	490 (272)	0.020
129	Test with cold igniter	Oxidizer valve did not open - fuel only flowed																
130	Test with cold igniter	0.106	0.095	0.008	265 (183)	0.121 (54.81)	0.031 (14.04)	3.90	0.36 (0.248)	311 (173)	245 (136)	322 (179)	261 (145)	413 (229)	462 (256)	413 (229)	462 (256)	0.095
131	Repeat Test 130	0.023	0.172	0.004	244 (168)	0.113 (51.19)	0.028 (12.68)	4.04	0.34 (0.235)	309 (171)	247 (137)	343 (190)	288 (160)	442 (245)	458 (254)	442 (245)	458 (254)	0.015

(1) Response: First pressure response in fuel manifold to establishment of full P_c, including fuel lead shown.(2) Duration: Time of full P_c.

(3) Temperatures of conditioned propellants.

(4) Temperatures of propellants flowing into catalytic igniter.

(5) Pretest hardware temperatures on fuel side of igniter body.

(6) Pretest hardware temperatures on oxidizer side of igniter body.

(7) Response time to 90% P_c less fuel lead time.

TABLE IV-10

CATALYTIC IGNITER TEST SUMMARY (COMPLETE THRUSTER MODE)

Exit Area Ratio = 3.0

<u>Parameter</u>	<u>Test 120</u>	<u>Test 136</u>
Duration (sec)	1.2	1.1
Igniter response (sec) ^a	0.025	0.028
Igniter ignition delay (sec) ^b	0.003	0.002
Engine start transient (sec) ^c	0.080	0.063
Engine ignition delay (sec) ^d	0.006	0.002
\dot{w}_{ox} (lb/sec) (Kgm/sec)	2.715 (1.230)	3.045 (1.379)
\dot{w}_f (lb/sec) (Kgm/sec)	0.683 (.309)	0.599 (.271)
\dot{w}_{oi} (lb/sec) (Kgm/sec)	0.0777 (.0352)	0.0773 (.0350)
\dot{w}_{fi} (lb/sec) (Kgm/sec)	0.0156 (.0071)	0.0158 (.0071)
MR _{core}	3.98	5.08
MR _i	4.99	4.88
MR _{thruster}	4.00	5.08
P _c (psia) (N/cm ²)	302 (208)	319 (220)
T _{propellants} (°R) (°K)	492 (273)	492 (273)

- (a) Response: First pressure response in oxidizer manifold to establishment of full igniter P_c.
- (b) Ignition Delay: First pressure response in oxidizer manifold to igniter ignition.
- (c) Start Transient: First pressure response in igniter fuel manifold to establishment of full thruster P_c.
- (d) Ignition Delay: First pressure response in thruster oxidizer manifold to thruster ignition.

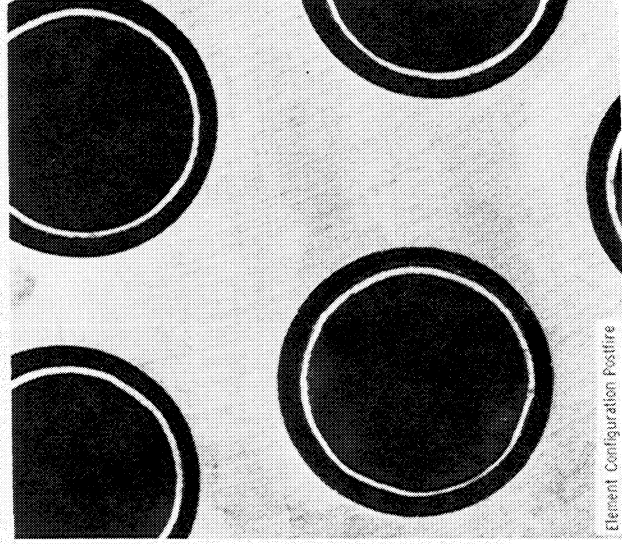
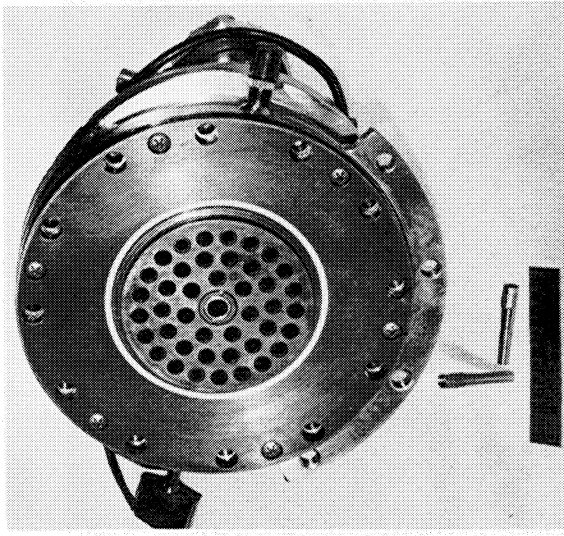
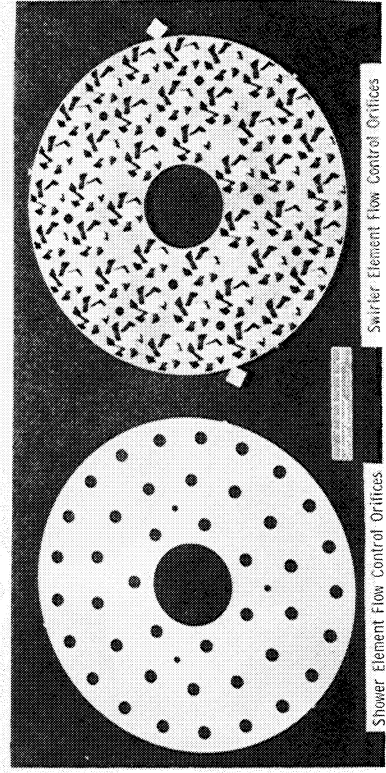
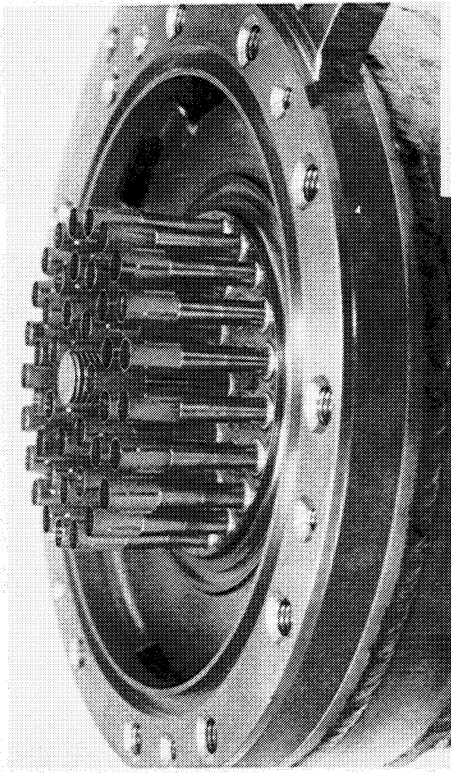
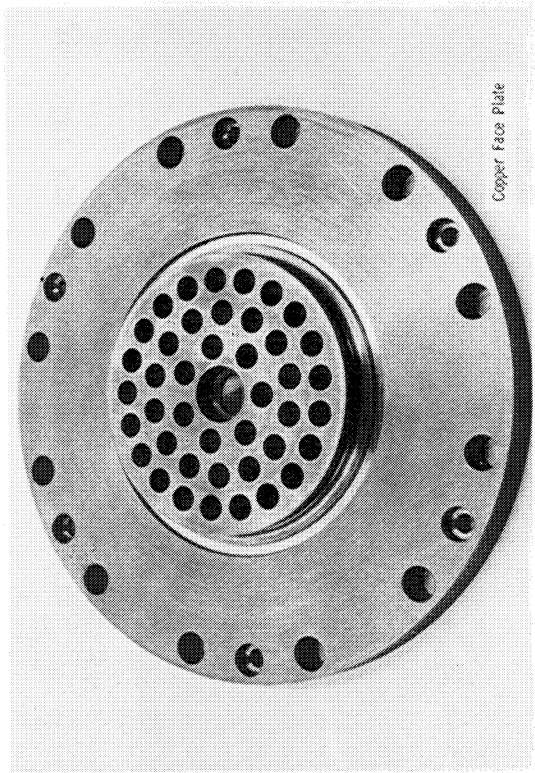


Figure IV-1. Coaxial Element Injector Components and Assembly

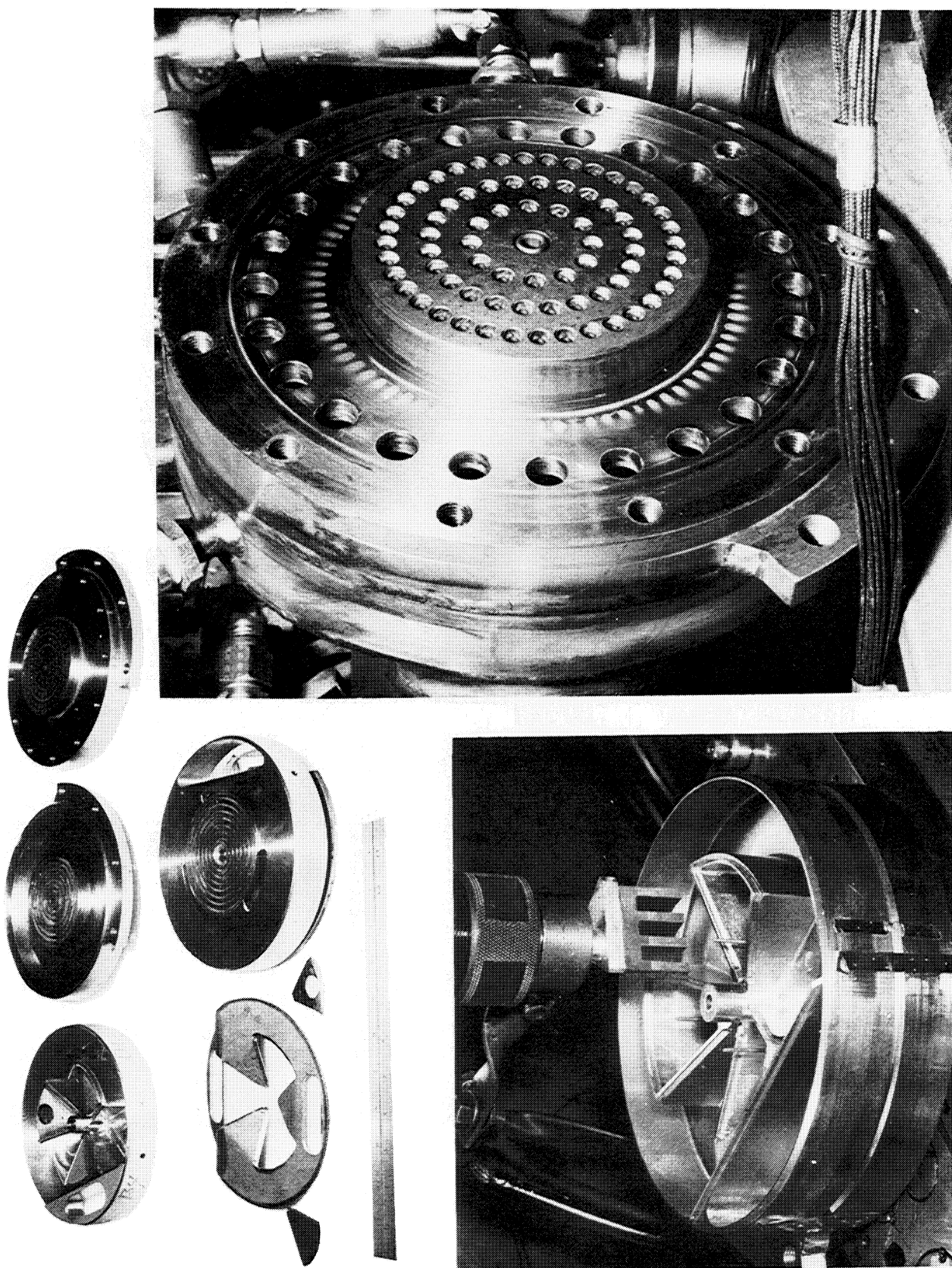
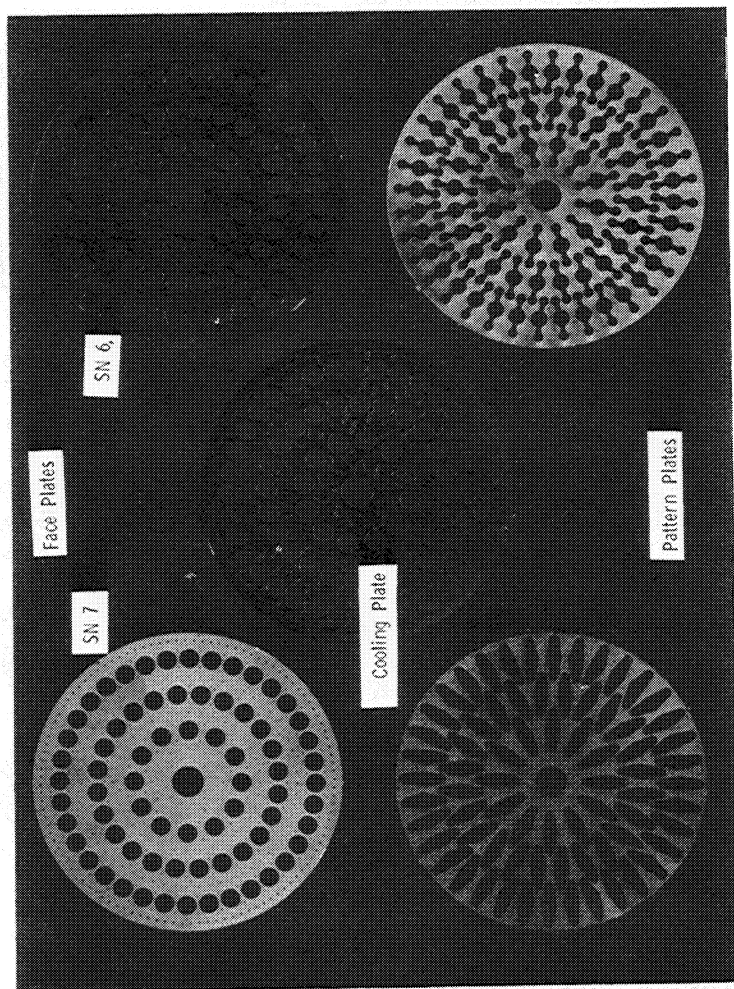
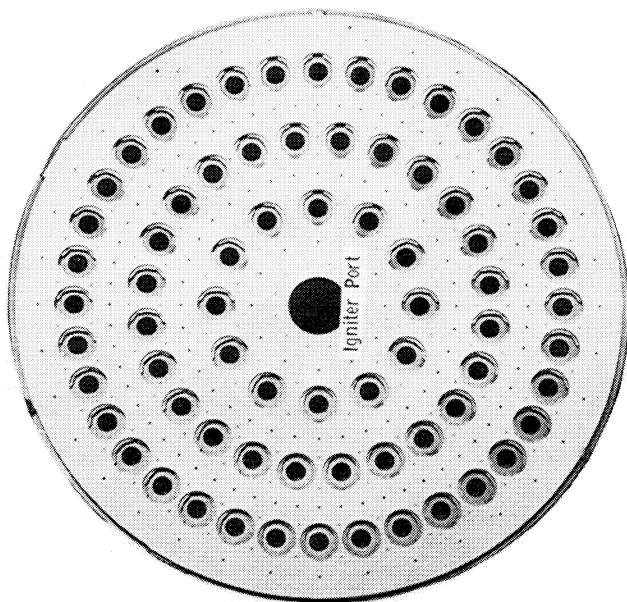
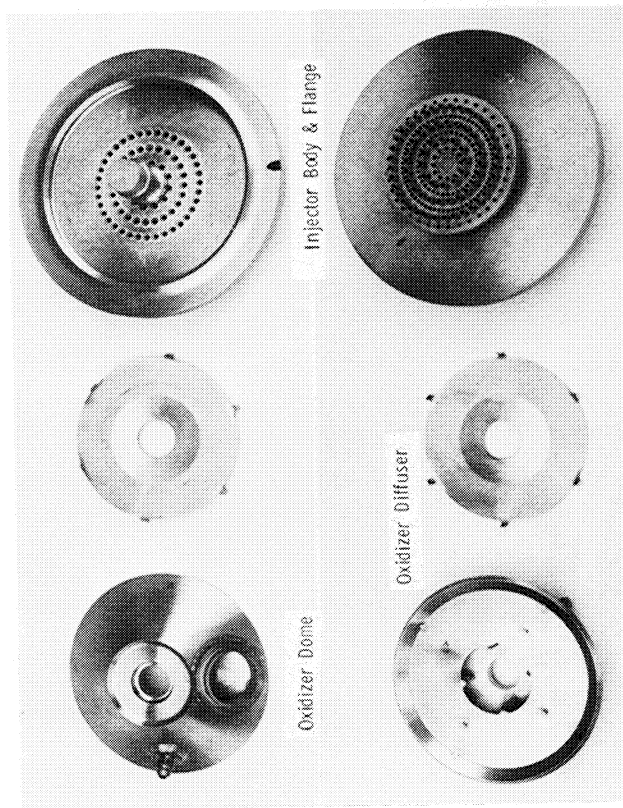


Figure IV-2. Phase I Premix Injector Components and Assembly



Premix "I" Triplet

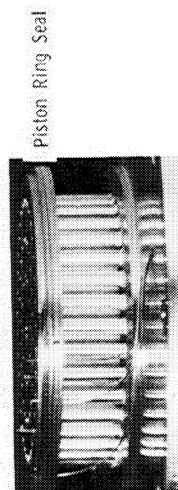
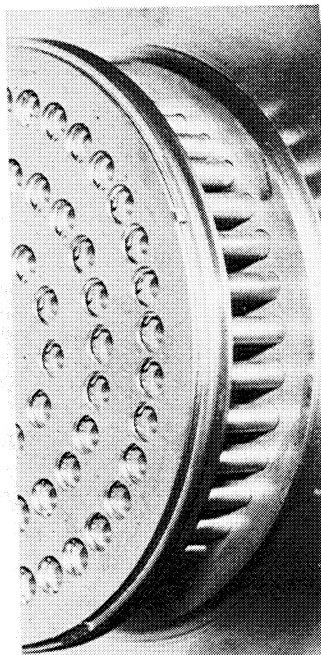


Figure IV-3. Phase II Premix Injector Components and Assembly

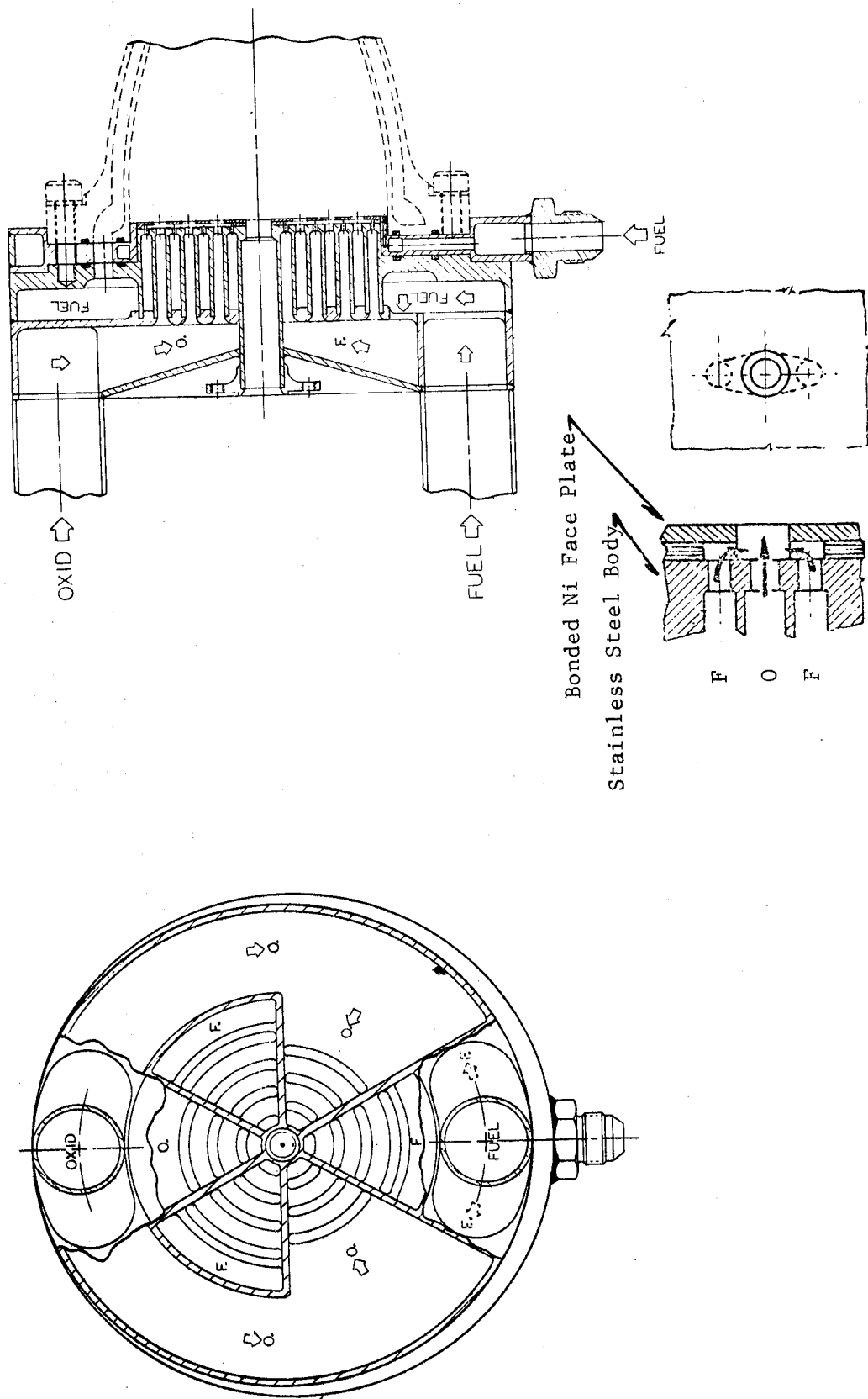
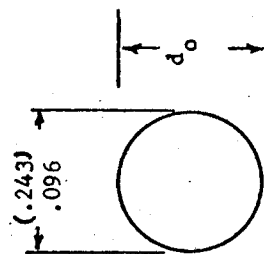


Figure IV-4. Phase I Premix Element Injector Manifolding and Flow Schematic

Note: All dimensions
in inches (cm)

Triplet

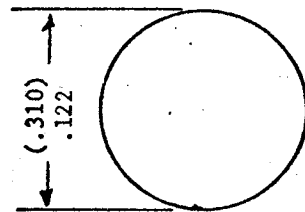
S/N-3 & -4



Oxidizer
Orifice

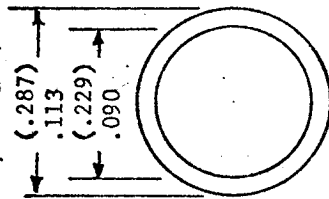
"I" Triplet

S/N-5

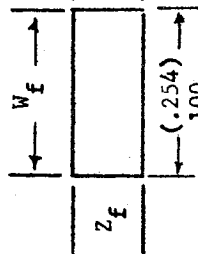
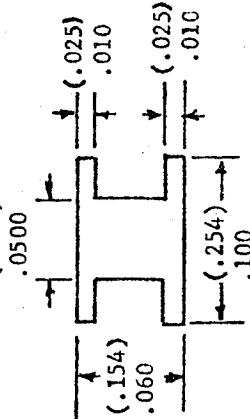


Modified
"I" Triplet

S/N-6 & -7

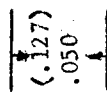
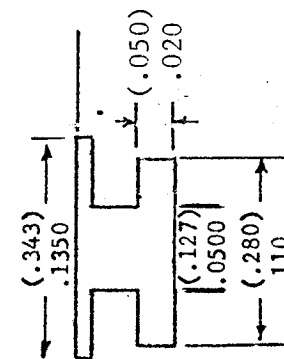


(.127)



Fuel Orifice

Z_f

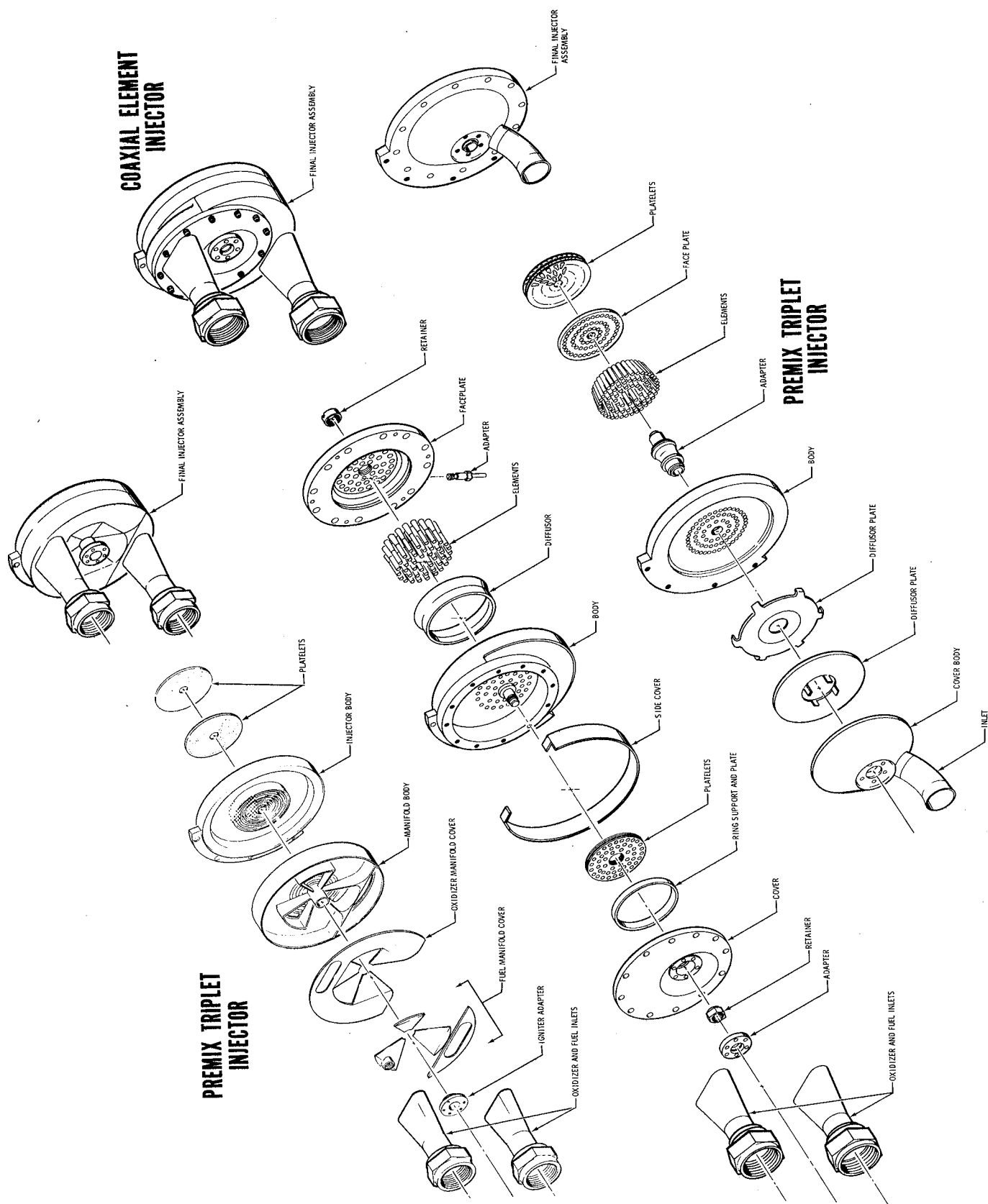


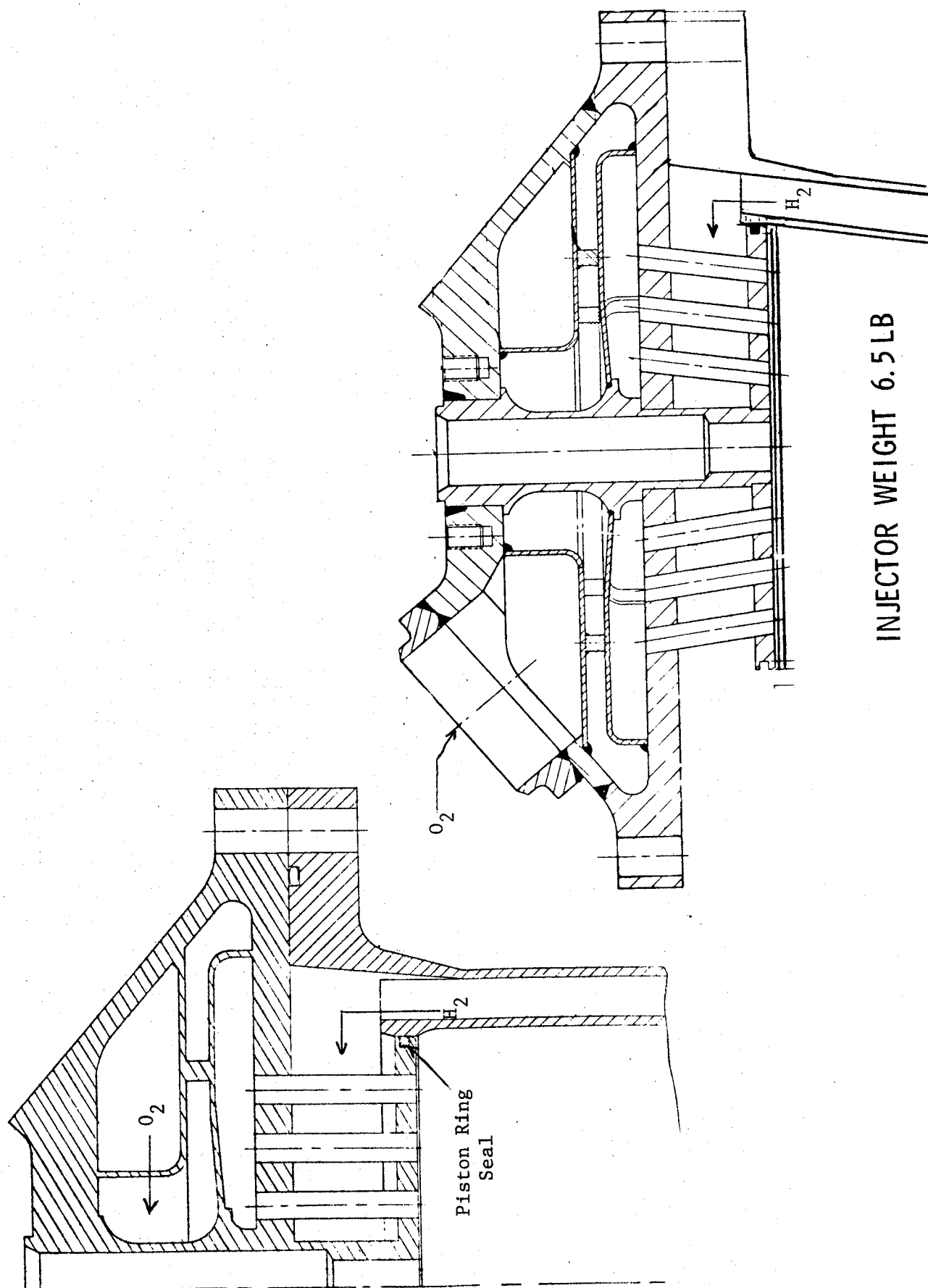
Fuel Temp.	Amb.	200° R	Amb.	200° R	Amb.	200° R
Face Temp, * O_F	(470-565) 387-558	--	(799) 979	--	(547-708) 525-815	(360-405) 188-270
ΔP Fuel, * (N/cm^2) psia	(39.35) 57	(15.9) 23	(48.3) 70	--	(49.7) 72	(24.8) 36
ΔP Oxidizer, (N/cm^2) psia	(42.8) 62	(24.8) 36	(33.8) 49	--	(53.2) 77	(27.6) 40

* MR = 4.0 @ 300 psia - 20% film cooling

Figure IV-5. Premix Injector Element Configurations

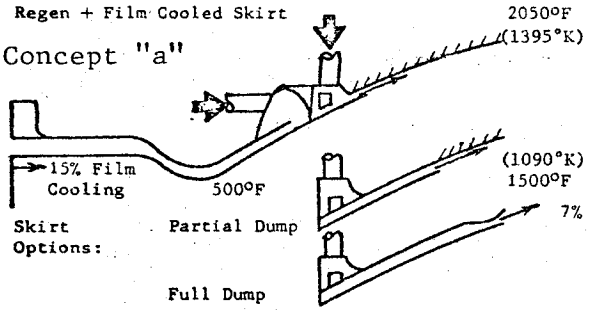
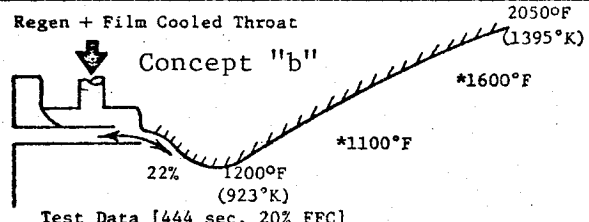
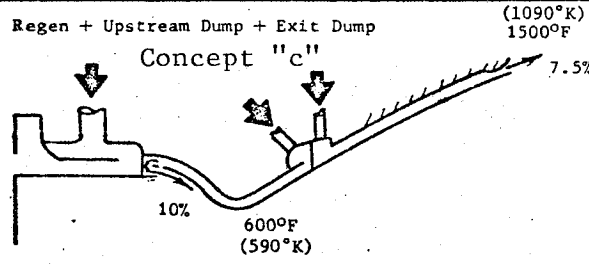
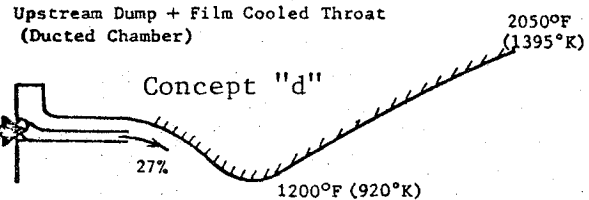
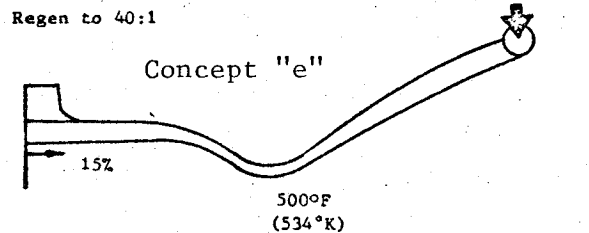
COAXIAL ELEMENT INJECTOR





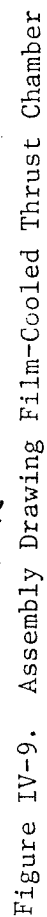
INJECTOR WEIGHT 6.5 LB

Figure IV-7. 72-Element Premix Injector Manifolding

Design	Predicted I_s , sec ΔP_{cool}	Pulsing Response	Weight	Cost	Nozzle Scarfining
Regen + Film Cooled Skirt Concept "a"  15% Film Cooling 500°F Partial Dump Full Dump 7%	ERF-99° 445 448	psi 35 Acceptable	Moderate High	Moderate High	All angles Some Separate skirt design for each angle
Regen + Film Cooled Throat Concept "b"  2050°F (1395°K) *1600°F *1100°F 22% 1200°F (923°K) Test Data [444 sec, 20% FFC]	443	22 Fast	Light	Low	All angles
Regen + Upstream Dump + Exit Dump Concept "c"  1090°K (1500°F) 10% 600°F (590°K) 7.5%	449	22 Fast	Moderate	High	Separate skirt design for each angle
Upstream Dump + Film Cooled Throat (Ducted Chamber) Concept "d"  2050°F (1395°K) 27% 1200°F (920°K)	441	0 Very fast	Minimum	Low	All angles
Regen to 40:1 Concept "e"  15% 500°F (534°K)	449	35 Slow	Maximum	High	Not adaptable

*Test Data

Figure IV-8. Thrust Chamber Cooling Evaluation



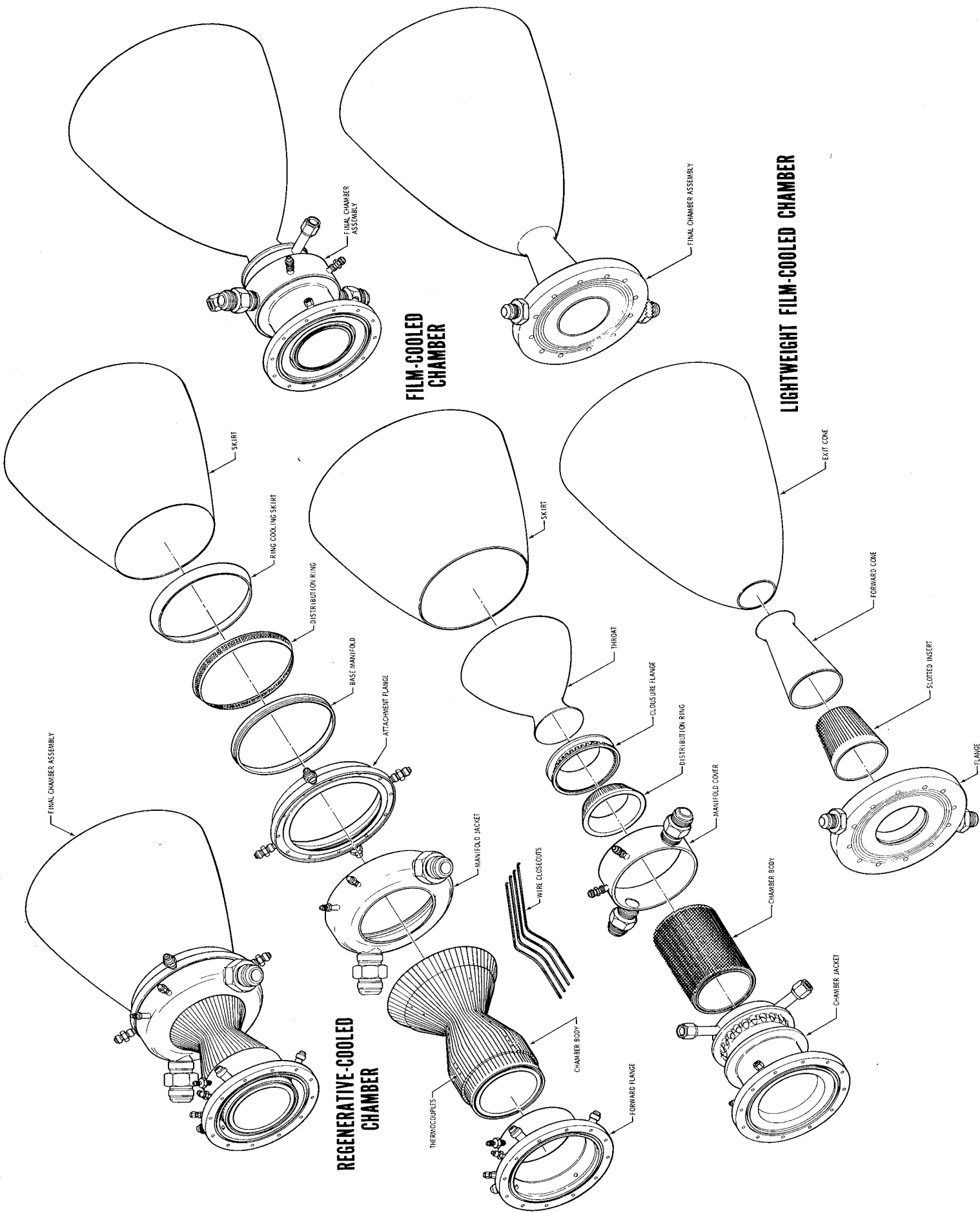
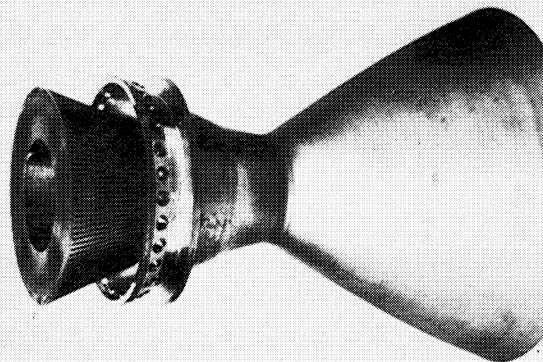
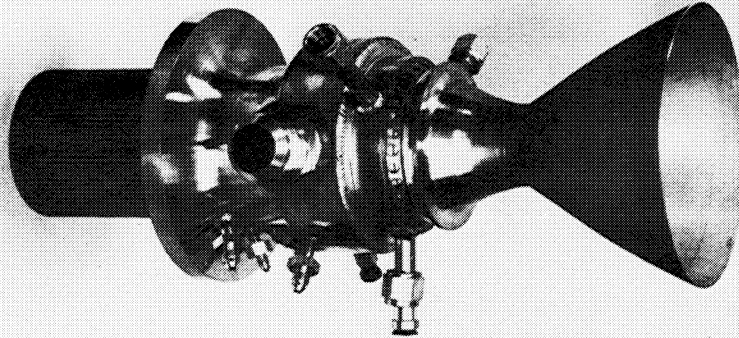


Figure IV-10. Thrust Chamber Assembly Schematic

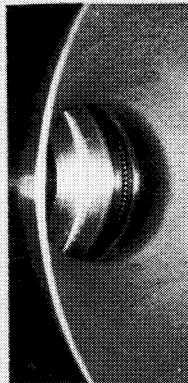
SUBASSEMBLIES



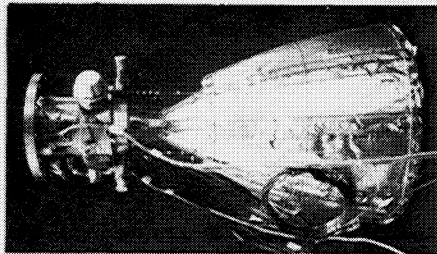
FILM COOLING INJECTOR
AND HAYNES 188 THROAT



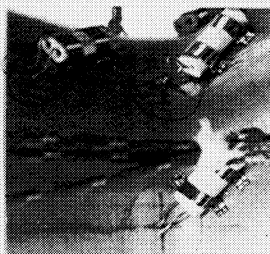
REGENERATIVE CHAMBER
SECTION AND MANIFOLD



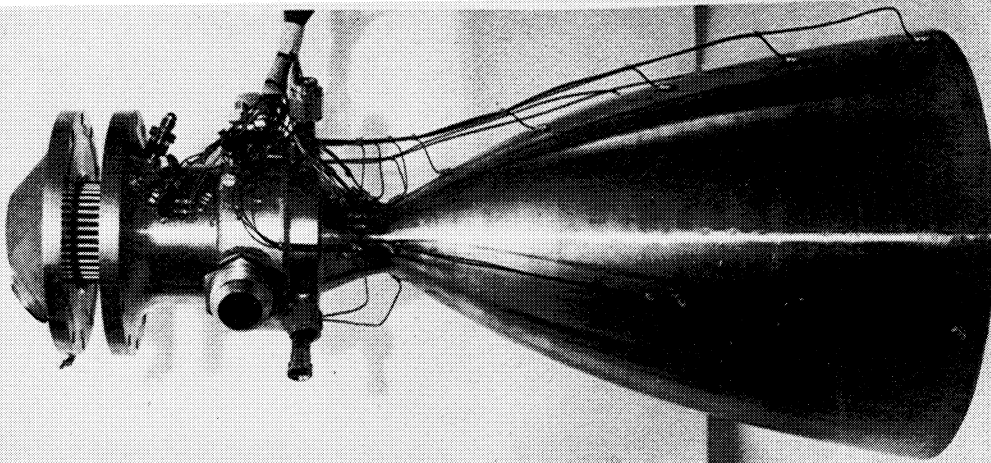
FILM COOLANT INJECTION PATTERN



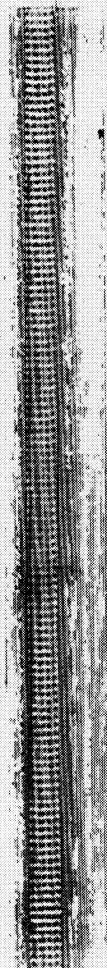
FINAL ASSEMBLY
WITH SKIRT
INSULATION



THROAT REGION,
THERMOCOUPLE



FINAL ASSEMBLY
BEFORE SKIRT
INSULATION



ULTRASONIC INSPECTION OF
FILM COOLANT INJECTOR BOND
LINE

3/25/54 4/1/54
Positive Recording
3/25/54

Center Body Mounted To Thrust Chamber

Fig. 10-234-1 4/1/54 4/1/54

Figure IV-11. Film-Cooled Thrust Chamber Components and Assembly

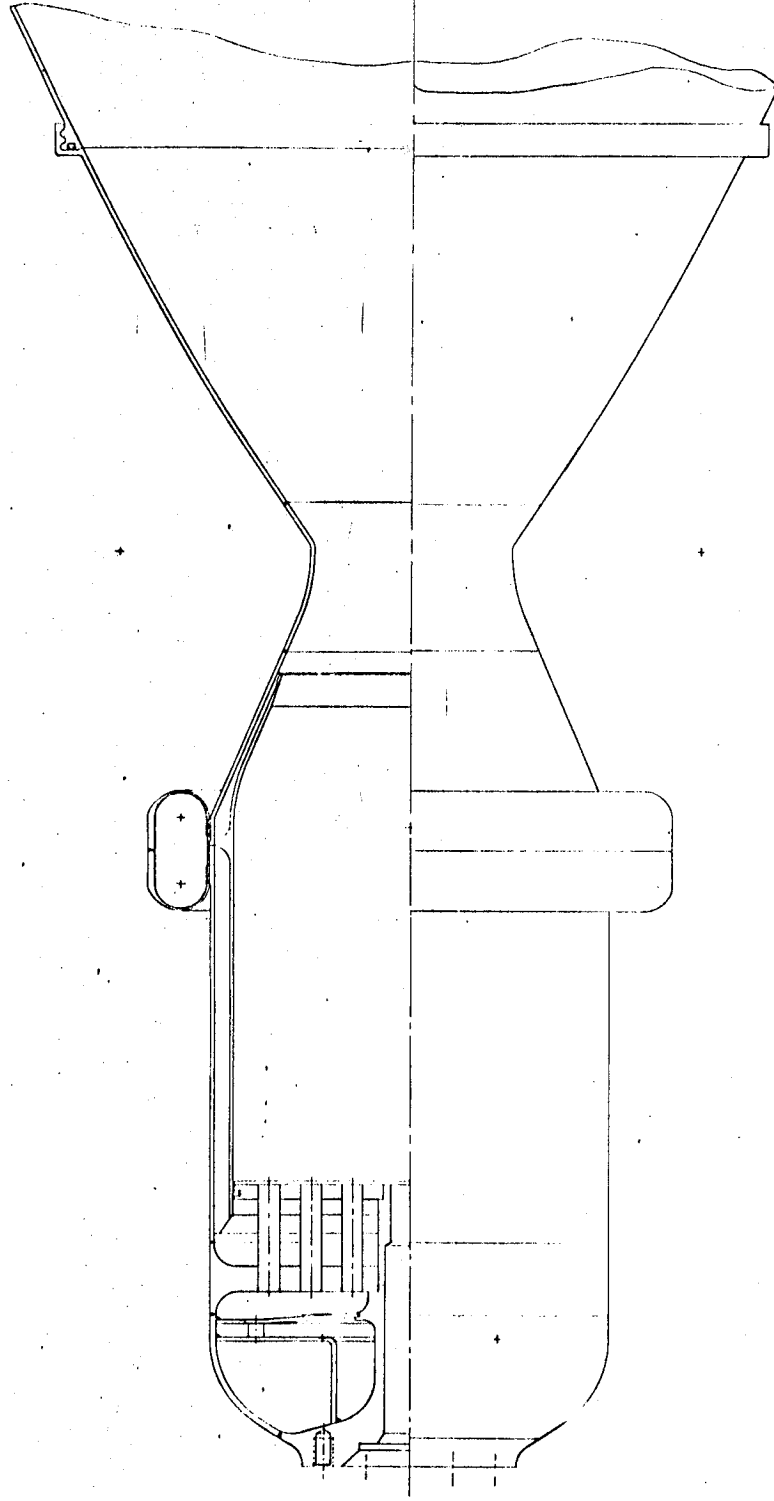


Figure IV-12. Phase II Film-Cooled Chamber

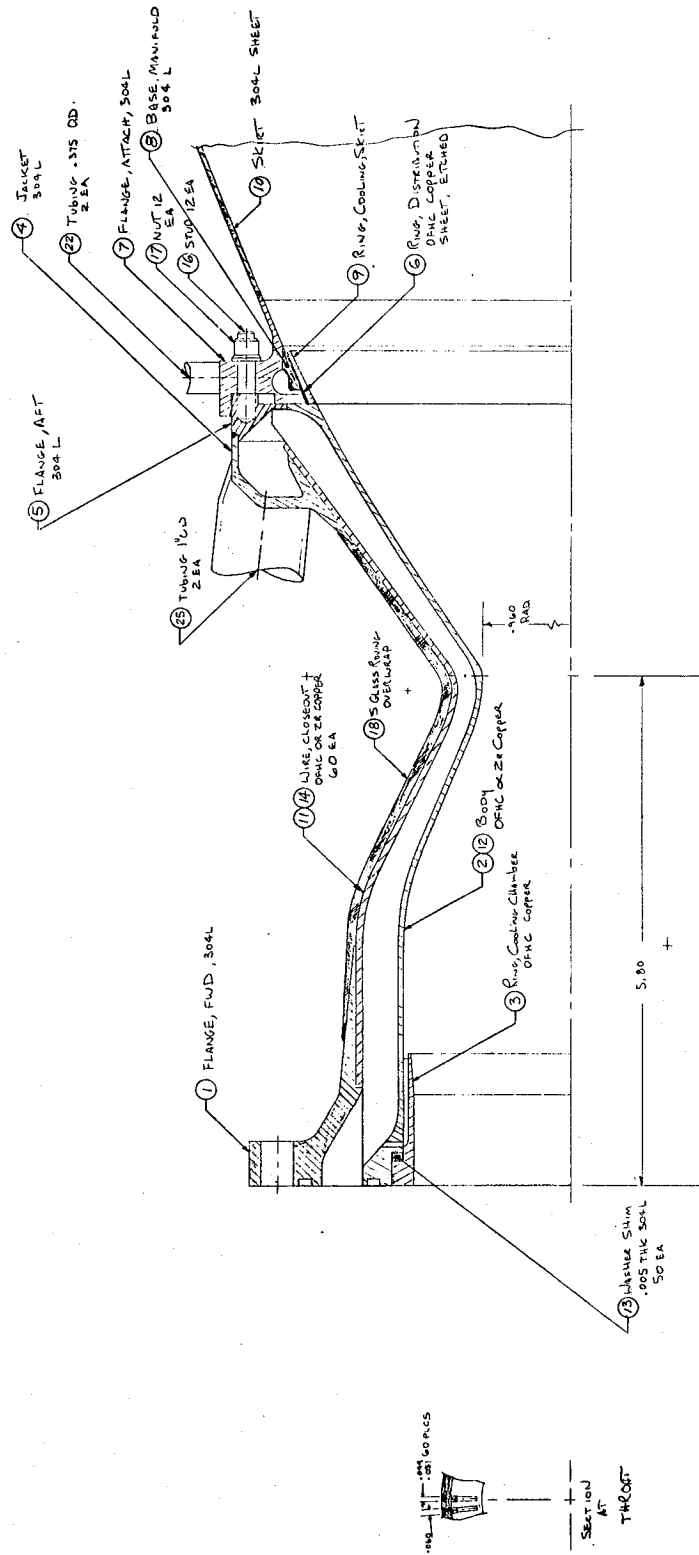
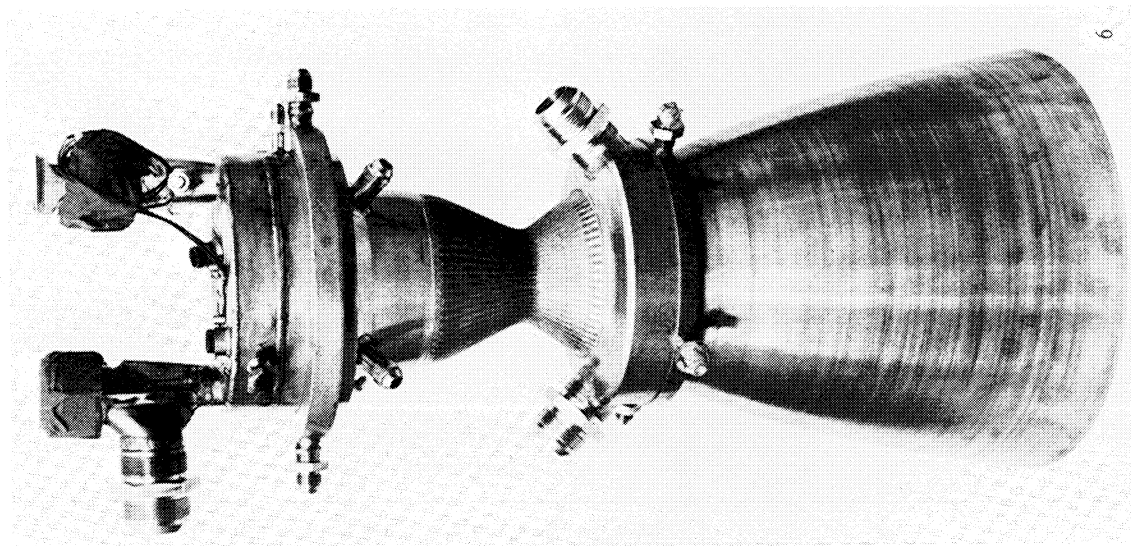
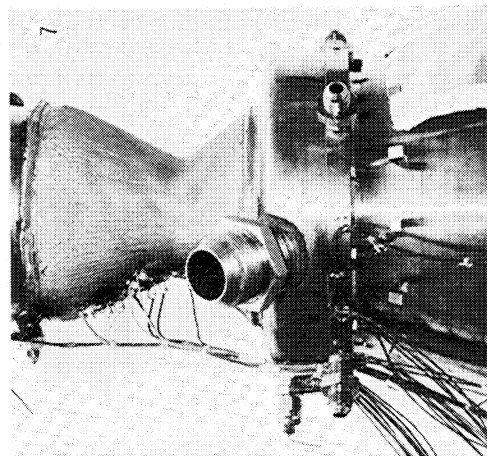
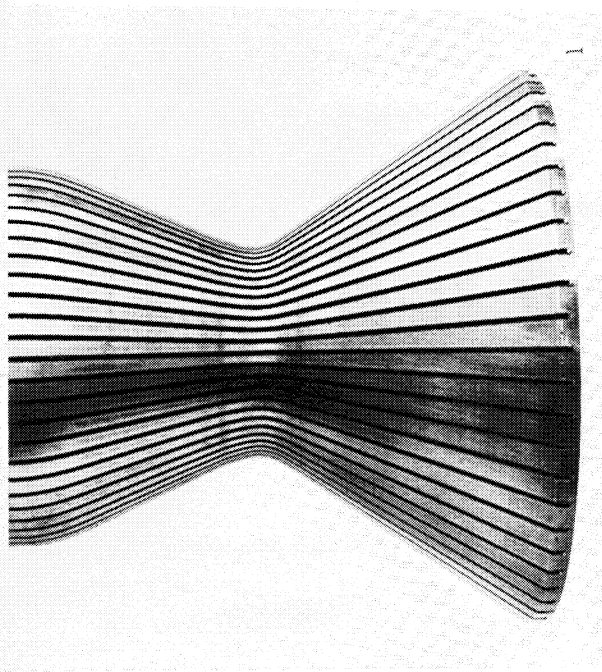
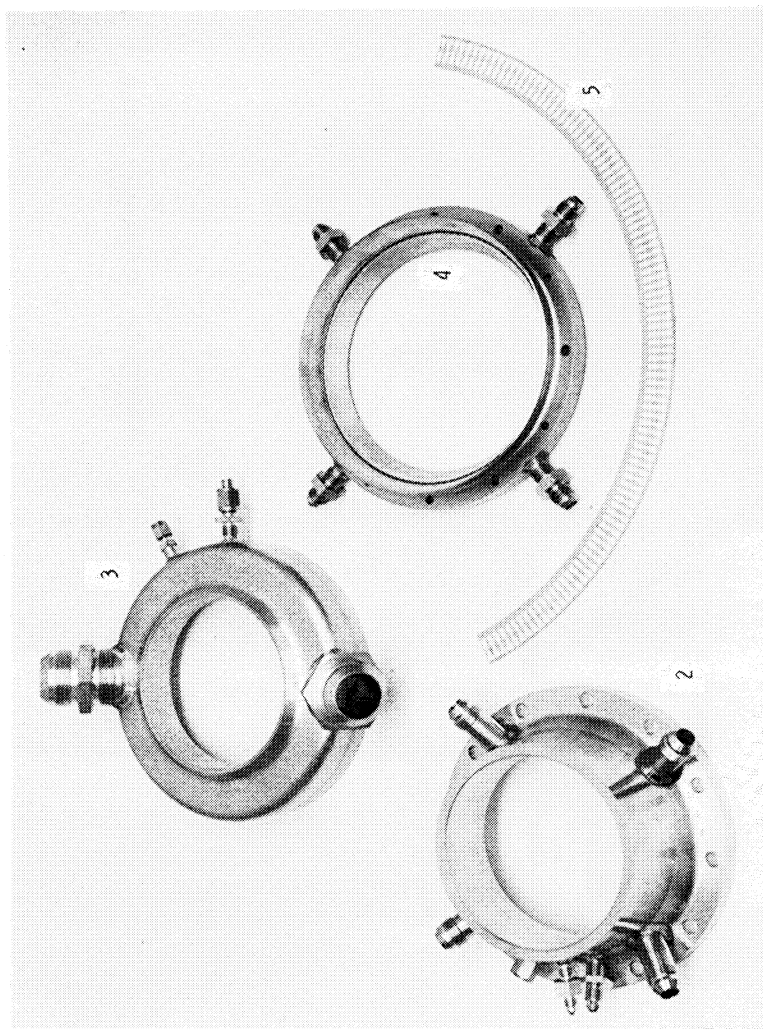


Figure IV-13. Assembly Drawing, Phase I Regeneratively Cooled Chamber

- 1 Slotted Copper Chamber
- 2 Forward Flange
- 3 Aft Flange & Manifold
- 4 Skirt Flange & Coolant Injectors
- 5 Coolant Injection Nozzles Prior to Assembly
- 6 Assembly Prior to Application of Electroformed Ni Case
- 7 Final Assembly Following Electroforming & Instrumentation



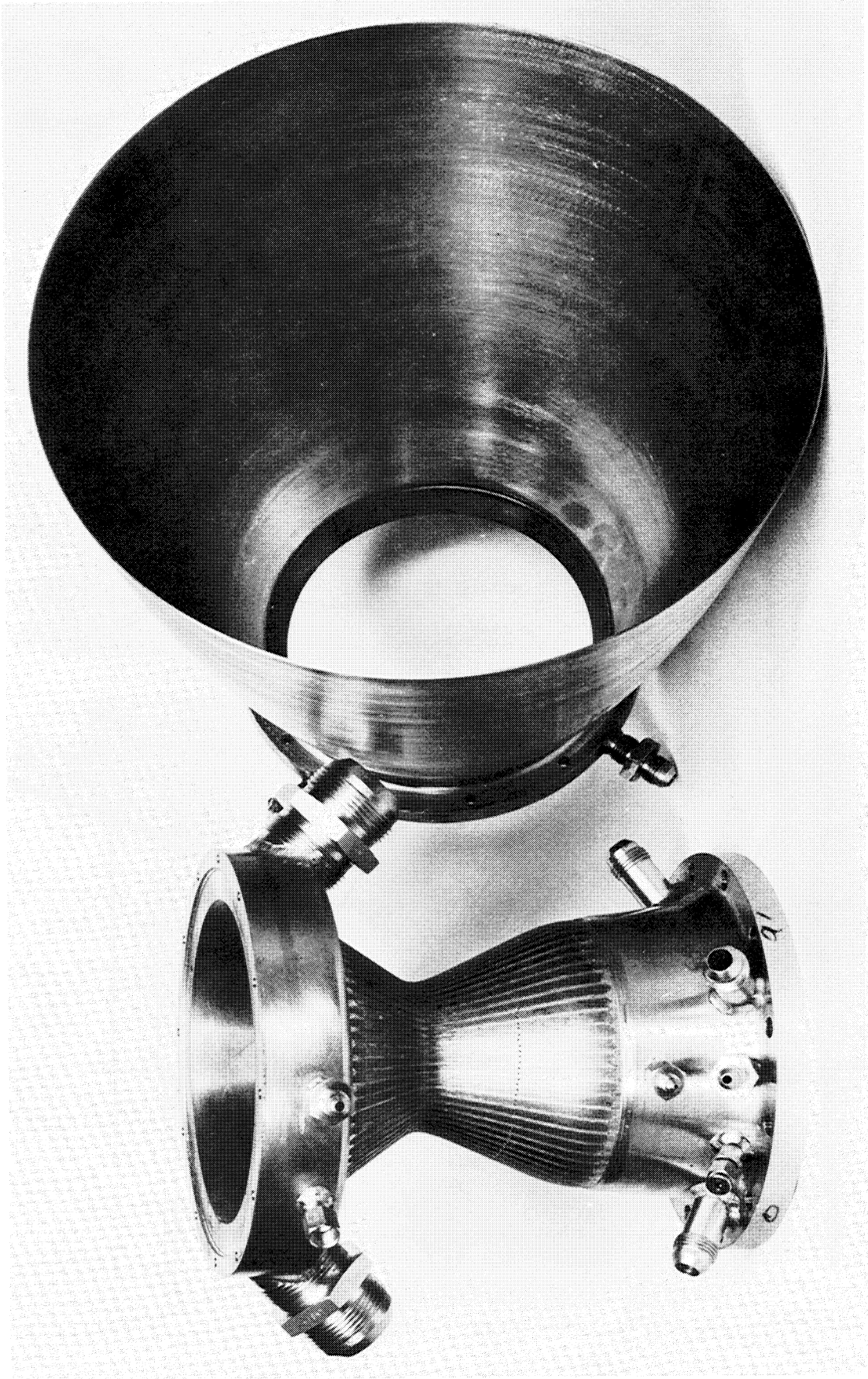


Figure IV-15. Phase I Regeneratively Cooled Chamber Prior to Electroforming

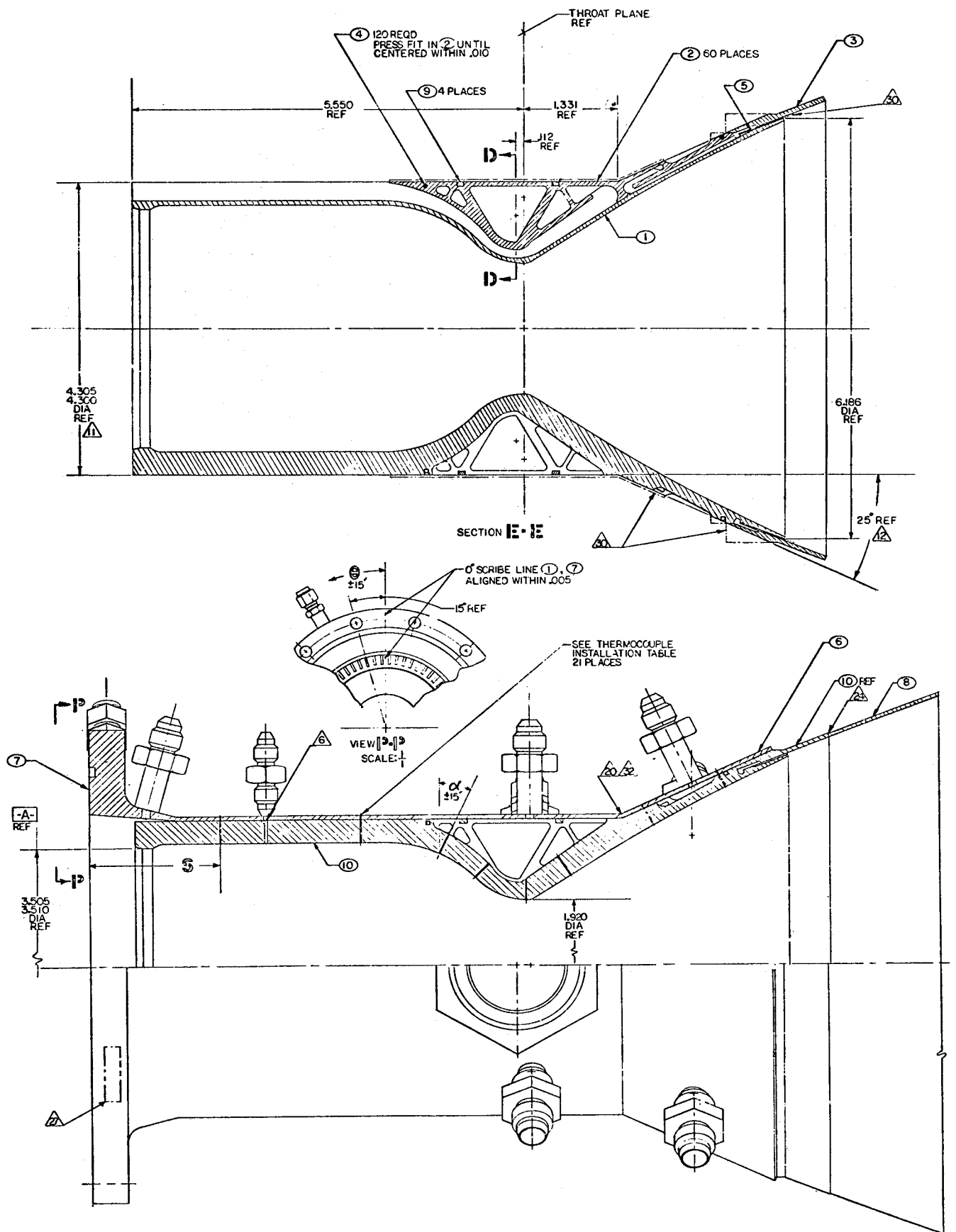
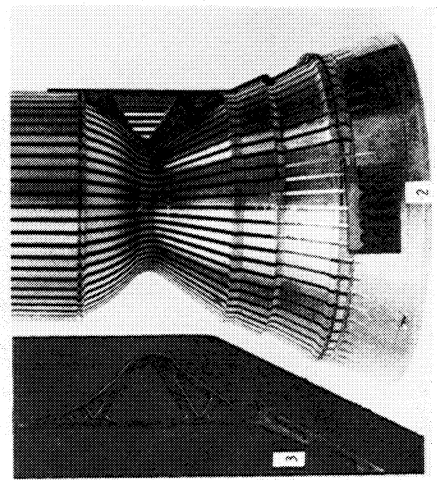
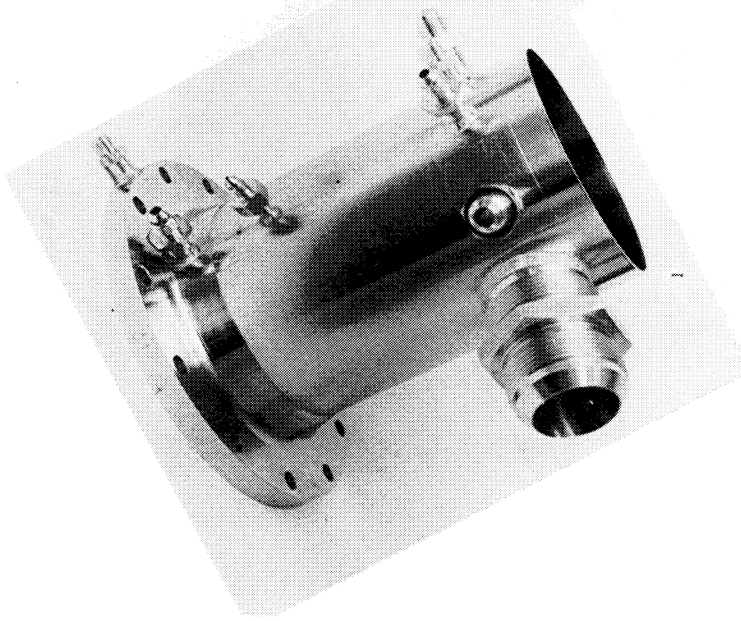
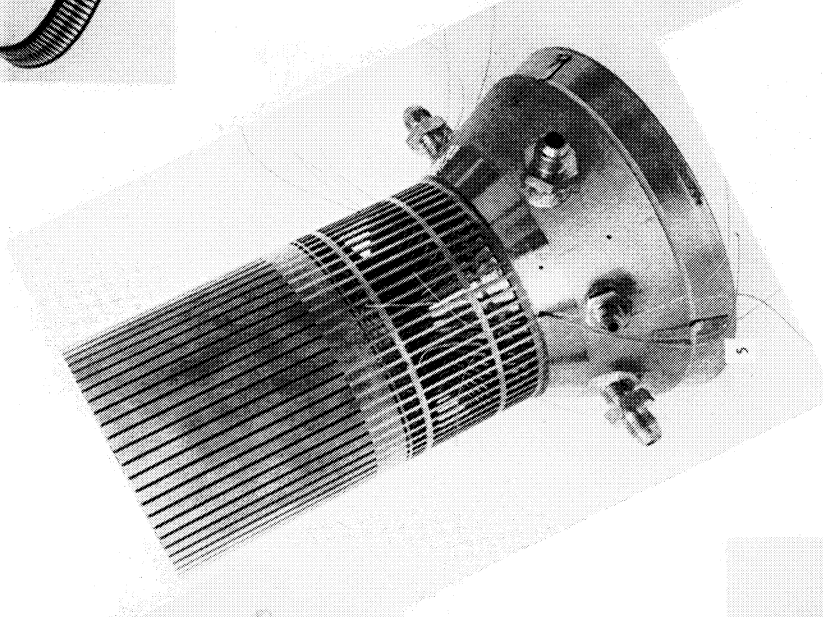
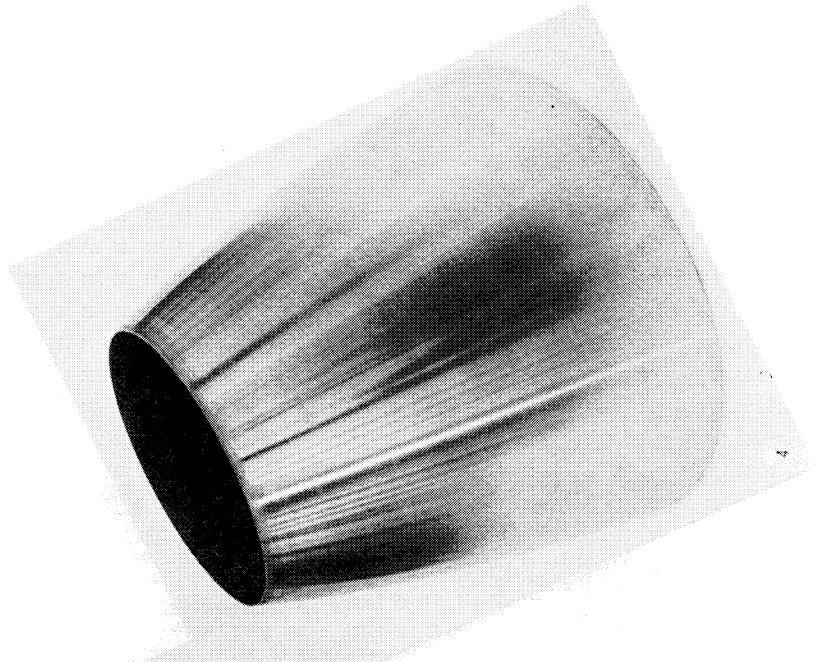
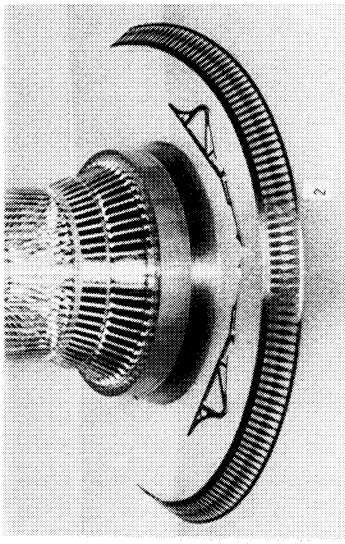


Figure IV-16. Phase II Regeneratively Cooled Chamber Section



- 1 304 Jacket
- 2 Skirt Film Cooling Nozzles
- 3 Photoetched Rib Closeout
- 4 Spun Skirt
- 5 Spun Skirt Weld-On Point

Figure IV-17. Phase II Regeneratively Cooled Chamber Components

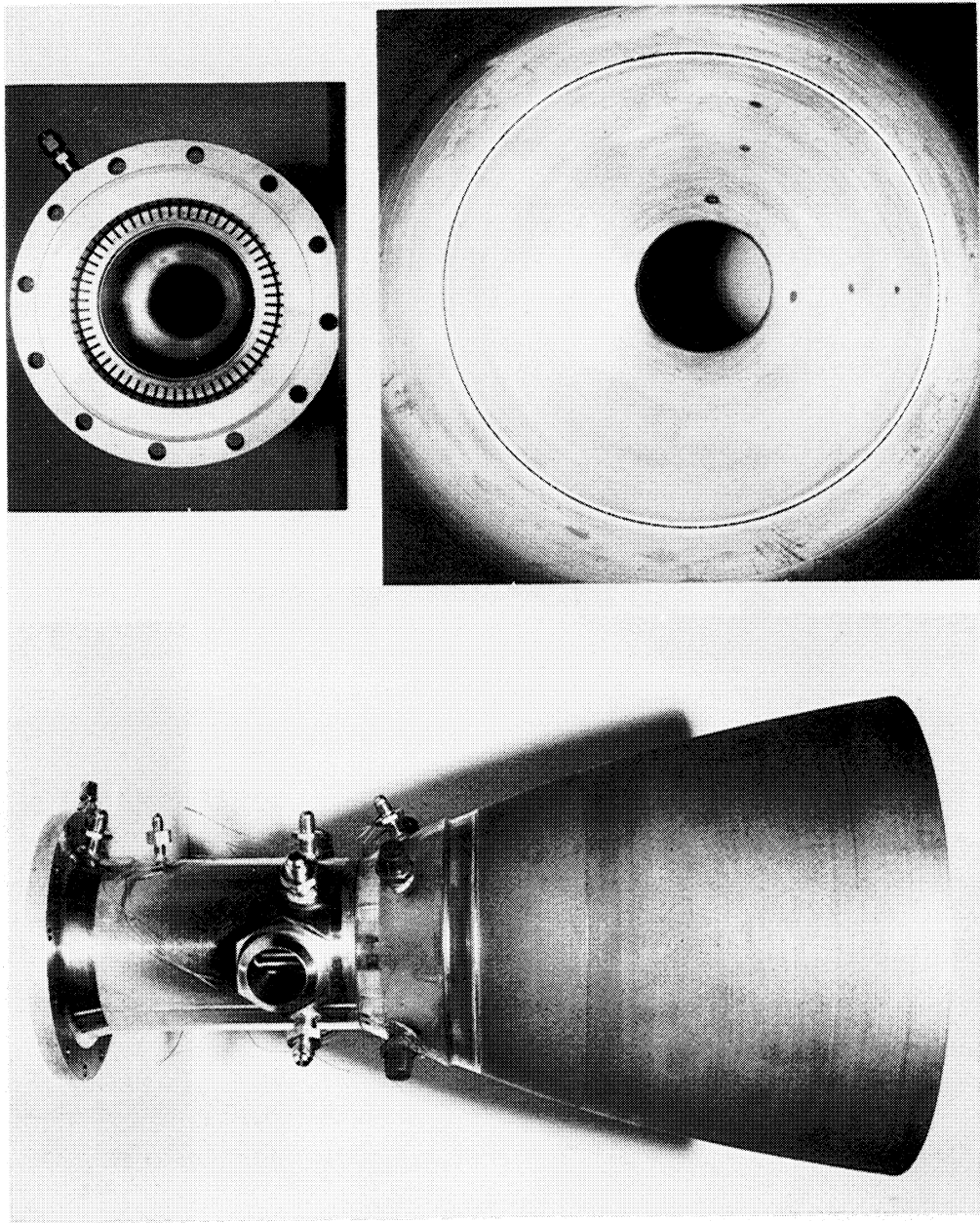


Figure IV-18. Phase II Regeneratively Cooled Chamber Assembly

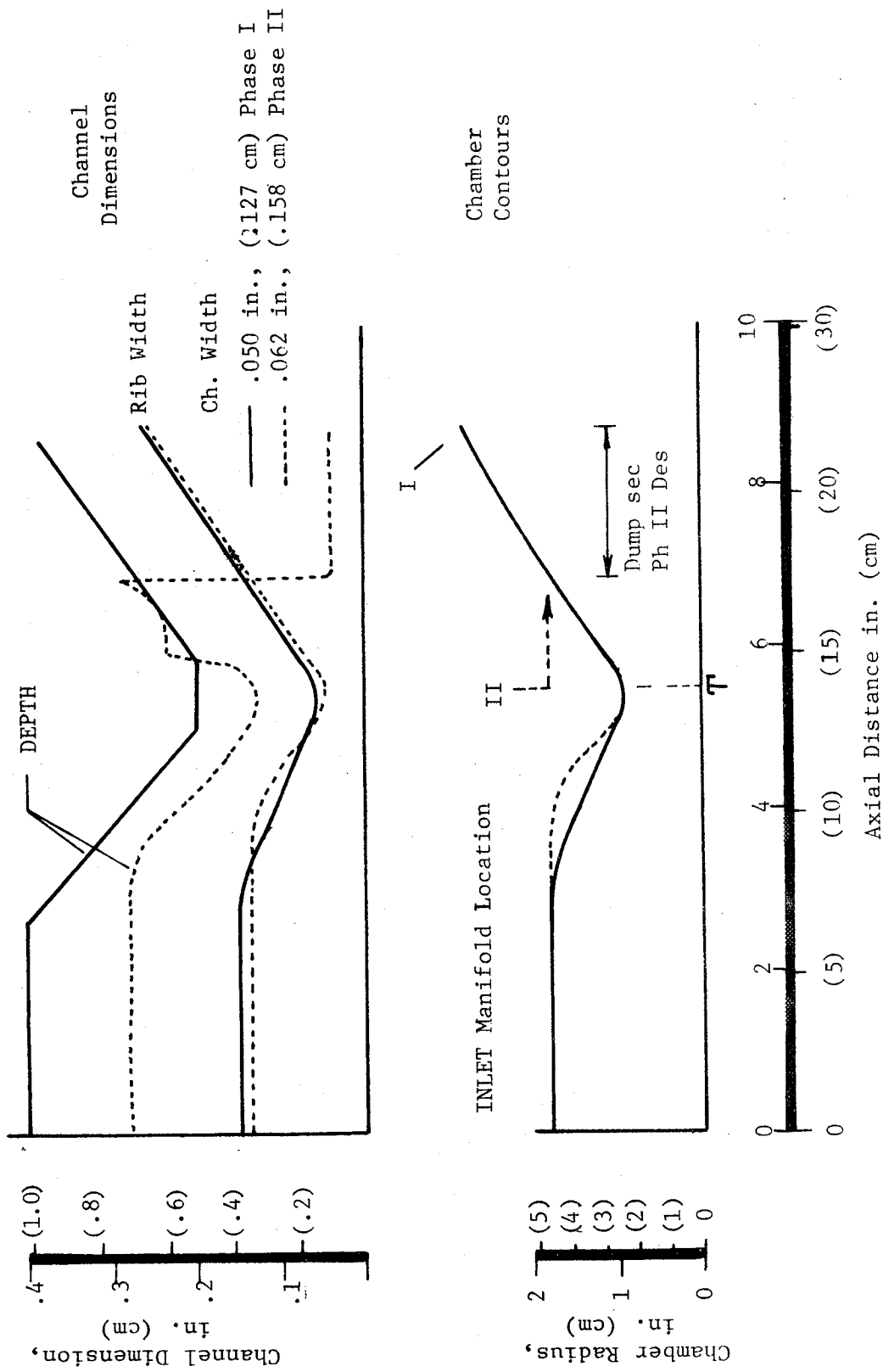
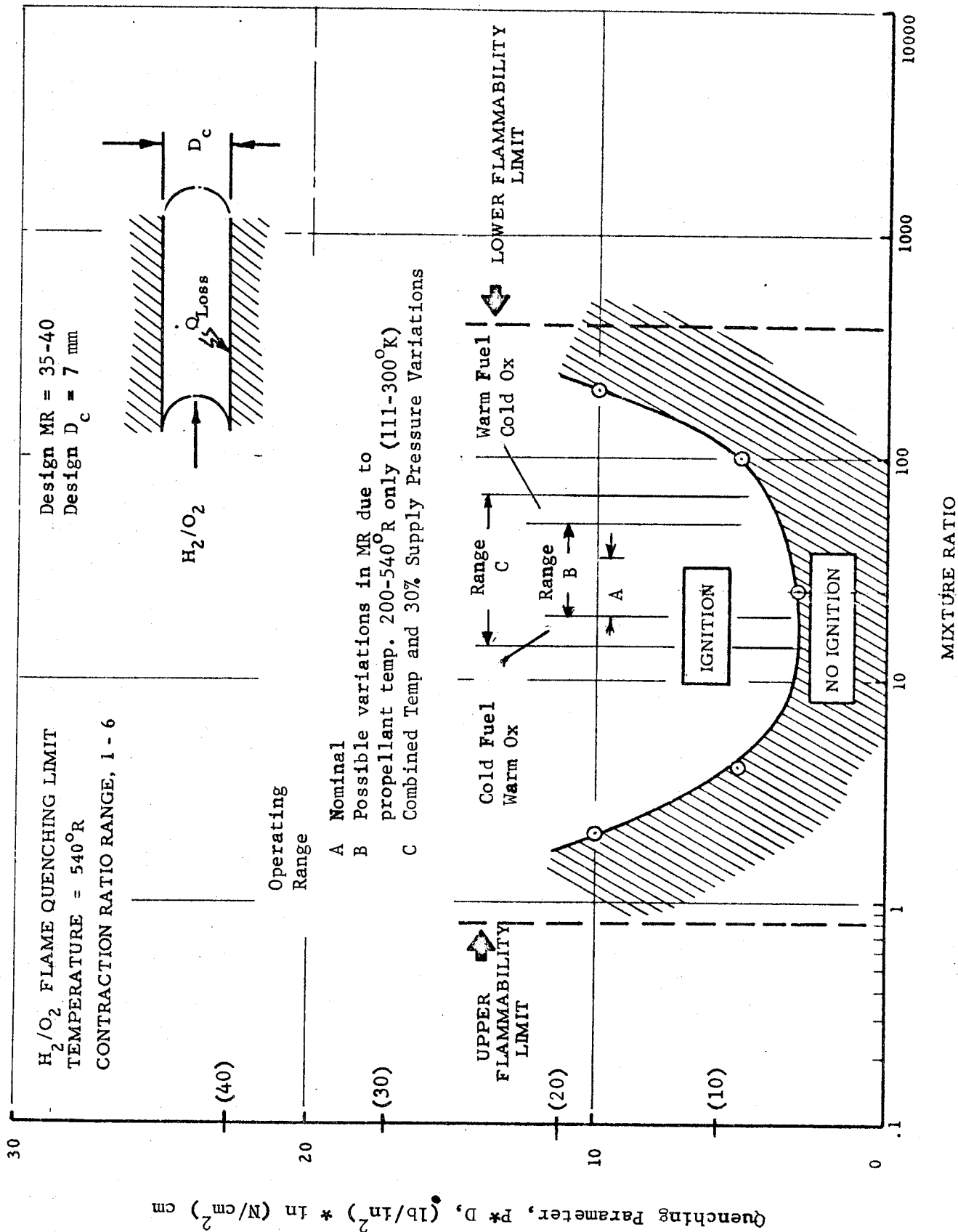


Figure IV-19. Comparison of Phase I and II Nozzle Contours and Coolant Channel Configurations



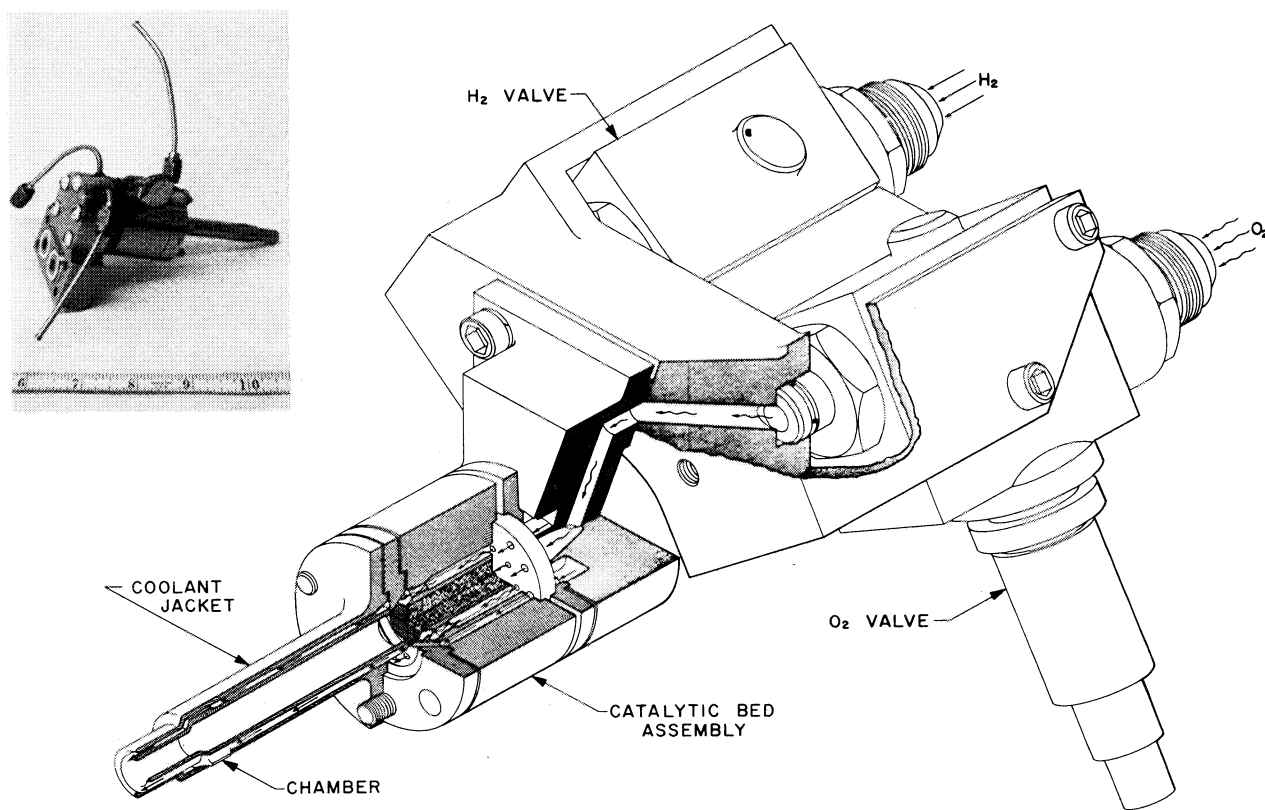
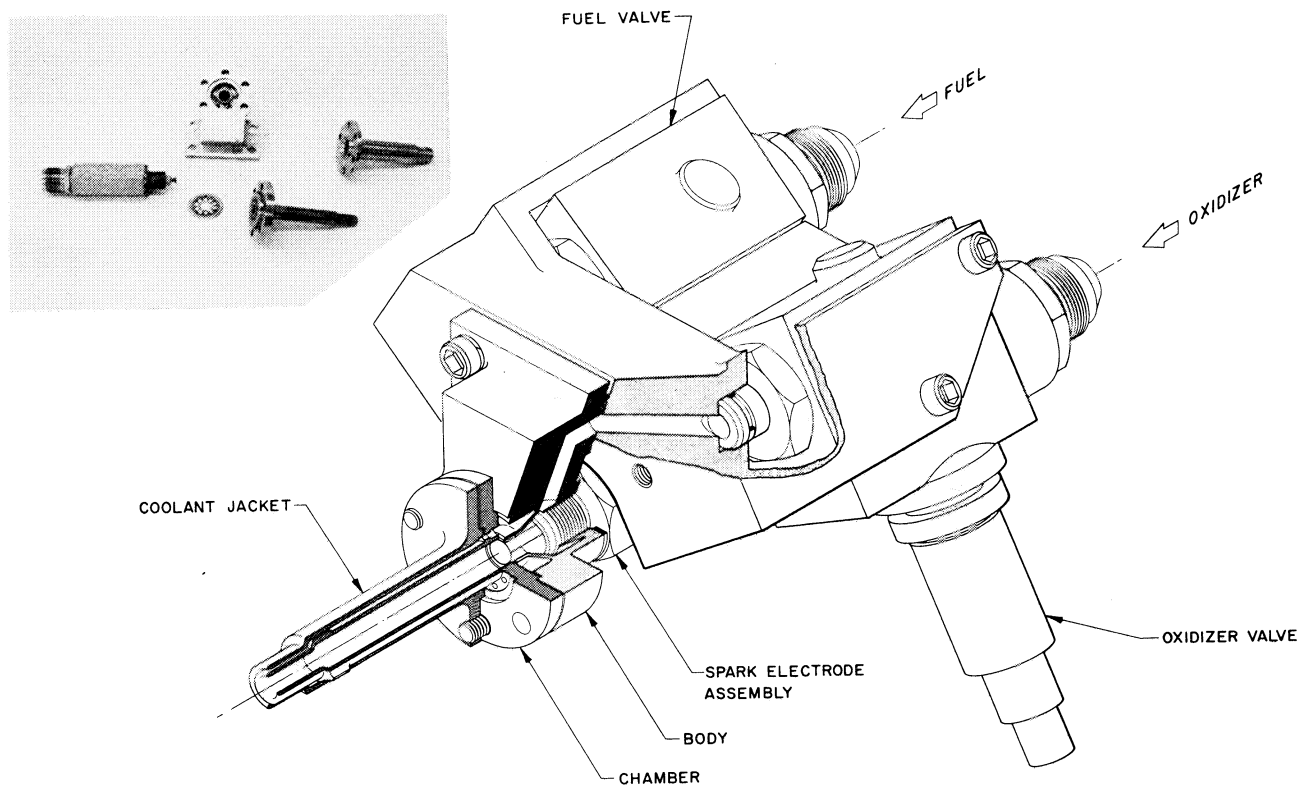
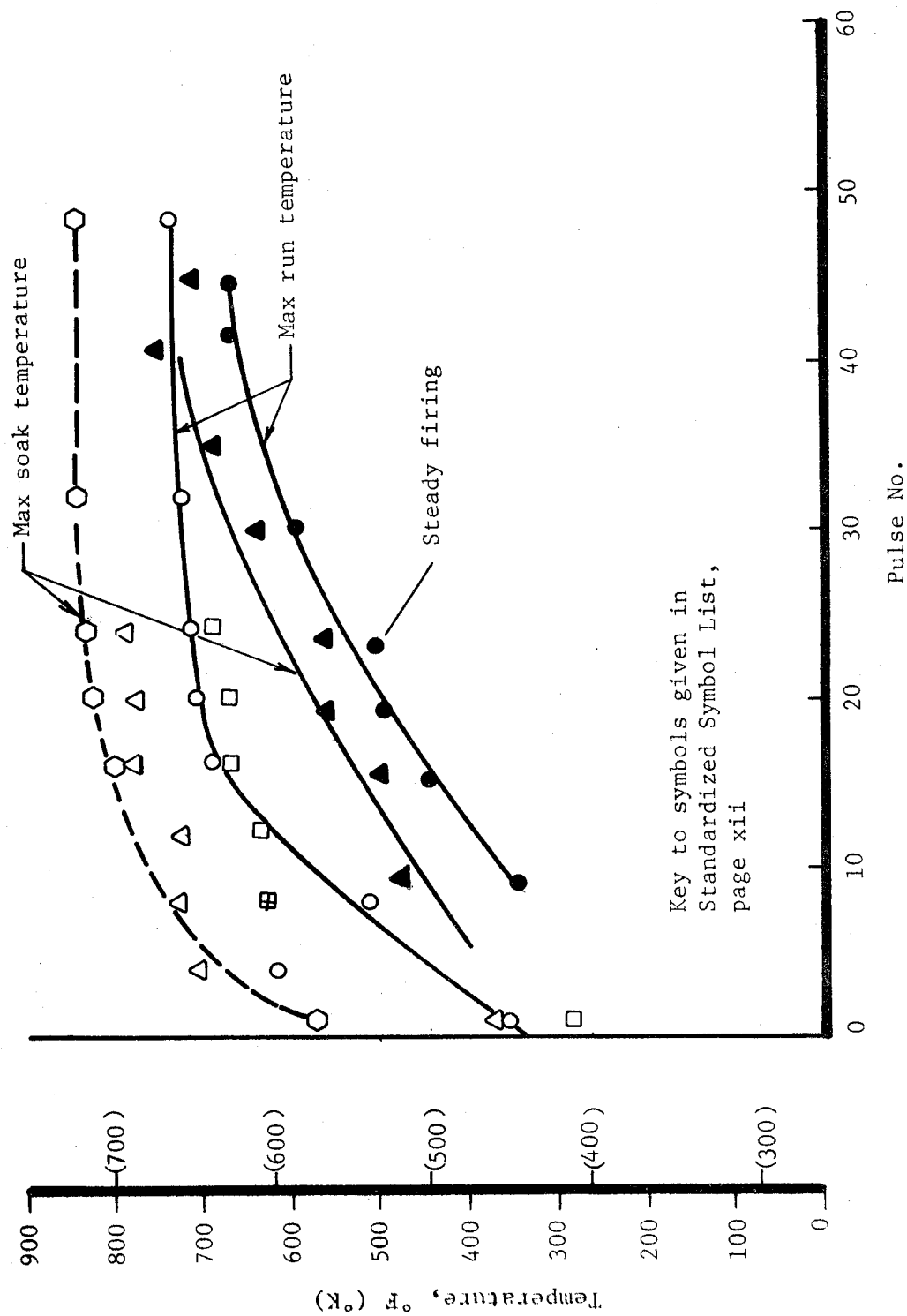


Figure IV-21. Igniter Isometric Drawings and Photographs



Key to symbols given in
Standardized Symbol List,
page xii

Pulse No.

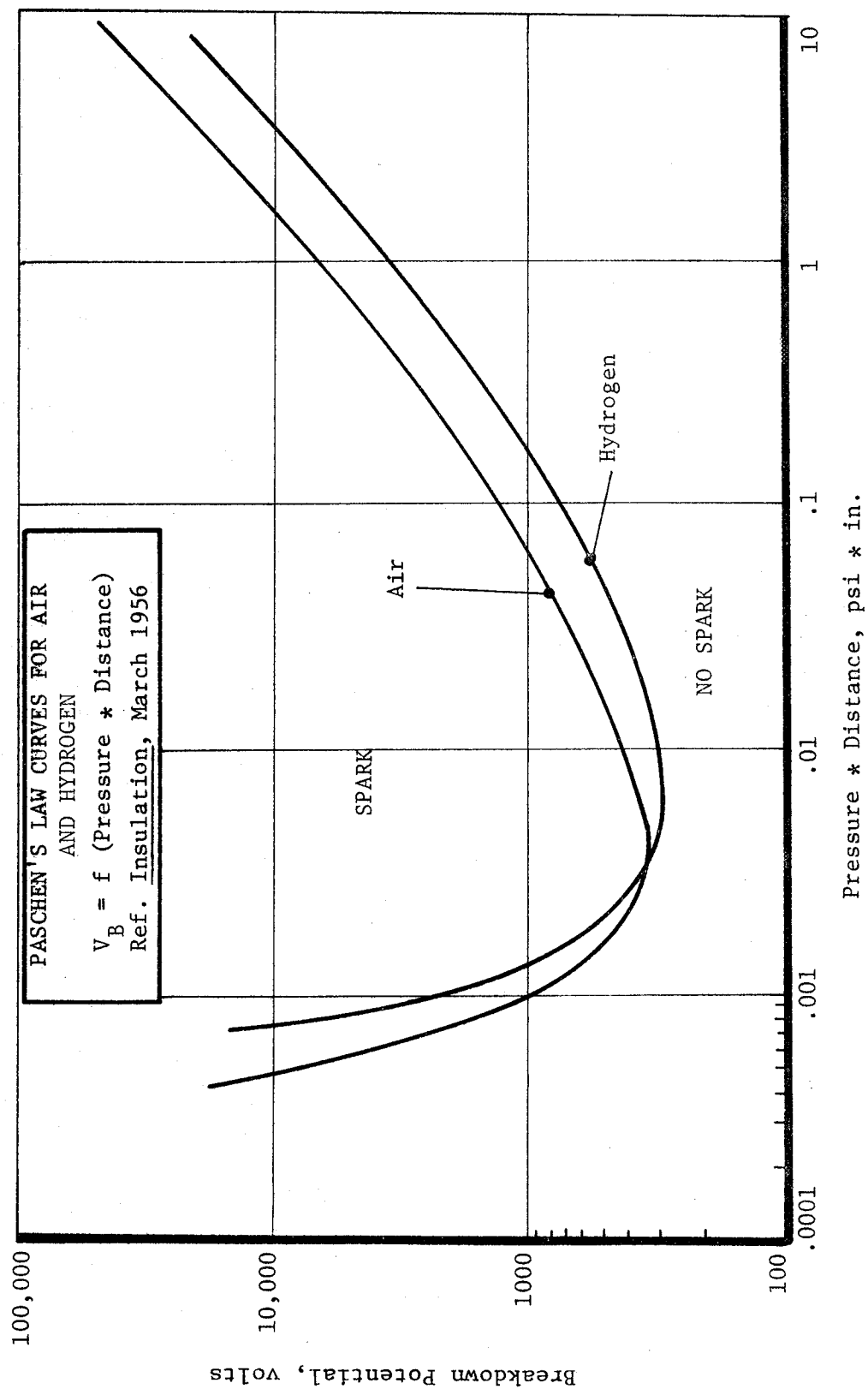


Figure IV-23. Paschen's Law Curves

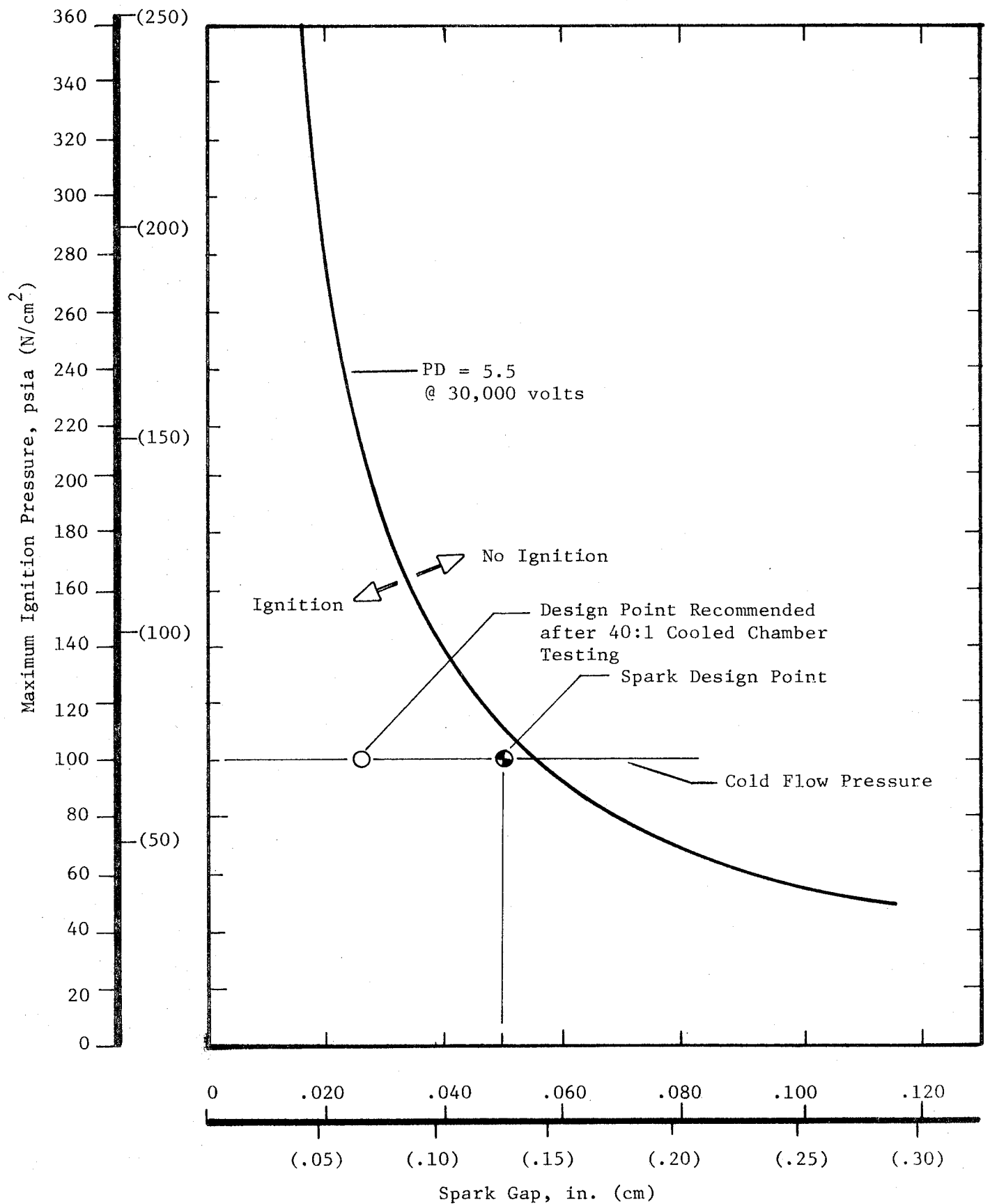


Figure IV-24. Electrical Igniter Maximum Ignition Pressure Limits

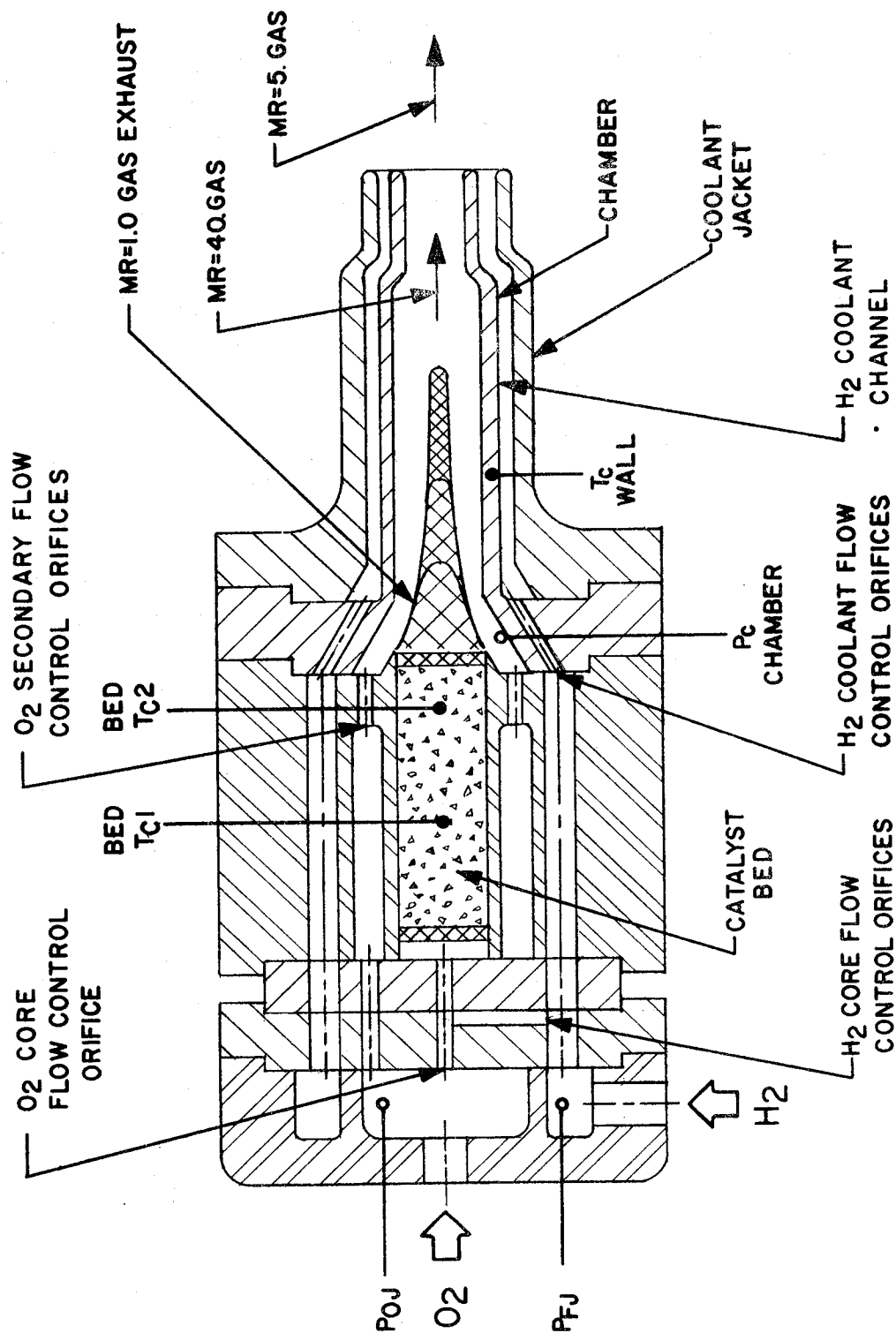


Figure IV-25. Schematic Drawing of Catalytic Igniter

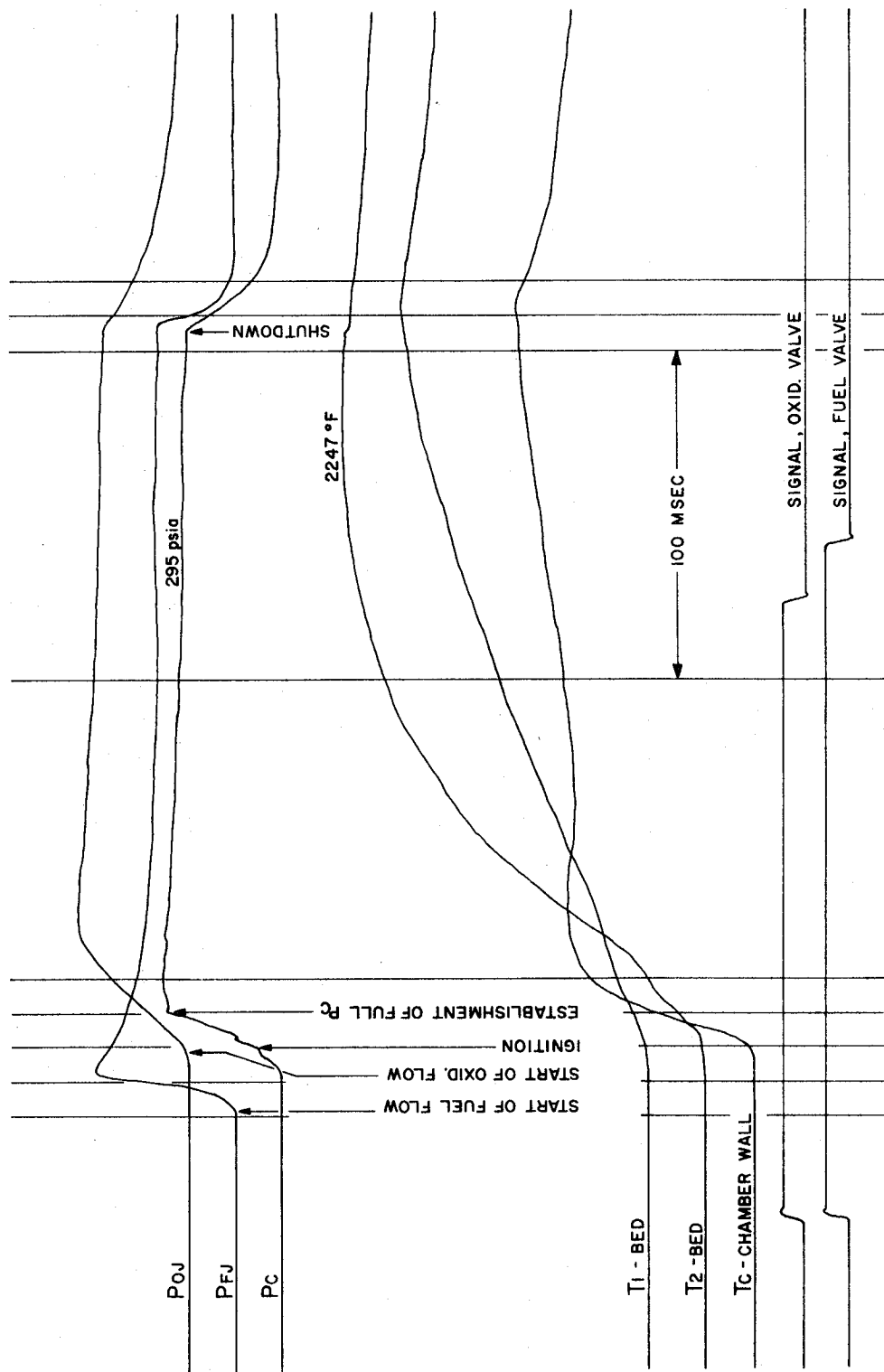


Figure IV-26. Oscilloscope Trace, Catalytic Igniter-Only Test No. 110

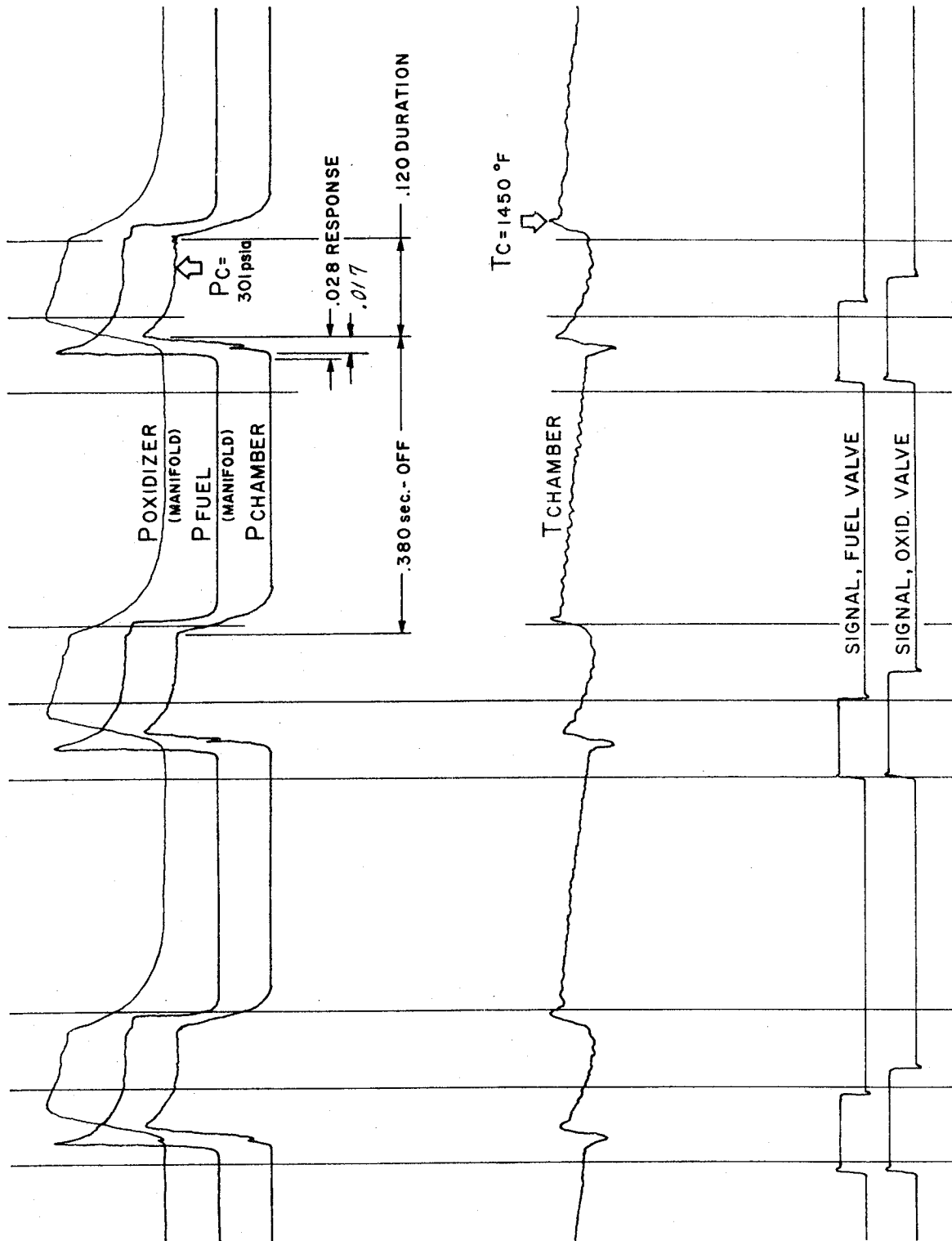


Figure IV-27. Oscilloscope Trace, Catalytic Igniter-Only Pulse Test No. 115

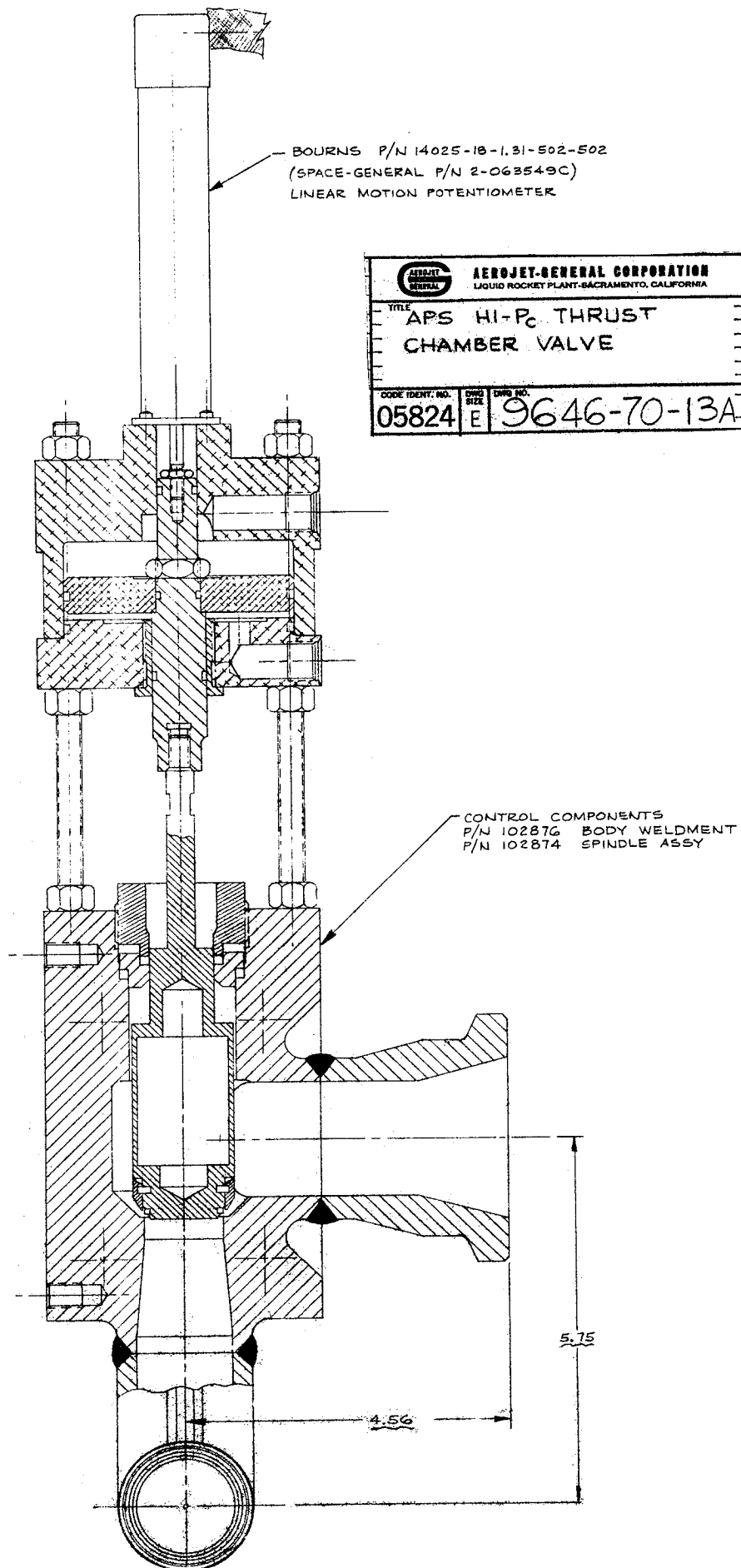


Figure IV-28. Valve and Valve Actuator Cross Section

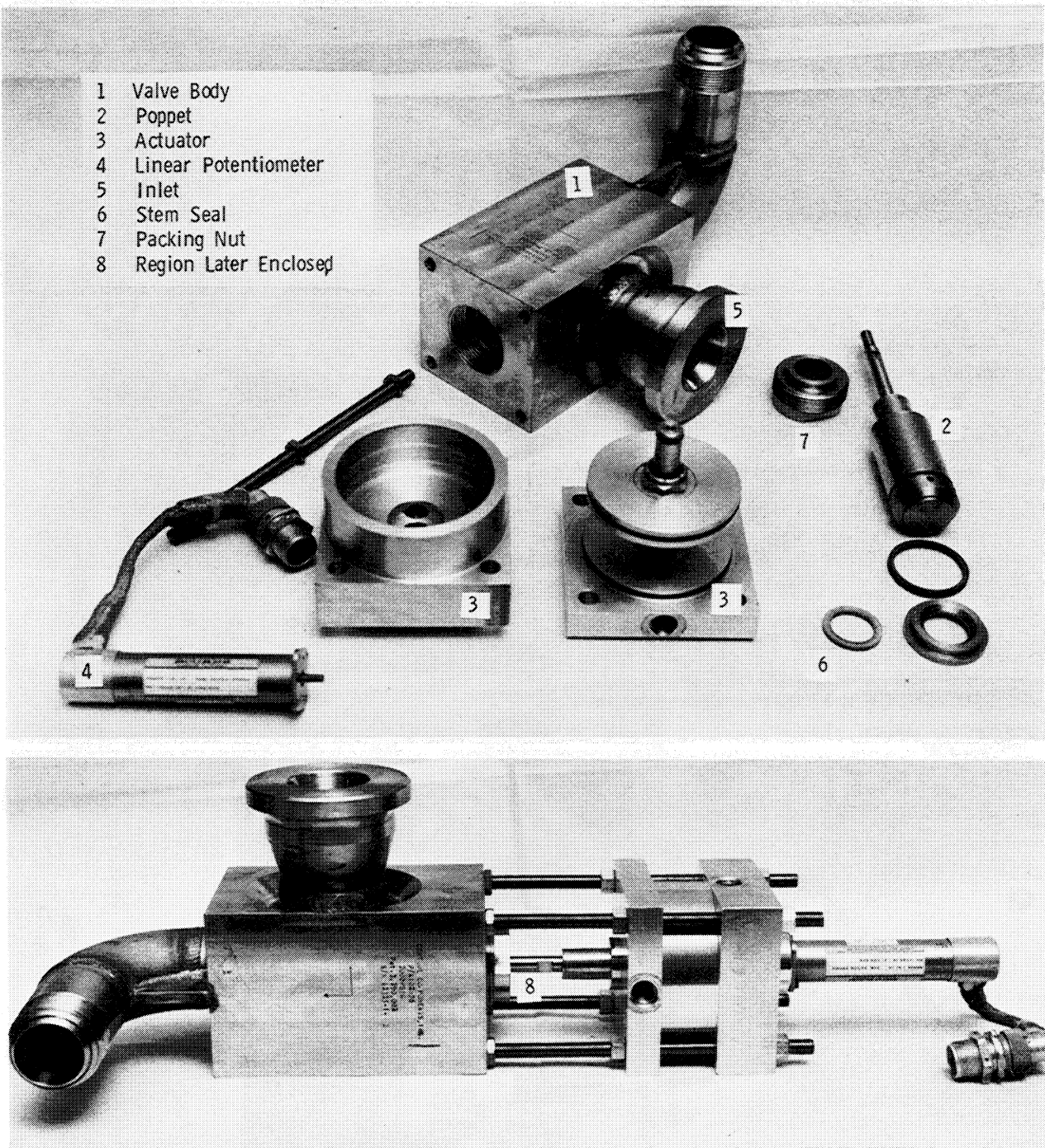
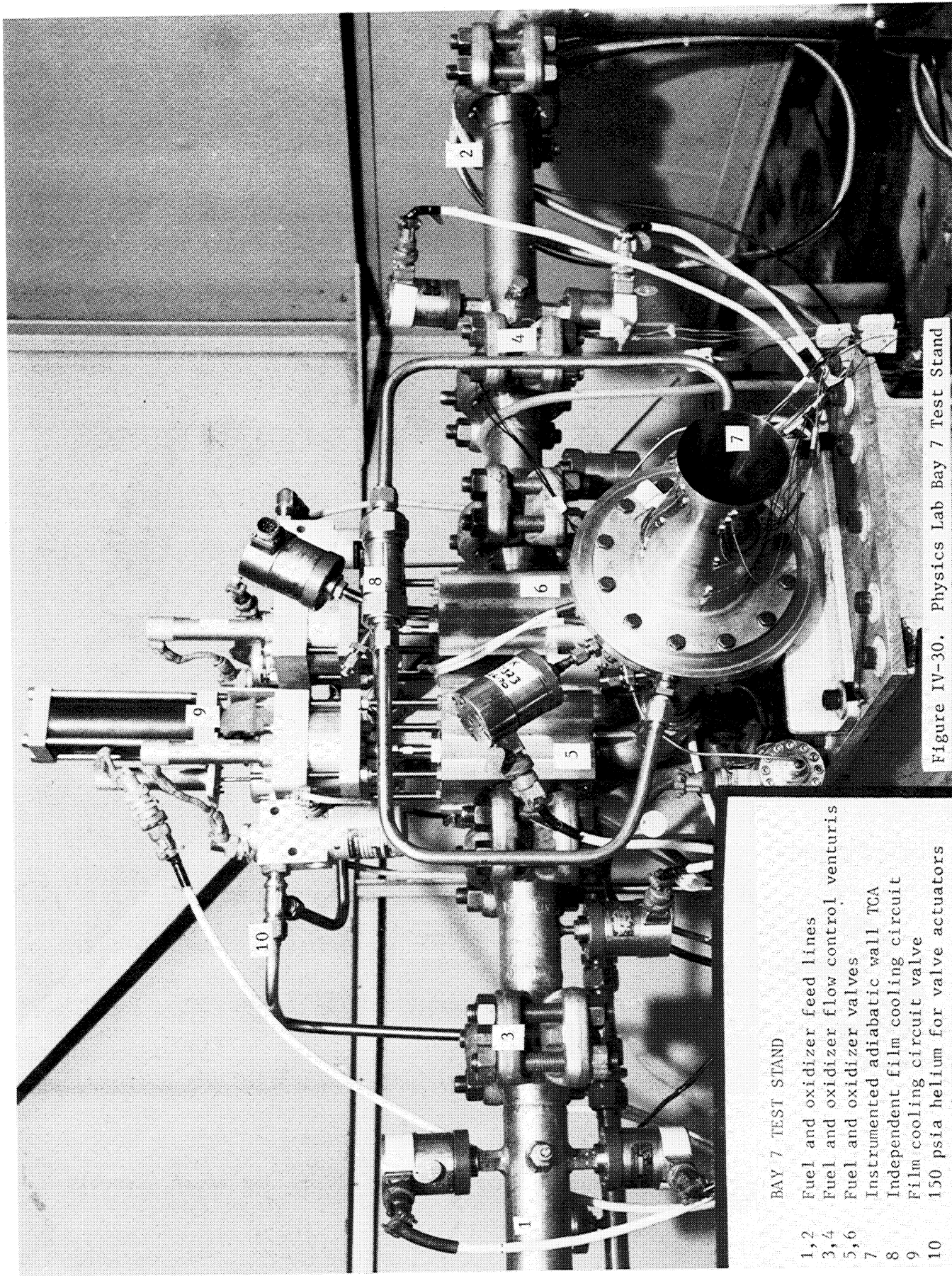


Figure IV-29. Fast Response Poppet Valves Before and After Assembly



BAY 7 TEST STAND

- 1,2 Fuel and oxidizer feed lines
- 3,4 Fuel and oxidizer flow control venturis
- 5,6 Fuel and oxidizer valves
- 7 Instrumented adiabatic wall TCA
- 8 Independent film cooling circuit
- 9 Film cooling circuit valve
- 10 150 psia helium for valve actuators

Figure IV-30. Physics Lab Bay 7 Test Stand

V. THRUST CHAMBER TESTING CONDITIONS AND DATA

A. SEA LEVEL TESTS

The purpose of the sea level testing was to: (1) obtain comparative performance and thermal data for the injectors discussed in Section IV,A; (2) to determine the influence of chamber length, mixture ratio, chamber pressure, propellant temperatures, and film cooling on the performance and chamber wall heat flux of each design; (3) to investigate injector streaking characteristics; and (4) to record the relative merits of the two igniter designs presented in Section IV,C. Combustion stability tests were also conducted on the premix "I" triplet injector with cold propellants.

1. Test Hardware

Injector testing was conducted using either a thick-wall copper heat sink chamber (exit area ratio = 3.0), an ablative (streak) chamber, or a thin-wall 0.040-in. (0.102 cm) stainless steel chamber. Copper chambers were available in 15 and 25 in. (38 and 63 cm) L^* configurations with injector face to throat lengths of 5.5 and 8.3 in. (14 and 21 cm). Cylindrical sections having L^* 's of 5 and 15 in. (12.7 and 38 cm) were also available which allowed a chamber with an L^* of 40 in. (102 cm) to be assembled.

Experimental heat flux and recovery temperature data were derived from the following sources: (1) a thick-wall copper chamber (Figure V-1) containing both brazed-in, surface temperature measuring thermocouples and adiabatic wall probes (insulated from the copper wall) and (2) a thin-wall stainless steel chamber (Figure IV-30) of the same contour with spot welded backside thermocouples. By testing both chambers at approximately the same conditions, it was possible to evaluate and compare the consistency of the experimental results.

V, A, Sea Level Tests (cont.)

Injector compatibility data were obtained from short duration firings (0.55 sec) in a 15-in. (38 cm) L^* chamber containing a replaceable chopped and molded silica phenolic liner of the design shown in Figure V-2. Injector compatibility was determined on the basis of the sensitivity of the silica phenolic material to temperature. At temperatures between 600 and 1000°F (587 to 810°K), the phenolic chars and turns black, thus showing cool zones which are presumably fuel rich. Between 1000 and 3200°F (810 and 2030°K), the phenolic vaporizes, leaving a gray-colored silica residue; and above 3200°F (2030°K), the silica starts to flow and develops a white crystalline surface. Discussions of the signatures provided by each of the injectors tested are provided in a later section covering injector compatibility.

Film coolant was injected via the interchangeable film coolant ring shown in Figure V-3. These rings are essentially short, convectively cooled sections whose effluent subsequently serves as film coolant for the downstream chamber. Nine of these nickel rings containing rectangular coolant passages formed by milling grooves in the outer periphery were available in lengths of 0.0, 1.0, and 2.5 in. (0.0, 2.54, and 6.25 cm) and three cross-sectional coolant flow areas.

The coolant rings were designed to yield minimum core-cooling mixing at injection at a given film coolant flow rate, within the constraints imposed by temperature and stress limitations of the ring material. This is achieved by matching the coolant injection velocity to the core velocity and pressure.

V, A, Sea Level Tests (cont.)

COOLANT RING GEOMETRY

Number of Channels	Flow Area, in. ² (cm)	Channel Width, in. (cm)	Coolant-to-Core Velocity Ratio	% Fuel Film Cooling in Ring Length of	
				1 in. (2.54 cm)	2.5 in. (6.25 cm)
160	0.2218 (1.43)	0.02773 (0.0705)	0.8	11.0	6.8
			1.0	14.0	10.0
			1.3	18.5	14.0
120	0.3019 (1.99)	0.05031 (0.128)	0.8	17.0	12.3
			1.0	21.0	17.0
			1.3	26.4	23.2
72	0.3979 (2.57)	0.11053 (0.281)	0.8	22.1	18.4
			1.0	26.8	23.6
			1.3	34.0	30.0

Channel depth = 0.050 in. (0.127 cm)

Land width = 0.040 in. (0.104 cm)

2. Measurements and Calibration

a. Thrust

Figure IV-30 shows the firing fixture as positioned in Bay 7 of the Physics Laboratory. Thrust was measured via a dual bridge, 2000 lb (8880 N) load cell. Lines feeding the main TC valves, film cooling valves, and igniter valves were mounted and supported such that pressurization, heating, and cooling of these supply lines did not result in force components along the axis of thrust.

The test stand thrust measuring load cell was calibrated preceding and following each test series by applying a known external force while the propellant feed lines were temperature conditioned and pressurized. This was accomplished via a remotely actuated hydraulic loader in line with the thrust and a second reference load cell.

V, A, Sea Level Tests (cont.)

b. Flow Measurements

Separate flow measurements were made for the following propellant circuits: oxidizer, fuel, fuel film cooling, igniter fuel and oxidizer. Flow in each circuit was regulated by a critical flow venturi. The two critical flow sections and nozzles regulating the main fuel and oxidizer flow were flow calibrated at the Colorado Experimental Station at Boulder. Flow through each critical nozzle was determined from the upstream temperature and pressure and nozzle calibration corrected to account for real gas effects for oxygen and hydrogen via Johnson coefficients (C_j) discussed in a following section.

Dual temperature and pressure measurements were made at the venturi inlets which control the main oxidizer and fuel flow. A third pressure measurement downstream of the thrust chamber oxidizer fuel and fuel film cooling venturi provided data to ensure nozzles were flowing critical. (Downstream pressure must be less than 85% of upstream pressures.) Where dual temperature and pressure measurements were recorded, flow was calculated from the average of the two measurements. If during a test series deviations exceeded 0.5%, the accuracy of the two measurements were compared with a third pressure measurement, namely the pressure downstream of the venturi in the locked-up condition. Performance was then computed based on the more appropriate of the two values and suspect instrumentation replaced or recalibrated on subsequent tests.

Weight Flow Calculations with Real Gas Corrections

In gas flow measurement using critical flow nozzles, the critical flow factor (C_j) provides a correction for real gas effects and is a function of inlet pressure and temperature. At sonic flow conditions the throat

V, A, Sea Level Tests (cont.)

pressure, temperature, and flow velocity are derived from the inlet environment using the P-V-T equation of state and its partial derivatives, as well as values and integrals of specific heat at constant pressure. The basic method of solution is to determine what throat conditions must be necessary with respect to inlet conditions in order to achieve exactly sonic velocity in the throat. This is accomplished by a two-level iterative process yielding the parameters required to compute C_j .

A computer program was written to compute C_j for oxygen, nitrogen, normal hydrogen, and parahydrogen over the regions defined in Figure V-4. For oxygen, densities have been computed over an extended range of temperatures using Johnson's equation of state, and the results compared with recent N.B.S. data. Over the defined region, differences approach 0.5% at temperature edges. The computed oxygen C_j error should correspond to this percentage.

In the case of both normal and parahydrogen, the P-V-T equation of state is from a recent N.B.S. general properties system (Ref 3) with an expected maximum deviation from the true surface of 0.8% for two sigma (2σ), or a 95% confidence interval. This equation is published for pressures up to 5000 psia.

The low temperature limit of the N.B.S. hydrogen equation is 240°R as applied to inlet conditions. In the 1 to 2000 psia pressure range, C_j 's were computed down to 170°R for comparison with C_j 's published by Johnson. The N.B.S. equation introducing differences in C_j approaching 3.0%. This was a direct result of extending the use of the N.B.S. equation past the limits of the original fit. A linear transformation was employed in this region to bring deviations from Johnson's tables down to less than 0.3%. Since the temperature range has not been significantly extended, Johnson's equations for specific heat were retained.

V, A, Sea Level Tests (cont.)

Propellant flow rates were calculated by

$$\dot{w} = \frac{C_d A \cdot C_j P}{\sqrt{R(T+459.7)}} [1 + \beta (T-T')]^2$$

where:

- $C_d A$ = the nozzle flow coefficient, a function of Reynolds number, determined from the calibration test at the Colorado Experimental Station
- C_j = the real gas correction, a function of propellant temperature and pressure
- β = the thermal expansion coefficient of the nozzle
- T = propellant stagnation temperature
- $(T-T')$ = the difference in temperature during a test from the calibration conditions
- P = the nozzle plenum pressure
- R = the gas constant

3. Vacuum Start Conditions

Vacuum start conditions were obtained within the 3:1 area ratio hardware by use of a vacuum pump and blow off cover which allowed high vacuum conditions to be obtained within the thruster during the start transient.

4. Summary of Test Conditions and Results

This section summarizes the sea level testing, performance results, and conclusions drawn prior to the 40:1 chamber altitude testing. Detailed discussion of the performance and thermal characteristics can be found in Section VII,A. The results of the electrical igniter lead-lag and flow relationship are contained in Reference 1, and complete thruster tests with the catalytic igniter are presented in Section IV,C.

V, A, Sea Level Tests (cont.)

5. Injector Performance Summary

The energy release efficiency of the four Phase I injector configurations, including the reduction in efficiency due to the use of up to 30% fuel film cooling, is summarized in Figures V-5 and V-6. Table V-1 provides a tabulation of the test conditions, test hardware, and measured performance for the test data points employed in preparing these figures. The upper part of Figure V-5 provides a data plot of injector efficiency for each design over a range of thrust chamber mixture ratios for various film cooling percentages. The loss in performance due to the diversion of a fixed percentage of the fuel to separate film cooling rings at the injector periphery is treated as a mixture ratio distribution loss which is additive to energy release loss of the core. The lower part of this figure is a cross plot of the data in the respective upper figures at a thrust chamber mixture ratio of 4.0. The upper dashed line at 98% ERE is the maximum reproducible performance for the most efficient injector configuration tested (the "I" triplet at 20 L*). The relative ranking of the remaining injector configurations indicates the triplet and showerhead coaxial to be close seconds and the swirler coaxial to be lowest ranking.

The second dashed line at 94.8% ERE indicated the lowest predicted injector energy release plus mixture ratio distribution efficiency which could be employed in conjunction with the selected 40:1 Rao nozzle contour and still maintain the performance goal of 435 sec. The intersection of this line with the experimental performance line for each injector at the respective L* values determines the maximum amount of fuel which can be employed as fuel film coolant for extending chamber life at a nominal thrust chamber mixture ratio of 4.0. Longer L* values allow additional film cooling to be employed. The swirler coaxial design allows the least amount of film cooling (approximately 12%), while the maximum amounts range between 22 and 25% for the other injectors, depending on L*.

V, A, Sea Level Tests (cont.)

Figure V-6 shows: (1) the influence of characteristic chamber length (L^*) for each design at mixture ratios of 4 and 5, (2) the effect of chamber pressure at mixture ratio of 4.0, and (3) the influence of oxidizer temperature on the 0% film cooling energy release efficiency. Energy release efficiency is noted to increase with chamber pressure and remain unaffected by oxidizer inlet temperature.

The premix "I" pattern was recommended for use in the 40:1 chamber altitude tests on the basis of the above data.

6. Stability Testing

A series of combustion stability tests were conducted prior to committing the selected injector concept (premix triplet) to altitude thruster testing.

Stability Tests 2K8-187, -188, and -189 were conducted in a 15 L^* copper heat sink chamber instrumented with two flush-mounted Photocon 307 transducers located 120 degrees apart and 1 in. (2.54 cm) downstream of the injector as shown schematically in Figure V-7. All tests were conducted with SN 2 ("I" pattern) premix element injector using cold propellants. The test conditions are summarized below. The combustion dynamic stability was evaluated by perturbing the chamber pressure with a thermally detonated 2-grain Teflon-encased RDX charge. The results of one of these stability tests are displayed in Figures V-7 and V-8. Prior to bomb detonation, peak-to-peak pressure amplitude oscillations are approximately 5% of chamber pressure, otherwise stated as 300 psia \pm 7.5 psi. The bomb detonation resulted in a nominal 200% overpressure as recorded by the Photocon pressure transducers. From Figure V-7, in which each major time division represents 0.001 sec, it can be seen that the pressure oscillations decay to within a few percent of

V, A, Sea Level Tests (cont.)

the pre-excited state in 0.006 sec. Figure V-8 shows the results of a spectral density analysis of the chamber pressure oscillations at all frequencies. Also shown are the predicted frequencies at which some resonance could be expected.

SUMMARY OF STABILITY TESTING

$MR_E = 4.0$, 10% Fuel Film Cooling

<u>Test No.</u>	<u>Propellant Temp, °R(°K)</u>		<u>P_c 2K*</u>	<u>P_c 1K</u>
	<u>Oxidizer</u>	<u>Fuel</u>		
2K-8-187	408 (227)	400 (222)	680/680	580/670
2K-8-188	360 (200)	390 (217)	230/370	510/540
2K-8-189	377 (210)	384 (213)	720/720	650/810

*Overpressure due to bomb

Initial ΔP /maximum ΔP , psia (N/cm²)

V, Thrust Chamber Testing Conditions and Data (cont.)

B. COOLED CHAMBER ALTITUDE TESTING

1. Introduction

The purpose of this test series was to evaluate the cooled chamber designs at nominal and off-design conditions and to establish a relationship between vacuum performance and chamber cooling. This section provides a chronological documentation of the testing events related to the following hardware buildups:

<u>Test Series</u>	<u>Chamber</u>	<u>Injector</u>
D03	SN 1 film-cooled	SN 5 premix "I"
D03	SN 1 film-cooled	SN 4 premix triplet
D04	SN 2 film-cooled	SN 6 modified premix "I"
D03	SN 1 regeneratively cooled	SN 3 premix triplet
D04	SN 1 regeneratively cooled	SN 6 modified "I"
D06	SN 3 film-cooled	SN 7 modified "I"
D06	SN 3 regeneratively cooled	SN 7 modified "I"

Table V-2 provides a summary of the test conditions for each hardware buildup. Tables V-3 through V-6 provide the exact test conditions, raw test data, computed performance, and measured chamber and injector temperatures.

2. APS Altitude Test Facility Description

APS hardware development testing was accomplished in the ALRC capital-owned altitude facility in Test Zone J. Test Stand J-3, an 8-ft-dia by 130-ft-long (2.44 m x 39.5 m) altitude chamber was used for all testing. The entire test setup including the test article, firing fixture, thrust calibration assembly, flow measuring devices, and approximately 24 ft (7.3 m) of

V, B, Cooled Chamber Altitude Testing (cont.)

both the fuel and oxidizer feed lines are located inside the test cell and are subjected to the simulated altitude environment as shown in Figure V-9. The propellant supply tankage, heat exchangers, and ullage tanks are located adjacent to and outside of the vacuum chamber.

Test Stand J-3 can be operated in several steam ejector configurations, depending on the desired altitude and engine mass flow conditions. The ejector configuration that yields the highest altitude and longest sustained duration utilizes the three-stage ejector system located at the end of the altitude chamber. This configuration consumes approximately 32 lb/sec of steam and will provide a maximum altitude, no flow, of 150,000 ft for 2000 sec. The sustaining altitude during engine flow conditions is not only dependent on the mass flow of the hardware and cell leakage but the resultant gas density. It can be seen on Figure V-10 that the test cell pressure is a function of both P_c and MR. As an example, a test with the $P_c = 300$ psia (206 N/cm^2) and $\text{MR} = 6.0$, the ejector system will maintain approximately 85,000 ft for 2000 sec of steady firing. Keeping everything the same and changing to a $\text{MR} = 4.0$, the altitude will change to 57,000 ft in 12 sec. To allow testing of this hardware through the entire range of conditions, a second ejector configuration was employed. This configuration utilized the second and third stages of the J-3 ejector system and a 4-ft-dia (1.2 m) cross-over direct to a 10 lb/sec two-stage ejector on Test Stand J-4. Figure V-10 shows this configuration, which is capable of handling the entire range of flow and MR; however, its sustained altitude is approximately 66,000 ft with a duration of 500 sec.

In both ejector configurations the propellant bleed-in, temperature stabilization, and in-place thrust calibrations are accomplished utilizing the second and third stage ejectors which only consume 6 lb/sec of steam, allowing that entire operation to be conducted under a vacuum condition. After the propellant is bled in and the temperature throughout the system has

V, B, Cooled Chamber Altitude Testing (cont.)

stabilized, the feed system is pressurized up to the thrust chamber valves and a remote thrust calibration is accomplished with the entire system under a vacuum environment. This in-place force stimulus calibration identifies the system bias caused by the propellant feed system growth as a result of both pressure and temperature effects as well as any interaction introduced by the altitude chamber to firing fixture movement caused by the low ambient pressure inside the cell. The calibration is accomplished by physically pulling the fixture/TCA on the centerline of thrust from 0 up to 2500 lbf and then back to 0 in 500 lbf steps. The thrust stand accuracy over 102 calibrations yields a bias of -2.54% with an accuracy of $\pm 0.4\%$ (95% confidence level).

The curve in Figure V-10 indicates the distribution about the mean thrust bias obtained from the thrust calibrations made during the period June through September 1971 on the J-3 thrust fixture. These calibrations were made under various conditions:

Propellants bleed-in:	Pressure range - 200 to 1000 psia
	Temperature range - 250 to 600°R
	Cell vacuum pressure - 0.9 to 9.0 psi
Without propellants:	Pressure - atmospheric
	Temperature - ambient

V, B, Cooled Chamber Altitude Testing (cont.)

The J-3 fuel (GH_2) propellant system was designed to deliver 1.5 lb/sec GH_2 from two 110,000 scf (at 2250 psi [1550 N/cm^2]) "over the road" trailers to the test hardware with a ΔP of 300 psi (207 N/cm^2).

The propellant line is 2-in. sch 40 pipe with a 10μ stainless steel filter located between the heat exchanger and the thruster. The oxidizer (GO_2) propellant system is designed to deliver 40 lb/sec GO_2 from an 81,000 scf (at 2250 psi) cascade to the test hardware. The GO_2 propellant line is 2-in. sch 40 pipe with two 10μ monel filters. One filter was located immediately downstream of the cascade but upstream of the propellant heat exchangers. The second filter was added to the line between the heat exchanger and thrust chamber valves following Test 03-015, during which an injector failure due to plugging was experienced.

The facility contains two heat exchangers in each of the propellant systems. One is of the pool boiling type. It is open to atmosphere and uses LN_2 for a cooling medium. The propellant outlet temperature is determined by the level of LN_2 in the heat exchanger. The level is maintained by a remotely operated supply valve. The LN_2 source is a 13,000-gal storage tank with a 120 gpm pump. The other heat exchanger is a counterflow tube in shell type that uses steam for the heating medium. The outlet temperature is controlled by a temperature feedback control regulator. The steam source is five 4550 ft³ accumulators (400 psi at 400°F). The heat exchangers are capable of delivering either hot (800°R) or cold (200°R) conditioned propellants for an unlimited test duration.

Control of the propellant mass flow rates was accomplished by three Hammel-Dahl hydraulic operated flow control valves (fuel, oxidizer and film coolant). The valves have a response time from full closed to full open of 0.075 sec. Nominal operating range for the APS program was approximately 20 to 50% open. The facility also contained an on-line E.A.I. Pace

V, B, Cooled Chamber Altitude Testing (cont.)

TR-48 analog computer which controlled the engine flow rates by monitoring the venturi inlet pressure and temperature and adjusting the flow control valves accordingly through a feedback loop. The TR-48 was capable of using linear and nonlinear functions in calculating flow rate and was programmed to provide a variety of mixture ratio, combustion chamber pressures, and coolant system flow rates during the test. The changes were made from the control console on demand while the engine was firing. The computer also had the capability of monitoring 16 pressures and temperatures and could terminate the test within 0.020 sec if valves were not within a predetermined safe operating range. The safe operating range was determined by a failure mode analysis of the test hardware and facility.

The facility was setup for two types of flow measurements: high recovery critical flow venturis or constant temperature anemometers. The venturi flowmeters were used for steady-state testing and were located just upstream of the thrust chamber valves. The venturis were calibrated at the Colorado Engineering Experimental Station, Inc., Boulder, Colorado. The accuracy of the oxygen flow at 310°R is 0.64% (95% confidence level) and for hydrogen flow at 200°R is 0.93% (95% confidence level).

The anemometer flow measuring system was used for the pulse testing. The anemometers were located immediately upstream of the thrust chamber valves while the venturis were moved from their location just upstream of the valves to a position upstream of the 17 ft³ accumulators. The anemometers which were employed had a full-scale response of 2 millisec. The anemometer type flowmeters were selected for gas flow measurement in the pulse test phase of the program to meet the need for very high response and reasonable accuracy. These flowmeters were calibrated in the test configuration against sonic nozzles traceable to N.B.S. Calibration results were fitted to fourth degree polynomial equations with standard deviations ranging from 0.45% to 0.75% with the exception of two oxygen flowmeters which were not

V, B, Cooled Chamber Altitude Testing (cont.)

fully temperature-compensated. These had standard deviations of 1.9% and 2.7% of full scale. The estimated accuracy of the temperature-compensated models within their operating flow and temperature range is 1.6% at the 95% confidence level. Though mechanically delicate and sensitive to careless handling, these flowmeters proved rugged in high velocity gas streams and exhibited the requisite high response to the very rapidly varying flow encountered in the pulse test program. Development of improved calibration methods to collect data over a wider range of flow and temperature should increase the accuracy of these flowmeters.

3. Summary of Altitude Testing

a. Facility Calibration and Checkout Tests (Series 1680-D03)

The initial J-3 tests were conducted with residual injectors and 3:1 area ratio film-cooled steel chambers in order to check out the dynamics of the computer-controlled system during mixture ratio changes and obtain a performance base point for comparison of J-3 altitude vs Physics Lab Bay 7 data.

Tests 001 through 004 were valve, igniter sequence, and cold flow tests.

Tests 005 through 009 were system debugging and calibration tests with SN 2 "I" premix injector, a 3:1 area ratio film-cooled chamber, and a 25 lb (111 N) thrust spark igniter. Tests were conducted at partial altitude conditions to prevent accumulation of combustible gases in the test cell.

V, B, Cooled Chamber Altitude Testing (cont.)

Tests 005, 006 and 007 were terminated between 0.6 and 1.0 sec by computer because of programming errors in the temperature shutdown criteria.

Tests 008 and 009 with the same hardware were of 23 and 28 sec duration in which both film cooling and mixture ratio were varied while the engine was firing. Test 008 and Test 009 proceeded as follows:

<u>Test</u>	<u>Period, sec</u>	<u>MR</u>	<u>% Cool</u>
008	0 - 6	3.0	33
	7 - 11	3.0	30
	12 - 16	3.0	25.5
	17 - 20	3.0	33
	21 - 23	4.0	37
009	0 - 14	3.0	30
	15 - 28	4.0	35

Accumulation of moisture in the load cell due to operation at partial vacuum resulted in questionable thrust measurements in the latter tests of this series. The facility, however, appeared to be operational at this point.

b. 40:1 Film-Cooled Chamber Tests

Tests 010 through 015 were conducted with SN 5A premix "I" triplet injector, SN 1 film-cooled 40:1 nozzle, and the same spark igniter. Figure V-11 provides an instrumentation schematic for this test setup. Test 010 consisted of three igniter-only firings prior to evacuating the cell. Normal ignition was achieved in each case. Test 011 was a repeat series at altitude of 69,000 ft. The igniter was fired three times in series and three normal ignitions were achieved. Test 012 was a 1-sec thrust chamber firing, MR = 4.0,

V, B, Cooled Chamber Altitude Testing (cont.)

30% film cooling. Real time data playback indicated that all thermal and pressure parameters appeared to function as predicted. The same test conditions were immediately repeated without hardware inspection in Run 013 for a 10-sec duration. Postfire inspection following the 10-sec test revealed the hardware to be in excellent condition.

The above test conditions were repeated for a 37-sec run (Test 014) during which steady-state temperatures were achieved throughout the nozzle.

Test 015 was initiated immediately following a brief data review and lasted for 278 sec. During this continuous fire period, the 11 following nominal balance conditions were evaluated:

<u>MR</u>	<u>Data Points</u>	<u>% Film Cooling</u>
4	(a - d)	30, 25, 20, 30
3	(e - h)	30, 25, 20, 30
4	i	30
5	j, k	30, 25

Testing was terminated due to a significant rise in cell pressure caused by depleted steam levels in the facility accumulator/ejector system. Steady-state thermal conditions were achieved at each condition except the last. Postfire hardware inspection revealed major local damage to the injector face under the oxidizer inlet, but no damage to the chamber, igniter, facility, or instrumentation. Data analysis revealed failure was initiated 18.5 sec prior to shutdown and was undetected because of only minor changes in the temperature, pressure, and performance parameters being monitored. The failure is believed to have resulted from foreign material which came from the oxygen heat exchanger and lodged in the injector during the high oxygen flow (MR = 5) testing.

V, B, Cooled Chamber Altitude Testing (cont.)

Figure V-9 shows a photograph of the film-cooled thrust chamber assembly mounted on the test stand within the J-3 altitude test cell prior to testing. Figure V-12 shows the same nozzle after Test 015 at which time four restarts and 326 sec of duration had been accumulated. Figures V-13 through V-16 provide a graphical record of the propellant flow rates and some of the pressure and temperature parameters monitored during Test 015. Instrumentation location and nomenclature is identified in Figure V-11. Changes in flows, and thus chamber wall temperatures, throughout the run are initiated by the pre-programmed computer control system.

Runs 016 through 021 employed the same hardware except the SN 5A injector was replaced by SN 4 premix triplet, which was employed earlier in the 2500-pulse test series for contract NAS 3-14358 (Ref 1) in Bay 7 of the Physics Lab. Run 016, a repeat test at MR = 3.0, 20% film cooling, was computer terminated due to an amplifier malfunction in one of the throat temperature circuits.

Runs 017, 018 and 019 were short (5 sec) tests to obtain repeat performance with the SN 4 injector at the following conditions:

<u>Run</u>	<u>MR</u>	<u>% Cooling</u>
017	3	30
018	3	25
019	4	25
	4	20

Run 020 was of approximately 50 sec duration during which near steady wall temperatures were reached at the following conditions:

V, B, Cooled Chamber Altitude Testing (cont.)

<u>MR</u>	<u>% Cooling</u>
4	25,20,30
5	30

Limiting wall temperatures were approached at the last test condition.

Run 021 was at reduced chamber pressure (100 psia [69 N/cm^2]) for a duration of 109 sec. Steady-state thermal conditions were achieved at a mixture ratio of 4.0 with 21 and 26% film cooling.

Tests 022 and 023 were low temperature propellant tests with the same hardware. A considerable amount of heat exchanger cold flow testing and evaluation of procedures for facility chilldown was conducted prior to this first cold propellant test series. The method of controlling propellant temperature was to adjust the LN_2 levels in the pool boiling heat exchangers. Cold flow tests showed that 200°R (111°K) hydrogen could be delivered to the thrust chamber valve at fire switch and thereafter when the accumulator and feed lines were preconditioned with a LN_2 purge and the heat exchanger operated at maximum cooling capacity. The oxidizer heat exchanger had a much larger cooling capacity and care had to be taken not to condense the GO_2 in the LN_2 bath. The initial oxygen circuit cold flow test was conducted with 50% of the pool boiling surface immersed in LN_2 . Two-phase flow was experienced in this run. Levels corresponding to 25 and 10% surface coverage were then flowed at nominal GO_2 flow rates. The latter coolant level provided the lower temperature limit of 320°R (178°K) at the inlet of the critical flow venturi. Temperatures at the oxidizer valve were 12°F (7°K) lower due to the pressure loss in the flow nozzle. Test 022 was a 15-sec burn at mixture ratio = 4 with 30% film cooling flow. The fuel temperature was 200°R (111°K) and the oxidizer nominally 260°R (200°K) throughout the run. Performance data on this test was of questionable value because of high test cell pressures resulting from the GN_2 cell purges which were left on during the test.

V, B, Cooled Chamber Altitude Testing (cont.)

Test 023 was a repeat test of 58-sec duration. The nominal test objectives were MR = 4.0, 30 and 25% cooling. A wider range of test conditions were actually demonstrated due to an invalid temperature signal to the computer. Nominal flow conditions experienced in this test were as follows:

<u>Period,</u> <u>sec</u>	<u>MR</u>	<u>% Cooling</u>	<u>T_{fuel},</u> <u>°R(°K)</u>	<u>T_{ox},</u> <u>°R(°K)</u>
0-15	4	28	200(111)	320(178)
15-25	5	28	200(111)	320(178)
30-45	4	20	200(111)	320(178)

Test 024 was a high pressure (500 psia [345 N/cm^2]) ambient temperature propellant run of 34-sec duration. Nominal test conditions were:

<u>MR</u>	<u>% Cooling</u>
4	30,25,30

Limiting skirt temperatures of 1850°F (1280°K) were approached at the 25% coolant flow conditions.

Hardware inspections following each of the three preceding tests showed all components to be in excellent condition. Figure V-17 shows the SN 4 triplet injector following these tests; at this time, the injector had accumulated over 700 sec duration and 2600 restarts. The radial markings around the periphery of the injector which can be observed in Figure V-17 (and were generally noted throughout the program) correspond to the chamber coolant channels. These fine pitting marks were apparently due to mechanical erosion caused by the impact of particles carried in the high velocity hydrogen discharging from the coolant jacket. These particles are probably from the "over the road" gas delivery trailer and smaller in size than the 10-micron filter.

V, B, Cooled Chamber Altitude Testing (cont.)

In the process of temperature conditioning the feed system prior to Run 025, which was to be a 500 psia (345 N/cm^2) cold propellant test, a small H_2 pop outside of the altitude cell ruptured a facility hydraulic line and caused a small oil fire outside the cell. This resulted in some damage to facility equipment located nearby. There was no damage within the test cell since it was sealed and at high vacuum conditions.

c. Checkout Tests of Modified "I" Premix SN 6 Film-Cooled Chamber (Test Series 1680-D04)

The improved Phase II modified "I" pattern design became available at this point in the program and the SN 4 triplet injector was replaced. The hardware buildup in this phase consisted of:

- SN 6 modified "I" premix triplet injector
- SN 1 film-cooled chamber
- 25-lb thrust spark igniter
- Spacer ring which adapts SN 6 injector to SN 1 film-cooled chamber

Facility operation and valves and chamber instrumentation were identical to those shown in Figure V-11 with the exception that the injector instrumentation consisted of six face and one flange thermocouples designated as TJ-1 through 4-10 and TJ-1 and 2-20 and the flange TJF.

Testing on the D04 series proceeded as follows:

Tests 001 through 006 included facility checkout tests and a series of short 1-sec firings to check out the new injector face temperatures.

Test 007 was a nominal 300 psia (207 N/cm^2) test at TCA MR of 4.0 and 25% fuel film cooling. Steady-state thermal conditions were achieved throughout the chamber in this test.

V, B, Cooled Chamber Altitude Testing (cont.)

Tests 008 and 009 were to be MR and film cooling survey tests. These were both terminated early because of an inoperative fuel film cooling valve.

(In the MR - film cooling survey tests, a separate flow circuit and valve was employed to vary film cooling flow.) Failure of the valve to function in the latter test resulted in a burnout of the steel wall immediately downstream of the film cooling injection ring and damage to the tip of the copper ring.

Test 012 - The damaged SN 1 film-cooled chamber was replaced with the SN 2 unit which differed from SN 1 in that it contained a zirconium copper liner rather than OFHC and had an uninsulated skirt. Test 012 was of 100-sec duration and provided the following nominal data points at 300 psia (207 N/cm^2) chamber pressure.

<u>MR</u>	<u>% FFC</u>
4	29,24,19,17
5	29,24

Test 014 was conducted with the same hardware at a chamber pressure of 500 psia (345 N/cm^2) for approximately 12 sec. Data points on this test include:

<u>MR</u>	<u>% Cooling</u>
4	25
5	25

Test 015 was a low temperature propellant test at 300 psia (207 N/cm^2). This test was terminated by computer malfunction detection system at $FS_1 + 0.150 \text{ sec}$ because the desired chamber pressure was not achieved. Failure to achieve ignition and thus chamber pressure was a result of not having the igniter power supply turned on. The preprogrammed computer monitoring system functioned exactly as expected.

V, B, Cooled Chamber Altitude Testing (cont.)

Test 017 was a cold propellant test of 20-sec duration at 300 psia (207 N/cm^2). Testing was terminated early because the mixture ratios could not be controlled by the computer due to very low oxidizer temperature. Temperatures below 320°R (178°K) produce two-phase flow in the critical flow venturis. Propellant temperatures experienced during this test were 170°R (94°K) for the fuel and 280°R (155°K) for the oxidizer.

Test 018 was a 100-sec repeat test at 300 psia (207 N/cm^2) with slightly warmer oxidizer. Data points obtained were as follows:

<u>Data Period,</u> <u>sec</u>	<u>MR</u>	<u>% FFC</u>
5-12	3	18.9
16-24	3	13.9
25-27	3	19.4
30-33	3	24.7
35-45	4	24.6
47-58	4	19.9
60-70	4	17.7
72-74	4	20.3
76-79	4	24.7
81-91	5	22.7
94-101	5	18.7

Hardware inspection following this series of tests showed all components in good condition. Photographs of the injector are shown in Figure V-18. The changes in color in the skirt correspond to the 304 - Haynes 188 joint and an axial weld in the 304 material. There were no streaks.

V, Thrust Chamber Testing Conditions and Data (cont.)

C. REGENERATIVELY COOLED CHAMBER TESTING

The first hardware buildup consisted of SN 3 triplet injector, a zero length "10%" film cooling ring, and a 25-lbf spark igniter.

The face plane film cooling ring was supplied from the coolant flow control valve such that the upstream film coolant could be reduced while the engine was firing. The downstream supersonic coolant injector, integral with the skirt, was fed from the main fuel circuit. The downstream flow was maintained at a fixed percentage of the flow going through the regenerative jacket and injector. Flow in the three respective fuel circuits (main flow, upstream coolant and downstream coolant) was controlled and measured via separate critical flow, high recovery venturis.

The 25-lbf spark igniter was that employed in earlier tasks and in the APS ignition contract, NAS 3-14348. The spark, set at a power level of 0.01 joules, gap of 0.025 in. (0.063 cm), was sequenced on 0.015 sec prior to actuation of the igniter valves. In these tests, the igniter was sequenced on 0.050 sec prior to main TCV opening and operated for a period of 0.170 sec at which time the spark and igniter oxidizer were sequenced off. Figure V-19 provides a flow and instrumentation schematic drawing of this test setup.

1. Testing Summary

Test 03-026 was the first test on the above buildup. The test was a 2-sec checkout run at 300 psia (207 N/cm^2), $\text{MR} = 4.0$, 20%* upstream and 7.4%* downstream cooling. The system and hardware performed flawlessly. Test 03-027 followed immediately after hardware inspection and lasted for a duration of 58 sec at which time steady-state thermal conditions were achieved throughout the chamber. The following conditions were achieved in this test.

*Percent of total fuel flow.

V, C, Regeneratively Cooled Chamber Testing (cont.)

<u>Time, sec</u>	<u>MR</u>	<u>% Upstream Cooling</u>	<u>% Downstream Cooling</u>
5-30	3.1	20.0	7.4
35-54	3.2	13.1	8.1
55-57	3.3	17.1	7.8

Test 03-028 was of 18-sec duration at the following conditions:

3-12	4.1	13.6	7.5
12-18	4.2	0	9.4

At this point in the test program, the SN-3 triplet injector was replaced with the higher performing SN-6 modified "I" triplet. Additional testing was conducted without upstream film cooling since thermal data from preceding tests confirmed that addition of up to 13% face plane film cooling did little to reduce throat plane heat flux and wall temperatures. Upstream film cooling flow rates in excess of 20% are required to provide significant improvements in chamber life. The use of upstream film cooling flows in excess of 20% was considered unrealistic since the film cooled chamber had already been demonstrated to operate satisfactorily with less total film cooling than 20%.

Test 04-019, the first test with the new buildup, was of 60-sec duration. No upstream cooling was used. Downstream cooling was varied using the system coolant flow control circuit to regulate and measure flow rates.

This test was programmed to provide downstream coolant flows starting at 15%. However, a reversal of upstream and downstream pressure transducer signals being fed to the computer resulted in actual coolant flow rates of 23.8%. The overall mixture ratio was 4.1. Skirt temperatures in this test reached maximum recorded steady-state values of 1000°F (810°K).

V, C, Regeneratively Cooled Chamber Testing (cont.)

Test 04-020 was a repeat test with corrected flows for a duration of 97 sec. The following conditions were evaluated.

<u>Time, sec</u>	<u>MR</u>	<u>% Cooling</u>
0-24	4.0	14.6
30-54	4.1	10.4
60-71	3.1	10.3
74-78	4.2	10.4
82-86	5.1	10.3
90-96	5.2	15.3

All test objectives were achieved and it was demonstrated that the minimum skirt film coolant flow rate required for steady-state operation on this design is about 10%.

Test 04-021 was a 500 psia (345 N/cm^2) test of 28-sec duration. Test conditions were:

<u>Time, sec</u>	<u>MR</u>	<u>% Cooling</u>
0-15	3.6	10.1
16-28	4.1	10.1

The test was terminated by a computer temperature shutdown shortly after the TCA MR was increased to 5.0. The shutdown was a result of a throat temperature exceeding the preprogrammed conservative 1100°F (865°K) operating limit. Post-fire inspection revealed all hardware to be in good condition. The only abnormal condition to be reported upon this inspection was that a .125 in. (.317 cm) dia. thermocouple which monitored the fuel bulk temperature leaving the chamber and entering the injector (TFM-2) was ejected from its friction-held and sealed retainer, thus allowing a small amount of overboard fuel leakage. The loss,

V, C, Regeneratively Cooled Chamber Testing (cont.)

estimated to be 1/2 to 3/4 of one percent, was not accounted for in calculating performance, thus actual performance will be higher than the reported values.

Test 03-029 was a 100 psia (69 N/cm^2) 5% film coolant test with the same hardware. This test was terminated by the computer logic which requires a minimum coolant manifold pressure to insure flow. The combination of low chamber pressure and flow rates resulted in failure to meet the specified criteria.

Test 03-030 was a repeat 100 psia (69 N/cm^2) test of 70-sec duration which evaluated the following conditions.

<u>MR</u>	<u>% Film Cooling</u>
4.4	4.0, 6.8, 9.7

All test objectives were achieved and it was determined that approximately 10% cooling was also required to allow steady-state operation at 100 psia.

Test 03-031 was an 8-sec 100 psia (69 N/cm^2) performance only test at MR = 3.1, 9.4% film cooling.

Test 03-032 was terminated at .14 sec due to a control system malfunction which could not be identified.

Test 03-033 was a 48-sec 100 psia (69 N/cm^2) test at mixture ratio 5.5 with 9.3% cooling. Testing continued to depletion of facility steam supply, giving a rise in cell pressure and nozzle flow separation. Postfire hardware inspection showed all components to be in good condition with the exception of an internal teflon O-ring which extruded from its retaining groove. The seal failure allowed some fuel leaving the regenerative cooling jacket to

V, C, Regeneratively Cooled Chamber Testing (cont.)

flow directly into the chamber without going through the injector; thus reducing performance and providing a degree of film cooling. This leakage was thought to be very small because the forward end of the copper chamber and the steel adapter ring which it contacts constitute a near zero clearance joint.

Test 04-022 was the first low temperature propellant test on this chamber. The test was run at 300 psia (207 N/cm^2) for 40 seconds. Test conditions were:

<u>MR</u>	<u>% FFC</u>	<u>O/F Temp, °R</u>	<u>(°K)</u>
4.5	11	350/200	(195/111)

The test was terminated short of the planned duration by the computer due to a slight shift in the ground voltage which in effect lowered all the shutdown temperatures. The test objectives were achieved; satisfactory data was obtained.

Test 04-023, 72 seconds, was an extension of the above conditions to other coolant flow rates and mixture ratios as follows:

<u>MR</u>	<u>% FFC</u>	<u>O/F Temp, °R</u>	<u>(°K)</u>
4.4	8.1	375/190	(208/105)
4.5	10.8	330/180	(183/100)
3.3	10.2	307/243	(170/135)
4.4	10.3	309/221	(171/122)
5.6	15.5	325/188	(180/104)

The test proceeded routinely and all systems and components functioned normally. Coolant flow rates of 10% were found to be marginal for steady-state operation above mixture ratios of 5.0.

V, C, Regeneratively Cooled Chamber Testing (cont.)

Test 04-024 was a 500 psia (345 N/cm^2) cold propellant test on the same hardware. A slug of very cold oxygen (possibly liquid) was experienced several seconds after ignition resulting in a very high oxygen flow rate and accompanying high engine mixture ratio. Although the precise oxygen flow rate could not be determined, the chamber pressure during the short run was approximately 650 psia (450 N/cm^2). Shutdown was initiated by the computer when the throat thermocouples reached the 1100°F (867°K) limit. All components were able to withstand this abnormal start and overpressure condition without damage.

Test 04-025 was a repeat of the above conditions for 35 seconds. Test points included:

<u>MR</u>	<u>% Cooling</u>	<u>O/F Temp, °R</u>	<u>(°K)</u>
3.6	7.2	415/189	(230/105)
4.2	8.5	419/260	(233/144)

All test objectives were achieved and systems and components functioned normally.

Test 03-035 was a 300 psia (207 N/cm^2) heated propellant test which lasted 250 seconds. The engine was started with the feed system and thrust chamber assembly preheated to approximately $600\text{--}700^\circ\text{R}$ ($330\text{--}390^\circ\text{K}$). The propellant heaters were kept on for about 23 seconds into the firing at which time the fuel and oxidizer entering the thrust chamber were 772°R (430°K) 682°R (379°K). At this time the heaters were sequenced off from the control room and propellant temperatures slowly decayed to ambient, as shown in Figure V-20. This cooldown of the feed system mass took about 100 seconds. The firing continued beyond 100 seconds with ambient temperature propellant until the duration goal of 250 sec was attained. Postfire inspection (Figure V-21) showed all components to be in good condition with the exception of the teflon O-ring which failed in the same manner as in Test 03-033. The manner in which this

V, C, Regeneratively Cooled Chamber Testing (cont.)

particular seal is retained represents a departure from standard practice for confined seals in order to allow use of a standard size. This failure is not considered significant to the program objectives. Postfire inspection of the injector fuel manifold (Figure V-21) revealed significant deposits of very fine powder (talc-like consistency) which was very dark in color (dark brown to grey). The chamber inlet manifold and feed system were clean. Chemical analysis of the deposits revealed the composition to be copper, copper oxide and a trace of SiO_2 . Since the propellant feed system contains no copper, it must be presumed that the source of deposits is the copper thrust chamber. Review of the fabrication and cleaning procedures on this chamber revealed internal manifold areas were at one time coated with a green and brown salt following the electroforming of the outer nickel pressure case. Additional investigation would be required to determine the precise source and mechanism causing these deposits; however, incomplete removal of these deposits from the cooling channels is believed to be the most likely source of the copper and copper oxide at this time. The SiO_2 trace may be from another source since small amounts of pitting (no deposits) were noted in high velocity turn areas in the fuel circuit on earlier film cooled chamber tests.

V, Thrust Chamber Testing Conditions and Data (cont.)

D. PHASE II - FILM COOLED CHAMBER TEST CONDITIONS - SERIES 1680-006

Additional low temperature propellant tests were conducted with the following hardware build up using the mass flow controller and a separately supplied film cooling circuit and valve.

SN 7 I premix injector
SN 3 Film cooled chamber
25 lbF Spark igniter

The function of this test series was to (1) obtain additional data using a chamber in which the film coolant injection orifices were reoptimized for the low temperature propellants, (2) to further explore the off design operating conditions and potential failure modes, and (3) to obtain better resolution of the axial wall temperature profiles in the region behind and immediately downstream of the film cooling ring. A flow and instrumentation schematic for this hardware build up is shown in Figure V-22.

Tests 001-003 were single short pulse tests with cold propellants at nominal conditions.

Tests 004 and 005 were each 8 sec tests in which cold propellants were supplied from the 17 cu ft accumulator tanks in a blowdown mode. This mode simulated failure of the vehicle propellant supply system to recharge the accumulator tanks. During this period, chamber pressure decayed from 312 to 209 psia, mixture ratio increased from 4.0 to 5.6 and the % cooling flow remained approximately constant at 19%. The maximum injector, throat, and skirt temperatures, respectively, achieved during this simulated excursion were 282, 1540, and 1400°F (411, 1110, and 1033°K), and no hardware damage was encountered.

V, D, Phase II - Film Cooled Chamber Test Conditions - Series 1680-006 (cont.)

Test 006 was a 38-sec cold propellant test at 20% film cooling which provided film cooling and heat transfer data at mixture ratios between 4 and 5.

Tests 007 through 011 were pulse tests and are discussed in Section V,C.

Test 012 was a 24-sec ambient fuel and cold oxidizer test with the oxidizer accumulator tank operating in the blowdown mode, simulating a partial system failure. In this test, chamber pressure dropped from 320 to 216 psia (221 to 149 N/cm²) and MR dropped from 3.8 to 2.6; film cooling remained constant at 19%. This simulated excursion resulted in a maximum injector face temperature of 314°F (430°K) and all chamber temperatures dropped.

Test 013 started out with both propellants at ambient temperatures. The fuel circuit was chilled to 220°R (122°K) during the first 10 sec of the firing. Chilling of the oxidizer was started after about 15 sec and reached a minimum value of 397°R (220°K) after 95 sec. At about 60 sec into the run, the propellant supply pressures were ramped up to increase the chamber pressure to 360 psia (248 N/cm²) and ramped again at 97 sec to 400 psia (276 N/cm²). In the period between 97 and 142 sec, the thruster mixture ratio was increased from 4.4 to 5.7 to examine the effect of very high oxidizer flows. The results of these test conditions are provided in Tables V-3 and V-4. All temperatures were found to be within safe operating limits.

V, Thrust Chamber Testing Conditions and Data (cont.)

E. PHASE II - REGENERATIVELY COOLED CHAMBER TESTS - SERIES 1680-006

The next series of tests were conducted using the SN-3 regeneratively cooled chamber and the same injector and igniter used in the previous test. All tests were conducted without the use of upstream film cooling. The skirt dump-film cooling injected downstream of the throat was supplied via a separately controlled circuit which allowed the cooling to be varied during each test. Figure V-23 shows an instrumentation and propellant flow schematic for this hardware build up.

Test 014 was a 2 sec checkout test at nominal condition.

Test 015 was a 128 sec ambient propellant test which explored 9 combinations of pressure and mixture ratios. The objective of this test was to explore the limits of boundary layer laminarization with the revised nozzle contour. Testing was started at 100 psia (69 N/cm^2) and data obtained at mixture ratios of 4, 5 and 6. Pressure was then increased to 200 psia (138 N/cm^2) and then 300 psia (207 N/cm^2) with MR surveys at each pressure level.

Test 016 was a 48 sec test which provided repeat data at 200 psia (138 N/cm^2) and additional data at 400 psia (276 N/cm^2).

Test 017 provided data at 500 psia (345 N/cm^2).

Test 018 was the final test of the program. The objectives of this test were to obtain repeat thermal data with cold propellants and to demonstrate hardware durability. The test duration was 1976.5 sec. The test started at nominal conditions with ambient propellants. First the fuel and then the oxidizer temperatures were reduced from ambient to cold while the engine was fired. Twelve data points at chamber pressures of 100, 200, 300, 400 psia ($69, 138, 207, 276 \text{ N/cm}^2$)

V, E, Phase II - Regeneratively Cooled Chamber Tests - Series 1680-006 (cont.)

MR 4, 5, and 6 were recorded in the 100 to 500 sec data period. Durability testing with cold propellants continued at various combinations of pressures, and coolant flow rates at MR = 6 until the duration limits of the altitude facility were reached at approximately 2000 sec. All components were found to be in excellent condition following this test. Post-fire inspection showed that several peripheral locations at the throat were marked from impingement of un-combusted oxidizer on the sharper convergent angle of this particular design. The effect was not noted in the previous test and is believed to be a result of the combination of very cold fuel and warm oxidizer which results in a less favorable propellant momentum ratio. The results of this test can be found in Tables V-5 and V-6.

V, Thrust Chamber Testing Conditions and Data (cont.)

F. PULSE TESTING

1. Test Objectives

The premix "I" triplet injector, film-cooled thrust chamber, and 25-lbf (106 N) spark igniter were selected for pulse testing based on the high performance and excellent durability this combination exhibited in the long duration firings. The objectives of this test series were to:

- (1) Investigate the start transient dynamics of a soft system (no mass flow controller) with ambient temperature propellants.
- (2) Investigate thermal characteristics and heat soak under various duty cycle modes.
- (3) Investigate bit impulse repeatability for values down to 50 lbf-sec (212 N sec) and bit specific impulse for various pulse widths.
- (4) Demonstrate thruster durability in a series of firings involving 2500 pulses.
- (5) Investigate in Phase II the start transient dynamics of a mass flow controlled system with cold propellants.

2. System Description

A simplified schematic drawing of the J-3 Altitude Testing Facility as configured for the ambient temperature pulse test series is shown in Figure V-24. The features of this test setup are as follows:

V, F, Pulse Testing (cont.)

(1) One fuel and one oxidizer accumulator tank (17 cu ft [0.47 cu m] each) located 23 ft (7 m) upstream of the thrust chamber valves were the source of all engine propellants (including those flowing to the igniter)

(2) The oxidizer and fuel accumulator tanks were maintained at pressures of 430 (297 N/cm²) and 466 psia (322 N/cm²) in order to provide nominal thrust and chamber pressure of 1500 lbf (6720 N), 300 psia (207 N/cm²) at a mixture ratio of 4.0.

(3) The flow to the igniter was regulated by high recovery venturis which choked during the igniter start transient.

(4) The fuel and oxidizer flows were measured by hot wire anemometers located 10.5 in. (26.5 cm) upstream of the thrust chamber valves, with redundant measurements provided by critical flow control orifices located upstream of the accumulator tanks.

(5) Thrust on the firing fixture (100 cps natural frequency) was measured via a dual bridge 5000-lbf (22,200 N) load cell.

The duty cycle and valve sequencing for pulse mode operations were established by a preprogrammed analog computer located in the test area control room. The computer regulated throttling valves which maintained accumulator pressure via a pressure feedback loop. The analog computer was also programmed to monitor critical engine parameters and terminate a pulse train should a malfunction occur. Potential failure modes and parameters monitored to detect such failures are provided in the following table.

V, F, Pulse Testing (cont.)

<u>Potential Malfunction Mode</u>	<u>Parameter Monitored and Criteria for Continued Firings</u>
Failure of a thrust chamber valve to open or failure to achieve ignition.	<u>Thrust</u> must be greater than 750-lbf (3360 N) at .075 sec after first electrical signal.
Shift in valve response or actuation resulting in overpressures or hard starts.	Injector manifold pressures must be less than 400 psia (276 N/cm ²) at all times.
Component overheating.	Injector face, throat, and skirt temp. less than 1000, 1500 and 2000°F (810, 1045, 1370°K), respectively.

3. Data Acquisition and Analysis

Temperature and pressure measurements were made on the cooled thrust chamber, injector and valves throughout the pulsing test series. These measurements were essentially the same as described earlier in the cooled chamber testing with the exception that data were recorded during pulsing, between pulses, and after shutdown.

Special consideration was given to define thrust and performance during single and multiple pulses. The system was evaluated on two parameters:

$$\text{Bit impulse (BI)} = \int_{T_1}^{T_2} F \, dT \quad (\text{Force} \times \text{Time})$$

$$\text{Bit specific impulse (ISPB)} = \frac{\int_{T_1}^{T_2} F \, dT}{\int_{T_1}^{T_2} \dot{w}_T \, dT} \quad \left(\frac{\text{Force} \times \text{Time}}{\text{Mass}} \right)$$

V, F, Pulse Testing (cont.)

Mixture ratio is defined as

$$MR = \frac{\int_{T_1}^{T_2} \dot{w}_o dT}{\int_{T_1}^{T_2} \dot{w}_f dT}$$

Data analysis was facilitated by computing three summation parameters through each pulse train which are close approximations of the integral values of BI and ISPB. The summation parameters are:

$$\sum_{T_1}^{T_2} F_{a,b} \Delta T; \quad \sum_{T_1}^{T_2} \dot{w}_o \Delta T; \quad \sum_{T_1}^{T_2} \dot{w}_f \Delta T$$

In order to obtain the data required to calculate these parameters, the following special measurements were made:

Thrust via a thermally isolated, vented to vacuum, 5K lbf (22,200 N) dual bridge load cell, with data from each channel recorded on a Millisadic type digital recorder at 500 samples per second. Backup recording systems employed were a continuous direct write type oscillograph and high frequency FM tape. The thrust stand frequency was ≈ 100 Hz. Figure V-25 provides a graphical representation of the two digitized thrust measurements from the dual bridge load cell. These are seen to be in excellent agreement and properly zeroed before and after the single pulse shown. In multiple pulses, the thrust zero was found to shift from the precalibrated value and appropriate thrust shift corrections applied.

Flow rates - Primary fuel and oxidizer flow measurements were by precalibrated hot wire anemometers in each propellant circuit. These anemometers are capable of providing full-scale deflections in 0.001 sec. Flow data for each

V, F, Pulse Testing (cont.)

propellant were also recorded on FM tape, direct write oscillograph, and digital format at 500 samples per second. Graphical representation of these digital traces are also shown in Figure V-25 and are noted to respond rapidly and return to a proper zero position following the pulse. The average flow rate recorded by the fuel anemometer was compared to the fuel flow determined by the critical nozzle located upstream of the fuel accumulator during the last several hundred pulses of a long pulse train (Test 038) and found to agree within 1.3%. No comparable evaluation could be made for the oxidizer flow because of low amplitude, low frequency pressure oscillations in the feed system and accumulator tank. These low amplitude (30 to 40 Hz) oscillations were sensed by the anemometers as can be noted in Figure V-25 and other reproductions of the oxidizer flow traces presented in this report. The oscillations were due to the movement of the flow control valve. The quality of the oxidizer flow measurement was not as good as the fuel flow measurement.

Additional parameters recorded or computed at the 500 sps rate were: (1) altitude pressure (P_{alt}) and (2) injector fuel manifold pressure (P_{fm2}). The rapid sampling altitude pressure was used to compute the vacuum thrust and the injector fuel manifold pressure was employed to compute c^* with appropriate injector ΔP corrections.

The lower portion of Figure V-25 provides a graphical representation of the flow and thrust integral approximation by summation. In each case, ΔT was 0.0020 sec and $F_{a,b}$, \dot{w}_o , and \dot{w}_f were the instantaneous measurement of thrust, oxidizer flow, and fuel flow. Bit impulse for any single pulse or group of pulses was obtained by the increase of the ΣF parameter between any time 1 and time 2. Individual and total flows were obtained in the same manner and ISPB was calculated by dividing the summation parameters. In evaluating individual pulses, the following time criteria for T_1 and T_2 were established:

V, F, Pulse Testing (cont.)

SO-SO	Spark signal on, to next spark signal on.
EPWV	Electrical pulse width based on valve signals. First igniter on signal to main valve off signal.
VPWO	Valve pulse width, initial main O ₂ valve opening movement to initial O ₂ valve closing movement.
PSS	Pulsing steady state; narrow time band which avoids the start and shutdown transients.

Typical use of these integral data (Figure V-25) is as follows: t BI for the pulse is obtained directly from the vacuum thrust integral scale as being 262 lb-sec (1082 N sec). The amount of impulse generated after the oxidizer valve is closed due to propellant venting is the change in the thrust integral between 0.281 sec and 0.337 sec. In this case, it equals 262-243 or 19 lb-sec for the particular design, mixture ratio, and shutdown sequence. The same approach was employed to evaluate the start sequence and average steady state thrust during the pulse, the average mixture ratios and average specific impulse throughout each grouping of pulses.

4. Summary of Pulse Testing Events - Ambient Temperature Propellants

Pulse testing was divided into five categories:

- (a) Hot wire anemometer flow calibration
- (b) Igniter sequencing and repeatability tests
- (c) Igniter-thruster sequencing tests
- (d) Pulse performance
- (e) Pulse repeatability test with low temperature propellants

A summary listing of the individual tests is given in Table V-7.

V, F, Pulse Testing (cont.)

a. Calibration Tests

Test 001 was an oxidizer anemometer flow calibration test in which three transducers were successfully calibrated in oxygen. The calibrations were accomplished in the test circuit with each anemometer in the correct run position for pulse flow. A downstream orifice was employed to simulate the thruster. The calibrations were made with ambient temperature propellants in a five-step flow range for the purpose of linearizing the transducer output. The flow measuring standard in these runs were the critical flow nozzles positioned upstream of the anemometers. Approximately 20 flow points were made on each anemometer. A typical analog output curve obtained during earlier calibrations can be found in Figure V-26, which shows excellent full-scale response of approximately 10 millisecc and a minimum overshoot. It is felt that this curve represents the actual flow transient in the system during the 10 millisecc valve opening and closing for the system in which the mass flow control venturi is employed. This no-overshoot start can be compared to the significant flow overshoot experienced in the soft system start shown in Figure V-25 in which the mass flow control device is removed.

Test 002 was a comparable test in which four fuel anemometers were successfully calibrated in the correct run position.

b. Igniter Sequencing and Repeatability Tests

Test 003 was an igniter only pulse series test in which fuel and oxidizer lead sequences were investigated. The conditions investigated were .010 sec fuel lead, a simultaneous pressurization of fuel and oxidizer manifolds, and .010 sec oxidizer lead. A significant number of 1, 10, and 20 pulse trains in the igniter only mode were run during this period. Data acquisition was in the form of oscillograph traces, in which only the longer 20-pulse

V, F, Pulse Testing (cont.)

sequences were given run numbers, 003 a, b, and c. Typical results of these tests are shown in Figure V-27, which depicts the igniter start transients with various valve sequencings. This test series demonstrated that it is possible to achieve satisfactory igniter ignition with a variety of valve sequences. A .010 sec fuel lead was selected for the pulse test series based on a vast backlog of experience indicating that this sequence is least sensitive to potential high voltage electrical shorts. It also requires the lowest spark power level. Spark gaps of .025 and .050 in. (.063 and .127 cm) were briefly evaluated during this period and the smaller gap was found to provide greater reliability because it insures that the spark discharge does take place at the spark gap.

During the course of these multiple igniter-only mode firings at the nominal 25-lbf (106 N), MR = 6 for .20 sec (5-lbf sec impulse), the tip of the copper film cooling injection ring overheated and flowed slightly. The damage was at this point apparently was so minor that it was not detected in normal hardware inspection. However, based on these test results and hardware damage, igniter only mode operation must be considered limited. Several pulses per minute for short periods are probably acceptable, while the two pulse per second rate evaluated is not.

c. Igniter Main Stage Sequencing

The next series of tests investigated the relationship between igniter ignition and main stage valve sequencing in an attempt to minimize the time from first electrical signal to full thrust. Ignition delay times (lagging propellant flow to observable ignition) were found to be in the order of 0.001 → 0.002 sec. With a fuel lead on the igniter, igniter ignition occurs as soon as the oxidizer reaches the spark gap. Main stage ignition, with the igniter running, can be detected within .005 sec after initial movement of the lagging valve. Most of this ignition delay time probably results from fill times and delays in sensing ignition due to transducer line lengths.

V, F, Pulse Testing (cont.)

Four values of igniter leads (igniter ignition to TC oxidizer valve movement "LOV") were investigated in this series, three of which are shown in Figure V-28. The normal ignition sequence (left), Run 04-012, employed in the previous long duration firings provided a .050 sec igniter lead with the igniter oxidizer sequenced off .04 sec after main stage ignition. Experience on hundreds of earlier firings demonstrated this to be a 100% reliable sequence. The first reduction in this igniter lead period investigated in pulse test 004 was a .020 sec igniter lead. Satisfactory ignition was achieved. Test 005 was a repeat with comparable results. In Test 006 two sequencing change errors were made which (1) reverted the igniter to .002 sec oxidizer lead and (2) gave a .02 sec delay between main fuel and oxidizer valve opening (oxidizer lag). This sequence resulted in failure of the igniter to ignite and there was a low thrust shutdown. Failure appeared to be due to a lack of spark at the spark gap. Test 007 corrected the sequence error and reduced the igniter lead to .012 sec. Satisfactory ignition was achieved. Tests 008 through 012 (see Table V-7) were final sequence adjustments to further reduce the igniter leads, to look at multiple pulses and investigate variable off times. Coast times between pulses were started at 10 minutes and reduced to 0.3 sec. Two and five pulse train series were conducted. The final igniter sequencing used in the pulse series, shown on the right of Figure V-28, was a .007 sec lead to LOV start. A difference in the thrust and P_c rise rates, thrust overshoots and general flow characteristics is noted between the .050 sec igniter lead and other two sequences shown. This is due to the use of a mass flow controlled feed system in the long duration tests (left) and a soft or non-flow controlled supply in the fixed pressure tank system shown center and right. The thrust rise rate (0 to max. thrust) is slightly faster in the soft system for the flow configuration tested.

The igniter only mode damage to the tip of the film cooling ring was discovered during a normal hardware inspection following Test 012. The damaged area was removed by machining approximately .080 in. (.203 cm) off the tip, and normal testing was resumed.

V, F, Pulse Testing (cont.)

Test 013 was a 0.2 sec pulse sequence check on the re-assembled hardware with repeatable satisfactory ignition. In Test 014 the fuel valve was advanced an additional 0.01 sec (0.02 from LFV to LOV) to determine the effect of a significant fuel lead. In this sequence the main fuel valve was sequenced to open prior to flow of the igniter oxidizer, i.e., 0.005 sec igniter lag. This resulted in a back pressure within the entire thruster. The injector and igniter were filled with H_2 when the oxidizer igniter valve opened, thus increasing the time for the oxidizer to reach the spark gap. This resulted in an igniter ignition delay of 0.02 sec. Igniter ignition occurred about the time of the opening of the main stage oxidizer valve, and there was a very rapid rise in POJ but no overpressure. This sequence is shown in Figure V- 29.

Test 015 reverted to the normal sequence, and 100 pulses were executed "all alike". Test 016 provided an additional 110 pulses. The computer terminated the pulse train on the 110th pulse due to low thrust. Normal ignition was attained but oxidizer flow was low. Tests 017 and 018 investigated the reason for the low flow and it was determined that there was flashback and overpressure in the oxidizer manifold starting at around the 100th pulse. This deformed a sheet metal diffuser plate in the manifold, obstructing the oxidizer orifices. Oxidizer manifold overpressures (POJ) of approximately 50 to 100% were recorded on the direct write oscillograph for 15 pulses prior to this failure as follows:

Peak Oxidizer Manifold Pressures with Fuel Lead (Normal 387 psia)

<u>Pulse</u>	<u>% Overpress.</u>	<u>Pulse</u>	<u>% Overpress.</u>	<u>Pulse</u>	<u>% Overpress.</u>
Last (N)	105	N-5	0	N-10	0
N-1	55	N-6	0	N-11	0
N-2	0	N-7	50	N-12	0
N-3	0	N-8	0	N-13	24
N-4	66	N-9	0	N-15	34

$$\text{Overpressure} \equiv \left(\frac{\text{Maximum}}{\text{Nominal}} - 1 \right) \times 100$$

V, F, Pulse Testing (cont.)

The overpressures appear to be the result of a backflow of fuel into the oxidizer manifold during the start sequence when operating with the fuel lead. For a short time after the oxygen valve is opened, a combustible mixture exists in the oxidizer manifold, giving rise to the flashback condition. There appears to be no reason a similar situation could not be encountered in the fuel manifold given a sufficient oxidizer lead. This problem is probably characteristic of all gaseous propellant thrusters and is best solved either by closely controlling sequencing or else simply making the manifold structurally capable of withstanding the overpressure.

Following the flashback, the SN 7 injector was placed on the stand and the sequence changed to provide a very slight oxidizer lead on injector manifold fill and the pulse counter was reset from "220" back to "0" so that a full 2500 pulses would be demonstrated on a single injector. Table V-8 provides a comparison of the time vs event for the two start sequences. Figure V-30 shows the dynamic response of the significant parameters after several hundred pulses were recorded on the high frequency FM tape. The flashbacks were eliminated. The valve traces and additional pulse characteristic parameters for a .200 sec pulse are shown in Figure V-31.

The pulsing was resumed with Test 019 and continued through 021 during which 269 identical 0.2-sec pulses were accumulated. A "no light" condition was encountered on the 266th pulse of Run 021 which caused a low thrust shutdown. This "no light" was attributed to a failure of the igniter power supply. While testing on Contract NAS 3-14348, it was found that, during repeated operation, a solenoid in the power supply box would overheat, producing intermittent sparking. Test 022 was a single pulse with high recording speed on the oscillograph to obtain better data resolution. Response and ignition were normal. Testing resumed with Run 023 for 259 pulses, all normal and repeatable. In Test 024, the pulse width was reduced to 0.1 sec, which was

V, F, Pulse Testing (cont.)

continued through Test 028, during which 770 additional pulses were executed without difficulty, all being repeatable. Test 028 involved 760 continuous pulses. A representation of the significant oscillograph traces for this pulse width is shown in Figure V-32.

Tests 029 through 037 further reduced the pulse widths to 0.035 sec and added an additional 395 pulses. Representative individual traces and a series of pulses are shown in Figures V-33 and V-34. The first pulse on Test 037 failed to ignite. The following pulses were normal until the 250th pulse in Test 037. The main stage fuel valve operation became irregular due to overheating of a pilot valve. At this point in time the thruster was executing 10 pulses per second which exceeded the cooling capability of the pilot valve electronics. All pulses were repeatable except for those associated with the irregular fuel valve actuation. In these cases, the thrust and pressures did not zero between pulses but returned to the fuel cold flow conditions. There were no adverse start conditions due to the continuous fuel flow.

In Test 039, the duty cycle was returned to the 0.10 pulse width and 840 additional firings executed in rapid succession. All pulses were normal.

5. Pulse Repeatability Tests with Low Temperature Propellants

An additional series of pulse tests were conducted with cold propellants. The same injector, igniter and valves were employed as in the ambient propellant pulse tests. The chamber, however, was the film-cooled SN 3 unit which contained the film coolant injection orifices which were optimized for the cold propellants. These tests differed from the ambient series in that pulsing was accomplished with a mass flow controlled feed system, as described in the long-duration cooled chamber tests, rather than with the soft tank supplied system. All pulsing was conducted with 20% fuel film cooling. Accurate

V, F, Pulse Testing (cont.)

flow measurements could not be obtained because the low temperature anemometers were not available in time for testing.

Seven test series were conducted. Three were single pulses of 0.200 sec duration (Tests 06-001 through -003). The next four tests were comprised of 8-sec steady burns followed by a 10-sec coast period and immediately thereafter by a preprogrammed four-pulse sequence which was repeated either four or eight times to give pulse trains of 16 or 32 pulses. The long burns were conducted prior to pulsing to ensure that all propellant circuits were adequately chilled in. These four tests were as follows:

Test No.	MR	Duration, sec		No. of Pulses	Prop. Temp* H ₂ /O ₂ , °F (°K)	Spark Power, mj
		Steady State Firing	Coast			
06-007	4.0	7.24	9.0	16	-201/-56 (144)/(224)	10
06-008	4.0	8.40	10.5	16	-201/-49 (149)/(218)	10
06-009	3.0	8.0	~10	33	-228/-53 (129)/(226)	10
06-010	4.0	8.0	~10	25	-258/-41 (106)/(233)	30

*Last pulse.

Test 010 was terminated by a no-ignition shutdown.

The variation of propellant temperature with time was significant in the oxidizer circuit while fuel temperature variation was less than 14°F (8°K).

V, F, Pulse Testing (cont.)

	Oxidizer Temperatures (ToV1), °F(°K)			
	<u>007</u>	<u>008</u>	<u>009</u>	<u>010</u>
T _{O2} at end of steady burn	-95(202)	-100(200)	-79(212)	-44(231)
T _{O2} first pulse	-29(239)	-24(242)	-35(236)	-15(247)
T _{O2} last pulse	-56(224)	-49(228)	-53(226)	-41(233)

The four-pulse repeatable sequence consisted of:

<u>Pulse No.</u>	<u>Electrical Pulse Width (sec)</u>	<u>Electrical Pulse Width (Valves) (sec)</u>	<u>Off-Time (sec)</u>
1	0.234	0.214	0.200
2	0.128	0.108	0.200
3	0.074	0.054	0.145
4	0.055	0.035	0.068

A reproduction of this pulse sequence is shown in Figure V-35. The results of the pulse test series is discussed in Section VI,A. A photograph of the injector following the 2500-pulse test series is shown in Figure V-36. The chamber condition was the same as shown in Figure V-18.

SEA LEVEL PERFORMANCE SUMMARY

Test Series	2K-6	2K-9	2K-12	2K-15	2K-18	2K-21	2K-24	2K-27	2K-30	2K-33	2K-36	2K-39	2K-42	2K-45	2K-48	2K-51	2K-54	2K-57	2K-60	2K-63	2K-66	2K-69	2K-72	2K-75	2K-78	2K-81	2K-84	2K-87	2K-90	2K-93	2K-96	2K-99	2K-102	2K-105	2K-108	2K-111	2K-114	2K-117	2K-120	2K-123	2K-126	2K-129	2K-132	2K-135	2K-138	2K-141	2K-144	2K-147	2K-150	2K-153	2K-156	2K-159	2K-162	2K-165	2K-168	2K-171	2K-174	2K-177	2K-180	2K-183	2K-186	2K-189	2K-192	2K-195	2K-198	2K-201	2K-204	2K-207	2K-210	2K-213	2K-216	2K-219	2K-222	2K-225	2K-228	2K-231	2K-234	2K-237	2K-240	2K-243	2K-246	2K-249	2K-252	2K-255	2K-258	2K-261	2K-264	2K-267	2K-270	2K-273	2K-276	2K-279	2K-282	2K-285	2K-288	2K-291	2K-294	2K-297	2K-300	2K-303	2K-306	2K-309	2K-312	2K-315	2K-318	2K-321	2K-324	2K-327	2K-330	2K-333	2K-336	2K-339	2K-342	2K-345	2K-348	2K-351	2K-354	2K-357	2K-360	2K-363	2K-366	2K-369	2K-372	2K-375	2K-378	2K-381	2K-384	2K-387	2K-390	2K-393	2K-396	2K-399	2K-402	2K-405	2K-408	2K-411	2K-414	2K-417	2K-420	2K-423	2K-426	2K-429	2K-432	2K-435	2K-438	2K-441	2K-444	2K-447	2K-450	2K-453	2K-456	2K-459	2K-462	2K-465	2K-468	2K-471	2K-474	2K-477	2K-480	2K-483	2K-486	2K-489	2K-492	2K-495	2K-498	2K-501	2K-504	2K-507	2K-510	2K-513	2K-516	2K-519	2K-522	2K-525	2K-528	2K-531	2K-534	2K-537	2K-540	2K-543	2K-546	2K-549	2K-552	2K-555	2K-558	2K-561	2K-564	2K-567	2K-570	2K-573	2K-576	2K-579	2K-582	2K-585	2K-588	2K-591	2K-594	2K-597	2K-600	2K-603	2K-606	2K-609	2K-612	2K-615	2K-618	2K-621	2K-624	2K-627	2K-630	2K-633	2K-636	2K-639	2K-642	2K-645	2K-648	2K-651	2K-654	2K-657	2K-660	2K-663	2K-666	2K-669	2K-672	2K-675	2K-678	2K-681	2K-684	2K-687	2K-690	2K-693	2K-696	2K-699	2K-702	2K-705	2K-708	2K-711	2K-714	2K-717	2K-720	2K-723	2K-726	2K-729	2K-732	2K-735	2K-738	2K-741	2K-744	2K-747	2K-750	2K-753	2K-756	2K-759	2K-762	2K-765	2K-768	2K-771	2K-774	2K-777	2K-780	2K-783	2K-786	2K-789	2K-792	2K-795	2K-798	2K-801	2K-804	2K-807	2K-810	2K-813	2K-816	2K-819	2K-822	2K-825	2K-828	2K-831	2K-834	2K-837	2K-840	2K-843	2K-846	2K-849	2K-852	2K-855	2K-858	2K-861	2K-864	2K-867	2K-870	2K-873	2K-876	2K-879	2K-882	2K-885	2K-888	2K-891	2K-894	2K-897	2K-900	2K-903	2K-906	2K-909	2K-912	2K-915	2K-918	2K-921	2K-924	2K-927	2K-930	2K-933	2K-936	2K-939	2K-942	2K-945	2K-948	2K-951	2K-954	2K-957	2K-960	2K-963	2K-966	2K-969	2K-972	2K-975	2K-978	2K-981	2K-984	2K-987	2K-990	2K-993	2K-996	2K-999	2K-1002	2K-1005	2K-1008	2K-1011	2K-1014	2K-1017	2K-1020	2K-1023	2K-1026	2K-1029	2K-1032	2K-1035	2K-1038	2K-1041	2K-1044	2K-1047	2K-1050	2K-1053	2K-1056	2K-1059	2K-1062	2K-1065	2K-1068	2K-1071	2K-1074	2K-1077	2K-1080	2K-1083	2K-1086	2K-1089	2K-1092	2K-1095	2K-1098	2K-1101	2K-1104	2K-1107	2K-1110	2K-1113	2K-1116	2K-1119	2K-1122	2K-1125	2K-1128	2K-1131	2K-1134	2K-1137	2K-1140	2K-1143	2K-1146	2K-1149	2K-1152	2K-1155	2K-1158	2K-1161	2K-1164	2K-1167	2K-1170	2K-1173	2K-1176	2K-1179	2K-1182	2K-1185	2K-1188	2K-1191	2K-1194	2K-1197	2K-1200	2K-1203	2K-1206	2K-1209	2K-1212	2K-1215	2K-1218	2K-1221	2K-1224	2K-1227	2K-1230	2K-1233	2K-1236	2K-1239	2K-1242	2K-1245	2K-1248	2K-1251	2K-1254	2K-1257	2K-1260	2K-1263	2K-1266	2K-1269	2K-1272	2K-1275	2K-1278	2K-1281	2K-1284	2K-1287	2K-1290	2K-1293	2K-1296	2K-1299	2K-1302	2K-1305	2K-1308	2K-1311	2K-1314	2K-1317	2K-1320	2K-1323	2K-1326	2K-1329	2K-1332	2K-1335	2K-1338	2K-1341	2K-1344	2K-1347	2K-1350	2K-1353	2K-1356	2K-1359	2K-1362	2K-1365	2K-1368	2K-1371	2K-1374	2K-1377	2K-1380	2K-1383	2K-1386	2K-1389	2K-1392	2K-1395	2K-1398	2K-1401	2K-1404	2K-1407	2K-1410	2K-1413	2K-1416	2K-1419	2K-1422	2K-1425	2K-1428	2K-1431	2K-1434	2K-1437	2K-1440	2K-1443	2K-1446	2K-1449	2K-1452	2K-1455	2K-1458	2K-1461	2K-1464	2K-1467	2K-1470	2K-1473	2K-1476	2K-1479	2K-1482	2K-1485	2K-1488	2K-1491	2K-1494	2K-1497	2K-1500	2K-1503	2K-1506	2K-1509	2K-1512	2K-1515	2K-1518	2K-1521	2K-1524	2K-1527	2K-1530	2K-1533	2K-1536	2K-1539	2K-1542	2K-1545	2K-1548	2K-1551	2K-1554	2K-1557	2K-1560	2K-1563	2K-1566	2K-1569	2K-1572	2K-1575	2K-1578	2K-1581	2K-1584	2K-1587	2K-1590	2K-1593	2K-1596	2K-1599	2K-1602	2K-1605	2K-1608	2K-1611	2K-1614	2K-1617	2K-1620	2K-1623	2K-1626	2K-1629	2K-1632	2K-1635	2K-1638	2K-1641	2K-1644	2K-1647	2K-1650	2K-1653	2K-1656	2K-1659	2K-1662	2K-1665	2K-1668	2K-1671	2K-1674	2K-1677	2K-1680	2K-1683	2K-1686	2K-1689	2K-1692	2K-1695	2K-1698	2K-1701	2K-1704	2K-1707	2K-1710	2K-1713	2K-1716	2K-1719	2K-1722	2K-1725	2K-1728	2K-1731	2K-1734	2K-1737	2K-1740	2K-1743	2K-1746	2K-1749	2K-1752	2K-1755	2K-1758	2K-1761	2K-1764	2K-1767	2K-1770	2K-1773	2K-1776	2K-1779	2K-1782	2K-1785	2K-1788	2K-1791	2K-1794	2K-1797	2K-1800	2K-1803	2K-1806	2K-1809	2K-1812	2K-1815	2K-1818	2K-1821	2K-1824	2K-1827	2K-1830	2K-1833	2K-1836	2K-1839	2K-1842	2K-1845	2K-1848	2K-1851	2K-1854	2K-1857	2K-1860	2K-1863	2K-1866	2K-1869	2K-1872	2K-1875	2K-1878	2K-1881	2K-1884	2K-1887	2K-1890	2K-1893	2K-1896	2K-1899	2K-1902	2K-1905	2K-1908	2K-1911	2K-1914	2K-1917	2K-1920	2K-1923	2K-1926	2K-1929	2K-1932	2K-1935	2K-1938	2K-1941	2K-1944	2K-1947	2K-1950	2K-1953	2K-1956	2K-1959	2K-1962	2K-1965	2K-1968	2K-1971	2K-1974	2K-1977	2K-1980	2K-1983	2K-1986	2K-1989	2K-1992	2K-1995	2K-1998	2K-2001	2K-2004	2K-2007	2K-2010	2K-2013	2K-2016	2K-2019	2K-2022	2K-2025	2K-2028	2K-2031	2K-2034	2K-2037	2K-2040	2K-2043	2K-2046	2K-2049	2K-2052	2K-2055	2K-2058	2K-2061	2K-2064	2K-2067	2K-2070	2K-2073	2K-2076	2K-2079	2K-2082	2K-2085	2K-2088	2K-2091	2K-2094	2K-2097	2K-2100	2K-2103	2K-2106	2K-2109	2K-2112	2K-2115	2K-2118	2K-2121	2K-2124	2K-2127	2K-2130	2K-2133	2K-2136	2K-2139	2K-2142	2K-2145	2K-2148	2K-2151	2K-2154	2K-2157	2K-2160	2K-2163	2K-2166	2K-2169	2K-2172	2K-2175	2K-2178	2K-2181	2K-2184	2K-2187	2K-2190	2K-2193	2K-2196	2K-2199	2K-2202	2K-2205	2K-2208	2K-2211	2K-2214	2K-2217	2K-2220	2K-2223	2K-2226	2K-2229	2K-2232	2K-2235	2K-2238	2K-2241	2K-2244	2K-2247	2K-2250	2K-2253	2K-2256	2K-2259	2K-2262	2K-2265	2K-2268	2K-2271	2K-2274	2K-2277	2K-2280	2K-2283	2K-2286	2K-2289	2K-2292	2K-2295	2K-2298	2K-2301	2K-2304	2K-2307	2K-2310	2K-2313	2K-2316	2K-2319	2K-2322	2K-2325	2K-2328	2K-2331	2K-2334	2K-2337	2K-2340	2K-2343	2K-2346	2K-2349	2K-2352	2K-2355	2K-2358	2K-2361	2K-2364	2K-2367	2K-2370	2K-2373	2K-2376	2K-2379	2K-2382	2K-2385	2K-2388	2K-2391	2K-2394	2K-2397	2K-2400	2K-2403	2K-2406	2K-2409	2K-2412	2K-2415	2K-2418	2K-2421	2K-2424	2K-2427	2K-2430	2K-2433	2K-2436	2K-2439	2K-2442	2K-2445	2K-2448	2K-2451	2K-2454	2K-2457	2K-2460	2K-2463	2K-2466	2K-2469	2K-2472	2K-2475	2K-2478	2K-2481	2K-2484	2K-2487	2K-2490	2K-2493	2K-2496	2K-2499	2K-2502	2K-2505	2K-2508	2K-2511	2K-2514	2K-2517	2K-2520	2K-2523	2K-2526	2K-2529	2K-2532	2K-2535	2K-2538	2K-2541	2K-2544	2K-2547	2K-2550	2K-2553	2K-2556	2K-2559	2K-2562	2K-2565	2K-2568	2K-2571	2K-2574	2K-2577	2K-2580	2K-2583	2K-2586	2K-2589	2K-2592	2K-2595	2K-2598	2K-2601	2K-2604	2K-2607	2K-2610	2K-2613	2K-2616	2K-2619	2K-2622	2K-2625	2K-2628	2K-2631	2K-2634	2K-2637	2K-2640	2K-2643	2K-2646	2K-2649	2K-2652	2K-2655	2K-2658	2K-2661	2K-2664	2K-2667	2K-2670	2K-2673	2K-2676	2K-2679	2K-2682	2K-2685	2K-2688	2K-2691	2K-2694	2K-2697	2K-2700	2K-2703	2K-2706	2K-2709	2K-2712	2K-2715	2K-2718	2K-2721	2K-2724	2K-2727	2K-2730	2K-2733	2K-2736	2K-2739	2K-2742	2K-2745	2K-2748	2K-2751	2K-2754	2K-2757	2K-2760	2K-2763	2K-2766	2K-2769	2K-2772	2K-2775	2K-2778	2K-2781	2K-2784	2K-2787	2K-2790	2K-2793	2K-2796	2K-2799	2K-2802	2K-2805	2K-2808	2K-2811	2K-2814	2K-2817	2K-2820	2K-2823	2K-2826	2K-2829	2K-2832	2K-2835	2K-2838	2K-2841	2K-2844	2K-2847	2K-2850	2K-2853	2K-2856	2K-2859	2K-2862	2K-2865	2K-2868	2K-2871	2K-2874	2K-2877	2K-2880	2K-2883	2K-2886	2K-2889	2K-2892	2K-2895	2K-2898	2K-2901	2K-2904	2K-2907	2K-2910	2K-2913	2K-2916	2K-2919	2K-2922	2K-2925	2K-2928	2K-2931	2K-2934	2K-2937	2K-2940	2K-2943	2K-2946	2K-2949	2K-2952	2K-2955	2K-2958	2K-2961	2K-2964	2K-2967	2K-2970	2K-2973	2K-2976	2K-2979	2K-2982	2K-2985	2K-2988	2K-2991	2K-2994	2K-2997	2K-3000	2K-3003	2K-3006	2K-3009	2K-3012	2K-3015	2K-3018	2K-3021	2K-3024	2K-3027	2K-3030	2K-3033	2K-3036	2K-3039	2K-3042	2K-3045	2K-3048	2K-3051	2K-3054	2K-3057	2K-3060	2K-3063	2K-3066	2K-3069	2K-3072	2K-3075	2K-3078	2K-3081	2K-3084	2K-3087	2K-3090	2K-3093	2K-3096	2K-3099	2K-3102	2K-3105	2K-3108	2K-3111	2K-3114	2K-3117	2K-3120	2K-3123	2K-3126	2K-3129	2K-3132	2K-3135	2K-3138	2K-3141	2K-3144	2K-3147	2K-3150	2K-3153	2K-3156	2K-3159	2K-3162	2K-3165	2K-3168	2K-3171	2K-3174	2K-3177	2K-3180	2K-3183	2K-3186	2K-31
-------------	------	------	-------	-------	-------	-------	-------	-------	-------	-------	-------	-------	-------	-------	-------	-------	-------	-------	-------	-------	-------	-------	-------	-------	-------	-------	-------	-------	-------	-------	-------	-------	--------	--------	--------	--------	--------	--------	--------	--------	--------	--------	--------	--------	--------	--------	--------	--------	--------	--------	--------	--------	--------	--------	--------	--------	--------	--------	--------	--------	--------	--------	--------	--------	--------	--------	--------	--------	--------	--------	--------	--------	--------	--------	--------	--------	--------	--------	--------	--------	--------	--------	--------	--------	--------	--------	--------	--------	--------	--------	--------	--------	--------	--------	--------	--------	--------	--------	--------	--------	--------	--------	--------	--------	--------	--------	--------	--------	--------	--------	--------	--------	--------	--------	--------	--------	--------	--------	--------	--------	--------	--------	--------	--------	--------	--------	--------	--------	--------	--------	--------	--------	--------	--------	--------	--------	--------	--------	--------	--------	--------	--------	--------	--------	--------	--------	--------	--------	--------	--------	--------	--------	--------	--------	--------	--------	--------	--------	--------	--------	--------	--------	--------	--------	--------	--------	--------	--------	--------	--------	--------	--------	--------	--------	--------	--------	--------	--------	--------	--------	--------	--------	--------	--------	--------	--------	--------	--------	--------	--------	--------	--------	--------	--------	--------	--------	--------	--------	--------	--------	--------	--------	--------	--------	--------	--------	--------	--------	--------	--------	--------	--------	--------	--------	--------	--------	--------	--------	--------	--------	--------	--------	--------	--------	--------	--------	--------	--------	--------	--------	--------	--------	--------	--------	--------	--------	--------	--------	--------	--------	--------	--------	--------	--------	--------	--------	--------	--------	--------	--------	--------	--------	--------	--------	--------	--------	--------	--------	--------	--------	--------	--------	--------	--------	--------	--------	--------	--------	--------	--------	--------	--------	--------	--------	--------	--------	--------	--------	--------	--------	--------	--------	--------	--------	--------	--------	--------	--------	--------	--------	--------	--------	--------	--------	--------	--------	--------	--------	--------	--------	--------	--------	--------	--------	--------	--------	--------	--------	--------	--------	--------	--------	--------	--------	--------	--------	--------	--------	--------	--------	--------	--------	--------	--------	--------	--------	--------	--------	--------	--------	--------	--------	---------	---------	---------	---------	---------	---------	---------	---------	---------	---------	---------	---------	---------	---------	---------	---------	---------	---------	---------	---------	---------	---------	---------	---------	---------	---------	---------	---------	---------	---------	---------	---------	---------	---------	---------	---------	---------	---------	---------	---------	---------	---------	---------	---------	---------	---------	---------	---------	---------	---------	---------	---------	---------	---------	---------	---------	---------	---------	---------	---------	---------	---------	---------	---------	---------	---------	---------	---------	---------	---------	---------	---------	---------	---------	---------	---------	---------	---------	---------	---------	---------	---------	---------	---------	---------	---------	---------	---------	---------	---------	---------	---------	---------	---------	---------	---------	---------	---------	---------	---------	---------	---------	---------	---------	---------	---------	---------	---------	---------	---------	---------	---------	---------	---------	---------	---------	---------	---------	---------	---------	---------	---------	---------	---------	---------	---------	---------	---------	---------	---------	---------	---------	---------	---------	---------	---------	---------	---------	---------	---------	---------	---------	---------	---------	---------	---------	---------	---------	---------	---------	---------	---------	---------	---------	---------	---------	---------	---------	---------	---------	---------	---------	---------	---------	---------	---------	---------	---------	---------	---------	---------	---------	---------	---------	---------	---------	---------	---------	---------	---------	---------	---------	---------	---------	---------	---------	---------	---------	---------	---------	---------	---------	---------	---------	---------	---------	---------	---------	---------	---------	---------	---------	---------	---------	---------	---------	---------	---------	---------	---------	---------	---------	---------	---------	---------	---------	---------	---------	---------	---------	---------	---------	---------	---------	---------	---------	---------	---------	---------	---------	---------	---------	---------	---------	---------	---------	---------	---------	---------	---------	---------	---------	---------	---------	---------	---------	---------	---------	---------	---------	---------	---------	---------	---------	---------	---------	---------	---------	---------	---------	---------	---------	---------	---------	---------	---------	---------	---------	---------	---------	---------	---------	---------	---------	---------	---------	---------	---------	---------	---------	---------	---------	---------	---------	---------	---------	---------	---------	---------	---------	---------	---------	---------	---------	---------	---------	---------	---------	---------	---------	---------	---------	---------	---------	---------	---------	---------	---------	---------	---------	---------	---------	---------	---------	---------	---------	---------	---------	---------	---------	---------	---------	---------	---------	---------	---------	---------	---------	---------	---------	---------	---------	---------	---------	---------	---------	---------	---------	---------	---------	---------	---------	---------	---------	---------	---------	---------	---------	---------	---------	---------	---------	---------	---------	---------	---------	---------	---------	---------	---------	---------	---------	---------	---------	---------	---------	---------	---------	---------	---------	---------	---------	---------	---------	---------	---------	---------	---------	---------	---------	---------	---------	---------	---------	---------	---------	---------	---------	---------	---------	---------	---------	---------	---------	---------	---------	---------	---------	---------	---------	---------	---------	---------	---------	---------	---------	---------	---------	---------	---------	---------	---------	---------	---------	---------	---------	---------	---------	---------	---------	---------	---------	---------	---------	---------	---------	---------	---------	---------	---------	---------	---------	---------	---------	---------	---------	---------	---------	---------	---------	---------	---------	---------	---------	---------	---------	---------	---------	---------	---------	---------	---------	---------	---------	---------	---------	---------	---------	---------	---------	---------	---------	---------	---------	---------	---------	---------	---------	---------	---------	---------	---------	---------	---------	---------	---------	---------	---------	---------	---------	---------	---------	---------	---------	---------	---------	---------	---------	---------	---------	---------	---------	---------	---------	---------	---------	---------	---------	---------	---------	---------	---------	---------	---------	---------	---------	---------	---------	---------	---------	---------	---------	---------	---------	---------	---------	---------	---------	---------	---------	---------	---------	---------	---------	---------	---------	---------	---------	---------	---------	---------	---------	---------	---------	---------	---------	---------	---------	---------	---------	---------	---------	---------	---------	---------	---------	---------	---------	---------	---------	---------	---------	---------	---------	---------	---------	---------	---------	---------	---------	---------	---------	---------	---------	---------	---------	---------	---------	---------	---------	---------	---------	---------	---------	---------	---------	---------	---------	---------	---------	---------	---------	---------	---------	---------	---------	---------	---------	---------	---------	---------	---------	---------	---------	---------	---------	---------	---------	---------	---------	---------	---------	---------	---------	---------	---------	---------	---------	---------	---------	---------	---------	---------	---------	---------	---------	---------	---------	---------	---------	---------	---------	---------	---------	---------	---------	---------	---------	---------	---------	---------	---------	---------	---------	---------	---------	---------	---------	---------	---------	---------	---------	---------	---------	---------	---------	---------	---------	---------	---------	---------	---------	---------	---------	---------	---------	---------	---------	---------	---------	---------	---------	---------	---------	---------	---------	---------	---------	---------	---------	---------	---------	---------	---------	---------	---------	---------	---------	---------	---------	---------	---------	---------	---------	---------	---------	---------	---------	---------	---------	---------	---------	---------	---------	---------	---------	---------	---------	---------	---------	---------	---------	---------	---------	---------	---------	---------	---------	---------	---------	---------	---------	---------	---------	---------	---------	---------	---------	---------	---------	---------	---------	---------	---------	---------	---------	---------	---------	---------	-------

NOTES: (1) 25 or 50 denotes nominal igniter thrust (lbf)
S: Spark igniter
P: Plasma igniter
C: Catalytic igniter
(2) Cu: Denotes copper heat sink chamber
FFC: Denotes adiabatic film cooled chamber
Abl: Denotes ablative streak chamber

TABLE V-1 (cont.)

Test Series	2K-7	2K-8	102	103	104	105	107	108	109	110	111	112	113	114	115	116	117
Run No.	102	103	102	103	104	105	107	108	109	110	111	112	113	114	115	116	117
Injector Type	"I" Triplet						Swirl Coax										
Igniter (lbf, Type)	20-S																
L* (Chamber Type), in.	15 (Cu)						25 (Cu)									40 (Cu)	40 (Cu)
\bar{c}	2.89	2.89	2.92				2.88			2.90	2.90	2.91					
Test Duration, sec	1.0			0.5			1.0			2.0	2.0	2.0	0.5			1.0	1.0
Data Summary, sec	1.46-1.66	1.46-1.66	1.46-1.66	0.98-1.18	0.98-1.18	0.98-1.18	1.5-1.7	1.5-1.7	1.5-1.7	1.5-1.7	2.4-2.6	2.4-2.6	1.0-1.2	1.0-1.2	1.0-1.2	1.5-1.7	1.5-1.7
P_c , psia	313	309	308	467	460	489	303	308	316	99	102	99	480	468	469	311	318
\dot{w}_o , lbm/sec	2.581	3.002	2.698	4.102	4.348	3.920	2.687	2.532	3.079	0.930	0.868	0.993	4.205	3.816	4.410	2.750	3.076
\dot{w}_f , lbm/sec	0.845	0.587	0.689	1.051	0.868	1.340	0.716	0.877	0.607	0.228	0.293	0.198	1.113	1.252	0.934	0.742	0.619
\dot{w}_{f1} , lbm/sec	0.013	0.013	0.013	0.020	0.020	0.020	0.013	0.013	0.013	0.004	0.004	0.004	0.020	0.020	0.020	0.013	0.013
$(O/F)_{eng} = (O/F)_{core}$	3.01	5.01	3.85	3.83	4.90	2.88	3.68	2.84	4.97	4.01	2.92	4.92	3.65	3.00	4.63	3.64	4.86
\dot{w}_T , lbm/sec	3.439	3.602	3.400	5.173	5.236	5.280	3.416	3.422	3.699	1.162	1.165	1.195	5.358	5.088	5.364	3.505	3.708
F_{SL} , lbf	1197.5	1191.3	1151.5	1837.0	1797.6	1918.1	1135.8	1154.3	1195.2	291.9	306.4	299.5	1872.2	1795.3	1834.7	1161.4	1198.0
P_{Ae} , lbf	120.3	120.3	120.4	120.7	120.6	120.6	121.2	121.2	121.2	120.7	120.7	120.5	120.4	120.4	120.4	120.4	120.4
F_{vac} , lbf	1317.8	1311.6	1271.9	1957.7	1918.2	2038.7	1257.0	1275.5	1316.4	412.6	427.1	420.0	1992.6	1915.7	1955.1	1281.8	1318.4
$I_{sp,vac}$, sec	383.2	364.1	374.1	378.5	366.4	386.1	368.0	372.8	355.9	355.1	366.5	351.5	371.9	376.5	364.5	365.7	355.6
$I_{sp,theo}$, sec	399.6	383.8	395.7	396.4	386.5	400.6	397.1	400.7	385.2	392.4	399.4	381.8	397.1	399.7	389.2	396.7	385.6
I_{sp}	95.9	94.9	94.5	95.5	94.8	96.4	92.7	93.0	92.4	90.5	91.8	92.1	93.7	94.2	93.7	92.2	92.2
P_{CSA} , lbf	8287	7818	8172	8188	7954	8400	8201	8334	7896	7819	8087	7665	8291	8516	8100	8212	7925
c^* , theo, fps	8165	7950	8241	8259	8003	8391	8272	8289	7961	8154	8369	7886	8287	8370	8071	8277	7984
c^*	99.1	98.3	99.2	99.1	99.4	100.1	99.1	99.3	99.2	95.9	96.6	97.2	100.0	101.7	100.4	99.2	99.3
Δ_{cyl} , sec	5.1	4.6	4.9	5.0	4.6	5.2	4.9	5.1	4.5	4.7	4.9	4.5	4.9	5.1	4.7	4.8	4.5
Δ_{cyl} , sec	5.7	6.3	6.2	5.7	5.9	5.3	10.0	9.4	7.7	12.7	12.0	9.8	9.3	9.1	8.4	11.3	9.0
Δ_{cyl} , sec	1.0	1.7	1.6	1.1	1.3	0.6	1.6	0.8	1.6	5.0	2.5	5.5	1.0	0.7	1.1	1.6	1.8
Δ_{cyl} , FL, sec	0.6	1.8	1.0	1.0	1.8	0.6	0.9	0.6	1.7	1.0	0.6	1.7	0.8	0.6	1.5	0.9	1.6
Δ_{FFCL} , sec	0.0																
Δ_{FFCL} , sec	3.9	5.3	7.9	5.1	6.5	2.9	11.7	12.0	13.7	13.9	12.9	8.8	9.2	7.7	9.0	12.5	13.2
$\% (ERE + MRD - FFCL)$	98.9	98.2	97.8	98.4	97.9	99.1	96.8	96.9	96.0	96.2	96.6	97.3	97.5	97.9	97.3	96.6	96.2
$\% ERE$	99.0	98.6	98.0	98.7	98.3	99.3	97.1	97.0	96.5	96.5	96.8	97.7	97.7	98.1	97.7	96.8	96.6
T_{ov} , °R	517	516	517	523	526	523	506	508	506	510	510	508	508	510	510	506	503
T_{iv} , °R	525	524	519	526	525	528	520	521	519	515	516	515	517	514	513	511	515

TABLE V-1 (cont.)

Test Series	2K-8	118	120	121	122	123	124	125	126	128	129	131	132	133	134	135	136	137
Run No.	118	120	121	122	123	124	125	126	128	129	131	132	133	134	135	136	137	
Injector Type	Swirler Coax	SN 3														Showerhead Coax		
Igniter (lbf, Type)	25-S	25-C	25-S	25-S	25-S	25-S	25-S	25-S	25-S	25-S	25-S	25-S	25-S	25-S	25-S	25-S	25-S	25-S
L* (Chamber Type), in.	15 (Alb)	25 (Cu)	15 (Alb)	25 (Cu)	15 (Alb)	25 (Cu)	15 (Alb)	25 (Cu)	15 (Alb)	25 (Cu)	15 (Alb)	25 (Cu)	15 (Alb)	25 (Cu)	15 (Alb)	25 (Cu)	15 (Alb)	25 (Cu)
% FFC	0	0	0	0	0	0	0	0	0	0	0	0	0	0	0	0	0	0
FFC - Plane, in.	N/A																	
\bar{C}	3.05	2.90	2.90	3.00	3.07	3.07	3.07	3.07	3.07	3.07	3.07	3.07	3.07	3.07	3.10	2.93	3.10	2.93
Test Duration, sec	0.5	1.0	1.0	1.0	1.0	1.0	1.0	1.0	1.0	1.0	1.0	1.0	1.0	1.0	1.0	1.0	1.0	1.0
Data Summary, sec	1.0-1.2	1.5-1.7	1.5-1.7	1.1-1.3	1.1-1.3	1.1-1.3	1.1-1.3	1.1-1.3	1.1-1.3	1.0-1.2	1.2-1.4	5.0-5.2	1.3-1.3	1.3-1.5	0.97-1.17	1.4-1.6	1.4-1.6	1.1-1.3
P_c , psia	318	302	310	345	333	337*	335	328	318*	316*	316*	316*	316*	316*	316*	316*	316*	316*
(O/F) eng	4.81	3.89	2.98	3.62	4.10	3.59	3.76	4.18	3.67	3.64	3.64	3.64	3.64	3.64	3.64	3.64	3.64	3.64
\dot{W}_o , lbm/sec	3.026	2.715	2.558	3.091	3.073	3.072	3.097	3.089	3.111	3.061	3.061	3.061	3.061	3.061	3.061	3.061	3.061	3.061
\dot{W}_i , lbm/sec	0.617	0.683	0.842	0.592	0.593	0.592	0.592	0.584	0.586	0.581	0.711	0.587	0.577	0.590	0.720	0.559	0.519	0.519
\dot{W}_{fic} , lbm/sec	0	0	0	0.249	0.143	0.252	0.242	0.142	0.249	0.247	0.302	0.250	0.145	0	0	0	0	0
\dot{W}_{fi} , lbm/sec	0.013	0.016	0.016	0.013	0.013	0.013	0.013	0.013	0.013	0.013	0.013	0.013	0.013	0.013	0.016	0.016	0.016	0.016
\dot{W}_{Ti} , lbm/sec	3.656	3.414	3.416	3.945	3.822	3.928	3.920	3.828	3.959	3.902	3.829	3.893	3.778	3.676	3.469	3.659	3.775	3.775
(O/F) core	4.81	3.89	2.98	5.11	5.07	5.08	5.33	5.18	5.20	5.15	3.87	5.07	4.96	5.10	3.71	4.95	6.05	6.05
P_{st} , lbf	1217.4	1137.8	1163.1	1290.1	1245.2	1281.0	1271.3	1246.1	1287.0	1275.5	1286.4	1294.4	1262.4	1205.1	1160.8	1191.8	1184.5	1184.5
P_{at} , lbf	129.4	120.0	120.0	123.4	123.4	123.6	123.6	123.6	132.2	130.9	130.7	122.2	122.2	131.6	121.9	122.0	122.0	122.0
P_{vac} , lbf	1346.8	1257.8	1283.1	1413.5	1368.6	1404.6	1394.9	1369.7	1419.2	1406.4	1417.1	1416.6	1384.6	1336.7	1282.7	1313.8	1306.5	1306.5
$I_{sp,vac}$, sec	368.4	368.4	375.6	358.3	358.1	357.6	355.9	357.8	358.4	360.4	370.1	363.9	366.5	363.6	369.8	359.0	346.1	346.1
$I_{sp,theo}$, sec	388.8	394.9	399.3	398.4	395.1	398.6	397.6	394.4	399.2	399.4	402.8	397.4	394.6	386.0	396.4	384.8	370.9	370.9
\dot{W}_{sp}	94.8	93.3	94.1	90.0	90.6	89.7	89.5	90.7	89.8	90.2	91.9	91.6	92.9	94.2	93.3	93.3	93.3	93.3
$P_c \& A_T$, fps	8172	8137	8348	7868	7847	7732	7691	7724	7549	7619	7866	7897	7971	7839	8220	7936	7936	7936
\dot{W}_{theo} , fps	8001	8226	8367	8282	8184	8288	8257	8167	8272	8279	8392	8286	8204	7914	8258	7954	7932	7932
\dot{W}_c	102.1	98.9	99.8	95.0	95.9	93.3	93.1	94.6	91.3	92.0	93.7	95.3	97.2	99.1	99.5	99.8	106.0	106.0
Δ_{DL} , sec	4.6	4.9	5.1	4.7	4.6	4.7	4.6	4.6	4.6	4.7	4.9	4.8	4.8	4.5	4.9	4.5	4.3	4.3
Δ_{LL} , sec	4.1	6.9	6.3	3.7	4.8	2.5	2.4	3.2	2.0	2.0	1.9	3.0	4.2	3.5	7.4	7.6	6.1	6.1
Δ_{NL} , sec	1.9	1.7	1.0	1.3	1.6	1.4	1.5	1.7	1.6	1.5	0.7	1.4	1.6	1.9	1.6	1.8	1.6	1.6
Δ_{FL} , sec	1.6	1.2	0.7	0.8	1.0	0.8	0.8	1.1	0.8	0.8	0.5	0.8	1.0	1.8	1.1	2.1	3.0	3.0
Δ_{FFCL} , sec	0.0			19.0	13.5	19.9	21.6	14.5	20.6	19.5	10.7	18.3	10.7	0.0				
Δ_{ERL} , sec	8.2	11.7	10.5	10.5	11.4	13.4	10.8	11.6	11.2	10.6	14.0	6.3	5.9	10.7	11.6	9.7	9.8	9.8
Σ (ERE + VRD - FFCL)	97.5	96.7	97.2	92.4	93.4	91.5	91.6	93.1	91.8	92.3	93.8	93.6	95.6	96.8	96.8	96.9	96.6	96.6
Σ ERE	97.9	97.0	97.4	97.4	97.1	96.7	97.3	97.1	97.2	97.3	96.5	98.4	98.5	97.2	97.1	97.5	97.4	97.4
T_{ov} , OR	511	501	501	497	498	500	502	503	503	505	499	503	502	503	498	498	501	501
T_{iv} , OR	511	511	512	507	507	509	510	510	511	512	514	511	511	508	508	507	507	507

*Based on $P_{c,0}$

TABLE V-1 (cont.)

Test Series	2K-8	138	139	140	141	142	143	145	146	148	149	150	151	152	153	154	157	158
Run No.	138	139	140	141	142	143	145	146	148	149	150	151	152	153	154	157	158	
Injector Type	Showerhead Coax								SN 3-D				"I" Triplet					
Igniter (lbf, Type)	25-S								50-P				25-P					
L* (Chamber Type), in.	25 (Cu)				15 (Cu)						15 (FFC) 15 (Cu)					15 (FFC) 15 (Ab1)		
1/2 FFC	30	20	30	20	0						30	0				30	0	
FFC - Plane, in.	0	0	2.5	2.5	N/A						2.5	N/A				2.5	N/A	
C	2.93				2.92	2.92	2.92	2.94	2.96	3.00	2.97					3.00	3.10	
Test Duration, sec	1.0															5.0	0.5	
Data Summary, sec	1.35-1.55	1.35-1.55	1.35-1.55	1.35-1.55	1.35-1.55	1.35-1.55	1.35-1.55	1.35-1.55	1.1-1.5	1.3-1.5	1.35-1.55	1.35-1.55	1.35-1.55	1.35-1.55	1.35-1.55	5.5-5.7	0.92-1.62	
P _c , psia	346*	338*	344*	337*	311	311	300	293	314	315*	309	317	164	106	101	321*	312	
(Q/F) _{eng}	3.67	4.14	3.59	4.17	3.88	6.21	4.30	5.37	3.93	2.75	3.87	5.05	3.90	5.07	6.05	3.47	4.93	
W _o , lbm/sec	3.062	3.067	3.036	3.058	2.736	3.235	2.712	2.897	2.791	2.747	2.729	3.049	0.932	1.033	1.054	3.049	2.934	
W _i , lbm/sec	0.577	0.585	0.584	0.580	0.692	0.508	0.608	0.517	0.687	0.685	0.694	0.59	0.228	0.193	0.163	0.608	0.584	
W _{ffc} , lbm/sec	0.246	0.142	0.248	0.141	0.0					0.292	0.0					0.259	0.0	
W _{ff} , lbm/sec	0.013	0.013	0.013	0.013	0.013	0.013	0.022	0.022	0.023	0.023	0.011	0.011	0.011	0.011	0.011	0.011	0.011	
W _{ff} , lbm/sec	3.898	3.807	3.881	3.792	3.441	3.756	3.343	3.436	3.501	3.746	3.434	3.652	1.171	1.236	1.228	3.926	3.529	
W _{ff} , lbm/sec	5.19	5.13	5.08	5.16	3.88	6.21	4.30	5.37	3.93	3.88	3.87	5.05	3.90	5.07	6.05	4.93	4.93	
(Q/F) core	1291.8	1259.1	1289.2	1256.9	1145.2	1158.0	1110.9	1083.4	1168.6	1251.0	1148.2	1183.9	306.9	312.9	294.3	1291.9	1154.7	
F _{SL} , lbf	120.0	120.0	119.8	119.8	118.9	118.9	120.3	120.3	121.6	128.3	120.8	120.7	120.7	120.7	120.7	129.4	132.2	
F _{Ao} , lbf	1411.8	1379.1	1409.0	1376.7	1264.1	1276.9	1231.2	1203.7	1290.2	1379.3	1269.0	1304.6	427.6	433.6	415.0	1421.3	1325.9	
F _{vac} , lbf	362.3	362.3	363.0	363.0	367.4	340.0	368.3	350.3	368.6	368.2	369.5	357.3	365.2	350.7	338.0	362.0	375.0	
I _{sp,vac} , sec	306.8	303.4	307.1	303.2	395.2	368.6	388.0	376.6	395.8	401.7	396.2	384.5	394.5	380.9	367.3	399.3	388.6	
I _{sp,theo} , sec	01.3	02.1	01.4	02.3	03.0	02.2	04.0	03.0	03.1	01.7	03.3	02.9	02.6	02.6	02.0	00.7	06.7	
I _{sp}	8044	8047	8043	8062	8138	7471	8069	7666	8061	7908	8034	7734	7965	7651	7349	7879	8230	
F _u , S _u A _u , fps	8268	8169	8282	8165	8223	7584	8047	7770	8224	8389	8230	7931	8182	7845	7538	8307	7974	
C _t , theo, fps	97.3	98.5	97.1	98.7	99.0	98.5	100.3	98.7	98.0	94.3	97.6	97.5	97.4	97.5	97.5	94.9	103.2	
C _t	4.8	4.7	4.8	4.7	4.8	4.2	4.8	4.4	4.8	4.9	4.8	4.5	4.8	4.4	4.2	4.7	4.6	
C _u , sec	5.4	6.5	3.6	4.8	6.8	5.2	6.5	6.1	6.3	1.9	6.1	6.1	7.9	7.8	6.7	2.0	3.4	
C _u , sec	1.4	1.6	1.3	1.6	1.7	1.7	1.9	2.0	1.6	0.7	1.6	1.6	4.8	5.4	5.4	1.3	1.8	
C _u , sec	0.8	1.1	0.8	1.1	1.0	2.6	2.2	3.7	1.8	2.8	0.9	1.5	2.7	4.5	6.5	0.6	1.5	
C _u , Ft., sec	12.1	7.4	13.5	8.1	0.0					10.4	0.0					17.8	0.0	
ΔFFCL, sec	10.0	9.9	10.0	9.9	13.6	14.9	4.3	10.1	12.8	12.9	13.3	13.5	9.1	8.1	6.5	10.9	1.3	
ΔFRL, sec	94.2	95.3	93.9	95.1	96.3	95.3	98.3	96.3	96.3	92.5	96.4	96.1	97.0	96.7	96.5	92.7	99.3	
Δ (ERE + MKD - FFCL)	97.5	97.5	97.5	97.5	96.6	96.0	98.9	97.3	96.8	96.8	96.6	96.5	97.7	97.9	98.2	97.3	99.7	
Δ ERE	496	497	498	499	498	498	329	334	505	510	507	509	511	511	509	512	528	
T _{ov} , or	505	506	507	507	507	507	344	344	512	514	513	513	515	515	514	514	528	
T _{fo} , or																		

TABLE V-1 (cont.)

Test Series	159	160	161	163	166	167	169	170	171	172	173	174	175	176	177	178	179
Run No.	159	160	161	163	166	167	169	170	171	172	173	174	175	176	177	178	179
Injector Type	"I" Triplet																
Igniter (lb, Type)	25-S																
L* (Chamber Type), in.	15 (Cu) → 20 (FFC) → 15 (Cu) → 20 (Cu) 15 (Cu)																
% FFC	0	0	0	30	30	0	30	20	30	30	30	30	30	20	20	30	20
FFC - Plane, in.	N/A	2.95	2.95	2.5	2.5	N/A	1.0	2.92	2.94	2.5	2.5	2.5	2.5	1.0	1.0	0	0
C	2.95	2.95	2.95	3.03	3.03	2.96	2.92	2.92	2.94	2.5	2.5	2.5	2.5	1.0	1.0	0	0
Test Duration, sec	2.0	2.0	2.0	10.0	1.0	2.0	2.0	2.0	2.0	2.0	2.0	2.0	2.0	2.0	2.0	2.0	2.0
Data Summary, sec	2.3-2.5	2.3-2.5	2.3-2.5	10.3-10.5	1.2-1.4	2.5-2.7	2.2-2.4	2.2-2.4	2.2-2.4	2.2-2.4	2.2-2.4	2.2-2.4	2.2-2.4	2.2-2.4	2.2-2.4	2.2-2.4	2.2-2.4
P _c , psia	310	314	313	331*	473*	318	298	295	467	488	301	297	99	288	284	310	298
(O/F)	3.82	4.87	5.89	3.45	3.52	2.96	2.97	3.42	3.34	3.63	3.34	3.55	3.47	3.59	4.22	4.16	3.62
u _o , lbm/sec	2.719	2.984	3.178	3.152	4.516	2.566	2.612	2.668	4.255	4.554	2.767	2.786	0.938	2.675	2.771	3.040	2.761
u _f , lbm/sec	0.701	0.602	0.528	0.633	0.888	0.855	0.610	0.619	0.882	0.867	0.574	0.544	0.187	0.595	0.521	0.506	0.595
u _{ff} , lbm/sec	0.0	0.0	0.0	0.268	0.377	0.0	0.259	0.150	0.376	0.368	0.243	0.230	0.080	0.140	0.124	0.214	0.143
u _{ff} , lbm/sec	0.011	0.011	0.011	0.011	0.019	0.011	0.011	0.011	0.018	0.018	0.011	0.011	0.004	0.011	0.011	0.012	0.011
u _{ff} , lbm/sec	3.431	3.597	3.717	4.064	5.800	3.432	3.492	3.448	5.531	5.807	3.595	3.571	1.209	3.421	3.427	3.772	3.510
u _f , lbm/sec	3.82	4.87	5.89	4.89	4.98	2.96	4.21	4.24	4.72	5.14	4.73	5.02	4.91	4.42	5.21	5.88	4.55
(O/F) core	1158.7	1176.8	1171.5	1360.2	2007.0	1186.4	1150.3	1143.7	1880.1	1985.0	1177.3	1162.8	370.9	1103.9	1094.8	1189.3	1139.3
F _{SL} , lbf	121.3	121.3	121.3	130.4	130.4	121.4	124.8	124.8	125.1	125.1	125.0	125.0	125.0	124.0	124.0	125.5	125.5
P _A , lbf	1280.0	1298.1	1292.8	1490.6	2137.4	1307.8	1275.1	1268.5	2005.2	2110.1	1302.3	127.8	35.9	1227.9	1218.8	1314.8	1264.8
F _{vac} , lbf	373.0	360.9	347.8	366.7	368.5	381.0	365.2	367.9	362.5	363.4	362.3	360.7	160.5	358.9	355.6	348.6	360.3
I _{sp,vac} , sec	306.0	386.1	373.3	399.7	399.3	400.4	399.2	397.5	398.0	396.9	398.2	397.2	396.7	390.5	388.7	392.2	395.3
I _{sp,theo} , sec	34.2	91.5	91.2	91.8	92.3	95.1	91.5	92.6	91.1	91.6	91.0	90.8	90.9	91.9	91.5	88.9	91.1
I _{sp}	8105	7830	7543	7654	7650	8288	7985	7998	7906	7870	7856	7802	7673	7885	7755	7689	7925
P _c g A _T , fps	8236	7978	7680	8307	8300	8369	8355	8299	8309	8271	8311	8279	8266	8139	8059	8139	8237
c* theo, fps	98.4	98.2	98.2	92.1	92.2	99.0	95.6	96.4	95.1	95.2	94.5	94.2	92.8	96.9	96.2	94.5	96.2
c*	4.9	4.6	4.3	4.8	4.8	5.1	4.9	4.9	4.8	4.8	4.8	4.8	4.8	4.7	4.6	4.6	4.6
ΔCDL, sec	5.8	6.1	5.4	2.1	2.0	5.5	3.2	4.2	2.9	2.5	1.4	1.6	4.2	3.6	3.5	3.7	4.8
ΔALL, sec	1.7	1.8	1.7	1.3	1.0	1.0	1.1	1.5	0.9	1.0	0.6	0.7	0.7	1.7	2.0	1.8	1.7
ΔKL, sec	0.9	1.4	2.0	0.6	0.7	0.5	0.5	0.7	0.7	0.7	0.6	0.7	0.7	0.8	1.1	1.0	0.8
ΔI _s FL, sec	0.0	0.0	0.0	17.9	17.6	0.0	13.0	9.6	17.6	17.9	16.8	18.8	21.3	10.1	13.5	23.7	10.9
ΔFFCL, sec	9.7	11.3	12.2	6.3	4.7	7.4	11.3	8.7	8.6	6.6	9.8	8.1	2.1	10.7	8.4	8.8	12.2
ΔERL, sec	97.3	96.7	96.2	93.8	94.2	98.0	93.8	95.0	93.3	93.7	93.2	93.1	93.9	94.5	94.1	91.4	93.9
% (ERE + MRD - FFCL)	97.5	97.1	96.7	98.4	98.8	98.2	97.2	97.8	97.8	98.3	97.5	98.0	99.5	97.3	97.8	97.7	96.9
% ERE	492	499	507	500	491	499	356	371	341	326	358	365	359	347	363	316	352
I _{ov} , °R	505	506	508	513	506	513	519	519	513	522	523	522	523	289	353	491	494
I _{ov} , °R																	

*Based on P 011

TABLE V-1 (cont.)

Test Series	2K-8						
Run No.	180	181	182	183	184	185	186
Injector Type	Recessed	Swirl	Coax				I-Triplet
Igniter (lbf, Type)	25-S						
L* (Chamber Type), in.	15 (Cu)	15 (Ab1)	20 (Cu)				15 (Cu)
% FFC	20	10	0	0	30	30	20
FFC - Plane, in.	0	0	N/A	N/A	2.5	2.5	0
\bar{C}	2.93	3.09	2.93				
Test Duration, sec	2.0	0.5	2.0				1.0
Data Summary, sec	2.2-2.4	0.8-1.0	2.2-2.4	2.2-2.4	1.4-1.5	2.2-2.4	1.2-1.4
P_c , psia	449	333	284	278	307	300	314
(O/F) _{eng}	3.75	4.72	4.65	5.65	3.31	3.71	4.09
\dot{w}_o , lbm/sec	4.169	3.212	2.789	2.926	2.821	2.860	3.018
\dot{w}_f , lbm/sec	0.880	0.606	0.589	0.506	0.593	0.534	0.587
\dot{w}_{ffc} , lbm/sec	0.214	0.064	0	0	0.249	0.226	0.140
\dot{w}_{fI} , lbm/sec	0.018	0.011					
\dot{w}_T , lbm/sec	5.281	3.893	3.389	3.443	3.674	3.631	3.756
(O/F) _{core}	4.64	5.20	4.65	5.65	4.67	5.24	5.05
F_{SL} , lbf	1781.8	1281.6	1089.5	1069.8	1170.4	1145.7	1222.1
$P_{a'e}$, lbf	125.5	131.7	125.3				125.2
F_{vac} , lbf	1907.3	1413.3	1214.8	1195.1	1295.7	1271.0	1347.3
$I_{sp,vac}$, sec	361.2	363.0	358.5	347.1	352.6	350.1	358.7
$I_{sp,theo}$, sec	395.6	390.1	387.6	375.0	393.8	393.5	390.7
% I_{sp}	91.3	93.1	92.5	92.6	89.5	89.0	91.8
$\frac{P_c g A_T}{\dot{w}_T}$, fps	7948	7958	7837	7551	7807	7723	7837
c^*_{theo} , fps	8239	8011	8022	7726	8205	8189	8107
% c^*	96.5	99.3	97.7	97.7	95.1	94.3	96.7
Δ_{CDL} , sec	4.5	4.5	4.5	4.5	4.7	4.6	4.7
Δ_{BLL} , sec	4.4	3.6	8.0	6.5	2.7	2.7	4.8
Δ_{KL} , sec	1.1	1.8	2.0	2.0	1.4	1.7	1.7
$\Delta_{I_g FL}$, sec	0.9	1.3	1.4	2.1	0.6	0.8	0.9
Δ_{FFCL} , sec	10.1	7.1	0	0	16.2	19.9	12.9
Δ_{ERL} , sec	13.4	8.8	13.2	12.8	15.6	13.7	7.0
% (ERE + MRD - FFC)	93.8	95.6	96.2	96.0	91.8	91.3	94.7
% ERE	96.6	97.7	96.6	96.6	96.0	96.5	98.2
T_{ov} , °R	370	342	369	370	371	389	379
T_{fv} , °R	492	503	508	506	341	399	376

*Based on P_{OJI}

TABLE V-2

SUMMARY OF 40:1 TEST CONDITIONS AND HARDWARE

Test No.	Date	Injector SN	Chamber	Data Summary Period, sec	P _c psia	TCA MR O/F	% FFC	Prop. Temp. O ₂ /H ₂ O _R /O _R
1680-D03-0A-001								
			System and Igniter Checkout Tests					
-002			System and Igniter Checkout Tests					
-003			System and Igniter Checkout Tests					
-004			System and Igniter Checkout Tests					
-005	4/30/71	2 I	3:1 FC	.4-.6	256	3.99	32.7	Amb.
-006	4/30/71	2 I	3:1 FC	.4-.96	269.4	3.000	32.05	
-007	4/30/71	2 I	3:1 FC	.4-.91	268.0	3.022	31.4	
-008	4/30/71	2 I	3:1 FC	15.0-20.0	250*	3.00	30.2	
-009	4/30/71	2 I	3:1 FC	5-10	258*	2.93	29.7	
-010	5/12/71	5 I	40:1 SN-1 FC		Sea Level - Igniter Only			
-011	5/12/71				Altitude - Igniter Only			
-012	5/12/71				P _{Alt} 1A Bad No Perf. Dam.			
-013	5/12/71	5 I	40:1 SN-1 FC	6.0-9.6	284.9	3.87	31.8	Amb.
-014	5/14/71	5 I		30-35	290.2	3.96	30.6	
-015	5/14/71	5 I		20-50	290.0	3.93	30.6	
				60-90	295.0	3.88	24.9	
				100-130	298.4	3.86	19.4	
				143-165	303.1	2.93	29.5	
				173-193	306.1	2.92	25.3	
				200-225	307.7	2.95	20.3	
				245-270	278.3	4.84	30.0	
-016	5/21/71	4 Trip		Computer shutdown due to amplifier malfunction				
-017	5/21/71	4 Trip	40:1 SN-1 FC	4.0-5.0	291.0	2.95	28.6	Amb.
				4.5-5.0	291.4	2.95	28.6	
-018				4.0-4.5	296.5	2.94	25.4	
				4.0-5.5	297.5	2.95	25.3	
-019				.5-1.5	276.0	4.00	23.7	
				3-8	284.4	3.98	25.1	
				9.2-11.5	289.2	3.94	19.1	
-020				.6-1.0	279.2	4.02	24.5	
				4.0-6.0	285.4	4.00	24.9	
				10.0-14.0	289.4	3.95	19.1	
				17.0-22.0	279.5	4.03	30.5	
				30-50.0	268.4	4.86	28.6	
-021				5-50	93.9	4.44	21.4	
				55-105	93.1	4.39	26.6	
-022	6/15/71			8-13	293.2	3.93	28.2	Cold
-023				9-14	287.4	4.05	28.0	
				19-23	256.4	5.18	29.5	
				30-34	284.3	4.05	24.1	
				36-50	282.7	4.13	20.0	
				54-58	285.7	4.08	23.9	
-024	6/18/71			5-16	479.5	3.95	29.0	Amb.
				19-23	486.1	3.92	24.3	
				26-34	480.3	3.95	29.0	

* Data questionable. Instrumentation calibration shift during test.

TABLE V-2 (cont.)

Test No.	Date	Injector SN	Chamber	Data Summary Period, sec	P _c , psia	TCA MR O/F	% FFC	Prop. Temp. O ₂ /H ₂ °R/°R
1680-D04-0A-001-006	7/15/71	6 I	40:1 SN-1 FC	None	Checkout Tests			Amb.
-007	↓	↓	↓	↓	No valid perf data due to open check valve			↓
-008-009	↓	↓	↓	↓	No data - Film cooling valve failed to open			↓
-010-011	↓	↓	↓	↓	Computer shut down at .150 sec			↓
-012	7/16/71	↓	40:1 SN-2 FC	5-25	298.9	3.8	18.9	Amb.
↓	↓	↓	↓	30-45	302.5	3.8	18.9	↓
↓	↓	↓	↓	49-59	302.6	3.8	16.9	↓
↓	↓	↓	↓	63-65	292.2	3.9	29.8	↓
↓	↓	↓	↓	68-73	281.7	4.8	29.0	↓
↓	↓	↓	↓	78-94	284.7	4.9	24.1	↓
-013	↓	↓	↓	No test				↓
-014	7/21/71	↓	↓	2-6	448.8	3.4	24.1	↓
↓	↓	↓	↓	7-11	468.7	4.9	25.2	↓
-015	↓	↓	↓	Igniter power not activated				↓
-016	↓	↓	↓	Computer shutdown due to low P _c in FFC manifold				↓
-017	8/3/71	↓	↓	0-20	Very low GO ₂ temp - no flow data			280/170
-018	↓	↓	↓	5-12	285.7	3.0	18.9	Cold
↓	↓	↓	↓	16-24	285.8	3.0	13.9	↓
↓	↓	↓	↓	25-27	281.0	3.1	19.4	↓
↓	↓	↓	↓	30-32	276.1	3.1	24.7	↓
↓	↓	↓	↓	35-45	276.7	4.1	24.6	↓
↓	↓	↓	↓	47-58	266.3	4.2	19.9	↓
↓	↓	↓	↓	60-70	267.5	4.2	17.7	↓
↓	↓	↓	↓	72-74	266.2	4.2	20.3	↓
↓	↓	↓	↓	76-79	268.9	4.0	24.7	↓
↓	↓	↓	↓	81-91	262.3	4.9	22.7	↓
↓	↓	↓	↓	94-101	268.0	4.8	18.7	↓
-D03-0A-026	8/5/71	3	40:1 SN-1 Regen	0-2.0	300	4	20/7.4	Amb.
-027	↓	↓	+10% FFC Ring	0-30	↓	3.1	20/7.4	↓
↓	↓	↓	↓	35-54	↓	3.1	13.1/8.1	↓
↓	↓	↓	↓	55-57	↓	3.3	17.1/7.8	↓
-028	↓	↓	↓	0-12	293	4.1	13.6/7.5	↓
↓	↓	↓	↓	12-18	295	4.2	0/9.4	↓
-D04-0A-019	8/11/71	6 I	40:1 SN-1 Regen	0-60	300	4.1	0/23	↓
↓	↓	↓	↓	↓	↓	↓	0/15	↓
-020	↓	↓	↓	0-24	290	4.1	0/14.6	↓
↓	↓	↓	↓	30-54	295	4.1	0/10.4	↓
↓	↓	↓	↓	60-71	304	3.1	0.10.3	↓
↓	↓	↓	↓	74-78	297	4.2	0/10.4	↓
↓	↓	↓	↓	82-86	284	5.1	0/10.3	↓
↓	↓	↓	↓	90-96	275	5.2	0/15.3	↓
-021	↓	↓	↓	0-15	497	3.6	0/10.1	↓
↓	↓	↓	↓	16-28	485	4.1	0/10.1	↓
-D03-0A-029	↓	↓	↓	Computer shutdown - low coolant manifold pressure				↓
-030	↓	↓	↓	0-19	96	4.4	0/4.0	↓
↓	↓	↓	↓	20-22	95		0/6.8	↓
↓	↓	↓	↓	24-58	94		0/9.7	↓
↓	↓	↓	↓	65-70	96		0/6.7	↓
-031	↓	↓	↓	0-8	99	3.1	0/9.4	↓
-032	↓	↓	↓	Facility malfunction - no test				↓
-033	↓	↓	↓	0-48	90	5.5	0/9.3	↓

Figure V-2 (Sheet 2 of 4)

TABLE V-2 (cont.)

Test No.	Date	Injector SN	Chamber	Data Summary Period, sec	P _c , psia	TCA MR, O/F	% FFC	Prop. Temp. O ₂ /H ₂ °R/°R
1680-D04-OA-022	8/18/71	6 I	40:1 SN-1 Regen	0-40	291	4.5	11	Cold
-023				0-15	289	4.4	8.1	
				18-24	297	4.5	10.8	
				36-47	310	3.3	10.2	
				50-56	305	4.4	10.3	
				64-72	282	5.6	15.5	
-024	8/20/71		2-phase Oxidizer Flow	0-10	480	3.6	7.2	
-025				18-35	460	4.2	8.5	
-D03-OA-035	8/26/71			0-25	300	3.9	10	Hot
				25-250	300	3.9	12	Variable
					300	3.9	10	
-D06-OA-001	10/7/71	7	SN-3 Film Cooled	0-.2	300	4.0	20	Cold/Cold
-002				0-.2			20	
-004				0-8			20	
-005	10/8/71			1-2.25			18.9	
				4-7.5				
-006				2-4		3.7	17.8	
				4-23		4.0	19.2	
				27-37		5.0	21.1	
-007				0-8	300	4.0	20	
				8-18	Coast			
				18-22	16 pulses of varying duration			
-008				0-8	300	4.0	20	
				8-18	Coast			
				18-22	16 pulses of varying duration			
-009				0-8	300	3.0	20	
				8-18	Coast			
				18-26	32 pulses of varying duration			
-010				0-8	300	4.0	20	
				8-18	Coast			
				18-24	25 pulses of varying duration			
-011			Six igniter-only tests with cold propellant					
-012	10/11/71	7	SN-3 Film Cooled	2-12	300	3.7	19	Amb/Cold
				12-24	230	3.3-2.6	19	
-013				0-60	294	4.0	19.3	Amb/Cold
				60-96	358	3.7	23.3	Cold/Cold
				97-110	397	4.4	27.1	
				112-117	400	4.7	26.5	
				117-122	400	5.2	24.2	
				122-142	400	5.7	24.2	
-014	11/2/71		SN-3 Regen	0-2	300	4.0	10	Amb/Amb

TABLE V-2 (cont.)

Test No.	Date	Injector SN	Chamber	Data Summary Period, sec	P _c , psia	TCA MR, O/F	% FFC	Prop. Temp. O ₂ /H ₂ °R/°R
1680-D06-0A-015	11/2/71	7	SN-3 Regen	0-128	100	4.0	10	Amb/Amb
-016					100	5.0		
					100	6.0		
					200	4.0		
					200	5.0		
					200	6.0		
-017				0-5	200	4.0		
				6-10	200	6.0		
				11-22	400	6.0		
				23-48	400	5.0		
				0-10	400	4.0		
-018	11/3/71			10-20	200	6.0		
				20-30	500	6.0		
				32-36	500	5.0		
				1976.5 sec continuous fire durability test.				
				Combinations of MR, P _c and propellant temperatures as follows:				

Fuel temp = 530-200°R
 Ox temp = 530-365°R
 100-400 psia
 4-6 MR

TABLE V-3

SUMMARY OF FILM-COOLED CHAMBER TEST CONDITIONS AND PERFORMANCE

HI PRESSURE APS TEST SUMMARY AND PERFORMANCE DATA

TEST INQ	DATE	DATA	TIME	MRE	MRC	PC	TH2	TO2	TFC	WT	WFT	WO	%FC	XIG	FVAC	PA	ISV	CSTAR	XISV	%C*	ERE	KL	RL	FCL	DL	ERI	
03-013	5	05-12-71	6.-	10.	3.9	5.9	285.	545.	534.	545.	3.52	72	2.80	32.	5	1355.	1.0	429.	7563.	80.7	91.8	97.2	4.	8.	15.	3.	13.
03-014	5	05-14-71	5.-	35.	4.0	5.9	290.	539.	533.	539.	3.52	71	2.81	31.	5	1294.	1.1	423.	7711.	89.5	93.8	96.2	4.	9.	15.	3.	18.
03-015	5	05-14-71	29.-	50.	3.9	5.9	289.	532.	533.	550.	3.50	71	2.79	31.	5	1369.	1.1	432.	7711.	91.2	93.8	97.8	4.	9.	15.	3.	10.
03-015	5	05-14-71	60.-	90.	3.9	5.3	295.	547.	532.	548.	3.51	72	2.79	25.	5	1369.	1.2	438.	7857.	92.5	95.4	98.2	4.	9.	10.	3.	9.
03-015	5	05-14-71	100.-	130.	3.9	4.9	298.	542.	532.	544.	3.51	72	2.79	19.	5	1401.	1.2	441.	7935.	93.3	96.3	98.2	4.	9.	7.	3.	8.
03-015	5	05-14-71	143.-	165.	2.9	4.3	303.	533.	527.	530.	3.52	90	2.62	30.	5	1385.	1.2	439.	8054.	93.3	95.1	97.3	2.	7.	6.	3.	13.
03-015	5	05-14-71	173.-	193.	2.9	4.0	306.	529.	528.	529.	3.52	90	2.62	25.	5	1384.	1.2	444.	8139.	94.4	97.1	98.2	2.	7.	5.	3.	9.
03-015	5	05-14-71	200.-	225.	3.0	3.8	308.	522.	527.	525.	3.51	89	2.62	20.	5	1381.	1.2	448.	8201.	95.2	97.9	98.9	2.	7.	4.	4.	5.
03-015	5	05-14-71	245.-	270.	4.8	7.2	278.	523.	523.	523.	3.51	60	2.91	30.	5	1263.	1.2	414.	7400.	87.9	92.6	96.8	6.	9.	22.	3.	15.
03-017	4	05-21-71	4.-	5.	2.9	4.2	291.	532.	517.	530.	3.36	85	2.51	29.	5	1390.	1.6	434.	8082.	92.3	95.5	96.2	2.	7.	6.	3.	18.
03-017	4	05-21-71	4.-	5.	2.9	4.2	291.	532.	516.	531.	3.37	85	2.52	29.	5	1389.	1.7	436.	8084.	92.7	96.5	96.6	2.	7.	6.	3.	16.
03-017	4	05-21-71	4.-	4.	2.9	4.0	297.	530.	514.	530.	3.41	87	2.54	25.	5	1405.	1.7	437.	8130.	92.8	97.0	96.6	2.	7.	5.	3.	16.
03-018	4	05-21-71	4.-	5.	2.9	4.0	297.	530.	514.	531.	3.41	87	2.55	25.	5	1387.	1.9	436.	8142.	92.8	97.2	96.6	2.	7.	5.	3.	16.
03-019	4	05-21-71	1.-	1.	4.0	5.4	276.	515.	509.	509.	3.33	65	2.66	24.	5	1391.	1.2	425.	7755.	89.8	93.5	95.6	4.	9.	11.	3.	21.
03-019	4	05-21-71	3.-	8.	4.0	5.5	284.	523.	508.	526.	3.43	69	2.74	25.	5	1421.	1.3	426.	7751.	90.0	94.4	95.9	4.	9.	11.	3.	19.
03-019	4	05-21-71	9.-	11.	3.9	5.0	289.	528.	511.	527.	3.43	69	2.74	19.	5	1413.	1.6	430.	7876.	91.0	95.8	96.0	4.	9.	7.	3.	19.
03-020	4	05-21-71	1.-	1.	4.0	5.5	279.	515.	503.	513.	3.37	67	2.70	25.	5	1404.	1.2	423.	7752.	89.8	94.5	95.4	4.	9.	11.	3.	22.
03-020	4	05-21-71	4.-	6.	4.0	5.5	285.	522.	507.	525.	3.44	69	2.75	25.	5	1399.	1.7	428.	7863.	90.5	95.7	95.6	4.	9.	7.	3.	21.
03-020	4	05-21-71	10.-	14.	4.0	5.0	289.	529.	511.	531.	3.44	69	2.75	19.	5	1399.	1.7	428.	7863.	90.5	95.7	95.6	4.	9.	7.	3.	21.
03-020	4	05-21-71	17.-	22.	4.0	5.0	279.	532.	516.	534.	3.42	60	2.74	31.	5	1304.	1.0	414.	7634.	87.4	93.1	94.3	4.	9.	16.	3.	27.
03-020	4	05-21-71	39.-	50.	5.0	7.3	268.	532.	517.	532.	3.43	58	2.86	30.	5	1345.	1.6	411.	7303.	87.3	91.0	96.4	6.	9.	23.	3.	17.
03-021	4	05-21-71	5.-	50.	4.5	5.9	284.	519.	501.	519.	1.15	21	94	21.	5	1464.	1.1	415.	7641.	87.9	94.4	95.0	5.	11.	13.	3.	24.
03-021	4	05-21-71	55.-	105.	4.4	6.2	293.	519.	493.	519.	1.15	21	94	27.	5	1484.	1.1	404.	7554.	85.4	93.1	93.0	5.	11.	16.	3.	33.
03-022	4	05-15-71	8.-	13.	3.9	5.6	293.	509.	341.	211.	3.67	75	2.93	28.	4	1377.	1.5	420.	7461.	90.6	92.3	96.7	3.	8.	13.	3.	15.
03-023	4	05-15-71	9.-	14.	4.0	5.8	287.	199.	321.	198.	3.68	73	2.95	28.	4	1364.	1.3	412.	7309.	89.9	93.7	95.3	4.	8.	14.	3.	22.
03-023	4	05-15-71	19.-	23.	5.2	7.7	256.	329.	319.	226.	3.51	57	2.94	29.	5	1221.	1.2	392.	6833.	85.0	91.6	95.2	6.	8.	28.	3.	22.
03-023	4	05-15-71	36.-	34.	4.1	5.5	284.	235.	325.	247.	3.65	72	2.93	24.	4	1399.	1.1	421.	7275.	90.8	94.3	96.5	4.	8.	11.	3.	16.
03-023	4	05-15-71	36.-	50.	4.1	5.3	283.	232.	331.	245.	3.63	71	2.92	29.	4	1349.	1.5	424.	7279.	91.3	98.5	96.8	4.	8.	9.	3.	15.
03-023	4	05-15-71	54.-	58.	4.1	5.5	286.	228.	339.	230.	3.63	72	2.92	24.	4	1368.	1.7	423.	7352.	91.2	91.3	97.0	4.	8.	11.	3.	14.
03-024	4	05-18-71	5.-	16.	4.0	5.7	439.	542.	531.	544.	5.801	17	4.63	29.	4	2415.	1.8	432.	7724.	91.2	93.8	96.9	2.	8.	13.	3.	15.
03-024	4	05-18-71	19.-	23.	5.9	9.3	436.	543.	529.	546.	5.811	18	4.63	24.	4	2460.	1.7	438.	7824.	92.5	94.9	97.5	2.	8.	9.	3.	12.
03-024	4	05-18-71	26.-	34.	4.0	5.7	480.	542.	528.	546.	5.801	17	4.63	29.	4	2439.	1.7	435.	7736.	91.8	93.0	97.5	2.	8.	13.	3.	12.
04-012	6	07-16-71	5.-	25.	3.9	5.2	299.	550.	531.	550.	3.59	74	2.85	24.	5	1458.	1.0	439.	7810.	92.7	94.7	98.1	4.	8.	6.	3.	9.
04-012	6	07-16-71	30.-	45.	3.0	4.8	302.	547.	521.	547.	3.60	75	2.85	19.	5	1510.	1.8	444.	7879.	93.9	95.6	98.7	4.	8.	6.	3.	6.
04-012	6	07-16-71	49.-	59.	3.8	4.7	303.	544.	517.	545.	3.60	75	2.86	17.	5	1524.	1.7	446.	7883.	94.2	95.6	98.8	4.	8.	5.	4.	6.
04-012	6	07-16-71	63.-	65.	3.9	5.7	292.	543.	516.	542.	3.59	73	2.86	30.	5	1481.	1.7	435.	7639.	91.9	92.8	98.3	4.	8.	14.	3.	8.
04-012	6	07-16-71	66.-	73.	4.8	7.1	222.	542.	516.	542.	3.61	62	2.89	24.	5	1449.	1.7	423.	7331.	89.7	91.6	98.3	6.	9.	21.	3.	8.
04-012	6	07-16-71	70.-	74.	4.9	6.7	285.	542.	515.	541.	3.60	61	2.93	24.	5	1468.	1.6	429.	7429.	91.0	93.0	98.8	6.	9.	17.	3.	6.
04-014	6	07-21-71	8.-	6.	3.4	4.6	449.	546.	545.	545.	5.201	19	4.03	24.	5	2190.	1.3	450.	8094.	95.2	97.2	99.1	2.	7.	5.	4.	4.
04-014	6	07-21-71	8.-	11.	4.9	6.8	469.	545.	545.	545.	5.201	19	4.03	24.	5	2190.	1.3	450.	8094.	95.2	97.2	99.1	2.	7.	5.	4.	4.
04-016	6	08-03-71	5.-	12.	3.0	3.8	286.	184.	454.	257.	3.32	82	2.80	19.	5	1360.	1.2	434.	7548.	92.1	94.4	98.5	4.	8.	18.	3.	3.
04-016	6	08-03-71	16.-	24.	3.0	3.5	286.	191.	433.	274.	3.31	94	2.48	14.	5	1347.	1.8	434.	8092.	94.9	99.1	98.2	1.	7.	4.	3.	7.
04-016	6	08-03-71	25.-	27.	3.1	3.9	281.	208.	424.	254.	3.27	81	2.46	19.	5	1324.	1.8	432.	8059.	94.3	98.9	97.9	1.	7.	3.	3.	10.
04-016	6	08-03-71	30.-	32.	3.1	4.3	276.	213.	420.	242.	3.23	78	2.45	25.	5	1310.	1.8	433.	8022.	94.3	98.3	98.3	1.	7.	6.	3.	8.
04-016	6	08-03-71	35.-	45.	4.1	5.7	277.	199.	412.	256.	3.25	63	2.61	25.	5	1306.	1.7	428.	7737.	92.2	96.1	98.5	4.	9.	12.	3.	7.
04-016	6	08-03-71	47.-	58.	4.2	5.5	266.	183.	407.	260.	3.20	61	2.59	20.	5	1304.	1.7	432.	7803.	93.2	97.2	99.0	4.	9.	10.	3.	5.
04-016	6	08-03-71	50.-	70.	4.2	5.3	267.	191.	404.	257.	3.20	61	2.53	18.	5	1310.	1.7	434.	7850.	93.7	97						

Table V-3
(Sheet 1 of 2)

TABLE V-3 (cont.)

HI PRESSURE APS TEST SUMMARY AND PERFORMANCE DATA

TEST INJ	DATE	DATA TIME	MRE	MRC	PC	TH2	TO2	TFC	WT	WFT	WO	%FC	%IG	FVAC	PA	ISV	CSTAR	NISV %*	ERE	KL	RL	FCL	DL	ERL	
06-005	7 10-08-71	0.-	1.	4.0	5.2	308.	310.	405.	523.	3.70	.74	2.96	20.	.5	1493.	1.1	430.	7852.	92.4	93.6	97.8	4.	9.	8.	3. 11.
06-005	7 10-08-71	1.-	2.	4.0	5.1	302.	266.	377.	522.	3.70	.73	2.96	19.	.5	1469.	1.1	433.	7738.	93.4	93.9	98.5	4.	9.	8.	3. 7.
06-005	7 10-08-71	2.-	3.	4.2	5.4	280.	255.	374.	517.	3.47	.66	2.81	19.	.4	1369.	1.0	423.	7659.	93.1	93.4	98.7	4.	9.	9.	3. 6.
06-005	7 10-08-71	4.-	8.	4.8	6.1	244.	239.	364.	499.	3.12	.54	2.58	18.	.4	1184.	1.0	423.	7433.	91.4	91.2	98.1	5.	9.	12.	3. 9.
06-005	7 10-08-71	8.-	8.	5.2	6.5	221.	229.	353.	485.	2.88	.46	2.42	18.	.3	1082.	.9	419.	7299.	90.7	93.7	98.1	5.	9.	14.	3. 9.
06-005	7 10-08-71	9.-	9.	5.6	6.9	200.	226.	352.	478.	2.76	.42	2.34	18.	.3	1017.	.8	411.	7184.	89.4	93.3	97.4	7.	9.	16.	3. 12.
06-006	7 10-08-71	1.-	2.	3.4	4.1	314.	268.	447.	507.	3.76	.66	2.90	16.	.6	1501.	1.1	435.	7937.	94.3	97.4	97.9	2.	8.	3.	3. 10.
06-006	7 10-08-71	2.-	4.	3.7	4.6	305.	266.	440.	504.	3.70	.79	2.91	16.	.5	1483.	1.1	432.	7834.	93.4	96.6	97.7	3.	8.	3.	3. 11.
06-006	7 10-08-71	4.-	12.	4.1	5.2	299.	216.	414.	477.	3.71	.73	2.98	19.	.4	1463.	1.0	426.	7655.	91.8	95.0	97.1	4.	8.	8.	3. 14.
06-006	7 10-08-71	12.-	14.	4.0	5.1	300.	198.	408.	427.	3.67	.73	2.94	19.	.4	1489.	.8	434.	7768.	93.6	96.3	98.8	4.	9.	8.	3. 5.
06-006	7 10-08-71	14.-	23.	4.0	5.1	301.	190.	383.	379.	3.67	.73	2.94	19.	.4	1506.	.8	439.	8021.	94.4	99.5	99.6	4.	9.	8.	3. 2.
06-006	7 10-08-71	23.-	27.	4.5	6.0	298.	192.	390.	361.	3.76	.67	3.10	21.	.3	1510.	.7	428.	7725.	92.3	97.3	99.0	5.	9.	13.	3. 5.
06-006	7 10-08-71	27.-	37.	5.0	6.5	294.	184.	379.	356.	3.78	.63	3.15	21.	.3	1500.	.7	422.	7557.	91.3	95.7	98.8	5.	9.	16.	3. 5.
06-006	7 10-08-71	37.-	38.	5.5	7.1	291.	162.	373.	352.	3.81	.53	3.23	20.	.3	1498.	.7	419.	7454.	90.9	96.0	99.3	7.	9.	18.	3. 3.
06-012	7 10-11-71	2.-	4.	3.5	4.8	290.	276.	539.	541.	3.51	.73	2.77	19.	.5	1412.	1.0	436.	7685.	94.2	94.8	98.8	3.	8.	6.	3. 6.
06-012	7 10-11-71	4.-	9.	3.7	4.7	289.	233.	537.	503.	3.51	.74	2.77	19.	.5	1408.	1.0	435.	7675.	93.9	94.7	98.4	3.	8.	6.	3. 7.
06-012	7 10-11-71	6.-	10.	3.8	4.8	285.	236.	536.	443.	3.48	.73	2.76	19.	.5	1396.	.9	435.	7637.	93.9	94.3	98.6	3.	8.	6.	3. 7.
06-012	7 10-11-71	10.-	12.	3.6	4.6	277.	238.	539.	417.	3.35	.72	2.62	19.	.5	1344.	.9	437.	7693.	94.4	91.7	98.8	3.	8.	5.	3. 6.
06-012	7 10-11-71	12.-	14.	3.4	4.3	265.	236.	541.	405.	3.18	.72	2.46	19.	.5	1279.	.9	439.	7737.	95.1	93.0	99.1	2.	8.	4.	3. 4.
06-012	7 10-11-71	14.-	16.	3.2	4.1	256.	234.	539.	400.	3.05	.73	2.33	19.	.5	1225.	.9	440.	7772.	95.6	93.3	99.3	2.	8.	4.	3. 3.
06-012	7 10-11-71	16.-	18.	3.0	3.9	246.	236.	533.	397.	2.93	.72	2.20	19.	.5	1172.	.9	441.	7801.	96.1	93.6	99.7	1.	7.	4.	3. 1.
06-012	7 10-11-71	18.-	20.	2.9	3.7	238.	236.	535.	398.	2.81	.73	2.09	19.	.6	1123.	.9	441.	7820.	96.7	93.9	100.2	1.	7.	4.	3. -1.
06-012	7 10-11-71	20.-	22.	2.7	3.5	230.	236.	535.	396.	2.72	.73	1.99	19.	.6	1081.	.9	441.	7831.	97.1	96.1	100.6	1.	7.	4.	3. -3.
06-012	7 10-11-71	22.-	24.	2.6	3.3	223.	236.	533.	396.	2.63	.73	1.90	19.	.6	1041.	.9	442.	7831.	97.6	95.2	101.2	1.	7.	5.	3. -5.
06-012	7 10-11-71	24.-	26.	2.4	3.1	218.	247.	539.	515.	2.51	.74	1.77	19.	.5	1409.	1.0	435.	7679.	94.0	94.7	96.5	3.	8.	6.	3. 7.
06-012	7 10-11-71	26.-	28.	2.1	2.9	208.	236.	537.	407.	2.35	.74	2.23	19.	.5	1181.	.9	440.	7778.	95.9	95.3	99.5	1.	7.	4.	3. 2.
06-013	7 10-11-71	3.-	10.	3.8	4.8	289.	225.	516.	475.	3.52	.73	2.79	19.	.4	1386.	1.2	433.	7672.	93.5	94.7	98.1	3.	8.	6.	3. 9.
06-013	7 10-11-71	13.-	22.	3.9	4.9	289.	225.	483.	383.	3.53	.73	2.80	19.	.4	1409.	1.0	433.	7637.	93.6	94.3	98.4	3.	8.	7.	3. 7.
06-013	7 10-11-71	22.-	65.	3.9	5.0	292.	245.	429.	380.	3.58	.73	2.85	19.	.4	1435.	.9	434.	7621.	93.6	94.3	98.6	3.	8.	7.	3. 7.
06-013	7 10-11-71	70.-	95.	3.5	4.7	364.	264.	399.	368.	4.39	.97	3.42	22.	.5	1783.	1.0	435.	7729.	94.2	95.0	98.1	1.	7.	5.	3. 9.
06-013	7 10-11-71	98.-	112.	4.4	6.2	402.	261.	393.	359.	5.02	.93	4.09	27.	.4	2027.	1.0	431.	7477.	92.9	93.3	99.3	2.	8.	15.	3. 3.
06-013	7 10-11-71	112.-	117.	4.8	6.7	439.	276.	403.	353.	5.17	.90	4.27	27.	.4	2027.	1.0	413.	7231.	90.3	91.0	97.5	3.	8.	18.	3. 11.
06-013	7 10-11-71	117.-	122.	5.2	7.1	407.	276.	403.	349.	5.36	.86	4.50	24.	.4	2071.	1.0	412.	7076.	89.1	90.4	97.1	4.	8.	21.	3. 13.
06-013	7 10-11-71	122.-	142.	5.7	7.8	407.	272.	419.	359.	5.49	.82	4.67	24.	.4	2081.	1.0	404.	6920.	87.9	89.8	97.2	4.	8.	26.	3. 13.

Table V-3
(Sheet 2 of 2)

TABLE V-4

SUMMARY OF FILM-COOLED CHAMBER THERMAL PROFILES

FILM COOLED CHAMBER

											AREA RATIO (--)										AXIAL DISTANCE (IN)																			
											3.14					3.14					3.14					1.25					1.25					1.25				
											3.14					3.14					3.14					1.25					1.25					1.25				
											3.14					3.14					3.14					1.25					1.25					1.25				
											3.14					3.14					3.14					1.25					1.25					1.25				
											3.14					3.14					3.14					1.25					1.25					1.25				
											3.14					3.14					3.14					1.25					1.25					1.25				
											3.14					3.14					3.14					1.25					1.25					1.25				
											3.14					3.14					3.14					1.25					1.25					1.25				
											3.14					3.14					3.14					1.25					1.25					1.25				
											3.14					3.14					3.14					1.25					1.25					1.25				
											3.14					3.14					3.14					1.25					1.25					1.25				
											3.14					3.14					3.14					1.25					1.25					1.25				
											3.14					3.14					3.14					1.25					1.25					1.25				
											3.14					3.14					3.14					1.25					1.25					1.25				
											3.14					3.14					3.14					1.25					1.25					1.25				
											3.14					3.14					3.14					1.25					1.25					1.25				
											3.14					3.14					3.14					1.25					1.25					1.25				
											3.14					3.14					3.14					1.25					1.25					1.25				
											3.14					3.14					3.14					1.25					1.25					1.25				
											3.14					3.14					3.14					1.25					1.25					1.25				
											3.14					3.14					3.14					1.25					1.25					1.25				
											3.14					3.14					3.14					1.25					1.25					1.25				
											3.14					3.14					3.14					1.25					1.25					1.25				
											3.14					3.14					3.14					1.25					1.25					1.25				
											3.14					3.14					3.14					1.25					1.25					1.25				
											3.14					3.14					3.14					1.25					1.25					1.25				
											3.14					3.14					3.14					1.25					1.25					1.25				
											3.14					3.14					3.14					1.25					1.25					1.25				
											3.14					3.14					3.14					1.25					1.25					1.25				
											3.14					3.14					3.14					1.25					1.25					1.25				
											3.14					3.14					3.14					1.25					1.25					1.25				
											3.14					3.14					3.14					1.25					1.25					1.25				
											3.14					3.14					3.14					1.25					1.25					1.25				
											3.14					3.14					3.14					1.25					1.25					1.25				
											3.14					3.14					3.14					1.25					1.25					1.25				
											3.14					3.14					3.14					1.25					1.25					1.25				
											3.14					3.14					3.14					1.25					1.25					1.25				
											3.14					3.14					3.14					1.25					1.25					1.25				
											3.14					3.14					3.14					1.25					1.25					1.25				
											3.14					3.14					3.14					1.25					1.25					1.25				
											3.14					3.14					3.14					1.25					1.25					1.25				
											3.14					3.14					3.14					1.25					1.25					1.25				
											3.14					3.14					3.14					1.25					1.25					1.25				
											3.14					3.14					3.14					1.25					1.25					1.25				
											3.14					3.14					3.14					1.25					1.25					1.25				
											3.14					3.14					3.14					1.25					1.25					1.25				
											3.14					3.14					3.14					1.25					1.25					1.25				
											3.14					3.14					3.14					1.25					1.25					1.25				
											3.14					3.14					3.14					1.25					1.25					1.25				
											3.14					3.14					3.14					1.25					1.25					1.25				
											3.14					3.14					3.14					1.25					1.25					1.25				
											3.14					3.14					3.14					1.25					1.25					1.25				
											3.14					3.14					3.14					1.25					1.25					1.25				
											3.14					3.14					3.14					1.25					1.25					1.25				
											3.14					3.14					3.14					1.25					1.25					1.25				
											3.14					3.14					3.14					1.25					1.25					1.25				
											3.14					3.14					3.14					1.25					1.25					1.25				
											3.14					3.14					3.14					1.25					1.25					1.25				
											3.14					3.14					3.14					1.25					1.25					1.25				
											3.14					3.14					3.14					1.25					1.25					1.25				
											3.14					3.14					3.14					1.25					1.25					1.25				
											3.14					3.14					3.14					1.25					1.25					1.25				
											3.14					3.14					3.14					1.25					1.25					1.25				
											3.14					3.14					3.14					1.25					1.25					1.25				
											3.14					3.14					3.14					1.25					1.25					1.25				
											3.14					3.14					3.14					1.25					1.25					1.25				
											3.14					3.14					3.14					1.25					1.25					1.25				
											3.14					3.14					3.14					1.25					1.25</									

TABLE V-4 (cont.)

FILM COOLED CHAMBER

		AREA RATIO (--)										AXIAL DISTANCE (IN)										
		TC-11 TC-10 TC-9 TC-8 TC-7 TC-6 TC-5 TC-4 TC-3 TC-2 TC-1										TC-11 TC-10 TC-9 TC-8 TC-7 TC-6 TC-5 TC-4 TC-3 TC-2 TC-1										
		(F) (F) (F) (F) (F) (F) (F) (F) (F) (F)										(F) (F) (F) (F) (F) (F) (F) (F) (F) (F)										
TEST NO.	DT1 DT2 SEC	MR MR CORE TCA	PC	WT	WFC	FEC TH2	T02	(R)	(R)	ROW	(F)	TC-11	TC-10	TC-9	TC-8	TC-7	TC-6	TC-5	TC-4	TC-3	TC-2	TC-1
03-023	19.	23.	7.65	5.18	256.	3.507	.167	29.5	202.	319.	A 363.	409.	304.	304.	187.	177.	567	1049	1146.	1355.	1344.	1221.
											D 231.	332.	407.	407.	167.	307.	709	1191	1274.	1353.	1318.	0.
03-023	30.	34.	5.50	4.05	284.	3.652	.174	24.1	235.	325.	A 343.	506.	348.	322.	334.	793.	1175.	1040.	1414.	1421.	1295.	0.
											D 492.	483.	334.	313.	361.	785.	1231.	1349.	1448.	1455.	0.	0.
03-023	36.	50.	5.32	4.13	283.	3.629	.141	20.0	232.	331.	A 445.	467.	331.	415.	439.	973.	1376.	1120.	1591.	0.	1380.	0.
											D 389.	454.	310.	423.	445.	1021.	1478.	1567.	1614.	1585.	0.	0.
03-023	54.	58.	5.52	4.08	286.	3.631	.171	23.9	228.	339.	A 430.	452.	303.	333.	299.	724.	1097.	785.	1467.	1494.	1358.	0.
											D 537.	461.	336.	298.	304.	681.	1142.	1375.	1537.	1567.	0.	0.
03-024	5.	15.	5.73	3.95	480.	5.801	.339	29.0	542.	531.	A 739.	663.	716.	488.	456.	744.	1150.	1309.	1378.	1408.	0.	0.
											D 708.	813.	617.	498.	506.	805.	0.	1514.	1603.	1600.	1592.	0.
03-024	19.	23.	5.32	3.92	486.	5.805	.206	24.3	543.	529.	A 741.	669.	744.	608.	562.	922.	1305.	1460.	1547.	1564.	0.	0.
											D 722.	830.	832.	635.	650.	1012.	0.	1726.	1816.	1830.	1800.	0.
03-024	26.	34.	5.73	3.95	480.	5.801	.339	29.0	542.	528.	A 739.	661.	714.	497.	448.	732.	1119.	1274.	1390.	1455.	0.	0.
											D 700.	809.	812.	512.	500.	800.	0.	1540.	1675.	1740.	1725.	0.
04-012	5.	25.	5.21	3.83	299.	3.591	.180	24.2	550.	531.	A 610.	616.	550.	592.	555.	807.	1168.	1337.	1423.	1449.	1423.	0.
											D 696.	618.	0.	583.	546.	809.	1147.	1320.	1410.	1419.	1436.	0.
04-012	30.	45.	4.64	3.32	302.	3.602	.141	18.9	547.	521.	A 594.	600.	0.	718.	742.	1090.	1410.	1559.	1620.	1631.	1615.	0.
											D 677.	597.	567.	706.	763.	1119.	1404.	1547.	1600.	1590.	1617.	0.
04-012	49.	59.	4.73	3.83	303.	3.602	.126	16.9	544.	517.	A 588.	595.	730.	701.	879.	1263.	1555.	1666.	1698.	1695.	1638.	0.
											D 671.	591.	577.	769.	915.	1305.	1555.	1665.	1686.	1656.	1626.	0.
04-012	63.	65.	5.75	3.90	292.	3.589	.218	29.8	543.	516.	A 629.	595.	590.	492.	440.	689.	1080.	1360.	1418.	1545.	1485.	0.
											D 711.	627.	532.	492.	460.	678.	1054.	1358.	1418.	1504.	1550.	0.
04-012	68.	73.	7.05	4.81	282.	3.606	.180	29.0	542.	515.	A 689.	0.	508.	544.	513.	761.	1168.	1315.	1407.	1430.	1448.	0.
											D 757.	665.	565.	539.	513.	763.	1141.	1311.	1396.	1420.	1465.	0.
04-012	78.	94.	6.65	4.87	285.	3.596	.148	24.1	542.	515.	A 661.	0.	430.	639.	628.	935.	1328.	1480.	1552.	1564.	1553.	0.
											D 742.	656.	583.	634.	646.	964.	1328.	1495.	1554.	1547.	1577.	0.
04-014	2.	6.	4.63	3.42	449.	5.203	.204	24.1	546.	548.	A 550.	0.	0.	621.	523.	758.	1083.	1180.	1140.	1070.	1027.	0.
											D 681.	622.	593.	576.	479.	722.	1007.	1135.	1130.	1040.	1004.	0.
04-014	8.	11.	6.84	4.95	469.	5.828	.247	25.2	545.	546.	A 631.	0.	0.	701.	624.	916.	1318.	1459.	1493.	1457.	1430.	0.
											D 762.	711.	668.	684.	553.	870.	1243.	1403.	1440.	1395.	1354.	0.

Table V-4
(Sheet 2 of 13)

TABLE V-4 (cont.)

FILM COOLED CHAMBER

		AREA RATIO (--)										AXIAL DISTANCE (IN)										
		3.14		3.14		3.14		1.89		1.22		1.20		4.43		10.94		21.01		30.48		
		1.25		2.35		4.76		6.25		6.25		9.25		11.35		14.75		18.06		21.42		
TEST NO.	DT1 DT2 SEC	MR CORE	TCA	PC	WT	WFC	FFC	TH2	T02	(R)	ROW	TC-11	TC-10	TC-9	TC-8	TC-7	TC-6	TC-5	TC-4	TC-3	TC-2	TC-1
												(F)	(F)	(F)	(F)	(F)	(F)	(F)	(F)	(F)	(F)	(F)
04-018	5.	12.	3.82	3.03	286.	3.323	.156	18.9	184.	454.	A	175.	0.	0.	430.	380.	793.	1059.	1148.	1166.	1134.	1115.
											D	280.	253.	0.	427.	415.	816.	1063.	1153.	1163.	1116.	1094.
04-018	16.	24.	3.51	2.95	286.	3.313	.116	13.9	191.	433.	A	176.	0.	0.	601.	640.	1105.	1353.	1443.	1462.	1450.	1436.
											D	245.	242.	0.	588.	674.	1045.	1372.	1416.	1433.	1406.	1413.
04-018	25.	27.	3.69	3.05	281.	3.266	.157	19.4	208.	424.	A	177.	0.	0.	405.	334.	725.	1037.	1305.	1379.	1400.	1460.
											D	257.	267.	0.	410.	330.	683.	993.	1297.	1347.	1363.	1397.
04-018	30.	32.	4.27	3.13	276.	3.228	.194	24.7	213.	420.	A	214.	0.	0.	207.	222.	550.	855.	1085.	1240.	1320.	1322.
											D	300.	280.	0.	210.	223.	532.	1030.	1060.	1207.	1255.	1308.
04-018	35.	45.	5.65	4.12	277.	3.246	.156	24.6	199.	412.	A	270.	0.	0.	335.	307.	708.	1035.	1200.	1304.	1343.	1368.
											D	310.	307.	0.	360.	338.	739.	1052.	1213.	1297.	1320.	1356.
04-018	47.	58.	5.45	4.23	266.	3.202	.122	19.9	188.	407.	A	295.	0.	0.	455.	500.	951.	1281.	1405.	1455.	1475.	1480.
											D	330.	310.	0.	490.	580.	1021.	1323.	1445.	1487.	1475.	1500.
04-018	60.	70.	5.28	4.22	267.	3.106	.108	17.7	191.	404.	A	291.	0.	0.	533.	630.	112.	1428.	1530.	1568.	1566.	1558.
											D	300.	273.	0.	567.	723.	1191.	1551.	1560.	1585.	1570.	1584.
04-018	81.	91.	6.56	4.89	262.	3.262	.126	22.7	184.	406.	A	296.	0.	0.	439.	450.	925.	1301.	1425.	1492.	1504.	1514.
											D	322.	322.	0.	457.	500.	959.	1273.	1419.	1477.	1483.	1510.
04-018	94.	101.	6.06	4.77	268.	3.279	.107	18.7	192.	408.	A	272.	0.	0.	582.	630.	1150.	1530.	1605.	1645.	1631.	1615.
											D	339.	330.	0.	577.	720.	1207.	1508.	1604.	1621.	1600.	1612.

Table V-4
(Sheet 3 of 13)

TABLE V-4 (cont.)

FILM COOLED CHAMBER										BACK-SIDE TEMP									
INJECTOR FACE TEMP																			
TEST NO.	DT1 SEC	DT2 SEC	MR CORE	MR TCA	PC PSIALR/SEC	WT WFC LB/SEC (%)	FFC TH2 (P)	T02 (R)	TJ-1 (F)	TJ-2 (F)	TJ-3 (F)	ROW	TS-11 (F)	TS-10 (F)	TS-9 (F)	TS-8 (F)	TS-7 (F)	TS-6 (F)	TS-5 (F)
03-015	20.	50.	5.86	3.93	289.	3.502	.217	30.6	552.	533.	0.	921.	0.	C 430.	383.				120
												L 501.	443.						
03-015	60.	90.	5.32	3.88	295.	3.509	.179	24.9	547.	532.	0.	952.	0.	C 399.	350.				142
												L 480.	420.						
03-015	100.	130.	4.92	3.86	298.	3.514	.140	13.4	542.	532.	0.	979.	0.	C 375.	335.				156
												L 462.	401.						
03-015	145.	165.	4.26	2.93	303.	3.516	.265	29.5	533.	527.	0.	1018.	0.	C 336.	295.				181
												L 365.	430.						
03-015	173.	193.	4.01	2.92	306.	3.515	.227	25.3	529.	528.	0.	1032.	0.	C 320.	277.				300
												L 414.	350.						
03-015	200.	225.	3.79	2.95	308.	3.506	.181	20.3	522.	527.	0.	1041.	0.	C 302.	259.				385
												L 396.	332.						
03-015	245.	270.	7.21	4.84	278.	3.514	.181	30.1	525.	528.	0.	920.	0.	C 401.	507.				536
												L 470.	414.						
03-020	4.	6.	5.51	4.00	285.	3.443	.172	25.0	522.	507.	396.	544.	0.	C 326.	300.				
												L 0.	0.						
03-020	10.	14.	5.03	3.95	289.	3.440	.133	19.1	529.	511.	389.	558.	0.	C 330.	306.				
												L 0.	0.						
03-020	17.	22.	6.01	4.03	279.	3.421	.208	30.5	532.	516.	400.	558.	0.	C 356.	331.				
												L 0.	0.						
03-020	30.	50.	7.35	4.96	268.	3.434	.170	29.6	532.	517.	400.	555.	0.	C 384.	360.				
												L 0.	0.						
03-021	5.	50.	5.90	4.47	94.	1.149	.045	21.4	519.	501.	399.	439.	0.	C 513.	453.				
												L 0.	0.						
03-021	55.	105.	6.22	4.39	93.	1.152	.057	26.6	519.	493.	401.	440.	0.	C 522.	464.				
												L 0.	0.						
03-022	8.	13.	5.64	3.93	293.	3.672	.210	20.2	200.	341.	0.	0.	0.	C 0.	0.				
												L 205.	0.						
03-023	9.	14.	5.60	4.05	287.	3.675	.204	28.0	195.	321.	0.	0.	0.	C 0.	0.				
												L 52.	100.						

TABLE V-4 (cont.)

FILM COOLED CHAMBER																	
INJECTOR FACE TEMP																	
BACK-SIDE TEMP																	
TEST NO.	LT1 SEC	DT2 SEC	MR CORE	MR TCA	PC PSIALB	WT	WFC LB/SEC	FEC TH2 (%)	T02 (R)	TJ-1 (F)	TJ-2 (F)	TJ-3 (F)	TS-11 (F)	TS-1 (F)	TS-8 (F)	TS-2 (F)	TS-1 (F)
03-023	19.	23.	7.65	5.16	256.	3.507	.167	29.5	202.	319.	0.	0.	0.	0.	0.	0.	0.
03-023	30.	34.	5.50	4.05	284.	3.652	.174	24.1	235.	325.	0.	0.	0.	0.	0.	0.	0.
03-023	36.	50.	5.32	4.13	283.	3.629	.141	20.0	232.	331.	0.	0.	0.	0.	0.	0.	0.
03-023	54.	58.	5.52	4.08	286.	3.631	.171	23.9	228.	339.	0.	0.	0.	0.	0.	0.	0.
03-024	5.	16.	5.73	3.95	480.	5.801	.339	29.0	542.	531.	0.	0.	0.	0.	0.	0.	0.
03-024	19.	23.	5.32	3.92	486.	5.805	.206	24.3	543.	529.	0.	0.	0.	0.	0.	0.	0.
03-024	26.	34.	5.73	3.95	480.	5.801	.339	29.0	542.	528.	0.	0.	0.	0.	0.	0.	0.

TABLE V-4 (cont.)

FILM COOLED CHAMBER														INJECTOR FACE TEMP				BACK-SIDE TEMP				
TEST	DT1	DT2	MR	MR	PC	WT	WFC	FFC TH2	T02TJ110	TJ220	TJ310	TJ410	TJ120	TS-11	TS-10	TS-9	TS-2	TS-1				
NO.	SEC	SEC	CORE	TCA	PSIALR/SEC	(%)	(R)	(R)	(F)	(F)	(F)	(F)	(F)	(F)	(F)	(F)	(F)	(F)	(F)	(F)	(F)	(F)
04-012	5.	25.	5.21	3.83	299.	3.591	.180	24.2	550.	531	546.	760.	529.	566.	555.	813.	C	462.	398.	0.	0.	0.
																	L	472.	396.	0.	0.	0.
04-012	30.	45.	4.84	3.82	302.	3.602	.141	18.9	547.	521	537.	766.	525.	560.	551.	815.	C	442.	378.	0.	0.	0.
																	L	450.	377.	0.	0.	0.
04-012	49.	59.	4.73	3.83	303.	3.602	.126	15.9	544.	517	529.	830.	526.	547.	553.	810.	C	436.	371.	0.	0.	0.
																	L	444.	371.	0.	0.	0.
04-012	63.	65.	5.75	3.90	292.	3.589	.218	29.8	543.	515	545.	815.	528.	567.	552.	807.	C	481.	415.	0.	0.	0.
																	L	491.	412.	0.	0.	0.
04-012	68.	73.	7.05	4.81	282.	3.606	.160	22.0	542.	516	560.	790.	538.	587.	570.	810.	C	535.	461.	0.	0.	0.
																	L	541.	456.	0.	0.	0.
04-012	78.	94.	6.65	4.87	285.	3.596	.148	24.1	542.	515	555.	805.	367.	381.	567.	808.	C	518.	445.	0.	0.	0.
																	L	528.	442.	0.	0.	0.
04-014	2.	6.	4.83	3.42	449.	5.203	.284	24.1	546.	549	555.	732.	505.	564.	547.	783.	C	370.	327.	0.	0.	0.
																	L	391.	341.	0.	0.	0.
04-014	8.	11.	6.84	4.95	469.	5.826	.247	25.2	545.	546	580.	754.	505.	601.	547.	806.	C	452.	404.	0.	0.	0.
																	L	474.	420.	0.	0.	0.
04-018	5.	12.	3.82	3.03	286.	3.323	.156	18.9	184.	454	0.	190.	230.	230.	240.	200.	C	62.	40.	0.	0.	0.
																	L	74.	48.	0.	0.	0.
04-018	15.	24.	3.51	2.95	206.	3.313	.116	13.9	191.	433	3.	200.	175.	230.	240.	190.	C	59.	30.	0.	0.	0.
																	L	66.	38.	0.	0.	0.
04-018	25.	27.	3.89	3.05	281.	3.266	.157	19.4	208.	424	0.	142.	260.	265.	200.	300.	C	80.	58.	0.	0.	0.
																	L	87.	58.	0.	0.	0.
04-018	30.	32.	4.27	3.13	276.	3.228	.194	24.7	213.	420	0.	178.	220.	250.	375.	340.	C	91.	72.	0.	0.	0.
																	L	101.	77.	0.	0.	0.
04-018	35.	45.	5.65	4.12	277.	3.246	.156	24.6	199.	412	0.	187.	209.	265.	260.	259.	C	116.	128.	0.	0.	0.
																	L	120.	113.	0.	0.	0.
04-018	47.	58.	5.45	4.23	266.	3.202	.122	19.9	188.	407	0.	200.	185.	260.	270.	260.	C	116.	131.	0.	0.	0.
																	L	135.	113.	0.	0.	0.
04-018	60.	70.	5.28	4.22	257.	3.196	.108	17.7	191.	404	0.	201.	205.	175.	374.	230.	C	117.	123.	0.	0.	0.
																	L	107.	95.	0.	0.	0.
04-018	81.	91.	8.56	4.89	262.	3.262	.126	22.7	194.	406	0.	190.	227.	268.	300.	193.	C	130.	155.	0.	0.	0.
																	L	112.	137.	0.	0.	0.
04-018	94.	101.	8.06	4.77	258.	3.279	.107	19.7	192.	408	0.	193.	268.	364.	300.	206.	C	115.	130.	0.	0.	0.
																	L	119.	131.	0.	0.	0.

TEST 1680-D06-0A-013

SN 3 FILM COOLED CHAMBER

TH2C = COOLANT SUPPLY TEMPERATURE

TABLE V-4 (cont.)

FILM COOLED CHAMBER - SJ UNITS

AREA RATIO (---)																					
AXIAL DISTANCE (CM)																					
TEST NO.	DT1 SEC	DT2 SEC	MR CORE	MR TCA	PC N/CW2KG/SEC	WT WFC KG/SEC	T02 (%)	TC-11 (K)	TC-10 (K)	TC-9 (K)	TC-8 (K)	TC-7 (K)	TC-6 (K)	TC-5 (K)	TC-4 (K)	TC-3 (K)	TC-2 (K)	TC-1 (K)			
03-015	20.	50.	5.06	3.93	199.	1.580	.099	30.6	307.	296.	A 700.	636.	585.	503.	524.	642.	836.	864.	985.	1011.	969.
								D 705.	711.	663.	511.	530.	650.	852.	908.	900.	1014.	805.			
03-015	60.	90.	5.32	3.88	203.	1.592	.081	24.9	304.	296.	A 680.	623.	587.	546.	583.	742.	921.	949.	1079.	1101.	1050.
								D 701.	704.	673.	558.	600.	742.	852.	1020.	1103.	1119.	777.			
03-015	100.	130.	4.92	3.86	206.	1.594	.064	19.4	301.	295.	A 666.	610.	589.	610.	746.	958.	1085.	1149.	1224.	1224.	1151.
								D 696.	697.	683.	625.	805.	991.	1166.	1246.	1273.	1267.	995.			
03-015	143.	165.	4.26	2.93	209.	1.595	.120	29.5	296.	293.	A 641.	581.	535.	464.	473.	578.	729.	821.	901.	939.	925.
								D 696.	674.	632.	469.	479.	576.	742.	833.	898.	928.	638.			
03-015	173.	193.	4.01	2.92	211.	1.594	.103	25.3	294.	293.	A 634.	570.	529.	491.	505.	629.	776.	875.	953.	986.	968.
								D 690.	665.	633.	495.	513.	625.	788.	888.	946.	974.	660.			
03-015	200.	225.	3.79	2.95	212.	1.590	.082	20.3	290.	293.	A 625.	556.	526.	536.	593.	758.	888.	965.	1054.	1075.	1061.
								D 673.	656.	636.	541.	594.	745.	898.	1000.	1048.	1069.	729.			
03-015	245.	270.	7.21	4.84	192.	1.594	.082	30.1	292.	294.	A 613.	719.	683.	541.	557.	704.	908.	1009.	1068.	1083.	1073.
								D 664.	658.	622.	533.	566.	712.	841.	1044.	1095.	1122.	759.			
03-020	4.	6.	5.51	4.00	197.	1.562	.078	25.0	290.	281.	A 613.	572.	613.	516.	533.	711.	903.	944.	772.	570.	739.
								D 608.	638.	494.	515.	554.	719.	981.	0.	881.	755.	683.			
03-020	10.	14.	5.03	3.95	200.	1.561	.060	19.1	294.	284.	A 623.	651.	630.	601.	697.	940.	1028.	1155.	1111.	804.	0.
								D 628.	578.	513.	607.	755.	970.	1186.	0.	1116.	1089.	950.			
03-020	17.	22.	6.01	4.03	193.	1.552	.094	30.5	296.	287.	A 622.	579.	494.	481.	481.	640.	874.	960.	1002.	770.	640.
								D 608.	634.	485.	430.	515.	663.	855.	0.	0.	0.	0.			
03-020	30.	50.	7.35	4.96	185.	1.558	.077	29.6	295.	287.	A 625.	613.	594.	496.	508.	696.	985.	1100.	1101.	1100.	805.
								D 592.	589.	476.	490.	535.	732.	992.	0.	1276.	1266.	1107.			
03-021	5.	50.	5.90	4.47	65.	.521	.021	21.4	288.	278.	A 649.	594.	489.	640.	679.	876.	1033.	1090.	1105.	1075.	0.
								D 620.	613.	422.	649.	700.	917.	1100.	0.	1215.	1186.	0.			
03-021	55.	105.	6.22	4.39	64.	.523	.026	26.6	289.	274.	A 651.	599.	410.	570.	569.	722.	805.	1022.	1033.	950.	876.
								D 623.	611.	475.	576.	598.	749.	944.	0.	1122.	1096.	846.			
03-022	6.	13.	5.64	3.93	202.	1.665	.095	24.2	111.	189.	A 700.	0.	418.	351.	527.	801.	954.	919.	880.	993.	847.
								D 0.	0.	432.	379.	558.	780.	929.	950.	955.	879.	0.			
03-023	9.	14.	5.60	4.05	198.	1.667	.092	23.0	111.	178.	A 423.	481.	416.	332.	324.	531.	735.	800.	876.	841.	850.
								D 413.	507.	431.	301.	425.	623.	798.	839.	859.	815.	0.			

TABLE V-4 (cont.)

FILM COOLED CHAMBER

AREA RATIO (---)													AXIAL DISTANCE (CM)												
TEST NO.													AXIAL DISTANCE (CM)												
TEST NO.													AXIAL DISTANCE (CM)												
TEST NO.													AXIAL DISTANCE (CM)												
TEST NO.													AXIAL DISTANCE (CM)												
TEST NO.													AXIAL DISTANCE (CM)												
TEST NO.													AXIAL DISTANCE (CM)												
TEST NO.													AXIAL DISTANCE (CM)												
TEST NO.													AXIAL DISTANCE (CM)												
TEST NO.													AXIAL DISTANCE (CM)												
TEST NO.													AXIAL DISTANCE (CM)												
TEST NO.													AXIAL DISTANCE (CM)												
TEST NO.													AXIAL DISTANCE (CM)												
TEST NO.													AXIAL DISTANCE (CM)												
TEST NO.													AXIAL DISTANCE (CM)												
TEST NO.													AXIAL DISTANCE (CM)												
TEST NO.													AXIAL DISTANCE (CM)												
TEST NO.													AXIAL DISTANCE (CM)												
TEST NO.													AXIAL DISTANCE (CM)												
TEST NO.													AXIAL DISTANCE (CM)												
TEST NO.													AXIAL DISTANCE (CM)												
TEST NO.													AXIAL DISTANCE (CM)												
TEST NO.													AXIAL DISTANCE (CM)												
TEST NO.													AXIAL DISTANCE (CM)												
TEST NO.													AXIAL DISTANCE (CM)												
TEST NO.													AXIAL DISTANCE (CM)												
TEST NO.													AXIAL DISTANCE (CM)												
TEST NO.													AXIAL DISTANCE (CM)												
TEST NO.													AXIAL DISTANCE (CM)												
TEST NO.													AXIAL DISTANCE (CM)												
TEST NO.													AXIAL DISTANCE (CM)												
TEST NO.													AXIAL DISTANCE (CM)												
TEST NO.													AXIAL DISTANCE (CM)												
TEST NO.													AXIAL DISTANCE (CM)												
TEST NO.													AXIAL DISTANCE (CM)												
TEST NO.													AXIAL DISTANCE (CM)												
TEST NO.													AXIAL DISTANCE (CM)												
TEST NO.													AXIAL DISTANCE (CM)												
TEST NO.													AXIAL DISTANCE (CM)												
TEST NO.													AXIAL DISTANCE (CM)												
TEST NO.													AXIAL DISTANCE (CM)												
TEST NO.													AXIAL DISTANCE (CM)												
TEST NO.													AXIAL DISTANCE (CM)												
TEST NO.													AXIAL DISTANCE (CM)												
TEST NO.													AXIAL DISTANCE (CM)												
TEST NO.													AXIAL DISTANCE (CM)												
TEST NO.													AXIAL DISTANCE (CM)												
TEST NO.													AXIAL DISTANCE (CM)												
TEST NO.													AXIAL DISTANCE (CM)												
TEST NO.													AXIAL DISTANCE (CM)												
TEST NO.													AXIAL DISTANCE (CM)												
TEST NO.													AXIAL DISTANCE (CM)												
TEST NO.													AXIAL DISTANCE (CM)												
TEST NO.													AXIAL DISTANCE (CM)												
TEST NO.													AXIAL DISTANCE (CM)												
TEST NO.													AXIAL DISTANCE (CM)												
TEST NO.													AXIAL DISTANCE (CM)												
TEST NO.													AXIAL DISTANCE (CM)												
TEST NO.													AXIAL DISTANCE (CM)												
TEST NO.													AXIAL DISTANCE (CM)												
TEST NO.													AXIAL DISTANCE (CM)												
TEST NO.													AXIAL DISTANCE (CM)												
TEST NO.													AXIAL DISTANCE (CM)												
TEST NO.													AXIAL DISTANCE (CM)												
TEST NO.													AXIAL DISTANCE (CM)												
TEST NO.													AXIAL DISTANCE (CM)												
TEST NO.													AXIAL DISTANCE (CM)												
TEST NO.													AXIAL DISTANCE (CM)												
TEST NO.													AXIAL DISTANCE (CM)												
TEST NO.													AXIAL DISTANCE (CM)												
TEST NO.													AXIAL DISTANCE (CM)												
TEST NO.													AXIAL DISTANCE (CM)												
TEST NO.													AXIAL DISTANCE (CM)												
TEST NO.													AXIAL DISTANCE (CM)												
TEST NO.													AXIAL DISTANCE (CM)												
TEST NO.													AXIAL DISTANCE (CM)												
TEST NO.													AXIAL DISTANCE (CM)												
TEST NO.													AXIAL DISTANCE (CM)												
TEST NO.													AXIAL DISTANCE (CM)												
TEST NO.													AXIAL DISTANCE (CM)												
TEST NO.													AXIAL DISTANCE (CM)												
TEST NO.													AXIAL DISTANCE (CM)												
TEST NO.													AXIAL DISTANCE (CM)												
TEST NO.													AXIAL DISTANCE (CM)												
TEST NO.													AXIAL DISTANCE (CM)												
TEST NO.													AXIAL DISTANCE (CM)												
TEST NO.													AXIAL DISTANCE (CM)												
TEST NO.													AXIAL DISTANCE (CM)												
TEST NO.													AXIAL DISTANCE (CM)												
TEST NO.													AXIAL DISTANCE (CM)												
TEST NO.													AXIAL DISTANCE (CM)												
TEST NO.													AXIAL DISTANCE (CM)												
TEST NO.													AXIAL DISTANCE (CM)												
TEST NO.													AXIAL DISTANCE (CM)												
TEST NO.													AXIAL DISTANCE (CM)												
TEST NO.													AXIAL DISTANCE (CM)												
TEST NO.													AXIAL DISTANCE (CM)												
TEST NO.													AXIAL DISTANCE (CM)												
TEST NO.													AXIAL DISTANCE (CM)												
TEST NO.													AXIAL DISTANCE (CM)												
TEST NO.													AXIAL DISTANCE (CM)												
TEST NO.													AXIAL DISTANCE (CM)												
TEST NO.													AXIAL DISTANCE (CM)												
TEST NO.													AXIAL DISTANCE (CM)												
TEST NO.													AXIAL DISTANCE (CM)												
TEST NO.													AXIAL DISTANCE (CM)												
TEST NO.													AXIAL DISTANCE (CM)												
TEST NO.													AXIAL DISTANCE (CM)												
TEST NO.													AXIAL DISTANCE (CM)												
TEST NO.													AXIAL DISTANCE (CM)												
TEST NO.													AXIAL DISTANCE (CM)												
TEST NO.													AXIAL DISTANCE (CM)												
TEST NO.													AXIAL DISTANCE (CM)												
TEST NO.													AXIAL DISTANCE (CM)												
TEST NO.													AXIAL DISTANCE (CM)												
TEST NO.													AXIAL DISTANCE (CM)												
TEST NO.													AXIAL DISTANCE (CM)												
TEST NO.													AXIAL DISTANCE (CM)												
TEST NO.													AXIAL DISTANCE (CM)												
TEST NO.													AXIAL DISTANCE (CM)												
TEST NO.													AXIAL DISTANCE (CM)												
TEST NO.													AXIAL DISTANCE (CM)												
TEST NO.													AXIAL DISTANCE (CM)												
TEST NO.													AXIAL DISTANCE (CM)												
TEST NO.													AXIAL DISTANCE (CM)												
TEST NO.													AXIAL DISTANCE (CM)												
TEST NO.													AXIAL DISTANCE (CM)												
TEST NO.													AXIAL DISTANCE (CM)												
TEST NO.													AXIAL DISTANCE (CM)												
TEST NO.													AXIAL DISTANCE (CM)												
TEST NO.													AXIAL DISTANCE (CM)												
TEST NO.													AXIAL DISTANCE (CM)												
TEST NO.													AXIAL DISTANCE (CM)												
TEST NO.													AXIAL DISTANCE (CM)												
TEST NO.													AXIAL DISTANCE (CM)												
TEST NO.													AXIAL DISTANCE (CM)												
TEST NO.													AXIAL DISTANCE (CM)												
TEST NO.													AXIAL DISTANCE (CM)												
TEST NO.													AXIAL DISTANCE (CM)												
TEST NO.													AXIAL DISTANCE (CM)												
TEST NO.													AXIAL DISTANCE (CM)												
TEST NO.													AXIAL DISTANCE (CM)												
TEST NO.													AXIAL DISTANCE (CM)												
TEST NO.													AXIAL DISTANCE (CM)												
TEST NO.													AXIAL DISTANCE (CM)												
TEST NO.													AXIAL DISTANCE (CM)												
TEST NO.													AXIAL DISTANCE (CM)												
TEST NO.													AXIAL DISTANCE (CM)												
TEST NO.													AXIAL DISTANCE (CM)												
TEST NO.													AXIAL DISTANCE (CM)												
TEST NO.													AXIAL DISTANCE (CM)												
TEST NO.													AXIAL DISTANCE (CM)												
TEST NO.													AXIAL DISTANCE (CM)												
TEST NO.													AXIAL DISTANCE (CM)												
TEST NO.													AXIAL DISTANCE (CM)												

TABLE V-4 (cont.)

FILM COOLED CHAMBER																				
		AREA RATIO (---)																		
		AXIAL DISTANCE (CM)																		
		3.14	3.14	3.14	1.89	1.22	1.00	4.43	10.94	21.01	30.48	38.93								
		3.17	5.97	12.09	15.87	17.40	123.4928	83	37.46	45.87	54.41									
TEST NO.	DT1 SEC	DT2 SEC	MR CORE	NR TCA	PC N/C42KG/SEC	WT WFC	FFC TH2 (%)	TO2 (K)	TC-11 (K)	TC-10 (K)	TC-9 (K)	TC-8 (K)	TC-7 (K)	TC-6 (K)	TC-5 (K)	TC-4 (K)	TC-3 (K)	TC-2 (K)	TC-1 (K)	
04-018	15	12	3.82	3.03	197	1.507	.071	18.9	102	252	A 353	0	494	466	696	839	893	903	885	875
									D 411	396	0	493	485	709	848	896	901	875	863	
04-018	16	24	3.51	2.95	197	1.503	.053	13.9	106	241	A 353	0	589	611	870	1008	1057	1068	1061	1053
									D 397	390	0	582	630	836	1018	1042	1051	1036	1040	
04-018	25	27	3.89	3.05	194	1.482	.071	19.4	116	236	A 354	0	480	441	659	831	980	1021	1033	1066
									D 398	404	0	483	439	636	810	976	1004	1013	1026	
04-018	30	32	4.27	3.13	190	1.464	.088	24.7	118	233	A 374	0	370	379	561	730	858	944	989	990
									D 422	411	0	372	379	551	828	844	926	958	982	
04-018	35	45	5.65	4.12	191	1.473	.071	24.6	110	229	A 405	0	441	426	547	830	922	980	1001	1015
									D 428	426	0	455	443	663	840	929	976	989	1009	
04-018	47	58	5.45	4.23	184	1.452	.055	19.9	105	226	A 419	0	508	533	786	967	1036	1069	1075	1078
									D 439	428	0	528	578	822	993	1058	1081	1075	1089	
04-018	60	70	5.26	4.22	184	1.450	.049	17.7	106	225	A 417	0	551	605	878	1049	1105	1126	1125	1121
									D 422	407	0	570	657	920	1116	1122	1136	1128	1135	
04-018	81	91	6.56	4.89	181	1.480	.057	22.7	108	225	A 420	0	499	505	770	978	1047	1084	1091	1096
									D 434	434	0	509	531	788	964	1044	1076	1079	1094	
04-018	94	101	6.06	4.77	185	1.467	.048	18.7	107	227	A 406	0	579	605	894	1105	1147	1169	1161	1153
									D 444	439	0	576	655	926	1093	1146	1156	1144	1151	

Table V-4
(Sheet 10 of 13)

TABLE V-4 (cont.)

FILM COOLED CHAMBER										INJECTOR FACE TEMP					BACK-SIDE TEMP				
TEST No.	DT1	DT2	MR	MR	PC	WT	WFC	FFC	TH2	T02	TJ-1 (°K)	TJ-2 (°K)	TJ-3 (°K)	ROW	TS-11 (°K)	TS-10 (°K)	TS-9 (°K)	TS-8 (°K)	TS-1 (°K)
03-015	20.	50.	5.86	3.93	199.	1.588	.099	30.6	307.	296.	0.	767.	0.	C	494.	468.			
														L	534.	501.			
03-015	50.	90.	5.32	3.88	203.	1.592	.061	24.9	304.	296.	0.	784.	0.	C	477.	450.			
														L	522.	489.			
03-015	100.	130.	4.92	3.86	206.	1.594	.064	19.4	301.	295.	0.	799.	0.	C	464.	441.			
														L	512.	478.			
03-015	143.	165.	4.26	2.93	209.	1.595	.120	29.5	296.	293.	0.	821.	0.	C	442.	412.			
														L	452.	404.			
03-015	173.	193.	4.01	2.92	211.	1.594	.103	25.3	294.	293.	0.	829.	0.	C	433.	409.			
														L	445.	450.			
03-015	200.	225.	3.79	2.95	212.	1.590	.082	20.3	290.	293.	0.	834.	0.	C	423.	399.			
														L	475.	440.			
03-015	245.	270.	7.21	4.84	192.	1.594	.082	30.1	292.	294.	0.	766.	0.	C	523.	537.			
														L	516.	483.			
03-020	4.	6.	5.51	4.00	197.	1.582	.076	25.0	290.	281.	475.	556.	0.	C	436.	424.			
														L	0.	0.			
03-020	10.	14.	5.03	3.95	200.	1.561	.060	19.1	294.	284.	471.	565.	0.	C	439.	421.			
														L	0.	0.			
03-020	17.	22.	6.01	4.03	193.	1.552	.094	30.5	296.	287.	478.	565.	0.	C	453.	439.			
														L	0.	0.			
03-020	30.	50.	7.35	4.96	185.	1.558	.077	29.6	295.	287.	478.	564.	0.	C	469.	455.			
														L	0.	0.			
03-021	5.	50.	5.90	4.47	65.	.521	.021	21.4	288.	278.	477.	499.	0.	C	540.	507.			
														L	0.	0.			
03-021	55.	105.	6.22	4.39	64.	.523	.026	26.6	289.	274.	478.	500.	0.	C	545.	513.			
														L	0.	0.			
03-022	8.	13.	5.64	3.93	202.	1.665	.095	24.2	111.	189.	0.	0.	0.	C	0.	0.			
														L	369.	0.			
03-023	9.	14.	5.80	4.05	198.	1.667	.092	25.0	111.	178.	0.	0.	0.	C	0.	0.			
														L	264.	311.			

Table V-4
(Sheet 11 of 13)

TABLE V-4 (cont.)

FILM COOLED CHAMBER - SI UNITS													
INJECTOR FACE TEMP													
BACK-SIDE TEMP													
TEST	UT1	DT2	MR	MR	PC	WT	WFC	FFC	TH2	T02	TJ-1	TJ-2	TJ-3
HO.	SEC	SEC	CORE	TCA	N/CH2	KG/SEC	KG/SEC	(%)	(°K)	(°K)	(°K)	(°K)	(°K)
03-023	19.	23.	7.65	5.18	177.	1.591	.076	29.5	112.	177.	0.	0.	0.
											C	L	0.
											287.	308.	0.
03-023	30.	34.	5.50	4.05	196.	1.657	.079	24.1	130.	180.	0.	0.	0.
											C	L	0.
											208.	318.	0.
03-023	36.	50.	5.32	4.13	195.	1.646	.064	20.0	129.	184.	0.	0.	0.
											C	L	0.
											306.	315.	0.
03-023	54.	58.	5.52	4.08	197.	1.647	.078	23.9	126.	188.	0.	0.	0.
											C	L	0.
											315.	319.	0.
03-024	5.	16.	5.73	3.95	331.	2.631	.154	29.0	301.	295.	0.	0.	0.
											C	L	0.
											0.	452.	0.
03-024	19.	23.	5.32	3.92	335.	2.633	.130	24.3	302.	294.	0.	0.	0.
											C	L	0.
											0.	450.	0.
03-024	26.	34.	5.73	3.95	331.	2.631	.154	29.0	301.	293.	0.	0.	0.
											C	L	0.
											0.	452.	0.

TABLE V-4 (cont.)

FILM COOLED CHAMBER - SI UNITS

BACK-SIDE TEMP

INJECTOR FACE TEMP

TEST NO.	DT1 SEC	DT2 SEC	MR CORE	MR TCA	PC N/CM2	WT KG/SEC	WFC KG/SEC	FEC TH2 (%)	T02TJ110 (%)	TJ220 (%)	TJ310 (%)	TJ410 (%)	TJ120 (%)	RQW (%)	TS-11 (%)	TS-10 (%)	TS-9 (%)	TS-2 (%)				
04-012	5.	25.	5.21	3.83	206.	1.629	.082	24.2	305.	295	553.	678.	549.	570.	564.	707.	C	512.	476.	0.	0.	0.
																	L	518.	475.	0.		
04-012	30.	45.	4.84	3.82	209.	1.634	.064	18.9	304.	290	554.	681.	547.	566.	561.	708.	C	501.	465.	0.	0.	0.
																	L	505.	465.	0.		
04-012	49.	59.	4.73	3.83	209.	1.634	.057	16.9	302.	287	549.	716.	548.	559.	563.	705.	C	498.	461.	0.	0.	0.
																	L	502.	461.	0.		
04-012	63.	65.	5.75	3.90	201.	1.628	.099	29.8	301.	287	558.	708.	549.	570.	562.	704.	C	523.	486.	0.	0.	0.
																	L	528.	484.	0.		
04-012	68.	73.	7.05	4.81	194.	1.636	.082	29.0	301.	287	566.	694.	554.	581.	572.	705.	C	553.	511.	0.	0.	0.
																	L	556.	509.	0.		
04-012	78.	94.	6.65	4.87	196.	1.631	.067	24.1	301.	286	564.	703.	459.	467.	570.	704.	C	543.	503.	0.	0.	0.
																	L	549.	501.	0.		
04-014	2.	6.	4.63	3.42	309.	2.360	.129	24.1	303.	304	564.	662.	536.	569.	559.	690.	C	461.	437.	0.	0.	0.
																	L	473.	445.	0.		
04-014	8.	11.	8.84	4.95	323.	2.643	.112	25.2	303.	303	578.	674.	536.	589.	559.	703.	C	506.	480.	0.	0.	0.
																	L	519.	489.	0.		
04-013	5.	12.	5.82	3.03	197.	1.507	.071	18.9	102.	252	0.	361.	383.	383.	389.	366.	C	290.	278.	0.	0.	0.
																	L	296.	282.	0.		
04-013	16.	24.	3.51	2.95	197.	1.503	.053	13.9	106.	241	257.	366.	353.	383.	389.	361.	C	288.	272.	0.	0.	0.
																	L	292.	276.	0.		
04-018	25.	27.	3.89	3.05	194.	1.482	.071	19.4	116.	236	0.	334.	400.	403.	366.	422.	C	300.	288.	0.	0.	0.
																	L	304.	288.	0.		
04-018	30.	32.	4.27	3.13	190.	1.464	.088	24.7	118.	233	0.	354.	378.	394.	454.	444.	C	306.	295.	0.	0.	0.
																	L	311.	298.	0.		
04-018	35.	45.	5.65	4.12	191.	1.473	.071	24.6	110.	229	0.	359.	371.	403.	400.	399.	C	320.	326.	0.	0.	0.
																	L	322.	318.	0.		
04-018	47.	55.	5.45	4.23	184.	1.452	.055	19.9	105.	226	0.	366.	358.	400.	405.	400.	C	320.	328.	0.	0.	0.
																	L	330.	318.	0.		
04-018	60.	70.	5.28	4.22	184.	1.450	.049	17.7	106.	225	0.	367.	369.	353.	463.	383.	C	320.	324.	0.	0.	0.
																	L	315.	308.	0.		
04-018	81.	91.	8.56	4.89	181.	1.480	.057	22.7	108.	225	0.	361.	381.	415.	422.	363.	C	328.	341.	0.	0.	0.
																	L	318.	331.	0.		
04-018	94.	104.	8.66	4.77	185.	1.487	.048	19.7	107.	227	0.	363.	404.	458.	422.	370.	C	319.	328.	0.	0.	0.

Table V-4
(Sheet 13 of 13)

TABLE V-5

SUMMARY OF REGENERATIVELY COOLED CHAMBER
TEST CONDITIONS AND PERFORMANCE

TEST INJ DATE	DATA TIME	MRE	MRC	PC	TH2	TO2	TFC	WT	WFT	WO	%FC	%IG	FVAC	PA	ISV	CSTAR	%ISV	%C*	ERE	KL	BL	FCL	DL	EPL	
03-027 4 08-05-71	5.-	30.	3.1	4.4	301.	550.	539.	549.	3.50	.85	2.66	27.	.5	1446.	.8	440.	7928.	93.3	94.0	96.2	2.7.	0.	3.	18.	
03-027 4 08-05-71	15.-	30.	3.1	4.4	301.	550.	536.	549.	3.50	.84	2.66	27.	.4	1450.	.8	440.	7924.	93.4	94.0	96.2	2.7.	0.	3.	18.	
03-027 4 08-05-71	35.-	54.	3.2	4.1	302.	551.	528.	549.	3.49	.84	2.66	21.	.4	1456.	.7	442.	7970.	93.8	95.5	96.7	2.7.	0.	3.	16.	
03-027 4 08-05-71	55.-	57.	3.3	4.4	299.	550.	526.	550.	3.48	.82	2.66	25.	.4	1443.	.7	441.	7932.	93.4	94.1	96.4	3.8.	0.	3.	17.	
03-028 4 08-05-71	3.-	12.	4.1	5.4	293.	553.	547.	554.	3.52	.69	2.83	21.	.4	1408.	.1	0	433.	7700.	91.6	94.1	95.3	4.9.	0.	3.	22.
03-028 4 08-05-71	5.-	12.	4.1	5.4	294.	553.	545.	553.	3.52	.69	2.83	21.	.4	1413.	.1	0	434.	7704.	91.7	94.1	95.4	4.9.	0.	3.	22.
03-028 4 08-05-71	13.-	14.	4.2	4.8	302.	553.	541.	543.	3.50	.67	2.83	9.	.4	1454.	.8	444.	7948.	93.9	91.5	97.8	5.9.	0.	3.	11.	
03-028 4 08-05-71	15.-	18.	4.2	4.8	291.	552.	539.	544.	3.51	.67	2.83	9.	.4	1426.	.8	434.	7656.	91.8	93.8	95.5	5.9.	0.	3.	21.	
03-026 4 08-05-71	13.-	18.	4.2	4.8	295.	553.	540.	544.	3.50	.67	2.83	9.	.4	1436.	.8	438.	77654	92.6	95.2	96.3	5.9.	0.	3.	17.	
04-020 6 08-11-71	8.-	24.	4.1	4.9	290.	554.	538.	552.	3.50	.69	2.81	15.	.4	1482.	.8	448.	7638.	94.7	93.3	98.4	4.9.	0.	4.	8.	
04-020 6 08-11-71	16.-	24.	4.1	4.9	289.	555.	535.	553.	3.50	.69	2.81	15.	.4	1489.	.7	449.	7632.	94.9	93.2	98.6	4.9.	0.	4.	7.	
04-020 6 08-11-71	30.-	54.	4.1	4.7	295.	556.	530.	552.	3.50	.69	2.82	10.	.4	1506.	.7	453.	7781.	95.7	91.0	99.5	4.9.	0.	4.	3.	
04-020 6 08-11-71	60.-	71.	3.1	3.6	304.	553.	528.	552.	3.48	.84	2.64	10.	.4	1496.	.7	454.	8049.	96.3	96.4	99.2	2.8.	0.	4.	4.	
04-020 6 08-11-71	74.-	78.	4.2	4.8	297.	553.	528.	550.	3.52	.68	2.84	10.	.4	1500.	.7	450.	7790.	95.1	95.3	98.8	5.9.	0.	4.	6.	
04-020 6 08-11-71	82.-	86.	5.1	5.9	294.	551.	523.	548.	3.51	.57	2.93	10.	.4	1461.	.7	439.	7480.	92.4	94.5	97.9	6.9.	0.	3.	10.	
04-020 6 08-11-71	90.-	96.	5.2	6.3	275.	551.	529.	550.	3.49	.56	2.93	15.	.4	1430.	.6	431.	7280.	91.8	92.3	96.3	7.9.	0.	3.	18.	
04-021 6 08-11-71	4.-	15.	3.6	4.1	497.	557.	557.	555.	5.701	.25	4.46	10.	.4	2491.	.1	0	457.	8042.	96.6	96.0	99.4	2.8.	0.	4.	3.
04-021 6 08-11-71	16.-	28.	4.1	4.7	485.	557.	551.	555.	5.681	.11	4.57	10.	.4	2491.	.1	0	455.	7886.	96.0	96.2	99.2	3.8.	0.	4.	4.
04-021 6 08-11-71	23.-	23.	4.1	4.7	495.	557.	552.	555.	5.681	.11	4.58	10.	.4	2488.	.8	454.	7883.	95.9	96.2	99.1	3.8.	0.	4.	4.	
03-030 6 08-11-71	4.-	8.	4.4	4.7	96.	557.	550.	567.	1.15	.21	.94	4.	.5	508.	.0	444.	7691.	93.9	91.0	98.3	5.11.	0.	3.	8.	
03-030 6 08-11-71	10.-	19.	4.4	4.7	96.	559.	547.	565.	1.15	.21	.94	4.	.5	518.	.0	451.	7720.	95.3	95.2	99.8	5.11.	0.	4.	1.	
03-030 6 08-11-71	20.-	22.	4.4	4.9	95.	559.	546.	566.	1.15	.21	.94	7.	.5	518.	.0	450.	7634.	95.2	91.3	99.7	5.11.	0.	4.	2.	
03-030 6 08-11-71	24.-	35.	4.5	5.1	94.	560.	544.	563.	1.15	.21	.94	10.	.5	516.	.0	448.	7552.	94.7	91.3	99.2	5.11.	0.	4.	4.	
03-030 6 08-11-71	40.-	58.	4.5	5.1	94.	560.	541.	564.	1.15	.21	.94	10.	.4	498.	.1	443.	7575.	93.9	91.6	98.3	5.11.	0.	3.	8.	
03-030 6 08-11-71	65.-	70.	4.5	4.9	96.	561.	540.	564.	1.15	.21	.94	7.	.4	497.	.1	440.	7691.	93.0	95.0	97.5	5.11.	0.	3.	12.	
03-031 6 08-11-71	1.-	8.	3.1	3.5	99.	561.	547.	564.	1.16	.26	.88	9.	.4	487.	.4	445.	7887.	94.4	94.3	97.6	2.9.	0.	3.	11.	
03-033 6 08-11-71	6.-	9.	5.5	6.3	91.	557.	544.	560.	1.16	.18	.94	9.	.5	485.	.1	419.	7174.	89.7	92.1	94.9	7.11.	0.	3.	24.	
03-033 6 08-11-71	11.-	15.	5.5	6.3	90.	558.	543.	560.	1.15	.18	.97	9.	.5	490.	.1	421.	7224.	90.1	92.5	95.3	7.11.	0.	3.	22.	
03-033 6 08-11-71	15.-	48.	5.5	6.3	91.	559.	541.	558.	1.15	.18	.98	9.	.5	494.	.3	422.	7246.	90.4	92.8	95.6	7.11.	0.	3.	21.	
04-022 6 08-13-71	10.-	20.	4.5	5.1	292.	201.	385.	505.	3.57	.65	2.91	11.	.4	1458.	.7	430.	7551.	92.8	94.6	96.6	4.9.	0.	3.	16.	
04-022 6 08-13-71	14.-	20.	4.5	5.2	292.	200.	379.	494.	3.57	.65	2.92	11.	.4	1460.	.7	429.	7543.	92.6	94.6	96.5	4.9.	0.	3.	16.	
04-022 6 08-13-71	10.-	40.	4.5	5.1	292.	206.	363.	475.	3.56	.65	2.91	11.	.4	1463.	.7	430.	7556.	92.8	94.7	96.6	4.9.	0.	3.	16.	
04-022 6 08-13-71	20.-	40.	4.4	5.1	292.	209.	353.	460.	3.56	.65	2.91	11.	.4	1466.	.7	430.	7559.	92.8	94.7	96.6	4.9.	0.	3.	16.	
04-023 6 08-19-71	6.-	15.	4.4	5.0	298.	197.	377.	488.	3.58	.66	2.92	8.	.4	1471.	.8	438.	7683.	94.4	96.2	98.2	4.9.	0.	3.	8.	
04-023 6 08-19-71	18.-	24.	4.5	5.2	297.	180.	331.	438.	3.60	.66	2.95	11.	.4	1496.	.7	438.	7592.	94.5	95.2	98.3	4.9.	0.	3.	8.	
04-023 6 08-19-71	36.-	47.	3.3	3.8	311.	244.	308.	377.	3.64	.84	2.80	10.	.6	1539.	.7	446.	7871.	96.7	96.5	99.7	2.8.	0.	4.	2.	
04-023 6 08-19-71	50.-	56.	4.4	5.0	305.	222.	310.	374.	3.70	.69	3.01	10.	.4	1559.	.7	442.	7880.	95.4	94.8	99.1	2.8.	0.	4.	2.	
04-023 6 08-19-71	64.-	72.	5.6	6.7	262.	188.	326.	382.	3.63	.55	3.06	15.	.3	1459.	.6	420.	7161.	91.4	93.0	95.9	7.9.	0.	3.	19.	
04-025 6 08-20-71	6.-	10.	3.6	4.0	481.	189.	419.	505.	5.501	.22	4.38	7.	.4	2354.	.1	0	440.	7913.	95.2	97.3	97.9	1.7.	0.	3.	10.
04-025 6 08-20-71	30.-	35.	4.2	4.7	455.	262.	419.	426.	5.411	.04	4.37	8.	.4	2296.	.8	438.	7762.	94.5	96.4	97.6	2.8.	0.	3.	11.	
04-025 6 08-20-71	18.-	35.	4.1	4.6	460.	260.	416.	429.	5.451	.07	4.33	8.	.4	2316.	.8	440.	7791.	94.9	95.6	98.0	2.8.	0.	3.	10.	
03-035 6 08-26-71	20.-	25.	3.9	4.5	299.	772.	682.	641.	3.50	.71	2.79	12.	.3	1515.	.7	457.	7898.	96.5	96.1	100.0	4.9.	0.	4.	-0.	
03-035 6 08-26-71	35.-	45.	3.9	4.5	298.	705.	663.	655.	3.50	.71	2.79	12.	.3	1504.	.7	453.	7870.	95.8	95.7	99.3	4.9.	0.	4.	3.	
03-035 6 08-26-71	46.-	45.	3.9	4.5	298.	696.	658.	651.	3.51	.71	2.79	12.	.3	1504.	.7	453.	7872.	95.7	95.7	99.3	4.9.	0.	4.	3.	
03-035 6 08-26-71	120.-	135.	3.9	4.6	298.	555.	542.	566.	3.54	.72	2.82	12.	.3	1509.	.7	450.	7795.	95.1	94.8	98.6	4.9.	0.	4.	7.	
03-035 6 08-26-71	136.-	155.	3.9	4.6	298.	555.	534.	565.	3.54	.72	2.82	12.	.3	1509.	.7	450.	7794.	95.0	94.8	98.6	4.9.	0.	4.	7.	
03-035 6 08-26-71	200.-	200.	3.9	4.6	298.	562.	551.	570.	3.54	.72	2.82	12.	.3	1507.	.7	450.	7795.	95.1	94.8	98.6	4.9.	0.	4.	7.	
03-035 6 08-26-71	150.-	200.	3.9	4.6	298.	545.	527.	557.	3.54	.72	2.83	12.	.3	1500.	.7	447.	7773.	94.4	94.5	98.0	4.9.	0.	4.	10.	
03-035 6 08-26-71	190.-	200.	3.9	4.6	298.	542.	524.	554.	3.55	.72	2.83	12.	.3	1497.	.7	446.	7766.	94.2	94.5	97.7	4.9.	0.	4.	11.	
03-035 6 08-26-71	210.-	250.	3.9	4.4	301.	537.	524.	549.	3.55	.72	2.83	10.	.3	1503.	.7	447.	7840.	94.5	95.3	98.0	4.9.	0.	4.	9.	
03-035 6 08-26-71	245.-	250.	3.9	4.4	301.	536.	524.	549.	3.55	.72	2.83	10.	.3	1503.	.7	447.	7840.	94.5	95.3	98.0	4.9.	0.	4.	9.	

SUMMARY OF REGENERATIVELY COOLED CHAMBER THERMAL PROFILES

Table V-6
(Sheet 1 of 26)

TABLE V-6 (cont.)

REGENERATIVELY COOLED CHAMBER

TEST NO.	11 SEC	12 SEC	MK CORE	TCA	MR	PC	WT	WFC	FFC	TH2 (R)	T02 (R)	AREA RATIO										
												AXIAL DISTANCE (IN)										
													TC-10 (F)	TC-9 (F)	TC-8 (F)	TC-7 (F)	TC-6 (F)	TC-5 (F)	TL-4 (F)	TL-3 (F)	TL-2 (F)	TL-1 (F)
03-028	13.	18.	4.77	4.22	295.	3.504	.063	9.4	553.	540.		A	245.	1503.	1752.	1746.						
												B	0.	980.	361.	399.	0.	1554.				
												D					236.	1564.	1786.	1766.		
												L	669.		881.	350.		1500.				
04-020	8.	24.	4.94	4.10	290.	3.500	.100	14.6	554.	538.		A					160.	916.	1253.	1353.		
												B	0.	1035.	895.	413.	0.	1306.				
												D					150.	924.	1229.	1349.		
												L	743.		862.	336.		910.				
04-020	16.	24.	4.94	4.10	289.	3.500	.100	14.6	555.	536.		A					161.	943.	1333.	1456.		
												B	0.	1035.	896.	413.	0.	1416.				
												D					151.	952.	1305.	1453.		
												L	744.		862.	337.		937.				
04-020	30.	54.	4.69	4.10	295.	3.501	.071	10.4	556.	530.		A					209.	1284.	1687.	1778.		
												B	0.	1034.	888.	404.	0.	1743.				
												D					202.	1284.	1650.	1752.		
												L	733.		854.	329.		1278.				
04-020	60.	71.	3.58	3.15	304.	3.483	.086	10.3	553.	528.		A					168.	1067.	1512.	1623.		
												B	0.	938.	791.	337.	0.	1619.				
												D					160.	1071.	1493.	1602.		
												L	628.		736.	275.	1059.					
04-020	74.	78.	4.75	4.16	297.	3.519	.071	10.4	553.	528.		A					200.	1182.	1578.	1690.		
												B	0.	1037.	892.	403.	0.	1660.				
												D					192.	1177.	1543.	1597.		
												L	721.		853.	326.	1169.					
04-020	82.	86.	5.87	5.12	284.	3.505	.059	10.3	551.	528.		A					259.	1473.	1853.	1970.		
												B	0.	1046.	925.	440.	0.	1917.				
												D					249.	1456.	1792.	1787.		
												L	778.		904.	365.	1450.					
04-020	90.	96.	6.34	5.21	275.	3.490	.066	15.3	551.	528.		A					191.	1297.	1798.	1854.		
												B	0.	1021.	915.	442.	0.	1736.				
												D					180.	1288.	1742.	1740.		
												L					1274.					

TABLE V-6 (cont.)

REGENERATIVELY COOLED CHAMBER

TEST NO.	I1	I2	SEC	CORE	MR	PC	WT	WFC	FFC	TH2	T02	AREA RATIO											
												AXIAL	DISTANCE (IN)		3.59		2.66		1.48		1.00		2.77
04-021	4.	15.	4.05	3.57	497.	5.705	.126	10.1	557.	557.	557.	A	B	0.	1116.	962.	402.		190.	1035.	1320.	1396.	
												D	K										
												L	788.	989.	347.								
04-021	16.	28.	4.70	4.13	483.	5.680	.112	10.1	557.	551.	551.	A	B	0.	1194.	1037.	440.		208.	1222.	1625.	1735.	
												D	K										
												L	785.	1015.	366.								
04-021	23.	28.	4.71	4.14	485.	5.683	.111	10.1	557.	552.	552.	A	B	0.	1183.	1029.	433.		211.	1259.	1683.	1791.	
												D	K										
												L	779.	1007.	365.								
03-030	4.	8.	4.73	4.42	96.	1.148	.009	4.0	557.	550.	550.	A	B	0.	521.	458.	242.		211.	925.	793.	709.	
												D	K										
												L	534.	430.	202.								
03-030	10.	19.	4.72	4.41	96.	1.150	.009	4.0	559.	547.	547.	A	B	0.	519.	455.	240.		265.	1455.	1440.	0.	
												D	K										
												L	594.	436.	201.								
03-030	20.	22.	4.91	4.45	95.	1.149	.014	6.8	559.	546.	546.	A	B	0.	526.	461.	243.		271.	1609.	1722.	0.	
												D	K										
												L	604.	440.	203.								
03-030	24.	35.	5.08	4.46	94.	1.148	.020	9.7	560.	544.	544.	A	B	0.	540.	473.	1414.		206.	1425.	1758.	1640.	
												D	K										
												L	623.	451.	206.								
03-030	40.	58.	5.08	4.46	94.	1.147	.020	9.7	560.	541.	541.	A	B	0.	540.	474.	252.		191.	1235.	1742.	1688.	
												D	K										
												L	642.	456.	208.								

TABLE V-6 (cont.)

REGENERATIVELY COOLED CHAMBER

TEST NO.	T1 SEC	T2 SEC	CORE	MR	TCA	PC	WT	PSIA	L3/SEC	WFC	FEC	TH2 (R)	T02 (R)	ROW	AXIAL DISTANCE (IN)										AREA RATIO																																																																																																																																																																																																																																																																																																																																																																																																																																																																																																																																																																																																																																																																																																																																																																																																																																																																																																																																																																																																																																																																																																																																																																																																																																	
															TC-10 (F)	TC-9 (F)	TC-8 (F)	TC-7 (F)	TC-6 (F)	TC-5 (F)	TL-4 (F)	TL-3 (F)	TL-2 (F)	TL-1 (F)	A	B	D	K	L	A	B	D	K	L	A	B	D	K	L	A	B	D	K	L	A	B	D	K	L																																																																																																																																																																																																																																																																																																																																																																																																																																																																																																																																																																																																																																																																																																																																																																																																																																																																																																																																																																																																																																																																																																																																																																																																									
03-030	65.	70.	4.89	4.46	96.	1.148	.014	6.7	561.	540.				A		528.	464.	1367.						235.	1382.	1827.	1755.																																																																																																																																																																																																																																																																																																																																																																																																																																																																																																																																																																																																																																																																																																																																																																																																																																																																																																																																																																																																																																																																																																																																																																																																																															

TABLE V-6 (cont.)

REGENERATIVELY COOLED CHAMBER

AXIAL DISTANCE (IN)													AREA RATIO									
													3.59 2.66 1.48 1.00 2.77 5.48 11.3 21.0 30.7 38.5									
													2.80 4.40 5.20 5.80 6.90 7.70 9.80 13.1 16.4 19.9									

TABLE V-6 (cont.)

REGENERATIVELY COOLED CHAMBER

AXIAL DISTANCE (IN)													AREA RATIO													
TEST NO.	I1 SEC	I2 SEC	MR CORE	TCA	MR	PC	WT	Lb/SEC	WFC	FFC	TH2 (R)	T02 (R)	ROW	TC-10 (F)	TC-9 (F)	TC-8 (F)	TC-7 (F)	TC-6 (F)	TC-5 (F)	TL-4 (F)	TL-3 (F)	TL-2 (F)	TL-1 (F)			
04-025	18.	35.	4.56	4.08	460.	5.447	.088	8.2	250.	416.	A	B	572.	1039.	855.	1324.		106.	1324.	1708.	1763.	0.	0.			
																								D	K	L
03-035	20.	25.	4.46	3.95	299.	3.500	.071	10.0	772.	682.	A	B	959.	1228.	1057.	617.		260.	1333.	1679.	1719.	0.	0.			
																								D	K	L
03-035	35.	45.	4.54	3.92	298.	3.504	.087	12.3	705.	663.	A	B	846.	1148.	986.	533.		257.	1238.	1602.	1761.	0.	0.			
																								D	K	L
03-035	40.	45.	4.54	3.92	296.	3.505	.087	12.2	686.	658.	A	B	827.	1136.	974.	521.		255.	1204.	1666.	1743.	0.	0.			
																								D	K	L
03-035	120.	135.	4.56	3.94	298.	3.540	.088	12.2	556.	542.	A	B	679.	1018.	861.	399.		181.	1108.	1540.	1638.	0.	0.			
																								D	K	L
03-035	130.	135.	4.56	3.94	296.	3.539	.088	12.3	555.	539.	A	B	679.	1018.	861.	389.		180.	1106.	1540.	1638.	0.	0.			
																								D	K	L
03-035	60.	200.	4.55	3.93	299.	3.536	.088	12.2	562.	551.	A	B	697.	1031.	872.	396.		186.	1119.	1557.	1653.	0.	0.			
																								D	K	L
03-035	160.	200.	4.56	3.94	298.	3.545	.088	12.2	545.	527.	A	B	686.	1020.	961.	382.		174.	1115.	1555.	1646.	0.	0.			
																								D	K	L
03-035	160.	200.	4.56	3.94	298.	3.545	.088	12.2	545.	527.	A	B	686.	1020.	961.	382.		174.	1115.	1555.	1646.	0.	0.			
																								D	K	L
03-035	160.	200.	4.56	3.94	298.	3.545	.088	12.2	545.	527.	A	B	686.	1020.	961.	382.		174.	1115.	1555.	1646.	0.	0.			
																								D	K	L
03-035	160.	200.	4.56	3.94	298.	3.545	.088	12.2	545.	527.	A	B	686.	1020.	961.	382.		174.	1115.	1555.	1646.	0.	0.			
																								D	K	L
03-035	160.	200.	4.56	3.94	298.	3.545	.088	12.2	545.	527.	A	B	686.	1020.	961.	382.		174.	1115.	1555.	1646.	0.	0.			
																								D	K	L
03-035	160.	200.	4.56	3.94	298.	3.545	.088	12.2	545.	527.	A	B	686.	1020.	961.	382.		174.	1115.	1555.	1646.	0.	0.			
																								D	K	L
03-035	160.	200.	4.56	3.94	298.	3.545	.088	12.2	545.	527.	A	B	686.	1020.	961.	382.		174.	1115.	1555.	1646.	0.	0.			
																								D	K	L
03-035	160.	200.	4.56	3.94	298.	3.545	.088	12.2	545.	527.	A	B	686.	1020.	961.	382.		174.	1115.	1555.	1646.	0.	0.			
																								D	K	L
03-035	160.	200.	4.56	3.94	298.	3.545	.088	12.2	545.	527.	A	B	686.	1020.	961.	382.		174.	1115.	1555.	1646.	0.	0.			
																								D	K	L
03-035	160.	200.	4.56	3.94	298.	3.545	.088	12.2	545.	527.	A	B	686.	1020.	961.	382.		174.	1115.	1555.	1646.	0.	0.			
																								D	K	L
03-035	160.	200.	4.56	3.94	298.	3.545	.088	12.2	545.	527.	A	B	686.	1020.	961.	382.		174.	1115.	1555.	1646.	0.	0.			
																								D	K	L
03-035	160.	200.	4.56	3.94	298.	3.545	.088	12.2	545.	527.	A	B	686.	1020.	961.	382.		174.	1115.	1555.	1646.	0.	0.			
																								D	K	L
03-035	160.	200.	4.56	3.94	298.	3.545	.088	12.2	545.	527.	A	B	686.	1020.	961.	382.		174.	1115.	1555.	1646.	0.	0.			
																								D	K	L
03-035	160.	200.	4.56	3.94	298.	3.545	.088	12.2	545.	527.	A	B	686.	1020.	961.	382.		174.	1115.	1555.	1646.	0.	0.			
																								D	K	L
03-035	160.	200.	4.56	3.94	298.	3.545	.088	12.2	545.	527.	A	B	686.	1020.	961.	382.		174.	1115.	1555.	1646.	0.	0.			
																								D	K	L
03-035	160.	200.	4.56	3.94	298.	3.545	.088	12.2	545.	527.	A	B	686.	1020.	961.	382.		174.	1115.	1555.	1646.	0.	0.			
																								D	K	L
03-035	160.	200.	4.56	3.94	298.	3.545	.088	12.2	545.	527.	A	B	686.	1020.	961.	382.		174.	1115.	1555.	1646.	0.	0.			
																								D	K	L
03-035	160.	200.	4.56	3.94	298.	3.545	.088	12.2	545.	527.	A	B	686.	1020.	961.	382.		174.	1115.	1555.	1646.	0.	0.			
																								D	K	L
03-035	160.	200.	4.56	3.94	298.	3.545	.088	12.2	545.	527.	A	B	686.	1020.	961.	382.		174.	1115.	1555.	1646.	0.	0.			
																								D	K	L
03-035	160.	200.	4.56	3.94	298.	3.545	.088	12.2	545.	527.	A	B	686.	1020.	961.	382.		174.	1115.	1555.	1646.	0.	0.			
																								D	K	L
03-035	160.	200.	4.56	3.94	298.	3.545	.088	12.2	545.	527.	A	B	686.	1020.	961.	382.		174.	1115.	1555.	1646.	0.	0.			
																								D	K	L
03-035	160.	200.	4.56	3.94	298.	3.545	.088	12.2	545.	527.	A	B	686.	1020.	961.	382.		174.	1115.	1555.	1646.	0.	0.			
																								D	K	L
03-035	160.	200.	4.56	3.94	298.	3.545	.088	12.2	545.	527.	A	B	686.	1020.	961.	382.		174.	1115.	1555.	1646.	0.	0.			
																								D	K	L
03-035	160.	200.	4.56	3.94	298.	3.545	.088	12.2	545.	527.	A	B	686.	1020.	961.	382.		174.	1115.	1555.	1646.	0.	0.			
																								D	K	L
03-035	160.	200.	4.56	3.94	298.	3.545	.088	12.2	545.	527.	A	B	686.	1020.	961.	382.		174.	1115.	1555.	1646.	0.	0.			
																								D	K	L
03-035	160.	200.	4.56	3.94	298.	3.545	.088	12.2	545.	527.	A	B	686.	1020.	961.	382.		174.	1115.	1555.	1646.	0.	0.			
																								D	K	L
03-035	160.	200.	4.56	3.94	298.	3.545	.088	12.2	545.	527.	A	B	686.	1020.	961.	382.		174.	1115.	1555.	1646.	0.	0.			
																								D	K	L
03-035	160.	200.	4.56	3.94	298.	3.545	.088	12.2	545.	527.	A	B	686.	1020.	961.	382.		174.	1115.	1555.	1646.	0.	0.			
																								D	K	L
03-035	160.	200.	4.56	3.94	298.	3.545	.088	12.2	545.	527.	A	B	686.	1020.	961.	382.		174.	1115.	1555.	1646.	0.	0.			
																								D	K	L
03-035	160.	200.	4.56	3.94	298.	3.545	.088	12.2	545.	527.	A	B	686.	1020.	961.	382.		174.	1115.	1555.	1646.	0.	0.			
																								D	K	L
03-035	160.	200.	4.56	3.94	298.	3.545	.088	12.2	545.	527.	A	B	686.	1020.	961.	382.		174.	1115.	1555.	1646.	0.	0.			
																								D	K	L
03-035	160.	200.	4.56	3.94	298.	3.545	.088	12.2	545.	527.	A	B	686.	1020.	961.	382.		174.	1115.	1555.	1646.	0.	0.			
																								D	K	L
03-035	160.	200.	4.56	3.94																						

Table V-6 (cont.)

REGENERATIVELY COOLED CHAMBER

TEST NO.	I1 SEC	I2 SEC	MR CORE	TCA	MR TCA	PC	WT	WFC LB/SEC	FFC (%)	TH2 (R)	T02 (R)	AXIAL DISTANCE (IN)										AREA RATIO	
												TC-10 (F)	TC-9 (F)	TC-8 (F)	TC-7 (F)	TC-6 (F)	TC-5 (F)	TL-4 (F)	TL-3 (F)	TL-2 (F)	TL-1 (F)	3.59	2.66
03-035	195.	200.	4.57	3.95	293.	3.547	.089	12.3	542.	524.	A	171. 1114. 1555. 1644. 0. 170. 1164. 1609. 1713. 1119.										1.48	
												171. 1114. 1555. 1644. 0. 170. 1164. 1609. 1713. 1119.										5.80	
												171. 1114. 1555. 1644. 0. 170. 1164. 1609. 1713. 1119.										5.80	
												171. 1114. 1555. 1644. 0. 170. 1164. 1609. 1713. 1119.										5.80	
03-035	210.	250.	4.44	3.93	301.	3.548	.072	10.0	537.	523.	A	199. 1285. 1701. 1726. 0. 199. 1364. 1743. 1838. 1316.										1.00	
												199. 1285. 1701. 1726. 0. 199. 1364. 1743. 1838. 1316.										1.00	
												199. 1285. 1701. 1726. 0. 199. 1364. 1743. 1838. 1316.										1.00	
												199. 1285. 1701. 1726. 0. 199. 1364. 1743. 1838. 1316.										1.00	
03-035	245.	250.	4.44	3.93	301.	3.547	.072	10.0	536.	522.	A	200. 1294. 1718. 1724. 0. 200. 1374. 1803. 1950. 1329.										1.00	
												200. 1294. 1718. 1724. 0. 200. 1374. 1803. 1950. 1329.										1.00	
												200. 1294. 1718. 1724. 0. 200. 1374. 1803. 1950. 1329.										1.00	
												200. 1294. 1718. 1724. 0. 200. 1374. 1803. 1950. 1329.										1.00	

Table V-6 (cont.)

REGENERATIVELY COOLED CHAMBER													INJECTOR FACE TEMP				BACK-SIDE TEMP			
TEST NO.	T1 SEC	T2 SEC	MR CORE	MR TCA	PC PSIALB/SEC	WT	WFC LB/SEC	FFC (%)	TH2 (R)	T02 (R)	INJECTOR FACE TEMP				BACK-SIDE TEMP					
											TJ110 (F)	TJ220 (F)	TJ310 (F)	TJ410 (F)	TJ120 (F)	ROW A	TS-9 (F)	TS-8 (F)	TS-2 TS-1 (F)	
03-027	5.	30.	4.45	3.14	301.	3.503	.232	27.4	550.	539.	0.	442.	0.	0.	431.	A	328.	311.	113. 104.	
																L	369.	351.		
03-027	15.	30.	4.45	3.15	301.	3.501	.231	27.3	550.	536.	0.	442.	0.	0.	433.	A	328.	311.	121. 105.	
																L	370.	351.		
03-027	35.	54.	4.13	3.18	302.	3.494	.177	21.2	551.	528.	0.	451.	0.	0.	441.	A	329.	311.	198. 143.	
																L	374.	355.		
03-027	55.	57.	4.44	3.25	299.	3.478	.204	24.9	550.	526.	0.	445.	0.	0.	437.	A	331.	315.	253. 183.	
																L	377.	359.		
03-028	3.	12.	5.36	4.11	293.	3.516	.145	21.1	553.	547.	0.	469.	0.	0.	469.	A	398.	388.	105. 100.	
																L	442.	429.		
03-028	5.	12.	5.36	4.11	294.	3.519	.145	21.1	553.	545.	0.	474.	0.	0.	474.	A	402.	390.	107. 101.	
																L	448.	431.		
03-028	13.	14.	4.80	4.24	302.	3.502	.063	9.4	553.	541.	0.	481.	0.	0.	479.	A	392.	374.	120. 103.	
																L	436.	409.		
03-028	15.	18.	4.76	4.21	291.	3.505	.063	9.4	552.	539.	0.	507.	0.	0.	510.	A	399.	371.	127. 103.	
																L	422.	397.		
03-028	13.	18.	4.77	4.22	295.	3.504	.063	9.4	553.	540.	0.	496.	0.	0.	497.	A	396.	373.	124. 103.	
																L	427.	402.		
04-020	8.	24.	4.94	4.10	290.	3.500	.100	14.6	554.	538.	0.	1018.	992.	862.	877.	A	423.	399.	116. 102.	
																L	433.	408.		
04-020	16.	24.	4.94	4.10	289.	3.500	.100	14.6	555.	536.	0.	1023.	994.	855.	873.	A	424.	399.	125. 102.	
																L	434.	409.		
04-020	30.	54.	4.69	4.10	295.	3.501	.071	10.4	556.	530.	0.	985.	1005.	852.	844.	A	415.	390.	222. 171.	
																L	424.	397.		

Table V-6 (cont.)

REGENERATIVELY COOLED CHAMBER

TEST NO.	T1 SEC	T2 SEC	MR CORE	MR TCA	PC PSIALB/SEC	WT LB/SEC	WFC %	FFC %	TH2 (R)	TC2 (R)	INJECTOR FACE TEMP					BACK-SIDE TEMP					
											TJ110 (F)	TJ220 (F)	TJ310 (F)	TJ410 (F)	TJ120 (F)	ROW A	TS-9 (F)	TS-8 (F)	TS-2 (F)	TS-1 (F)	
04-020	60.	71.	3.58	3.15	304.	3.483	.086	10.3	553.	528.	0.	758.	1040.	801.	524.	A	B	350.	322.	387.	394.
																L	B	351.	318.		
04-020	74.	78.	4.75	4.16	297.	3.519	.071	10.4	553.	529.	0.	924.	1020.	838.	809.	A	B	413.	389.	459.	495.
																L	B	418.	395.		
04-020	82.	86.	5.87	5.12	284.	3.505	.059	10.3	551.	528.	0.	985.	1006.	867.	866.	A	B	460.	431.	511.	550.
																L	B	473.	451.		
04-020	90.	96.	6.34	5.21	275.	3.490	.086	15.3	551.	528.	0.	1027.	1000.	871.	890.	A	B	473.	440.	575.	608.
																L	B	491.	467.		
04-021	4.	15.	4.05	3.57	497.	5.705	.126	10.1	557.	557.	0.	646.	878.	630.	501.	A	B	344.	307.	204.	189.
																L	B	371.	323.		
04-021	16.	28.	4.70	4.13	485.	5.680	.112	10.1	557.	551.	0.	652.	833.	653.	545.	A	B	382.	345.	299.	213.
																L	B	398.	352.		
04-021	23.	28.	4.71	4.14	485.	5.683	.111	10.1	557.	552.	0.	583.	829.	651.	490.	A	B	381.	344.	328.	226.
																L	B	397.	350.		
03-030	4.	8.	4.73	4.42	96.	1.148	.009	4.0	557.	550.	0.	777.	1296.	678.	711.	A	B	396.	342.	106.	104.
																L	B	385.	334.		
03-030	10.	19.	4.72	4.41	96.	1.150	.009	4.0	559.	547.	0.	878.	1411.	735.	815.	A	B	407.	343.	111.	112.
																L	B	410.	342.		
03-030	20.	22.	4.91	4.45	95.	1.149	.014	6.8	559.	546.	0.	895.	1408.	747.	833.	A	B	413.	349.	123.	128.
																L	B	417.	347.		
03-030	24.	35.	5.08	4.46	94.	1.148	.020	9.7	560.	544.	0.	1758.	1839.	1425.	1433.	A	B	431.	363.	0.	0.
																L	B	435.	360.		
03-030	40.	58.	5.08	4.46	94.	1.147	.020	9.7	560.	541.	0.	921.	1430.	773.	838.	A	B	434.	365.	375.	370.
																L	B	447.	368.		

Table V-6 (cont.)

REGENERATIVELY COOLED CHAMBER													INJECTOR FACE TEMP					BACK-SIDE TEMP				
TEST NO.	11 SEC	T2 SEC	MR CORE	MR TCA	PC PSIALR/SEC	WT	WFC LB/SEC	FFC (%)	TH2 (R)	T02 (R)	INJECTOR FACE TEMP					BACK-SIDE TEMP						
											TJ110 (F)	TJ220 (F)	TJ310 (F)	TJ410 (F)	TJ120 (F)	ROW A	TS-9 (F)	TS-8 (F)	TS-2 TS-1 (F)			
03-030	65.	70.	4.89	4.46	96.	1.148	.014	6.7	561.	540.	1760.	1700.	1930.	1440.	1375.	A	423.	355.	1700.			
																B	437.	360.				
																L						
03-031	1.	8.	3.48	3.09	99.	1.163	.027	9.4	561.	547.	0.	356.	1311.	626.	409.	A	321.	288.	372.			
																B	348.	303.	137.			
																L						
03-033	6.	9.	6.35	5.54	91.	1.165	.017	9.3	557.	544.	0.	534.	984.	690.	547.	A	490.	425.	161.			
																B	506.	427.	104.			
																L						
03-033	11.	15.	6.25	5.46	90.	1.153	.017	9.3	558.	543.	0.	814.	1111.	762.	779.	A	499.	418.	146.			
																B	505.	417.	90.			
																L						
03-033	15.	48.	6.27	5.47	91.	1.154	.017	9.3	559.	541.	0.	919.	1258.	805.	874.	A	509.	422.	124.			
																B	509.	419.	75.			
																L						
04-022	10.	20.	5.14	4.46	292.	3.569	.072	11.0	201.	385.	0.	331.	295.	276.	261.	A	190.	167.	108.			
																B	192.	171.	104.			
																L						
04-022	14.	20.	5.18	4.49	292.	3.572	.072	11.0	200.	379.	0.	317.	290.	272.	255.	A	187.	166.	114.			
																B	189.	170.	103.			
																L						
04-022	10.	40.	5.14	4.45	292.	3.562	.071	10.9	206.	363.	0.	330.	297.	274.	264.	A	187.	161.	153.			
																B	191.	162.	124.			
																L						
04-022	20.	40.	5.13	4.45	292.	3.558	.071	10.9	209.	353.	0.	329.	298.	273.	266.	A	186.	158.	176.			
																B	190.	157.	134.			
																L						
04-023	6.	15.	4.96	4.44	298.	3.580	.053	8.1	197.	377.	0.	294.	291.	265.	245.	A	171.	149.	104.			
																B	181.	163.	103.			
																L						
04-023	18.	24.	5.17	4.49	297.	3.603	.071	10.8	190.	331.	0.	286.	276.	250.	225.	A	166.	144.	164.			
																B	179.	159.	115.			
																L						
04-023	36.	47.	3.82	3.32	311.	3.641	.086	10.2	244.	308.	0.	318.	303.	264.	215.	A	116.	87.	331.			
																B	137.	103.	305.			
																L						

Table V-6 (cont.)

REGENERATIVELY COOLED CHAMBER														INJECTOR FACE TEMP						BACK-SIDE TEMP					
TEST NO.	T1 SEC	T2 SEC	MR CORE	MR TCA	PC PSIALB/SEC	WT	WFC LB/SEC	FFC (%)	TH2 (R)	T02 (R)	TJ110 TJ220 TJ310 TJ410 TJ120						TS-9 TS-8 TS-2 TS-1								
											(F)	(F)	(F)	(F)	(F)	A	(F)	(F)	(F)	(F)	(F)	(F)	(F)	(F)	(F)
04-023	50.	56.	4.99	4.37	305.	3.703	.071	10.3	222.	310.	0.	352.	322.	289.	200.	A	182.	144.	407.	416.					
																B	205.	170.							
04-023	64.	72.	6.75	5.56	282.	3.632	.086	15.5	188.	326.	0.	323.	324.	306.	297.	A	241.	219.	549.	557.					
																B	266.	246.							
04-025	6.	10.	3.95	3.60	481.	5.604	.088	7.2	189.	415.	0.	184.	324.	299.	142.	A	71.	41.	96.	100.					
																B	74.	34.							
04-025	30.	35.	4.70	4.20	455.	5.407	.088	8.5	262.	419.	0.	253.	305.	297.	204.	A	147.	119.	165.	100.					
																B	174.	121.							
04-025	18.	35.	4.56	4.08	460.	5.447	.088	8.2	260.	416.	1807.	1708.	1713.	1324.	881.	A	143.	113.	0.	1823.					
																B	162.	114.							
03-035	20.	25.	4.46	3.95	299.	3.500	.071	10.0	772.	682.	0.	1094.	988.	937.	1043.	A	616.	582.	108.	112.					
																B	630.	600.							
03-035	35.	45.	4.54	3.92	298.	3.504	.087	12.3	705.	663.	0.	680.	863.	819.	677.	A	533.	502.	234.	243.					
																B	548.	518.							
03-035	40.	45.	4.54	3.92	296.	3.505	.087	12.2	696.	659.	0.	591.	843.	803.	603.	A	521.	490.	260.	268.					
																B	536.	507.							
03-035	120.	135.	4.56	3.94	290.	3.540	.088	12.2	556.	542.	0.	421.	663.	615.	439.	A	396.	368.	639.	737.					
																B	410.	384.							
03-035	130.	135.	4.56	3.94	290.	3.539	.088	12.3	555.	539.	0.	416.	662.	614.	439.	A	395.	367.	644.	748.					
																B	409.	382.							
03-035	60.	200.	4.55	3.93	299.	3.536	.088	12.2	562.	551.	0.	601.	676.	626.	477.	A	403.	374.	613.	706.					
																B	415.	389.							
03-035	160.	200.	4.56	3.94	290.	3.545	.088	12.2	545.	527.	0.	611.	662.	607.	469.	A	391.	362.	666.	774.					
																B	405.	379.							

Table V-6 (cont.)

REGENERATIVELY COOLED CHAMBER

TEST NO.	T1 SEC	T2 SEC	MR CORE	MR TCA	PC PSIALB/SEC	WT LB/SEC	WFC LB/SEC	FFC (%)	TH2 (R)	T02 (R)	INJECTOR FACE TEMP					BACK-SIDE TEMP				
											TJ110 (F)	TJ220 (F)	TJ310 (F)	TJ410 (F)	TJ120 (F)	ROW	TS-9 (F)	TS-8 (F)	TS-2 (F)	TS-1 (F)
03-035	195.	200.	4.57	3.95	298.	3.547	.0033	12.3	542.	524.	0.	609.	659.	603.	457.	A	389.	350.	668.	785.
																B	402.	376.		
																L				
03-035	210.	250.	4.44	3.93	301.	3.548	.072	10.0	537.	523.	0.	604.	650.	592.	441.	A	378.	349.	677.	816.
																B	391.	364.		
																L				
03-035	245.	250.	4.44	3.93	301.	3.547	.072	10.0	536.	522.	0.	603.	648.	589.	416.	A	377.	347.	688.	844.
																B	389.	362.		
																L				

Table V-6 (cont.)

SN 3 REGENERATIVELY COOLED CHAMBER SUMMARY

DATA		DISTANCE FROM INJECTOR (IN.)							TEMPERATURE (°F)											
TEST NO.	PERIOD SEC	MR CORE	MR TCA	PC PSIA	WT LB/SEC	WFC LB/SEC (%)	FFC (%)	TH2/T02 (°R)	.97	2.96	4.07	4.57	5.50	5.92	7.07	8.07	9.20	12.53	13.86	19.19
06-015	9-13	4.10	3.77	94.8	1.12	.019	8.1		666	477	428	434	224	179	175	210	144	575	--	--
									635	481	446	221	389	189	210	274	165	580	--	--
06-015	20-28	5.16	4.76	91.3	1.12	.015	7.7	515/	714	530	517	517	304	221	252	261	188	820	--	--
									711	546	584	253	461	233	253	327	216	835	--	1125
06-015	35-40	6.19	5.73	88.1	1.12	.012	7.4		776	590	586	602	273	269	260	327	238	912	--	--
									777	607	554	287	534	279	300	387	266	983	--	1422
06-015	45-52	4.22	3.81	195	2.29	.045	9.5		741	566	533	502	254	240	267	324	206	760	--	--
									702	580	508	258	576	268	349	420	244	777	--	1397
06-015	60-66	5.30	4.81	187	2.29	.036	9.2	525/	761	609	589	562	295	258	255	315	205	903	--	--
									754	624	553	280	625	287	349	440	264	879	--	1497
06-015	80-85	6.37	5.80	180	2.29	.030	8.9		784	643	640	627	336	274	267	330	221	1126	--	--
									798	662	597	309	674	306	358	461	289	1086	--	1716
06-015	95-100	5.45	4.92	287	3.51	.058	9.8	525/	800	689	664	642	327	360	382	439	276	909	--	--
									799	718	617	331	813	390	456	532	291	910	--	1612
06-015	110-116	6.57	5.94	276	3.52	.049	9.6		801	712	706	690	352	351	386	458	299	1087	--	--
									821	745	651	356	845	396	480	479	326	1046	--	1733
06-015	123-127	4.34	3.91	301	3.51	.071	9.9		791	649	609	595	301	347	364	402	236	723	--	--
									755	674	575	310	770	367	405	454	234	727	--	1433
06-017	34-47	5.65	5.09	389	6.68	.079	10.3	526/490	827	765	676	741	389	458	454	491	284	912	--	1671
									831	799	734	410	984	474	507	565	283	881	--	1642
06-017	32-36	5.61	5.0	490	5.97	.094	9.6	532/	856	833	796	836	451	557	539	576	323	1058	--	--
									863	865	734	--	1171	563	598	669	327	1029	--	1736
06-018	140-150	5.77	5.19	295	3.69	.060	10.1	217/375	419	461	451	475	185	199	175	296	120	916	--	1600
									473	495	382	--	654	180	289	390	125	887	--	1700
06-018	174-179	5.45	4.94	191	2.38	.038	9.4	194/359	374	363	320	341	120	140	130	135	93	936	--	1544
									393	376	310	--	469	116	147	297	127	883	--	1646
06-018	214-217	4.06	3.70	99	1.16	.022	9.0	235/366	393	282	220	200	91	90	83	89	18	719	--	1287
									375	267	212	125	227	81	80	91	33	697	--	1360
06-018	241-245	4.10	4.06	100	1.16	.022	8.9	229/360	389	283	213	199	80	80	86	89	25	673	--	1231
									250	264	218	117	209	80	80	91	89	638	--	1274
06-018	255-258	5.08	4.63	98	1.17	.018	8.7	229/346	390	298	255	221	103	100	96	97	27	833	--	1309
									397	300	242	--	271	100	98	100	39	834	--	1367
06-018	281-284	5.79	5.24	413	5.05	.078	9.7	258/367	510	565	515	578	214	275	286	333	122	982	--	1677
									535	585	477	--	807	264	340	418	124	931	--	1790
06-018	298-304	7.25	6.36	389	5.08	.084	12.3	244/361	488	568	561	600	256	287	290	330	127	939	--	1707
									542	600	478	--	858	288	358	429	135	902	--	1820
06-018	322-329	7.13	6.35	283	3.68	.054	10.9	246/355	468	495	487	488	200	224	261	344	171	1062	--	1706
									518	525	428	--	713	232	353	465	198	1000	--	1790

Table V-6
(Sheet 13 of 26)

Table V-6 (cont.)

SN 3 REGENERATIVELY COOLED CHAMBER SUMMARY

TEST NO.	DATA PERIOD SEC	MR		PC	WT		WFC	FFC (%)	TS-12	TS-11	TL-10	TL-8	TL-7	S-6	S-5
		CORE	TCA		LB/SEC	LB/SEC									
06-015	9-13	4.10	3.77	94.8	1.12	.019	8.1	501 471	355	185	137	177	174	239	
06-015	20-28	5.16	4.76	91.3	1.12	.015	7.7	554 548	407	230	176	--	213	289	
06-015	35-40	6.19	5.73	88.1	1.12	.012	7.4	621 619	464	272	219	--	258	344	
06-015	45-52	4.22	3.81	195	2.29	.045	9.5	479 446	349	172	124	--	246	343	
06-015	60-66	5.30	4.81	187	2.29	.036	9.2	510 505	391	201	142	158	254	362	
06-015	80-85	6.37	5.80	180	2.29	.030	8.9	557 557	432	230	166	216	269	381	
06-015	95-100	5.45	4.92	287	3.51	.058	9.8	489 482	419	190	142	184	303	423	
06-015	110-116	6.57	5.94	276	3.52	.049	9.6	519 528	418	212	152	201	332	471	
06-015	123-127	4.34	3.91	301	3.51	.071	9.9	450 426	345	166	131	165	267	362	
06-016	34-47	5.65	5.09	389	6.68	.079	10.3	454 461	384	192	148	190	--	--	
06-017	32-36	5.61	5.07	490	5.97	.094	9.6	490 490	464	203	161	211	372	514	
06-018	140-150		5.19	295				169 199	153	-56	-100	-32	137	228	
06-018	174-179		4.94	191				197 204	152	-62	-99	-28	88	180	
06-018	214-217		3.70	99				250 251	157	-47	-70	-18	47	67	
06-018	214-245		4.06	100				243 205	150	-56	-81	-25	45	64	
06-018	255-268		4.63	98				260 256	171	-28	-57	-7	71	76	
06-018	281-284		5.24	413				197 189	164	-40	-95	-31	119	159	
06-018	298-304	6.	6.36	389				209 232	191	-17	-77	-6	179	273	
06-018	322-329		6.35	283				232 258	195	-15	-70	11	200	279	

21:13:18

SY UNITS: 73

Table V-6
(Sheet 15 of 26)

21:13:19

09 MAR 72

Table V-6 (cont.)

REGENERATIVELY COOLED CHAMBER - SI UNITS

TEST NO.	T1 SEC	T2 SEC	MR CORE	MR TCA	PC N/CM2	WT KG/SEC	WFC KG/SEC	FFC (%)	TH2 (K)	T02 (K)	AXIAL DISTANCE (CM)										AREA RATIO																																																																																																																																																																																																																																																																																																																																																																																																																																																																																																																																																																																																																																																																																																																																																																																																																																																																																																																																																																																																																																																																																																																																																																																																																																																																																																												
											TC-10 (K)	TC-9 (K)	TC-8 (K)	TC-7 (K)	TC-6 (K)	TC-5 (K)	TL-4 (K)	TL-3 (K)	TL-2 (K)	TL-1 (K)	A	B	D	K	L	A	B	D	K	L																																																																																																																																																																																																																																																																																																																																																																																																																																																																																																																																																																																																																																																																																																																																																																																																																																																																																																																																																																																																																																																																																																																																																																																																																																																																																																			
03-028	13.	18.	4.77	4.22	203.	1.590	.028	9.4	307.	300.	A						391.	1090.	1229.	1225.																																																																																																																																																																																																																																																																																																																																																																																																																																																																																																																																																																																																																																																																																																																																																																																																																																																																																																																																																																																																																																																																																																																																																																																																																																																																																																													</

Table V-6
(Sheet 16 of 26)

Table V-6 (cont.)

REGENERATIVELY COOLED CHAMBER - SI UNITS

TEST No.	I1 SEC	I2 SEC	CORE TCA	MR N/CM2	PC WT	WEC KG/SEC	FFC (%)	T02 (K)	AREA RATIO									
									AXIAL DISTANCE (CM)	3.59	2.66	1.48	1.00	2.77	5.44	11.3	21.0	30.7
TEST No.	I1 SEC	I2 SEC	CORE TCA	MR N/CM2	PC WT	WEC KG/SEC	FFC (%)	T02 (K)	ROW (K)	TC-9 (K)	TC-8 (K)	TC-7 (K)	TC-6 (K)	TC-5 (K)	TL-4 (K)	TL-3 (K)	TL-2 (K)	TL-1 (K)
04-021	4.	15.	4.05	3.57	343.	2.588	.057	10.1	309.	310.	A	0.	875.	790.	478.	361.	830.	989.
04-021	16.	28.	4.70	4.13	335.	2.577	.051	10.1	309.	306.	A	0.	919.	832.	500.	371.	934.	1158.
04-021	23.	28.	4.71	4.14	335.	2.578	.051	10.1	310.	307.	A	0.	912.	827.	498.	372.	955.	1190.
03-030	4.	8.	4.73	4.42	66.	.521	.004	4.0	309.	306.	A	0.	545.	510.	390.	372.	769.	649.
03-030	10.	19.	4.72	4.41	60.	.522	.004	4.0	310.	304.	A	0.	544.	508.	389.	402.	1064.	1055.
03-030	20.	22.	4.91	4.45	60.	.521	.007	6.8	311.	303.	A	0.	548.	512.	391.	406.	1149.	1212.
03-030	24.	35.	5.08	4.46	65.	.521	.009	9.7	311.	302.	A	0.	555.	518.	1041.	370.	1047.	1232.
03-030	40.	58.	5.03	4.46	65.	.520	.009	9.7	311.	300.	A	0.	555.	519.	395.	362.	942.	1223.

Table V-6 (cont.)

REGENERATIVELY COOLED CHAMBER - SI UNITS

AREA RATIO																							
AXIAL DISTANCE (CM)																							
TEST NO.	T1 SEC	T2 SEC	MR CORE	MR TCA	PC N/CM2	WT KG/SEC	WFC KG/SEC	FFC (%)	TH2 (K)	T02 (K)	AXIAL DISTANCE (CM)												
											TC-10 (K)	TC-9 (K)	TC-8 (K)	TC-7 (K)	TC-6 (K)	TC-5 (K)	TL-4 (K)	TL-3 (K)	TL-2 (K)	TL-1 (K)			
03-030	65.	70.	4.49	4.46	66.	.521	.006	6.7	312.	300.	A												
											B	0.	549.	513.	1015.								
											D												
											K	606.											
03-031	1.	8.	3.40	3.09	69.	.528	.012	9.4	312.	304.	A												
											B	0.	503.	471.	386.								
											D												
											K												
03-033	6.	9.	6.35	5.54	62.	.528	.008	9.3	310.	302.	A												
											B	0.	503.	471.	386.								
											D												
											K												
03-033	11.	15.	6.25	5.46	62.	.523	.008	9.3	310.	302.	A												
											B	0.	503.	471.	386.								
											D												
											K												
03-033	15.	48.	6.27	5.47	62.	.523	.007	9.3	311.	301.	A												
											B	0.	503.	471.	386.								
											D												
											K												
04-022	10.	20.	5.14	4.46	201.	1.619	.033	11.0	112.	214.	A												
											B	527.	723.	640.	340.								
											D												
											K												
04-022	14.	20.	5.18	4.49	201.	1.620	.033	11.0	111.	210.	A												
											B	525.	722.	639.	339.								
											D												
											K												
04-022	10.	40.	5.14	4.45	201.	1.616	.032	10.9	115.	202.	A												
											B	528.	722.	639.	339.								
											D												
											K												

Table V-6
(Sheet 18 of 26)

Table V-6 (cont.)

REGENERATIVELY COOLED CHAMBER - SI UNITS

[illegible]

Table V-6 (cont.)

REGENERATIVELY COOLED CHAMBER - SI UNITS

[illegible]

Table V-6 (cont.)

REGENERATIVELY COOLED CHAMBER - SI UNITS																			
		AREA RATIO		AXIAL DISTANCE (CM)		TC-1		TC-2		TC-3		TC-4		TC-5		TC-6		TC-7	
		3.59 2.66		1.48 1.00		2.77 5.48		11.3 21.0		30.7 38.5		41.7 50.5							
		7.11 11.1A		13.21 14.73		17.53 19.56		24.89 33.3		33.3 41.7		41.7 50.5							
TEST NO.	T1 SEC	T2 SEC	MR CORE	TCA	PC	WT	WFC	FFC	TH2	TH1	TC-1 (K)	TC-2 (K)	TC-3 (K)	TC-4 (K)	TC-5 (K)	TC-6 (K)	TC-7 (K)	TC-8 (K)	TC-9 (K)
03-035 195. 200. 4.57 3.95 205. 1.609 .040 12.3 301. 291.																			
		A		B		C		D		E		F		G		H		I	
		635.		821.		732.		466.		351.		874.		1119.		1169.			
		D		K		L				350.		902.		1149.		1207.			
		K		L				432.											
		A		B		C		D		E		F		G		H		I	
		630.		817.		727.		461.		366.		969.		1200.		1214.			
		D		K		L				366.		1013.		1246.		1276.			
		K		L				427.											
		A		B		C		D		E		F		G		H		I	
		630.		816.		727.		460.		366.		975.		1210.		1213.			
		D		K		L				366.		1019.		1257.		1283.			
		K		L				426.											
		A		B		C		D		E		F		G		H		I	
		644.		708.		426.													
		K		L															

Table V-6 (cont.)

REGENERATIVELY COOLED CHAMBER														INJECTOR FACE TEMP						BACK-SIDE TEMP					
TEST NO.	T ₁ SEC	T ₂ SEC	MR CORE	MR TCA	PC N/CM ²	WT KG/SEC	WFC KG/SEC	FFC (%)	TH ₂ (°K)	T _{O2} (%)	INJECTOR FACE TEMP						BACK-SIDE TEMP								
											TJ110 (°K)	TJ220 (°K)	TJ310 (°K)	TJ410 (°K)	TJ120 (°K)	ROW	TS-9 (°K)	TS-8 (°K)	TS-2 (°K)	TS-1 (°K)					
03-027	5.	30.	4.45	3.14	207.	1.589	.105	27.4	306.	300.	0.	501.	0.	0.	495.	A	437.	428.	318.	313.					
																B	461.	450.							
																L									
03-027	15.	30.	4.45	3.15	207.	1.588	.105	27.3	306.	298.	0.	501.	0.	0.	496.	A	438.	428.	323.	314.					
																R	461.	451.							
																L									
03-027	35.	54.	4.13	3.18	208.	1.585	.080	21.2	306.	293.	0.	506.	0.	0.	501.	A	438.	428.	366.	335.					
																B	463.	453.							
																L									
03-027	55.	57.	4.44	3.25	206.	1.578	.093	24.9	306.	292.	0.	503.	0.	0.	498.	A	440.	431.	306.	357.					
																B	465.	455.							
																L									
03-028	3.	12.	5.36	4.11	202.	1.595	.056	21.1	307.	304.	0.	516.	0.	0.	516.	A	476.	471.	314.	311.					
																B	501.	494.							
																L									
03-028	5.	12.	5.36	4.11	202.	1.596	.056	21.1	307.	303.	0.	519.	0.	0.	519.	A	479.	472.	315.	311.					
																B	504.	495.							
																L									
03-028	13.	18.	4.80	4.24	208.	1.588	.028	9.4	307.	300.	0.	523.	0.	0.	522.	A	473.	463.	322.	312.					
																B	497.	483.							
																L									
03-028	15.	18.	4.76	4.21	200.	1.590	.029	9.4	307.	300.	0.	537.	0.	0.	539.	A	477.	462.	326.	313.					
																B	490.	476.							
																L									
03-028	13.	18.	4.77	4.22	203.	1.590	.028	9.4	307.	300.	0.	531.	0.	0.	531.	A	475.	462.	324.	313.					
																B	492.	479.							
																L									
04-020	8.	24.	4.94	4.10	200.	1.587	.045	14.6	308.	299.	0.	821.	806.	734.	743.	A	490.	477.	320.	312.					
																B	496.	482.							
																L									
04-020	16.	24.	4.94	4.10	199.	1.588	.045	14.6	309.	298.	0.	824.	807.	736.	740.	A	491.	477.	325.	312.					
																B	497.	483.							
																L									
04-020	30.	54.	4.69	4.10	203.	1.588	.032	10.4	309.	295.	0.	803.	814.	728.	724.	A	486.	472.	379.	350.					
																B	491.	476.							
																L									

Table V-6 (cont.)

REGENERATIVELY COOLED CHAMBER

TEST NO.	T1 SEC	T2 SEC	MR CORE	MR TCA	PC N/CM2	WT KG/SEC	WFC KG/SEC	FFC (%)	TH2 (°K)	TO2 (°K)	INJECTOR FACE TEMP					BACK-SIDE TEMP				
											TJ110 (°K)	TJ220 (°K)	TJ310 (°K)	TJ410 (°K)	TJ120 (°K)	ROW	TS-9 (°K)	TS-8 (°K)	TS-2 (°K)	TS-1 (°K)
04-020	60.	71.	3.58	3.15	209.	1.569	.039	10.3	307.	294.	0.	677.	833.	701.	546.	A	450.	434.	470.	474.
																B	451.	432.		
																L				
04-020	74.	78.	4.75	4.16	205.	1.596	.032	10.4	307.	293.	0.	769.	822.	721.	705.	A	485.	472.	510.	530.
																B	488.	475.		
																L				
04-020	82.	86.	5.87	5.12	190.	1.590	.027	10.3	306.	294.	0.	803.	814.	737.	737.	A	511.	495.	539.	561.
																B	518.	506.		
																L				
04-020	90.	96.	6.34	5.21	190.	1.583	.039	15.3	306.	294.	0.	826.	811.	739.	750.	A	518.	500.	575.	593.
																B	528.	515.		
																L				
04-021	4.	15.	4.05	3.57	343.	2.588	.057	10.1	309.	310.	0.	614.	743.	605.	534.	A	447.	426.	369.	360.
																B	461.	435.		
																L				
04-021	16.	28.	4.70	4.13	335.	2.577	.051	10.1	309.	306.	0.	618.	718.	618.	558.	A	468.	447.	421.	374.
																B	477.	451.		
																L				
04-021	23.	28.	4.71	4.14	335.	2.578	.051	10.1	310.	307.	0.	579.	716.	617.	527.	A	467.	446.	438.	381.
																B	476.	450.		
																L				
03-030	4.	8.	4.73	4.42	60.	.521	.004	4.0	309.	306.	0.	687.	976.	632.	651.	A	476.	445.	314.	313.
																B	469.	441.		
																L				
03-030	10.	19.	4.72	4.41	60.	.522	.004	4.0	310.	304.	0.	743.	1039.	663.	708.	A	482.	446.	317.	318.
																B	483.	445.		
																L				
03-030	20.	22.	4.91	4.45	60.	.521	.007	6.8	311.	303.	0.	753.	1038.	670.	718.	A	485.	449.	324.	326.
																B	487.	448.		
																L				
03-030	24.	35.	5.03	4.46	65.	.521	.009	9.7	311.	302.	0.	1232.	1277.	1047.	1052.	A	485.	457.	0.	0.
																B	497.	456.		
																L				
03-030	40.	50.	5.03	4.46	65.	.520	.009	9.7	311.	300.	0.	767.	1050.	685.	721.	A	497.	459.	464.	461.
																B	504.	460.		
																L				

Table V-6 (cont.)

REGENERATIVELY COOLED CHAMBER

TEST NO.	T1 SEC	T2 SEC	MR CORE	MR TCA	PC N/CM2	WT KG/SEC	WFC KG/SEC	FFC (%)	TH2 (°K)	T02 (°K)	INJECTOR FACE TEMP					BACK-SIDE TEMP				
											TJ110 (°K)	TJ220 (°K)	TJ310 (°K)	TJ410 (°K)	TJ120 (°K)	ROW	TS-8 (°K)	TS-9 (°K)	TS-2 (°K)	TS-1 (°K)
03-030	65.	70.	4.09	4.46	60.	.521	.006	6.7	312.	300.	1233.	1200.	1320.	1055.	1019.	A	491.	453.	1200.	1231.
																B	498.	455.		
03-031	1.	8.	3.48	3.09	64.	.528	.012	9.4	312.	304.	0.	453.	984.	603.	483.	A	434.	415.	462.	332.
																B	449.	424.		
03-033	6.	9.	6.35	5.54	62.	.528	.008	9.3	310.	302.	0.	552.	802.	639.	559.	A	528.	492.	345.	313.
																B	537.	492.		
03-033	11.	15.	6.25	5.46	62.	.523	.008	9.3	310.	302.	0.	708.	873.	679.	589.	A	533.	488.	336.	305.
																B	536.	487.		
03-033	15.	48.	6.27	5.47	62.	.523	.007	9.3	311.	301.	0.	766.	955.	703.	741.	A	538.	490.	324.	297.
																B	538.	488.		
04-022	10.	20.	5.14	4.46	201.	1.619	.033	11.0	112.	214.	0.	439.	419.	409.	400.	A	361.	348.	316.	313.
																B	362.	351.		
04-022	14.	20.	5.18	4.49	201.	1.620	.033	11.0	111.	210.	0.	431.	417.	406.	397.	A	359.	347.	319.	313.
																B	361.	350.		
04-022	10.	40.	5.14	4.45	201.	1.616	.032	10.9	115.	202.	0.	439.	420.	408.	402.	A	359.	345.	341.	324.
																B	361.	345.		
04-022	20.	40.	5.13	4.45	201.	1.614	.032	10.9	116.	196.	0.	438.	421.	407.	403.	A	359.	343.	353.	330.
																B	361.	343.		
04-023	6.	15.	4.96	4.44	206.	1.624	.024	8.1	109.	209.	0.	419.	417.	403.	392.	A	350.	338.	313.	313.
																B	356.	346.		
04-023	18.	24.	5.17	4.49	204.	1.634	.032	10.8	100.	184.	0.	414.	409.	394.	380.	A	347.	336.	347.	319.
																B	355.	344.		
04-023	36.	47.	3.82	3.32	214.	1.652	.039	10.2	135.	171.	0.	432.	423.	402.	375.	A	320.	304.	439.	425.
																B	332.	313.		

Table V-6 (cont.)

REGENERATIVELY COOLED CHAMBER																			
INJECTOR FACE TEMP										BACK-SIDE TEMP									
TEST NO.	T1 SEC	T2 SEC	MR CORE	MR TCA	PC N/CM2	WT KG/SEC	WFC KG/SEC	FFC (%)	TH2 (°K)	T02 (°K)	TJ110 (°K)	TJ220 (°K)	TJ310 (°K)	TJ410 (°K)	TJ120 (°K)	ROW	TS-9 (°K)	TS-8 (°K)	TS-2 TS-1 (°K)
04-023	50.	56.	4.99	4.37	210.	1.679	.032	10.3	123.	172.	0.	451.	434.	416.	411.	A	357.	336.	482.
																B	369.	350.	487.
04-023	64.	72.	6.75	5.56	195.	1.647	.039	15.5	105.	181.	0.	435.	435.	425.	420.	A	389.	377.	560.
																R	403.	392.	565.
04-025	6.	10.	3.95	3.60	332.	2.542	.040	7.2	105.	231.	0.	357.	436.	422.	334.	A	295.	278.	309.
																R	297.	274.	311.
04-025	30.	35.	4.70	4.20	314.	2.453	.040	8.5	145.	233.	0.	396.	425.	420.	363.	A	337.	322.	347.
																R	352.	323.	311.
04-025	18.	35.	4.56	4.00	317.	2.471	.040	8.2	144.	231.	1259.	1204.	1207.	991.	745.	A	335.	318.	0.
																R	346.	319.	1268.
03-035	20.	25.	4.46	3.95	200.	1.588	.032	10.0	429.	379.	0.	863.	804.	776.	835.	A	597.	579.	315.
																R	605.	589.	318.
03-035	35.	45.	4.54	3.92	200.	1.569	.040	12.3	392.	363.	0.	633.	735.	711.	631.	A	552.	534.	386.
																R	560.	543.	391.
03-035	40.	45.	4.54	3.92	200.	1.590	.040	12.2	386.	366.	0.	584.	724.	702.	590.	A	545.	528.	400.
																R	553.	537.	404.
03-035	120.	135.	4.56	3.94	200.	1.606	.040	12.2	309.	301.	0.	489.	624.	597.	500.	A	475.	460.	610.
																R	483.	469.	665.
03-035	130.	135.	4.56	3.94	200.	1.606	.040	12.3	308.	300.	0.	486.	623.	596.	499.	A	475.	459.	613.
																R	483.	468.	671.
03-035	60.	200.	4.55	3.93	200.	1.604	.040	12.2	312.	306.	0.	589.	631.	603.	521.	A	479.	463.	596.
																R	486.	471.	647.
03-035	160.	200.	4.56	3.94	200.	1.608	.040	12.2	303.	293.	0.	595.	623.	593.	516.	A	473.	456.	626.
																R	480.	466.	685.

Table V-6 (cont.)

REGENERATIVELY COOLED CHAMBER																				
INJECTOR FACE TEMP											BACK-SIDE TEMP									
TEST NO.	T1 SEC	T2 SEC	MR CORE	MR TCA	PC N/CM2	WT KG/SEC	WFC KG/SEC	FFC (%)	TH2 (°K)	TO2 (°K)	TJ110 (°K)	TJ220 (°K)	TJ310 (°K)	TJ410 (°K)	TJ120 (°K)	ROW	TS-9 (°K)	TS-8 (°K)	TS-2 (°K)	TS-1 (°K)
03-035	195.	200.	4.57	3.95	205.	1.609	.040	12.3	301.	291.	0.	594.	621.	590.	509.	A	471.	455.	626.	691.
																B	479.	464.		
																L				
03-035	210.	250.	4.44	3.93	207.	1.609	.033	10.0	298.	290.	0.	591.	616.	585.	501.	A	465.	449.	632.	709.
																B	473.	458.		
																L				
03-035	245.	250.	4.44	3.93	207.	1.609	.033	10.0	298.	290.	0.	590.	615.	583.	437.	A	465.	448.	638.	724.
																B	471.	457.		
																L				

TABLE V-7

PULSE TEST SUMMARY

Series 1680-DOA-05-

Test No.	Date	Function	No. of Pulses	Pulse Width, sec	Off-Time	Results
001		Anemometer calib. (Ox.)	4 units			One unit lost in handling.
002		Anemometer calib. (Fuel)	4 units			Four calibrated units obtained.
003	9/16	Igniter Only Sea Level	Many	.200	Variable	Electrical problems produced non repeatable igniter ignitions, changed spark plug, box & cables; increased power to .02 joules.
003a	9/17	.010 fuel lead	20	.20	.30 sec	Repeatable ignition.
b	9/17	Simultaneous fuel and ox.	20	.20	.30	Satisfactory ignition very repeatable
c		.010 fuel lag	20	.20	.30	Ignition in all cases but not as repeatable as simultaneous or fuel lead.
d		Selected .010 fuel lead for igniter start				
	9/17	Altitude test 100,000 ft	20	.20	.30	Reproducible igniter ignition with fuel lead.
004	9/17	Igniter/engine sequencing .020 sec igniter lead	1	.2	--	Normal thrust chamber ignition - no overpressure
005	9/17	.020 sec igniter lead	1	.2	--	Repeat of above results
006	9/17	Reduce igniter lead	1	.2	--	Error in sequence change - no ignition
007	9/17	Correct error igniter lead .120 sec	1	.2	--	Smooth ignition
008*	9/20	Final sequence adjustment variable off-times	1	.2	10 min	Satisfactory ignitions in all cases. Postfire inspection showed erosion of tip of film cooling sleeve.
009			1	.2	7 min	Damage attributed to 80 igniter only firings test 003 a-d.
010			1	.2	6 min	
011			2	.2	.3, 120 sec	
012*			5	.2	.3 sec	
013*	9/23	Recheck sequence with repaired chamber	2	.2	.3	Ignition and coolant flow satisfactory
014*		.010 sec fuel valve advance .010 igniter fuel lead LFV to LOV = .02 sec	2	.2	.3	Ignition O.K., sequence too slow; ignition delay in igniter .02 sec.
015*	9/23	Established sequence initiated rapid pulsing Performance & thermal characteristics for 2 cps	100	.2	.3	Steady state temperatures attained; all pulses repeatable
016*	9/23	Repeat of above for additional cycles	110	.2	.3	Computer shut down at 110 pulses due to failure to achieve thrust. Ignition normal, low thrust.
017	9/24	Investigate reason for low thrust	1	.2	--	See discussion
018						
019	9/27	Change TCV sequence to .005 sec ox. lead	1	.2	20 min	Smoother start - no overpressure in oxidizer manifold
020	9/27	Repeat of above performance,	2	.2	.3	Pulses repeatable
021	9/27	thermal & durability	266	.2	.3	Pulses repeatable, low thrust shutdown on pulse 266 (no igniter ignition).
022	9/27	Single pulse of above sequence	1	.2	--	Normal ignition and pulse.

TABLE V-7 (cont.)

Test No.	Date	Function	No. of Pulses	Pulse Width, sec	Off-Time	Results
023	9/27	Continuation of durability testing	259	.2	.3	2 cps 40% duty cycle satisfactorily completed.
024	9/27	3.3 cps 40% duty cycle investigation	4	.1	.15	Satisfactory ignition and repeatability.
025*	9/27	Repeat of above with variable off-times	1	.1	--	Normal ignition and repeatability in all tests
026*			1	.1	--	
027*			4	.1	.15	
028*	9/27	Performance repeatability and durability tests	760	.1	.15	Normal ignition and repeatability in all tests
029	9/28	10 cps 35% duty cycle	1	.035	10 min	Normal ignition and repeatability in all tests Minimum off-time between pulses for valve sequencing .065 sec.
030		low impulse bits	1	.035	5 min	
031		sequence evaluation	1	.035	5 min	
032		variable off-time	10	.035	.065 sec	
033			1	.035	3 min	
034			1	.035	7 min	
035			1	.		
036*		Repeatability & durability	100	.035	.065	Normal ignition and repeatability
037*		Continuation of durability testing	280	.035	.065	No igniter ignition first pulse. Fuel valve operation irregular due to pilot valve actuator overheating after approx 250 pulses.
038*		Continuation of durability testing	840	.100	.150	Satisfactory completion of pulse test series with over 2500 pulses on SN-7 injector and 2700 pulses on SN-2 film cooled chamber

TABLE V-8

SYSTEM SEQUENCING AND RESULTING EVENTS

<u>Time</u>	<u>Test -016 with Fuel Lead</u>	<u>Time</u>	<u>Test -036 with Oxidizer Lead</u>
<u>START</u>			
-0.020	Signal to spark power supply	-0.020	Signal to spark power supply
-0.010	Sparkling starts	-0.010	Sparkling starts
0.0	Signal to igniter fuel and main <u>fuel valve</u>	0.0	Signal to main <u>oxidizer valve</u>
0.010	Signal to main <u>oxidizer valve</u>	0.010	Signal to igniter fuel and main <u>fuel valve</u>
0.020	Signal to igniter oxidizer valve	0.020	Signal to igniter oxidizer valve
0.030	Fuel flow sensed at anemometer		
0.032	Fuel manifold pressure rise		
0.035	Igniter ignition and Poj rise due to fuel	00.034	Igniter ignition
0.040	Oxidizer flow sensed at anemometer	0.040	Oxidizer flow sensed at anemometer
		0.045	Poj rise due to oxidizer flow
		0.045	Fuel flow sensed at anemometer and manifold
0.045	Mainstage ignition	0.046	Mainstage ignition
0.047	Full thrust	0.051	Full thrust
<u>SHUTDOWN</u>			
0.090	Oxidizer igniter valve signaled closed	0.045	Oxidizer valve signaled closed
0.220	All valves and spark signaled closed (FS-2)	0.055	All valves and spark signaled closed (FS-2)
FS-2		FS-2	
+0.030	Oxidizer valve closed; flow stopped	+0.030	Oxidizer valve closed; flow stopped
+0.040	Fuel valve closed; flow stopped	+0.040	Fuel valve closed; flow stopped

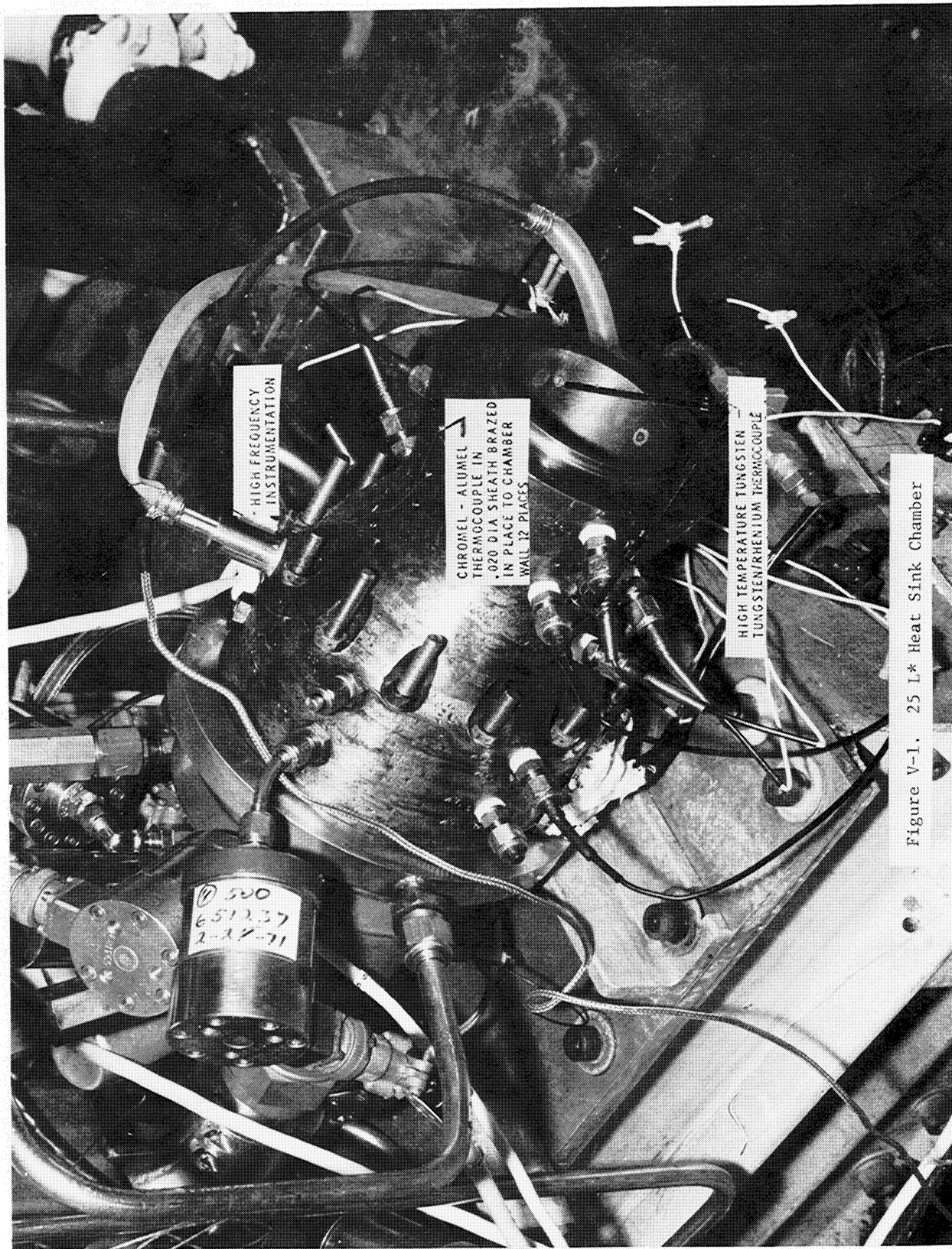


Figure V-1. 25 L* Heat Sink Chamber

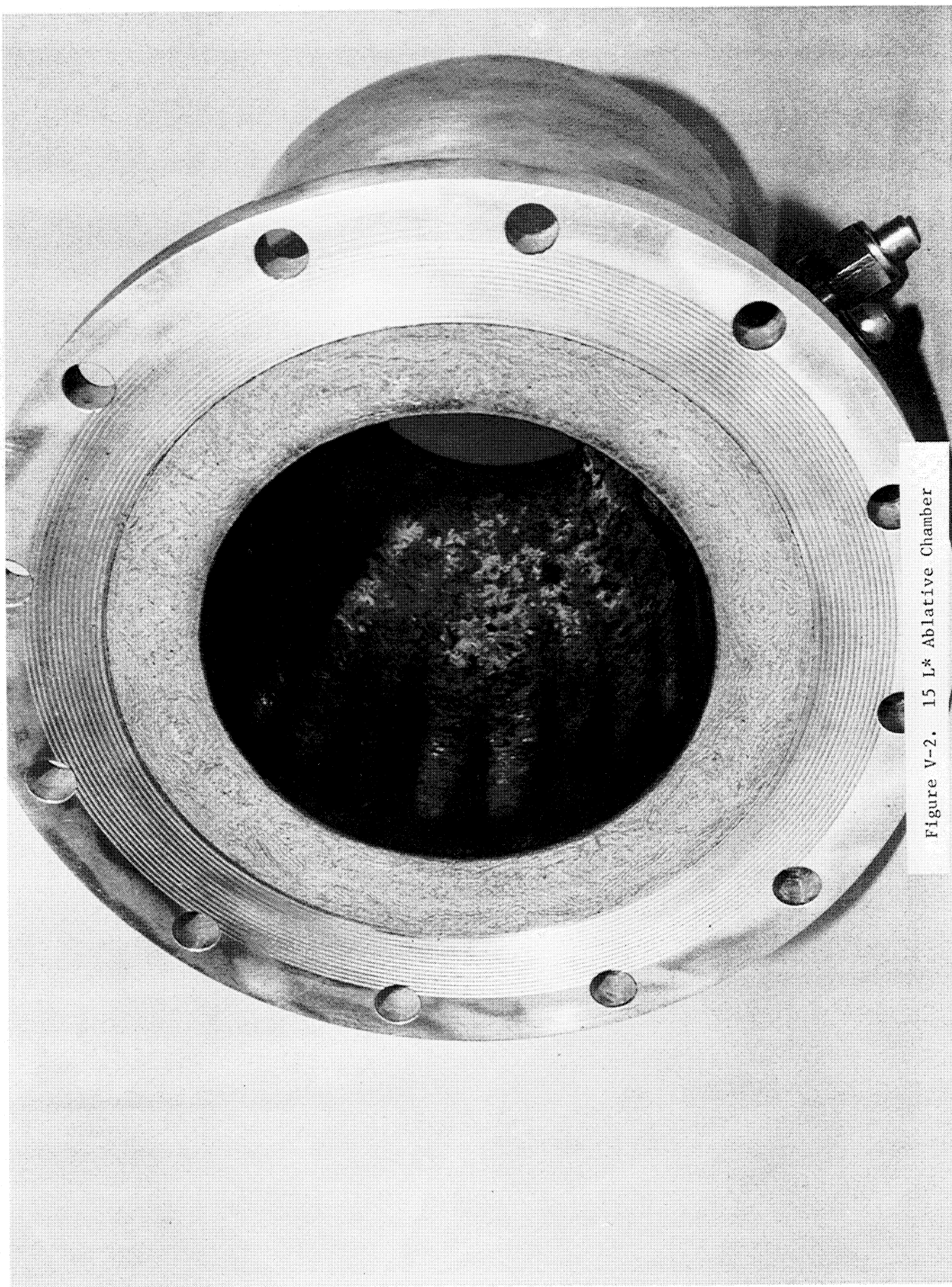


Figure V-2. 15 L* Ablative Chamber

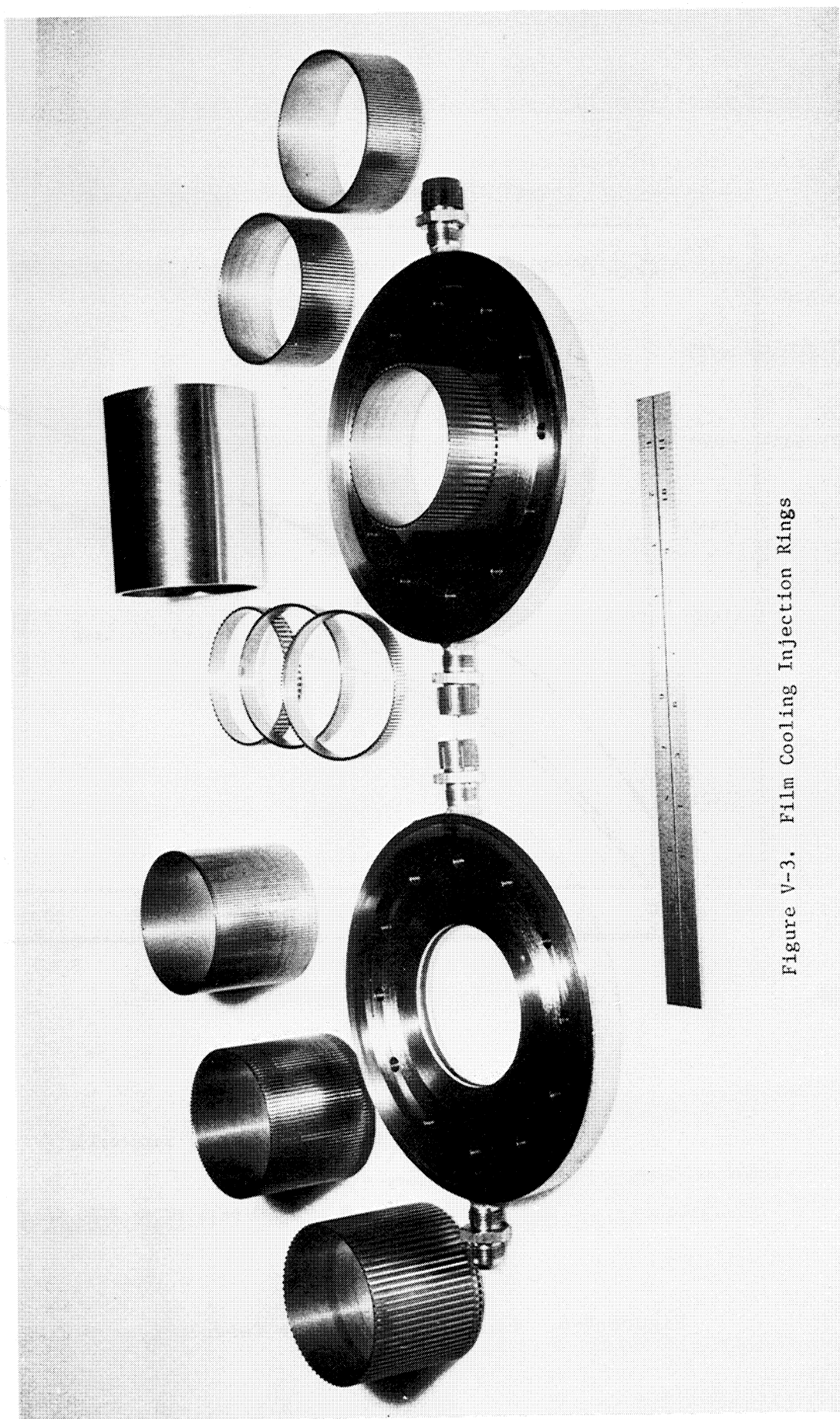
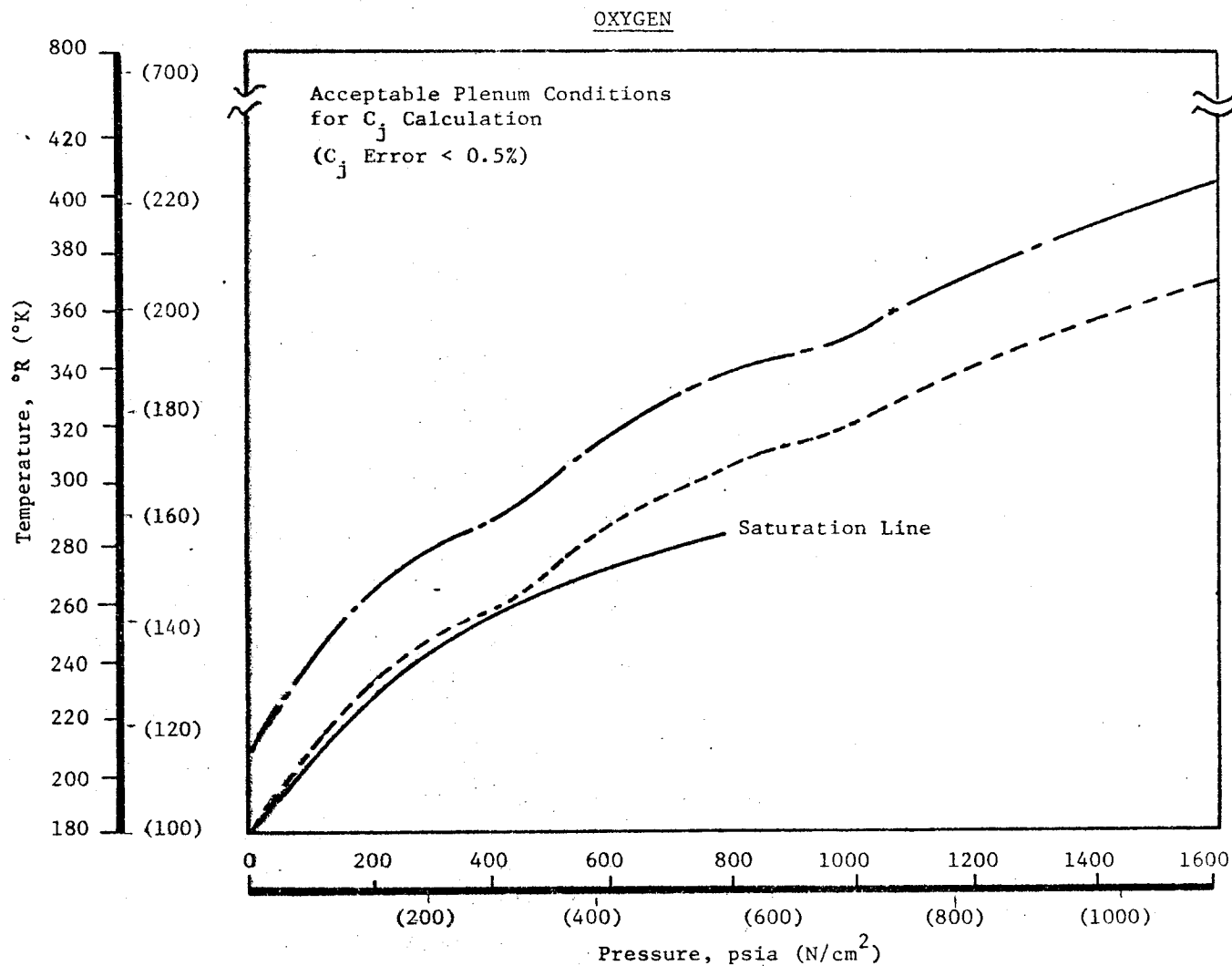


Figure V-3. Film Cooling Injection Rings



NORMAL AND PARA HYDROGEN

(C_j Error < 0.8% for 95% Conf. Interval)

Temperature = 170 to 800°R

Pressure = 0 to 2000 psia (0 to 1380 N/cm^2)

Figure V-4. Limits of Flow Rate Calculations for Real Gases

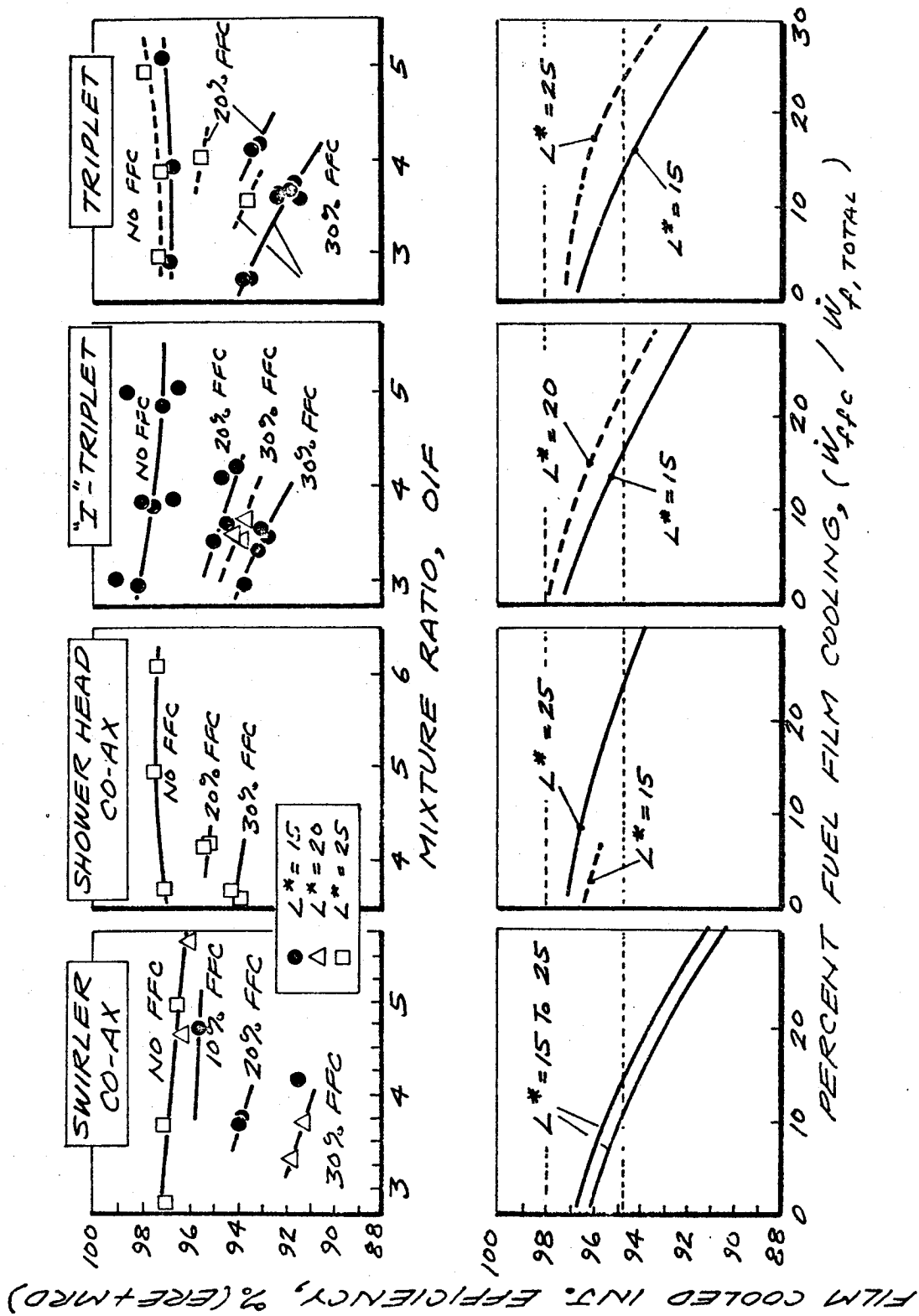


Figure V-5. Injector Energy Release Efficiency Comparison

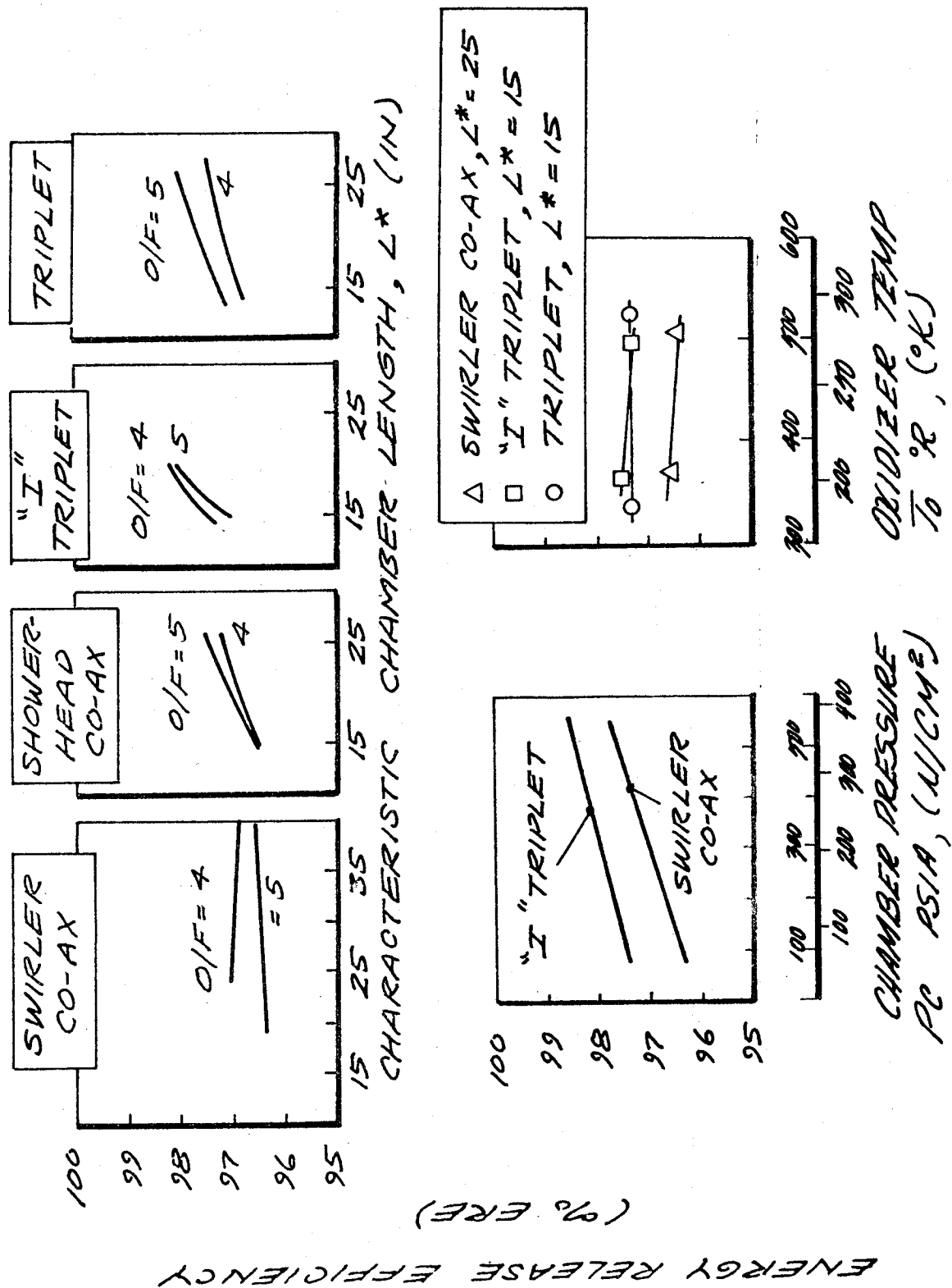


Figure V-6. Effect of L^* Propellant Temperature and Chamber Pressure on Injector Energy Release Efficiency

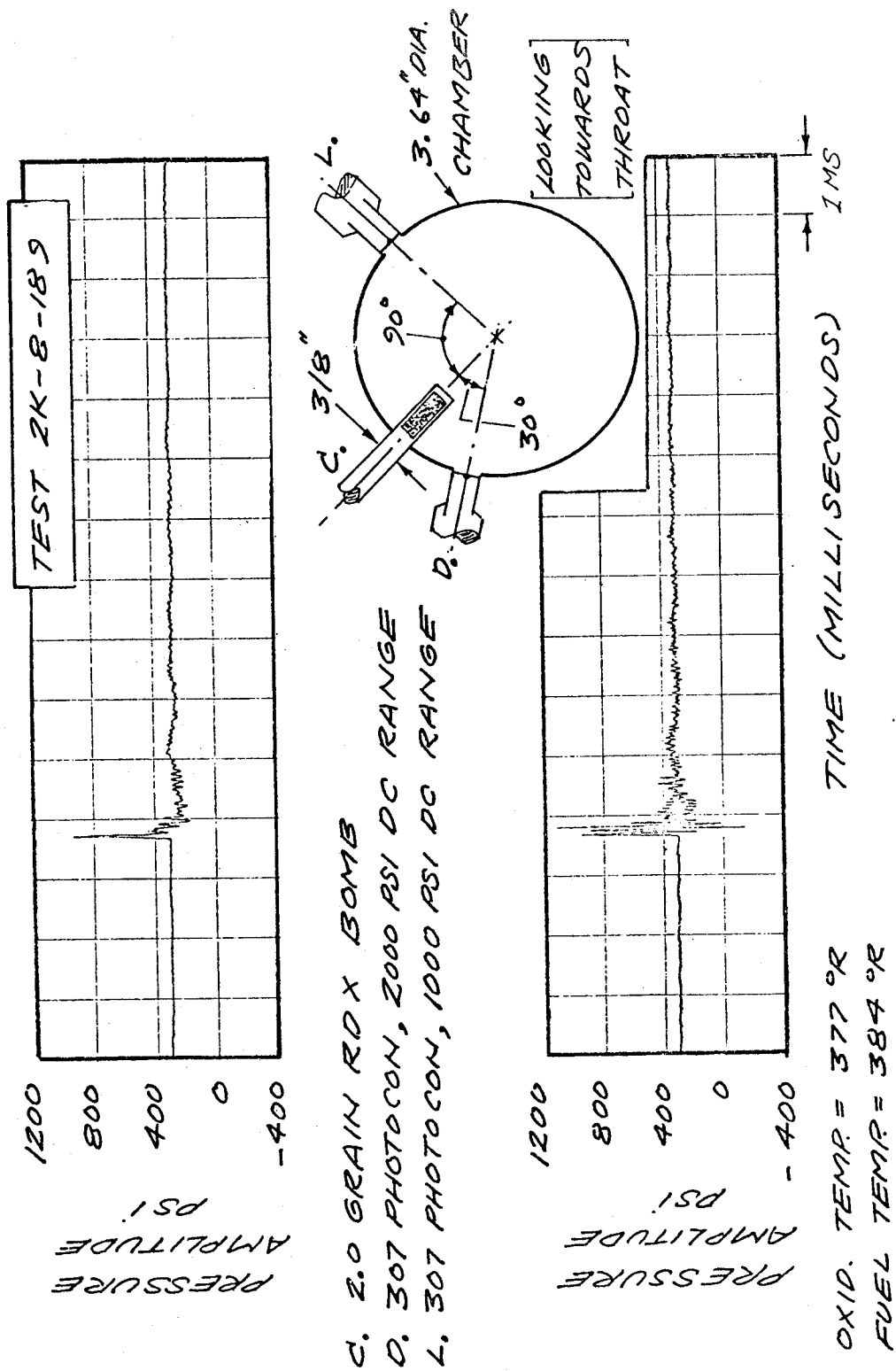


Figure V-7. Combustion Stability Bomb Test Results

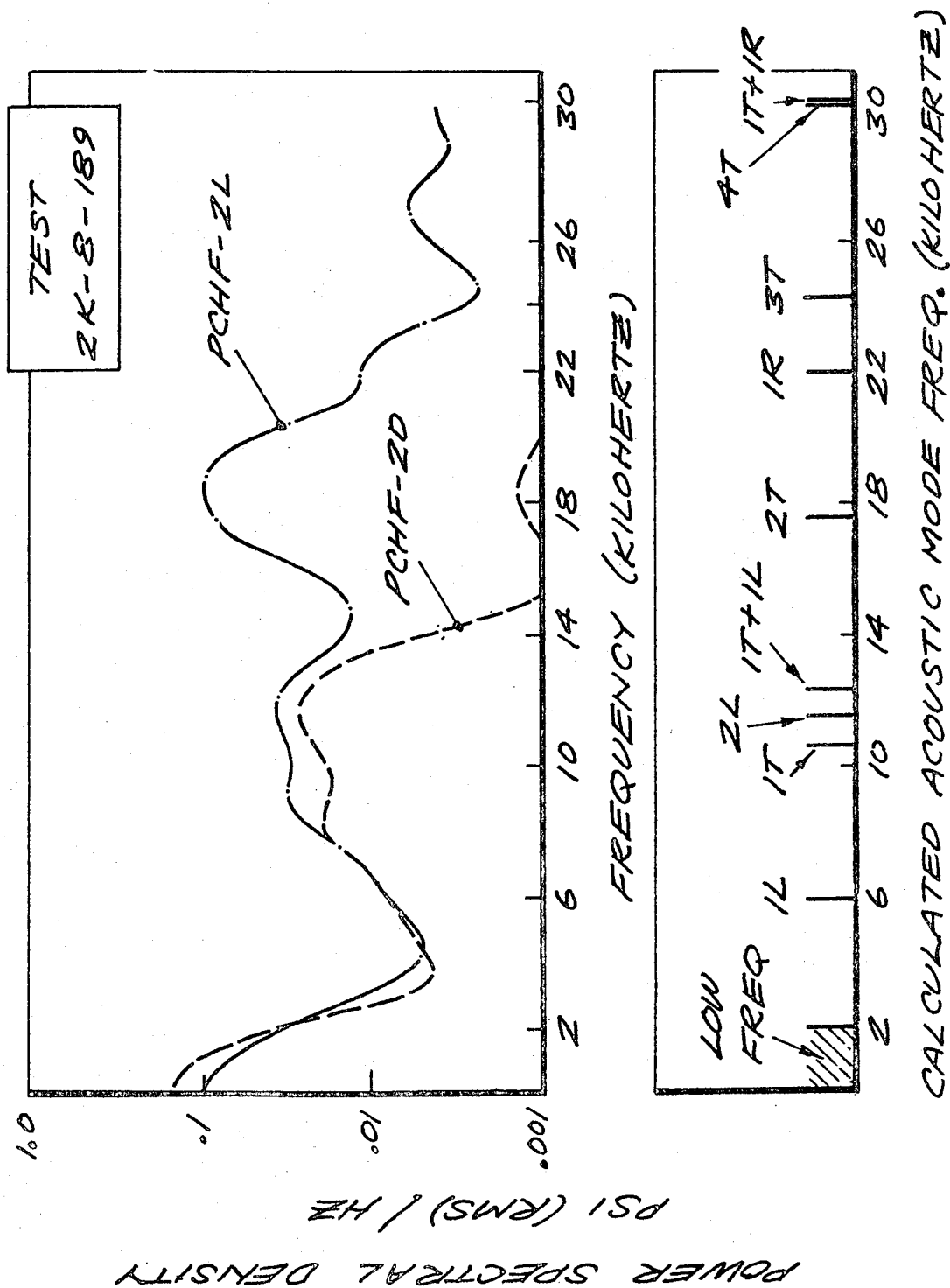


Figure V-8. Spectral Analysis of Bomb Test Data

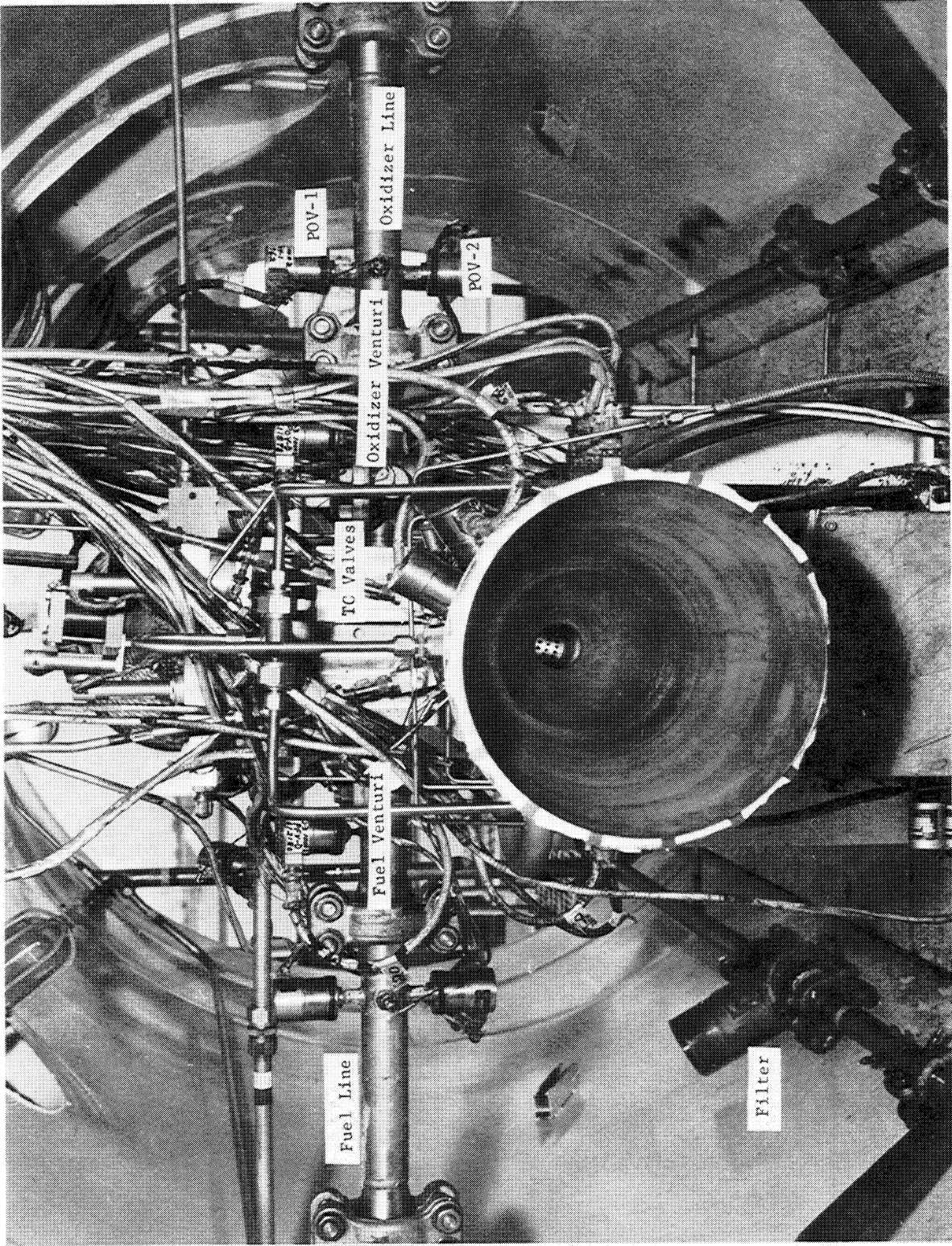


Figure V-9. Film-Cooled Thrust Chamber Assembly on J-3 Altitude Facility (Prefire)

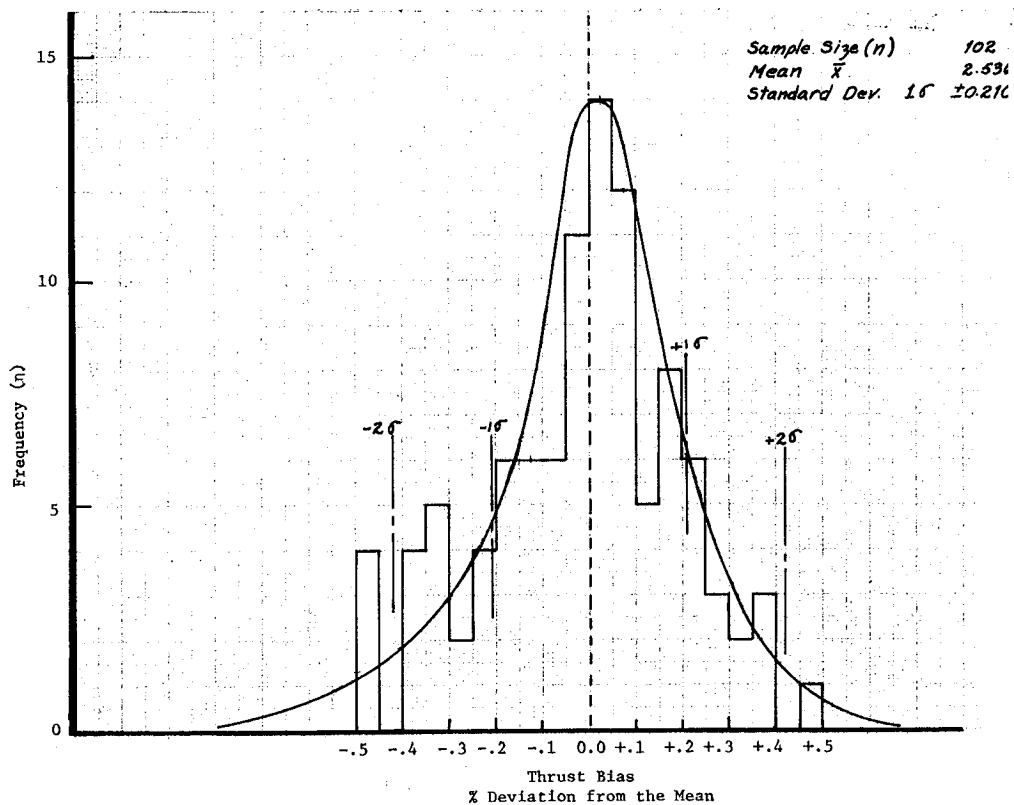
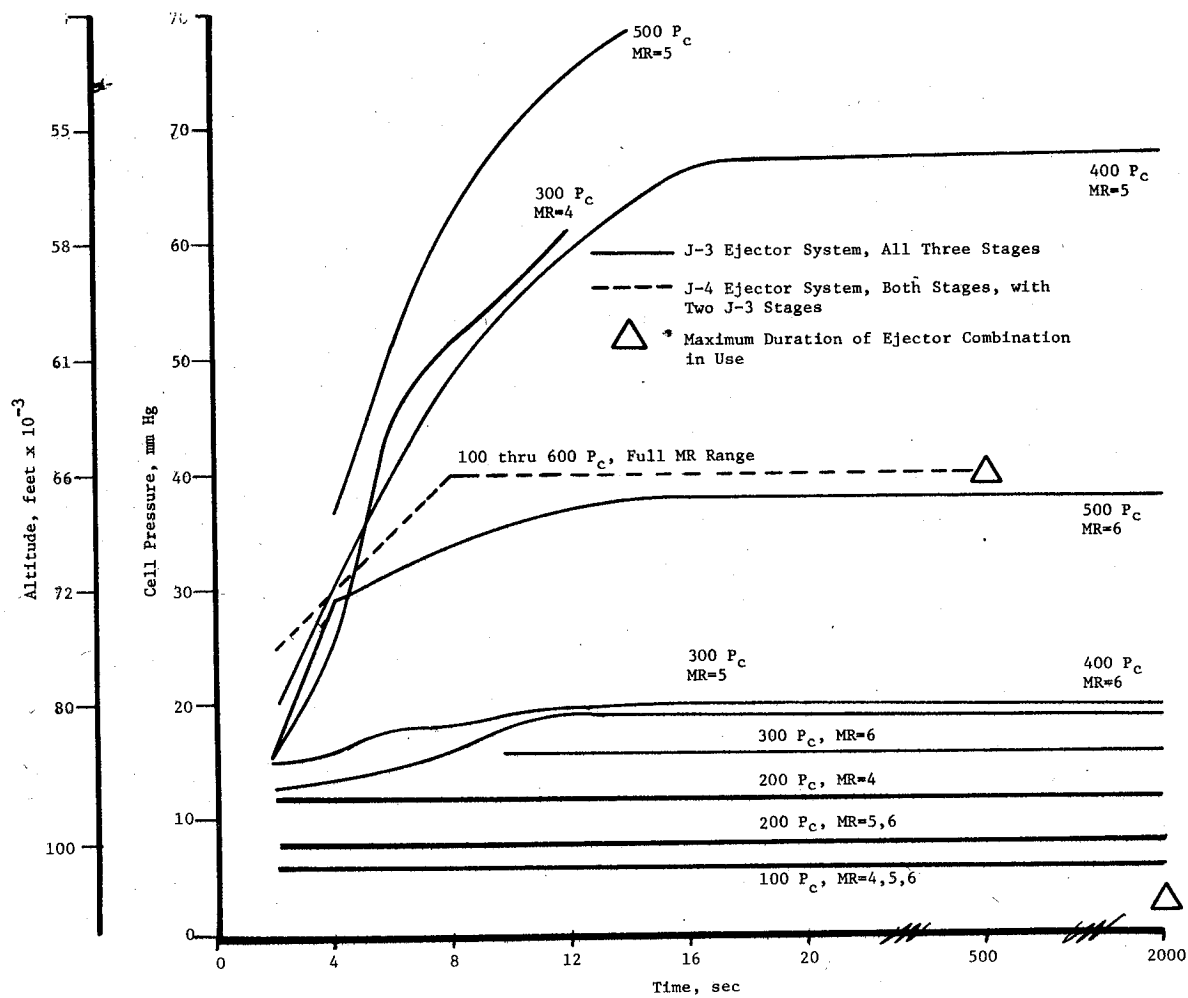
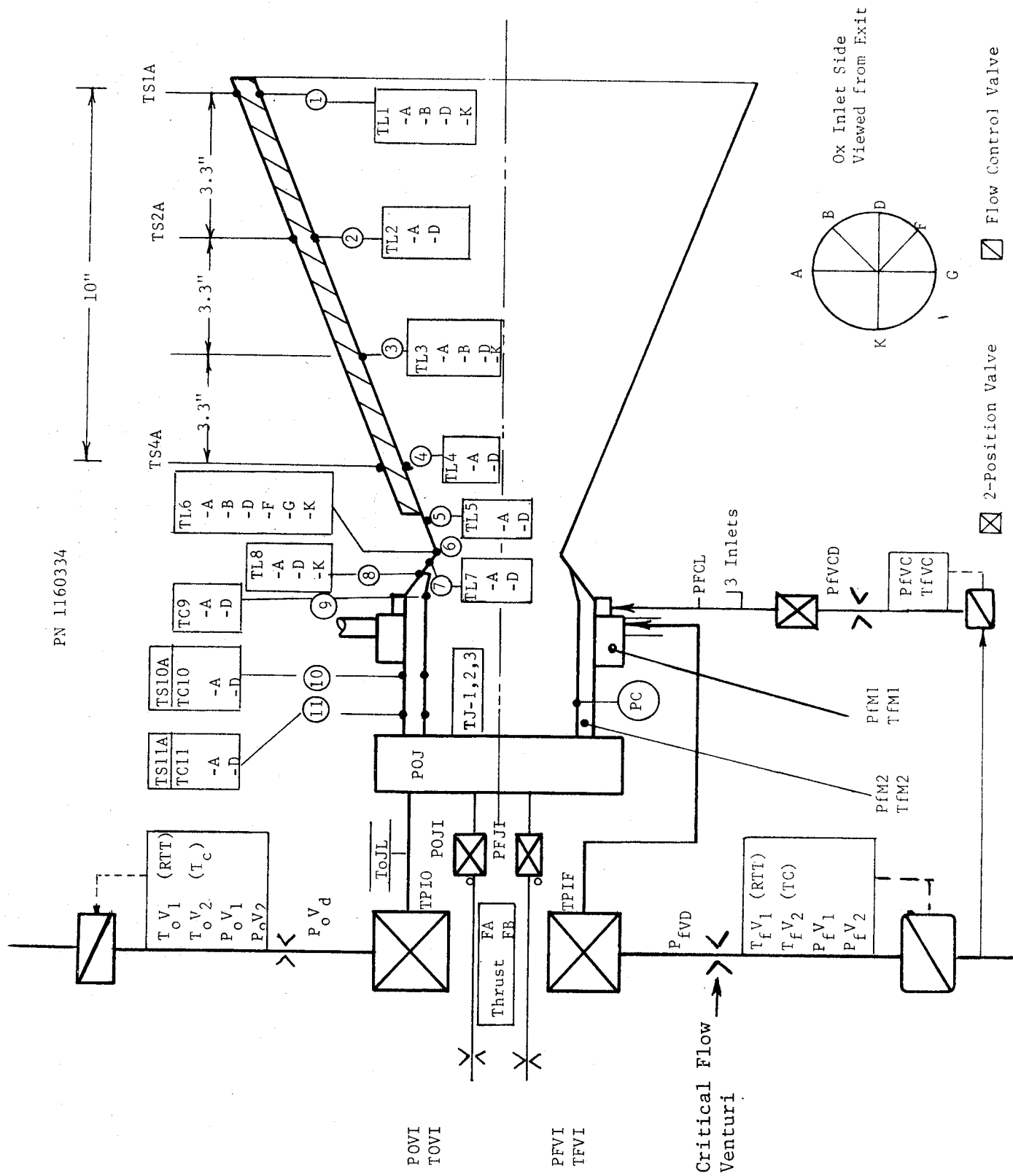


Figure V-10. Test Zone J Altitude System Capabilities

PN 1160334



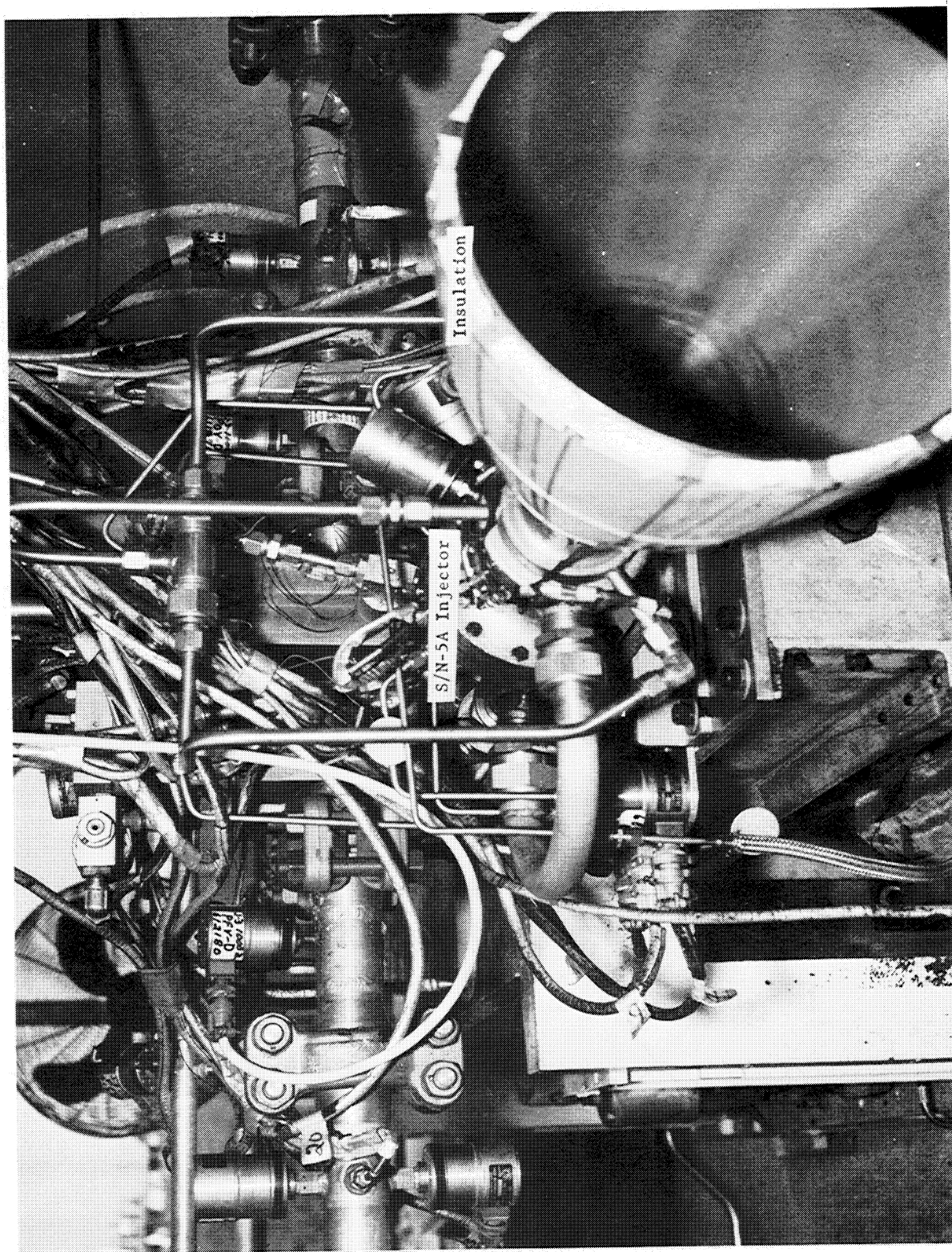


Figure V-12. Film-Cooled TCA in J-3 Altitude Facility (Postfire)

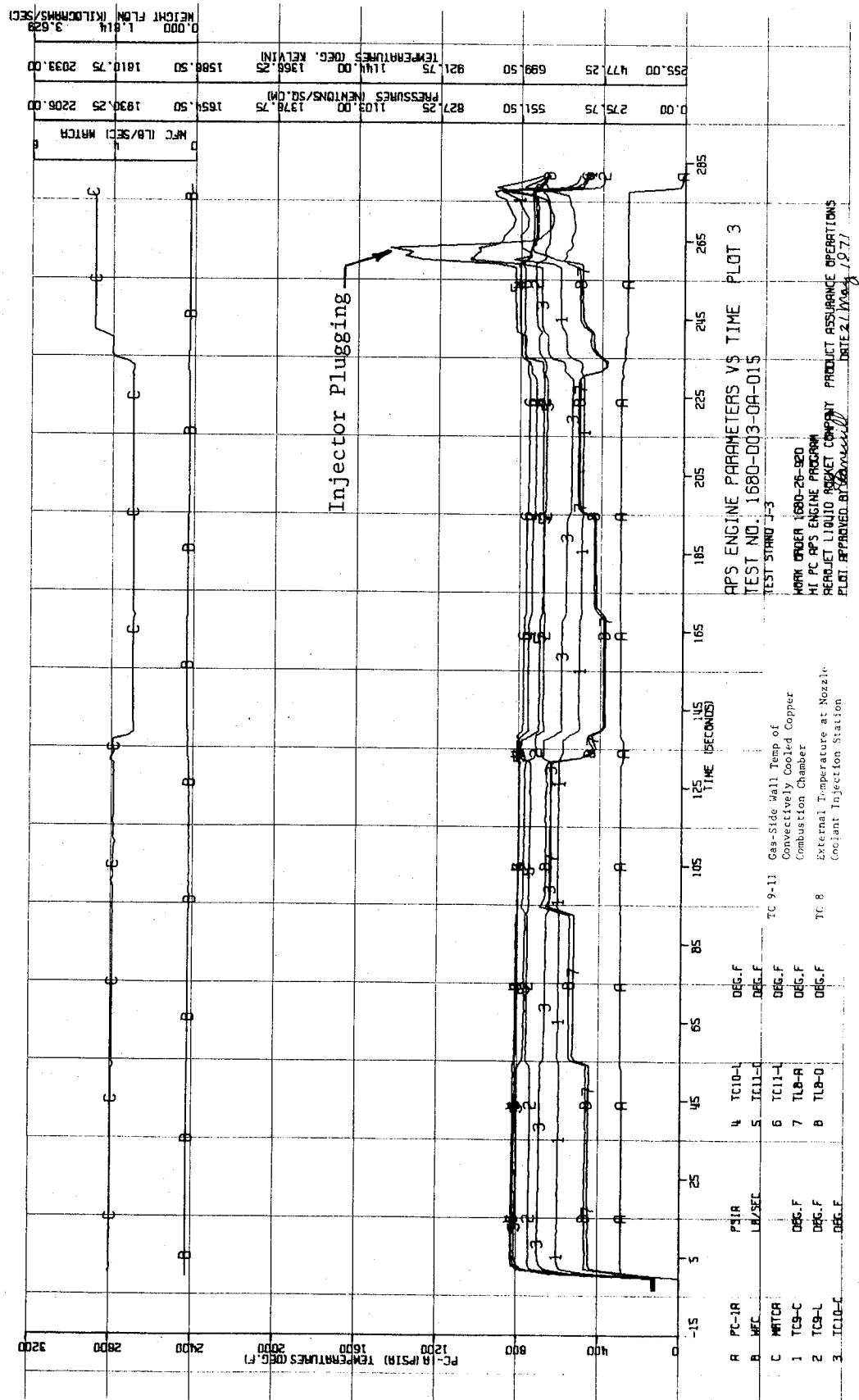


Figure V-14. Thruster Wall Temperatures - Chamber Region

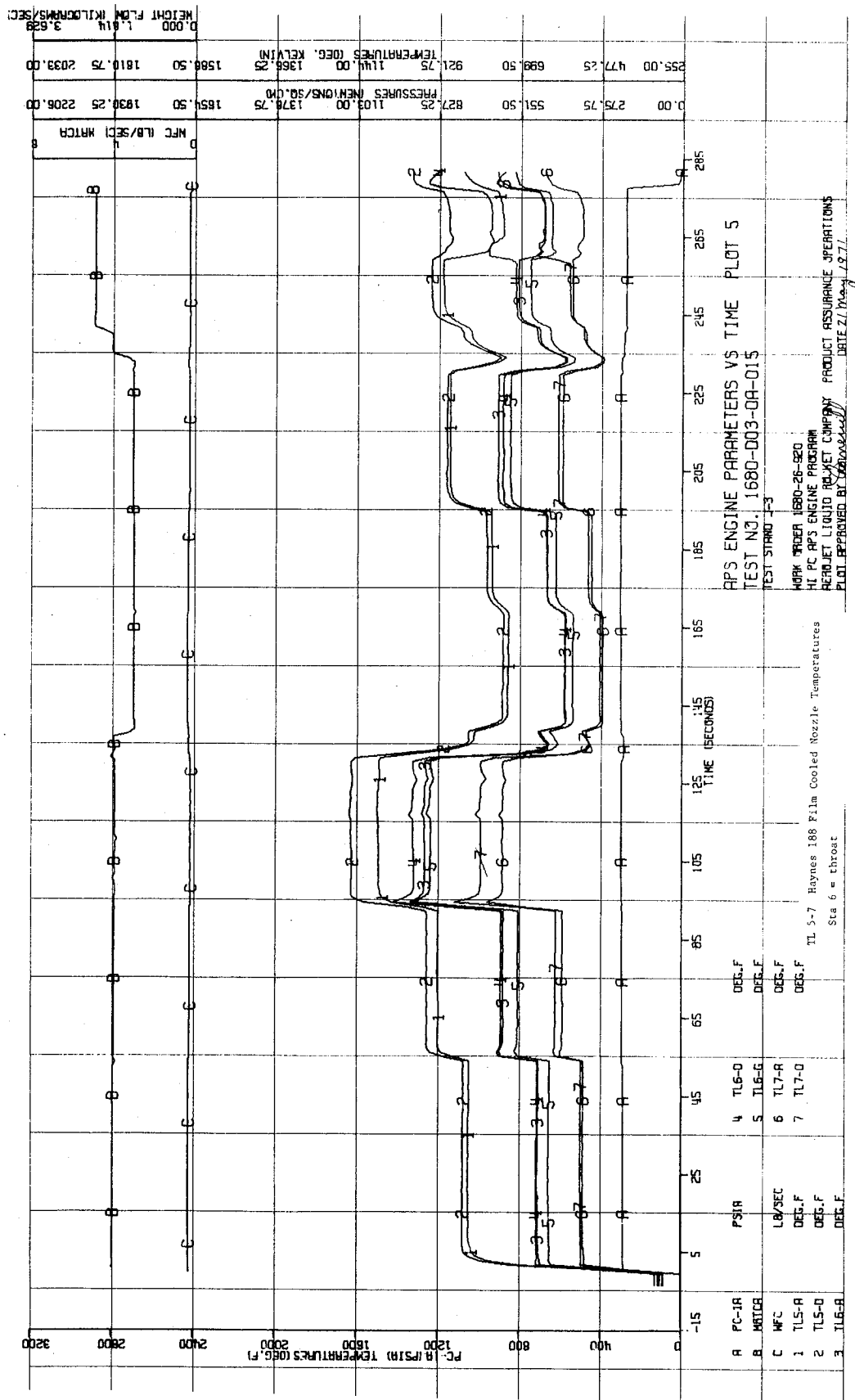


Figure V-15. Throat Wall Temperatures, Throat Region

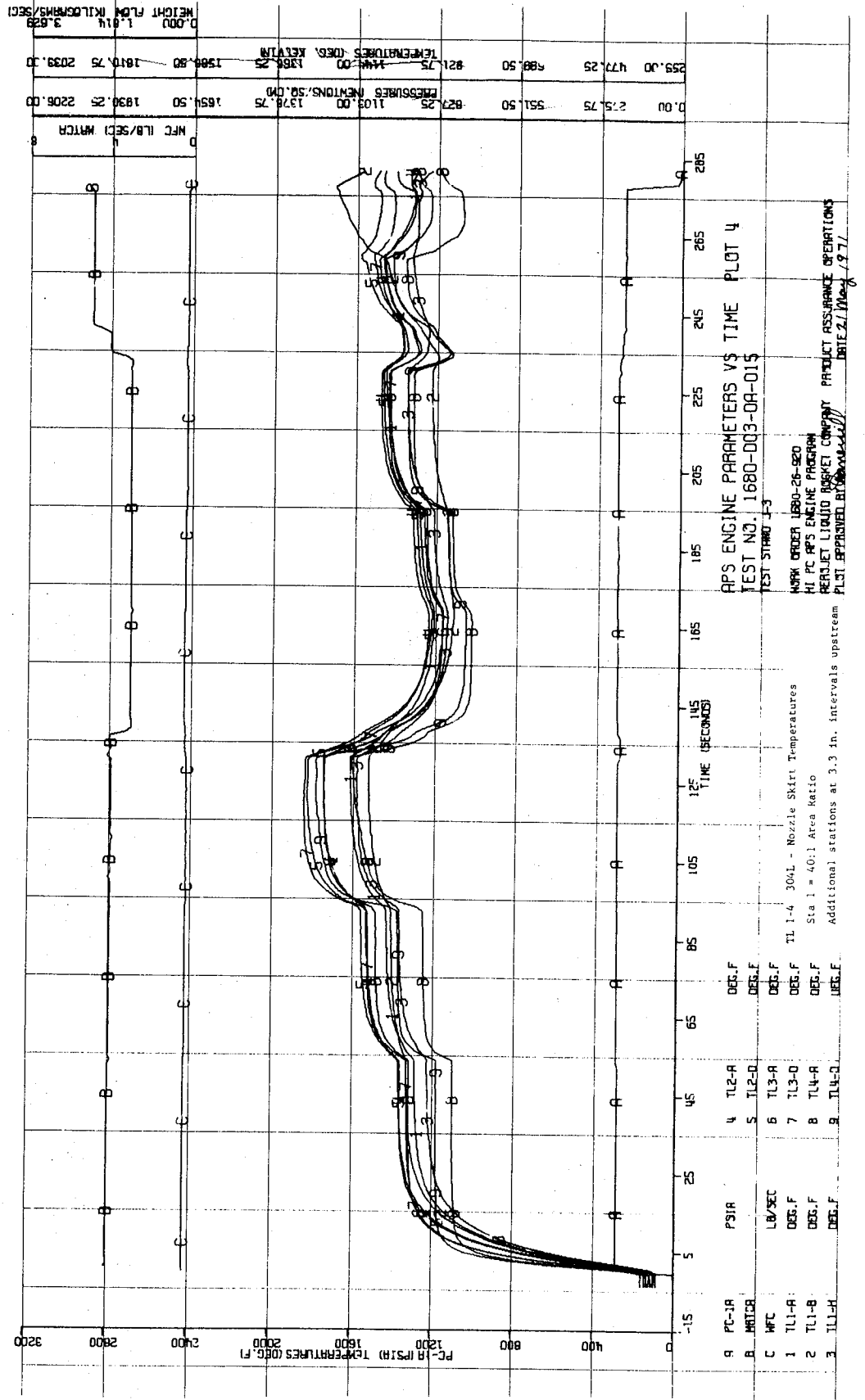


Figure V-16. Thruster Wall Temperatures - Skirt Region

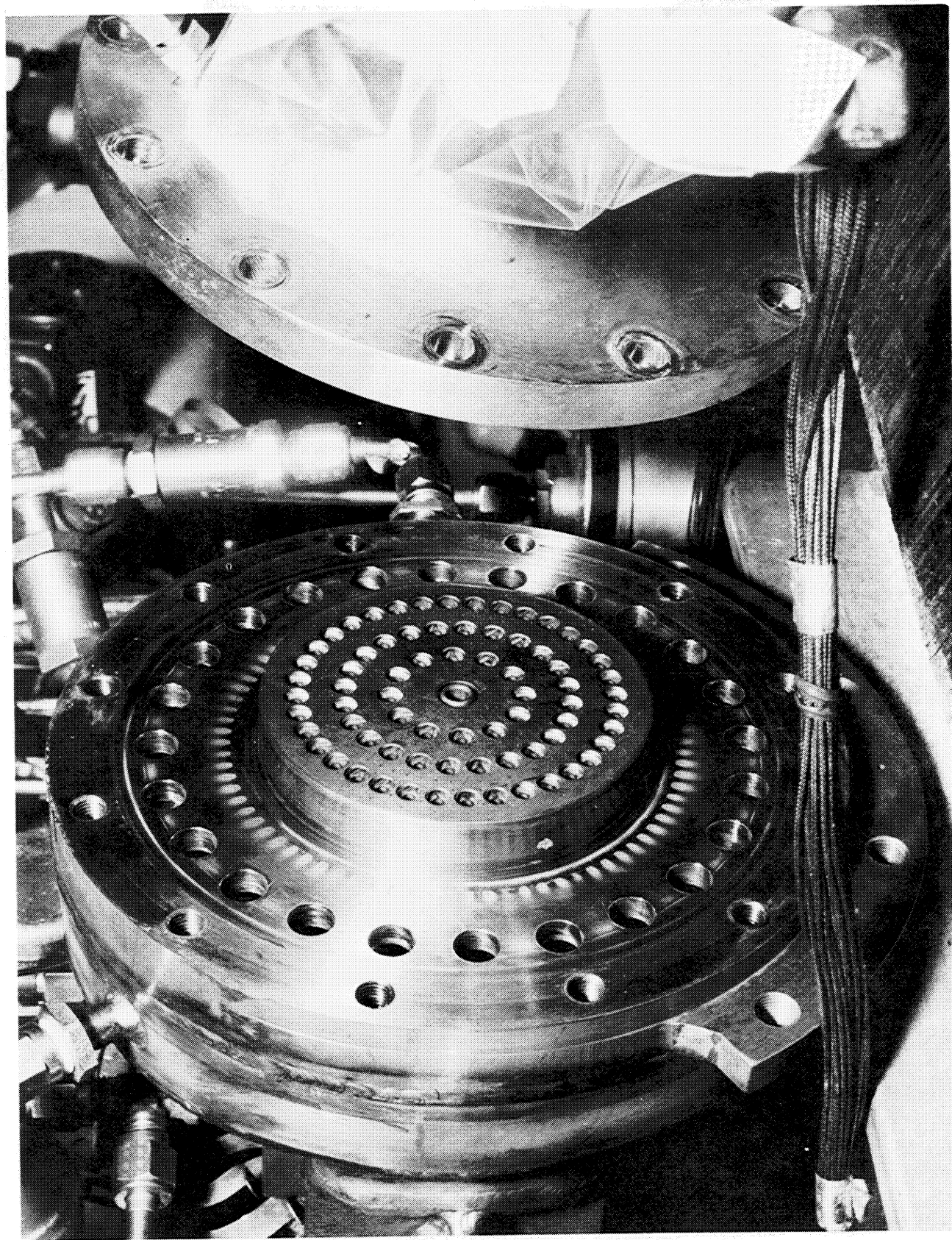


Figure V-17. SN 4 Triplet Injector After 2600 Restarts and 700 sec Firing

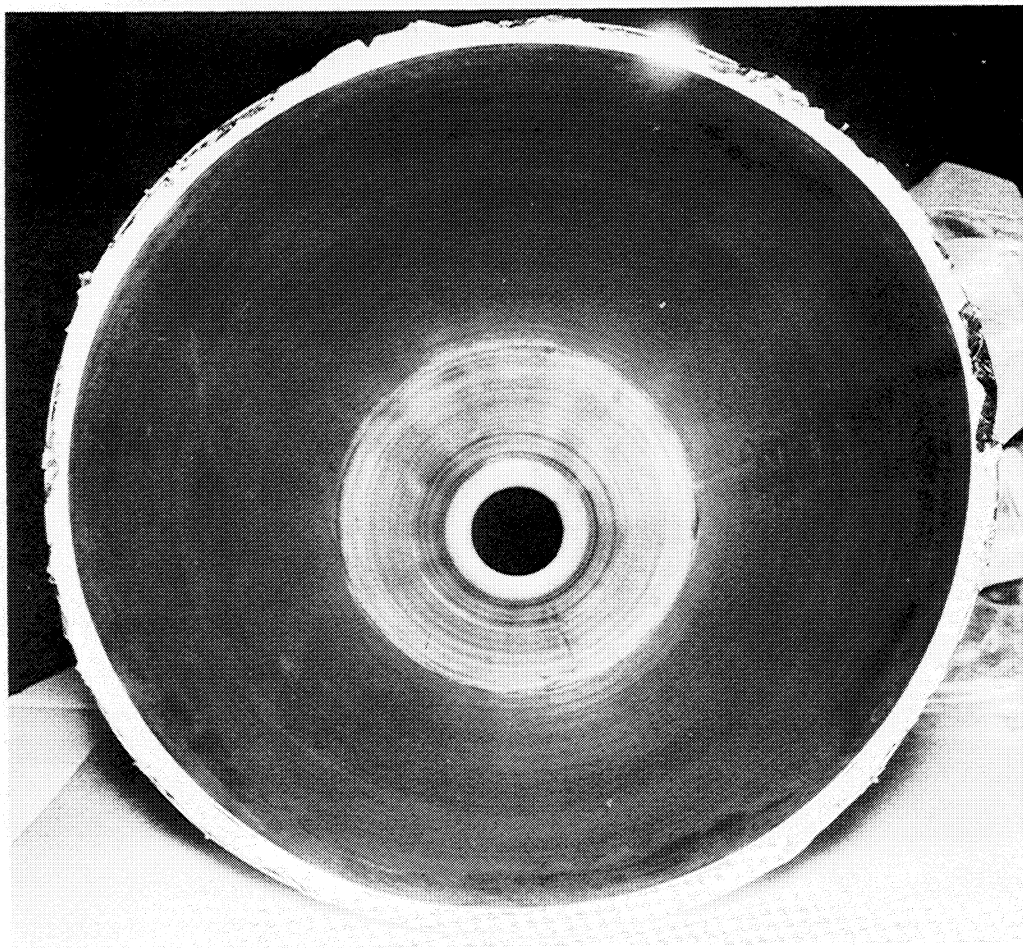
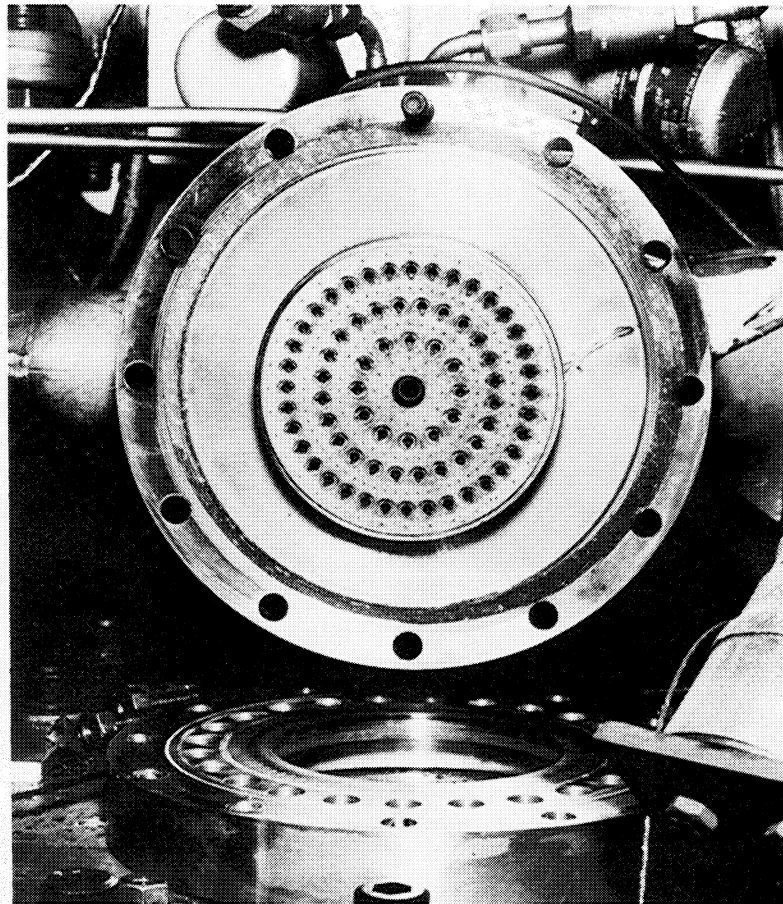


Figure V-18. Postfire Photograph, SN 6 Injector - SN 2 Film-Cooled Chamber

Figure V-19. Regeneratively Cooled Chamber Instrumentation

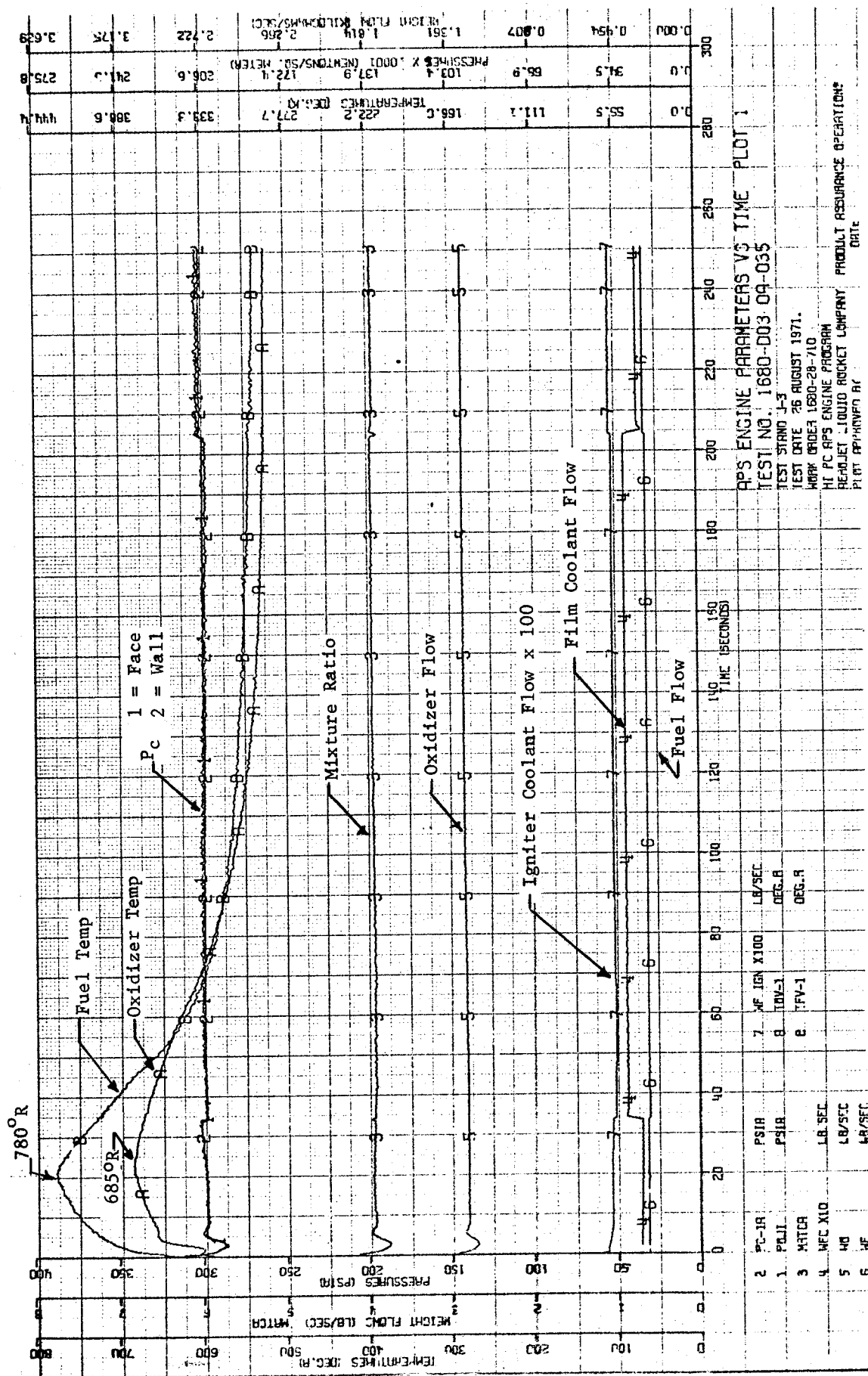


Figure V-20. Regeneratively Cooled Chamber Test with Variable Propellant Inlet Temperatures

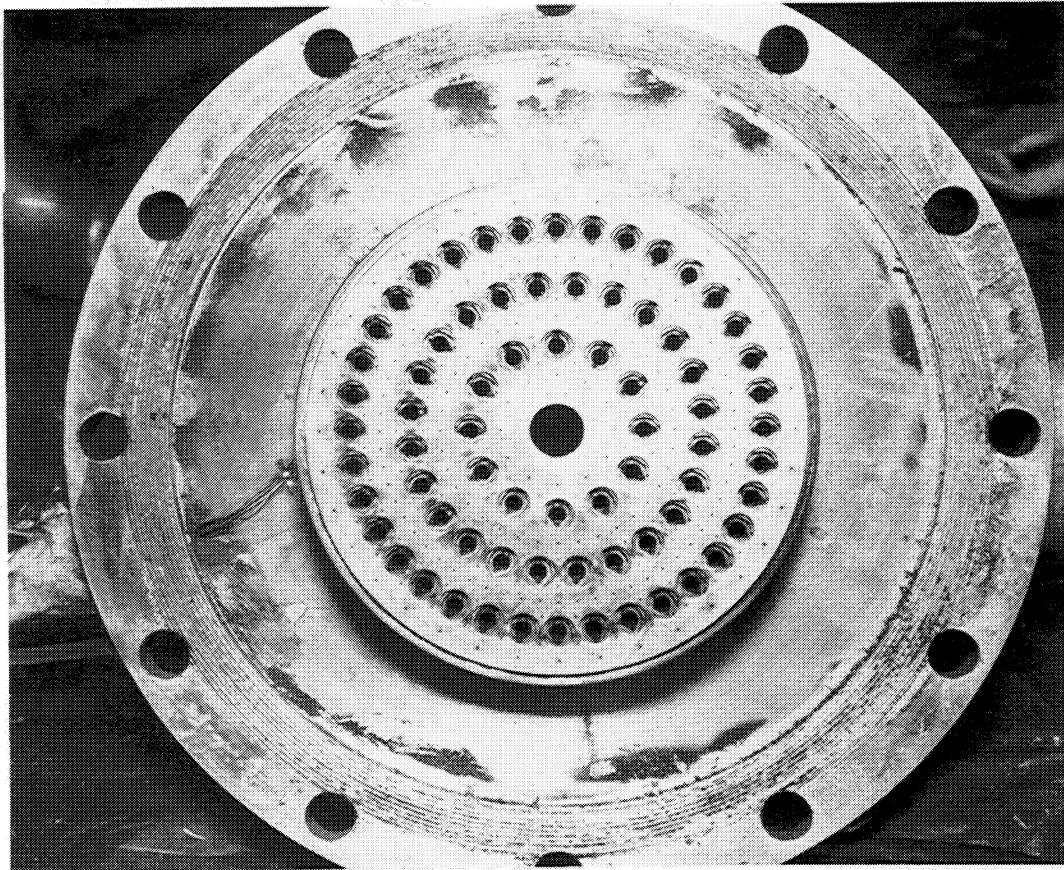
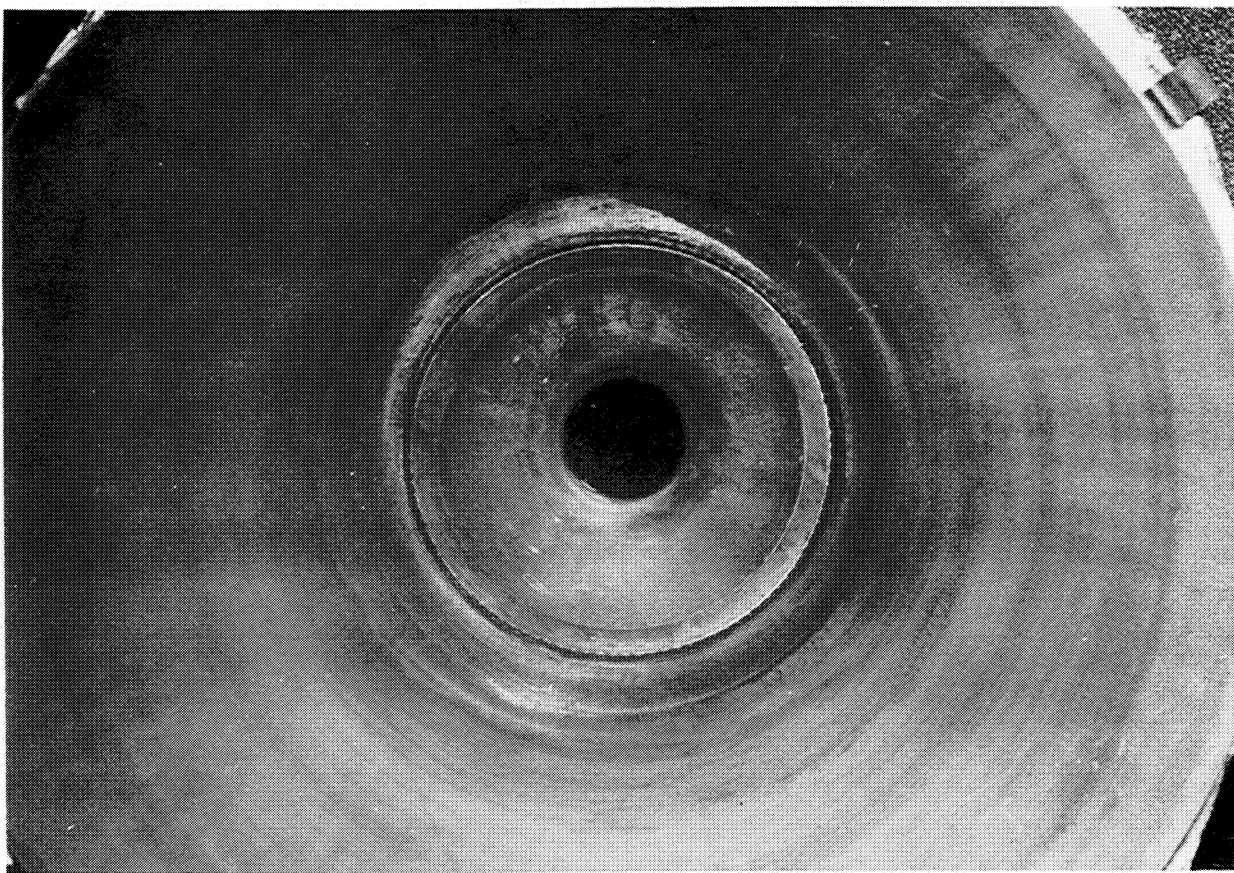


Figure V-21. Regeneratively Cooled Chamber Postfire Run 03-035

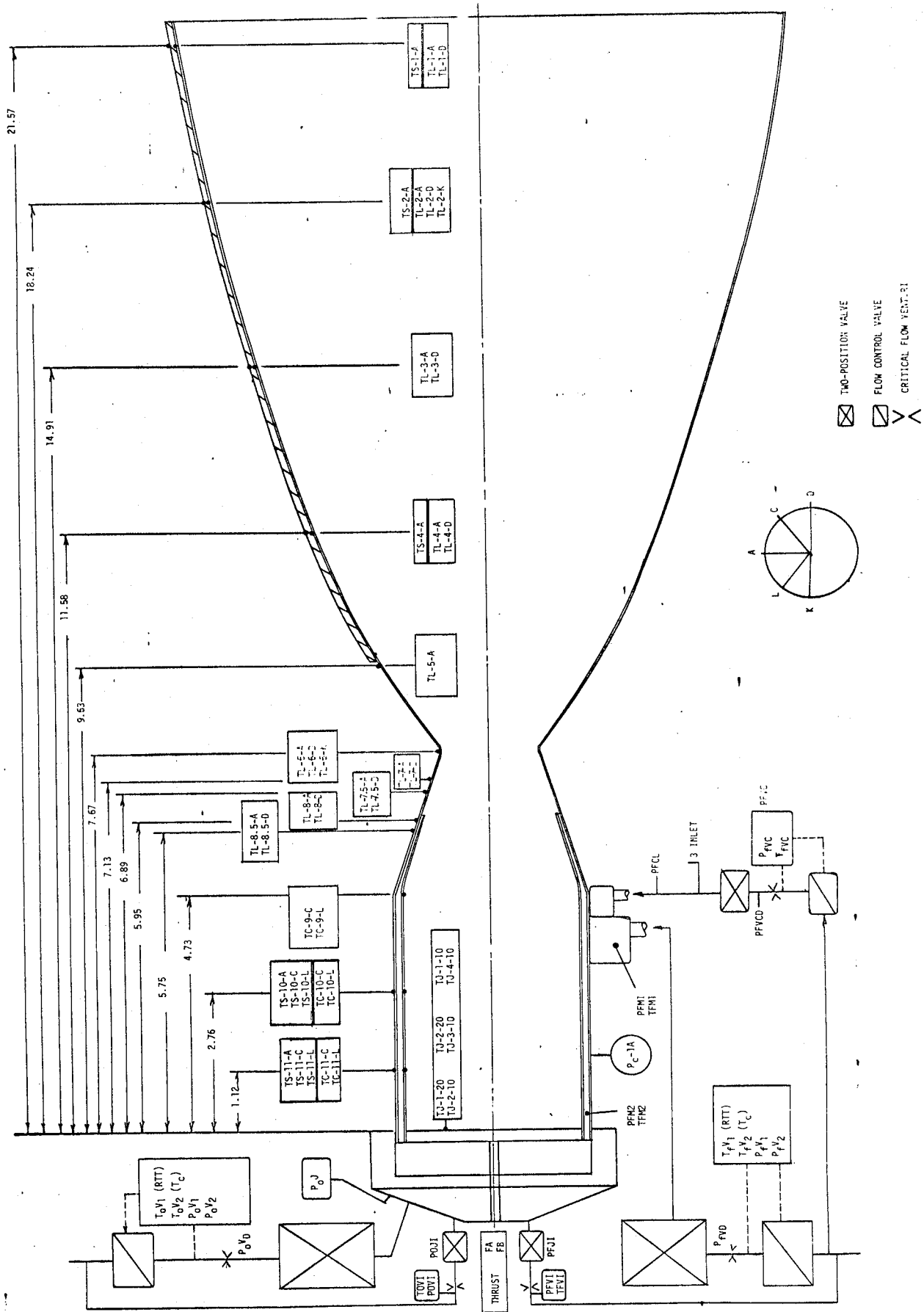


Figure V-22. SN 3 Film-Cooled Chamber and Flow Instrumentation

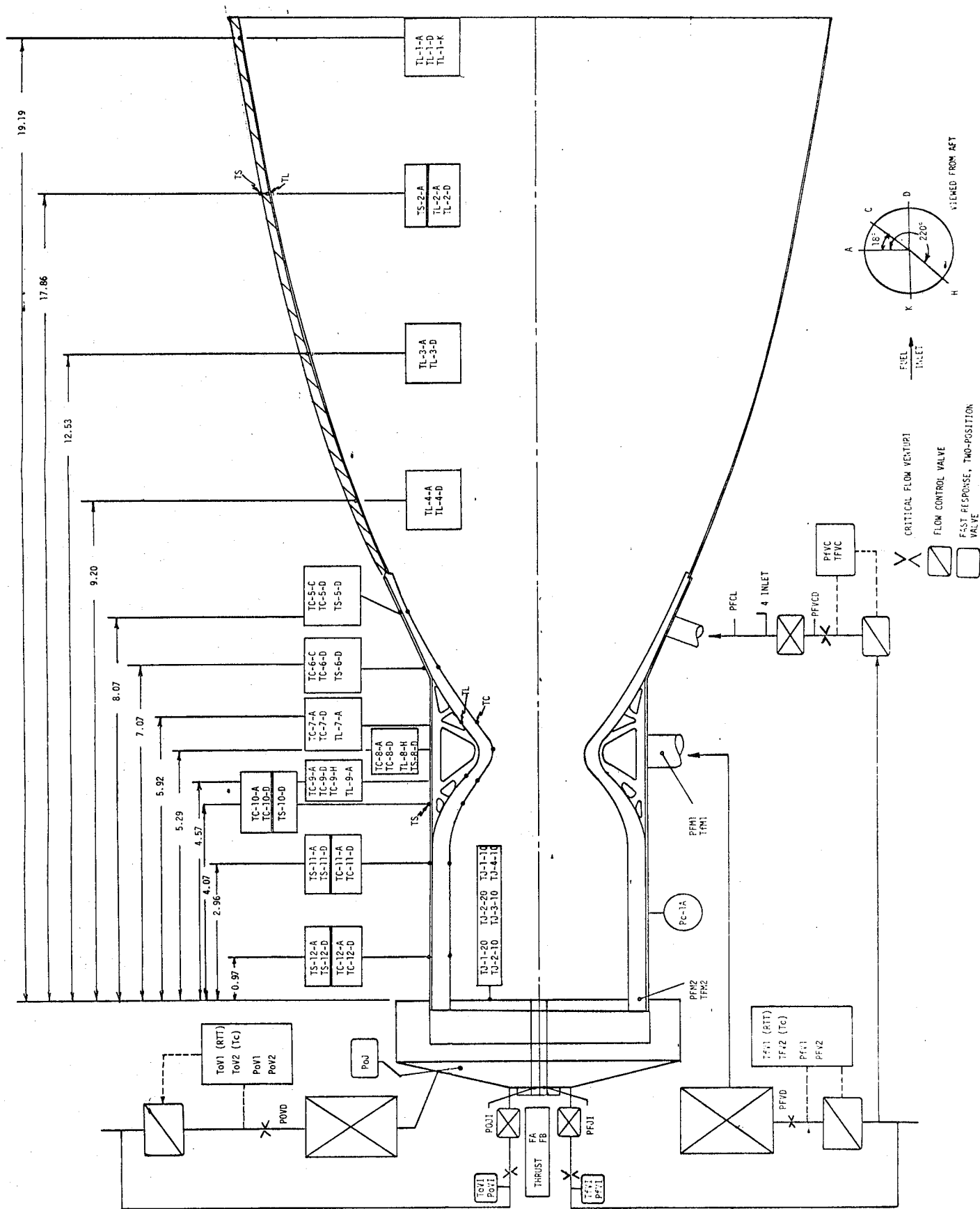


Figure V-23. SN 3 Regeneratively Cooled Chamber Instrumentation

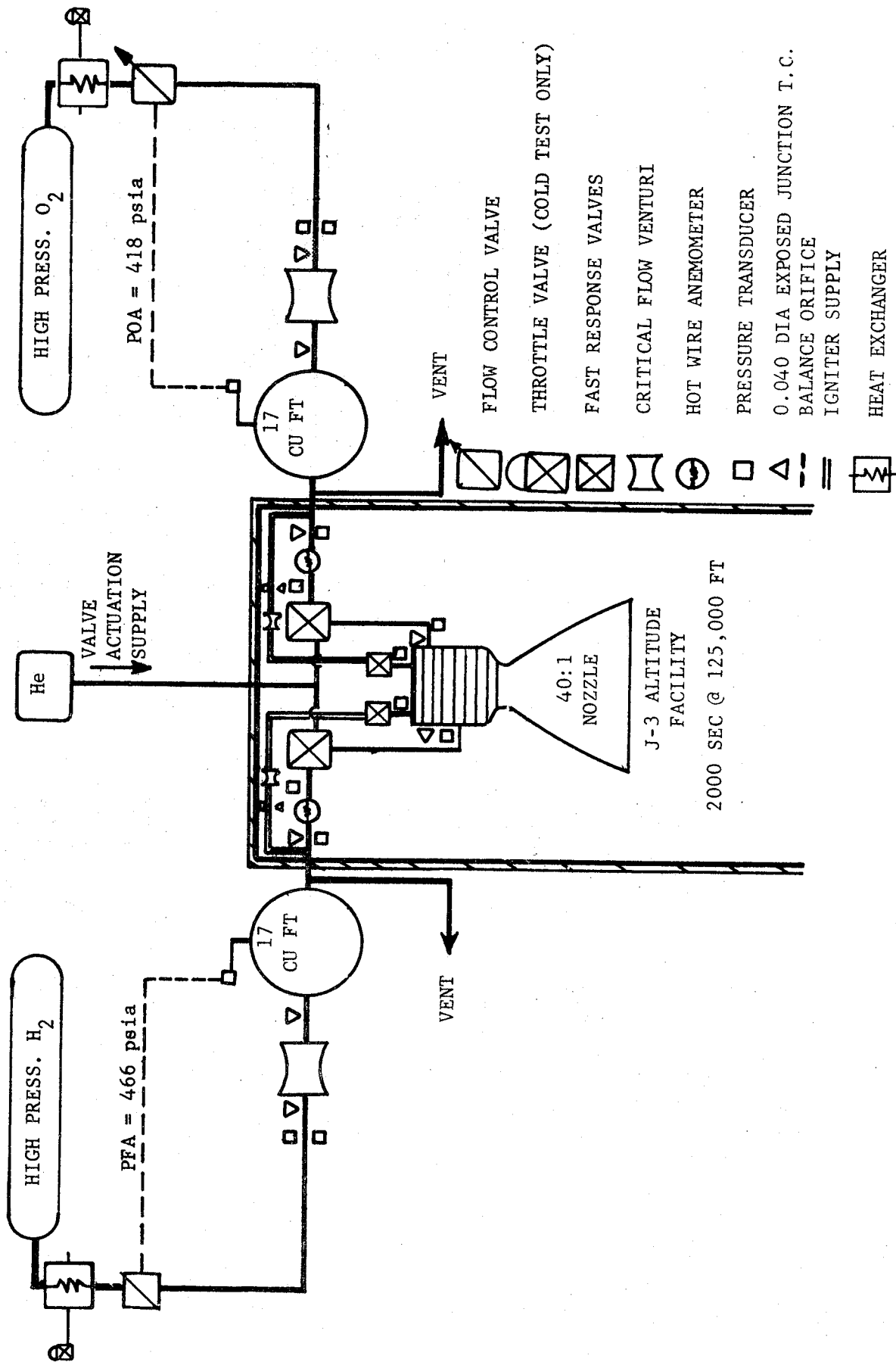


Figure V-24. Flow Schematic for Pulse Tests

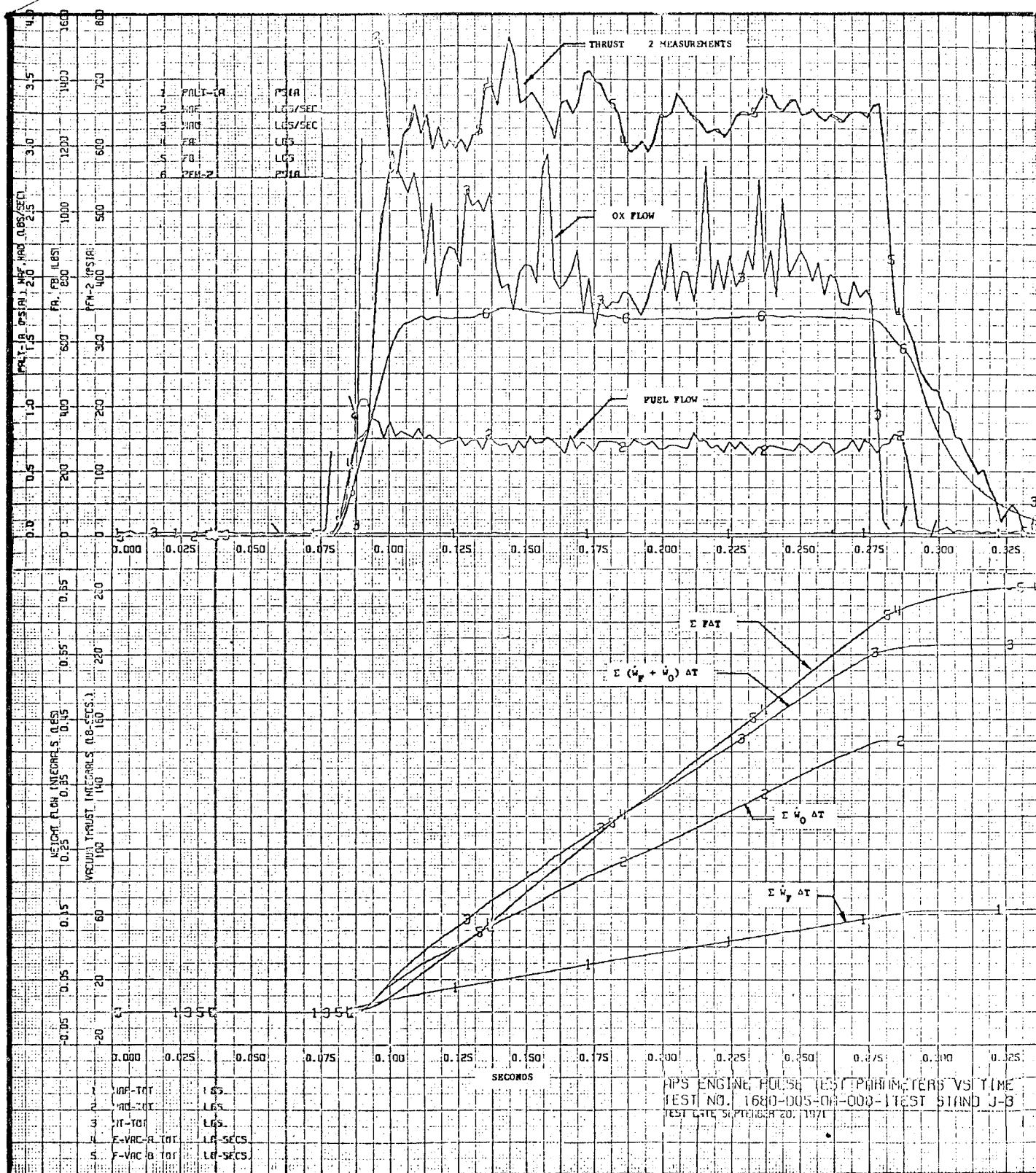


Figure V-25. Digitized Measurements and Integrals in Pulse Testing

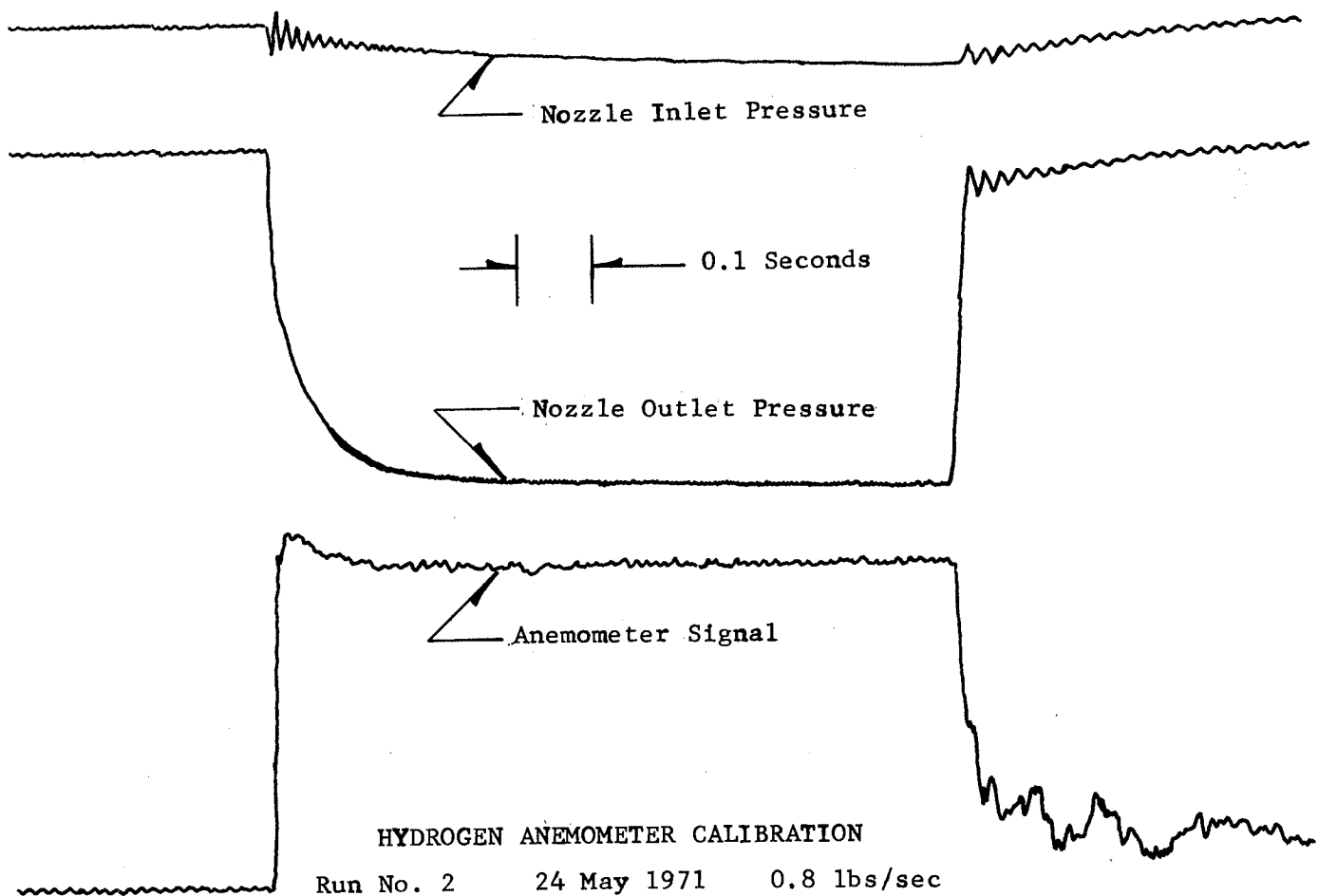
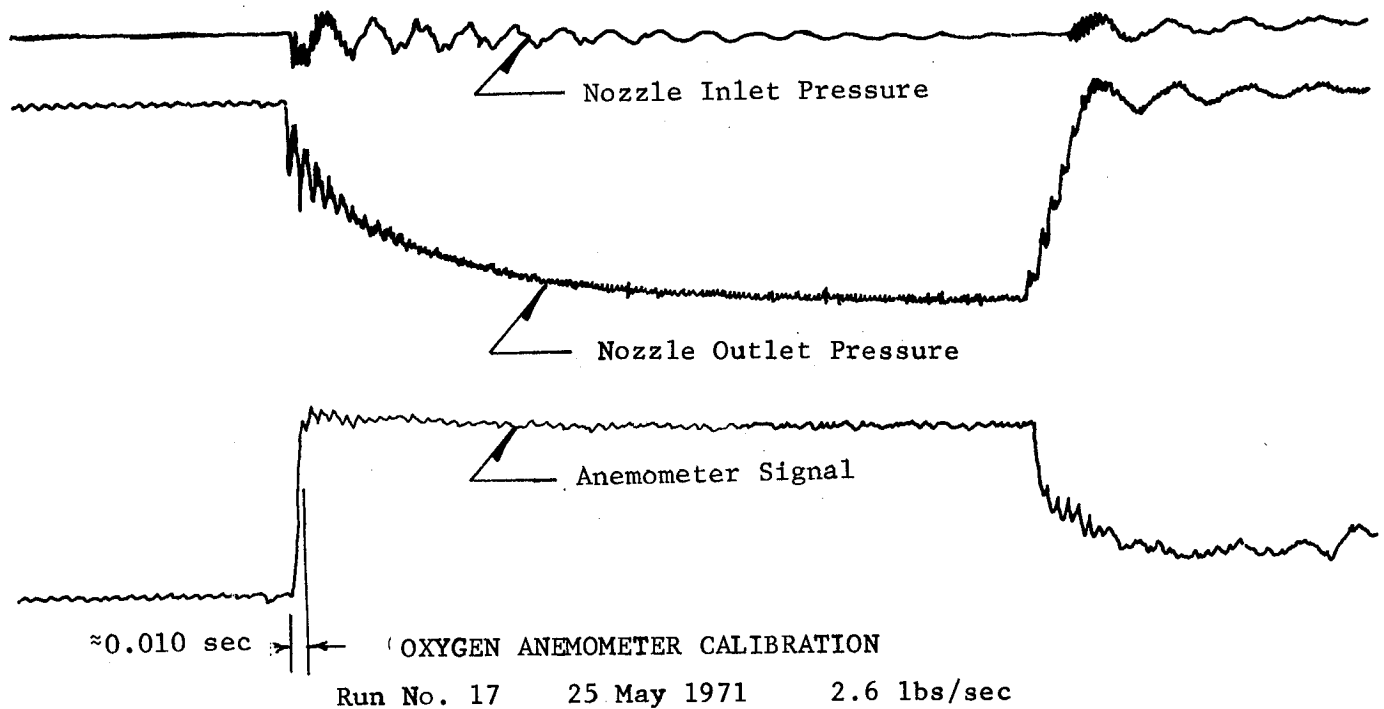


Figure V-26. Anemometer Response and Calibration for Pulse Testing

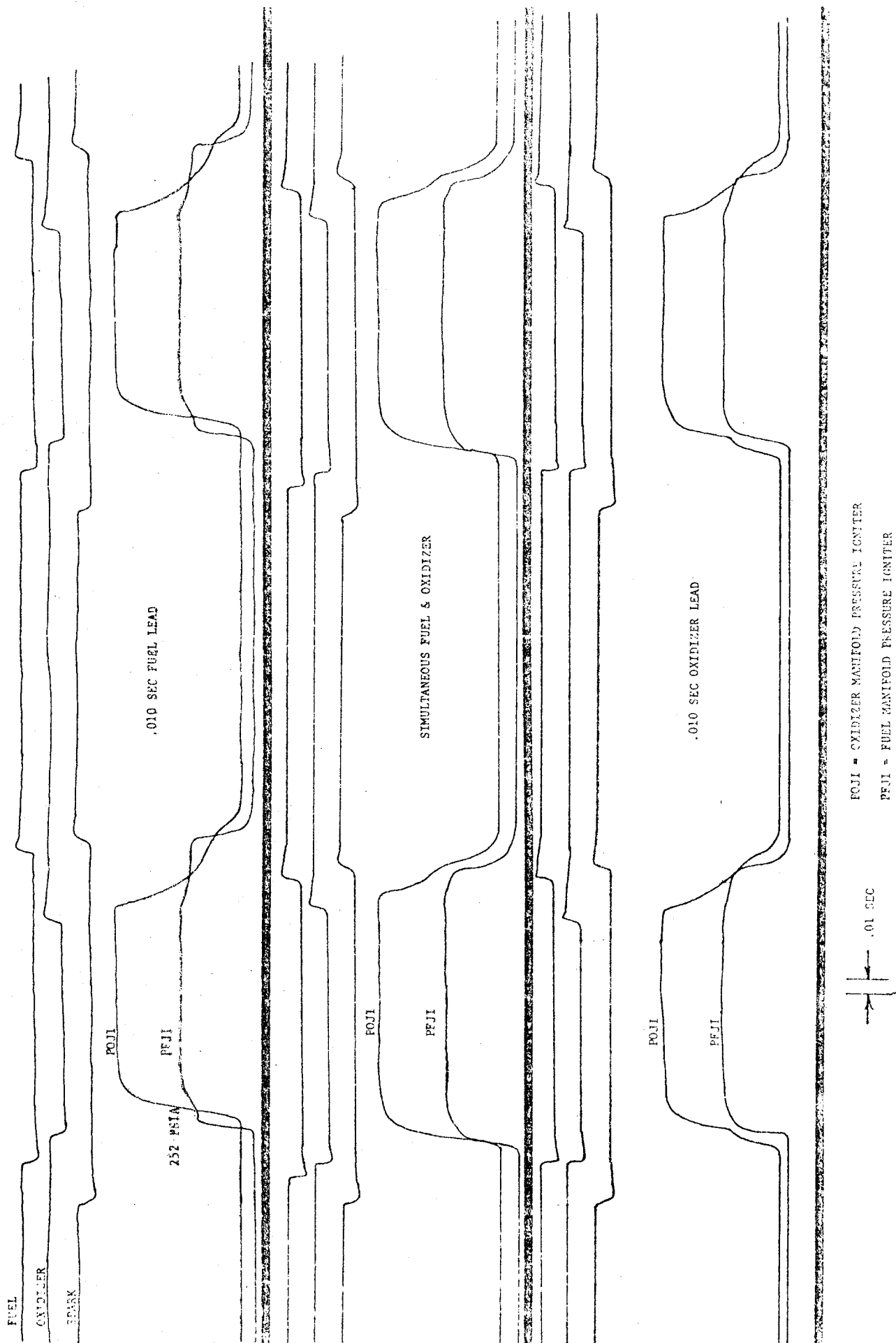


Figure V-27. Igniter Propellant Sequencing Tests

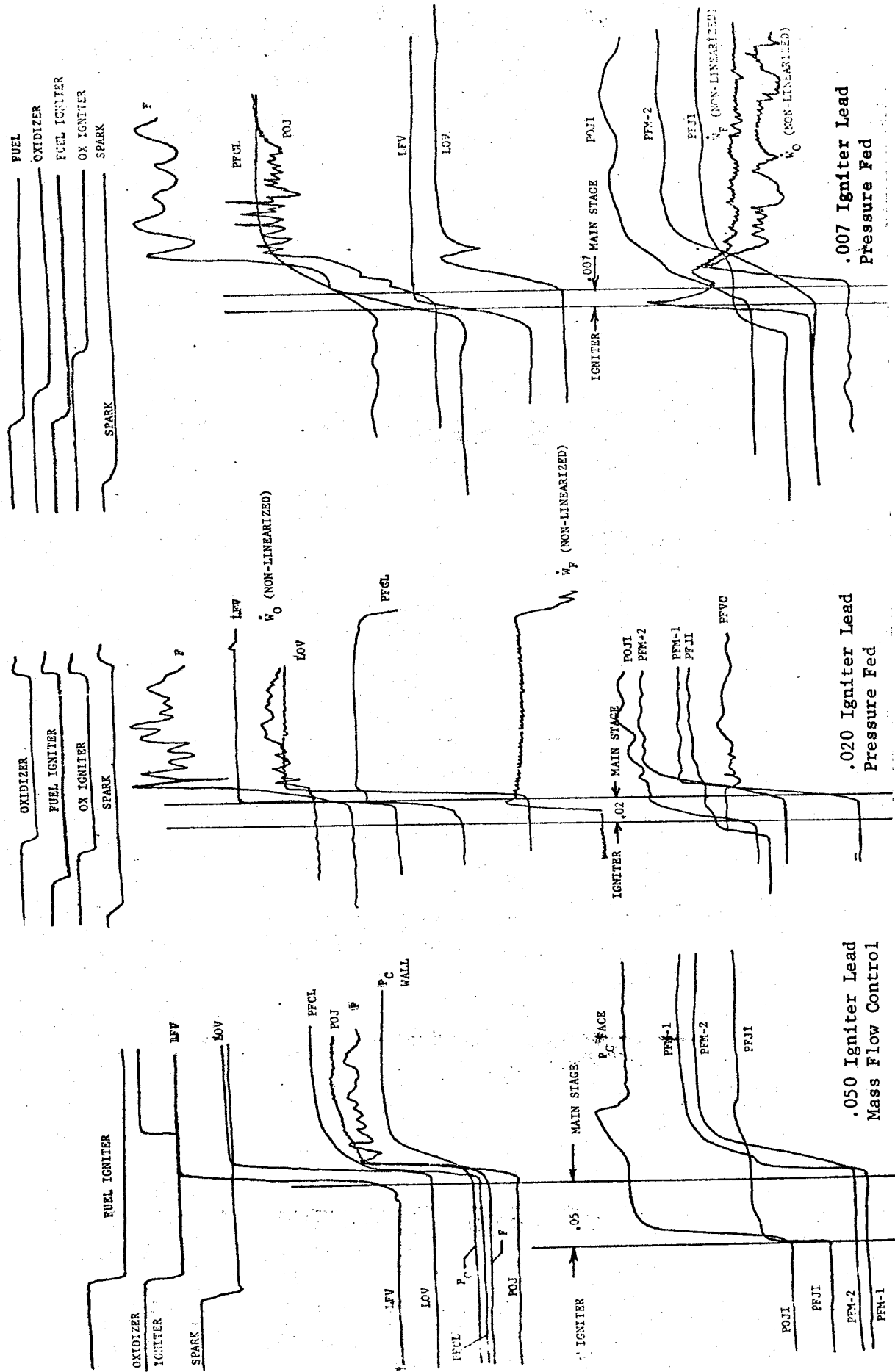


Figure V-28. Igniter Lead - Main Stage Sequencing Tests

ELECTRICAL PULSE WIDTH .23

ELECTRICAL
SYSTEM

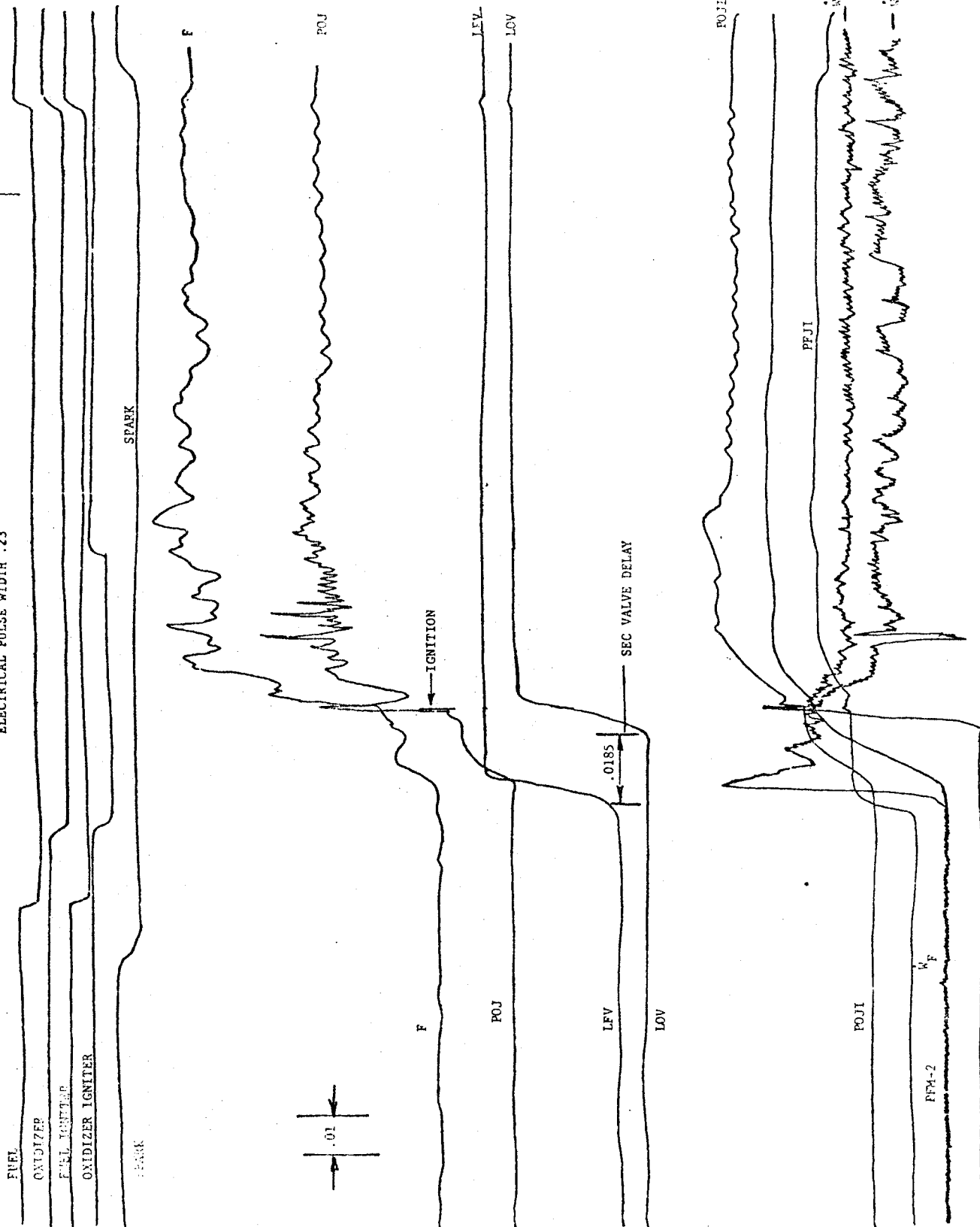


Figure V-29. Ignition Delay with Main Stage Fuel Leading Igniter Ignition
(1680-D05-0A-014)

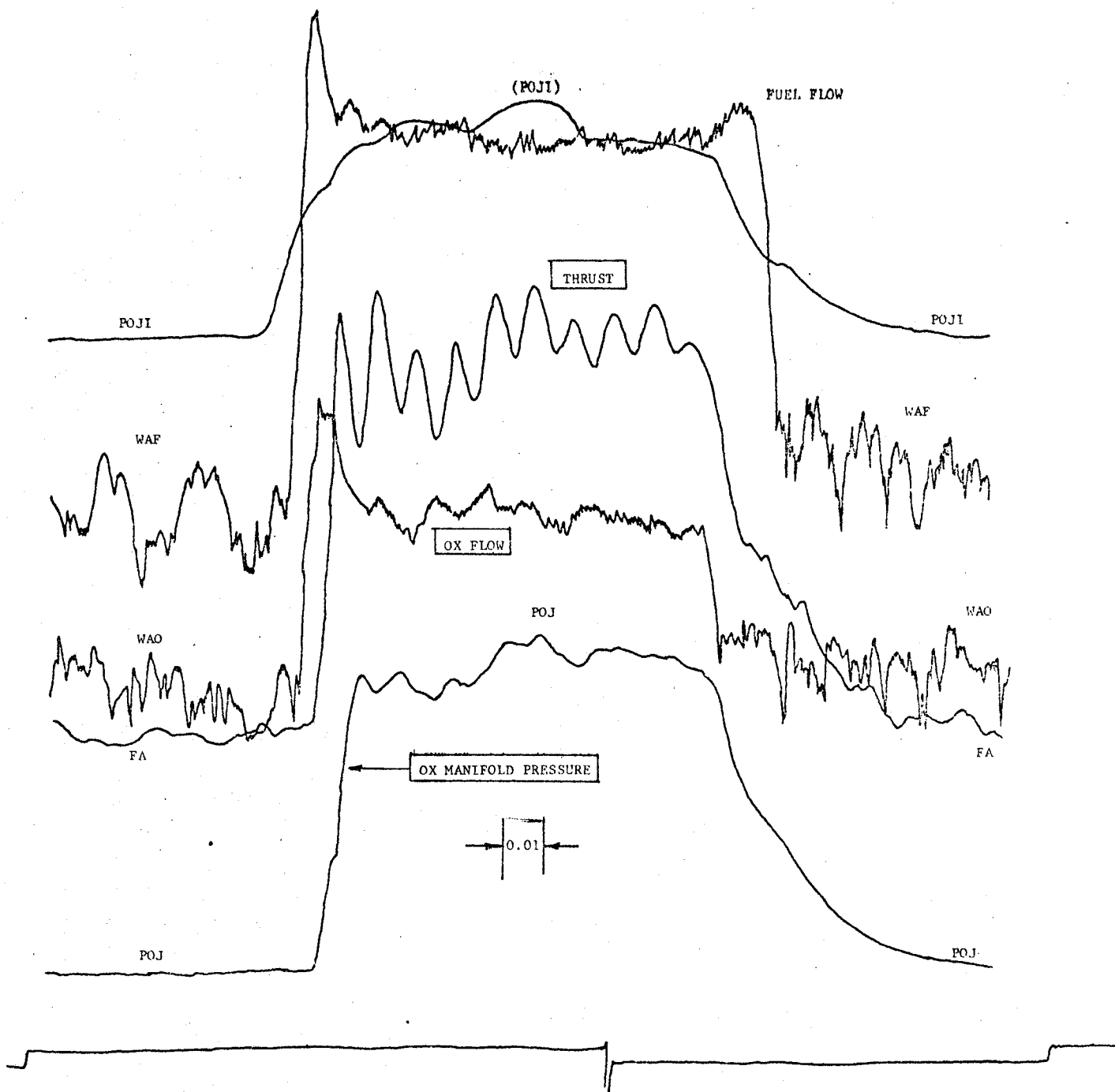


Figure V-30. Ignition Transient and Pulse Characteristics with Simultaneous Fuel and Oxidizer Flow

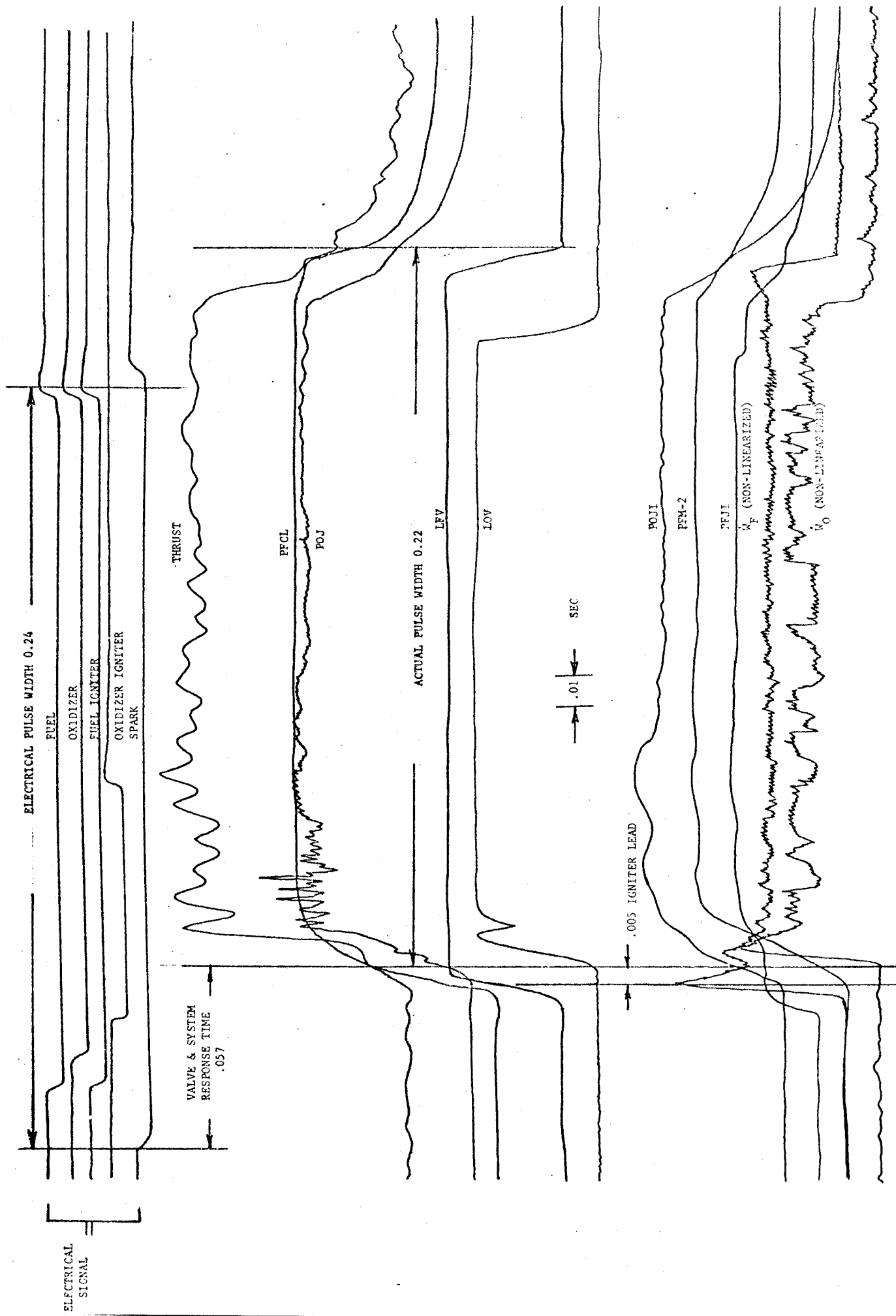


Figure V-31. Pulsing Characteristics for Nominal Pulse Width of 0.2 sec
(1680-D05-0A-016)

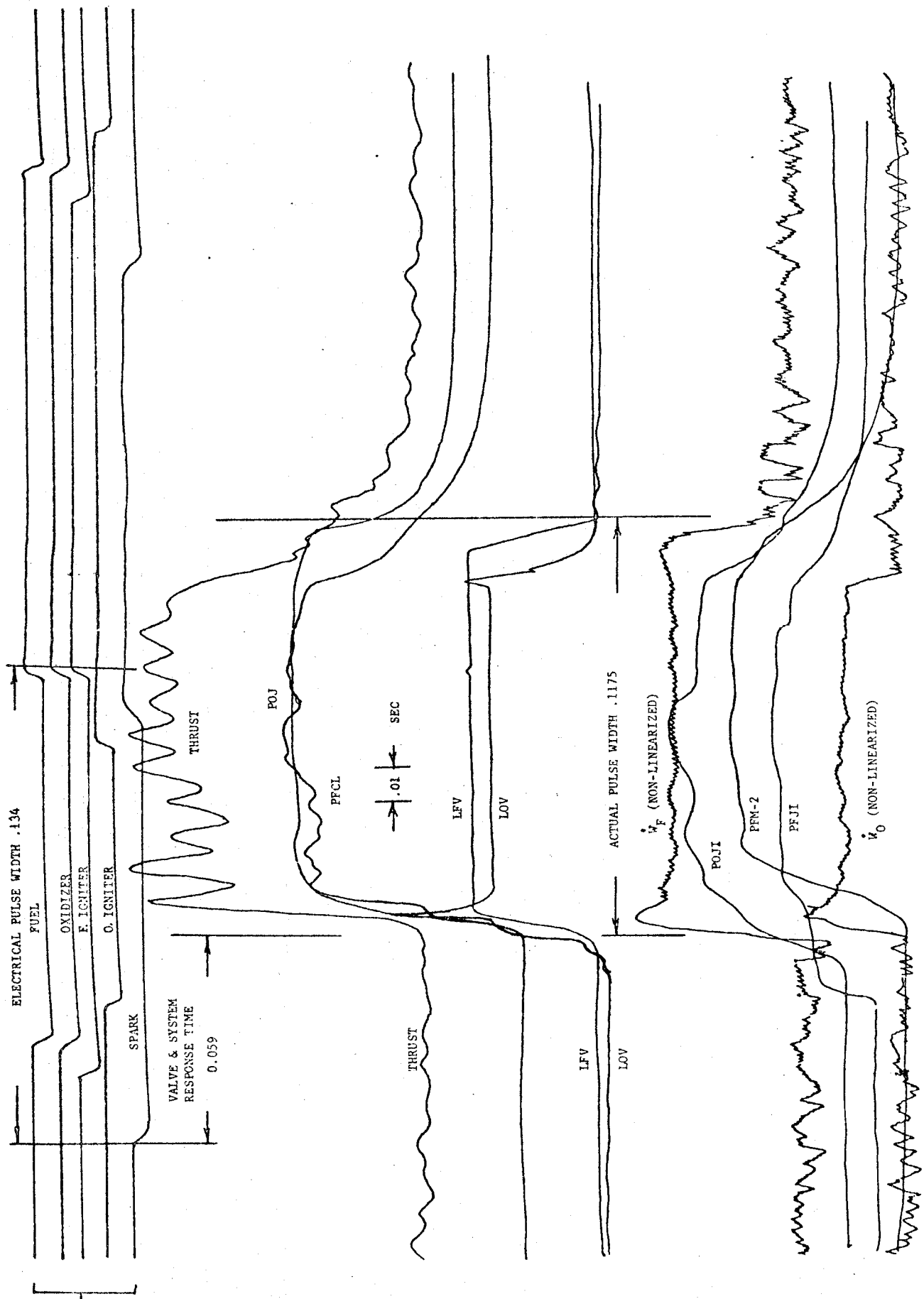


Figure V-32. Pulsing Characteristics for Nominal Pulse Width of 0.1 sec
(1680-D05-0A-028)

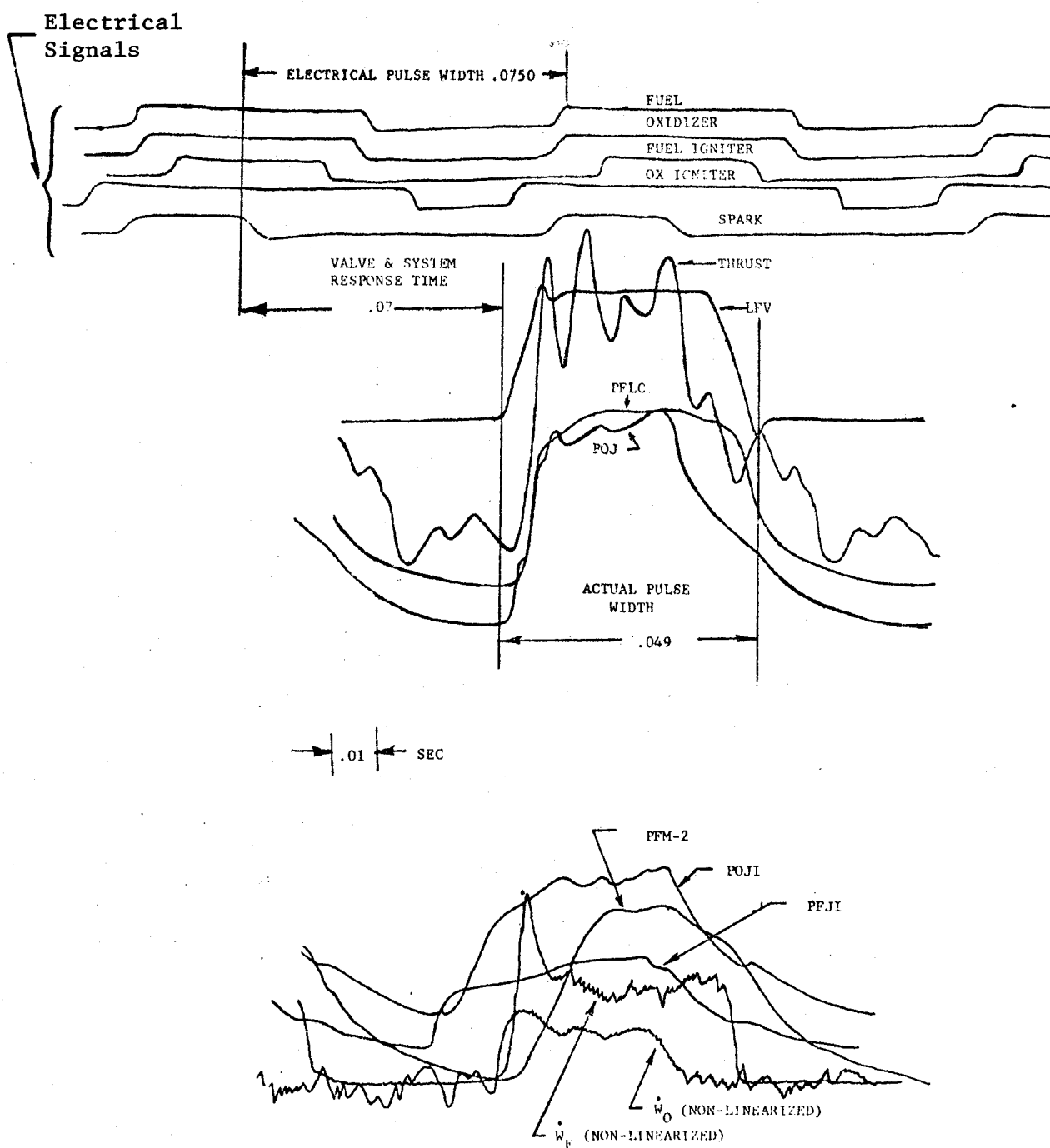
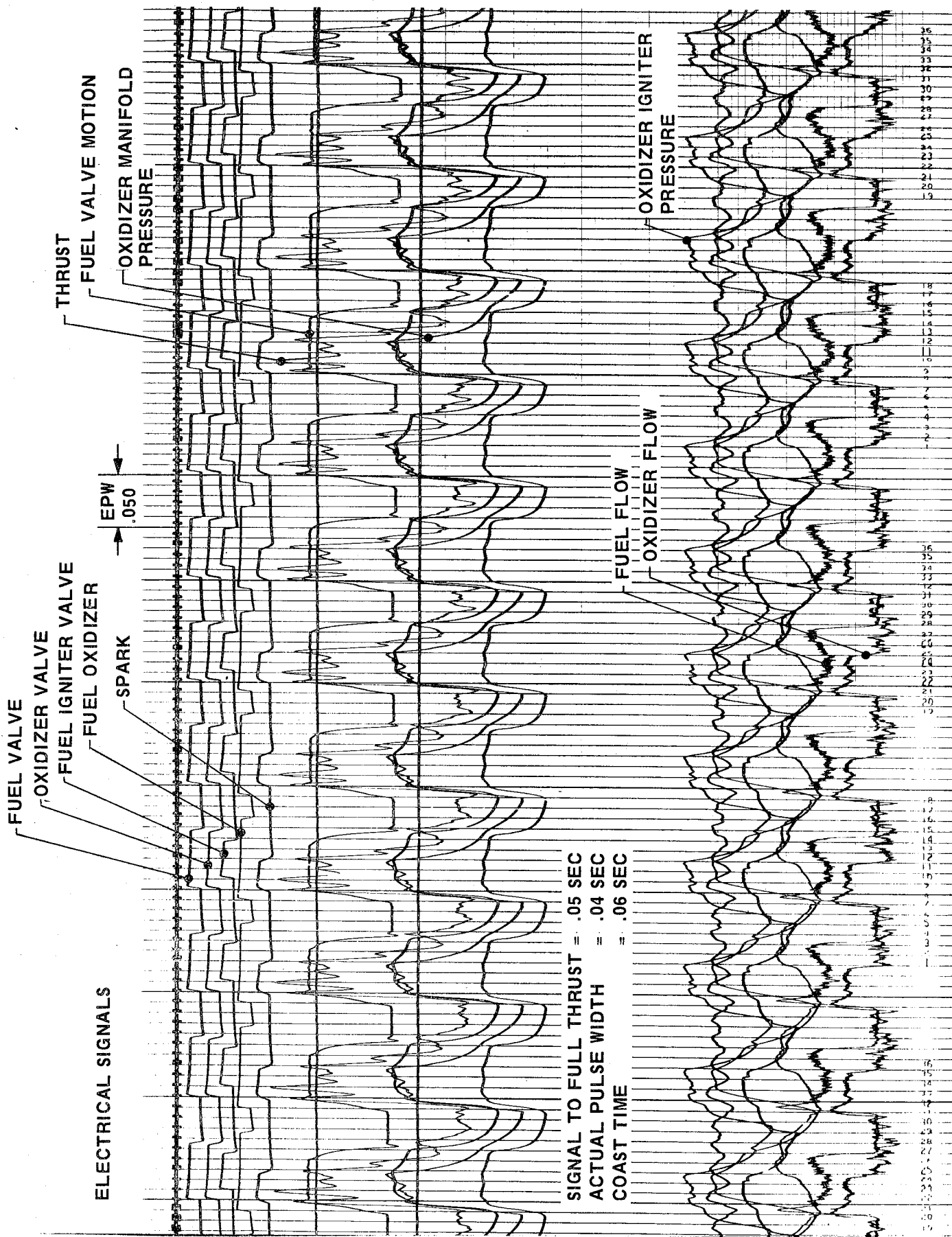


Figure V-33. Pulsing Characteristics for Nominal Pulse Width of 0.035 sec
(Actual Pulse Width = 0.049 sec) (1680-D05-0A-036)



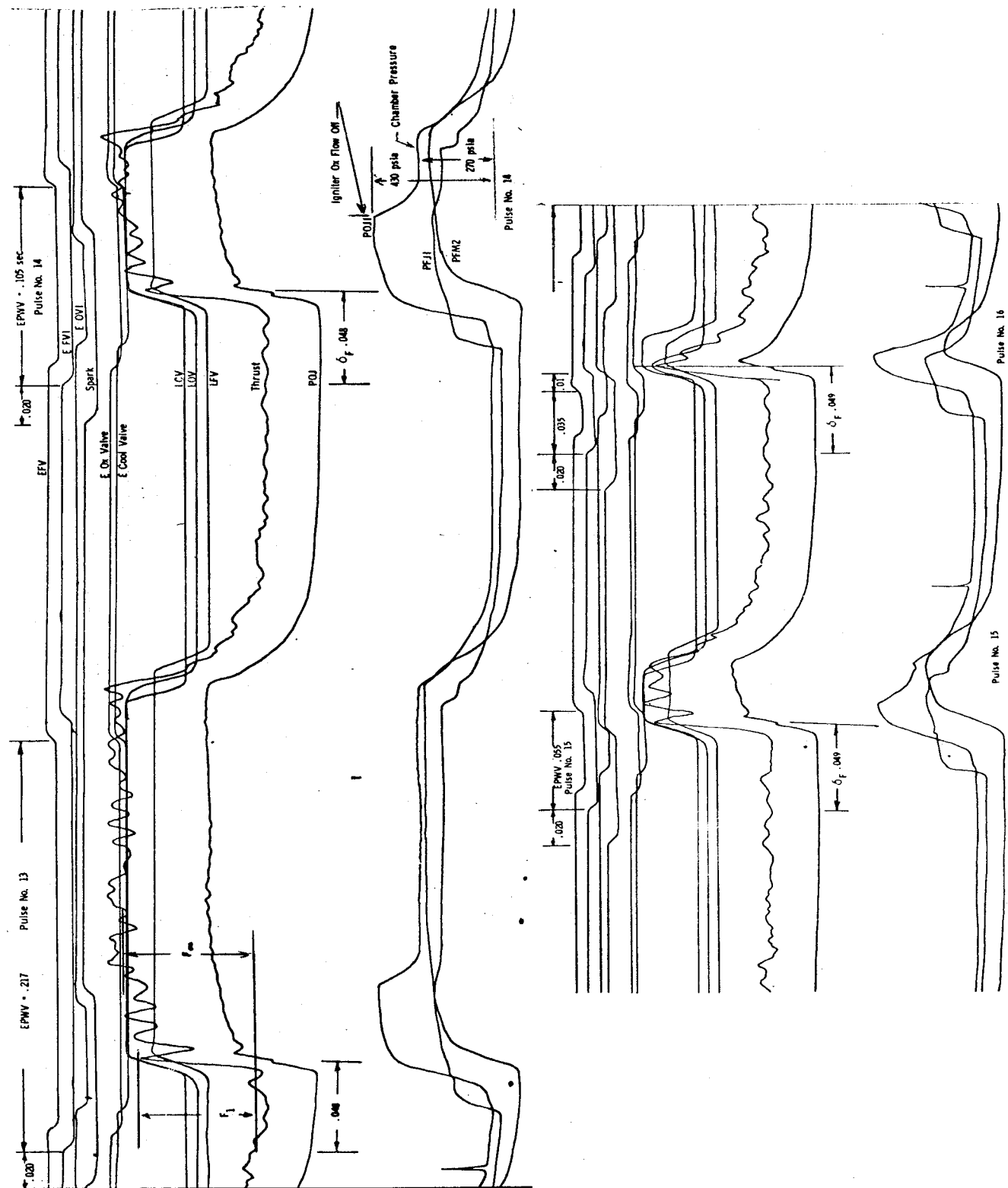


Figure V-35. Pulse Series with Cold Propellants



Figure V-36. Photograph of SN 7, Modified "I" Premix Following the
2500 Pulse Test Series

VI. 40:1 THRUSTER TEST RESULTS

A. STEADY STATE TESTS

1. Cold Flow Acceptance Tests

Prior to hot firing, each thruster was subjected to leak tests and pressure tests and was cold flowed with GN_2 to determine: (a) chamber flow coefficient, (b) flow uniformity within the coolant channels, and (c) to detect possible plugged channels. Uniformity was determined by collecting and measuring the flow from each of the channels.

a. Film-Cooled Chamber (SN 2)

Figure VI-1 shows the coolant channel flow distribution in the regenerative portion of SN 2 film-cooled chamber using a single inlet to feed a constant area manifold. The flow distribution falls within $\pm 10\%$ of the nominal values with the exception of several channels located on either side of the inlet line. The low flow condition on either side of the inlet port was determined to be a result of the manifold aerodynamics rather than obstructed channels because of its reproducibility in both SN 1 and SN 2 chambers. The locally low flow conditions, although acceptable for the technology program, will tend to result in undesirable thermal gradients around the chamber periphery and thus be detrimental to chamber life. When the chamber was flowed with double inlet ports (180 degrees apart), flow distribution was improved. A somewhat more elaborate manifold or baffling will be recommended for future single inlet designs to improve this condition.

The gas flow from individual slots in the film coolant injection circuit could not be collected because the discharge flow was attached to the chamber wall and the spacing between slots was very small. Flow uniformity was established visually with water and also with GN_2 . GN_2 flow was observed by applying a thin film of blackened oil with appropriate

VI, A, Steady State Tests (cont.)

viscosity to the film-cooled wall region between the coolant injection station and a station several inches downstream of the throat. When the GN_2 was turned on, a visual pattern was established by the shear forces which slowly moved the tracer fluid down the wall. This check showed all channels to be open and flowing approximately the same.

b. Regeneratively Cooled Chamber

The cold flow test data for the SN 1 60-channel regeneratively cooled chamber are also shown in Figure VI-1. The coolant inlet manifold in this design is fed at two locations spaced 180 degrees. All channels were found to be open and flowing uniformly within a range of $\pm 10\%$. This flow condition is considered satisfactory. The flow distribution in the skirt film cooling circuit was found to be uniform within 3%.

2. Altitude Performance Testing

Altitude performance data were obtained with three different premix type injector designs using both regenerative and film-cooled chambers. Evaluation of the data indicated that the only real influence which chamber type had upon the delivered performance was in terms of the amount of film cooling required to cool the chamber. At comparable coolant flow rates (independent of the point of injection) with a given injector, both chamber types gave the same delivered performance, all other factors being the same (i.e., mixture ratio, P_c , etc.). Such was not the case, however, with injectors. Distinct performance differences were found to exist between the SN 4 triplet, the SN 5 "I" triplet, and the SN 6 (and SN 7) modified "I" triplet. As a result of the insensitivity of chamber type and the strong influence which injector design had upon performance, the altitude performance will be discussed with the primary hardware emphasis being on injector type. The delivered specific impulse was not influenced by the chamber redesigns for Phase II propellant conditions.

VI, A, Steady State Tests (cont.)

All tests were conducted in the ALRC J-3 vacuum facility at altitude equivalents from 60,000 to 100,000 feet, with a full 40:1 area ratio expansion nozzle. All tests were analyzed using the standardized JANNAF-approved performance evaluation procedure in order to obtain the component losses which describe the performance difference between measured and theoretical. Since all tests were performed using fuel film cooling to demonstrate full duration capability, the injector performance loss could only be inferred from the combination of cooling and energy release losses. Consequently, energy release loss was inferred by using ALRC's thermal exchange cooling model to define the portion of the combined loss attributable to fuel film cooling. Due to the uncertainty of this approach, the bulk of the data portrayed in this report is in terms of delivered vacuum specific impulse rather than correlation of component performance losses.

Delivered vacuum specific impulse exceeded contract goals with both chamber configurations using the SN 6 and 7 premix injectors over the entire coolant fraction range tested. Using design coolant fractions based on heat transfer analysis of chamber and nozzle wall temperature profiles, the following table of design point performance is given for all injector/chamber combinations.

<u>Injector</u>	<u>MR</u>	<u>Film-Cooled</u>			<u>Regenerative</u>		
		<u>% FFC</u>	<u>I_{sp}</u>		<u>% FFC</u>	<u>I_{sp}</u>	
			<u>Amb</u>	<u>Cold</u>		<u>Amb</u>	<u>Cold</u>
SN 6 & 7 (Mod I)	4	18	444	436	10	451	442
SN 5 (I)	4	18	441	--	10	--	--
SN 4 (Triplet)	4	18	432	--	10	438	--

Because the modified "I" injectors (SN 6 and 7) represent the final design which evolved in the course of the program, these injectors will be emphasized in the subsequent detailed performance discussion. A summary of the test conditions, measured data, and calculated performance parameters is presented in Tables V-3 and V-5.

VI, A, Steady State Tests (cont.)

a. Injector SN 6

A total of 65 data points, obtained using both the film-cooled and regenerative chambers, were analyzed in detail to establish the performance characteristics of the modified "I" injector. Table VI-1 denotes the nominal performance values obtained at a design coolant fraction of 10% for the regenerative chamber and 18% for the film-cooled chamber. Also included on the table is the influence of low propellant temperature and high and low chamber pressure over a range of mixture ratios. A more detailed discussion of these summary performance numbers is included in the following paragraphs.

(1) Ambient Propellants

Delivered performance over a range of mixture ratios and coolant fractions is presented in Figure VI-2. The figure includes both the regenerative and film-cooled data. Superimposed on the figure are lines of constant coolant percentage from 30 to 10% in 10% increments. Also included are delivered performance lines corresponding to high chamber pressure (500 psia [345 N/cm^2]) operation which produced a delivered specific impulse increase of 5 sec over the nominal 300 psia (207 N/cm^2) point. Of particular significance is the data with reference to the contract goal of 435 sec at a mixture ratio of 4, which indicates an allowable coolant percentage of nearly 30% is possible without compromising the 435-sec goal. Thermal fatigue analyses show only 18% film cooling is required to meet the film-cooled chamber life requirements, resulting in an 8-sec performance margin. In addition, the relationship between the regenerative and film-cooled performance is particularly interesting since each chamber utilizes a different cooling technique. The regenerative system has downstream coolant injection from the throat with sonic nozzles, whereas the film-cooled engine has coolant injection just upstream of the throat with subsonic injection. In either case, the coolant performance loss is a sole function of coolant percentage rather than being dependent on point of coolant injection.

VI, A, Steady State Tests (cont.)

(2) Cold Propellants

Operation with cold propellants, nominally 220°R (122°K) H₂ and 340°R (189°K) O₂, was completed on both the regenerative and film-cooled chambers using the SN 6 injector. The corresponding performance delivery map for the film and regeneratively cooled chambers is shown in Figure VI-3 as a function of mixture ratio and fuel coolant fraction. At a mixture ratio of 4, the delivered performance corresponding to a 10⁶ cycle life is 436 sec on the film-cooled chamber and using cold propellants.

(3) Chamber Pressure

The influence of chamber pressure on performance (with nominal temperature propellants) was demonstrated on the regenerative chamber using 10% fuel film cooling. The resulting performance (on a mixture ratio base) is shown in Figure VI-4. At 500 psia (345 N/cm²), a 3-sec improvement is noted. This corresponds to the increased kinetic performance. The low pressure data indicate a 3-sec reduction compared to a theoretical kinetic reduction of nearly 7 sec.

(4) Propellant Temperature

Hydrogen propellant inlet temperature was varied from 200 to 800°R (111 to 444°K) using the regenerative chamber with approximately 10% cooling. The performance results are presented in Figure VI-5. The slope of the performance curve matches the theoretical slope, indicating the percent of theoretical specific impulse delivered is not dependent on propellant temperatures. This condition results since the premix "I" element is sensitive only to momentum and velocity ratios (rather than absolute momentum) which remain nearly constant with propellant temperature.

VI, A, Steady State Tests (cont.)

b. Injector S/N 5

A limited data sample was taken of tests conducted using the Phase I "I" triplet injector. All altitude tests with this injector were conducted with ambient propellants and the film-cooled combustion chamber. A performance level of 441 sec was obtained, which was slightly lower than that obtained with the Modified "I" injector (S/N 6) at the design mixture ratio. Comparable performance was achieved at a mixture ratio of 3, indicating the similarity of its mixing characteristics to S/N 6. Performance data over the complete O/F and % FFC operating map is shown in Figure VI-6.

c. Injector S/N 4

A portion of the altitude testing was conducted using a rectangular premix triplet pattern, Serial No. 4. This unit was tested over a range of coolant flows, propellant temperature, and engine mixture ratio. The results clearly indicated the performance superiority of the "I" triplet design. At the design mixture ratio and 18% fuel film cooling, S/N 4 injector developed twelve seconds less vacuum specific impulse than the S/N 6 or 7 Modified "I" triplet designs. This differential decreases to six as the fuel velocity is increased at a lower mixture ratio of 3. The performance data map is portrayed in Figure VI-7 over a range of coolant fractions and injector mixture ratios. With low temperature propellants, the injector demonstrated comparable efficiency without degradations due to reduced fuel velocities. The low temperature performance map is also shown in Figure VI-7.

d. Injector Comparison

Direct comparison of the performance of the injectors is particularly difficult due to the use of variable quantities of fuel film cooling. To decrease this uncertainty, the thermal exchange cooling model was

VI, A, Steady State Tests (cont.)

used to define the performance penalty attributable to fuel film cooling. This model is not an accepted part of the JANNAF Standard Performance Methodology, and is only used in this case as a means to differentiate the injector performance loss. Subtracting this loss and converting the remaining energy release loss to energy release efficiency results in the data comparison shown in Figure VI-8. At the normal design point of the regenerative and film cooled chamber, the following values of energy release efficiency were calculated, which have a $\pm 1\%$ data scatter:

<u>Injector (SN)</u>	<u>Energy Release Efficiency, %</u>	
	<u>Regen Chamber</u>	<u>Film Cooled Chamber</u>
4 Trip	96.3	96.0
5 I Trip	98.3	98.1
6 Mod I	98.8	98.7

Different slopes are noted for the influence of injector mixture ratio on Energy Release Efficiency for the three injectors tested. S/N 6 premix injector, with its optimized "I" fuel configuration and superior oxidizer manifolding, is fairly insensitive to injector mixture ratio showing only a one-half percent ERE variance from 3 to 5 MR. Serial numbers 4 and 5, on the other hand, denote a stronger influence of injector mixture ratio. S/N 5 injector utilized a "I" configuration fuel element but with the pie and concentric ring manifolding. With this combination a performance improvement of over two percent was noticed when the mixture ratio was reduced from 7 to 3. The normal premix injector, S/N 4, denoted consistently lower energy release. The S/N 4 fuel element was rectangular in shape, decreasing its core penetration potential and secondary mixing efficiency. A two percent lower performance was noted. With cold propellants and lower fuel momentum the S/N 4 premix exhibited an apparent gain in energy release efficiency as shown on the Figure VI-8.

VI, A, Steady State Tests (cont.)

To better understand the physical mechanism which produces this sensitivity to injection mixture ratio, Figure VI-9 was prepared defining the sensitivity of energy release efficiency to injection velocity ratio. Referring first to S/N 4 injector, an extreme dependence is noted on fuel to oxidizer velocity ratio. This reduction in mixing loss at high V_f/V_o results due to the increased momentum exchange (fuel/oxid) as the rectangular fuel channel impinges on the showerhead oxidizer. Since the fuel channel is not optimized for maximum confined penetration, the element is very sensitive to increased fuel flow.

S/N 5 and 6 injectors deliver higher efficiency due to their optimized fuel element mixing configuration. These "I" triplet designs achieve excellent penetration through the use of profiling of the fuel channels such that the fuel impinges on the showerhead oxidizer flow in a pattern that yields improved momentum exchange, and thus more effective mixing. The one percent data scatter trend of S/N 6 implies a variable performance of less than one percent over the entire velocity ratio test range. This insensitivity results due to two factors; (1) the optimized element and (2) the superior manifold distribution characteristic as compared to S/N 5. S/N 5 employed a high turning velocity at the entrance to the oxidizer injection orifice which no doubt distorted the distribution over the normal test range. This distortion in some instances may have overridden the beneficial mixing characteristic of the "I" element, thus producing a sensitivity similar to S/N 4, which employed the same manifolding.

e. Film Cooling Performance

As previously stated, the energy release was determined by using the thermal exchange model to predict the portion of the remaining loss which was attributable to fuel film cooling. Using the nominal values the energy release loss for each injector was defined as a unique value at each mixture ratio and the remaining loss was attributed to the cooling process. In so doing the uncertainty

VI, A, Steady State Tests (cont.)

was shifted to the cooling loss to check the data spread. These results are shown in Figure VI-10, as compared to the thermal exchange model prediction. Although this correlation is not necessarily a check of the validity of the model, it is important in terms of defining a loss method to predict injector performance. Using these models, the empirical data model for ERE, the thermal exchange model of cooling loss and the approved JANNAF loss models - the performance of APS thrusters can be predicted with an error of less than one percent over a wide range of operating conditions.

f. Delivered Performance

Up to this point, the performance of the two chambers has been presented in terms of nominal values based on interpolation of graphical presentation from several data points. True demonstration of the APS performance is, however, determined by conducting a test at design point operating condition. For the film cooled chamber, with S/N 6 injector, demonstrated compliance of contract performance was achieved on Test 1680 -D04-04 -012, and 04-018 ambient and cold propellant. A tabulation of the resulting performance is presented in Table VI-2. The demonstrated value at 18.9 percent fuel film cooling is 444.5 seconds of vacuum specific impulse with ambient propellants and 434.4 with cold propellants. This compares favorably with the nominal of 443 and 436 seconds respective values derived from all related tests. Regenerative performance was demonstrated on Tests 1680-D04-0A-020 and 023, with 10.4 percent coolant injected downstream of the throat. Measured vacuum specific impulse was 453 and 442 seconds, respectively, as noted in Table V-2.

VI, A, Steady State Tests (cont.)

3. Steady State Firing Temperature Measurements

a. Film Cooled Chambers

(1) Phase I Thermal Results

Figure VI-11 provides a summary of the measured temperature profiles at normal operating pressures (300 psia (207 N/cm^2) with 530°R (294°K) propellants). Data are shown for three premix injectors (triplet, "I" pattern, and modified "I" pattern), three film cooling flow rates (20, 25 and 30%), and three mixture ratios (3, 4 and 5). The temperature data shown are for the gas-side and backside of the regeneratively cooled cylindrical chamber section, the backside behind the film cooling injection ring (dump section), and the backside of the film-cooled, thin wall spun nozzle and skirt. The influence of the injector on the measured temperature profiles is noticeable. The "I" pattern runs slightly hotter in the forward chamber region because of the very rapid mixing and combustion. The triplet pattern provides lower forward end temperatures and average nozzle and skirt temperatures which are the same as the "I" pattern. However, the slower mixing and combustion rates, combined with propellant maldistribution, results in greater peripheral temperature variation in the throat and skirt. This adversely affects chamber life and causes local hot streaks, requiring more film cooling at higher mixture ratios. The modified "I" pattern (Phase II injector) provides a chamber region thermal load which falls between these two injectors and provides slightly lower maximum and average temperatures in the nozzle and skirt region because of the more uniform peripheral distributions.

The data shown in the left half of Figure VI-11 were generated at constant thrust and mixture ratio with a varying split of fuel between the short regenerative section and the dump film-cooled section. As coolant flow through the dump section is reduced from 30%, the nozzle temper-

VI, A, Steady State Tests (cont.)

atures rise, the chamber temperatures drop, and performance increases. Chamber temperatures drop because of the increased coolant flow through the regenerative section. Reducing the dump coolant flow from 30 to 17% results in a 40°F drop (22°K) in chamber temperatures. The exact variation in temperatures at other stations are provided in Table V-4. Sustained firing has been demonstrated with coolant flows down to 17% with SN 6 injector and Phase I nominal design conditions.

The right side of Figure VI-11 provides a parametric data presentation which identifies the relationship between mixture ratio and coolant flow. These curves are used later in design optimization and to determine the influence of off-design operation on chamber life. The conclusions to be drawn from this figure are:

- (1) The best performing injector (Modified "I") provides the coolest running nozzle and skirt because there is no unreacted oxidizer to cause streaking.
- (2) The chamber region is not influenced significantly by mixture ratio and only slightly by film coolant flow rates.
- (3) Maximum temperatures are attained midpoint in the skirt, 14 to 18 in. (35 to 45 cm) down from the injector face. Beyond this length, radiation cooling through the nozzle exit plane becomes significant and the exit area ratio can be increased with only slight need for additional coolant.
- (4) Under steady-state operation, the maximum axial temperature gradients occur between the film coolant injection plane and the throat.

VI, A, Steady State Tests (cont.)

(5) The radial temperature gradient, gas-side to backside, in the regeneratively cooled region is identified directly from test data.

Figure VI-12 shows the influence of chamber pressure, mixture ratio and propellant temperatures. Chamber pressure is not a significant thermal parameter in the film-cooled nozzle and skirt region except at the very high area ratios where radiation becomes important at the lower chamber pressures. This design does not depend on radiation cooling, and peak skirt temperatures change only slightly with chamber pressure. The regenerative portion of the chamber is only slightly influenced by chamber pressure except in the coolant inlet region where the additional cooling provided by peripheral flow in the fuel inlet manifold aids in reducing the gas-side wall temperatures at lower pressures. The regenerative portion of the chamber is not influenced by MR changes while the throat and skirt are influenced significantly. The mechanism behind this change of temperature with MR is not related to the propellant chemistry but to the reduction of the fuel flow (coolant). It is later shown that wall temperatures are dependent only on the coolant flow expressed as a fraction of total propellant flow and on propellant supply temperature.

The influence of propellant supply temperature depends on chamber location. The trends are independent of cooling percentage, mixture ratio, and chamber pressure. In the regenerative chamber region, a one-degree change in coolant temperature results in a one-degree change in wall temperature. The effect is less significant in the film-cooled nozzle region where a three-degree change in fuel temperature results in only a one-degree change in wall temperature.

The minimum film cooling flow which allows safe operation between mixture ratios of 3 to 5 is 17.5%, at which point the peak skirt

VI, A, Steady State Tests (cont.)

temperature is 2000°F (1370°K). The factors which determine the upper limit skirt temperatures over long durations are chemical attack and creep. The thermal and pressure induced stresses at this point are so low that most materials can operate satisfactorily almost to the melt point for short periods. A chamber balanced to operate with 20% film coolant at nominal design conditions can operate safely anywhere in the following matrix:

P_c	= 30% to 200% design value
MR	= 3 to 5
Propellant Temperatures	= 200°R (111°K) to 800°R (434°K)

The resulting nominal design and most severe temperatures derived from the experimental data for this operating envelope are given below. In this table the Design Phase I & II refers to the range of conditions listed in Table VI-1.

Design Phase:	<u>Nominal Design, °F (°K)</u>		<u>Maximum, °F (°K)</u>	
	<u>I</u>	<u>II</u>	<u>I</u>	<u>II</u>
Throat	1250 (950)	870 (740)	1460 (1070)	1360 (1010)
Maximum skirt	1800 (1260)	1450 (1060)	1930 (1330)	1820 (1270)
Chamber	650 (620)	350 (454)	920 (770)	650 (620)

Measured Start Transient Temperatures

The cyclic life of certain regions of the thrust chamber are determined by the thermal strains generated during rapid transient heating of the chamber wall. Temperature data obtained during the seconds following engine ignition were used to verify the thermal models discussed in Sections VII and VIII. The appropriate thermal models were employed to generate

VI, A, Steady State Tests (cont.)

comprehensive two- and three-dimensional thermal maps required for the finite element plastic structural analyses which identify surface and internal strains. Strain was then converted to cyclic life (N_f) using published or computed S-N curves for the particular material.

Figure VI-13 summarizes the transient characteristics based on data from two tests with ambient temperature propellants at nominal operating conditions. The upper insert on this figure compares the measured gas-side and backside temperature transients with a two-dimensional thermal model prediction. The predictions and data with the modified "I" pattern are in reasonable agreement. Both data and predictions demonstrate that, for this particular start condition, the maximum thermal gradient takes place 0.35 sec after ignition and that steady-state gradients are less severe. It is later shown that hot restarts or starts with cold propellants and ambient hardware are less severe in the transient than at steady state.

The mid-region of Figure VI-13 provides the temperature vs time history at six locations along the monowall film-cooled nozzle. The figure at the bottom identifies the maximum through-the-wall gradient for a 0.040 in. (0.1 cm) wall thickness design. The transient responses for the 0.040-in. (0.1 cm) wall were obtained from the 0.05-in. (0.127 cm) test condition data by computing the heat transfer coefficient and recovery temperature from the transient and steady-state temperatures. These boundary conditions were then used to compute the new profiles and heating rates with wall thickness as a parameter. Steady-state temperatures are not influenced by changes in wall thickness.

Stations 1, 2 and 3 at high exit area ratios heat slowly and have low gas-side to backside temperature differentials. Approximately 20 sec of firing and 300 sec of coast (cooldown) are required to achieve

VI, A, Steady State Tests (cont.)

a full thermal cycle of the skirt. Stations 4 and 5 are located downstream of the throat; station 7 is located upstream. The full thermal heating cycle times for these stations are 10, 3, and 1 sec, respectively. Since the backside and the gas-side conditions are approximately the same, only the gas-side values were shown. Maximum thermal gradients occur approximately 0.1 sec after ignition. These are noted to be small compared to the throat values, station 6. Both gas-side and backside temperatures are shown for the throat station since this is the critical design region for pulse mode operation. In the throat maximum gradients with cold wall starts occur between 0.05 and 0.10 sec; therefore, nearly all single firings will represent a thermal strain cycle for this location. A series of rapid pulses, however, will be less severe than a single, long burn because hot starts do not constitute a thermal cycle.

The lower left figure provides the information required for fatigue life and creep life analyses for nominal Phase I design conditions. Identified therein are: (1) axial temperature gradients at steady-state for creep analyses, and (2) maximum radial temperature gradients and the mean wall temperatures at the time these gradients occur. The latter parameter is required because the material properties employed for the transient life analysis are based on the actual wall temperatures at the time in the run when the stresses are developed. The creep life is based on properties evaluated at steady-state temperatures. The chamber life analyses are covered in Section VIII.

(2) Phase II Film Cooled Chamber Test Conditions

The start transient conditions with cold propellants (Phase II) were generally less severe since the hardware is not prechilled and therefore warm with respect to the incoming fuel. The experimental influence of propellant temperature on steady state wall temperatures in Phase II tests is documented in Table V-4. The influence on chamber life is covered in Section VIII.

VI, A, Steady State Tests (cont.)

The experimental temperatures measured with the SN 3 film cooled chamber (which had a reduced coolant injection area to compensate for the higher density of the Phase II propellant) is presented in the test data correlation of Section VII. The reduced injection area resulted in a slight reduction in chamber wall temperatures. However, analysis of the data suggested that the geometry of the tip of the cooling injector probably has as much influence on coolant effectiveness as does the coolant to core velocity ratio.

(3) Chamber Pressure Drop

The fuel pressure drop in the regenerative circuit of the film-cooled chamber designs is given for the nominal design point in the following table:

$$\Delta P^* = \text{psi (N/cm}^2\text{)}$$

<u>Propellant Temperature</u>	<u>Phase I Test Data</u>	<u>Phase II Predicted</u>
250°R (139°K)	20 (13)	35 (24)
530°R (295°K)	38 (26)	66 (46)

*80% flow through regen circuit, $MR = 4.0$, $P_c = 300 \text{ psia (207 N/cm}^2\text{)}$

The chamber pressure drop can be approximated at other conditions by the following expression:

$$\Delta P = C \frac{(\dot{w})^2}{\rho}$$

VI, A, Steady State Tests (cont.)

where: P = pressure drop, psi
 $\dot{w} = (1 - \frac{\% \text{ film cooling}}{100}) \dot{w}_f$, lb/sec
 ρ = density, lb/ft³
 C = the appropriate flow coefficient from the following table:

Chamber Flow Coefficient (C)

<u>Propellant Temperature</u>	<u>Phase I Design</u>	<u>Phase II Design</u>
250°R (139°K)	22	39
530°R (295°K)	20	35

The slight variation in flow coefficient with temperature is due to the heat addition to the fuel which is not accounted for in the highly simplified expression based on propellant density at the supply conditions.

b. Regeneratively Cooled Chambers

(1) Phase I Chamber Thermal Results

The steady state temperatures recorded in testing of this design are provided in Table V-6 and shown graphically in Figures VI-14 and VI-15.

Figure VI-14 illustrates the measured steady-state gas-side wall temperature in the regeneratively cooled chamber region and measured backside temperatures in the thin wall film cooled steel skirt at nominal chamber pressures of 100, 300, and 500 psia (69, 207, and 345 N/cm²). The injector employed was the SN 6 modified "I" premix pattern. These test data correspond to nominal mixture ratios (4.1-4.5), the minimum film cooling for steady-state operation (10%), and ambient temperature propellants. In these

VI, A, Steady State Tests (cont.)

tests all of the fuel film cooling was injected through nozzles located downstream of the throat to cool the 10-in. (25 cm) long 40:1 area ratio skirt. No head end film cooling was employed.

Phenomena of particular interest in these data are:

- (1) Chamber pressure has only a small influence on gas-side wall temperature in the chamber region, axial distance 2.5 in. (6.3 cm). The reason for this is that the coolant side and gas-side heat transfer coefficients increase with chamber pressure at the same rate while the wall conductance is large relative to the film coefficients.
- (2) The relationship between gas-side wall temperature and chamber pressure in the throat region (5.0-5.5 in.) (12.1-14 cm) is different from the chamber region. There is a considerable increase in throat temperature when the pressure is raised from 100 psia to 300 psia (69 to 207 N/cm²) because the gas-side coefficient has increased at a faster rate than the coolant side. Increasing the chamber pressure from 300 to 500 psia (207 to 345 N/cm²) caused the throat wall temperature to increase further but at a slower rate than occurred in going from 100 to 300 psia (69 to 207 N/cm²). This phenomena is attributed to laminarization of the throat boundary layer at the 100 psia (69 N/cm²) chamber pressure and then undergoing a transition to turbulent behavior in going to 300 psia (207 N/cm²). These results are in agreement with the predictions made earlier using heat sink data.
- (3) The film cooling requirements for the 40:1 skirt are nearly independent of chamber pressure. Approximately 10% of the fuel is required to maintain maximum temperatures below 1805°F (1280°K), which allows the use of a stainless steel skirt. Other materials such as Haynes 188 or columbium alloys would allow further reductions in skirt film cooling.

VI, A, Steady State Tests (cont.)

(4) Temperatures in the film-cooled skirt stabilized at their maximum values, starting at an axial distance of 16 in. (41 cm). Therefore, larger skirt area ratios and scarfed nozzle configurations can be employed without the use of additional film cooling.

(5) The following table summarizes the peak chamber temperatures and provides the estimated life based on the measured wall temperatures and temperature gradients with ambient temperature propellants.

Chamber pressure, psia (N/cm ²)	Peak Temp, °F (°K)	Location	N _f Life		
			Min. Prop.		Max. Prop.
			Steady State	Transient	Transient
100 (69)	632 (607)	Chamber	130,000		
300 (207)	1000 (811)	$\epsilon_c = 1.48$	3,000	2,000	7,000
500 (345)	1194 (918)	$\epsilon_c = 1.48$	1,500	1,300	6,000

At the two higher chamber pressures, the minimum life location was identified as occurring 0.6 in. (1.55 cm) upstream of the throat where the peak copper temperature is achieved. At the lower chamber pressure, minimum life is identified as being in the chamber region. Three values of N_f are indicated: one is based on the steady-state thermal profiles with minimum SN properties; the second at a time in the transient heating when the strain is slightly more severe than steady state (N_f transient); and the third is based on the same transient time, however, with S-N fatigue properties based on a second reference as discussed in the materials section VII. All S-N properties are based on the use of ZrCu. Chamber life and transient operation are discussed in further detail in Section VIII.

Figure VI-15A (top) shows the influence of film cooling introduced around the injector periphery on axial wall temperature profiles.

VI, A, Steady State Tests (cont.)

These results are summarized below along with the predicted cycle life (N_f) based on steady-state thermal profiles with min/max value ZrCu properties.

% FFC	Chamber Temp, °F (°K)	Max Temp., °F (°K)	Throat Temp, °F (°K)	N_f	
				Min	Max
0	700 (645)	1000 (811)	890 (750)	3000	12,000
13.6	600 (589)	940 (778)	870 (739)	4000	15,000
20	430 (495)	730 (661)	630 (605)	6500	25,000

The addition of 13.6% head-end film cooling does little to reduce maximum temperatures (60°F) (33°K) while 20% produces a significant reduction (270°F) (150°K). The addition of 20% film cooling does not provide a significant increase in the life based on steady-state operation.

Figure VI-15B (center) shows the influence of propellant inlet temperature without injector peripheral cooling. These results are also summarized in tabular form below:

H_2 Temp, °R (°K)	Chamber Temp, °F (°K)	Max Temp, °F (°K)	Throat Temp, °F (°K)	$N_{f_{ss}}$	
				Min	Max
201 (112)	490 (527)	830 (717)	690 (640)	3000	12,000
555 (308)	710 (850)	1000 (811)	860 (733)	3000	12,000
772 (429)	990 (805)	1230 (939)	1060 (844)	2000	8,000

At high fuel temperatures, the wall temperature varies at approximately the same rate as the fuel inlet temperature (i.e., a 100-degree change in coolant temperature produces a nearly like change in wall temperature). At low propellant temperature, the wall temperature variation is less than the variation in propellant inlet temperatures. Chamber life is not significantly impacted by propellant supply temperature.

VI, A, Steady State Tests (cont.)

It is not possible to comment on the influence of fuel inlet temperature on the film-cooled skirt region directly from the data since the small difference on test variables such as MR and percent cooling influence the relative values of these data. In general, however, propellant inlet temperature appears to have a second-order effect on the peak skirt temperatures.

Figure VI- 15C (bottom) illustrates the influence of mixture ratio as a variable with all other parameters held fixed. Higher mixture ratios result in higher wall temperatures. However, these differences are small in the regeneratively cooled chamber and throat region (approximately 150°F (83°K) variation in going from MR = 3 to MR = 5). In the film-cooled skirt region, the difference in wall temperature between MR = 4 and MR = 5 is also small (~100°F).

Figure VI-16 provides a comparison of the chamber and nozzle test data with thermal model predictions for nominal design conditions without injector plane film cooling. Shown in this figure are:

- (1) gas-side and backside measured temperatures
- (2) predictions from a 2-dimensional analysis using the SINDA Network Analyzer
- (3) predictions using a simplified 1-dimensional fin heat conduction model.

Both models are in reasonable agreement with each other and the test data. The 1-D model was employed for concept screening while the 2-D model was used to generate more detailed temperature distributions which were used in the structural and life analysis.

VI, A, Steady State Tests (cont.)

(2) Phase I Regenerative Skirt Temperature

Figure VI-17 shows the relationship between skirt film cooling and skirt steady-state wall temperatures, with no upstream film cooling injection. The figure on the left shows the axial profiles for Phase I nominal operating conditions with three values of downstream injection. In this design, maximum skirt temperatures are attained near the maximum nozzle area ratio, which is different from the peak measured in the film-cooled monowall throat design. A film cooling flow of 10% at 530°R (294°K) is required to achieve the design temperature of 1850°F (1280°K) for stainless steel. Through the use of a higher strength steel alloy, which would allow operation at 2000°F (1370°K), the flow requirements could be reduced to 8%. Even lower flows would be required if refractory metal alloys with appropriate coatings were selected. Thermal cycling is not a material selection criterion for the skirts because of the low heating rates.

The data on the right side of Figure VI-17 show the effects of varying MR, P_c , and propellant temperatures from the nominal conditions. The solid lines indicate ambient fuel injection while the dashed lines indicate cold propellants. Chamber pressure and MR are designated by the standard symbols except as otherwise noted. The conclusions which can be drawn from these data are:

- (1) P_c is not a significant parameter in skirt cooling.
- (2) Cold fuel injection (250°R [139°K]) will allow the downstream film cooling to be reduced to 8%.
- (3) Mixture ratio shifts have a measurable influence on skirt temperatures; however, shifts from 3 to 5 can be accommodated safely at the 8% balance point without the use of refractory materials.

VI, A, Steady State Tests (cont.)

(3) Phase II Regeneratively Cooled Chamber Test Results

Four long duration tests were conducted on the Phase II regeneratively cooled chamber with the objective of establishing the limits of laminarization with ambient and cold propellants. The first three tests (Series 06-015, 016 and 017) were with ambient temperature propellants. Pressures were increased from 100 to 500 psia (69 to 345 N/cm^2) in five equal steps with data obtained at mixture ratios of 4, 5 and 6 at the first three pressure levels and 5 and 6 at the two highest pressures. Test 06-018 was a 1976-sec run which provided a matrix of similar data in which propellant temperature, mixture ratio and chamber pressures were all variables. Most of the test duration was with cold propellants.

Figure VI-18 provides the measured (at MR = 5) gas-side and backside temperatures of the regeneratively cooled section of the chamber and a portion of the film-cooled skirt using 9% of the fuel as film cooling. These data were obtained in the upper limit of the Phase II propellant supply temperature range.

The temperature profiles at 100 psia (69 N/cm^2) were very similar to those measured in the Phase I chamber. The throat temperatures were lower than the chamber region temperatures due to laminarization. The redundant wall temperature measurements (90° apart at each axial station) are in excellent agreement except in the throat region where two significantly different temperature levels were recorded. These differences cannot be attributed to injector streaking since corresponding peripheral measurements upstream and downstream of that point show good agreement. The differences in throat region measurements as indicated by the shaded area, are small at low chamber pressures and increase with increasing chamber pressure. Postfire analyses at the design point pressure showed the higher of the two measured gas-side throat temperatures and temperatures in the region downstream of the throat to be in agreement with turbulent

VI, A, Steady State Tests (cont.)

boundary layer predictions. However, the lower of the throat region gas-side temperature measurements, the throat backside temperature, and coolant bulk temperature rise measurements were found to be in agreement with the computer analysis resulting from a laminarization hypothesis as shown in Figure VI-19. If the results are taken at face value, it must be concluded that some regions of the throat laminarized and some did not. The data also suggest the boundary layer undergoes a laminar to turbulent transition in the reduced pressure gradient region downstream of the throat.

The temperature profiles recorded with low propellant temperatures corresponding to the Phase II nominal conditions are shown in Figure VI-20 for three pressure levels. Reducing the propellant temperatures is noted to provide reductions in wall temperatures; however, the profiles and dual level throat measurements are similar to the ambient propellant results. The maximum copper temperatures range between 500 and 600°F (531 and 388°K) at nominal operating conditions.

Figure VI-21 shows the measured axial gas-side temperature profiles for the complete Phase II chamber pressure-propellant temperature matrix, at a mixture ratio of 5. The regeneratively cooled region temperatures are nearly independent of mixture ratio over the 4 to 6 range tested in this series. These profiles are based on the higher values of measured throat temperature. Skirt data points corresponding to two thermocouple locations at the 15.8-in. (40-cm) location are not shown because the recorded temperatures drifted considerably when thrust and mixture ratio were changed. The temperature drift ranged between the curve value as a maximum and approximately 400°F (532°K) as a minimum. The consistency of the two measurements with each other suggest the instrumentation may be responding to a real physical phenomenon. Instrumentation upstream and downstream of this location was well behaved.

VI, A, Steady State Tests (cont.)

Figure VI-22 provides cross plots of the high throat, low throat, and chamber region temperatures vs chamber pressure, with mixture ratio and propellant temperature as parameters.

The figure in the lower left shows the increase in the two throat surface temperature measurements with increasing chamber pressure. The influence of mixture ratio is seen to be secondary. The lower recorded temperatures increase with P_c at a rate which is slightly faster than predicted for a fully laminarized condition. This is expected since the reverse transition is a very gradual process. These temperatures are very close to the dewpoint, indicating water condensation may be taking place. In contrast, the higher throat temperature measurements increase at a rate which is greater than predicted for turbulent flow, which would be a normal characteristic of the transitional region.

The curves on the lower right show the temperature vs pressure relation for the gas side approximately 3 in. (7.62 cm) downstream of the injector which corresponds to the beginning of the convergent nozzle. The slopes of these curves represent the normal relationship for fully developed turbulent flow. The influence of mixture ratio is small at all stations.

The upper half of Figure VI-22 provides the same comparison for cold propellants. It is significant to note that at low pressures the chamber region wall temperatures correspond to the dewpoint temperature while the throat values are below the dewpoint, suggesting a water covered wall. This may explain the lower Phase II skirt wall temperatures shown in the upper half of Figure VI-23. Water flowing off the regeneratively cooled region may be providing additional skirt cooling. The hypothesis of condensation is supported by the 12% higher coolant bulk temperature rise with cold propellants. These reduced skirt temperatures, however, could also be

VI, A, Steady State Tests (cont.)

due to a slight difference in the tip geometry of the supersonic coolant injectors, laminarization of the throat region boundary layer, or a combination of these effects.

The curves presented in the lower portion of this figure are the differences between the measured gas and measured backside temperatures. These are employed in the thermal fatigue life analysis. The coolant bulk temperature rise measurements showing a higher coolant temperature rise in the throttled condition is a normal characteristic for regeneratively cooled chambers.

Start Transients

Figure VI-24 shows the throat transient heating rates for both wall measurements. The left side presents data obtained at 100 and 200 psia (69 and 138 N/cm²) with ambient propellants while the right side presents data from an ambient start at 300 psia (207 N/cm²) with the fuel being chilled in while the engine is running. The cooldown rate of the fuel is noted to influence the measured wall temperatures.

c. Conclusions - Regenerative Chamber

The Phase II design represents an improvement over the Phase I design in that lower chamber wall temperatures were achieved with less coolant pressure drop while requiring lower skirt film cooling flows. Temperature measurements with the Phase II design gave a mixed reading on throat laminarization, some measurements indicating laminarization occurred over the entire pressure range while other measurements indicated only more limited laminarization occurred. The Phase I and Phase II designs are compared as follows for the nominal design point.

VI, A, Steady State Tests (cont.)

	Coolant ΔP , psi (N/cm ²)	T _{wg} Max, °F (°K)	% FFC	N _f *
Phase I	23	830 (717)	10	3000
Phase II	21	650/470 (617/517)	6.5	3000/8500

*Nominal design at steady state, minimum ZrCu properties.

If one assumes that very limited laminarization occurred with the Phase II chamber, then the life limiting portion of the design is the throat and the cycle life capability is the same as that of the Phase I design (i.e., 3000 cycles). If, on the other hand, the cycle life analysis is based upon the data which indicate complete laminarization did occur, the life limiting portion of the design no longer is the throat but switches to the chamber. The cycle life capability of this particular chamber design is 8500 full thermal cycles. However, slight modifications to the chamber portion of the design to make it more closely resemble the film-cooled chamber can raise the cycle life capability of the unit to over 30,000 full thermal cycles.

VI, 40:1 Thruster Test Results (cont.)

B. PULSE TESTING

1. Valve Response

The limiting factor in the response of the gas-gas propellant system was found to be the valve actuation time. In the test program conducted, the electrical signal to mainstage ignition period was approximately 0.045 sec with an additional 0.005 sec to full thrust. The limiting factor in valve actuation was the electrical power buildup rate in the main valve pilot valve. The following table summarizes the valve dynamic characteristics during three tests in the program with the indicated service background and operating conditions. Figure VI-25 shows the relation between valve actuation and total impulse for ambient and cold propellants.

(1) Test 05-015 - This test occurred after 5500 actuations with the main valve. The stem and seat seals had been replaced in a preventive maintenance servicing several hundred actuations prior to the data point shown. Propellants were at ambient temperature.

(2) Test 06-010 - This test took place after approximately 8500 total actuations with no additional inspection or servicing for the additional 3000 firings which occurred after Test 05-015. The propellants and the valve body were cold.

(3) Test 06-014 - Same life condition as Test 06-010 but with ambient temperature propellants.

Valve Response Characteristics, sec

<u>Condition</u>	<u>Test 05-015</u>		<u>Test 06-010</u>		<u>Test 06-014</u>	
	<u>Fuel</u>	<u>Oxid</u>	<u>Fuel</u>	<u>Oxid</u>	<u>Fuel</u>	<u>Oxid</u>
Electrical signal to full open	0.035	0.036	0.042	0.036	0.045	0.040
Electrical signal to full close	0.042	0.032	0.048	0.035	0.048	0.030
Travel time - open	0.008	0.008	0.011	0.012	0.012	0.010
Travel time - close	0.009	0.010	0.012	0.012	0.012	0.010

VI, B, Pulse Testing (cont.)

The valve travel time of 0.010 ± 0.002 sec is typical of the repeatability noted throughout the program under all combinations of propellant supply temperatures and pressures and under the very full operation conditions in the altitude cell (see valve section). The ± 0.002 sec variation from the nominal did not adversely affect system characteristics.

The fuel valve response was somewhat poorer than the oxidizer valve at the start of testing and the condition generally got worse during testing. This is attributed to the severe environment (consisting of sand and steam or ice) and aging of the pilot valves (which had over 5000 actuations coming into this series and were never inspected or serviced). At all times, however, the propellant valves were capable of providing the response necessary for the program objectives.

The valve sequencing on this program was never fully optimized because the valve electrical signals could only be advanced or regressed in increments of 0.010 sec. This limitation in valve vernier sequencing was due to the manner in which the electrical system had been set up to handle the long pulse trains. The electrically recognized time span was ranged from 0.010 to 999 sec. A more suitable choice would have been 0.001 to 99 sec which would have allowed valve sequencing increments of 0.001 sec to be available.

2. Minimum Impulse (Thrust Time Integral)

The minimum repeatable bit impulse obtainable was 27.5 lb-sec (122 N-sec) with the mass flow controlled system and cold propellants. The system is valve actuation limited. In this 0.035-sec pulse width, the fuel and coolant valve travel was fully closed to fully open to fully closed. The oxidizer valve travel was closed to 67% open to closed. Valve response times (in seconds) were as follows:

VI, B, Pulse Testing (cont.)

	<u>Signal to Max Open</u>	<u>Travel Open</u>	<u>Full Open Time</u>	<u>Travel Closed</u>	<u>Signal to Full Closed</u>
Fuel valve	0.044 (100%)	0.012	0.011	0.012	0.040
Oxidizer valve	0.042 (67%)	0.012	0	0.012	0.026
Coolant	0.030 (100%)	0.008	0.015	0.010	0.030

Additional system characteristics with the mass flow controller were:

	<u>Pulse Width, sec</u>			
<u>Test 06-010</u>	<u>0.214</u>	<u>0.108</u>	<u>0.054</u>	<u>0.035</u>
T_1 ; signal to igniter valves to F_1	(0.048 to 0.050 sec, all values of EPWV)			
F_1 , lb (N) (see Figure V-35)	1242 (5630)	1275 (5680)	1287 (5730)	1300 (5790)
F_1/F_∞ ; $F_\infty = 1515$ lbf (6730 N)	82%	83%	85%	86%

The lowest impulse demonstrated with ambient propellants without the mass flow controller was 74 lb-sec (330 N-sec); however, the system was not pushed to its minimum. Some comparisons of the shortest demonstrated pulse with and without the mass flow controller are as follows:

	<u>Minimum Demonstrated Impulse</u>	
	<u>With Mass Flow Control</u>	<u>Without Mass Flow Control</u>
Propellant temperature	Cold	Ambient
Signal to mainstage ignition, sec	0.044	0.045
Signal to F_1 , sec	0.050	0.049
F_1/F_∞	0.86	1.34
Time at full thrust, sec	0.0	0.032
Oxidizer valve electrical signal, sec	0.027	0.046
$\int f dT$ lb-sec (N-sec)	27.5 (122.5)	74.0 (329)

VI, B, Pulse Testing (cont.)

From the above data, it can be noted that the time to ignition is unaffected by the use of the mass flow controller or lowering propellant temperatures. This is a highly desirable feature of the spark/oxidizer torch design. The time from ignition to F_1 as defined in Figure V-35 is also unaffected. The main difference is the ratio of F_1 to steady-state thrust. The initial rise with the mass flow controller is much slower, such that there is no thrust overshoot (i.e., 86% vs 134%). These impulse results are in agreement with the anemometer starting weight flow measurements made with and without the mass flow controller.

The minimum impulse is controlled by the minimum time the oxidizer valve can be kept unseated. The minimum impulse without the mass flow controller and a 0.027-sec valve signal, estimated by the ratio of the peak thrust F_1 , is 44 lb-sec (196 N-sec).

Bit Impulse Repeatability

Tables VI-3 and 4 summarize the pulse tests, test conditions, and repeatability. The results are shown graphically in Figures VI-26 and VI-27. The pulses were generally reproducible within 5% of the average value. The results were more reproducible with the pressure-fed system and ambient propellant temperature than with the mass flow controller and cold propellants.

The change in the thrust integral with the pulse number is due to the characteristics of the mass flow controller with cold propellants. The first propellant to the thruster, particularly the oxidizer, is warmed because of the 10-sec coast time between the long burn and first pulse. The propellant temperatures drop $\approx 25^\circ\text{F}$ (14°K) with subsequent pulses and the mass flow controller attempts to adjust the feed system supply pressures (down) to maintain the programmed flow rates. The volume in the 17 cu ft accumulator

VI, B, Pulse Testing (cont.)

tanks between the flow control valve and the critical flow nozzles, however, limit the rate at which the system can respond. The first pulses therefore have a slightly higher bit impulse than the subsequent pulses. If the first pulses are excluded from consideration, the repeatability is within a 9% band for all thrust-time integrals. The variance, including the first pulses, is $\approx 13\%$. Variation of the thruster mixture ratio between 3 and 4 did not significantly influence the bit impulse and MR effects are included in the above-quoted variances. These are shown in Table VI-4.

Several aspects of the operational mode with cold propellants are significant. One is that no control was maintained over the igniter flow rates or mixture ratios after the initial balance point was set. The igniter venturis were sized to provide a specific flow at a particular upstream temperature and pressure condition. The temperatures of the propellants arriving at these venturis, however, are influenced by the supply condition which was noted to vary considerably with time. The heat addition to the two-meter line length between the igniter tapoff and the igniter venturis further influences the relative oxidizer and fuel flow rates. Propellant supply pressures to the igniter and mainstage were common and were controlled to maintain mainstage thrust and mixture ratio without regard to its influence on the igniter. As a result, the igniter had to be capable of operating over a wide range of conditions. The igniter oxidizer manifold pressure (POJI) test record shown in Figure V -35 demonstrates this aspect. The igniter was balanced to provide flows corresponding to 300 psia (207 N/cm^2) at a $\text{MR} = 6$ with 500°R (277°K) propellants, which would have been the condition if this was the first pulse after a very long period of inactivity. Since the fuel was actually very much colder and the oxidizer only slightly chilled, the measured POJI was 430 psia (297 N/cm^2) and the igniter mixture ratio was unknown (but probably less than 6). The influence of these events on igniter reliability is covered in a subsequent section.

VI, B, Pulse Testing (cont.)

3. Pulsing Performance

Bit specific impulse [thrust integral/flow integral] was computed for the various pulse widths. These data were generated by evaluating individual pulses in long pulse trains and by the average of a series of successive pulses. The computed bit specific impulse for the ambient propellant test series with the film-cooled chamber is provided in Figure VI-28. The bit specific impulse was found to be dependent mainly on valve sequencing for the very short pulses, 0.03 to 0.05 sec, whereas the pulsing performance was demonstrated to closely approximate the steady-state values at pulse widths of 0.1 sec or greater. Performance data was not obtained with cold propellants because the anemometer calibrations were invalid in the low temperature range.

4. Ignition Repeatability

A total of 89 pulses were conducted in this latter cold propellant series during which 16 no-ignitions and 7 delayed ignitions were noted. The distribution of these were as follows:

1) by pulse width

<u>Pulse No.</u>	<u>Electrical Pulse Width (sec)</u>	<u>Electrical Pulse Width (Valves) (sec)</u>	<u>Number No Ignitions</u>	<u>Igniter Ignition Delays (sec)</u>
1	0.234	0.214	1	None
2	0.128	0.108	5	0.045, 0.030, 0.030, 0.025
3	0.074	0.054	7	0.012
4	0.055	0.034	3	0.006, 0.012

VI, B, Pulse Testing (cont.)

2) by test number

<u>Test No.</u>	<u>Delays (sec)</u>	<u>No Ignitions</u>
007	1 @ 0.045	1
008	1 @ 0.006	None
009	3 @ 0.030, 0.012, 0.012	7
010	2 @ 0.030, 0.025	8

Some trends were apparent from these data as more nonignitions on the EPWV of .108 and .054, and increasing failures on the latter two tests. The mixture ratio of 3 used in Test -009 and the higher spark power level in Test -010 would on the surface appear to aggravate the situation.

On each of the ignition failures the cause was determined to be failure of the igniter to ignite. Unfortunately, there was no instrumentation to sense the high voltage discharge in the spark box or at the spark gap. Immediately following this series a sequence of igniter only tests were conducted in an attempt to further identify the possible reasons for the delayed and ignition failures. A total of six individual igniter only firings were conducted which reproduced the pulse test propellant supply conditions. This included changes in mixture ratio and absolute pressure levels up to 430 psia. In all cases the igniter experienced satisfactory ignition and it was not possible to produce a no-light situation.

Additional testing with an improved electrical system is required to determine if the nonignitions are due to electrical problems.

5. Thermal Characteristics

During thruster pulse testing, film coolant was supplied to the chamber from the main fuel valve via an external bypass line containing a

VI, B, Pulse Testing (cont.)

0.375-in. (.95 cm) -dia sharp-edge flow control orifice which limited the coolant flow to 20%. The thruster temperatures were lower during continuous pulsing than in continuous firing at all chamber and injector locations. Comparison of the ratio of pulsing to steady-state temperature are:

<u>Location</u>	Steady-state Temp, °F (°K)	Fraction of Steady State Temperature On Time/Off Time Duty Cycle		
		0.2/0.3	0.1/0.15	0.054/0.046
Injector face	550 (562)	0.91	0.82	0.76
Combustion chamber wall	600 (588)	0.87	0.87	0.79
Tip film cooling ring	710 (650)	0.84	0.99	0.93
Throat	1100 (867)	0.78	0.83	0.80
Skirt maximum	1620 (1155)	0.86	--	--

The thermal characteristics recorded on the control room Brown recorders are shown in Figures VI-29 and VI-30. Additional temperature measurements were made at the following locations to monitor heat soaks:

- Oxidizer and fuel igniter valve bodies
- Main stage oxidizer and fuel valve bodies
- Backside of injector
- Injector flange

During continuous pulsing, the igniter and main stage valve temperatures reflected the propellant temperatures flowing through the valves. All valve temperatures ranged between 40 and 80°F (277 and 300°K) even after 840 pulses. The injector back reached 150°F (339°K) in continuous pulsing while the flange reached 450°F (505°K), which are all within acceptable limits of the design. Postfire soaks were accomplished without purges or external cooling and ambient pressure was maintained at 0.5 psia or less to prevent convective cooling. As can be noted from the postfire soak traces and data provided in Figures VI-29 and VI-30. The injector face temperature drops almost immediately to 250 to 300°F (395 to 422°K). The chamber temperatures, including the throat

VI, B, Pulse Testing (cont.)

and skirt, drop to the 100 to the 225°F (311 to 380°K) range within 5 minutes after shutdown.

No thermal limitations were encountered in the 2800 pulses conducted in this program other than the coil overheating on the fuel pilot valve in Test 05-037, which was due to excessive electrical power input at ten firings per second.

TABLE VI-1

(1)
DELIVERED VACUUM SPECIFIC IMPULSE
lbf-sec/lbm (N-sec/Kg)

MR	Inj SN	Regenerative Chamber (2)				Film-Cooled Chamber (3)			
		Propellant Temperature and Pressure				Propellant Temperature & Pressure			
		P _c = 300 psia (207 N/cm ²)				P _c = 300 psia (207 N/cm ²)			
		High Temp	Amb Temp	Low Temp	High (4) Pressure	Los (4) Pressure	Amb Temp	Low Temp	High (4) Pressure
3	6 M "I"	--	455(253)	444(247)	458(316)	449(310)	449(249)	439(244)	454(313)
	5 "I"	--	--	--	--	--	449(249)	--	--
	4	--	--	--	--	--	443(246)	--	--
4	6 M "I"	456(253)	451(251)	441(246)	455(314)	449(310)	444(247)	436(242)	449(310)
	5 "I"	--	--	--	--	--	441(246)	--	--
	4	--	438(243)	--	--	--	432(240)	427(237)	440(304)
5	6 M "I"	--	440(244)	431(239)	446(308)	435(300)	432(246)	419(233)	439(303)
	5 "I"	--	--	--	--	--	430(239)	--	--
	4	--	--	--	--	--	411()	411()	--

- (1) Tested at vacuum with 40 area ratio nozzle
 (2) With 10% fuel film cooling injected in nozzle.
 (3) With 18% fuel film cooling injected in chamber.
 (4) Conducted at ambient temperature.

TABLE VI-2

40:1 ALTITUDE PERFORMANCE SUMMARY

Delivered performance

GO₂/GH₂ APS thruster

Injector SN 6

Combustion chamber	40:1 Film-Cooled Chamber		40:1 Regeneratively Cooled Chamber	
Propellant temperature	Ambient	Cold	Ambient	Cold
Test 1680-	04-012	04-018	04-020	04-023
Date	7/16/71	8/3/71	8/11/71	8/19/71
Data period, sec	30-45	60-70	30-54	50-56
Chamber pressure, psia (N/cm ²)	302.5 (208)	267.5 (184.6)	295.1 (203.6)	305.2 (210.6)
Thrust, lbf (N)	1601.1 (7121)	1383.5 (6156)	1586.3 (7055)	1639.0 (7290)
Mixture ratio, O/F	3.8	4.2	4.1	4.4
Percent fuel film cooling, W_{FC}/W_{FT}	18.9	17.7	10.4	10.3
Oxidizer temperature, °R (°K)	521.3 (289)	404.3 (224)	530.3 (278)	309.9 (172)
Fuel temperature, °R (°K)	547.4 (304)	190.8 (106)	555.9 (309)	221.9 (123)
Theoretical vacuum specific impulse, lbf-sec/lbm (N-s/kg)	473.3 (4635)	463.7 (4547)	473.2 (4635)	463.7 (4544)
Kinetic loss, lbf-sec/lbm (N-s/kg)	3.8 (37.24)	3.9 (38.22)	4.4 (43.12)	4.2 (41.16)
Igniter mixture ratio maldistribution, lbf-sec/lbm (N-s/kg)	0.6 (5.8)	0.9 (8.82)	0.7 (6.86)	0.8 (7.84)
Boundary layer loss, lbf-sec/lbm (N-s/kg)	8.4 (82.3)	9.1 (89.18)	8.9 (87.22)	7.5 (73.5)
Divergence loss, lbf-sec/lbm (N-s/kg)	3.5 (34.3)	3.4 (33.32)	3.6 (35.28)	3.5 (34.3)
Fuel film cooling loss, lbf-sec/lbm (N-s/kg)	6.2 (60.76)	8.1 (79.38)	2.6 (25.48)	5.4 (52.92)
Energy release loss, lbf-sec/lbm (N-s/kg)	6.3 (61.74)	3.9 (38.22)		
Delivered vacuum specific impulse (measured), lbf-sec/lbm (N-s/kg)	444.5 (4356)	434.4 (4257)	453.0 (4439)	442.3 (4335)

TABLE VI-3

BIT IMPULSE TEST CONDITIONS AND REPEATABILITY

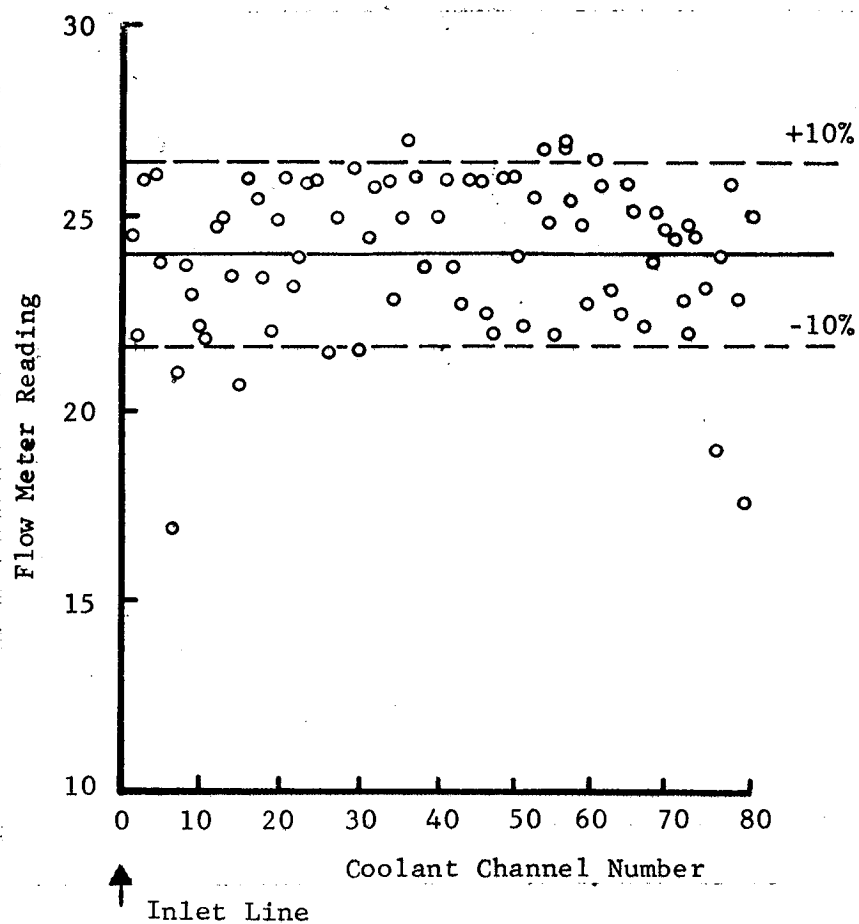
Test No.	EPWV, sec	Mass Flow Controller	Propellant Temperature	Total No. Pulses	MR	Test Results		
						Average Bit Impulse, lb-sec (N-s)	Low oxidizer flow	% Variation
05-008	0.216	No	Ambient	1	3	262		
05-015	0.216	No	Ambient	100	4	First 10	334 (1498)	+3, -5
						Middle 10	349 (1566)	
						Last 10	352 (1343)	
05-038	0.116	No	Ambient	840	4	First 10	185 (823)	+4, -2
						Middle 10	194 (863)	
						Last 10	183 (814)	
05-036	0.054	No	Ambient	100	4	First 10	73.4 (326)	+7, -2
						Middle 10	74.8 (333)	
						Last 10	74.1 (330)	
06-009	0.214	Yes	Cold	9	3	326.9 (1454)		+5, -3
	0.108			5		153.5 (683)		+5, -3
	0.054			4		73.1 (325)		+5, -2
	0.034			5		27.4 (122)		+5, -4
06-010	0.214	Yes	Cold	6	4	322.0 (1432)		+9, -5
	0.108			1		152.1 (676)		--
	0.054			2		76.1 (338)		--

TABLE VI-4

COLD PROPELLANT BIT IMPULSE DATA
Tests D06-0A-009, -010

Pulse Width:		EPW	0.234		0.128		0.074		0.054
		EPWV	0.214		0.108		0.054		0.034
Test No.	Pulse No.	lbf-sec (N-s)	Pulse No.	lbf-sec (N-s)	Pulse No.	lbf-sec (N-s)	Pulse No.	lbf-sec (N-s)	
-009 MR=3.0	1	344.6 (1544)	2	160.5 (716)	3	77.42 (347)	8	27.09 (121)	
	5	334.5 (1498)	6	153.0 (685)	19	72.28 (324)	12	26.48 (119)	
	9	325.7 (1459)	10	151.9 (681)	23	72.15 (323)	16	26.48 (119)	
	13	322.3 (1444)	14	152.4 (683)	31	70.53 (316)	20	28.24 (127)	
	17	327.2 (1466)	22	149.8 (671)			24	28.91 (129)	
	21	326.8 (1464)							
	25	321.8 (1442)							
	29	322.0 (1443)							
	33	317.2 (1422)							
	Average	326.9 (1465)		153.5 (688)		73.1 (327)		27.4 (123)	
-010 MR=4.0	1	349.6 (1566)	14	152.1 (681)	3	79.04 (354)			
	5	336.6 (1508)			15	73.23 (328)			
	9	317.0 (1420)							
	13	305.8 (1370)							
	17	312.2 (1398)							
	21	310.7 (1392)							
	Average	322.0 (1443)		152.1 (681)		76.1 (341)			
Min/Max Deviation (MR=3-4)									
All pulses		13.4%		6.9%		11.8%		8.9%	
Pulse 2 to N		8%		2.1%		3.8%		8.9%	

Film-Cooled Chamber Coolant Jacket Flow Distribution



SN 1 Regeneratively Cooled Chamber Coolant Channel Flow Distribution

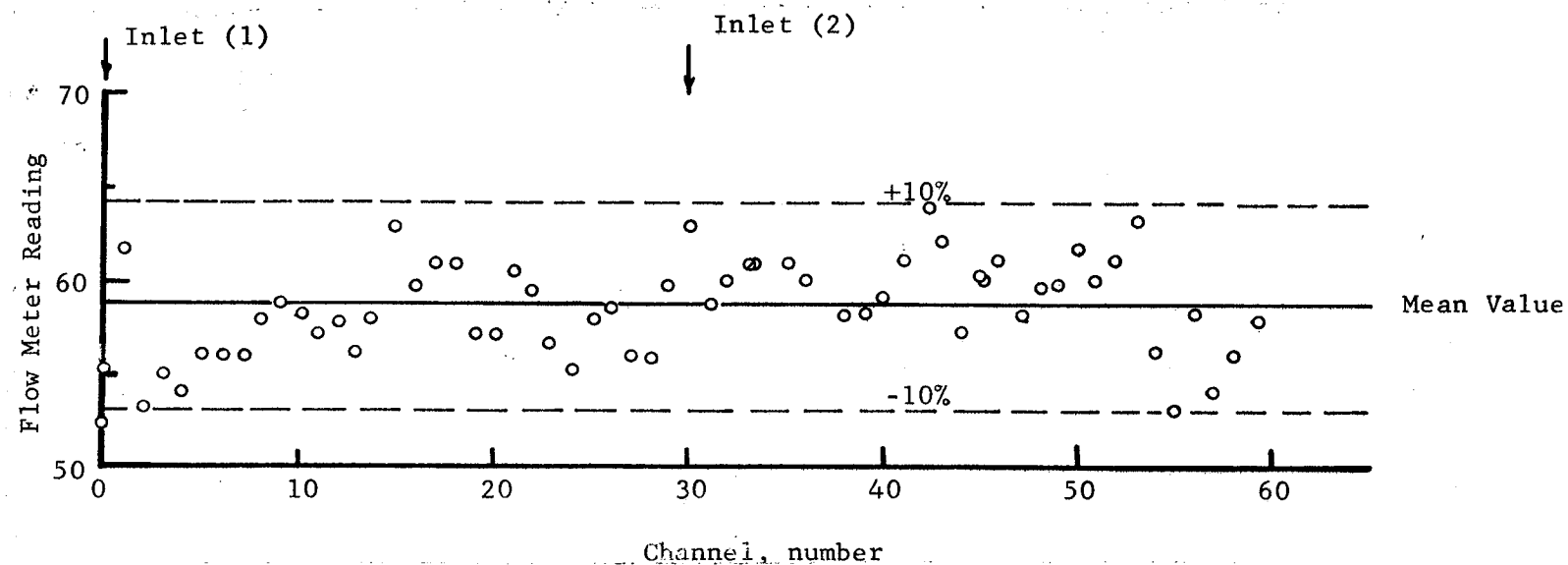
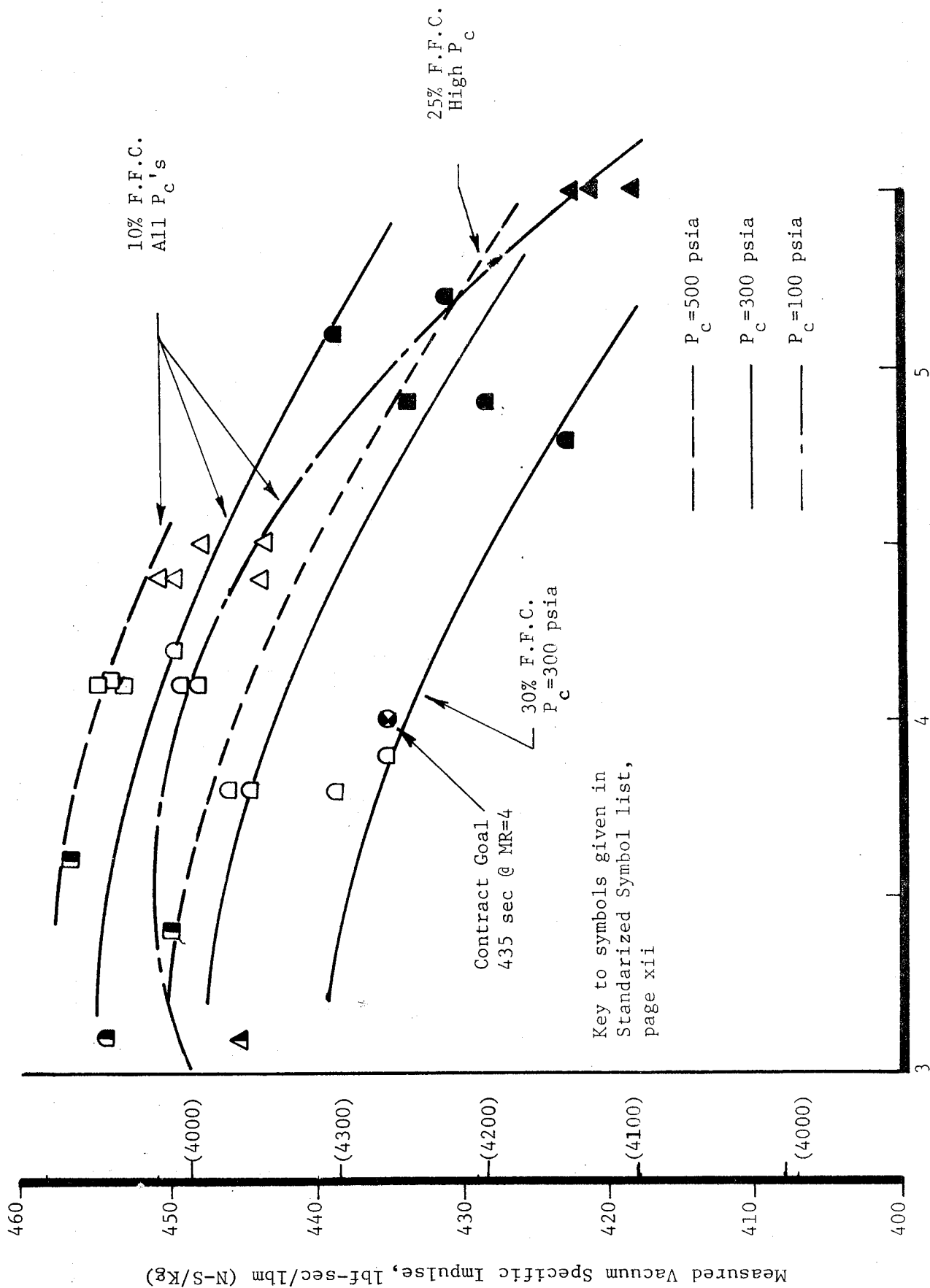


Figure VI-1. Coolant Channel Flow Distribution



Overall Mixture Ratio

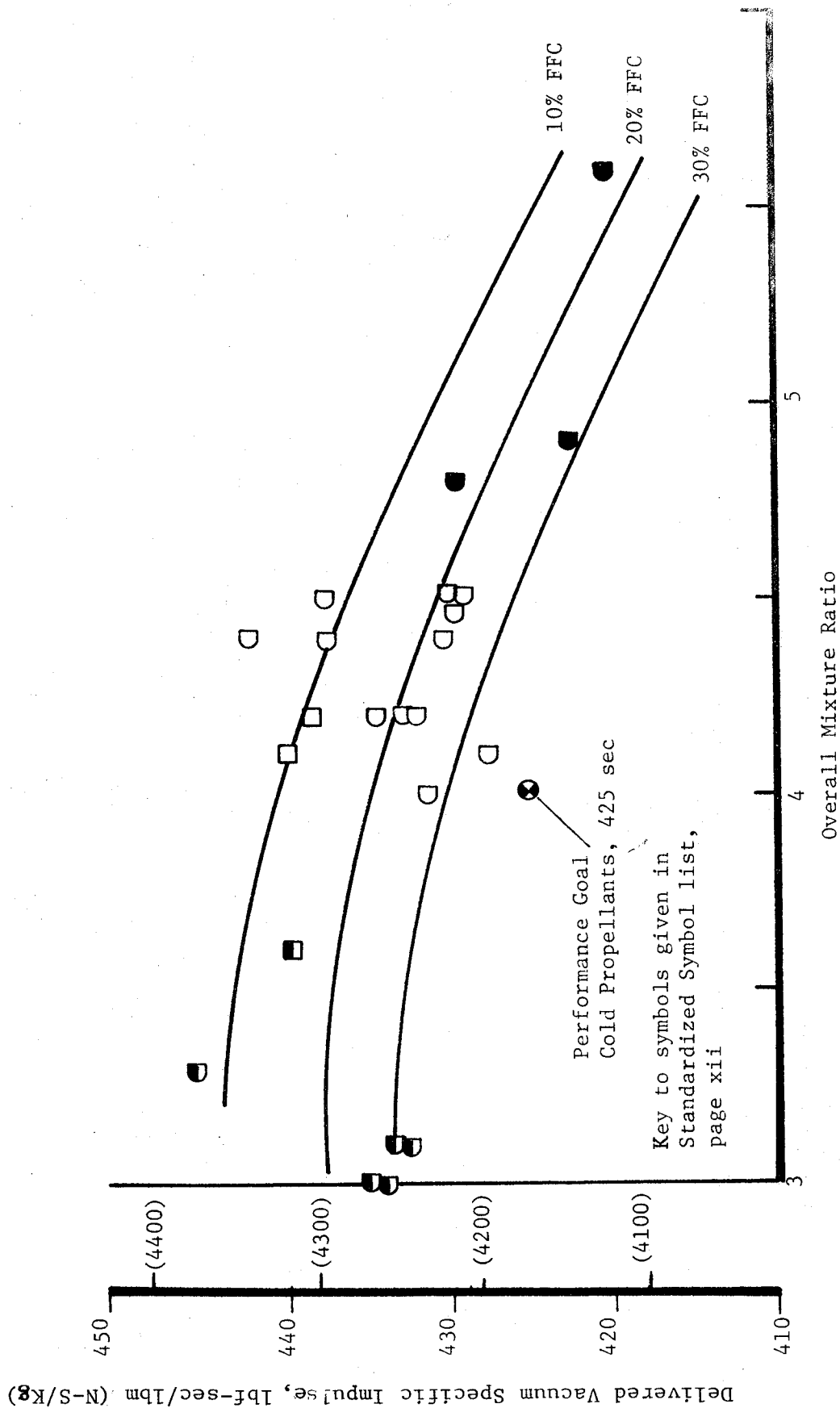


Figure VI-3. Vacuum Specific Impulse, SN 6 and 7 Modified "I" Premix Injector, Cold Propellants, 40:1 Regenerative and Film Cooled Chambers

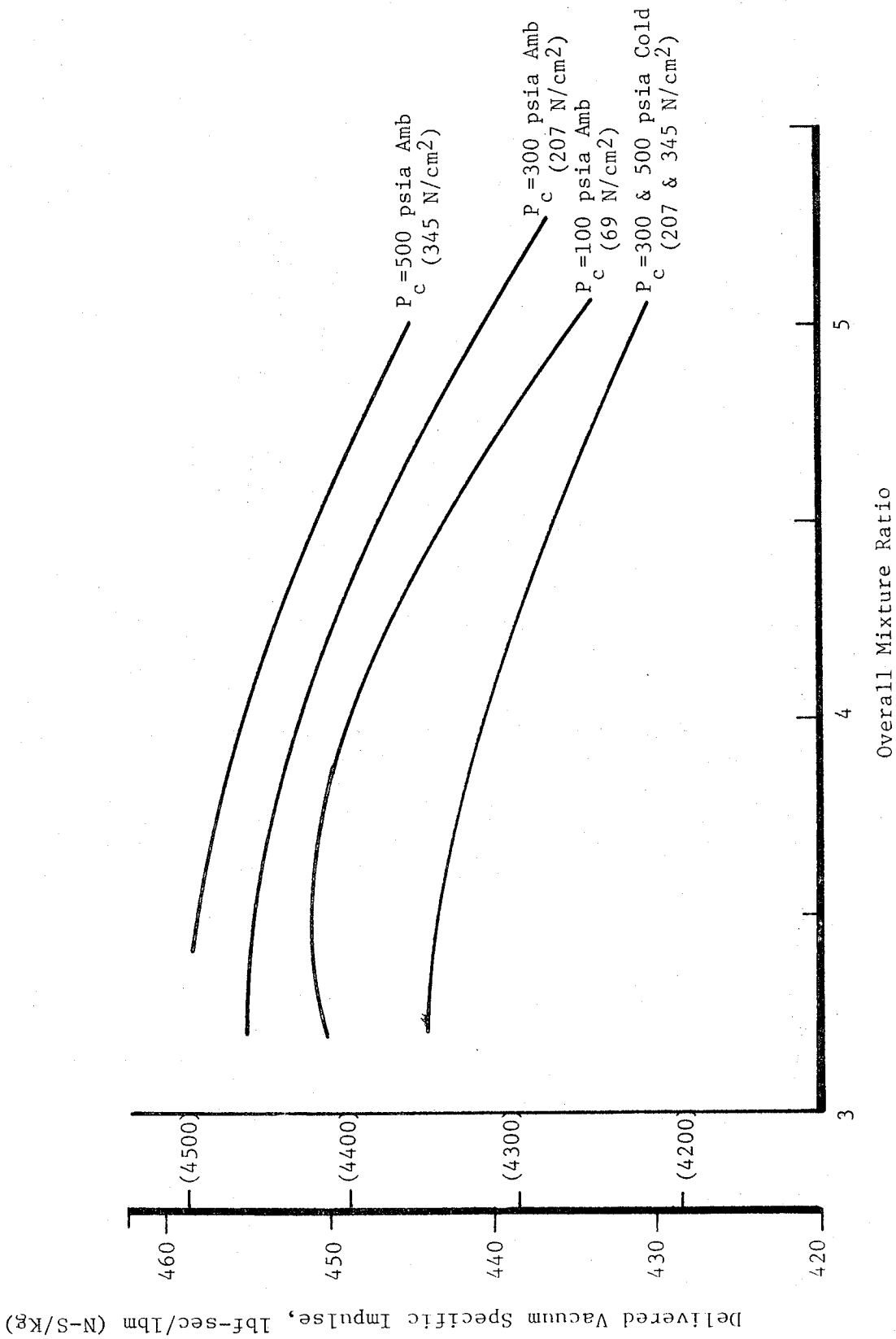


Figure VI-4. Vacuum Specific Impulse, SN 6 and 7 Modified "I" Premix Injector, Regeneratively Cooled Chambers, 10% Supersonic Film Cooling

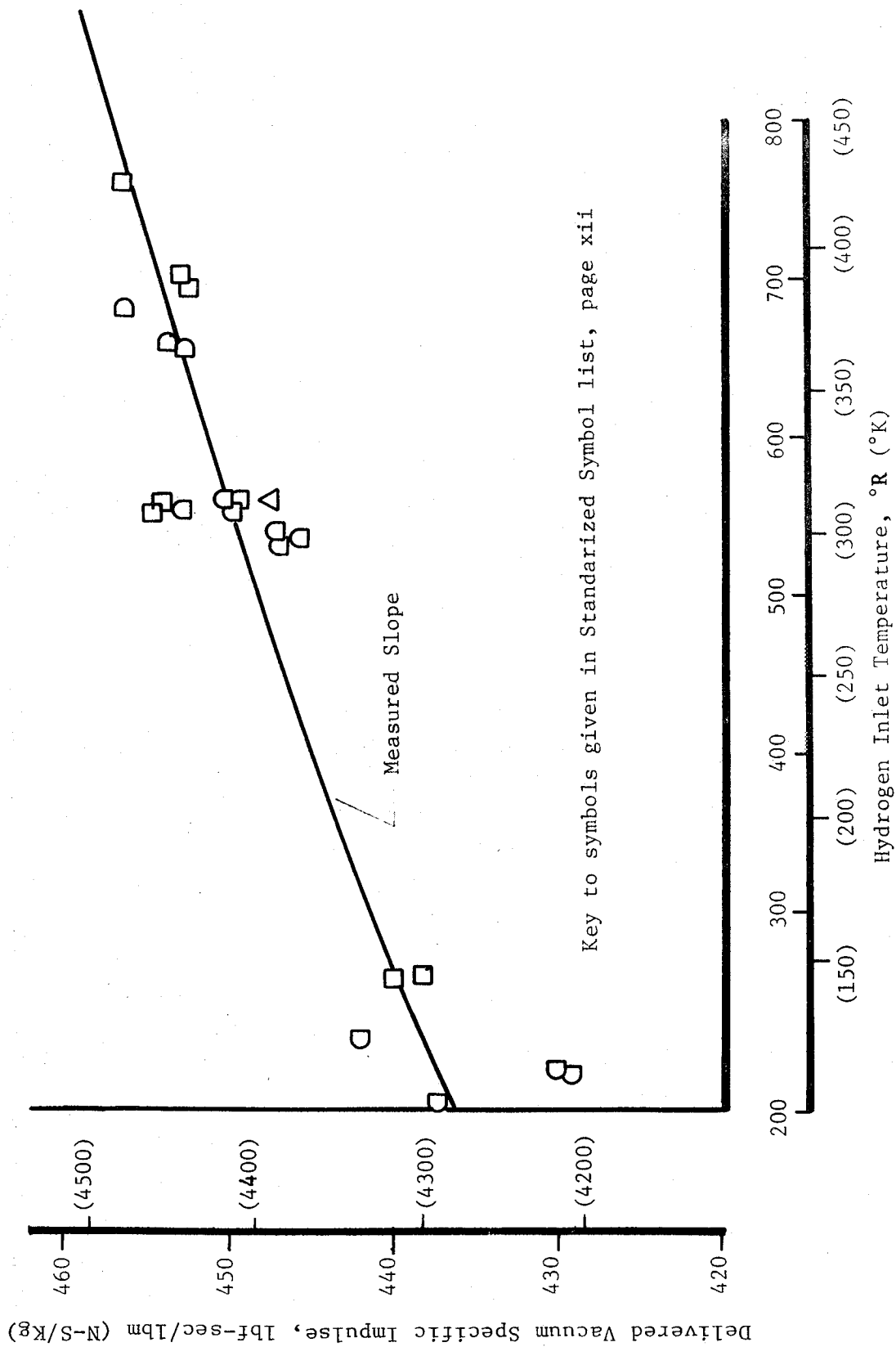


Figure VI-5. Influence of Hydrogen Supply Temperature on Measured Vacuum Specific Impulse, SN 6 Modified "I" Premix Injector, Regeneratively Cooled Chamber, 10% FFC

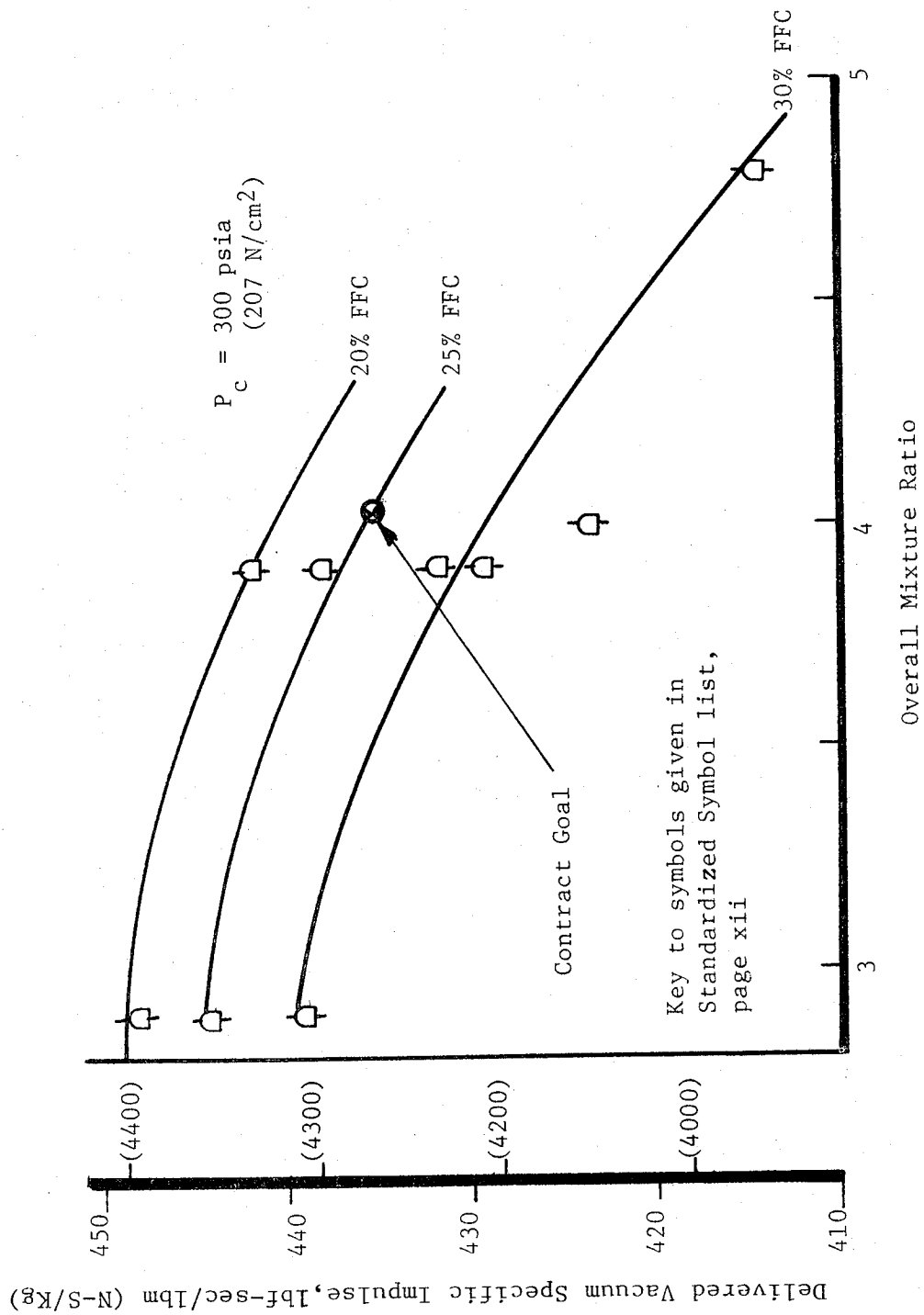


Figure VI-6. Vacuum Specific Impulse, SN 5 "I" Injector, Film Cooled Chamber, Ambient Temperature Propellants

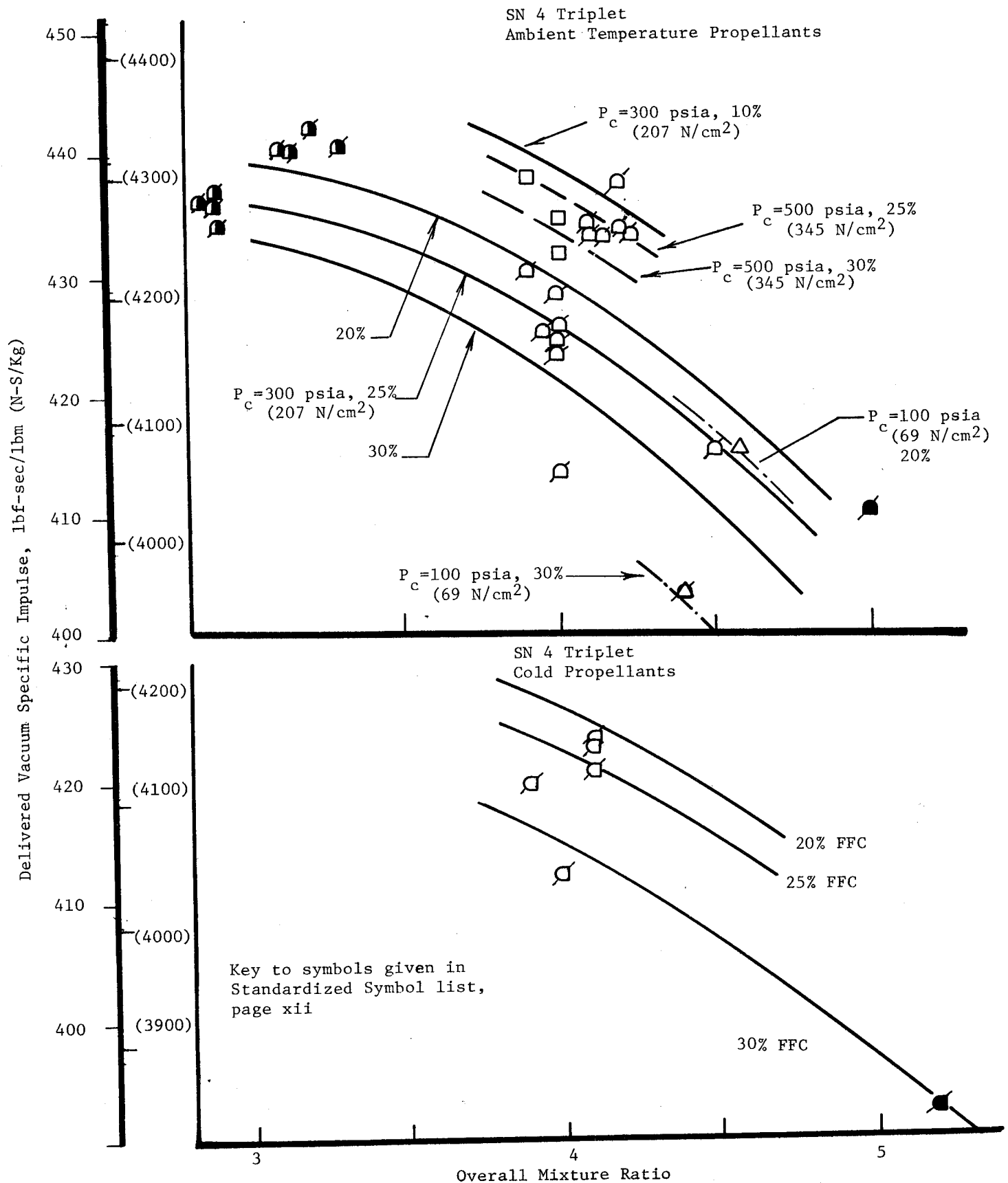


Figure VI-7. Vacuum Specific Impulse, SN 4 Premix Triplet Injector, All Test Conditions

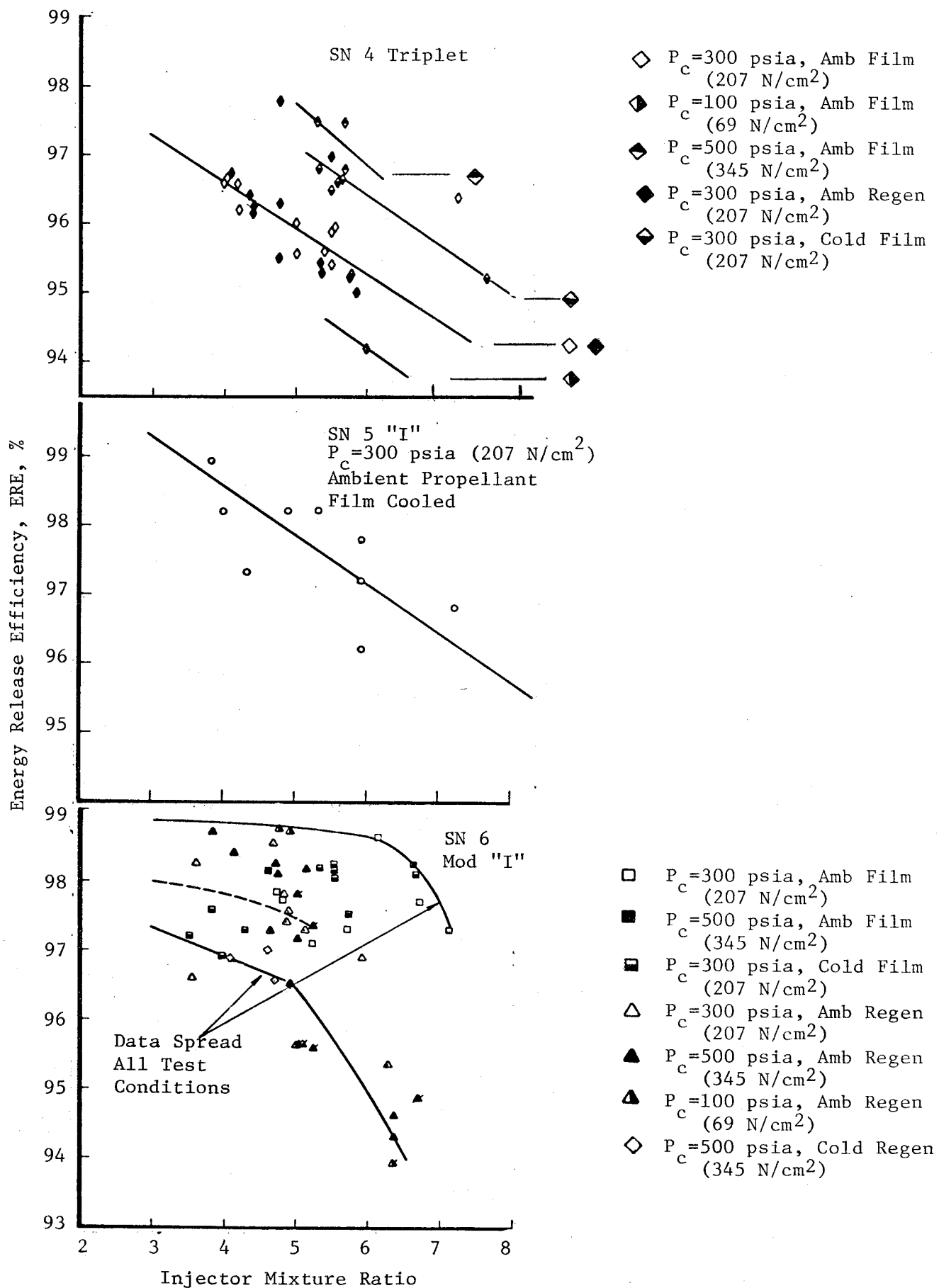


Figure VI-8. Energy Release Efficiency, Premix Triplet Type Injectors

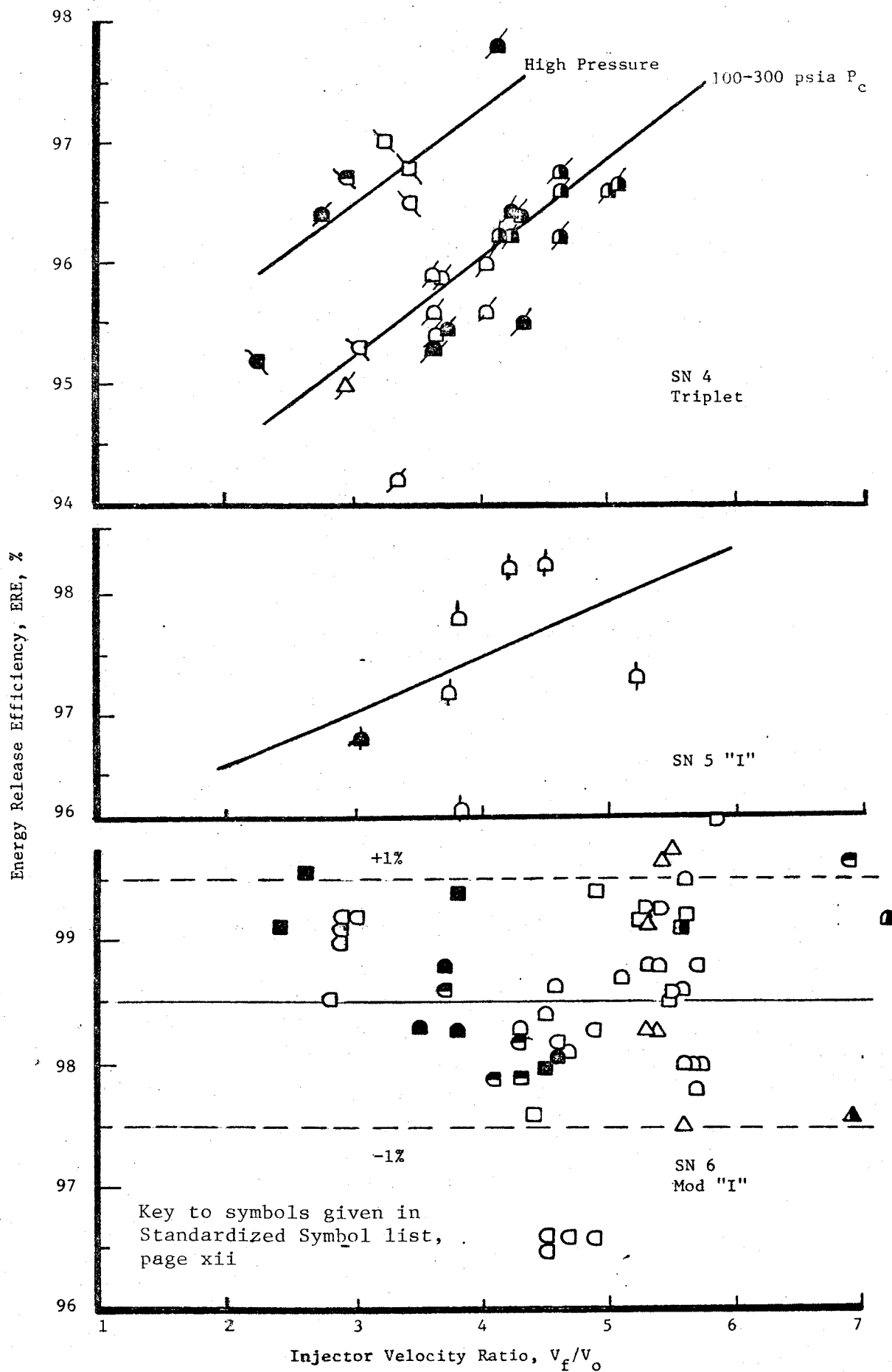


Figure VI-9. Influence of Velocity Ratio on Injector ERE

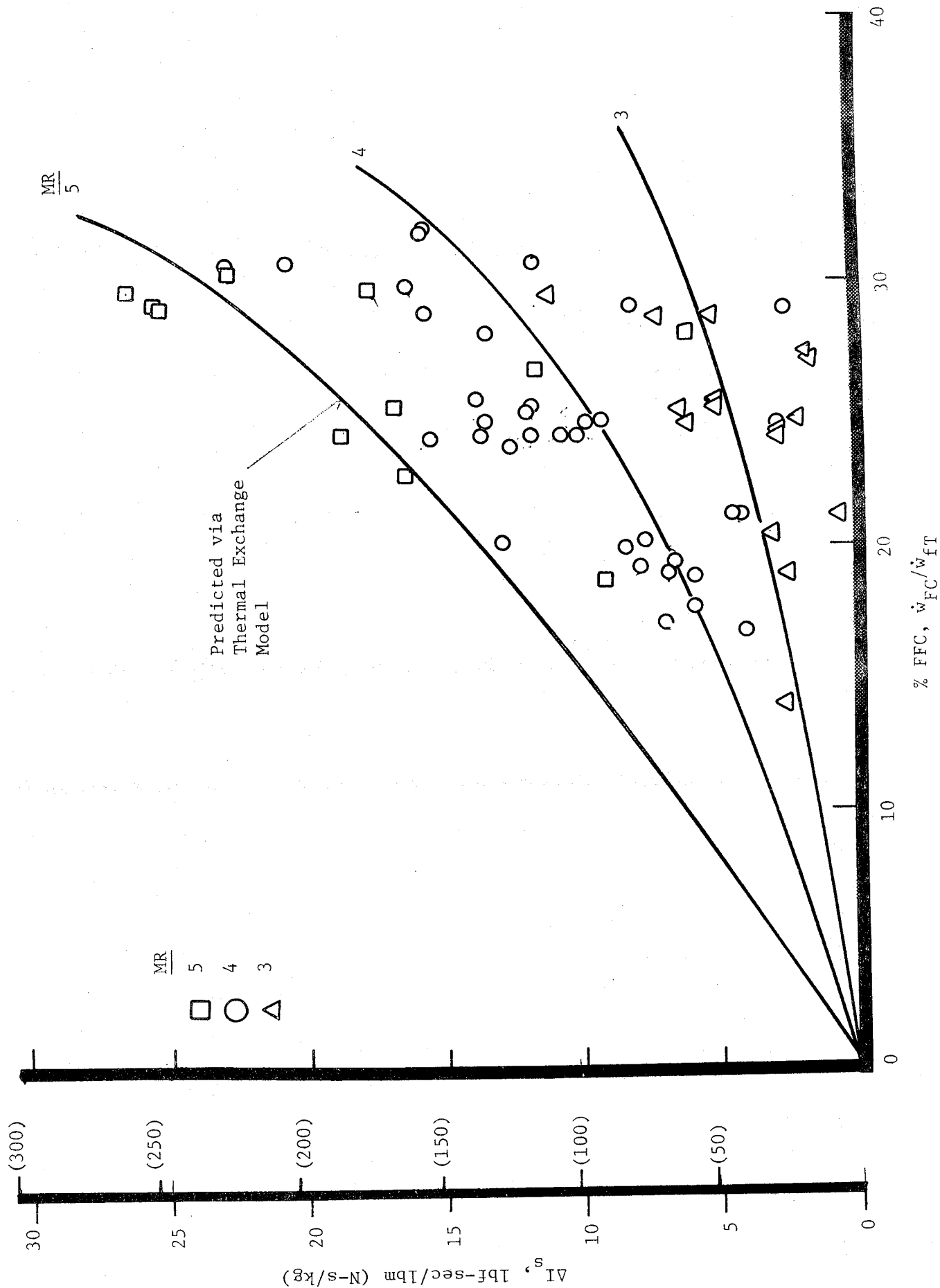


Figure VI-10. Experimental and Predicted Specific Impulse Loss vs % Film Cooling

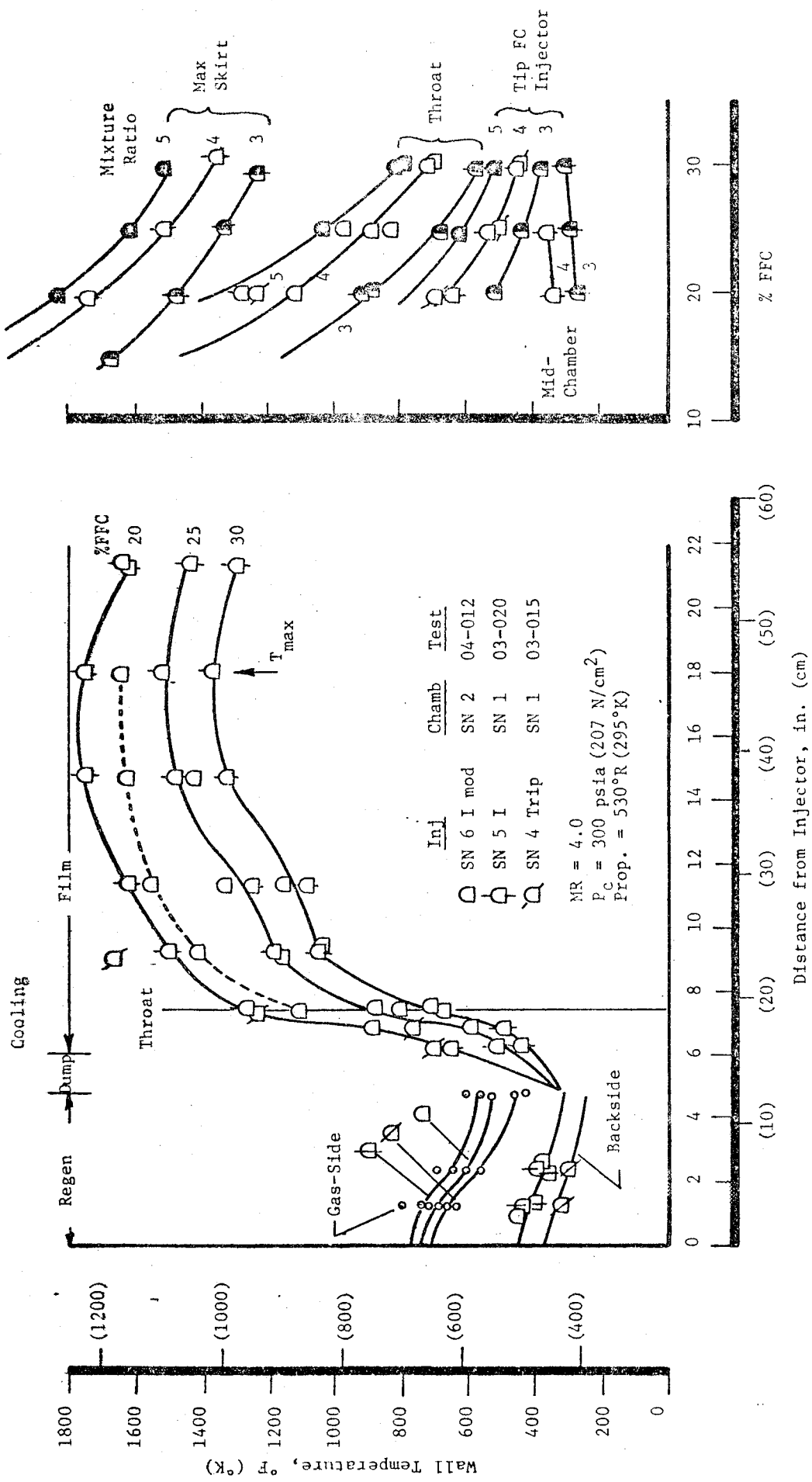


Figure VI-11. Film Cooled Chamber Measured Steady State Wall Temperature vs Injector Mixture Ratio and % Film Cooling

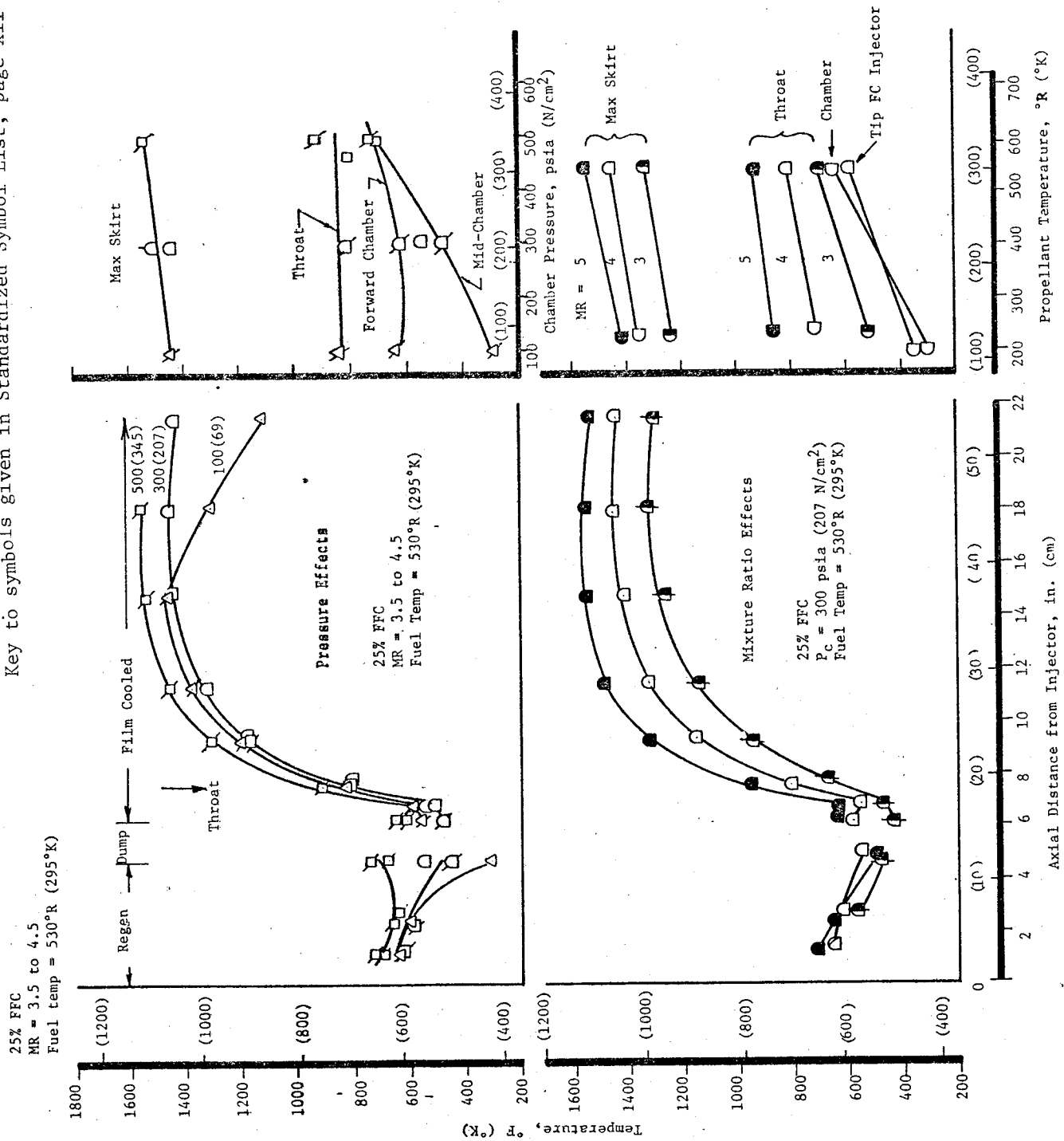


Figure VI-12. Film Cooled Chamber Measured Steady State Wall Temperatures vs Pressure, Mixture Ratio, and Propellant Temperature

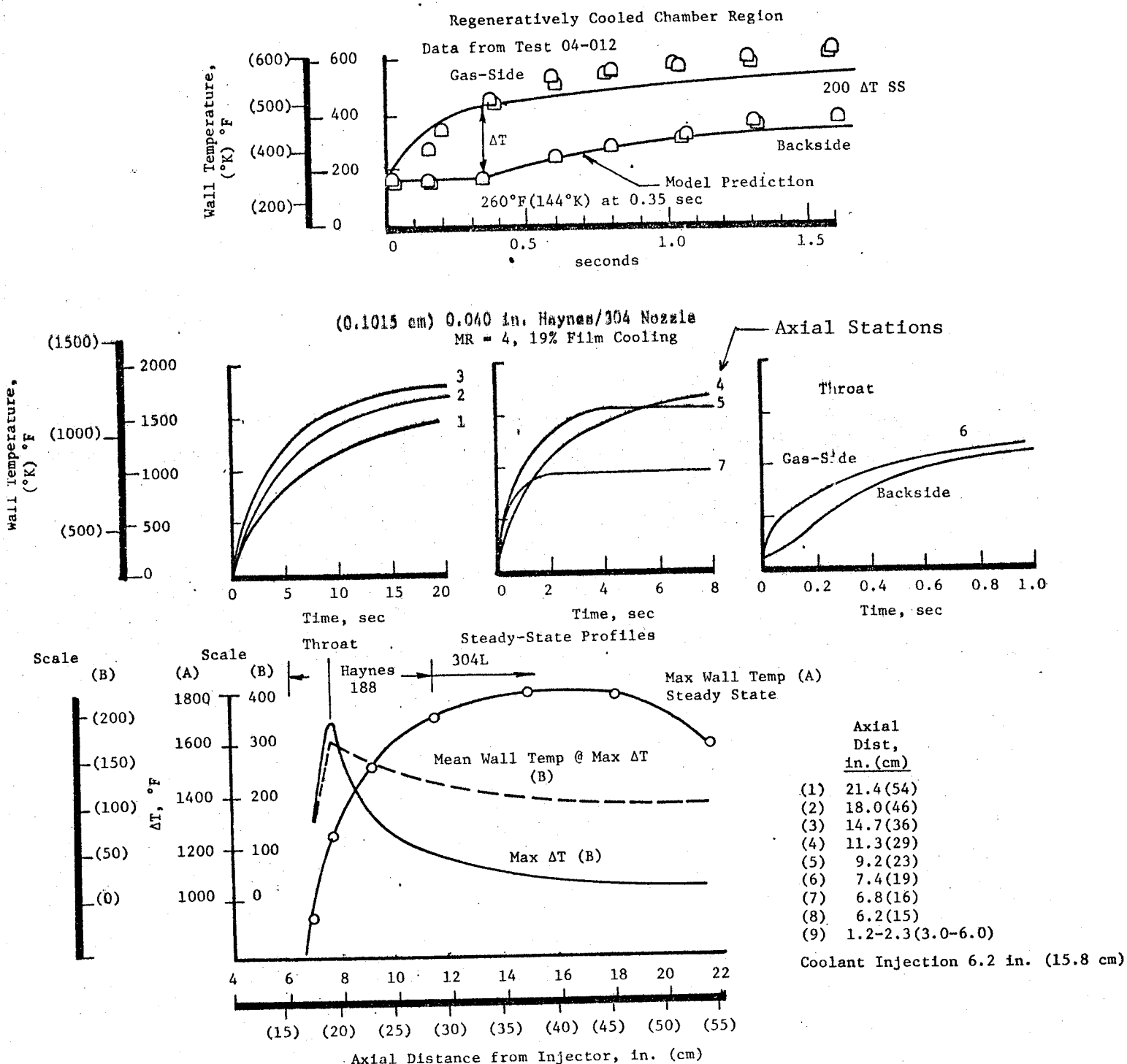
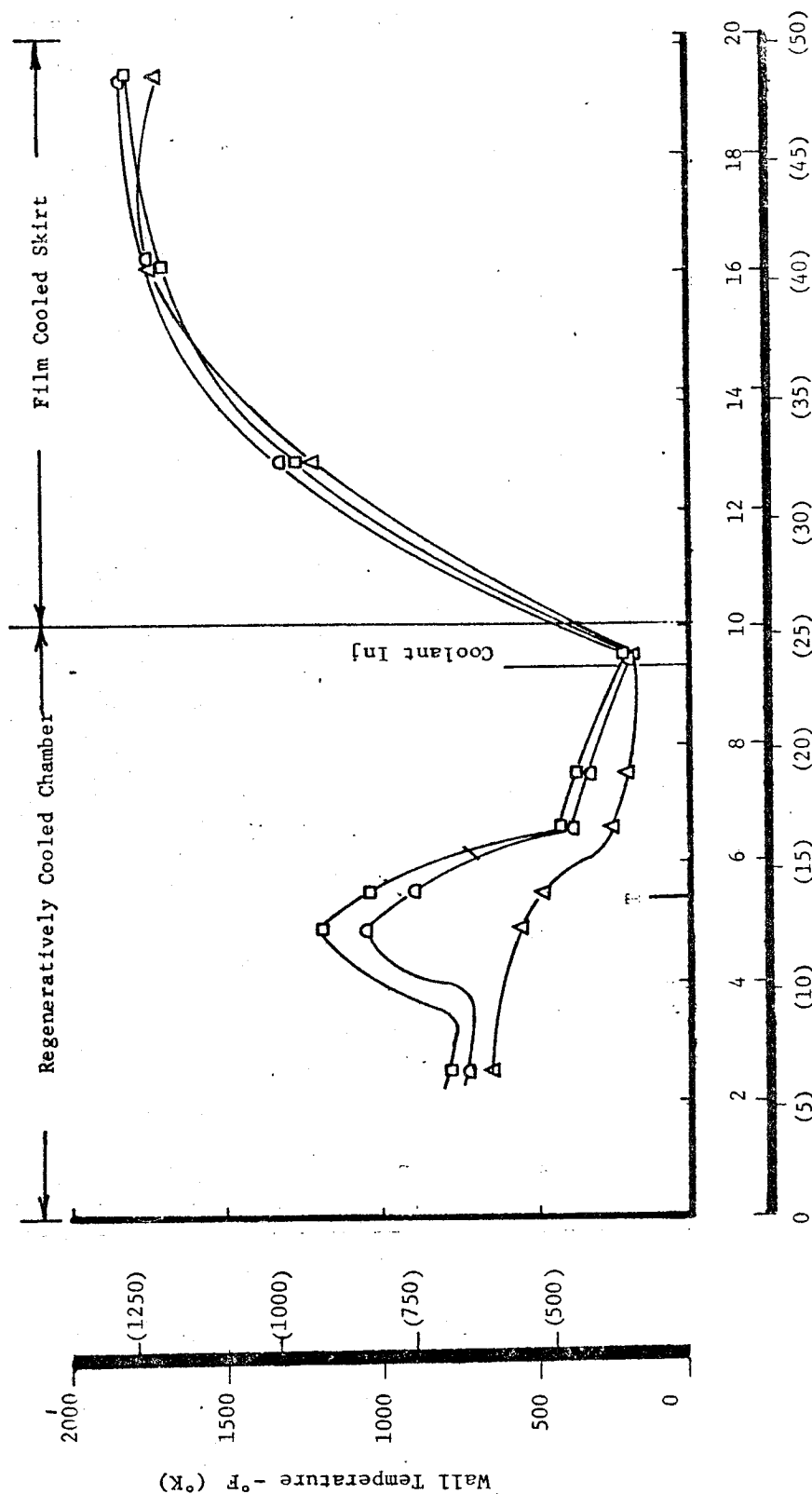


Figure VI-13. Film Cooled Chamber Transient Thermal Characteristics with Ambient Temperature Propellants, Tests 03-012 and 015

Test	MR	P _c	TH ₂	% FFC
Δ 03-030	4.47	94 (64.9)	Amb.	9.75
□ 04-020	4.10	295 (204)	↓	10.38
□ 04-021	4.12	485 (335)	↓	10.07



Regeneratively Cooled Chamber Wall Temperatures

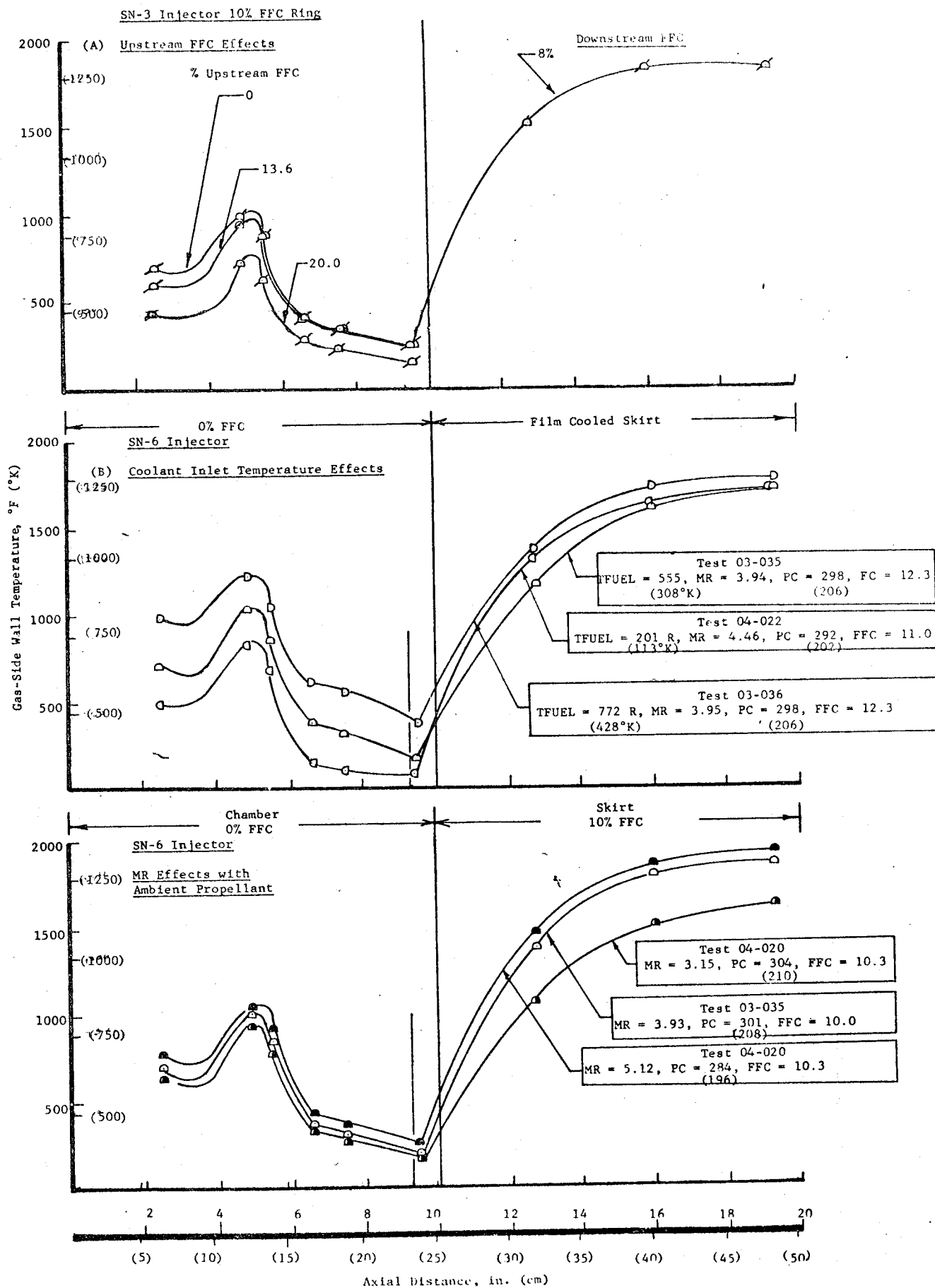


Figure VI-15. Experimental Wall Temperature, Phase I Regeneratively Cooled Chambers vs % Film Cooling, Coolant Supply Temperatures and Mixture Ratio

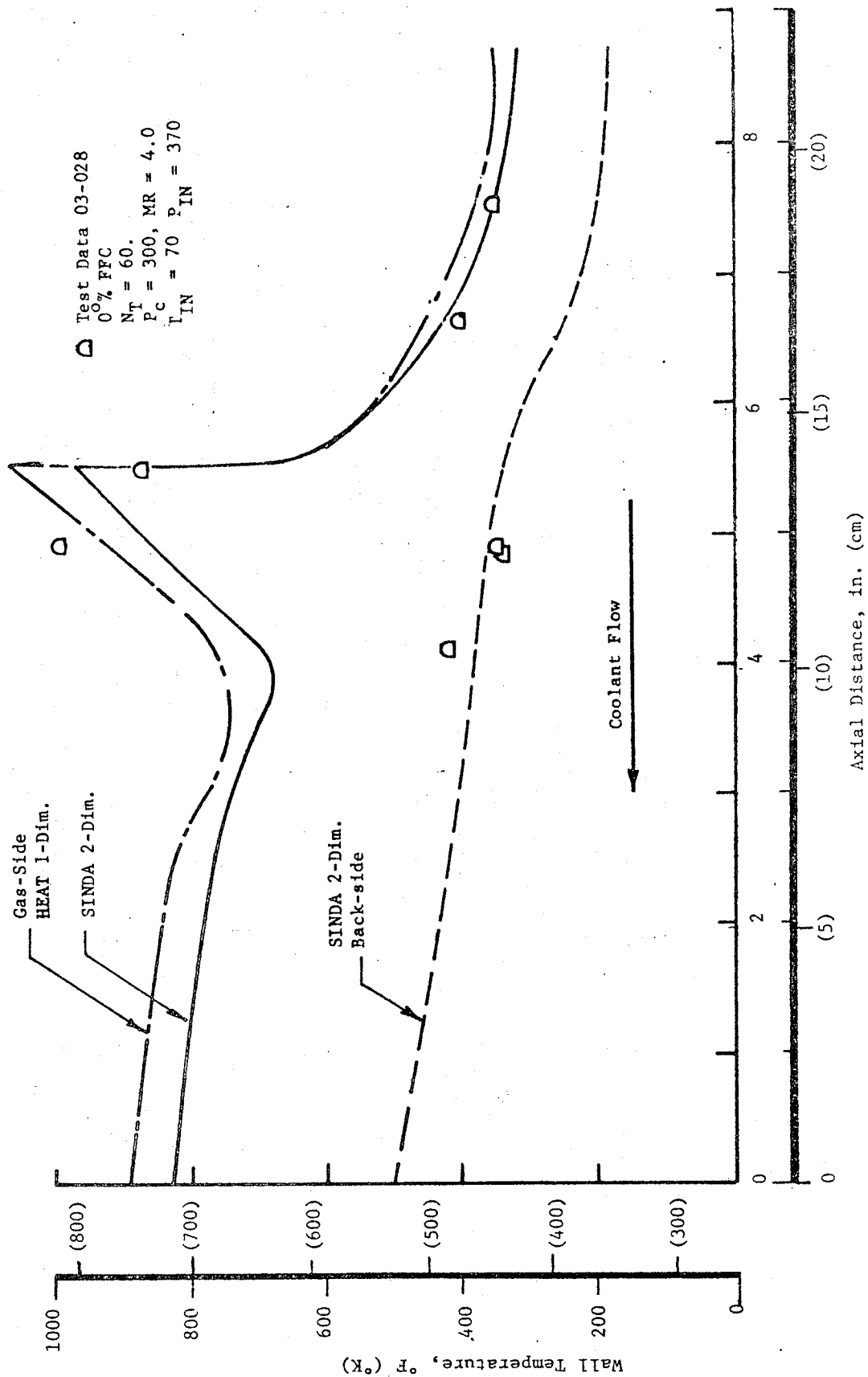


Figure VI-16. Comparison of Predicted and Measured Gas and Backside Wall Temperatures, Phase I Regeneratively Cooled Chambers

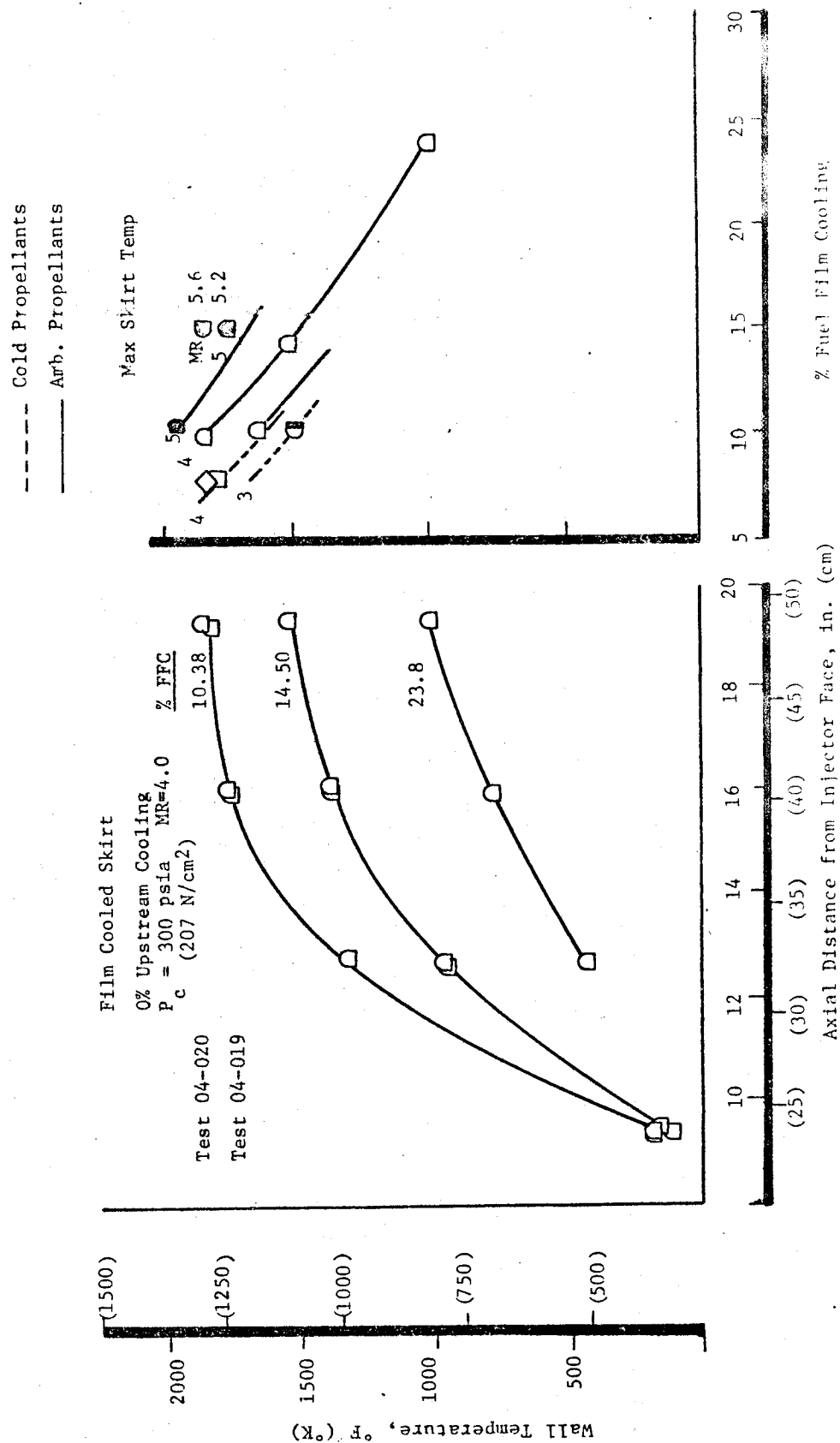


Figure VI-17. Skirt Temperature Profile, Phase I Regeneratively Cooled Chamber
 vs MR and % Film Cooling

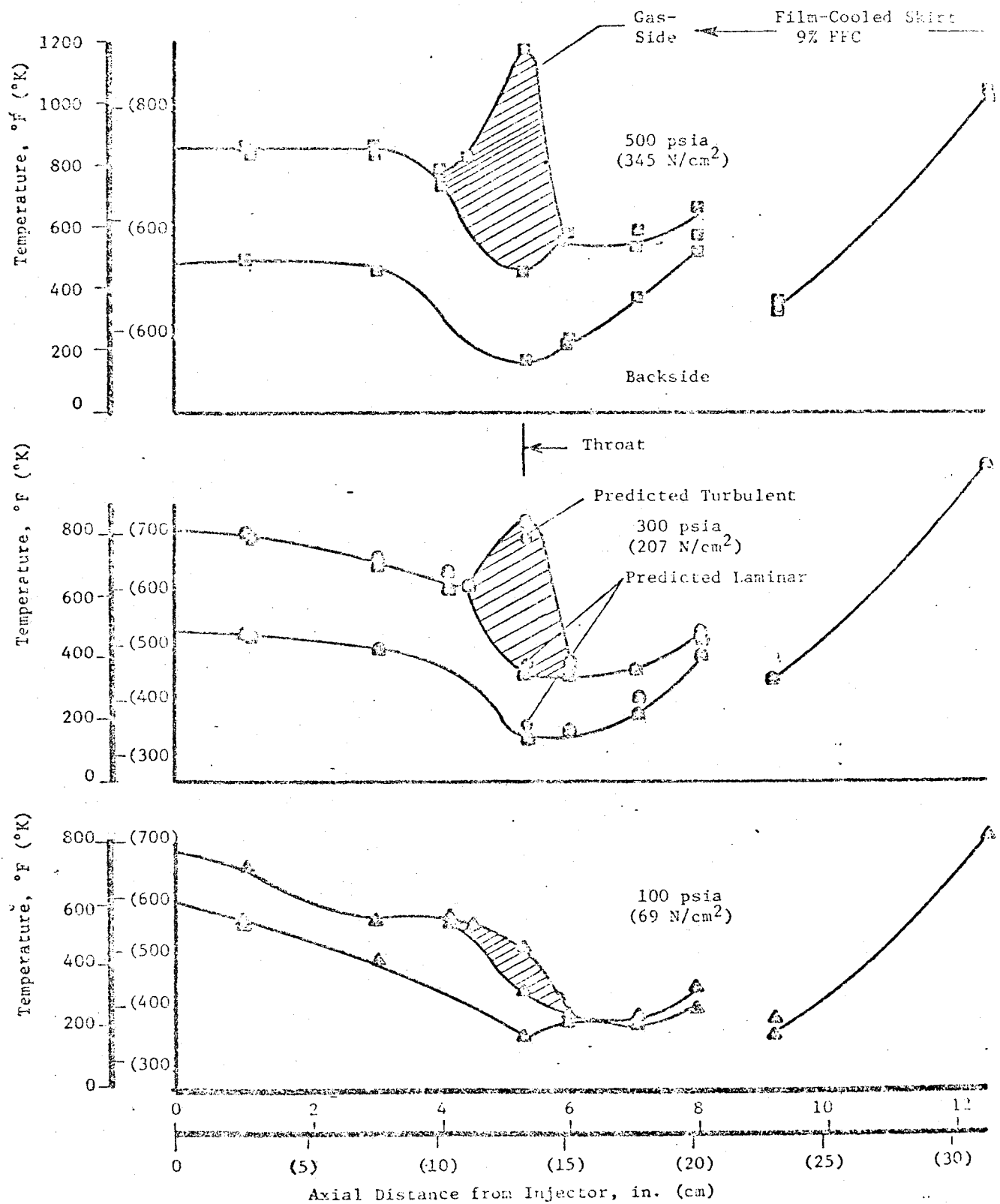


Figure VI-18. Phase II Regeneratively Cooled Chamber Wall Temperatures vs Chamber Pressure, Ambient Temperature Propellants

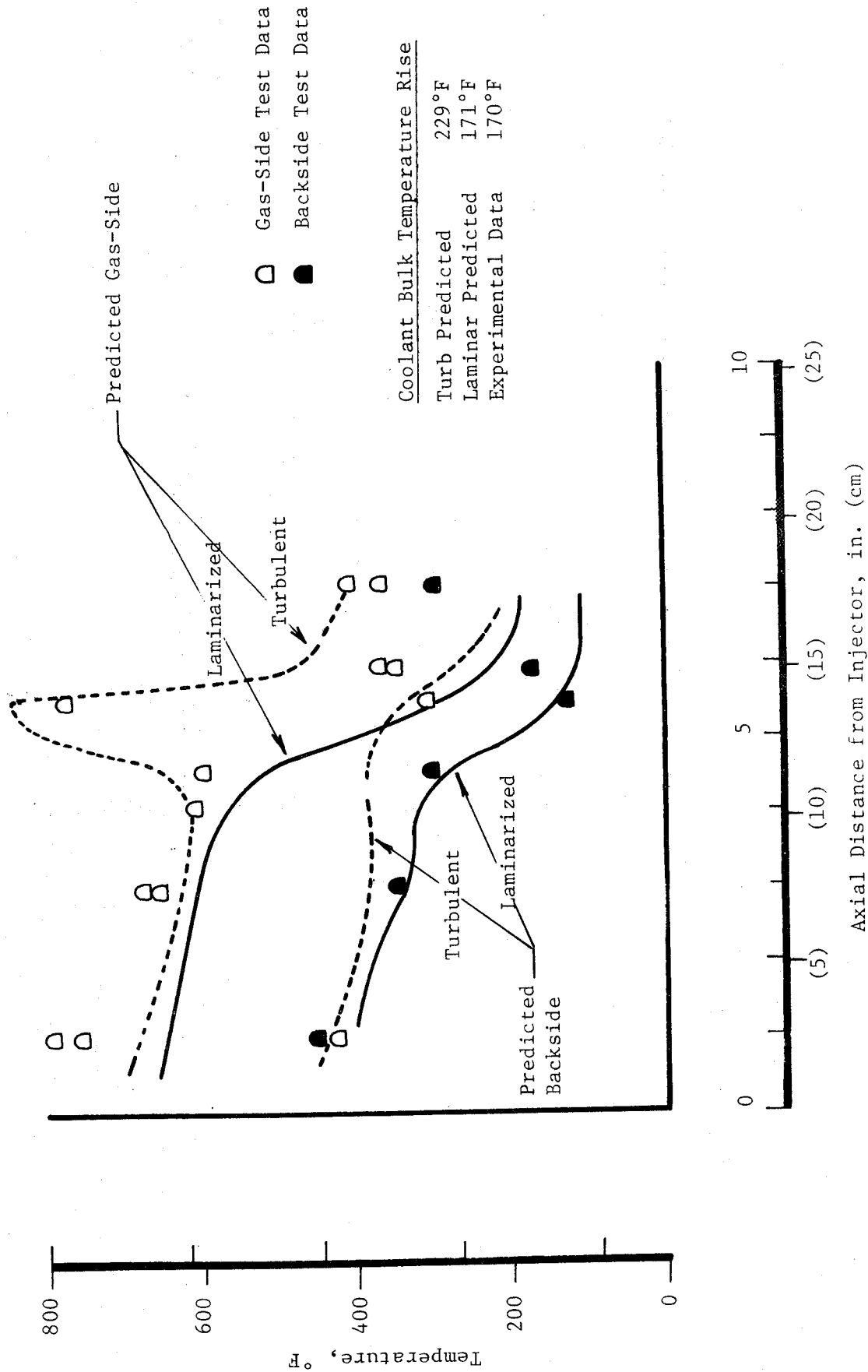


Figure VI-19. Comparison of Measured and Predicted Wall Temperature Profiles, Phase II Regeneratively Cooled Chamber

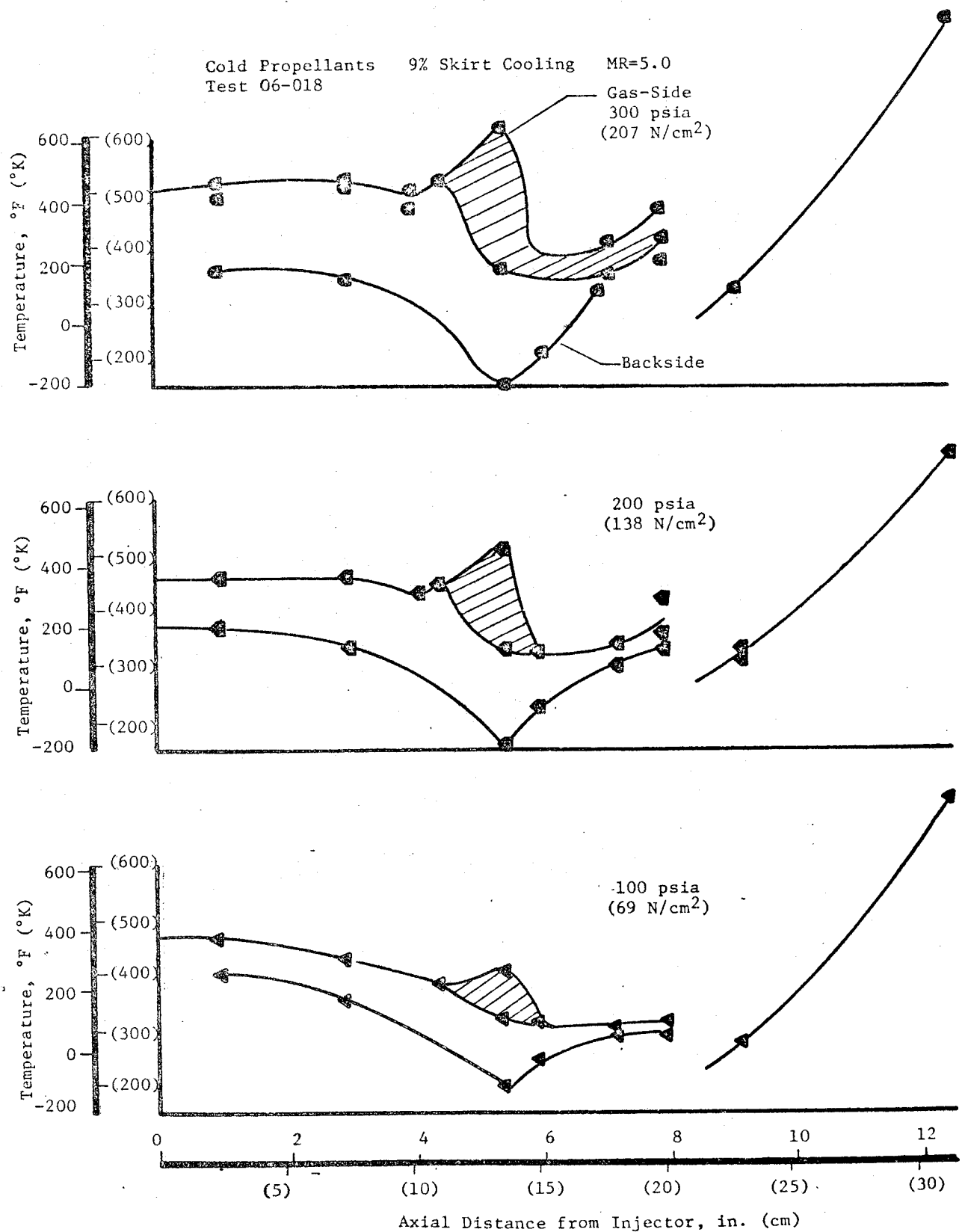


Figure VI-20. Phase II Regeneratively Cooled Chamber Wall Temperature Profiles vs Chamber Pressure, Cold Propellants

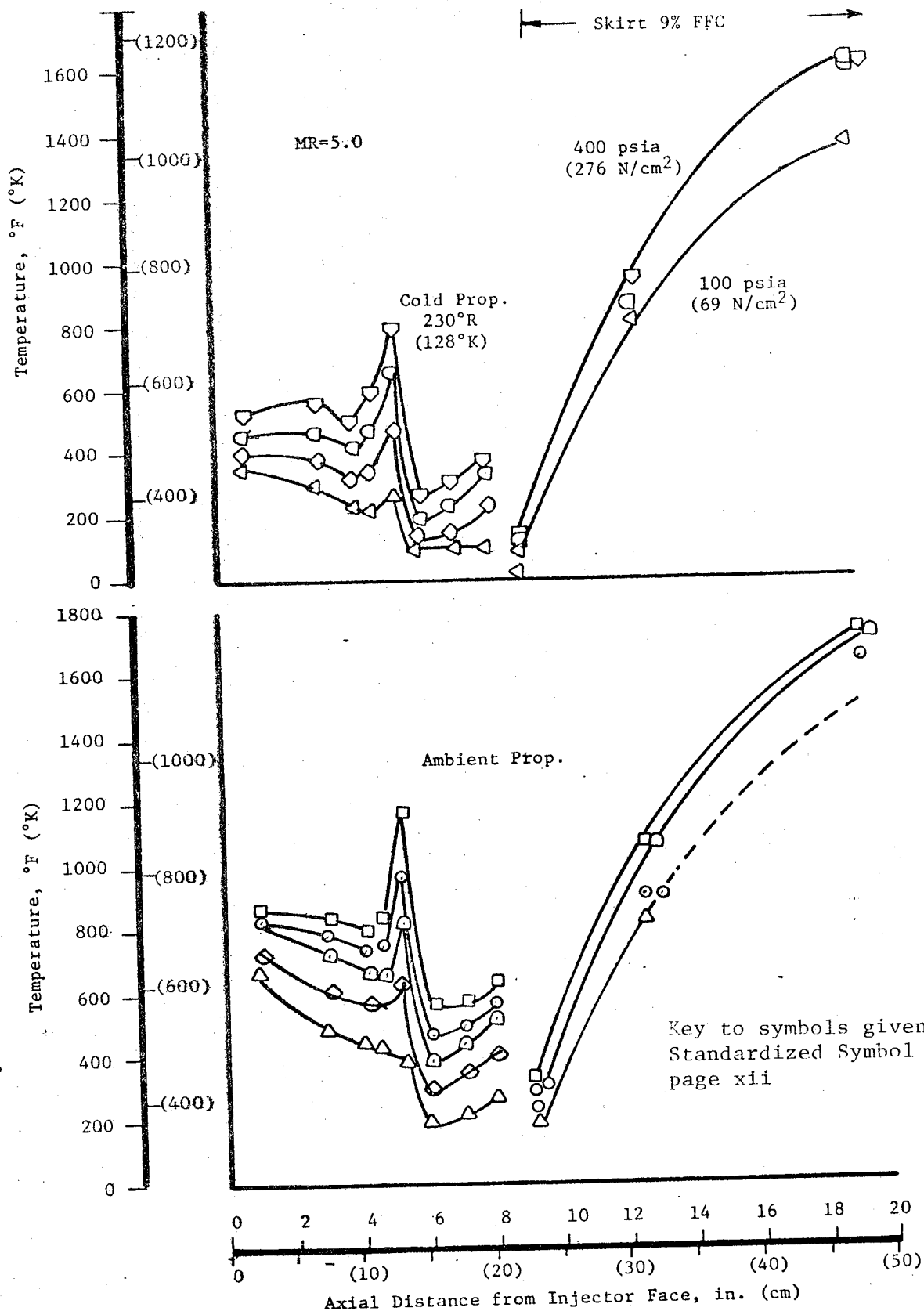


Figure VI-21. Summary of Upper Limit Experimental Gas-Side Wall Temperatures for Phase II Regeneratively Cooled Chamber vs Pressure and Propellant Temperature

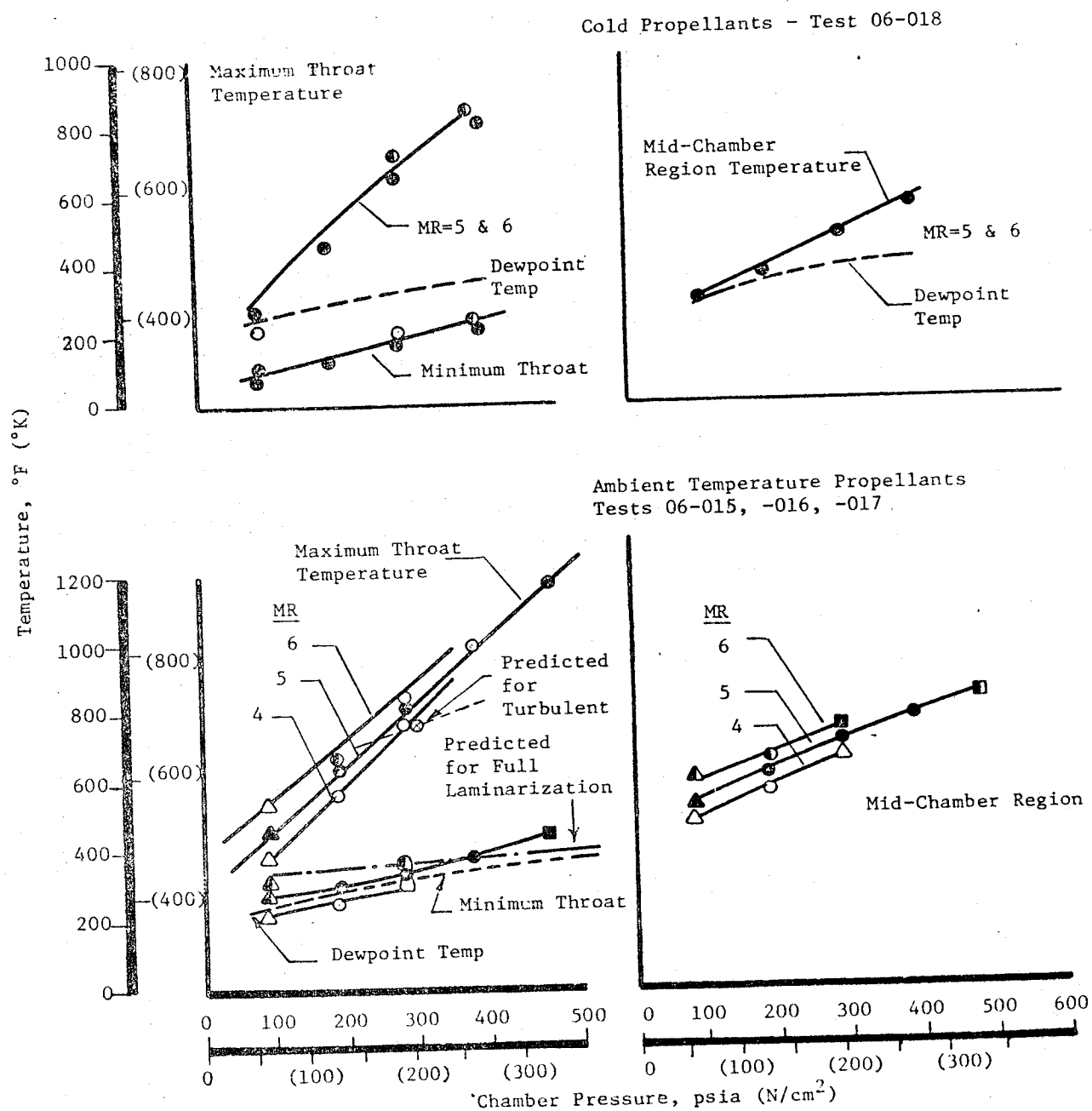


Figure VI-22. Summary of Steady State Gas-Side Thermal Data for Phase II Regeneratively Cooled Chamber

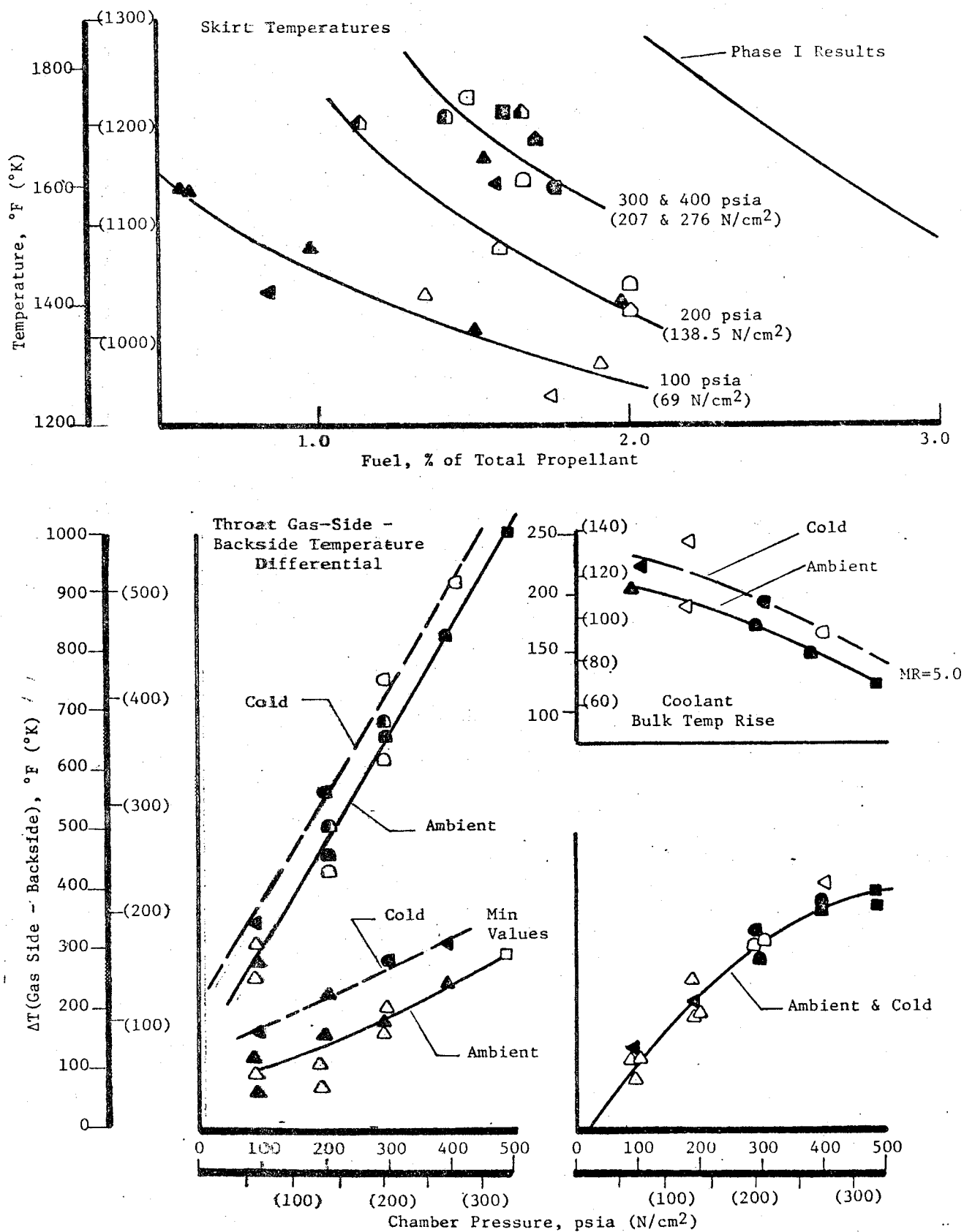


Figure VI-23. Summary of Steady State Skirt Temperatures and Chamber Thermal Gradients for Phase II Regeneratively Cooled Chamber

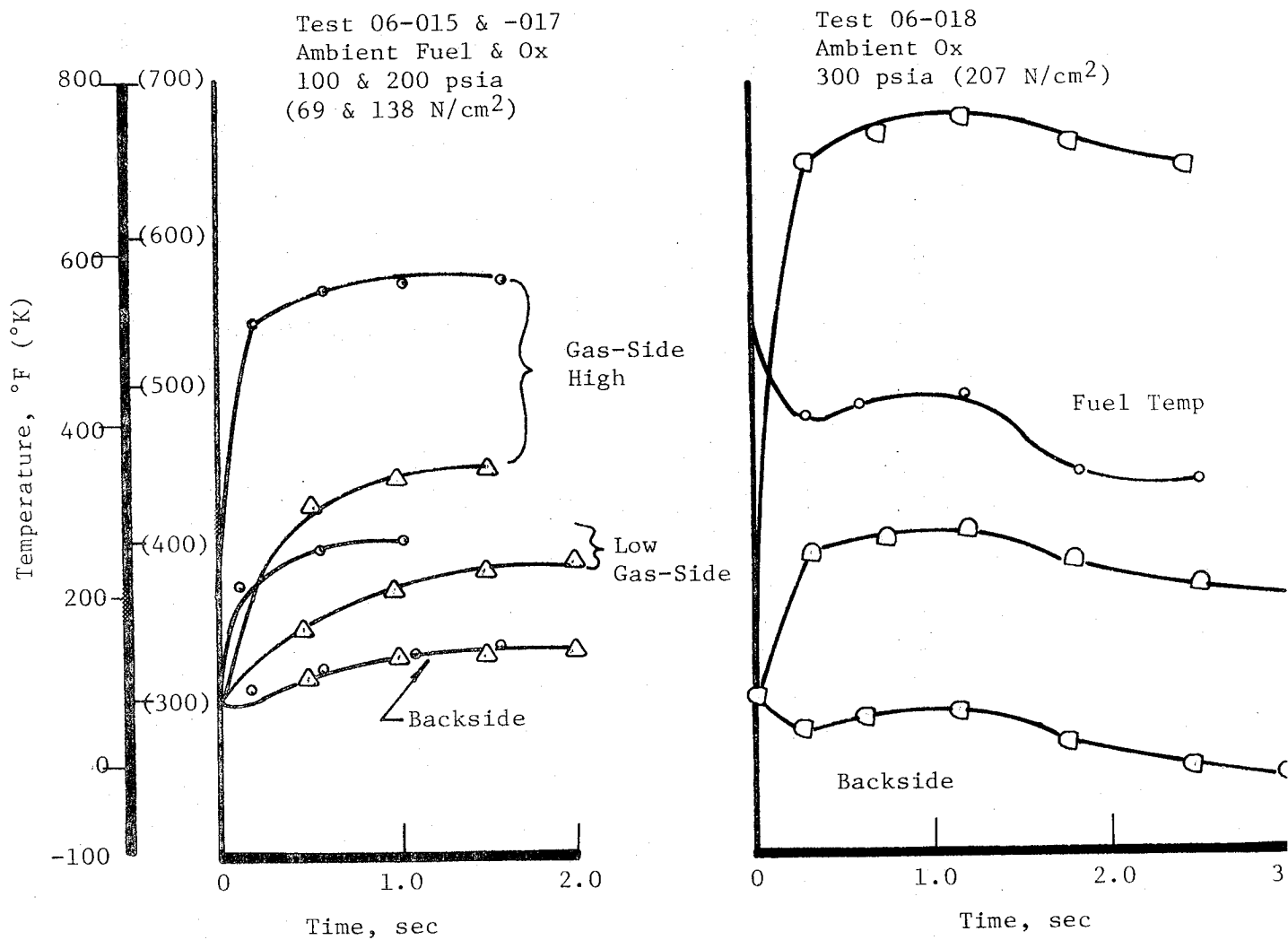


Figure VI-24. Transient Thermal Data for Phase II Regeneratively Cooled Chamber

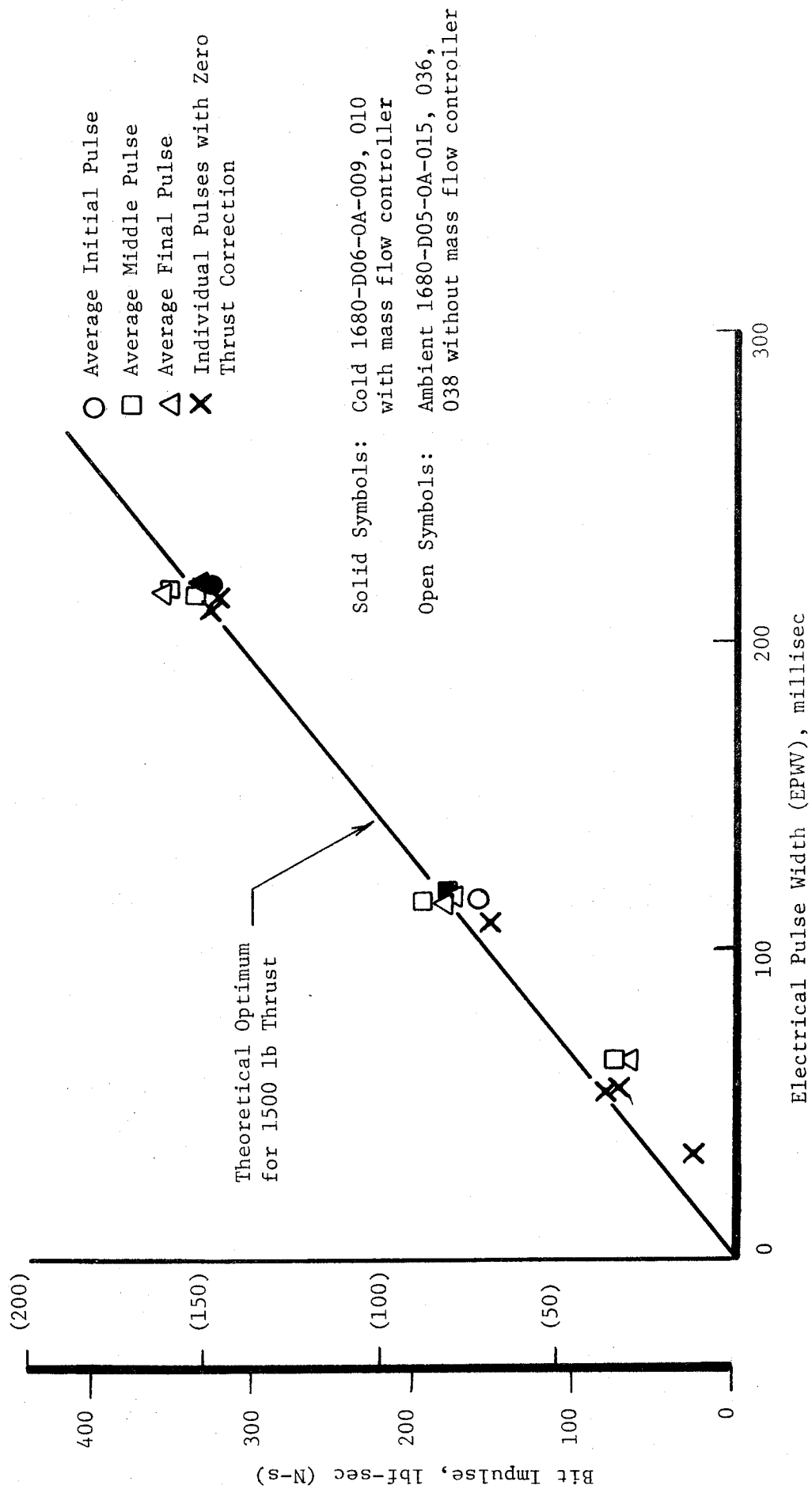


Figure VI-25. Film Cooled Chamber Bit Impulse

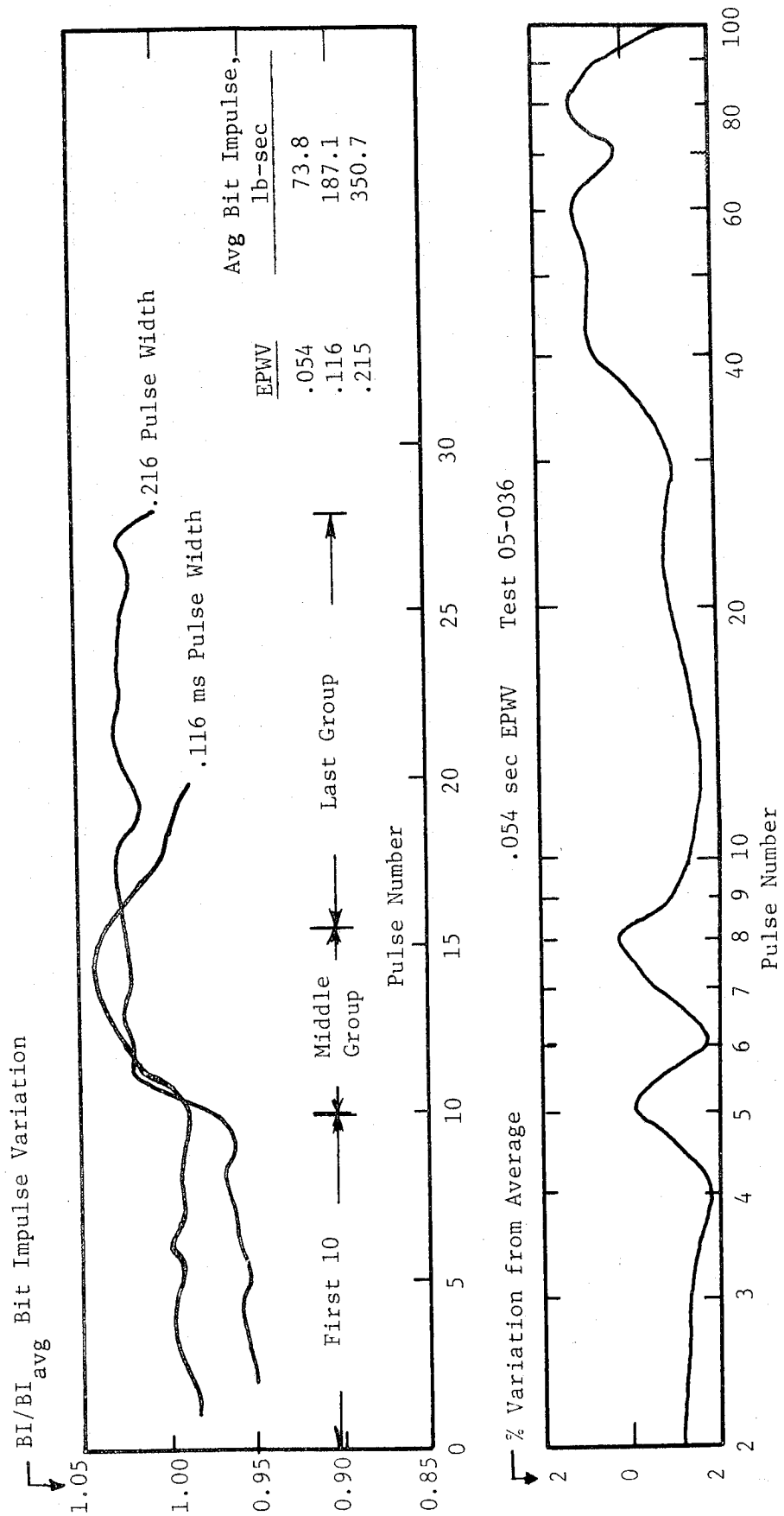


Figure VI-26. Film Cooled Chamber Bit Impulse Repeatability, Ambient Temperature Propellants (Constant Pressure Supply)

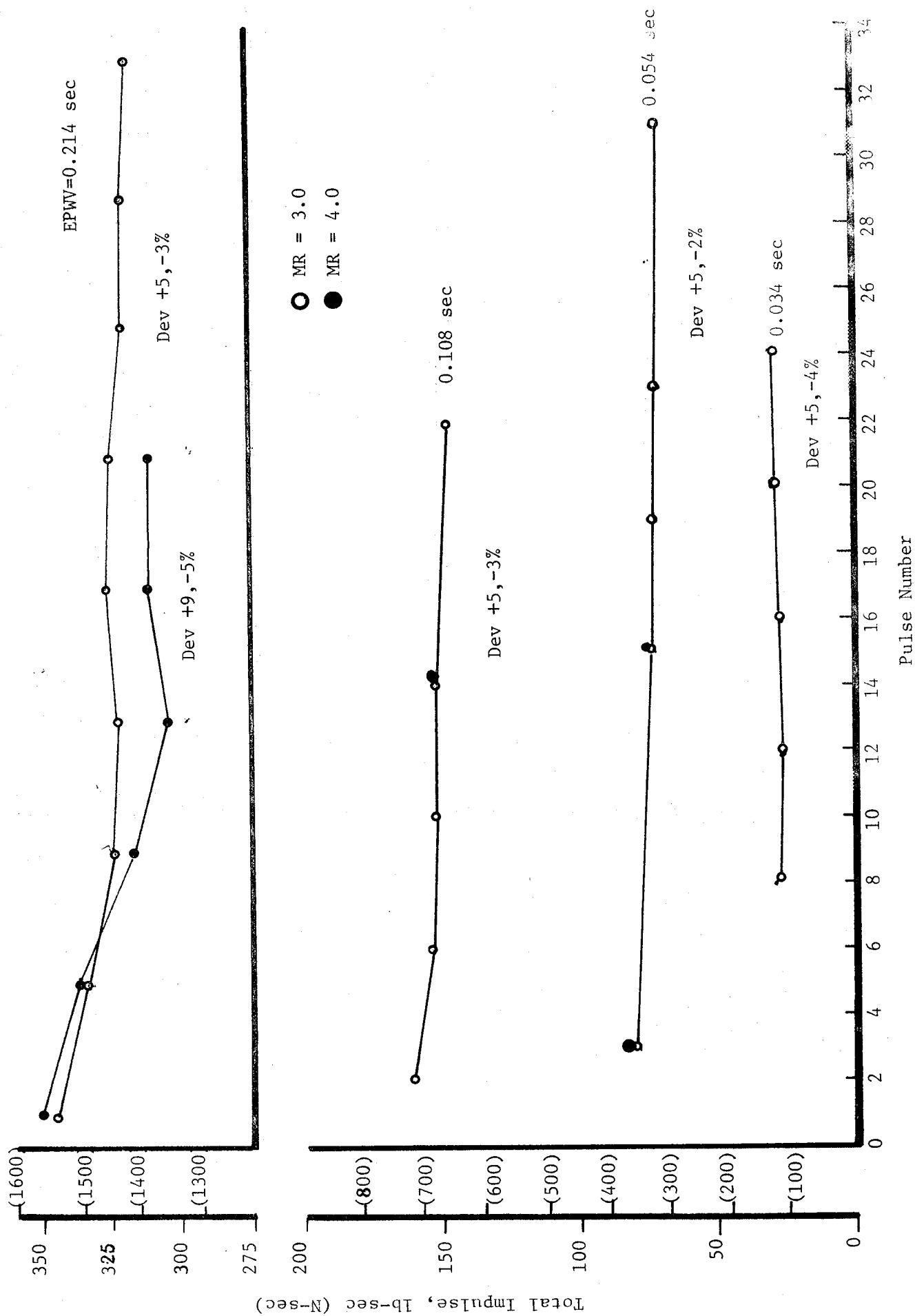
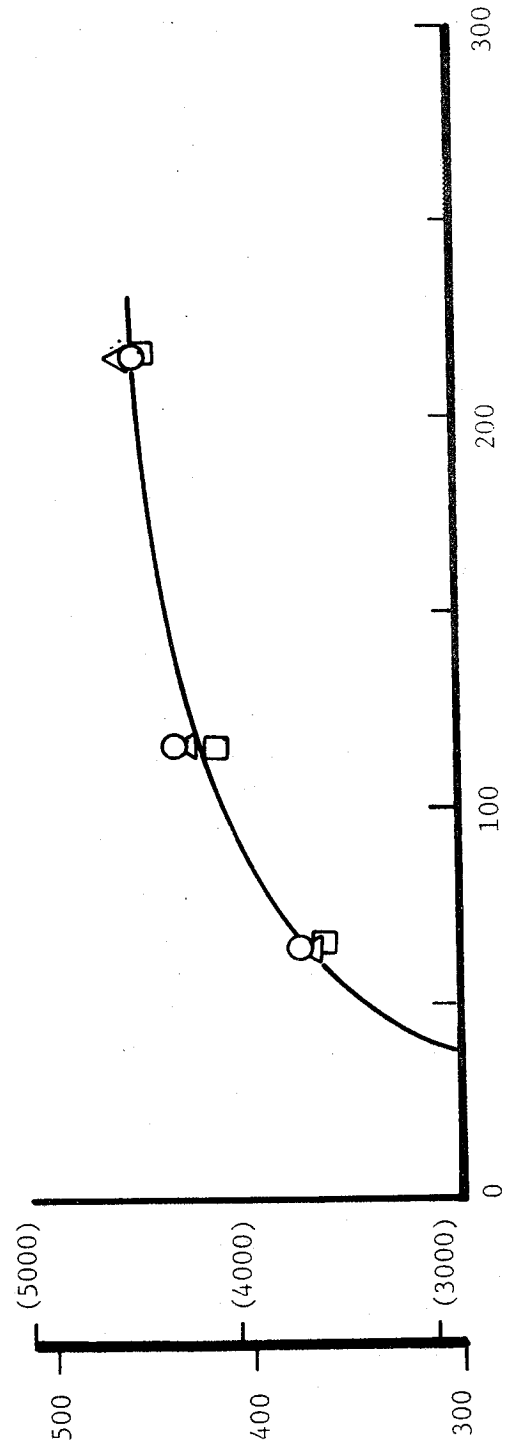
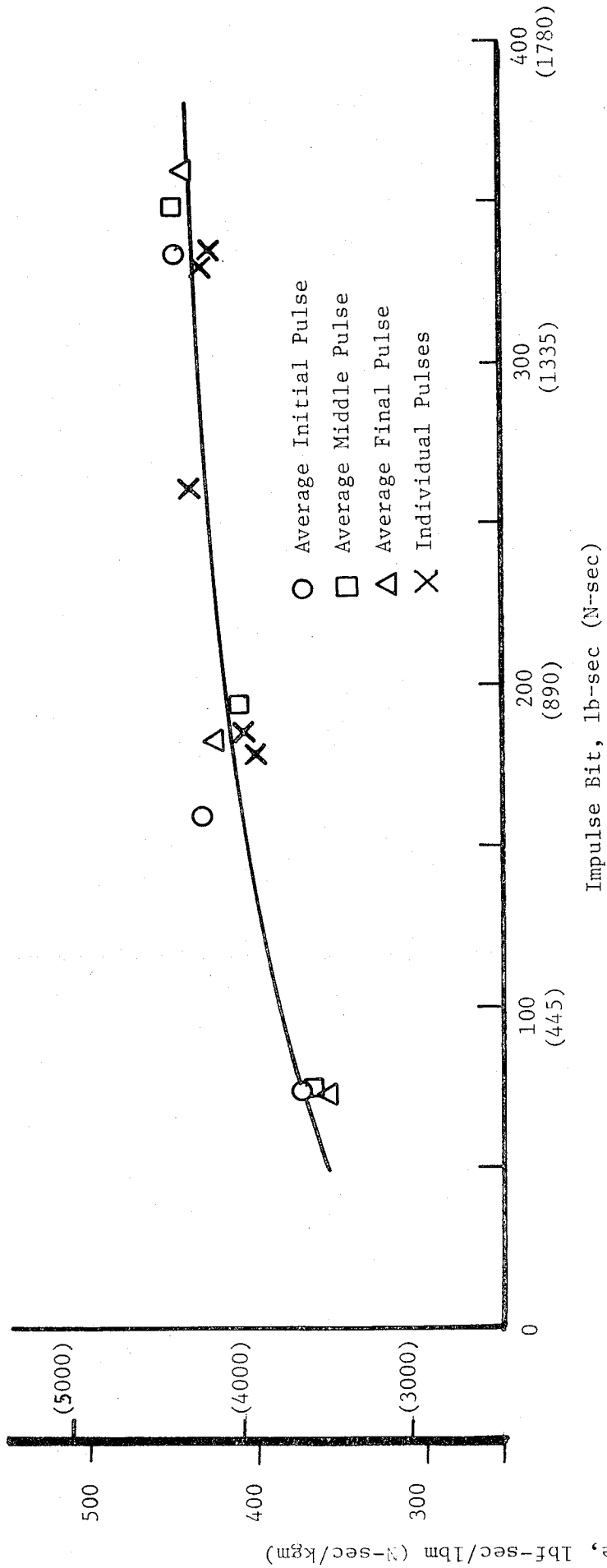


Figure VI-27. Film Cooled Chamber Bit Impulse Repeatability with Cold Propellants (Mass Flow Controlled System)



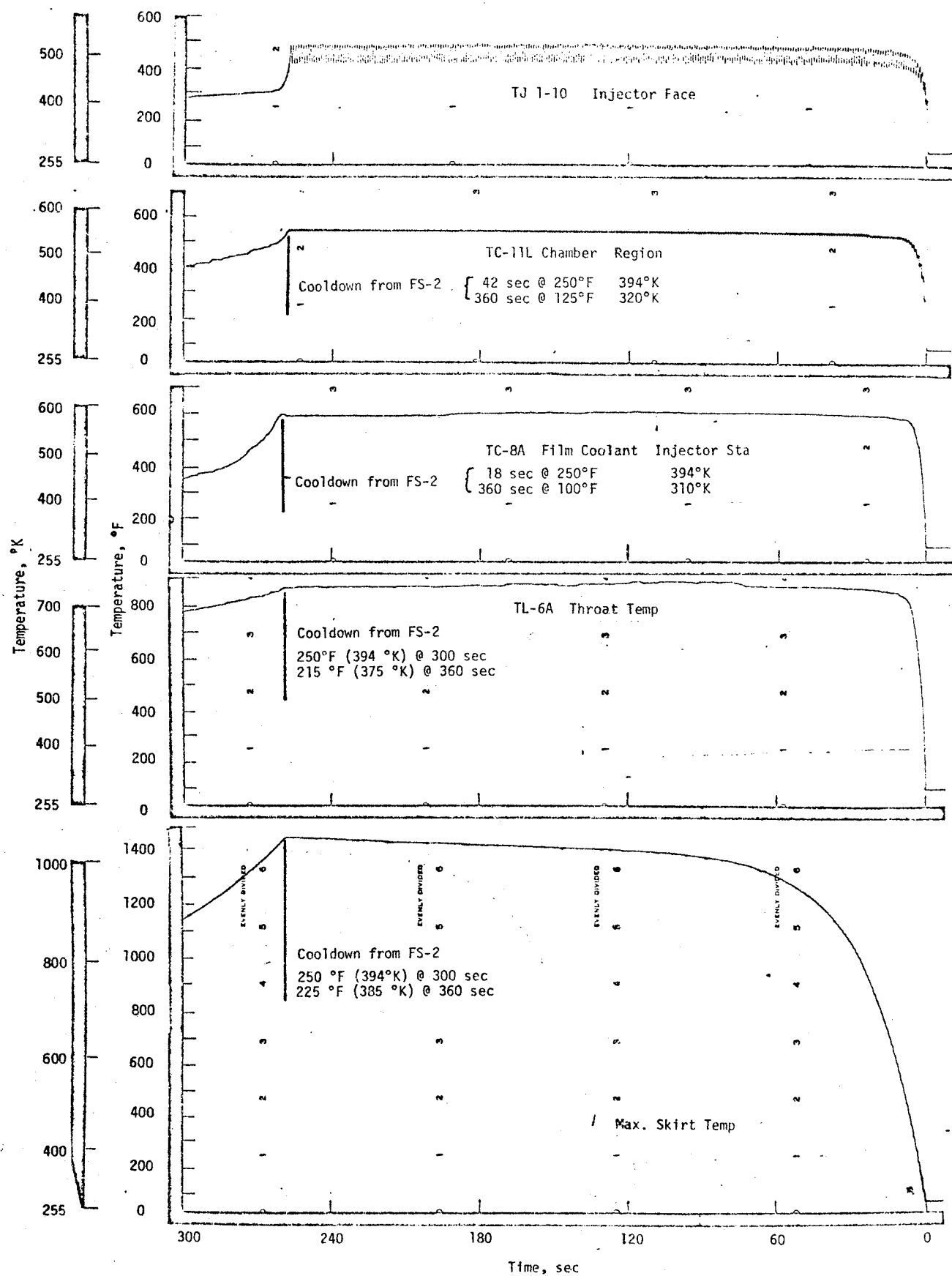


Figure VI-29. Film Cooled Chamber Temperatures in Pulse Mode Operation, Test 05-021, 266 Pulses, 0.2 sec On - 0.3 sec Off

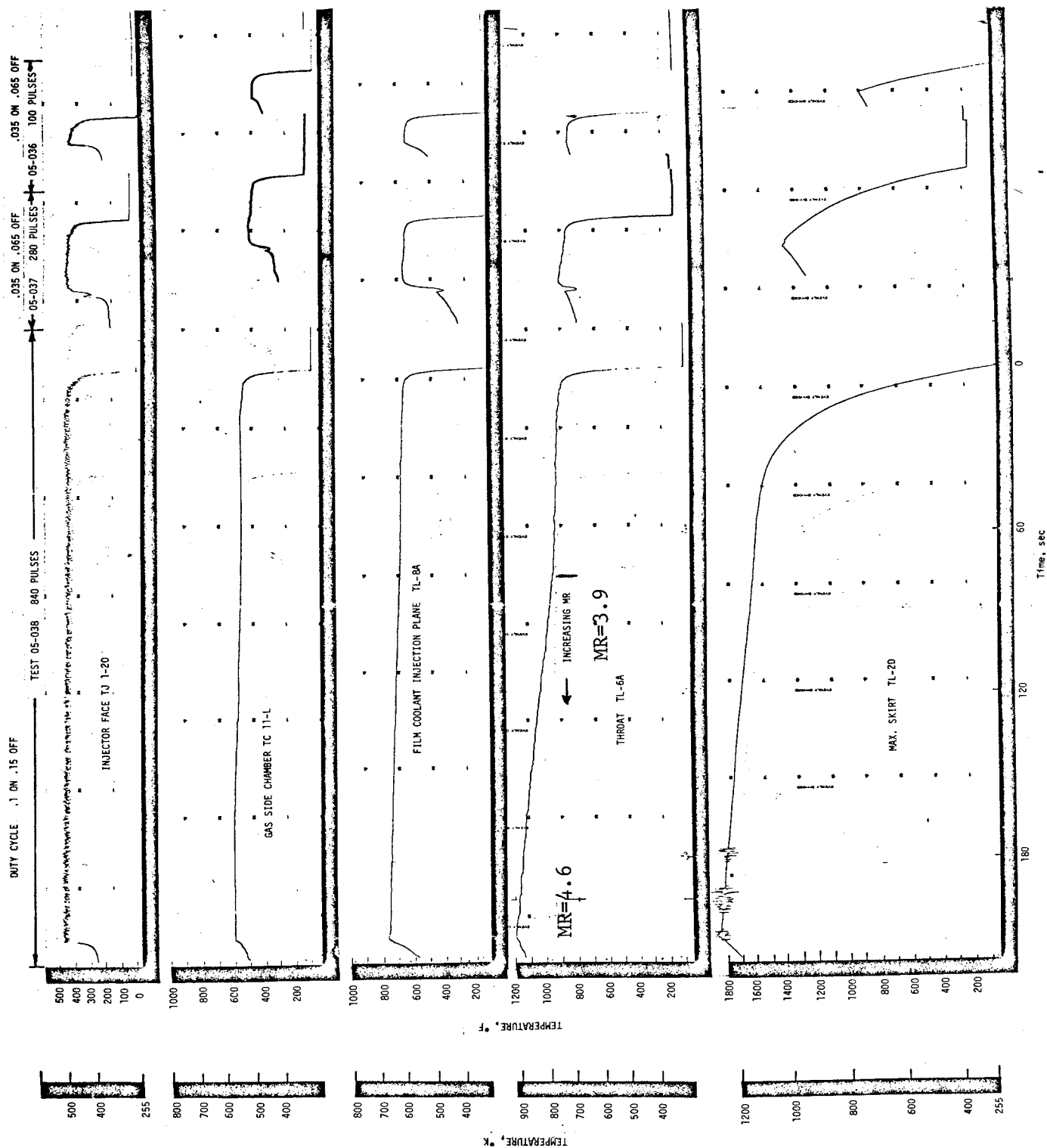


Figure VI-30. Film Cooled Chamber Temperatures in Pulse Mode Operation,

VII. SUPPORTING ANALYSES AND DATA CORRELATION

This section summarizes the supporting laboratory cold flow tests, analytical methods employed in the thermal, structural, material, and performance analyses and provides a comparison of the predicted and experimental results.

A. INJECTOR PERFORMANCE AND COMPATIBILITY

This first section includes the results of unielement cold flow tests, injector manifold design and cold flow studies and the results of the sea level performance and compatibility testing.

1. Injector Element Cold Flow Testing

Cold flow testing of the selected injector elements was conducted to evaluate their mixing and compatibility characteristics and to provide the data required to allow near optimum hardware to be fabricated in the initial injector fabrication. The basic data required was the mixture ratio/mass flux profile generated by the injector element for each of the flow and geometry conditions tested.

a. Experimental Approach

The definition of the mass and mixture ratio profiles for candidate premix and coaxial flow element configurations was accomplished in an experimental test facility which delivered a measured quantity of hot helium and cold nitrogen to the element under evaluation. A temperature rake was used to measure the effluent temperature profile and a pressure rake was used to define the mass profile. A noncombustible mixture of hot helium and cold nitrogen was used for this testing because the hot helium (+200°F (367°K) and cold nitrogen (-200°F) (144°K) closely simulate the respective densities of room temperature hydrogen and oxygen. The temperature difference between the simulants allows a

VII, A, Injector Performance and Compatibility (cont.)

temperature profile in the mixed stream to be measured, from which a local mixture ratio can be inferred. Assuming heat is transferred by turbulent transport rather than by conduction, a temperature above the equilibrium mixed mean temperature indicates a fuel-rich mixture ratio and a temperature reading below the mixed mean temperature indicates an oxygen-rich condition.

The measured temperatures are related to the local mixture by the following equation:

$$OFL = \frac{(CPF * OFO) (1 + \theta) + \theta}{(1 - \theta - \theta * CPR \text{ I } OFO) CPR}$$

where:

OFL = local mixture ratio

OFO = overall mixture ratio

CPR - specific heat ratio = $\frac{C_p N_2}{C_o He}$

and

$$\theta = \frac{T_L - T_{mix}}{T_{N_2} - T_{He}}$$

where:

T_L = local temperature

T_{mix} = mixed mean temperature (equilibrium)

T_{N_2} = nitrogen inlet temperature (injector face)

T_{He} = helium inlet temperature (injector face)

The mass flow associated with each temperature and corresponding mixture ratio zone was obtained in a manner similar to the temperature profile by measuring local static and total pressures with a pitot tube pressure rake. The local mass flux is related to the pitot tube total to static pressure ratio by the following equation:

VII, A, Injector Performance and Compatibility (cont.)

$$W/A = \frac{P_o}{(\bar{R}T_o/\gamma g)^{1/2}} \left| \frac{\left(\frac{2}{\gamma-1}\right) (P_o/P_s)^{\frac{\gamma-1}{\gamma}} - 1}{(P_o/P_s)^{\frac{\gamma-1}{2}}} \right|^{1/2}$$

where:

W/A = mass flux, lb/sec-in.²

P_o = measured local total pressure, psia

P_s = measured local static pressure, psia

γ = average ratio of specific heat

\bar{R} = average gas constant, ft/°R

T_o = measured local total temperature, °R

g = acceleration of gravity, ft/sec²

The average values of specific heat and molecular weight used in the calculation are obtained by mass weighting the simulant specific heats and molecular weights derived from the temperature-inferred local mixture ratio calculation.

A mixing efficiency parameter was used to assess the merit of any individual injector element design. This parameter, which expresses the deviation of the local mixture ratio from the average inlet mixture ratio, is obtained from the following equation.

$$E_m = 100 \left[1 - \sum_o \left[\frac{A_i M_{ti}}{\dot{w}_o} \left(\frac{\dot{w}_o}{\dot{w}_t} - \frac{M_{oi}}{M_{ti}} \right) + \sum_o \frac{A_i M_{ti}}{-\dot{w}_f} \left(\frac{\dot{w}_o}{\dot{w}_t} - \frac{M_{oi}}{M_{ti}} \right) \right] \right]$$

VII, A, Injector Performance and Compatibility (cont.)

where:

E_m	= mixing efficiency
M_{ti}	= local total mass flux, lb/sec-in. ²
A_i	= local area, in. ²
\dot{w}_o	= oxidizer flow rate, N ₂ , lb/sec
\dot{w}_f	= fuel flow rate, He, lb/sec
\dot{w}_t	= total flow rate, lb/sec
M_{oi}	= local oxidizre mass flux, N ₂ , lb/sec-in. ²

The experimental test facility is illustrated schematically in Figure VII-1. Helium is routed from the high pressure storage facility through a steam heat exchanger into the fuel side of the test article. Gaseous nitrogen is cooled by liquid nitrogen in an open bath heat exchanger and routed into the oxygen side of the injection element. Temperature and pressure data which define the flow rates of the simulants are measured with appropriate transducers and recorded with real time digital instrumentation.

The pressure and temperature rakes are 2 in. (5.08 cm) wide. The temperature rake contains 21 chromel-alumel thermocouples, supported in insulated 0.050-in. (.127 cm) tubes while the pressure probe is comprised of fifteen total and fourteen static pressure probes located on 0.060-in. (.152 cm) centers. Rake pressures (both static and total) are recorded via a scanning valve and a single pressure transducer that sequentially samples each probe.

Both probes can be adjusted radially, rotationally, and axially with respect to the chamber face using a traversing optical bench.

In the case of the coaxial flow element where oxidizer tube recess is a parameter, thermocouples were also installed on the thin-wall tubing which forms the outside of the fuel annulus. These provide adiabatic wall temperature measurements which allow an evaluation of the wall mixture ratio within the injection orifice when the oxygen tube is recessed.

VII, A, Injector Performance and Compatibility (cont.)

b. Coaxial Jet Element

(1) Background

Traditionally, the coaxial element has been characterized by its excellent chamber compatibility and relatively slow interpropellant mixing, which is usually overcome by the use of longer combustion chamber lengths. Frequently, in liquid-liquid or gas-liquid injectors, performance has been improved by (1) introducing a swirl component into the oxidizer and/or (2) recessing the center spud approximately one oxidizer tube diameter. These parameters were logical starting points for the gas-gas element as well.

The technology available when the current series of gas-gas cold flow tests were first designed indicated that high fuel to oxidizer velocity ratios enhanced both performance and combustion stability and that fuel to oxidizer velocity ratios of 10 to 15 were historically most successful in past coaxial element development work. However, earlier works investigating the influence of oxygen port recess, oxygen swirlers, and specialized elements such as the scarfed tip were confined to gaseous fuel and liquid oxidizer. The current program was therefore directed toward providing similar mixing and compatibility data with both propellants in the gaseous state. In this light a cold flow program was structured to investigate: (1) three different recess lengths, (2) swirl elements with and without recess, (3) oxidizer inlet characteristics, and (4) scarfed swirler element characteristics. Additional objectives of cold flow testing were to investigate the thermal risk to the injector face that could result as the oxidizer tube recess is increased and to investigate various methods of increasing the stiffness (pressure drop) through the oxidizer injection orifices without increasing the injection velocity.

VII, A, Injector Performance and Compatibility (cont.)

(2) Test Hardware and Conditions

The test hardware employed to simulate the coaxial element fuel and oxidizer manifolds is shown in Figure VII-2. For cold flow testing, a threaded section was added to the full-scale oxygen tube. This allowed recesses to be varied by screwing the element in or out relative to the outer fuel tube. Flow control devices employed on the oxidizer inlet to increase pressure drop and/or promote propellant mixing include:

- (a) Single orifice at element inlet
- (b) Multiple (smaller) orifices at element inlet
- (c) Swirler at element inlet

Additional test variables include the use of recessed and scarfed elements as shown schematically in Figure VII-3.

The test condition which best simulated H_2 and O_2 density, velocity, Mach and Reynolds numbers at ambient temperature, and the nominal Hi P_c chamber pressure of 300 psia (207 N/cm^2) was: 250°F (395°K) helium, -150°F (207°K) nitrogen, and a cold flow chamber pressure of 150 psia (103 N/cm^2).

In total, 95 pressure rake and 57 temperature rake surveys were obtained. Cup premix data were obtained on all 152 tests. The test matrix included three types of oxidizer flow control orifices and one with the oxygen post inlets unrestricted, oxidizer tube recess of 0.0, 0.12, and 0.25 in. (0, 0.31 and 0.63 cm), 0.0 to 1.0 in. (2.54 cm) tube diameters. Additional tests with element tips scarfed at 22° and 45° were conducted with the swirl oxidizer inlet configurations. Table VII-1 provides a summary of the test conditions.

VII, A, Injector Performance and Compatibility (cont.)

(3) Coaxial Cold Flow Testing Results

The initial phase of cold flow testing investigated the flow characteristics (spreading or coring) of the oxygen elements as a function of the element inlet conditions. The results of this series, presented in Figure VII-4, shows the oxygen stream velocity profile at three locations downstream of the oxidizer element discharge. The station nearest the injection plane (top) provides the best picture of the flow distribution. This curve shows there is a significant difference between the swirl and nonswirl inlets, the swirl showing more rapid spreading and loss of axial velocity. By comparison to the swirl flow, differences between the other flow control devices are small. The addition of a single orifice at the inlet to increase the pressure drop produced a higher central core velocity than the nonorificed or 6-orifice inlet configurations. This high velocity persists at the second axial station 1.31 in. (3.34 cm) downstream.

The results of the bipropellant mixing tests are presented in Figure VII-5. The left side of the figure contains mass flux profiles--top for swirler, bottom for the open inlet (showerhead) reference case. The right side provides the normalized mixture ratio profiles--top for swirl, bottom for open inlet. Superimposed on each of the four plots are the influence of element recess and data from three of the axial stations investigated. The dashed lines represent a zero flux in the mass flux plots and the fully mixed state for the mixture ratio profile plots and are located at the axial station at which the data were obtained. In the case of the mixture ratio profiles, points to the left of the line are rich in fuel, while points to the right are oxidizer rich. The performance goal is to have the reference line and data coincide in the shortest possible length. The swirl flow design is seen to best accomplish this objective.

VII, A, Injector Performance and Compatibility (cont.)

The mass flux plots with both fuel and oxidizer flowing retain characteristics similar to the oxidizer only flow, indicating the importance of the oxidizer flow to the mixing process. In the upper left figure, the swirl element mass flux 0.31 in. (0.80 cm) from the injection plane is low over the center of the element, peaks at radius = 0.15 in. (0.38 cm), and decays to zero at 0.25-in. (0.63 cm) radius. This flow profile is characteristic of the vortexing oxidizer. As expected, the flux shows improving uniformity with increasing length.

The normalized mixture ratio profile for the swirl element (upper right) showed the expected oxidizer-rich center and fuel-rich zone surrounding it at a length 0.31 in. (0.80 cm) from injection but again with uniformity improving with length. The profile at the outer radius approaches the nominal O/F from the fuel-rich side, indicating a desirable characteristic from a compatibility standpoint.

In comparing the swirl flow results with those obtained with no inlet flow control, it is apparent that the open inlet element is much less effective in mixing the propellants. High core mass velocities and mixture ratios noted at short downstream distances still persist as far downstream as two to three inches. The presence of excess fuel at the outer periphery of the jet is expected to improve the element compatibility near the injector over the swirl element, which mixes more rapidly. However, the persistence of an oxidizer-rich core for long distances increases the likelihood of incompatibilities in the convergent nozzle if the jets impact on the wall.

The effect of oxidizer tube recess on element mixing is also shown in these data. The data indicate very little, if any, additional mixing can be attributed to recess and that, compared to the effects of swirl, the recess has only a second-order effect.

VII, A, Injector Performance and Compatibility (cont.)

The integrated influence of the mass and mixture ratio distribution, defined in an earlier equation as E_m , provides an analytical approach to evaluating the mixing efficiency. Figure VII-6 summarizes the calculated mixing efficiency as a function of length and mixture ratio. The plot of mixing efficiency vs. axial distance does show a slight advantage for a non-recessed element at axial stations greater than about 1.0 in. (2.54 cm). This is unlike the classic gas-liquid or liquid-liquid elements. This suggests that recess in liquid-phase propellants affects the atomization rather than mixing process.

The effect of varying the flow rates of each propellant through a fixed geometry (thus changing both mixture and velocity ratio) is shown in the lower half of Figure VII-6. The dashed line represents the swirl element and the solid line the nonswirl. Lines to the left correspond to the nominal oxidizer flow, while lines to the right correspond to 1.55 times nominal oxidizer flow. The nominal test condition mixture ratio is 4.85. These data show the mixing efficiency of the swirl element to continuously improve as the oxidizer to fuel ratio is increased because of the added swirl mixing. The non-swirl element peaks out and decreases as oxidizer to fuel flow ratio increases because of a loss in shear mixing efficiency. A flat mixing efficiency curve over a wide mixture ratio range is a desirable characteristic.

Scarfed Coaxial Element

Hot fire chamber heat flux data presented in Reference 4 indicate significant reductions in chamber wall heat flux through the addition of scarfed elements. Cold flow liquid tests reported in Reference 4, show the scarf, in combination with the swirler, to throw the oxidizer radially inboard, thus providing a more fuel-rich environment near the chamber wall. Figure VII-7 provides a comparison of the mixture ratio profiles for the scarfed and nonscarfed

VII, A, Injector Performance and Compatibility (cont.)

swirl elements with both propellants in the gas phase. The profiles appear to be similar with only a small amount of oxidizer thrown into the upper right-hand quadrant as a result of a combined scarfed tip and swirl flow inlet. Significant compatibility advantages of this type of element with gas-gas injection are not demonstrated by these data.

Mixing Within the Recess Zone

A second phase of the cold flow tests was devoted to studying the mixing which takes place in the recessed area of the coaxial element. The amount of mixing occurring within the recess was a matter of concern in that excessive recess could result in a combustible mixture reaching the element wall.

The degree of mixing occurring within the recess was determined through the use of thermocouples spot welded to the outside of the fuel tube at 0.1-in. (.25 cm) increments along the length of the tube (Figures VII-2 and VII-3). The local mixture ratio along the tube wall could be calculated from the temperature data. The effect of increasing the exposure length (greater recess) of the fuel tube to the mixed hot fuel and cold oxidizer is shown in Figure VII-8. The upper figure presents the data in terms of local mixture ratio and shows the pronounced effect of recess on mixture ratio. The plots on the lower part of Figure VII-8 are a cross plot of the mixture ratio at the plane of injection (axial distance 0.0 on the upper plot). The results of these tests show that a substantial risk in the ability to adequately cool the face is being accepted when recesses of greater than about 0.1 in. (.25 cm) or about six times the fuel slot height are employed.

Conclusions for Coaxial Jet Element

The most significant conclusions reached following the coaxial element cold flow test program were:

VII, A, Injector Performance and Compatibility (cont.)

(1) The best propellant mixing in the shortest possible length is obtained by swirling the oxidizer.

(2) Varying the oxygen tube recess distance from zero to one tube diameter does little to improve the mixing efficiency measured 0.5 in. (1.27 cm) downstream of the discharge point.

(3) For the configuration tested, the risk of having elevated face temperatures increased significantly when recess lengths exceeded approximately 0.1 in. (.25 cm).

(4) The various types of inlet orifices employed to increase oxidizer pressure drop do influence element mixing efficiency. However, these effects are small compared to the marked improvement realized with swirlers.

(5) The addition of hydraulic swirlers will probably increase the chamber forward end heat flux because of more rapid mixing as compared to pure axial flow elements. Heat flux in the convergent nozzle, however, could be lower with the swirler because of a more uniform downstream mass flux and mixture ratio and, in particular, because of the absence of unreacted oxidizer cores which could impinge on the chamber wall.

(6) The use of swirlers with scarfed elements provides only small changes in the flow and mixture ratio distribution.

The above conclusions were those attained following the cold flow testing for this element. Many of the predicted results, however, did not materialize in full-scale hot fire tests. Several additional studies were conducted on a company-funded program to determine the reason for the inconsistent results. These included the use of hydrogen and oxygen in cold flow

VII, A, Injector Performance and Compatibility (cont.)

testing rather than heated simulants and use of a mass spectrometer to determine local mixture ratio. These results were in reasonable agreement with those reported above. The test employing the mass spectrometer and actual propellants were repeated, however, with the gases ignited and combusting. These data (presented in Reference 5) revealed that the mixing rates and efficiency are significantly reduced by the combustion process and that predictions based only on cold flow data are likely to be in error.

c. Premix Element Cold Flow Testing

(1) Background

Preliminary cold flow studies prior to initiation of this program established that fuel orifice geometry and relative propellant momentum were controlling parameters in injector mixing effectiveness. Three fuel orifice geometries were evaluated over a range of momentum ratios that encompassed the expected operating conditions of the full-scale hardware. Two basic techniques were used to evaluate the model injection element: Schlieren photograph and mass and mixture ratio surveys using thermocouple-pressure rakes.

Schlieren photographs were taken at ambient pressure with the intent of investigating the dimensional character of the gas body after impingement. The photographs revealed that elliptical spray fans are formed that are similar to the classic liquid-liquid fans.

The following table indicates the momentum range possible with the full-scale hardware consistent with available system pressure losses and the corresponding momentum ratio range of the model injector.

VII, A, Injector Performance and Compatibility (cont.)

	<u>Full-Scale Injector</u>	<u>Model Injector</u>
Oxidizer momentum, lb-ft/sec ²	11.7 to 18.8	2.4 to 23.4
Fuel momentum, lb-ft/sec ²	9.4 to 16.2	2.2 to 40.0
Momentum ratio, $(\dot{w} V)_f / (\dot{w} V)_o$	0.50 to 1.38	0.11 to 15.30

Approximate Mach number similarity was maintained by using heated helium as a H₂ propellant simulant and chilled N₂ as an oxygen propellant simulant.

The model injector element configuration was based on cold and hot flow testing completed prior to this work. This earlier testing revealed that the fuel orifice exit cross-section shape had a first-order effect on the mass and mixture ratio distribution. For the model testing, this parameter was varied as shown in Figure VII-9. The oxidizer orifice diameter was 0.469 in. (1.19 cm) in diameter in all cases. Modifications B and C, Figure VII-9, were designed to concentrate the available fuel momentum at the center of the oxidizer stream, thus increasing the penetration of the fuel into the oxidizer jet. Design A, however, attempts to suppress mixing by shrouding the oxidizer stream with fuel, thereby generating a benign flow boundary in the chamber.

(2) Premix Element Cold Flow Test Results

Optical Tests

In order to visualize the plume, a number of Schlieren photographs were taken with the injector flowing to ambient back pressure. For these tests, relative injection velocity and momentum were maintained by reducing the weight flow through the injector. Figure VII-10 provides Schlieren photographs of the triplet element with the camera oriented parallel and normal to the long

VII, A, Injector Performance and Compatibility (cont.)

axis of the fan. It can be seen that the fan aspect is approximately two and decreases with increasing momentum ratio. The decreasing aspect ratio of the fan with increasing momentum ratio is related to the relative penetration of the fuel into the oxidizer core. At low fuel momentum, the fuel divides and flows around the oxidizer, forming the high aspect ratio fan shape. Fuel penetration of the circular oxidizer jet improves as the fuel momentum is increased, resulting in higher entrained fuel fractions and decreasing the fan aspect ratio. Subsequent testing with pressure rakes in a confined environment indicated the same characteristics, i.e., elliptical fans at low fuel momentum approaching the circular jet shape at higher fuel momentum.

Pressure - Temperature Tests

A series of twenty tests was conducted varying oxidizer and fuel momentum using three different fuel geometries. For each injector type, the momentum ratio was varied over the expected range of real injector design conditions by changing both fuel and oxidizer weight flow. The results of this study are shown in Figure VII-9.

The "I" triplet is noted to mix considerably better than the triplet element over the momentum ratio range of interest (.9 - 2.0). It is apparent that the orifice geometry which concentrates the available fuel momentum at the center line of the oxidizer jet, penetrates the core of the jet and thus mixes effectively. The optimum ratio of oxidizer orifice diameter to fuel slot width (relative width R_w) is 2.0 - 2.25; the design point is 2.2. When the fuel slot width is greater than the oxidizer diameter the fuel sheet is penetrated by oxidizer and forms a fan with a fuel rich boundary and an oxidizer rich core. As the fuel slot width is decreased ($R_w = 2.0 - 2.25$), increasing quantities of fuel are injected into the center of the ox stream until in the limit most of the oxidizer surrounds the fuel, generating obviously bad compatibility characteristics. For this particular element a width ratio of 2.2 is a good compromise between performance and compatibility.

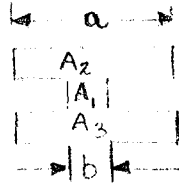
VII, A, Injector Performance and Compatibility (cont.)

In addition to the cold flow providing mixing efficiencies, information was obtained indicating the expected compatibility of each element, as shown in Figure VII-11, for the low (top) and high momentum ratio cases (bottom). The triplet element has a characteristically fuel-rich boundary and oxidizer rich core. Both the mass flux and mixture ratio profiles become more uniform as the relative oxidizer momentum is decreased by a factor of three. The characteristic of a fuel rich boundary however, remains. This element type would be excellent from an injector face and wall compatibility standpoint assuming the chamber was long enough to react to all of the oxygen before it impacted on the convergent nozzle wall.

With the "I" triplet design, the peripheral gas composition products contain a greater fraction of oxidizer. Depending on the shape of the element and momentum ratio the fuel can become concentrated in the center of the jet while the oxidizer tends to be oriented near the wall (high momentum ratio, high R_w). However, for the same element a fuel rich boundary is restored by lowering momentum ratio.

Cold flow testing revealed that the mixing efficiency of the premix element is a function of both the fuel orifice geometry and propellant momentum ratio. With the flat or conventional triplet, high mixing efficiencies can only be obtained with a momentum ratio approaching ten. However, as the fuel is concentrated upon the center of the oxidizer jet (e.g., the "I" triplet), mixing efficiencies improve dramatically and, in the optimum approach, 100% at momentum ratios near two. The data also indicate that momentum ratios below two have the characteristic of a fuel-rich boundary while those above two have the opposite characteristic. The recommended full-scale injector element, based on cold flow data, was an "I" triplet with oxidizer orifice diameter equal to 2.2 times the fuel leg width as shown below.

VII, A, Injector Performance and Compatibility (cont.)



Area split	$A_{\text{total}} = .6A_1 + .2A_2 + .2A_3$
b Dimension	= Oxidizer Jet Dia./2.2
a Dimension	= 1.1* Oxidizer Jet Dia.

2. Manifold Design and Flow Studies

Proper manifold design is essential if uniform propellant injection and mixture ratio is to be achieved within the allowable system pressure drop budgets. Uniform propellant injection is a prerequisite for high performance and for minimizing streaking which produces large peripheral thermal gradients that reduce chamber life.

Two types of manifolding arrangements were selected for study in this program. One was the conventional radial inflow fuel and flooded back oxidizer of the coaxial tube design, the other was a pie and concentric ring design for both fuel and oxidizer, wherein radial inflow is accomplished via six alternating fuel and oxidizer pies and peripheral distribution is accomplished via seven alternating fuel and oxidizer concentric rings which are fed from the pies. An understanding of the manifold designs can be obtained from Figures IV-1, -2, -4, and -6 and VII-12.

Flow distribution analyses and cold flow tests were conducted in support of each manifold design approach in an attempt to provide uniform flow conditions and pressures at the inlet to the propellant injection element.

VII, A, Injector Performance and Compatibility (cont.)

The cold flow tests involved flowing GN_2 in a mockup or actual hardware of each propellant circuit at simulated Mach number conditions. Distribution data were obtained by using a specially designed nonrestrictive flow collector to capture the flow as it discharged from each of the individual propellant injection orifice. A rotometer was employed to measure the flow. The design goal in Phase I was to provide an element to element flow deviation of less than $\pm 5\%$.

The manifold cold flow testing on the pie and concentric ring manifold was largely completed under a prior company funded effort. A number of modifications were made to the manifolding to improve the basic distribution. In general, these modifications consisted of rounding off sharp edges and chamfering inlets to keep flow from separating and to reduce the sensitivity to cross-flow. However, in spite of this the flow variation was never reduced below about $\pm 4\%$. A fundamental flaw in this manifolding approach is that the high and low flow rates occur under and between the pies respectively. This results in an out of phase condition wherein the point of maximum oxidizer corresponds to the point of minimum fuel and vice-versa. Thus, a 5% flow variation in each circuit produces a 10% mixture ratio maldistribution at six peripheral locations.

The flooded oxidizer/cross-fed fuel manifold design used first in the coaxial injector and later adapted to the Phase II premix injector was found to be satisfactory. On the coaxial injector this pattern was flowed with four different oxidizer tube inlet conditions (sharp edges orifices and high, medium, and low ΔP swirlers) deflector rings and approach baffles (Figure VII-12). The only variable which appreciably altered the flow distribution was the inlet on the oxidizer tubes. The various manifold baffles and deflector rings had no noticeable influence on either the fuel or oxidizer distribution. The oxidizer flow reached the goal of $\pm 5\%$ maldistribution with the medium pressure drop swirler and a maldistribution of less than $\pm 2\%$ with the sharp edged orifice plate inlet.

VII, A, Injector Performance and Compatibility (cont.)

The fuel circuit showed a persistent element to element flow deviation in excess of $\pm 10\%$ of nominal. This deviation was eventually traced to dimensional tolerances on the 0.017 -in. (.043 cm) fuel annuli. Critical dimensions (oxidizer tube "OD") on those elements which exhibited low fuel flow were rechecked and fabrication deviations were found to be the cause. After the dimensions of the low flow annuli were corrected the fuel flow uniformity approached the desired $\pm 5\%$.

The manifold configuration and propellant velocities employed with the Phase II premix injector design are shown in Figure VII-13. The flow control and distribution system of this injector combined the basic manifold configuration of the coaxial injector with the premix element Phase I design. The maximum measured element to element flow distributions for the final injector assemblies were as follows:

		Variance within the Row			Overall Variance
	SN	12 Elements Inner Row	24 Elements Center Row	36 Elements Outer Row	
Oxidizer	6	$\pm 1.7\%$	± 2.6	± 2.6	± 3.3
	7	± 1.6	± 3.5	± 3.0	± 3.7
Fuel	6	$\pm 1.3\%$	± 1.7	± 1.9	± 3.0
	7	± 3.0	± 2.5	± 3.0	± 3.1

Some of the flow variation can be attributed to the flow collecting and measurement techniques since what is being reported is small calculated differences between large measured numbers. Furthermore the above results encompass the data from all elements. The extreme conditions in most cases represent only one or two elements within a row. The general conclusion from these tests are that (1) the Phase II design is capable of providing uniform flow within about 3.5% (which has been demonstrated to be streak free in hot fire tests), and (2) that the selected fabrication approach is consistently reproducible.

VII, A, Injector Performance and Compatibility (cont.)

3. Injector Face Cooling and Cycle Life

a. Background

One of the main injector design objectives was to investigate and develop the technology required for 10^6 engine restarts. The concern for face cooling therefore went beyond the usual face cooling and structural analyses. In particular it was necessary to define the face temperature profiles and resulting strains during the pneumatic and thermal start transient, during steady state operation and during the thermal shutdown transient.

Cooling analyses for the injector face were initiated following definition of the propellant injection orifice configuration from the cold flow testing. The greatest single unknown in these analyses was the thermal environment at the injector face and certain assumptions had to be made on the basis of previous experience. Empirically it has been shown that injector face heat fluxes can range from 20 to 100% of the theoretical heat flux at the forward end of the chamber as calculated from equations presented in later sections. The precise magnitude of the face heat flux depends on three parameters: (1) the rapidity of propellant mixing, (2) the level of combustion turbulence, and (3) the hot gas cross flow and recirculation patterns between the injection orifices. In general the face thermal load is reduced by: (1) delaying inter-propellant mixing which translates to poor mixing efficiency and is therefore undesirable; (2) increasing the number and density of the propellant injection elements which also tends to improve performance, and (3) to provide a face bleed. The two latter approaches tend to reduce cross flow and recirculation of the combusted propellants, in addition to providing an active face cooling mechanism.

VII, A, Injector Performance and Compatibility (cont.)

b. Coaxial Injector

The selected cooling approach for this design employs a thick, highly conductive face material in which heat is removed convectively by the fuel flowing at high velocity through the closely spaced large diameter injection annuli. The approach to the face plate cooling analysis was to estimate the face heat flux and then compute the face temperatures for various thicknesses, element densities, and materials. Normally, the face flux for a coaxial (liquid oxidizer within gaseous fuel) jet, augmented by a porous face, would be estimated at 20% of the chamber wall flux. A more conservative estimate of 80% (5 Btu/sec-in.^2) (820 w/cm^2) was made for design purposes because of the solid face design and gas phase oxidizer injection. The design equations which led to the selection of the 0.5-in. (1.27 cm)-thick copper face plate having 42 orifices are provided below.

Equations 1, 2 and 3 (Table VII-2) define the variables which control the steady state injector face thermal gradients, the thermal stresses, and the ultimate cycle life of a conductively/convectively cooled injector face. Equation 1 provides an approximate general closed-form solution defining the temperature at any point within a circular plate of thickness (t) containing (N_e) uniformly spaced holes where the plate is exposed to a known flux on one face and is cooled by a convective coefficient (h) on the surface generated on the inside surface of each hole. The maximum temperature gradient (ΔT) which the face plate experiences (defined in Equation 2) is the difference between the local temperature at the heated face most remote from the cooled holes and the injector flange (which is assumed to be at the propellant inlet temperature). The maximum allowable temperature gradient the face plate can sustain, based on thermal stresses and cyclic life, is approximated by Equation 3. This equation assumes that the point on the face which reaches a maximum temperature is fully restrained from thermal expansion.

VII, A, Injector Performance and Compatibility (cont.)

The initial analyses were to establish a relationship between maximum temperature, quantity of injection elements and face plate thickness for a specified fuel and oxidizer injection velocity, and an assumed face heat flux and a given material thermal conductivity. The results of this study are given in Figure VII-14 (lower right) for a face plate thermal conductivity corresponding to either T-6063 aluminum or BeCu-10X and a face flux of 5 Btu/in.²-sec (820 w/cm²). The figure shows that, in terms of injector face cooling, little advantage is realized in increasing the number of elements beyond about 40 or the fuel-cooled face thickness above 0.25 in. (0.63 cm).

Application of Equation 2 to the selected 42-element design pattern provided an estimate of the face temperature gradient for several candidate face plate materials and thickness. These are shown on the left side of Figure VII-14. The face temperature gradient for a fully restrained plate is observed to decrease both as the thermal conductivity of the face plate material increases and as the cooling surface (plate thickness) is increased. The benefits of increased thickness diminish rapidly, however, after thicknesses of about 0.25 in. (0.63 cm). Since many assumptions were involved in the analysis, the initial selection of face plate material (OFHC copper) and thickness was very conservative, 0.5 in. (1.25 cm).

Test Results

The 0.5-in. (1.27-cm) thick OFHC copper face plate and a 0.55-in. (1.4-cm) thick aluminum face were instrumented with six gas-side thermocouples to obtain face temperature and heat fluxes. The experimental data from these tests are shown in Figure VII-15. The lower half shows the measured heating transients for the various thermocouple positions from firings at 30%, 100% and 166% of nominal chamber pressure. The outer periphery of the injector is hotter than the inboard positions because of recirculation of the partially combusted propellant. A small peripheral bleed or reduction of the distance

VII, A, Injector Performance and Compatibility (cont.)

between the outer elements and the wall will be required to eliminate this hotter area. The inboard temperature measurements are uniform which is essential for minimizing thermal strains. The transient measurements show that near steady-state temperatures are achieved in approximately 0.2 sec from ignition.

The upper half of the same figure shows the thermal sensitivity at steady state to design and operational variables to be as follows:

<u>Variable</u>	<u>Effect on Temperature</u>
Mixture ratio	Not significant at low and nominal pressures. Significant at higher pressures.
Chamber pressure	Temperature increases significantly with increasing pressure.
Fuel temperature	Face temperature proportional to fuel temperature.
Oxidizer injection	Swirl and shower are nearly the same.
Face thermal conductivity	Aluminum is slightly hotter; however, this may be due to slight tip recess.

The maximum face temperature was predicted to be about 280°F (155°R) higher than the fuel temperature. Actual test data from the thermal instrumentation presented in Figure VII-15 showed the prediction to be conservative by 80°F (44°K) ($\Delta T_{\text{exp}} = 200^\circ\text{F}$) based on maximum temperature and by 160°F (89°K) ($\Delta T = 120^\circ\text{F}$) based on inboard measurements. From these test results and Equation 2, it is inferred that the actual maximum face heat flux is approximately 3.6 Btu/sec-in.² (590 W/cm²) rather than the assumed value of 5. The experimental ΔT on the T-6061 aluminum face was 230°F (128°K) with cold propellants for which the inferred face heat flux was 2.7 Btu/sec-in.². One aspect of this injector design which could not be experimentally investigated for practical reasons was the thermal environment at the tip of the oxidizer injection tube. The tube tip thermal environment may be considerably more severe if they act as flame holders.

VII, A, Injector Performance and Compatibility (cont.)

Life Analyses

When the results of the thermal analysis are coupled with material structural properties, the upper right half of Figure VII-14 is obtained. These curves indicate the relative maximum face heat fluxes which various materials can withstand as a function of number of thermal cycles. The superiority of BeCu 10% and aluminum alloy T-6061 over nickel and OFHC copper for the thick face plate configuration is evident. A significant limitation of aluminum, however, is that it loses strength rapidly at temperatures above 400°F and its durability could be substantially reduced if propellant temperatures higher than ambient are sustained for any duration. This material is not compatible with the high reentry heating temperatures being projected for some of the APS thruster locations.

c Premix Pattern Face Cooling and Fatigue Life

Cooling of the premix element injector face is accomplished by a combination convective and dump cooling. The convective cooling results from the flow of the fuel at high velocity through channels oriented parallel to the injector face and 0.024 in. (0.06 cm) below the heated surface. The configuration of these coolant channels, which also serve as the propellant injection orifices, is optimized to maximize mixing efficiency and compatibility and minimize the injector face thermal load. Additional convective cooling is obtained by diverting a small percentage of the fuel to a network of smaller high velocity channels located 0.010 in. (0.025 cm) below the heated surface as shown in Figure IV-3. This supplemental coolant is then discharged through a network of orifices selectively located in the normally high heat flux zones usually found between and around each injection element. The face bleed minimizes recirculation of the hot combustion products and therefore reduces the face heat flux to levels which are compatible with high cyclic life.

VII, A, Injector Performance and Compatibility (cont.)

Initial design studies evaluated: element configurations, premixing cup geometries, materials, and bleed port locations. The end product of these activities evolved through three variations of the basic injection elements and one modification to the quantity and location of the bleed ports. These iterations resulted in an injector design providing the 10^6 life cycle requirement while still maintaining a 99% propellant mixing efficiency element configuration. The injector face material can be either copper or nickel. Nickel was selected mainly because of its greater oxidation resistance.

As in the case of previous injector face cooling analyses, the design activities related to the premix element were empirical. The face cooling is closely coupled with the premix element configuration and a considerable degree of element flow tailoring was accomplished to optimize both face cooling and propellant mixing efficiency. The cold flow test results presented in an earlier section provided the following design parameters for maximum mixing efficiency: (1) preferred propellant momentum ratios, (2) a relation between the width of the fuel orifice relative to the oxidizer jet, and (3) an insight into the flow recirculation patterns at the injector face. Sea level hot fire testing with prototype injectors and several pattern configurations showed the face thermal environment to be influenced by the depth to diameter ratio of the premix cup and the relative widths of the fuel and oxidizer jets. Figure IV-5 shows the element configurations tested in this program.

Injector Face Thermal Data

The face cooling and life analysis for the premix family of injectors is based on extensive test data and an injector face thermal model. Measurements of the injector face temperatures were made at the following six locations with the instrumentation as noted below and shown in Figure IV-3.

VII, A, Injector Performance and Compatibility (cont.)

- (1) Between injection orifice (mid row) at two locations (0.010 in. (0.025 cm) dia TC)
- (2) Between rows of orifices (mid and outboard) at two locations (0.010 in. (0.025 cm) dia TC)
- (3) At injector periphery at two locations (0.020 in. (0.051 cm) dia TC)

These thermocouples were inserted through the face to the gas-side surface and staked into position flush with the surface. Figure VII-16 shows 3 typical sets of recorded start transient, steady-state and shutdown temperature data obtained from the validated instrumentation for the following test conditions with the modified "I" pattern premix injector:

Top Figure:	Nominal pressure and mixture ratio with 200°R (111°K) propellants
Center Figure:	Nominal pressure and mixture ratio with 590°R (326°K) propellants
Lower Figure:	High pressure and nominal mixture ratio with 560°R (310°K) propellants

Comparable data were also obtained at high and low mixture ratios from the pre-mix triplet (SN 4), the initial "I" design (SN 5), and a very shallow cup canted "I" to evaluate element geometry effects. The center figure also provides three data points which are the face temperatures recorded following single pulses at 0.04, 0.10 and 0.20 sec duration in the pulse test series. These pulse data are in agreement with steady firings at the same point in time from ignition.

VII, A, Injector Performance and Compatibility (cont.)

Steady-State Measurements

The nominal and extreme thermal conditions were identified directly from the steady-state measurements for each of the design and operational variables of concern. Measured steady-state temperatures for the various element patterns are shown in the upper half of Figure VII-17. The left side shows the steady-state temperatures recorded for each of the patterns vs. core mixture ratio at nominal pressures and ambient propellant temperatures. Each of the three patterns is nearly insensitive to mixture ratio; however, there is a considerable difference in the absolute temperature level. The major difference between the two initial patterns tested (SN 5 "I" triplet and SN 4 triplet) was the depth of the premix cup and the ratio of fuel to oxidizer jet cross sections. The curves in the (upper right) show how the face temperature increases with cup depth. The modified "I" was configured in Phase II to have the same momentum and high mixing efficiency as the initial high performing "I" pattern; however, the cup depth was reduced to reduce the residence time. The SN 4 triplet pattern runs much cooler and is shown as a separate curve because the ratio of oxidizer (d_o) to fuel jet (w_f) width is different from the "I" family ratio (d_o/w_I).

A small physical difference exists between the two modified "I" patterns tested. The initial designs provided 5% bleed through 300 0.013-in. (0.033 cm) -dia ports located between injection elements and rows of elements. Because the two peripheral temperature measurements indicated the outboard region to be running about 200°F (111°K) hotter than the four inboard stations, the final design provided an additional 108 .02-in.-dia (.051 cm) ports around the periphery of the face. These can be seen in the photograph in Figure IV-3. This modification increased the peripheral face bleed to 2.5% and eliminated the difference.

VII, A, Injector Performance and Compatibility (cont.)

The two lower curves in Figure VII-17 show the influence of fuel supply temperature and chamber pressure on injector face temperatures. Different temperatures are shown for the regeneratively cooled and film-cooled chambers. Part of this is due to higher fuel bulk temperature rise in the regenerative chamber (125°F vs 200°F (70°K vs 111°K) at nominal conditions). The remainder is probably due to a small outflow component on the regeneratively cooled chamber because the head end film coolant injection ring was removed in these tests, thus increasing the chamber diameter by approximately 0.22 in. (0.56 cm). The dependency of injector face temperature on fuel inlet temperature is approximately one to one; i.e., a one-degree rise in fuel temperature results in a one-degree rise in face temperature. The effect of chamber pressure on injector face temperature is a second order effect with temperatures tending to drop as the chamber pressure is increased.

The conclusions on face steady-state thermal sensitivity are:

- (1) The design approach allows considerable flexibility to cool the face while maintaining high performance.
- (2) The design is not sensitive to MR variations.
- (3) The design is not sensitive to P_c ; the trend is toward lower temperatures at higher P_c .
- (4) Face temperatures are proportional to fuel supply temperature.

Transient Thermal Characteristics

The temperature data for the modified "I" premix pattern shown in Figure VII-16 include both the start and shutdown transients and some pulse data. These are significant data because most of the firings, in

VII, A, Injector Performance and Compatibility (cont.)

application, will be short and it is important to know what condition constitutes a full thermal cycle. It can be observed from these data that there is an initial rise concurrent with igniter ignition which, depending on the start sequence selected, may lead mainstage valve actuation by 0.0 to 0.050 sec. The lead was 0.050 sec for the tests shown. The face temperatures then rise rapidly following mainstage ignition. The injector pattern design controls the rate of temperature rise, the temperature level at steady state, and the uniformity across the surface. Typically, the premix injector face reaches 75% of its steady-state operating temperature in approximately 0.2 sec from the mainstage ignition. Short firings, therefore, do not constitute a full thermal cycle. Following shutdown, the injector face does not immediately return to its initial temperature. For example, Figure VII-16 (center) shows the face temperatures rise by about 400°F (222°K) on the long firing and experience a 200°F (111°K) drop on shutdown. In a subsequent firing, the face temperature will only increase by 200°F (111°K) to the steady-state value. This was demonstrated in actual pulse testing. Life is therefore duty-cycle sensitive. Another test variable identified by these data is the influence of valve sequencing and manifold venting at shutdown and its influence on injector face temperatures during this period. Several of the face temperature traces shown are noted to rise 50 to 100°F (28 to 56°K) following the valve closure. Valve sequencing was found to influence the magnitude of the postfire thermal rise and, thus, eventually the life. These specific data are covered in a later section.

Interpretation of the Data for Life Analysis

The data shown and discussed in Figure VII-16 were useful in both understanding the transient thermodynamic aspects of the system. A quantitative assessment of the magnitude of the thermally induced loads which affect the component life was obtained by processing the measured parameters through appropriate injector face structural and thermal models.

VII, A, Injector Performance and Compatibility (cont.)

The thermally induced strain levels within the injector face were obtained by the following equations and assumptions:

The nickel platelet stack and the 0.125-in. (0.32 cm) stainless steel plate to which it is bonded are subjected to a known, time-dependent temperature gradient which forces the material into the plastic range. The face is prevented from rotating by being rigidly attached to the injector body by 72 oxidizer posts and the central igniter adapter. The maximum thermal strains between injection elements and between rows of elements are determined by the following equations:

Region A between elements (1 degree of fixity) $\epsilon_{\max} = \alpha \Delta T$

Region B between rows of elements (2 deg of fixity) $\epsilon_{\max} = \frac{\alpha \Delta T}{1-u}$

where:

α = coefficient of thermal expansion of nickel

u = Poisson's ratio = 0.3

ΔT = maximum surface temperature - average temperature of face plate

Fatigue life of the face is based on the appropriate S-N curve for the material using the computed maximum thermal strains.

Thermal Input

The average face plate temperature was obtained by two independent procedures. One was from the postfire face plate soak temperature recorded approximately 2 sec after shutdown. The other was from the computer thermal model which generates the thermal profile through the face and then computes the average. Both approaches provide approximately the same results.

VII, A, Injector Performance and Compatibility (cont.)

The computer calculated temperature profiles and average temperature were generated from the thermal model having the following characteristics and boundary condition assumptions and inputs:

- The injector face assembly is treated as a two-material plate with distributed temperature-dependent resistances and capacitances.
- The combustion surface boundary condition is known (temperatures vs time from test measurements).
- Backside convective coefficients are computed based on local fuel mass velocity (internal cooling neglected).
- Backside fuel coolant temperature vs time is calculated from cooled chamber transient thermal model.

From these inputs, the network thermal model computed the temperature distribution, surface heat flux, and average temperature:

$$T_{avg} = \frac{\sum_{Node=1}^{Node=N} T_{node}}{N}$$

The three start transients shown in Figure VII-16 were analyzed in this manner. The program output is summarized in Figure VII-18. The through-the-face profiles (front to back) at several time periods following main-stage ignition are shown (top) for a nominal start (left) and a maximum propellant temperature start at nominal pressure (right). The lower figures provide the face heat flux and computed ΔT ($T_{max} - T_{avg}$) vs time that was employed in the structural analysis. The three operating conditions shown are the above two plus an additional high pressure (450 psia) (311 N/cm^2), high temperature (560°R) (311°K) start which represents an extreme thermal stress condition. The noteworthy results are as follows:

VII, A, Injector Performance and Compatibility (cont.)

(1) Maximum ΔT (strain) is at 0.3 to 0.4 sec (0.3 sec = full thermal cycle)

(2) Face heat flux at	<u>Btu/sec-in.</u> ²	<u>W/cm</u> ²
Nominal temperature and pressure	2.0	328
Maximum fuel temperature, nominal pressure	2.5	410
Maximum fuel temperature, maximum pressure	3.5	574

The decrease in heat flux with time is due to two factors: the low gas temperatures at the face due to the coolant bleed and simplifications in the analytical model which neglect the internal cooling and therefore make the flux calculations less accurate as time increases.

Material Properties

Figure VII-19 provides the S-N curve (total strain ϵ vs fatigue life N_f) for Nickel 200 for the temperature range of interest. Test data from several sources are presented along with a prediction line suggested by Manson. The Manson prediction indicates this material to be temperature insensitive between 500 and 1000°R (280 and 550°K). Test data from several sources show a sensitivity with experimental values falling above and below the Manson prediction. The relationship between ΔT , total strain (ϵ), and fatigue life (N_f) is as follows:

ΔT 1° Fixity	ΔT 2° Fixity	ϵ Maximum	N_f Manson 500-1000°R	Ref 1* N_f 500°R	Ref 2* N_f 1000°R
0	0	0	∞	∞	∞
200	140	0.148%	$>10^6$	No data	No data
250	175	0.186%	10^6	No data	No data
400	280	0.308%	5×10^4	No data	3×10^6
600	420	0.480%	1.1×10^4	3×10^4	0.6×10^4
800	560	0.655%	0.56×10^4	1.3×10^4	0.3×10^4

*References are those given in Figure VII-19

VII, A, Injector Performance and Compatibility (cont.)

At nominal operating conditions, the injector face temperatures are between 200 and 300°F (378 and 430°K) where the available ϵ vs N_f data and predictions are in approximate agreement. (A data point from an RPL test at 2000°R is in agreement with that of Reference 3* at the same temperature.)

The relationship between the temperature gradient parameter and N_f is shown in Figure VII-19 for the following situations:

- (1) Region A between elements where two temperature measurements are available and where the one-degree of fixity equations are applied.
- (2) Region B between rows of elements, where two additional temperature measurements are available and where the more severe two-degree of fixity equations are applied.

The latter situation is represented by the dashed curves of which three are shown. The upper- and lowermost dashed curves correspond to the experimental fatigue life data from the indicated references at ambient and elevated temperatures. The face temperature gradients required to achieve the desired life goals of the program are seen to be limited to approximately 200°F (110°K).

The initial Phase I testing showed the ΔT for the premix triplet pattern (SN 4) to be in the order of 150°F (83°K) with a corresponding $N_f > 10^6$. The Phase I "I" premix triplet (SN 5) had a maximum ΔT of 500°F which occurred between the elements where the one-degree of fixity equation applied. The N_f value at nominal pressures and ambient temperature propellants was 20,000 full thermal cycles. The Phase II modified "I" premix data shown in Figure VII-18 reveals ΔT values ranging from 150Δ°F (83Δ°K) to 200Δ°F (111Δ°K), depending on the pressure and fuel temperature supplied when the engine is started. These temperatures occur uniformly across the face and, therefore, the more conservative

VII, A, Injector Performance and Compatibility (cont.)

two-degree of fixity analysis is applied corresponding to Region B. The life under these circumstances ranges from 300,000 full thermal cycles (firings greater than 0.3 sec) under the most adverse start conditions to values in excess of 10^6 full thermal cycles with nominal starts.

Further definition of the life of the modified "I" premix pattern under off-design and transient operation is provided in Figure VII-20 which is based on the temperature data obtained through extensive testing of the SN 7 unit. Several values of life are indicated in the lower portion of this figure vs firing duration. The life for nominal pressures, mixture ratios, and optimum valve sequencing is greater than 10^6 thermal cycles for all anticipated propellant supply temperatures. The maximum gradient is influenced slightly by off-mixture ratio and higher pressure starts. This off-design sensitivity is shown by the scatter of steady-state data on the ΔT vs MR plot provided mid-page. The sensitivity of $+55^\circ\text{FA}$ (30.5°KA), -45°FA (25°KA) covers the deviation of data at all pressures, mixture ratios and surface locations from the average of the surface temperatures at a nominal mixture ratio of 4.0.

The MR, P_c , and location deviations with cold propellants are referenced to the nominal MR = 4.0, 300 psia (207 N/cm^2) average condition with cold propellants while the MR, P_c and location deviations with warm propellants are referenced to the nominal MR = 4.0, 300 psia (207 N/cm^2) average condition with warm propellants. These additional ΔT deviations have been added to the respective ΔT vs pulse width values experienced at nominal conditions to obtain an estimate of the life capabilities at off-design operation. The design is predicted to be suitable for the following:

- More than 1,000,000 full thermal cycles at nominal conditions.
- 100,000 full thermal cycles at the most severe off-design conditions.
- 1,000,000 pulses at the most severe off-nominal conditions for pulse widths up to 0.12 sec.

VII, A, Injector Performance and Compatibility (cont.)

The above cyclic life allows for some flexibility in valve sequencing at shutdown: namely, up to a 0.005-sec fuel valve delay. The sensitivity of valve delays beyond this period are shown in the valve shutdown sequence insert of Figure VII-20. The postfire soak rise is not equivalent to the ΔT used in the life analysis since the average mass of the face also rises. The significance is, however, that valve sequencing is a parameter which can influence injector life in a predictable manner.

4. Phase II Premix Injectors Structural Analysis

a. Design Criteria

The structural design criteria (per the contract requirements to obtain data are chamber pressures up to 500 psia (345 N/cm^2)) are as follows:

Chamber pressure, P_c	500 psi (345 N/cm^2) (nominal)
Oxidizer manifold pressure, P_{oj}	600 psi (414 N/cm^2) (nominal)
Fuel manifold pressure, P_{fj}	600 psi (414 N/cm^2) (nominal)
Proof	700 psi (483 N/cm^2)

The injector life analysis is based on nominal operating pressures of 300 psia (207 N/cm^2). The thermal strains are superimposed on the pressure-induced strains parametrically, such that the useful life can be easily calculated for a variety of injection element configurations and firing conditions.

VII, A, Injector Performance and Compatibility (cont.)

Factor of Safety

A 1.25 factor is applied to all nominal pressures to produce limit design loads.

Failure Criteria

The Huber-Von Mises-Hencky yield criterion was used as a basis for establishing the structural adequacy of the High P_c injector. This criterion states that, when the effective stress exceeds the uniaxial yield strength of an elastic material, yielding will occur. The effective stress is computed from the following expression:

$$\sigma_{\text{eff}} = \{1/2 [(\sigma_1 - \sigma_2)^2 + (\sigma_1 - \sigma_\theta)^2 + (\sigma_2 - \sigma_\theta)^2]\}$$

The margin of safety is:

$$\text{M.S.} = \frac{\sigma_{\text{allow}}}{\sigma_{\text{eff}}} - 1$$

where

- σ_1 = principal stress in the radial direction
- σ_2 = principal stress in the Z direction
- σ_θ = circumferential (hoop) stress
- σ_{allow} = uniaxial material allowable

Fatigue life of a component is established by comparing the total maximum strain to an S-N curve of the particular material.

Materials

All components are annealed Type 304 stainless steel except the face platelet stack which is annealed Nickel 200. The properties employed in

VII, A, Injector Performance and Compatibility (cont.)

the structural analysis are listed in the Materials Section

b. Method of Analysis

The structural components of the High P_c injector were analyzed as a figure of revolution loaded by pressure. To facilitate the analyses, the injector geometry was input to the AB5U Computer Program. This program is a finite element stress analysis of axisymmetric and plane structures.

The model shown in Figure VII-21 was subjected to three different loading conditions which correspond to the three possible operating modes. These modes are: (1) proof pressure in the chamber with the injector used as a closure (no ΔP across the face or injector plate), (2) oxidizer lead with full pressure in the oxidizer manifold and zero pressure in the fuel cavity and chamber, and (3) fuel lead with full pressure in the fuel manifold while pressure is zero in the chamber and oxidizer manifold. In all cases, the injector is fixed against axial deflection and rotation at the bolt circle.

c. Results of Structural Analyses

The effective stresses resulting from each of these loading conditions are shown in Figure VII-21. This analysis showed two highly stressed regions: (1) the igniter tube and (2) the weld area where the flange plate and oxidizer manifold cover are joined. The design drawings were modified prior to fabrication to eliminate these two highly stressed regions as follows: the igniter tube thickness was increased by 16% and large fillets added to the ends where the tube was joined to the oxidizer cover and flange plate. Large pre-machined fillets were added at the flange plate where the cover is welded on such that the weld was removed from what would have been an area of high stress concentration.

VII, A, Injector Performance and Compatibility (cont.)

The body flange and manifold operate in the elastic material range throughout. The maximum stress at the most severe proof or overpressure conditions is 83% of the material yield strength at 70°F. The design is even more conservative when components are at lower temperatures. Under normal 300 psia P_c (207 N/cm²) cyclic operation, maximum stress is 42% of yield (0.044% strain), thus ensuring a pressure cyclic life $>10^6$.

5. Hot Test Performance Evaluation Methodology

The performance model recommended by the JANNAF Performance Standardization Working Group⁽⁶⁾ was used on this program to the extent that it is applicable to the designs being evaluated. For the gaseous hydrogen, gaseous oxygen thruster, the JANNAF methodology is incomplete in modeling the combustion process and the film coolant process. In addition it does not specify a methodology based on the characteristic velocity, c^* , which is used to state a performance goal for this program. The following paragraphs will provide a discussion of the general methodology including the applicable portions of the JANNAF procedures. Following this, energy release (combustion) and coolant losses will be discussed in more detail since: (1) achievement of the program objectives was directly dependent on understanding the combustion and coolant flow processes within the thrust chamber and (2) the models have not been published in the open literature.

The technique used for evaluation and prediction of performance considers the one-dimensional equilibrium (ODE) flow conditions to be the base case. As seen in the following equations, all performance losses are subtracted from the base case:

$$I_{sp(\text{delivered})} = I_{sp(\text{ODE})} - \Sigma I_{sp \text{ losses}}$$

$$c^*_{(\text{delivered})} = c^* (\text{ODE}) - \Sigma c^* \text{ losses}$$

VII, A, Injector Performance and Compatibility (cont.)

Theoretical thermochemical performance is evaluated using the NASA-LeRC One Dimensional Equilibrium computer program.⁽⁷⁾ This documented program computes one-dimensional flow in chemical equilibrium and is the basis for all % I_{sp} and %C* quotations.

Six primary specific impulse losses are considered in the specific impulse performance methodology: kinetic (expansion), nozzle divergence, boundary layer, mixture ratio distribution, energy release, and coolant performance loss. Since c^* is a measure of injector - chamber performance, the nozzle divergence loss is not applicable, but the other five are included in evaluating c^* efficiency. The first four losses are evaluated in a manner similar to the JANNAF methodology. These will be briefly described along with specification of the applicable computer program(s) and required input assumptions.

The kinetic performance loss accounts for the performance degradation because of chemical recombination lag during the gas expansion process. It is calculated using either the JANNAF One Dimensional Kinetic Program⁽⁹⁾ (TDK). Both programs are input with the JANNAF recommended reaction rate constants⁽¹⁰⁾. TDK permits the kinetically controlled expansion to be evaluated for the axisymmetric flow field conditions rather than imposing the uniform lateral flow field restriction inherent in the ODK analysis. However, test case comparisons have indicated that the difference between ODK and TDK kinetic losses are usually within 1.0 sec of specific impulse. Choice of which program to use to evaluate the kinetic loss depends upon the desired accuracy versus the computer cost budget.

Nozzle divergence loss is a measure of the performance which is lost due to non-axially directed momentum at the nozzle exit. It is included in the TDK analysis described in the previous paragraph. If ODK is used, the divergence loss must be evaluated separately using either Aerojet's Equilibrium

VII, A, Injector Performance and Compatibility (cont.)

Expansion Nozzle Program No. 10009 or Frozen Flow Expansion Nozzle Program No. E21201. Both are method of characteristic programs and use either the Hall transonic flow model or the third order modification to the Hall transonic flow model developed by Kliegel⁽¹¹⁾.

The boundary layer loss accounts for the degradation in performance due to shear drag and nonrecoverable heat transfer at the thruster walls. The JANNAF Turbulent Boundary Layer Program⁽¹²⁾ (TBL) is used to evaluate this loss. It uses an integral solution to the boundary layer equations and has been modified by Aerojet to permit input of actual heat flux into the computer program logic as this data becomes available from thruster testing. The latter thermal loss is employed only in heat sink chamber tests.

If a nonuniform propellant injection occurs across the injector face, a performance loss will result (MRDL). This loss is primarily caused by uneven manifold flow paths and igniter cooling and it is evaluated using a stream tube model. The igniter loss is considered separately and is very small. The losses due to mixture ratio maldistribution caused by manifold folding related distribution is lumped into the injector (ERL) Energy Release Loss.

Energy Release Losses (ERL) account for all remaining losses caused by incomplete mixing of the gases due to the injector design and is a measure of the injector mixing efficiency. For the gaseous hydrogen - gaseous oxygen thruster, the incoming propellants are already completely vaporized, and it is not possible to incur a gas phase mass reduction as with liquid propellant injectors. Therefore, gaseous propellant thruster energy release performance losses can only be attributed to an enthalpy reduction which differs from the JANNAF methodology.

VII, A, Injector Performance and Compatibility (cont.)

If the local injection mixture ratio everywhere within the combustor were completely uniform and homogeneous in pressure, temperature and chemical species, the enthalpy reduction could only occur due to chemical reaction rate limitations. However, chemical reaction rates of gaseous hydrogen - gaseous oxygen are sufficiently fast above 4500°F (2760 °K) ($3 < O/F < 30$) that this would be a second order effect. On the other hand, deviations in local mixture ratio from the overall injection mixture ratio would result in incomplete combustion enthalpy release, added thermal dissociation, and nonoptimum chemistry so that the mass weighted sum of the enthalpies of all stream tubes is less than the enthalpy which would result from a homogeneous mixture. Thus, local micro-scale mixture ratio nonuniformity has a first-order effect on gaseous hydrogen - gaseous oxygen thruster energy release efficiently and is considered to be the rate controlling energy release mechanism.

Because of the complexity of the process, no analytical model is currently available which will reliably predict gas/gas energy release efficiency from design and operating conditions without empirical data. Therefore, the performance test data quoted in the next section are based on the assumption that the other performance losses--analytically evaluated from design and operating conditions--are accurate and the remaining performance loss is the energy release loss, ERL. This is expressed mathematically by the following relationships:

$$\text{ERL (sec)} = I_{sp(\text{ODE})} - I_{s_{\text{DEL}}} - \left[\Delta I_{sp_{\text{KL}}} + \Delta I_{sp_{\text{DL}}} + \Delta I_{sp_{\text{BL}}} + \Delta I_{sp_{\text{MRMD}}} + \Delta I_{sp_{\text{CL}}} \right]$$

and

$$\% \text{ ERE} = 1 - \frac{\text{ERL}}{I_{sp_{\text{ODE}}}} = \frac{I_{sp_{\text{DEL}}}}{I_{sp_{\text{ODE}}}} + \frac{1}{I_{sp_{\text{ODE}}}} \left[\Delta I_{sp_{\text{KL}}} + \Delta I_{sp_{\text{DL}}} + \Delta I_{sp_{\text{BL}}} + \Delta I_{sp_{\text{MRMD}}} + \Delta I_{sp_{\text{CL}}} \right]$$

VII, A, Injector Performance and Compatibility (cont.)

where

- $I_{sp_{ODE}}$ = One dimensional equilibrium specific impulse (theoretical), sec
- $I_{sp_{DEL}}$ = Delivered specific impulse, corrected to vacuum, sec
- $\Delta I_{sp_{KL}}$ = Specific impulse loss due to kinetic expansion
- $\Delta I_{sp_{DL}}$ = Specific impulse loss due to nozzle divergence
- $\Delta I_{sp_{BL}}$ = Specific impulse loss due to boundary layer effects
- $\Delta I_{sp_{MRMD}}$ = Specific impulse loss due to mixture ratio maldistribution
- $\Delta I_{sp_{CL}}$ = Specific impulse loss due to chamber coolant flow

ERE can also be evaluated from c^* test data in an analogous procedure to that outlined above for the I_{sp} test data. However, the inherent difficulty in determining precise throat stagnation pressure values make this calculation significant only if reliable thrust data is not available. Consequently, c^* data was not broken down into separate performance losses and the uncorrected c^* data is tabulated in the next section for information purposes only.

The coolant model described herein accounts for the performance penalty associated with the resultant nonuniform propellant mixture ratio distribution and the thermal energy transport from the high temperature core to the low temperature boundary flow. The basic assumptions are summarized as:

VII, A, Injector Performance and Compatibility (cont.)

1. Film bulk temperature is obtained from empirically measured thermal data.
2. Energy is assumed to be exchanged upstream of throat.
3. Energy is extracted uniformly from core.

$$4. \quad \Delta h = \int_{T_{IN}}^{T_B} C_p (dT)$$

$$5. \quad (\dot{w}\Delta h)_{core} = (\dot{w}\Delta h)_{coolant}$$

$$6. \quad I_{sp} = f \frac{[\dot{w} (h - \Delta h)_{core}^{1/2} + \dot{w} (h + \Delta h)_{coolant}^{1/2}]}{\dot{w}_T}$$

where:

Δh = enthalpy

C_p = specific heat at constant pressure

T_B = bulk film coolant temperature

T_{IN} = inlet film coolant temperature

Computationally, the heat is removed from the core by reducing the propellant heat of formation in the ODE computer program by an amount which exactly compensates for the total enthalpy gained in the coolant stream tube when it is heated from its inlet temperature to the final bulk coolant temperature. Both stream tubes--the heated coolant and reduced enthalpy core--are then expanded to the nozzle exit conditions using ODK/TDK computer program for the core and ODE for the film coolant. The coolant performance decrement ΔI_{sp} , coolant is then computed by using the following relationship:

VII, A, Injector Performance and Compatibility (cont.)

$$I_{sp, \text{coolant}} = I_{sp, O/F, \text{overall}} - \frac{\dot{w}_{\text{core}} I_{sp, \text{core } O/F} \Delta h + \dot{w}_{\text{coolant}} I_{sp, O/F} \Delta h}{\dot{w}_T}$$

The model assumes no species transport between the core and coolant stream tubes. However, parametric evaluation of this model with variable species transport and variable coolant bulk temperature rise show the coolant performance loss to be insensitive to these influences. The percentage of hydrogen coolant is the primary determinant of the coolant performance loss.

The sea level test setup test conditions and data are presented in Section IV,A.

a. Sea Level Testing Energy Release Efficiency (No Film Cooling)

I-Triplet Injectors

Three I-premix injector assemblies were tested. The thrust based ERE results in Table V-1 were shown graphically in Figure V-5. The first unit fired (SN 5) gave very high performance (98.0 to 99.3% ERE) at mixture ratios from 3 to 5 at both $P_c = 300$ and 500 psia (207 and 345 N/cm²). The second unit (SN 2A) was converted from a triplet pattern by bonding on a new set of face plates, while the third assembly was SN 5 with a second set of identical face plates, designated 5A. Experimental energy release efficiency of the three assemblies were reproducible within a 1% band with the exception of one data point at mixture ratio of 5.0. The first unit tested provided the upper limit, while the second provided the lower. The deviation of the first two about the nominal, or third assembly data, provided a variance of $\pm 0.5\%$, which is about equal to the level of experimental accuracy. SN 5A I-triplet operated at intermediate ERE's between 97 and 98% at 15 L* and is considered representative

VII, A, Injector Performance and Compatibility (cont.)

of Phase I "I" injector performance. ERE's backed out from three film-cooled tests at 20 L^* indicate as much as 1% higher ERE than for 15 L^* . This represents a higher gain with L^* than for any other injector.

Triplet Injectors

Two assemblies of the triplet pattern were tested (SN 3 and 4). A variation of the triplet pattern (SN 3D) was obtained by crimping the fuel element to bias the fuel impingement momentum inboard toward the chamber axis to improve chamber compatibility.

The normal triplet injectors deliver from 0 to 1% lower ERE than the "I" configuration, depending upon the mixture ratio and L^* . Although the triplet injectors at best can only approach the "I" performance, they have the advantage of operating at lower injector face temperatures due to the fuel-rich periphery around each element. Chamber compatibility and heat flux appear comparable for both normal and I-triplet injector patterns. Testing of the crimped injector to determine its success in improving chamber compatibility was very limited, although wall temperatures appeared to be more uniform in the few tests conducted. However, to take full advantage of this modification, it must be tested in a lower contraction ratio chamber with conical walls parallel to the resultant momentum of the injected stream.

Swirler Coaxial Injector

The swirler coaxial element injector was tested with both a shallow and a deep recess. Both configurations had identical (96.6 to 97.0%) ERE, indicating that the recess had no influence on performance. Furthermore, increasing L^* from 20 to 40 in. (51 to 102 Cm) merely resulted in lower engine performance due to an increase in chamber (boundary layer) heat loss with no

VII, A, Injector Performance and Compatibility (cont.)

discernible improvement in ERE. Besides being the lowest performer of any injector tested, the swirler coaxial also had the highest chamber heat flux. Because of these undesirable injector characteristics, the concept was dropped from further evaluation.

Showerhead Coaxial Injector

At 15 in. (38 cm) L^* , the showerhead coaxial operates at 0.5% lower ERE than the swirler coaxial. However, it delivers approximately 0.5% higher ERE than the swirler at 25 in. (63 cm) L^* . Chamber heat flux on the showerhead is intermediate between the swirler and the triplets. The showerhead coaxial continued to produce high heat fluxes in the nozzle convergent section upstream of the throat. This is attributed to the oxidizer-rich core within each element. The cooling performance loss is significantly lower per percent fuel film coolant on the showerhead design than for the triplets. This indicates the oxidizer-rich core from each element is reacting with the fuel coolant in the nozzle convergent zone. Although this may appear to be an advantage from the performance standpoint, the advantage is lost because the coolant reaction results in a slower rate of heat flux reduction per percent coolant.

b. Comparison of Cold Flow Data with Hot Test Results

The relative merits of the triplet and I-triplet element designs were identified reasonably well by the cold flow tests. The hot fire test results qualitatively substantiated the cold flow mass and mixture ratio profiles. This was especially true in its predicted enhancement of injector face and chamber wall compatibility. In absolute terms, however, the hot fire mixing efficiencies were considerably lower than those expected on the basis of cold flow testing. Cold flow testing indicated it was possible to achieve reasonably uniform mixture ratio distributions on the order of 1 in. (2.5 cm) from the injector face. Hot fire data, on the other hand, still indicate

VII, A, Injector Performance and Compatibility (cont.)

significant local mixture ratio gradients still exist 5 to 8 in. (13 to 20 cm) from the injector at the nozzle throat plane, as indicated from ERE data, if it is assumed that the injection mixture ratio distribution due to injector manifold folding was uniform.

An analytical energy release model formulated by dividing the injector into two stream tubes, one assumed to be lower than the nominal overall mixture ratio by the factor E_m , and the other to be higher by the reciprocal of E_m , were employed to predict energy release efficiencies for both sea level ($\epsilon = 3$) and vacuum ($\epsilon = 40$) nozzle exit area ratios for overall engine mixture ratios ranging from 3 to 6. The results are shown in Figure VII-22. By comparing the experimental ERE's with the model, the hot fire mixing efficiency (E_m) is seen to vary from approximately 0.6 to 0.7 for the triplet and .65 to .78 for the I pattern. The relative injector ranking is in agreement with cold flow results although the absolute values are lower than anticipated.

The lower hot fire mixing results have been found to be caused by the energy released by the combustion products which are not present during cold flow. The mechanism which suppresses the mixing in hot firing is discussed in References 5 and 14. The cold flow results showed the swirler coaxial injector efficiency to be comparable to the 99% "I" triplet element E_m . In reality, S/N 1 yielded only 97% ERE. The fact that negligible performance improvement was realized for longer L^* chambers however did substantiate that the type of element attains its maximum mixing efficiency in a short distance. At 25 in. (64 cm) L^* , S/N 1A showerhead coaxial injector ERE was identical to S/N 1 swirler coaxial performance. However, at 15 in. (38 cm) L^* the showerhead configuration was approximately 1% lower in ERE, thus supporting the cold flow data trends which predicted more rapid mixing with swirlers.

VII, A, Injector Performance and Compatibility (cont.)

The swirler coaxial element achieves its mixing outside of the injection element and within the combustor cross section where streams are not mechanically constrained. In Reference 5, it was shown that the combustion effects (which are not present during cold flow testing) influence the injection inertial effects and reduce their mixing efficiency. After the primary combustion occurs, the entire chamber cross section is filled with expanded hot gases which have achieved relatively stable static pressure equilibrium, accounting for their apparent stream tube behavior.

Historically, swirlers have been demonstrated to improve hydrogen/oxygen performance efficiencies, but these data were obtained with gaseous hydrogen and liquid oxygen. With a liquid oxidizer, ERE is not strictly mixing efficiency limited but is also influenced by the atomization and vaporization processes. The swirler contributes to the injector performance by spreading the liquid stream into a thin sheet which improves both atomization efficiency and vaporization efficiency. Furthermore, with a liquid oxidizer, vaporization must occur before combustion. As a result, combustion with liquid oxygen occurs more slowly than with gaseous oxygen, and combustion induced separation tendencies are reduced. This mechanism also explains the observed thermal results.

In summary, cold flow is useful in identifying the relative merits of momentum and geometry variables of a given class of elements, however, actual combustion tests are required in order to identify the absolute value of mixing efficiency.

c. Injector Performance with Film Cooling

The requirement for fuel film coolant penalizes the injector performance by the following physical mechanisms:

VII, A, Injector Performance and Compatibility (cont.)

- (a) At a given overall engine mixture ratio, provision for chamber film coolant raises the core mixture ratio which lowers the theoretical I_{sp} of the core.
- (b) Enthalpy is extracted from the core combustion gases to raise the temperature of the coolant which further reduces the core performance.
- (c) Higher core mixture ratio increases the nozzle kinetic loss due to greater thermal dissociation of the combustion gas products.
- (d) A higher core mixture ratio alters the element mixing efficiency (E_m).

Premix Triplet Injectors

Cooled injector performance efficiencies for the SN 3 and 4 triplets and the I-triplet injectors are shown in Figure V-5. The ERE for these injectors, which were backed out from film-cooled performance data, agree identically with uncooled ERE data below a core mixture ratio of 4.0, supporting the validity of the no interaction assumption. At a core mixture ratio of 5.0, the cooled performance efficiency is 0.5 to 1.0% higher than the sum of the uncooled ERE and the analytical no interaction film cooling performance decrement. This indicates a weak interaction at high core mixture ratios in which the fuel coolant chemically reacts with some portion of the core, improving performance. It is reasonable to expect the interaction to occur at high core mixture ratio since thermal dissociation and oxidizer-free radical concentrations increase as the stoichiometric mixture ratio is approached. The combined analytical/experimental cooled injector efficiency is shown vs % fuel film coolant at nominal engine mixture ratio for the various injectors on the bottom half of Figure V-5.

Showerhead Coaxial Injector

The film-cooled showerhead coaxial injector demonstrated 1.5 to 2.0% interaction gain between the fuel coolant and the core gases. This was two to three times the interaction of the triplet and I-triplet injectors.

VII, A, Injector Performance and Compatibility (cont.)

Swirler Coaxial Injector

The film-cooled swirler coaxial performance data indicate no coolant interaction similar to the triplet injectors. Besides having a lower uncooled injector ERE, no ERE improvement with longer chamber length, and the highest chamber heat flux, the lack of coolant interaction performance gain made the swirler coaxial injector the least attractive injector to develop from both injector performance and chamber compatibility standpoints.

d. Compatibility Results

The "I" triplet was designed to achieve a uniformly homogeneous mixture ratio prior to combustion. No effort was made to bias mixture ratios to achieve a fuel-rich periphery by each element. Streak chamber photographs are not included for the "I" premix with the pie and concentric manifolding; however, the test results were similar to the SN 4 premix photo shown in Figure VII-23. The main difference was a short blackened region near the injector, indicating more rapid mixing and combustion and a slightly more uniform downstream region. The chamber streaking tendencies mainly reflected the manifold flow maldistributions noted earlier in manifold cold flow tests.

The premix triplet was designed for a cool fuel-rich periphery with a compromise in performance. Low mixture ratio along the cylindrical chamber wall (black region) was verified by the streak chamber test (Figure VII-23). However, the mixture ratio is slightly higher in the convergent section than for the "I" triplet. This is attributed to the wider mixture ratio variation at the entrance to the convergent section because the mixing efficiency is lower than with the "I".

VII, A, Injector Performance and Compatibility (cont.)

The swirler coaxial injector compatibility results shown in Figure VII-23 indicated the fastest mixing rate of any injector tested. This occurs because the swirler throws the oxidizer out toward the wall, resulting in a relatively oxygen-rich wall mixture ratio. This is in agreement with heat sink measurements presented later. The swirler coaxial was retested with 10% fuel film cooling and reduced swirl obtained by lowering the oxidizer temperature (Test 2K8-181). The oxidizer is noted to penetrate the film cooling. The swirler did not achieve the desired objective of high ERE and could not be justified from a compatibility/coolant requirement standpoint except possibly at very short chamber lengths ($L' < 15$ in.).

There were no streak chamber tests with the shower coaxial; however, long cylindrical chamber lengths are required to complete turbulent shear mixing and prevent the oxidizer-rich core of each element from creating a chemical or thermal incompatibility condition in the nozzle convergent section. The oxidizer-rich cores would tend to partially consume the fuel film coolant, increasing the coolant flow rate requirement to achieve comparable convergent section compatibility as with a more uniformly mixed injector.

Streak chamber tests were not conducted with the Phase II modified premix design; however, an indication of the improvement that was achieved by changing the manifolding and adding the long L/D oxidizer tubes can be visualized in Figure VII-24 by comparing copper oxidation traces on the 40:1 cooled chamber which was tested with both Phase I and II injectors under similar conditions. The left side of Figure VII-24 shows the premix triplet and the right side shows the highly uniform condition attained by the modified "I" pattern.

VII, Supporting Analyses and Data Correlation (cont.)

B. THRUST CHAMBER COOLING

1. Analytical Approach

The thermal models significant to this program were those defining the transient and steady-state temperature profiles in a thin wall cylinder and also a thick bimetallic wall containing rectangular cooling channels. Several resistance-capacitance computer programs and thermal network generators, available throughout the industry, provide similar capabilities and results. The SINDA 3G system for the UNIVAC 1108 computer was employed in this contract. The availability of a variety of SINDA subroutines (including combustion gas and coolant properties; preformulated nodal networks for slotted, convectively cooled channels; and subroutines for computing heat transfer coefficients and pressure drop) greatly enhanced the designer's ability to investigate a large number of design variables with a minimum of programming effort.

Of more significance to this contract are the thermal boundary conditions derived from the test data, their relationship to existing analytical and empirical approaches, and the ability of the tuned-up computer models to accurately reproduce the observed test results.

Three models defining the thermal boundary conditions internal and external to the chamber wall were required. These systems of equations define the combustion-side boundary conditions in the various flow regimes, the coolant-side boundary conditions, and the entrainment and mixing of fuel film cooling along the nozzle wall as a function of varying design and operational conditions.

a. Wall Analysis

The temperature profiles (either transient or steady state)

VII, B, Thrust Chamber Cooling (cont.)

around the periphery of the slotted cooling channels were computed in a station-by-station marching manner, starting at the coolant inlet and proceeding to the injector face where the coolant enters the injector. Steady-state wall thermal solutions were obtained for varying channel depths until the desired wall temperatures were achieved.

b. Gas-Side Boundary Conditions

In the absence of film cooling, the heat flux to a wall of known temperature is computed by the following expression:

$$Q = \Delta T * hg$$

$$Q = [T_r - T_w] C_g \rho_{ref} V_{\infty} \left[\frac{i_r - i_w}{T_r - T_w} \right] Re_{d,ref}^{-0.2} Pr_{ref}^{-0.67}$$

where

C_g = experimental constant

hg = gas-side heat transfer coefficient

i = enthalpy of combustion products or film coolant

Pr = Prandtl number

Q = heat flux (for wall temperature of 500°F in all data shown)

Re_d = Reynolds number based on local diameter

V = velocity

ρ = density

Subscripts

r = recovery temperature -- $T_r = (ERE)^2 [T_o + Pr^{1/3} (T_o - T_{\infty})]$

ref = reference temperature for evaluating properties

w = wall temperature conditions

∞ = free stream

VII, B, Thrust Chamber Cooling (cont.)

In the case of a cooled wall where wall temperatures are an unknown or are changing with time, the solution becomes an iterative process involving wall geometries and coolant side conditions.

The value of C_g is input as a function of injector, chamber contour, and axial station using experimental data which are obtained from several sources. The ALRC data bank and heat sink chamber tests conducted on this program provide heat flux vs wall temperature for a fixed point in a chamber and therefore allow the C_g to be computed.

The reference temperatures at which the properties are evaluated will significantly influence the C_g value computed. Two reference temperatures were considered in data correlation: the adiabatic wall temperature recommended in Reference 15 and a film properties temperature which is the average of the adiabatic wall and cooled wall temperatures. The former approach provides a simple, noniterative solution to the gas-side heat transfer coefficient. While the latter is more involved, it provides C_g values which are in better agreement with laboratory data. The film reference condition applies to viscosity, density, and Prandtl number. The specific heat, represented by $\Delta \text{enthalpy} / \Delta \text{temperature}$, is an integral value and includes changes in chemical composition with temperature for the gas in the boundary layer, i.e., chemical as well as kinetic energy transport. The correction for boundary layer chemical reactions at mixtures below 4, however, is small for the O_2/H_2 propellants at the pressures of interest. The errors which result if this phenomenon is not included in the analysis are shown in Figure VII-25.

When film cooling is employed, it is necessary to account for the change in gas temperature and chemistry at the chamber wall when computing the local heat flux. The temperature influence is accounted for directly by employing the reduced adiabatic wall temperature as the driving temperature (T_r). The local wall chemistry is accounted for in the heat transfer

VII, B, Thrust Chamber Cooling (cont.)

coefficients by evaluating the properties μ , \bar{C}_p and Pr at the wall MR and applying the following factor to correct the density:

$$hg_{FC} = hg_{(no\ FC)} * \left[\frac{T_{fs}}{T_{ref}} * \frac{MW_w}{MW_{fs}} \right]^{0.8}$$

The relationship between adiabatic wall temperature and mixture ratio is shown in Figure VII-25. The local wall conditions are therefore obtainable experimentally from the adiabatic wall temperature measurements and analytically from the film cooling model.

c. Coolant Side Boundary Conditions

The coolant side heat transfer coefficients were calculated from the McCarthy-Wolf equation.

$$h_c = 0.025 \frac{K}{D} (Re_b)^{0.8} Pr_b^{0.4} \left(\frac{T_w}{T_b} \right)^{-0.55} \phi_1 \phi_2 \phi_3$$

which is a conventional Nusselt type equation for turbulent channel flow with a correction for high ratios of wall (T_w) to bulk (T_b) temperatures.

In this equation, D is based on the equivalent hydraulic diameter of the rectangular slot ($4 * \text{area/perimeter}$), ϕ_1 corresponds to an enhancement of the coolant effectiveness due to entrance effects and is generally equal to 1.3, ϕ_2 is the enhancement due to relative wall roughness in small channels and is computed by

$$\phi_2 = \sqrt{\frac{\text{friction factor for actual wall}}{\text{friction factor for smooth tube}}}$$

and ϕ_3 is the correction for channel curvature effects which were not considered in the analysis.

VII, B, Thrust Chamber Cooling (cont.)

d. Film Cooling Effectiveness Model for Chemical Reacting Accelerating Gases

The model employed in the film cooling analysis is essentially a boundary layer mixing model which relates, via an entrainment factor, the mass transfer normal to the flow direction to the local core mass velocity in the flow direction. The local film coolant mixture ratio and enthalpy is calculated, as the flow proceeds along the wall and through the nozzle, by integration of the entrainment mass flux area product. An entrainment factor derived from plane unaccelerated flow using laboratory data accounts for initial shear mixing via an empirical function of the coolant injection velocity, Reynolds Number, density, and slot height. An entrainment factor correction is available to account for alteration due to flow acceleration. Empirical multiplying factors accounting for combustion effects associated with specific injectors, coolant injector effects, and turning effects due to specific nozzle contours can be either input or computed, depending on the operating mode.

Forward mode operation of this film cooling computer program provides axial temperature and mixture ratio profiles for assigned coolant flow rates and input empirical multiplying factors. In the reverse or data mode, inputs consist of experimental data and test conditions and outputs are the empirical correlating factors required to make the model and data agree. The empirical factors calculated relate actual film cooling effectiveness in a rocket with combustion and real injector and coolant injection geometries to comparable data obtained in the laboratory with idealized injection and plane unaccelerated, nonreacting flow, thus providing a measure of the level of efficiency being achieved in actual chamber film cooling.

The basic analytical approach and a schematic drawing defining the experimental film cooling parameters are summarized in Figure VII-26.

VII, B, Thrust Chamber Cooling (cont.)

A more complete discussion of this model will be published in the final report to Contract NAS 3-14343, Ref. 16.

2. Experimental Results of Sea Level Testing

a. Heat Flux Measurements

Heat flux data at various axial stations were obtained from the thermal temperature transient measured by 0.020-in. (.051 cm) -dia stainless steel sheathed chromel/alumel thermocouples, flush mounted and brazed in position on the gas-side surface of a thick-walled copper chamber. Data reduction was accomplished by driving the experimental gas-side temperature vs time data in a thermal model representing the test hardware. The computer model recreates the thermal profiles in the chamber wall, assuming an insulated exterior and no axial conduction, from which the local surface gradients and heat flux are computed.

Heat flux from the thin-walled steel chamber backside measurements is also computed using the wall as a calorimeter; however, in this case, it is necessary to make an additional assumption. That is, the through-the-wall temperature profile is known and corresponds to a theoretical solution for a wall insulated on the backside, having constant material properties, and subjected to a convective heating condition on the other applied as a step function. In order to obtain useful test durations with this chamber, it is necessary to conduct all tests with large amounts of fuel film cooling.

Recovery temperature can be obtained in three ways: from steady-state operation of the thin-wall chamber, direct readings of the adiabatic wall probes, and extrapolation of the flux vs gas-side surface temperature measurements from the thick-wall copper chamber. The most reliable is considered to be from the steady-state measurements on the thin-wall steel chamber.

VII, B, Thrust Chamber Cooling (cont.)

b. Heat Sink Chamber Heat Flux Data Without Film Cooling (Phase I Chamber Contour)

Figure VII-27 shows some typical flux vs wall temperature curves derived from the copper chamber surface temperatures for 300 psia (207 N/cm^2) operation at nominal mixture ratios of 3, 4 and 5 with a premix injector. Both heat transfer coefficients and recovery temperatures can be obtained from the slopes and intercept of these curves. Variation of the throat flux and heat transfer coefficient with mixture ratio is seen to be small (less than 15%).

The experimental variation of heat flux as the wall heated during a test lasting 2 sec was employed to calculate local heat transfer coefficients as they varied both with wall temperature, peripheral and axial positions in the chamber. For the condition where there is no film cooling, the recovery temperature (T_r) is assumed to be equal to $T_o * \eta^2$, where T_o is the theoretical combustion temperature and η is the energy release efficiency. This approach is in good agreement with the recovery temperatures determined by the slope and intercept method. The coefficients calculated in this manner are shown in Figure VII-28. Data for two peripheral and four axial stations are shown as the wall heats from ambient to about 1000°F (810°K). Also shown in this figure are the predicted heat transfer coefficients for these test conditions and the equation from which they were calculated. The following points are to be noted about the information presented in Figure VII-28.

(1) The heat flux and resulting heat transfer coefficients are consistent and reproducible at peripheral stations D, G and K which are 90° apart.

(2) The simplified Bartz equation (a pipe flow equation) having a C_g of 0.026, when used with properties evaluated at a film temperature

VII, B, Thrust Chamber Cooling (cont.)

which is the average of the recovery and wall temperature, adequately predicts both the magnitude of the local heat transfer coefficients and variation with wall temperature at the low Mach number stations.

(3) As the flow approaches the throat and pressure gradients become significant, the familiar phenomenon (Ref 17) of having lower than predicted coefficients is once again observed. This is accounted for analytically by altering the correlating constant " C_g " as noted. This aspect is discussed in the following sections.

(4) The shape of the experimental coefficient vs temperature curves does not match the predicted curves at the throat and supersonic stations. This could be due either to axial conduction effects not taken into account in the data reduction or to alteration of the nature of the boundary layer as the wall cooling effects on the boundary layer diminish or a combination of both effects. The latter is highly suspect as the test conditions are in a region that has been characterized (Ref 18) as transitional between fully turbulent and relaminarized, in which wall cooling is an important parameter. Additional analysis of the sonic and supersonic flow conditions is warranted.

(5) The C_g values shown neglect the correction shown in Figure VII-25 for boundary layer composition changes due to wall cooling. Application of this factor would reduce the C_g values shown by approximately 17%.

Figure VII-29 shows the same type of analysis for the throat station at three chamber pressures. Note two different injectors have been employed. The point of interest is that the same C_g can be employed to predict the 300 (207 N/cm²) and 500 (345 N/cm²) psia data, while the C_g which matches the 100 psia (69 N/cm²) run is a factor of two lower. Earlier observations of similar effects in small nozzles (Ref 18) have led to the conclusion that the

VII, B, Thrust Chamber Cooling (cont.)

lower than expected throat heat transfer coefficients result from flow acceleration, which at low Reynolds numbers can result in relaminarization of a turbulent boundary layer. This is discussed in more detail in Section VII-C.

A C'_g value is also shown. This term includes the appropriate correlation to replace the frozen specific heat with the enthalpy function. When referring to Figure VII-55 (discussed in Section VII-C), it will be observed that the numerical values of C'_g are in better agreement with published data than are the uncorrected values of C_g .

c. Injector Effects

In order to conduct a realistic cooled chamber design analysis, it is necessary to account for the combustion characteristics of specific injectors. One aspect of the sea level injector checkout testing was to generate the data characterizing the thermal environment created by the selected injectors. These comparisons were made on the basis of measured heat flux profiles without film cooling and on flux and adiabatic wall temperature profiles in tests employing film cooling.

Tables VII-3 and VII-4 summarize the test conditions for which heat flux data are available and tabulate the experimental heat flux values. The first of these two tables contains data for tests without film cooling, while the second summarizes the heat flux to the noted wall temperatures for nominal, 20, and 30% cooling flow rates. The data presented in these tables represent the heat flux values obtained from the data reduction computer program.

Comparisons are made between the following injector types:

- (1) OMS 5000 lbf (22200 N), 72-element recessed coaxial tube with Rigimesh face (Contract NAS 9-8285)

VII, B, Thrust Chamber Cooling (cont.)

- (2) APS 1500 lbf (6660 N), 42-element coaxial tube
 - CA SN 1 - swirlers on oxidizer
 - CA SN 1A - shower oxidizer
- (3) APS 1500 lbf (6660 N), 72-element premix
 - SN 1, 3, 4 - triplet pattern
 - SN 5 - "I" triplet
 - SN 6 and 7 - modified "I" triplet

Figure VII-30 provides a comparison of the throat region heat flux data for three types of coaxial element injectors at several pressures. The heat flux profiles for the three injector types are quite similar at the throat and downstream at comparable chamber pressures. The shower type APS injector has a slightly higher throat heat flux than either the APS swirler element or the OMS shower recessed element. Some of the latter difference may be due to the contour and throat diameter differences. The no-film-cooling throat design heat flux for this type of injector at 300 psia (207 N/cm^2) is 16 Btu/sec-in.^2 (2626 W/cm^2). The flux at area ratio 2 upstream of the throat is considerably higher than would be theoretically predicted with a pipe flow type equation. The throat heat fluxes are noted to increase with chamber pressure. Between 100 (69 N/cm^2) and 300 (207 N/cm^2) psia, the throat flux increases at a rate greater than the 0.8 power of chamber pressure, while between 300 (207 N/cm^2) and 480 (331 N/cm^2) psi, the rate of increase is slightly less than the 0.8 power. The marked increase in throat flux (20 vs $27.5 \text{ Btu/sec-in.}^2$) as the chamber length is increased from 6 to 8 in. (15.3 to 20.4 cm) and the chamber pressure increased slightly with the OMS injector is not entirely explainable by the improved energy release efficiency. The mixture ratio is noted to have a second order influence.

VII, B, Thrust Chamber Cooling (cont.)

Figure VII-31 compares test data from the two APS coaxial jet configurations tested with the various analytical predictions available using a C_g of 0.026. Included are (1) film temperature properties $(T_r + T_w)/2$, (2) adiabatic wall temperature properties (T_r) , and (3) film properties--the latter two with a correction for chemical reactions. The latter method provides the most conservative approach.

Neither analysis satisfactorily predicts the experimental data in the combustion chamber region for these injectors, although the higher values generated by the film properties analysis come closer. The adiabatic wall temperature relationship does a satisfactory job in predicting the flux at the throat and in the supersonic nozzle. The deviations in the combustion chamber and convergent nozzle are attributed to injector-induced combustion and turbulence effects. The data from the injector incorporating hydraulic swirlers in the oxidizer circuit show a higher heat flux in the forward chamber region due to more rapid mixing. This high flux is a local phenomenon which appears to take place directly under the elements. The flux in between elements is 66% of the maximum value at the first measurement station 1.1 in. (2.8 cm) downstream of the injector face. This phenomenon is observed visually in the results of streak chamber tests, shown in Figure VII-23. The experimental heat flux becomes more uniform and approaches the theoretical values as the propellants mix and flow toward the throat. Removal of the swirlers is seen to markedly reduce the forward end heat flux, a phenomenon which is generally expected because of the slower mixing rates of the shower element. However, the heat flux further down in the combustion chamber and convergent nozzle increases for the shower injection configuration due to the delay in the combustion resulting from slower initial mixing.

In a third test with the tube slightly recessed and the oxidizer chilled to reduce the swirl component, as shown by the solid triangles,

VII, B, Thrust Chamber Cooling (cont.)

it was found that the heat flux in the convergent nozzle was reduced while the throat and downstream flux increased. This was accompanied by a drop in performance, thus suggesting that mixing was slow and that combustion continued in and downstream of the throat.

Figure VII-32 (top) provides a flux vs wall temperature history for the station nearest the injector face for the three test configurations. The shape (rapid decay of flux) of the flux curve under the injection elements suggests that the high local flux may be due to impingement of partially combusted hydrogen at high velocities rather than fully combusted gases on the chamber wall. Data for the reduced swirl velocity obtained by a 28% decrease in the absolute temperature of the oxidizer is shown to the right for a station slightly further downstream. These data, the data from the shower element, and the location between high velocity swirl elements are in approximate agreement.

Figure VII-33 provides a comparison of the experimental heat flux for the SN 5 "I" configuration premix element design (mixture ratio 3 through 5) with predicted values for mixture ratio 4, using the previously discussed methods. Also shown in this figure are some data inferred from the 40:1 film-cooled chamber test with the modified "I" pattern SN 6. The data shown are for the location upstream of the film coolant injection plane. The higher forward end flux for the latter configuration is due to the slightly smaller contraction ratio resulting from the elimination of the head-end film cooling injector. The thermal profiles for these two injectors are the same except that the peripheral data scatter for the modified "I" pattern is less due to the superior flow distribution.

The combustion chamber heat flux for the premix injector is lower than for the coaxial tube design and in better agreement with the theoretical predictions. The influence of mixture ratio changes between 3 and 5 ar

VII, B, Thrust Chamber Cooling (cont.)

small compared to injector effects and generally fall within the data scatter due to peripheral variations in this early design. Figure VII-34 shows comparable heat flux data for the triplet pattern premix injector for three mixture ratios and two chamber lengths. The significant aspect of these data is that increasing the distance between injector and throat by increasing the L^* reduces the heat flux in the convergent nozzle.

Figure VII-32 (bottom) provides a comparison of data from all injectors expressed in the form of " C_g ". The heat transfer coefficient correlating parameter is based on film reference properties and corrected for chemical reactions at a MR of 4.0. To be noted are: (1) the higher heat flux with the coaxial jet elements, (2) the reduced throat fluxes with longer chamber lengths in both the premix and coaxial elements, and (3) the peaking of the empirical (C_g) coefficient in the convergent nozzle for three of the four injectors.

The high flux level at the forward end of the chamber with the coaxial jet element is in conflict with nearly all previous data which show this type of element to provide a very low combustion chamber heat flux. However, it is evident that this major difference is due to the state of the oxidizer at injection, i.e., gas vs liquid. Based on the rather consistent data obtained in this program, it can be hypothesized that liquid-phase injection and the slow vaporization of the oxidizer is the mechanism providing the low heat flux, while with gas phase injection more immediate reaction occurs producing more severe chamber wall thermal loads.

d. Experimental Data with Film Cooling

The analysis in the previous section defined the thermal characteristics of the APS thrusters without film cooling. The addition of

VII, B, Thrust Chamber Cooling (cont.)

fuel film cooling to extend the chamber life alters the thermal characteristics by reducing the recovery temperature and making the boundary layer considerably more fuel rich, which in turn alters the heat transfer coefficients.

In the regeneratively cooled chamber, it is necessary to lower the throat heat flux to attain the desired life. However, it is the adiabatic wall temperature, rather than heat flux, which is the significant thermal parameter employed in the design of the film-cooled throat and nozzle.

In the sea level chamber tests employing film cooling, barrier probes containing tungsten/rhenium thermocouples (as shown in Figure VII-35) were inserted into the coolant film zone along the wall in order to obtain an estimate of the adiabatic wall temperatures. This additional instrumentation technique was employed since comparative data from adiabatic wall chambers show that the adiabatic wall temperature cannot always be reliably calculated from knowledge of the copper surface temperature vs heat flux profile alone. In the test program the test variables were injector, chamber length, film cooling injection velocity, and axial station at which coolant is injected. Coolant injection velocity and station were determined by selection of one of the nine film cooling rings (shown in a pre-assembled state in Figure V-3). These rings, which extend into the chamber, are available in three lengths: 0, 1.0, and 2.5 in. (0, 2.5, and 6.3 cm) --each length being available in one of three coolant channel geometries tabulated below. Figure IV-30 shows the adiabatic wall chamber. The copper heat sink was shown in Figure V-1.

The following table compares the recovery temperatures as determined from the probe data, by extrapolating to zero flux the heat flux vs wall temperature data from the copper chamber, and the steady-state adiabatic wall measurements.

VII, B, Thrust Chamber Cooling (cont.)

Boundary Layer Recovery Temperature in °F (°K) During
Film Cooling as Determined by Various Methods

		3K8-163				2K8-173				
		Steady State - Adiabatic Wall				Probe		Copper Wall		
Peripheral Station:		A	D	G	K	D	K	A	D	K
<u>Axial Distance, in.</u>										
	-1.5	956 (787)	1149 (894)	--	--	950 (783)	900 (755)	650 (617)	670 (628)	540 (556)
Throat	0	1313 (985)	1462 (1068)	1087 (860)	1056 (842)	1400 (1033)	1000 (811)	850 (728)	950 (783)	750 (673)
	1.1	1379 (1021)	1669 (1183)	1225 (935)	--	1200 (923)	800 (700)			900 (955)
	2.2	1466 (1070)	1902 (1313)	1243 (945)	1115 (875)					

Comparisons of the data presented in the above table show that:

(1) The steady-state wall temperatures recorded from the backside of the thin-wall steel chamber at subsonic and sonic conditions are in reasonable agreement with the adiabatic wall probe measurements obtained from the copper chamber at the same test conditions. The probes have consistently underpredicted the recovery temperature in the supersonic flow.

(2) Extrapolation of the heat flux vs wall temperature curve from the copper chamber indicates a much lower recovery temperature than either the probe or the adiabatic wall measurements,

Figure VII-36 displays these data and recovery temperatures derived from the various experimental techniques for two typical throat thermocouple stations. The open circles, representing the heat flux from the copper chamber, indicate a high flux at low temperatures, which decreases rapidly as the wall heats. The flux data derived from the steel adiabatic wall chamber, depicted by triangles, suggests a lower flux at the lower wall temperatures, which then diminishes more slowly as the wall heats. The heat flux data profiles and tabulations provided in Table VII-4 were obtained from the copper chamber at a wall temperature of 500°F (533°K), which in most cases, is a more conservative

VII, B, Thrust Chamber Cooling (cont.)

value than the backside steel data. The lower recovery temperature and steeper slope of the copper chamber data suggest a much higher heat transfer coefficient.

The shapes of these data curves, or rather the changes in shapes, are of considerable interest in that they represent a flux vs wall temperature history from ignition to the achievement of steady-state thermal conditions. The initial rise of flux with wall temperature represents the first 0.1 sec after the initial P_c rise (which occurs in 0.01 sec). A major portion of the hump corresponds to the next few tenths of seconds and the remainder of the data to about 2 sec of firing. Figure VII-37 compares the similarities of the shape of high and low P_c data with and without the use of film cooling. The hump in the flux curve at low wall temperatures consistently develops whenever film cooling is employed. The magnitude of the hump increases either as additional film cooling or higher injection velocities are employed. Additional analyses were conducted to determine if these indicated high heat fluxes at the low wall temperatures are real transient thermal affects, a phenomenon which is being generated by the instrumentation technique, a data reduction method, or a result of the engine start sequence being employed. These high early time fluxes, if real, are detrimental to chamber life.

The engine start transient dynamics of the sea level test facility, which employed critical flow nozzles fed through a pressure regulator, also shown in Figure VII-36. This plot shows the engine and facility flow parameters vs time in the upper half, throat heat flux vs time in the center, and flux vs wall temperature in the lower half. The prefire pressures at which the regulators are set are higher than steady state to accommodate regulator-to-venturi line losses. This results in a correspondingly higher propellant weight flow during the first few tenths of a second after the thrust chamber valves are opened. These initially higher weight flows, in turn, result in the momentarily higher heat flux. When the data (solid points) in Figure VII-36 are adjusted to the steady-state flow rate, a lower heat flux (half shaded points) results. This makes the copper and steel chamber data agree reasonably well.

VII, B, Thrust Chamber Cooling (cont.)

The feed system dynamics appear to be responsible for the high early time heat flux on the high pressure tests, but it is not clear why similar trends are not observed in the tests without film cooling. Additional phenomena may influence the low pressure tests.

The next three figures summarize a portion of the thermal data obtained with film cooling. The upper part of Figures VII-38 and VII-39 provide the film coolant temperature determined from the barrier probes, while the lower halves provide a comparison of heat flux with 0, 20, and 30% film cooling with core mixture ratios of 4, 5 and 5, respectively. Figure VII-38 provides a comparison of the premix triplet (left) and shower coaxial tube injectors (right) in a 25 L* (63 cm) chamber with the film cooling ring which extends 2.5 in. (6.3 cm) into the chamber. Figure VII-39 compares data from the premix triplet injector in a 15 L* (38 cm) chamber with a 2.5-in. (6.3 cm) -long film cooling ring and a zero length ring.

The probe data from the heat sink chamber is compared with the measured backside temperatures from a thin (0.040 in.) (0.102 cm) adiabatic wall chamber in the upper left quadrant of Figure VII-39. The probe data are found to be in good agreement with the adiabatic wall temperature measurements up to the throat station, thus demonstrating the validity of the technique in both subsonic and sonic flow. The deviation between probe and adiabatic wall data downstream of the throat is noted, again pointing out that the probe data are valid only to the throat station.

Figure VII-40 provides a cross plot of data presented in the previous two figures. This figure shows the reduction in heat flux at the throat (top) and midpoint in convergent nozzle (bottom) vs percent film cooling for the various injectors, chamber lengths, and film cooling ring lengths.

VII, B, Thrust Chamber Cooling (cont.)

The conclusions reached from this figure are:

(1) The 2.5-in. (6.3 cm) -long ring is more effective in reducing heat flux than injection at the plane of the injector (zero length ring).

(2) The premix element design produces lower heat fluxes than the coaxial tube element design at a given film coolant flow rate.

(3) Increasing the distance between the injector face and the throat appears to have a favorable influence on film cooling effectiveness at the throat station.

An additional conclusion reached from these data, but not indicated in the figures, is that the heat flux reductions due to film cooling are less than those predicted in the theoretical analyses. To date, this difference has been attributed to at least three factors:

(1) Mixing of the coolant with the core due to a non-optimum injection.

(2) Mixing and secondary combustion of the coolant and core due to turning of the flow in the convergent nozzle.

(3) An increase in the heat transfer coefficient as the boundary layer chemistry becomes more fuel rich.

3. Experimental Heat Transfer Coefficients with Film Cooling

Figure VII-41 provides a comparison of axial heat transfer coefficient profiles for a film cooled and several nonfilm-cooled sea level

VII, B, Thrust Chamber Cooling (cont.)

tests ($\epsilon = 3:1$, 15° conical nozzle). The nonfilm-cooled coefficients are for a 500°F (533°K) wall temperature, while the film-cooled coefficients are for the higher 1000°F (811°K) wall temperatures; the predictions and data agree. Throat heat transfer coefficients with film cooling in this comparison are about twice the nonfilm cooling experimental values - 0.006 vs 0.003 Btu/sec-in.²- $^\circ\text{F}$. If the comparison were made at a 500°K (533°K) wall temperature, the coefficient with film cooling would be 0.007 to 0.008 Btu/sec-in.²- $^\circ\text{F}$. The model which accurately predicts higher coefficients with film cooling employs the properties evaluated at the local wall mixture ratio and noted film temperature.

Additional heat transfer coefficients derived from the transient heating of the thin wall $40:1$ film-cooled Rao contour steel nozzle in Tests 3-015 (300 psia) (207 N/cm^2) and 3-021 (100 psia) (69 N/cm^2) are shown in Figure VII-42. These results are in agreement with the sea level tests as can be noted by comparing the data with the curves obtained using several prediction methods. In computing local heat transfer coefficients, the nozzle mass velocity ρV is determined from the two-dimensional flow conditions near the edge of the boundary layer for an axisymmetric Rao nozzle using the method of characteristics, assuming the film cooling does not influence the pressure profiles. The higher than predicted experimental coefficients at the high area ratios, especially in the low pressure tests, are probably due to the fact that the radiation from the water vapor in the stream was not accounted for in either the data reduction or predictions.

4. Film Cooling Effectiveness (Data Correlation)

The effectiveness of film cooling is best evaluated from the steady-state wall temperatures of the thin wall, $3:1$ and $40:1$ film-cooled chambers. Wall temperatures are expressed as the enthalpy effectiveness shown in Figure VII-26 and discussed in Reference 16. An additional parameter, which

VII, B, Thrust Chamber Cooling (cont.)

relates measured rate of core and coolant mixing along the contour length to mixing observed in nonreacting plane unaccelerated laboratory flow tests for idealized slot injection with identical coolant to core velocity ratios at injection, is also computed. This parameter, defined as the entrainment multiplying factor, identifies the magnitude of the mixing in the rocket which is in excess of that experienced under optimum conditions. The entrainment multiplying factor K_e is considered to be composed of three components:

(1) K_{inj} , mixing due to injector streaks and combustion turbulence.

(2) K_{FC} , mixing due to coolant injection from discrete orifices with a well-supported thick lip rather than continuous annulus with knife-edge separation, which is structurally impractical for the APS application with 10^6 cycle requirements.

(3) K_T , losses due to coolant turning caused by the nozzle contour.

5. Subsonic Coolant Injection

Figure VII-43 provides the results of the sea level tests in which the coolant was injected in the cylindrical chamber region. This figure contains the chamber geometry, coolant injection geometry, entrainment multiplying factors, and enthalpy cooling effectiveness.

The high mixing rate noted downstream of the injection station is attributed to the geometry of the downstream edge of the coolant injection ring. The peripheral variation in the mixing parameter reflects the manifold flow maldistribution in the Phase I injector designs.

VII, B, Thrust Chamber Cooling (cont.)

The mixing resulting from the coolant turning into the convergent nozzle is not particularly high. This is attributed to the favorable coolant to core density ratio which holds the coolant against the wall. The mixing rate approaches the laboratory values as the flow approaches the throat. The reason the parameter remains greater than one rounding the throat is thought to be the turning of the coolant in the reverse direction. The trends noted in these and subsequent figures are that colder fuel coolant rounding the throat results in greater mixing rates. The mixing rates downstream of the throat are noted to reduce as chamber L^* is increased or MR reduced and thus can be attributed to unreacted oxidizer combusting at or downstream of the throat. This leads to the conclusion that a high performing injector, 100% ERE, will provide the most favorable thermal environment in a film-cooled divergent nozzle.

The results of these early injector checkout tests led to:

- (1) a much tighter design criterion for injector manifold flow distribution,
- (2) the use of a 7.5-in. (19 cm) injector to throat length in the film-cooled design to prevent interaction of unreacted oxidizer with coolant on the convergent nozzle,
- (3) the coolant injection location moved from the end of the cylindrical section to a location on the conical nozzle 1.3 in. (3.4 cm) upstream of the throat,
- (4) a reduction of the step height from 0.110 in. (.28 cm) to 0.060 in. (.15 cm) and the coolant injection orifices made a larger percentage of the projected area of the step, and
- (5) the design optimization of the 40:1 cooled chamber.

Figures VII-45, VII-46, and VII-47 provide comparable experimental results from the 40:1 chamber under the following conditions:

Figure VII-44 - Phase I Injector, Ambient Temperature Propellant

Figure VII-45 - Phase II Modified "I" Injector, Ambient Temperature Propellant

VII, B, Thrust Chamber Cooling (cont.)

Figure VII-46 - Phase II Modified "I" Injector, Cold Propellants with Phase I and Phase II Film Coolant Injection Orifice Areas

The contour is shown in the upper portion of the figure, including the new coolant injection station. The following observations can be made by comparing the data in these three figures:

- (1) K_e remains high at the coolant injection station but drops from 3.5 to 2.5 when the Phase I "I" pattern is replaced by the Phase II modified "I" pattern with improved manifolding.
- (2) The solid symbols in Figure VII-46 were obtained with the Phase II film-cooled chamber which had reduced slot depth (0.030 vs 0.040 in. (.076 vs .102 cm)) and more extensive instrumentation immediately downstream of the injection station. These data show an improvement in the injection efficiency but indicate higher than flat plate mixing rates still exist in the in-the-throat curvature region.
- (3) Higher film cooling flows result in greater losses rounding the throat even though the injection velocity is more favorable. This is due to the reduced ability of the colder (higher density) coolant to make the small radius turn into the exit nozzle. The trend to higher mixing at higher flows continues into the skirt.
- (4) A peculiar, unexplainable flow pattern is noted midskirt in Test 03-015 and was noted in some other tests.
- (5) The coolant entrainment is greater than that found under laboratory conditions in the convergent nozzle and throat, less than laboratory (subsonic data) in the region downstream of the throat, and approaches zero at

VII, B, Thrust Chamber Cooling (cont.)

high area ratios. The latter infers that nozzle area ratios can be increased without need for additional cooling.

(6) The model accurately predicts the influence of coolant injection velocity since changes in flow and propellant injection temperatures do not measurably alter the K_e value at the injection station.

A direct comparison of the data from all film-cooled chamber tests is presented in Figure VII-47 by plotting the throat and peak skirt temperatures vs fuel film cooling expressed as a percent of total flow. The variables included are: injector type, MR, chamber pressure, percent coolant, and coolant temperature. The conditions can be identified by the standard symbol format. Two bands of data which show temperatures dropping with increasing coolant flow are observable, the upper being the peak skirt and the lower the throat temperatures. In this format, data at all chamber pressures and mixture ratios fall within a narrow band; however, a definite influence of propellant temperature is observable. An injector influence is not detected because only mean data points are shown. The main difference between injectors would be reflected in the deviation of the peripheral temperatures from the mean at any station. In this regard, the peripheral temperature variation has a direct relation to the flow uniformity provided by the injector manifolding and injection orifices. No significant differences are noted between the Phase I and II chamber configurations; therefore, parametric analyses presented in other sections were based on the best fit of all data at each axial station with the only distinction being propellant temperature.

6. Film Cooling Effectiveness with Supersonic Coolant Injection

a. Design Considerations

To minimize thruster weight and allow nozzle scarfing the regeneratively cooled chamber had a thin adiabatic wall film cooled skirt

VII, B, Thrust Chamber Cooling (cont.)

from an area ratio of 10.4 to the nozzle exit at area ratio 40. The fuel film coolant was injected through thin, two-dimensional supersonic nozzles at the nozzle attachment point. The details of the coolant injection nozzles and their general operating characteristics are given in Figure VII-48.

In the design of the coolant injection nozzles, it was recognized that the ideal injection condition would be to have the coolant match both the free stream velocity and static pressure at the point of injection. However, it was not possible to match coolant and core velocities in the design because the coolant injection temperature required to do so was found to be excessively high; the nozzles were therefore designed to match pressure only. The initial design was based on matching the static pressure of the coolant at the two-dimensional nozzle discharge to the free stream pressure computed for the Rao nozzle by the method of characteristics. The local wall pressure was 5.7 psia (3.94 N/cm^2) at nominal operating conditions. The coolant nozzles were sized to match these conditions with 8% fuel flow when propellants are supplied at ambient conditions. In the course of testing, propellant flows were varied from 23% of the fuel down to 5%. The minimum flow for steady-state operation was found to be approximately 8% at nominal conditions. The coolant to core velocity ratio which resulted was 0.55, was nearly independent of flow rate, and varied as the square root of the coolant supply temperature. The coolant Mach number at injection is 2.5 compared to a free stream Mach number of 3.1.

The axial stations downstream of the point of coolant injection at which the wall temperatures were measured are also shown in Figure VII-48. These correspond to length to slot height multiples of 73.4, 290, 524, and 745, where the slot height is 0.015 in. (0.388 mm). Also shown in the figure are the curves of coolant weight flow vs manifold pressure for various total coolant supply temperatures.

VII, B, Thrust Chamber Cooling (cont.)

b. Phase I Chamber Test Data

The test conditions and wall temperature measurements from the Phase I chamber tests are provided in Table V-5. Figure VII-49 provides a plot of the measured steady state wall temperatures vs the film coolant expressed as a % of total propellant flow. Data are shown for the 4 axial stations for all mixture ratios and propellant supply temperatures as indicated by the C, A and H (cold, ambient and hot) designations. The temperatures measured for each axial station correlate with flow rate independent of mixture ratio and chamber pressure except for one set of data at 100 psia (69 N/cm^2) and very low coolant flows. If the boundary layer remained laminarized along the entire length of the skirt, the lower skirt temperatures would be expected for several reasons: (1) the coolant mixing rates would be reduced, (2) the recovery factor for laminar flow is less, and (3) radiation out the exit plane would be more significant with the lower heat transfer coefficients. Changes in the propellant supply temperatures are noted to result in comparable changes in the wall temperatures along the entire skirt length.

Selected data for the supersonic injection were compared with published correlations as shown in Figure VII-50. Data of this type are generally presented using a dimensionless temperature effectiveness, a blowing parameter and distance to slot high ratio. The format adapted for this purpose was that recommended by Zakkay. This simple approach evaluates the conditions at the coolant injection stations and neglects the difference in heat capacities of the core and coolant flows. A second parameter was also generated which includes a specific heat ratio which is commonly employed for injection of foreign gases. Since the core mass velocity varied considerably along the length of the cooled wall as the area ratio increased from 10.4 to 40, the blowing parameter λ' was also modified to reflect the average hot gas condition between the coolant injection point and the station where the wall temperature

VII, B, Thrust Chamber Cooling (cont.)

was measured. Before comparing test results, it should be pointed out that differences exist in the experimental techniques, in the coolant injector design, and in the magnitude of the parameter λ with the present values being much higher than those of the laboratory tests. The data of References 1 and 3 in Figure VII-50 were inferred from cooled wall heat flux measurements and may be subject to error since it was necessary to use a computed heat transfer coefficient in order to estimate T_{aw} ; in the present data, these temperatures were measured directly.

In the format employed it is possible to present data from all axial stations, mixture ratios, chamber pressures and coolant flowrates and injection temperature as a single line. Since the specific heat ratio remained nearly constant in all tests, λ and λ' give equally good correlation. The latter is considered more universal since it would be applicable to other fluid combinations. The item most significant about the APS data in comparison with the reference data is that for a given λ , mixing starts at a much lower x/s value and proceeds at a much lower rate. This may be due to the many variables which are not considered in the simplified approach, the coolant injector geometry, or the great difference in λ values between the current data and the reference data. In terms of cooling effectiveness this means that at low values of λ' ($\frac{x}{s}$) the cooling effectiveness was much lower than presented by the various references. However, extrapolation of the test data to larger λ' ($\frac{x}{s}$) values (which means either lower cooling flows or a longer nozzle) indicates the current injection schemes are providing higher effectiveness in the downstream region.

ALRC Film Cooling Model

The rather elaborate computer model discussed in Ref. 16 and used extensively in design for film coolant injection upstream of the throat was not initially employed for the supersonic coolant injection. It was

VII, B, Thrust Chamber Cooling (cont.)

generally felt that the high Mach number correlations of References 1 through 3 of Figure VII-50 would be more appropriate since the ALRC model contains velocity ratio parameters, temperature and species concentration shape factors for the film layer which were derived specifically to match low Mach number cooling conditions. However, after data reduction was initiated, it was found that the ALRC model correlated the supersonic data in terms of an energy effectiveness parameter (η_T) better than the referenced supersonic models. The ALRC model was therefore adapted for the data reduction.

Before discussing the results, it is necessary to review the major differences between film cooling models. The ALRC model effectiveness is an enthalpy effectiveness and accounts for the difference in core/coolant total energy levels including sensible, chemical and kinetic energy differences. The mixing rates are calculated from the temperature measurements using a computer subroutine which defines the energy level of O-H at all mixture ratio and pressure states. The mixing rate is expressed by the dimensionless mixing parameter (κ) which is the ratio of the mass flux normal to the wall to the free stream mass flux as noted in Figure VII-26.

Figure VII-51 shows this computed mixing parameter κ for coolant injection upstream and downstream of the throat, i.e., film-cooled chamber and Phase I regeneratively cooled chamber test data. Data are shown for several coolant flow rates, pressures and injection temperatures. Two bands of data are noted: one for upstream injection, the other for downstream. The data are very consistent except for: (1) the low pressure regeneratively cooled chamber test which relaminarized, and (2) the high area ratio points where mixing rates are very low and small differences in the measured wall temperature due to radiation effects result in large apparent differences in the mixing rate.

Significant observation from these data are: (1) near the injection station the mixing ratio parameter κ is approximately the same for

VII, B, Thrust Chamber Cooling (cont.)

coolant injection upstream and downstream of the throat; (2) the rate of mixing decays more rapidly with length for upstream subsonic injection as noted from the slope of curves, thus resulting in greater mixing rates in the skirt for the downstream injection; (3) the coolant mixing rate in the test corresponding to the laminarized throat condition is markedly lower at the injection station.

Figure VII-52 shows the enthalpy cooling effectiveness for selected tests and the entrainment multiplying factor related to the K_o computed from subsonic laboratory conditions:

$$\text{Entrainment multiplying factor} = \frac{K_{\text{exp}}}{K_o}$$

This parameter is very sensitive to the mixing rates and is thus more suitable for evaluating differences in the flow and mixing phenomena. The mixing rates are noted to be slightly higher at the 15% flow rates and this may be due to the over-pressure condition at the injector point. The much lower mixing rates at the relaminarized 100 psia (69 N/cm^2) condition are obvious with the mixing rate being less than those obtained in the laboratory under idealized conditions.

Although not conclusive, these data suggests that a relaminarized condition in the nozzle, in addition to lowering throat heat fluxes, may allow a reduction in the amount of skirt film cooling which will lead to higher engine performance. Similar results were noted in the Phase II chamber test data.

C. NOZZLE CONTOUR SELECTION

The shape and length of the combustion chamber, throat region, and divergent nozzle were selected to provide the maximum performance

VII, C, Nozzle Contour Selection (cont.)

consistent with minimum length, weight, and cooling requirements. The selections made involved:

- (1) Chamber contour - cylindrical, conical, or other
- (2) Throat radius of curvature - upstream and downstream
- (3) Expansion angle and length of Rao nozzle

Additional restraints of the experimental program required variable L^* and the selection of a single contour for two cooling approaches. The preferred chamber contour for the film-cooled design was conical to minimize the coolant losses associated with turning the film coolant along a contoured chamber wall. The preferred contour for the regeneratively cooled chamber depended upon whether or not the throat boundary layer could be laminarized to reduce the heat flux at the nominal operating conditions. The requirements for laminarization are considerably different than those optimum for film cooling.

The conical contour was not selected because it was not compatible with the need for conducting chamber L^* surveys with a limited number of chambers and injectors. The idealized configuration requires that the propellant injection from the outer rows of the injector be parallel to the chamber wall, which means that the chamber length must be known to design the injector.

A cylindrical chamber was selected for Phase I to allow axial orientation of the injector elements and variable L^* . As a compromise, a short, straight section was followed by a 22° convergent nozzle with a large radii of curvature blending the cylindrical and conical sections ($R/R_T = 2.67$) and a large upstream throat radius of curvature ($R_v/R_T = 2.0$). The chamber L^* was selected based on the experimental results of the injector checkout tests. The 20 in. L^* (51 cm), 7.5-in. (19 cm) length was selected for the film-cooled

VII, C, Nozzle Contour Selection (cont.)

design, while a 15 L^* (38 cm), 5.5-in. (14 cm) length was selected for the regenerative design. Three chamber length selections were based mainly on thermal considerations, since performance was sufficiently high even at the lower L^* values. The underlying logic was to keep the film coolant injection station as close to the throat as possible without allowing the convergent nozzle to act as a splash plate for unreacted oxidizer. In the film-cooled design the coolant injection station was fixed in the converging portion of the nozzle and the chamber length could be increased without changing the position of the coolant injection relative to the throat. In the regeneratively cooled design, the film coolant was injected at the head end of the chamber and increases in chamber length resulted in increasing the distance from the injection point to the throat.

The Rao nozzle contour was selected by evaluating the combined frictional, kinetic, and divergence losses as a function of length and downstream radius of curvature as noted in Figure VII-53. Selection of the radius of curvature downstream of the throat was considered to have an impact on nozzle fabrication, performance, and heat transfer. Rapid expansion (small curvature) favored performance and minimized cooling loads in a nonfilm-cooled design. A large curvature simplified fabrication and might prove to be advantageous in a film-cooled design, although no data were available to either support or refute this hypothesis. The selection of $R_d/R_T = 0.2$ and $L/R_T = 15$, length = 14.4 in. (36.6 cm), was based on maximizing performance without film cooling as can be noted in Figure VII-53.

Comparisons were made of the wall mass flux and temperature profiles for six different divergent nozzle contours. Small differences were noted for a short distance downstream of the throat, but at large distances, all throat curvatures produced the same results. Figure VII-54 provides the gas temperatures and mass flux profiles and pressure profiles for the selected

VII, C, Nozzle Contour Selection (cont.)

contour. These were employed in the thermal analysis in evaluating data, in the structural analysis for computing skirt hoop pressure and thrust loads, and as a criterion for flow separation in altitude testing.

Comparison of frozen and equilibrium flow (Figure VII-54) showed chemical kinetics to be of second-order importance in terms of mass flux profiles at a MR = 4.0. Comparison of one-dimensional flow and two-dimensional nozzle flow computed by the method of characteristics, however, proved to be of great significance; therefore, two-dimensional gas flow parameters were included in all analyses of the 40:1 nozzle.

Effect of Nozzle Contour on Throat Heat Transfer and Boundary Layer Characteristics

Figure VII-55 shows that, at throat Reynolds numbers greater than 10^6 , throat Stanton*Prandtl Number products are satisfactorily estimated by turbulent boundary layer equations with a Reynolds number coefficient (C_g) of 0.016. At Reynolds numbers less than 2×10^5 , the throat Stanton number is best predicted assuming the boundary layer is laminar. The intermediate Reynolds number range may be either laminar, turbulent, or transitional. The heat transfer coefficients which materialize in the transitional range are dependent on nozzle contraction ratios, angles, throat curvature, and wall-to-free-stream temperature ratios. Data from References 15, 18, and 22 were correlated with adiabatic wall temperature properties. This contrasts to the film temperature properties, which appear more appropriate for the APS data obtained. Phase I contour heat transfer coefficients derived from heat sink copper chambers converted to dimensionless Stanton numbers for 100, 300 and 500 psia (69, 207 and 345 N/cm^2) were superimposed on existing data (large diamonds) using both adiabatic wall and film reference temperatures.

VII, C, Nozzle Contour Selection (cont.)

Based on the Phase I test results, additional analyses were undertaken to determine if the contour of the regeneratively cooled chamber could be modified to provide a reduced throat Stanton number at 300 psia (207 N/cm^2) operation without film cooling.

Moretti (Ref 19) suggested that laminarization is possible when

$$K = \frac{\mu}{\rho u} \left[\frac{1}{u} \frac{du}{dx} + 0.4 \frac{1}{r} \frac{dr}{dx} \right] \geq 3.3 \times 10^{-6}$$

where

- μ = viscosity
- ρ = density
- u = freestream velocity
- r = local chamber radius
- x = contour length

Figure VII-56 shows the magnitude of the K parameter for several convergent nozzle contours at 100 and 300 psia (69 and 207 N/cm^2) in comparison to the minimum value at which laminarization is expected to occur. Contour C was employed in Phase I testing, which demonstrated the reduced heat transfer rate associated with a laminarized condition at 100 psia (69 N/cm^2) but not at 300 psia (207 N/cm^2). This is consistent with the above prediction criterion which suggests the 300 psia (207 N/cm^2) condition is very marginal. The analysis showed that modification of the contour could bring about a twofold increase in the K parameter for 300 psia (207 N/cm^2) operation and a significantly improved the chance of a laminarized boundary layer at the throat. The Phase II regeneratively cooled chamber was therefore fabricated to contour B, shown in Figure VII-56. This was selected over contour A because it was anticipated that the coolant slots for the smaller throat radius of curvature would be very difficult to fabricate.

VII, C, Nozzle Contour Selection (cont.)

Figure VII-57 shows the predicted gas-side heat transfer coefficients for the two limiting cases, fully turbulent and fully laminarized flow, using the method of Reference 18. The chamber conditions are predicted to be the same while, in the throat, a significant reduction is noted for the fully laminarized condition. The coefficients can be expected to fall between these limits in transitional flow. A comparison of data and predictions is presented in Section VI.

D. MATERIALS EVALUATION

The preliminary search for materials that provide the greatest chamber life with the minimum of film cooling was conducted using a material unit of merit "M", which relates the ratio of a material's ability to withstand cyclic thermal stress to the properties which cause the thermal stresses to develop. This parameter is often referred to as a thermal shock sensitivity factor.

$$M = \frac{\sigma/E}{\alpha/K}$$

Desirable properties are:

- High allowable alternating stress amplitude, σ , at temperature
- Low Young's modulus, E
- Low expansion coefficient, α
- High thermal conductivity, K

The allowable alternating stress values for each material are computed based on ultimate strength, modulus, and reduction of area values, using the following NASA/Manson equation:

VII, D, Materials Evaluation (cont.)

$$\sigma = \frac{E}{2} \left[\frac{3.5 F_{tu}}{E N_f^{0.12}} + \frac{D^{0.6}}{N_f^{0.6}} \right]$$

where σ = critical alternating stress, psi

E = Young's modulus, psi

F_{tu} = ultimate tensile strength, psi

N_f = number of cycles to failure

D = ductility = $n \frac{100}{100-RA}$

RA = reduction of area

High strength superalloys, coppers, and refractory metals were considered in the materials selection study. Two high temperature alloys were considered particularly attractive for use in the film-cooled chamber design: Hastelloy X and Haynes Alloy No. 188. Hastelloy X is a nickel base alloy which possesses exceptional strength and oxidation resistance. The alloy has excellent forming characteristics and can be readily welded to itself and to stainless steel.

Haynes Alloy No. 188, a cobalt base material, is superior in strength and corrosion resistance to Hastelloy X at all temperatures. This alloy can be worked and welded similarly to Hastelloy X, but gives a very ductile condition following welding, air or water quenching from high temperature. The Haynes 188 alloy is higher in cost than Hastelloy X but the added reliability afforded by its high temperature mechanical properties and oxidation resistance provides compensatory advantages. S-N strength properties calculated from the NASA/Manson equation are shown in Figure VII-58. Another high strength alloy, A-286, was considered but not selected because of its poor welding characteristics.

VII, D, Materials Evaluation (cont.)

Copper and copper alloys were considered for the nonadiabatic portions of the chamber, mainly because of their high thermal conductivity which is more than an order of magnitude higher than the nickel-based superalloys. The lower value of Young's modulus enhances the merit of copper. The main limitation of copper is its low strength at elevated temperatures, which to a degree offsets the advantages of high thermal conductivity. The use of copper alloys containing silver, zirconium, and beryllium to improve the strength provides greater chamber life capabilities over unalloyed copper.

The problem of brittleness induced by heating copper and copper alloys containing oxygen (in the form of cuprous oxide) in atmosphere containing hydrogen is well known. This embrittling is encountered industrially when heating tough pitch copper (0.02% O_2) in hydrogen above 750°F (670°K). Embrittlement has not been encountered in oxygen-free copper alloys--including the ZrCu and BeCu alloys of less than 0.0001% O_2 --with hydrogen at pressures of 100 psi (69 N/cm²) and would not be expected at high hydrogen pressures as long as the low oxygen content is maintained.

Zirconium copper was selected as the best material for use in the high flux, convectively cooled regions because of its high resistance to thermal shock and its ability to provide an efficient fin which diffuses the heat being transferred to the coolant. ALRC experimental investigations in support of the SSME demonstrated that this alloy could be satisfactorily brazed to itself and other alloys without significant loss in strength and that the joint strength exceeded that of the copper when proper surface preparation and alloy application is employed.

Beryllium copper, in contrast, showed a significant reduction in ductility following the heating and cooling cycles required for brazing and therefore was not considered at this time. Another reason for not selecting

VII, D, Materials Evaluation (cont.)

beryllium copper, which has much greater strength than zirconium copper, was the unknown influence of reentry heating thermal cycling on the ductility since the brazing had produced a hot, short condition.

The high strength alloy Haynes 188 was selected for the throat of the film-cooled chamber because: (1) it can operate at higher temperatures than copper and still contain the chamber pressure loads, and (2) it can withstand the thermal shock associated with 10^6 thermal cycles because of its high fatigue strength characteristics. Film-cooled divergent nozzles, flanges, manifolds, and other structural components which are not subjected to high thermally induced stresses were fabricated from 304L stainless steel because of its excellent welding characteristics and compatibility with the propellants at elevated temperatures; however, a higher strength alloy, ARMC0 (22-13-5), is recommended for prototype designs because it will provide greater life and result in a reduction in chamber weight. The fatigue life properties of the chamber materials are shown in Figures VII-58 and VII-59.

The 22-13-5 strain-life data are based on an extrapolation of the experimental results reported in Reference 20. The Haynes 188 predictions were computed from the Manson equation using the manufacturer's quoted properties.

The data for various types of copper, presented in Figure VII-60, were obtained from several sources. A significant difference in life at a given strain is noted between the two references. This can be attributed to any of the following factors: the precise composition of the alloy, the method of testing, and differences in test environment. The specimens tested in an inert gas environment showed much greater life than those conducted by another experimenter in air. The test in air showed B-DCu, ZrCu, and AgZrCu to be comparable and superior to OFHC copper. The inert gas test produced greater life for ZrCu and AgZrCu with the latter being clearly superior.

VII, D, Materials Evaluation (cont.)

Additional testing by a single investigator using identical samples in air, H_2 , H_2O , and an inert atmosphere is warranted in order to make a proper selection of the best copper alloy.

Prediction of APS copper component life was based on minimum (air) properties as noted on appropriate figures ($N_{f(min)}$) except in situations where both minimum and maximum values were given.

Refractory materials such as columbium have high strength at elevated temperatures, a low modulus of elasticity, low expansion coefficients, and moderately good thermal conductivities, which are all highly favorable properties. This class of materials, including molybdenum and tantalum alloys, have severe oxidation limitations and would require protective coatings even if used at low temperatures. Many protective coatings, consisting mainly of complex metal silicides, are available and some have proven the ability to withstand hundreds of hours of exposure to oxidizing atmospheres at high temperature under laboratory conditions. Reliability is the main difficulty with these protective coatings. Data have shown premature failure of some specimens after a relatively low number (hundreds) of thermal cycles, while other samples provide many thousands. The solution to this material's limitation was considered to present a technical effort which is beyond the scope of the current program, although the recommended concepts could make use of this class of material at a later date to provide improved performance. The use of columbium or fibrous graphite skirt was evaluated, including methods of attachment, as shown in Figure VII-61.

VII, Supporting Analyses and Data Correlation (cont.)

E. STRUCTURAL AND LIFE ANALYSES

1. Design Loads

Nominal pressures and temperatures were used in all calculations of fatigue life; then the required factors of safety were applied to verify strength adequacy. The nominal pressures used are itemized below, and the associated thrust loads were also applied to the structure.

<u>Location</u>	<u>Pressure</u>
Main chamber	300 psia (207 N/cm ²)
Fuel inlet manifold (250°R)	390 psia (269 N/cm ²)
Channel section	360 psia (248 N/cm ²)
Throat region and skirt	Distributed two-dimensional pressure based on 300 psia (207 N/cm ²) chamber
Injector pressure	340 psia (235 N/cm ²)

A proof pressure for the entire structure was selected upon the basis of 500 psi (345 N/cm²) nominal chamber pressure and using a 1.25 factor of safety to obtain design limit load as follows:

Nominal chamber pressure	=	500 psia (345 N/cm ²)
Nominal injector pressure	=	600 psia (414 N/cm ²)
Proof pressure, all components	=	700 psia (483 N/cm ²)
Design limit pressure = 1.25 proof	=	875 psia (603 N/cm ²)

2. Thermal Environment

Mixture ratio	4.0
Film cooling	Variable
Temperature profiles	Per test data and thermal model predictions

VII, E, Structural and Life Analyses (cont.)

3. Life Goal

Anticipated fatigue life (cycles and duration) requirements for the APS thrusters are based upon a 100-mission goal, with a life safety factor of five. Although no official mission profile or thruster duty cycle was specified, it was possible to make some estimates with the assistance of the vehicle system analysts. The estimated thruster life requirements are:

50 full thermal cycles x 100 missions x 5 safety factor =
25,000 full thermal cycles

1000 short pulses x 100 missions x 5 safety factor =
500,000 short pulses

5 minutes x 100 missions x 5 safety factor =
2500 minute total duration

No information exists as to the duration of the short pulses or as to the sequence of application, so no interaction was assumed. Further data are needed if they are to be combined by a cumulative damage theory, especially if the short impulses are on the order of a minimum impulse bit (50 to 60 millisec range), since maximum copper thermal gradients occur later in the firing.

4. Methods of Analysis

Each major component of the thrust chamber assembly was analyzed with the aid of a finite element computer program. The nonlinear (plastic) plane-strain option was used to analyze the convectively cooled copper sections while the other regions were analyzed by use of elastic solutions with the appropriate secant moduli for copper material in the plastic range.

VII, E, Structural and Life Analyses (cont.)

The approach used in design optimization and life prediction was to identify the location and time of the limiting stresses in each component. Consideration of the strains in transient heating are essential since the location of life limiting transient strains may be at a different location and greater in magnitude than those computed for steady-state thermal operation. As noted under discussion of the individual designs, this process was an iterative one involving the investigation of several geometries until satisfactory results were attained.

The detailed computer analyses were conducted for the nominal design point. Computer costs prohibited repeat runs for off-design conditions. In order to provide the parametric results showing the influence of MR, P_c , propellant temperature, film cooling flow, etc., for a given design, simplified models were employed. The accuracy of the simplified approach was established by comparing these results with the detailed computer prediction available at the nominal design point. Where these results differed significantly, empirical correction factors were added to the simplified equation at the design point to make the simplified and computer solutions agree.

Transient thermal stresses in the single-layer shell and skirt regions were calculated by use of the following expressions, derived in Reference 21:

$$\sigma_1 = \frac{E \propto \Delta T_f}{(1 - \nu) \left(1.5 + \frac{3.25k}{ht}\right)}$$
$$\epsilon_T = \frac{0.5 (\tau_1 + \tau_p)}{1 - \frac{0.5 (\tau_1 + \tau_p)}{UTS}}$$

VII, E, Structural and Life Analyses (cont.)

where σ_1 = maximum surface stress level, psi (thermal)
 ϵ_T = total strain range, in./in.
 E = Young's modulus, psi, at point of maximum stress
 α = coefficient of thermal expansion, in./in./°F
 ΔT_f = suddenly applied temperature (film), °F - initial temperature
 ν = Poisson's ratio, dimensionless
 k = thermal conductivity, Btu-in./sec-in.²-°F
 h = heat transfer film coefficient, Btu/in.²-sec-°F
 t = material thickness, in.
 τ_p = stress from pressure loading
UTS = ultimate tensile strength

This expression allows a direct calculation of maximum thermal stress if either the flat plate Biot number ($\frac{ht}{k}$) or the film coefficient is known, without the intermediate heat transfer analysis to determine time of maximum thermal gradient. Stresses calculated by this technique agreed with computer solutions within 10% error.

The equation used for predicting thermal strains in the convectively cooled channel section is:

$$\epsilon_T = K \alpha \Delta T + \epsilon_p$$

where K = the empirical geometric constant determined for each component examined, either by means of analytical expressions or computer solution
 ϵ_p = strain due to pressure loading
 ΔT = temperature difference between hot structure and colder restraining material, °F

VII, E, Structural and Life Analyses (cont.)

The values of "K" were found to vary from a minimum of 1.35 for the regeneratively cooled chamber design considered, where the pressure case was provided by a glass wrap, to a maximum of 2.0 for a fully restrained cooling channel wall with an unfavorable channel to land width ratio and nonoptimum wall thickness. The "K" values for the selected wall construction varied from 1.7 to 1.8, depending on the location.

Creep rupture life was determined by comparison of the steady-state stress levels to the Larsen-Miller plots of stress-rupture data at elevated temperatures.

Fatigue life was determined using the results of the stress-strain solution to plot stress-strain history of a full thermal cycle, cold start firing to steady state and subsequent cooldown. The peak strain obtained in this manner was used to obtain the number of cycles to failure.

The linear cumulative damage rule was used for predicting the remaining life available following the accumulation of short and long burns.

$$\text{Residual life} = 1 - \left[\sum \frac{n}{N_f} + \sum \frac{t}{T_R} \right]$$

where $\sum \frac{n}{N_f}$ is the summation of the number of pulses at a given pulse width divided by the allowable for that duration and $\sum \frac{t}{T_R}$ is the accumulated firing duration (hr) divided by the allowable creep life (hr) for the operating temperature and stress. The latter term is a negligible factor in thruster life.

VII, E, Structural and Life Analyses (cont.)

5. Material Properties

Material fatigue life data were provided in Figures VII-58, VII-59, and VII-60. The structural properties employed in the analysis are as follows:

(1) Zirconium Copper (Basic)

<u>Property</u>	<u>Temperature, °F</u>					
	<u>-200</u>	<u>0</u>	<u>200</u>	<u>400</u>	<u>600</u>	<u>800</u>
Modulus ($\times 10^{-6}$)	17.3	17.2	16.5	14.5	11.8	8.9
Yield strength ($\times 10^{-3}$)	13.0	13.0	12.0	11.0	10.0	8.8
Modulus ratio	0.03	0.03	0.03	0.03	0.03	--
Thermal expansion ($\times 10^6$)	9.4	9.4	9.4	9.6	9.8	10.1
Poisson's ratio	0.3	0.3	0.3	0.3	0.35	0.35

See Figure VII-62 for zirconium copper stress-strain curves.

(2) Stainless Steel (22-13-5)

<u>Property</u>	<u>Temperature, °F</u>			
	<u>-200</u>	<u>70</u>	<u>200</u>	<u>400</u>
Modulus ($\times 10^{-6}$)	30.0	29.0	27.0	26.0
Yield strength ($\times 10^{-3}$)	76.0	57.0	46.0	41.0
Modulus ratio	0.013	0.013	0.013	0.013
Thermal expansion ($\times 10^6$)	8.3	8.8	9.0	9.2
Poisson's ratio	0.22	0.25	0.27	0.30

VII, E, Structural and Life Analyses (cont.)

(3) Haynes Alloy 188

<u>Property</u>	<u>Temperature, °F</u>						
	<u>0</u>	<u>200</u>	<u>400</u>	<u>600</u>	<u>800</u>	<u>1000</u>	<u>1200</u>
Modulus ($\times 10^{-6}$)	34.3	32.9	31.4	30.2	29.0	27.6	26.4
Yield strength ($\times 10^{-3}$)	77.0	61.0	53.0	48.0	46.0	44.0	43.0
Modulus ratio	0.005	0.005	0.005	0.005	0.005	0.005	0.005
Thermal expansion ($\times 10^6$)	6.2	6.6	7.0	7.4	7.8	8.2	8.6
Poisson's ratio	0.3	0.3	0.3	0.3	0.3	0.3	0.3

See Figure VII-63 for Haynes 188 creep-rupture life.

(4) Stainless Steel (CRES 304)

<u>Property</u>	<u>Temperature, °F</u>			
	<u>-100</u>	<u>0</u>	<u>100</u>	<u>200</u>
Modulus ($\times 10^{-6}$)	28.0	28.0	28.0	28.0
Yield strength ($\times 10^{-3}$)	32.0	31.0	30.0	28.0
Ultimate strength ($\times 10^{-3}$)	--	75.0	75.0	--
Thermal expansion ($\times 10^6$)	8.8	8.85	8.90	9.00
Poisson's ratio	0.3	0.3	0.3	0.3

(5) Nickel 200

<u>Property</u>	<u>Temperature, °F</u>		
	<u>70</u>	<u>600</u>	<u>1200</u>
Modulus ($\times 10^{-6}$)	30.0	--	--
Yield strength ($\times 10^{-3}$)	21.5	20.3	10.0
Ultimate strength ($\times 10^{-3}$)	67.0	66.2	21.5
Coefficient ($\times 10^6$)	7.4	8.0	8.7
Poisson's ratio	0.3	0.3	0.3

TABLE VII-1

COAXIAL ELEMENT COLD FLOW TESTS

Date	Run No.	Rake Station (in.)	\dot{w}_{N_2} (lb/sec)	\dot{w}_{He} (lb/sec)	Oxidizer		Element Tip	Test Function
					Inlet	Recess (in.)		
PRESSURE RAKE TESTS								
24-25 Aug	1-17	0,0.5,1,2,3	--	--	--	0-0.25	Normal	Flow system checkout
25 Aug	18-21	0,0.5,1,2,3	0.063	0.013	No orifice	0.25	Normal	Mass flux profiles (L)
25 Aug	22-25	0,0.5,2,3	0.063	0.013	No orifice	0	Normal	Mass flux profiles (L)
28 Aug	26-27	0,1	0.063	0	No orifice	0.12	Normal	Ox flow characteristics
28 Aug	29-34	0,0.5,2,3	0.063	0.013	No orifice	0.12	Normal	Mass flux profiles (L)
28 Aug	35-40	0.5	0.04-0.063	0.0077-0.021	No orifice	0.12	Normal	Velocity and mixture ratio effects
28 Aug	42-43	0,1,2	0.063	0	No orifice	0.12	Normal	
28 Aug	44-46	0,1,2	0.063	0	Single orifice	0.12	Normal	Effect of orifice on flow distribution
28 Aug	47-53	0,1,2	0.063	0	Six orifice	0.12	Normal	Same as above + 5 rotational positions
28 Aug	54-56	0,1,2	0.063	0	Swirler	0	Normal	Swirl characteristics
28 Aug	57-60	0,0.5,2,3	0.063	0.013	Swirler	0	Normal	Mass flux profiles (L)
31 Aug	61-65	0,0.5,2,3	0.063	0.013	Swirler	0.12	Normal	Mass flux profiles (L)
31 Aug	66-69	0.5	0.063	0.013	Swirler	0	Normal	Rotational survey(θ) Mass flux
31 Aug	70-75	0.5	0.04-0.063	0.0077-0.021	Swirler	0	Normal	Velocity and mixture ratio effects
31 Aug	76-79	0.5	0.063	0	Swirler	0	22° scarfed	Rotational mass flux profiles (θ)
31 Aug	80-83	0.5	0.063	0.013	Swirler	0	22° scarfed	
31 Aug	84-87	0.5	0.063	0	Swirler	0	45° scarfed	
31 Aug	88-95	0.5	0.063	0.013	Swirler	0	45° scarfed	

Table VII-1 (cont.)

Date	Run No.	Rake Station (in.)	\dot{w}_{N_2} (lb/sec)	\dot{w}_{He} (lb/sec)	Oxidizer		Element Tip	Test Function
					Inlet	Recess (in.)		
TEMPERATURE RAKE TESTS								
3 Sept	T1-T6	0	0.04-0.063	0.0077-0.021	No orifice	0	Normal	Temp calibration tests
3 Sept	T7-T9	0.5, 2, 3	0.063	0.013	No orifice	0	Normal	MR distribution (L)
3 Sept	T10-T13	0, 0.5, 2, 3	0.063	0.013	No orifice	0.25	Normal	MR distribution (L)
3 Sept	T14-T17	1	0.063	0.013	No orifice	0.25	Normal	Rotational survey (θ)
3 Sept	T18-T21	0, 0.5, 2, 3	0.063	0.013	No orifice	0.12	Normal	MR distribution (L)
3 Sept	T22-T27	0.5	0.04-0.063	0.0077-0.021	No orifice	0.12	Normal	Velocity and MR effects
3 Sept	T28-T31	0.5	0.063	0.013	Swirler	0	45° scarfed	Rotational survey (θ)
3 Sept	T32-T35	0, 0.5, 2, 3	0.063	0.013	Swirler	0.12	Normal	MR distribution (L)
3 Sept	T36-T39	0, 0.5, 2, 3	0.063	0.013	Swirler	0	Normal	MR distribution (L)
3 Sept	T40-T43	0.5	0.063	0.013	Swirler	0	Normal	Rotational survey (θ)
3 Sept	T44-T49	0.5	0.04-0.063	0.0077-0.021	Swirler	0	Normal	Velocity and MR effects
3 Sept	T50-T53	0, 0.5, 2, 3	0.063	0.013	Single orifice	0.12	Normal	MR distribution (L)
3 Sept	T54-T57	0, 0.5, 2, 3	0.063	0.013	Six orifice	0.12	Normal	MR distribution (L)

TABLE VII-2

EQUATIONS FOR ESTIMATING MAXIMUM AND ALLOWABLE
FACE TEMPERATURE GRADIENT

General Solution

$$\Delta T = \frac{Q \cosh \sqrt{A} Z}{K \sqrt{A} \sinh (\sqrt{A} t)} \left[1 - A \left[\frac{r_o^2}{2} \ln \frac{r_o}{r} - \frac{1}{4} (r_o^2 - r^2) \right] \right] \quad \text{Eq 1}$$

$$\text{Maximum } \Delta T_m = \frac{Q}{K \sqrt{A} \tanh \sqrt{A} T} \quad \text{Eq 2}$$

where $A = \frac{2r_i h/K}{r_o^2 - r_i^2 + 2r_i \frac{h}{K} \left[\frac{r_o^2}{2} \ln \frac{r_o}{r_i} - \frac{1}{4} (r_o^2 - r_i^2) \right]}$

$$r_o \approx \frac{r_f}{\sqrt{N_e}}$$

$$\text{Allowable } \Delta T_m = \frac{2(1 - u) (F_F - \sigma)}{\alpha E} \quad \text{Eq 3}$$

- where
- h = convective heat transfer coefficient in fuel annulus, Btu/sec-in.²-°F
 - K = face plate thermal conductivity, Btu/sec-in.-°F
 - N_e = number of coaxial elements
 - r = local radius from center of orifice
 - r_i = radius of fuel annulus in face plate, in.
 - r_f = radius of injector face, in.
 - Q = face heat flux, Btu/sec-in.²
 - t = H₂ cooled face plate thickness, in.
 - ΔT = local temperature - coolant inlet temperature
 - ΔT_m = maximum face temperature - injector body or propellant temperature,
 - Z = distance from adiabatic back face
 - E = elastic modulus, lb/in.²,
 - F_F = fatigue strength for specific number of cycles at temperature, lb/in.²
 - α = coefficient of thermal expansion, in./in.-°F
 - u = Poisson's ratio
 - σ = hydraulically induced stresses, lb/in.²

TABLE VII-3

SUMMARY OF NO FILM COOLING HEAT FLUX DATA

Nominal Chamber Pressure				T _o °R	Injector	Axial Station										Test No.					
P _c psia	MR	L', in.	W _q , lb/sec			P _{re} , %	Inches from Throat: Diameter, in.	Supersonic			Throat		Subsonic		15 L*		25 L*		40 L*		
								2.18	1.10	0.00	1.4	3.00	4.38	7.18	10.06		11.44	3.64	3.64	3.64	3.64
312.8	3.01	5.5	3.44	98.97	4850	SN 5	Peripheral Station:	A	7.5	12.8										7-102	
								D	6.5			6.0									
								G	4.4			10.0									
								K	6.5			10.1									
												5.2									
307.8	3.85	5.5	3.40	98.00	5500	SN 5		A	5.3	8.8	12.5									8-102	
								D	7.9			6.6									
								G	4.7	7.1	11.0	10.6									
								K				10.0	5.2								
309.1	5.01	5.5	3.60	98.79	5950	SN 5		A	10.0		14.0									7-103	
								D	8.7			6.6									
								G	5.5		11.5										
								K	8.3		10.0	4.7									
302.9	3.68	8.30	3.42	96.86	5320	CA SN 1		A	5.02	6.9	13.5	10.6	9.0	6.5	10.6					8-107	
								D			15.9										
								G			15.0			6.9	7.7						
308.4	2.85	8.30	3.42	96.75	4700	CA SN 1		A	4.4	6.2	12.6	10.2	8.6	6.3	9.0					8-108	
								D			14.9										
								G			13.0			6.7							
315.8	4.97	8.30	3.70	97.23	5930	CA SN 1		A	5.8	8.0	15.0	10.5	9.3	7.2	10.8					8-109	
								D			17.5										
								G			15.8			8.1	7.1						
297.0	3.85	5.5	3.36	96.56	5500	SN 3		D			14.0									9-102	
								G			8.3	12.0		5.0							
								K	5.0	7.8		10.6	6.4								
306.2	2.94	5.5	3.36	97.25	4800	SN 3		D	4.7	7.4	13.7	12.4		5.7						9-103	
								G	4.4	7.0	12.0	6.4		6.0							
								K													
299.1	5.02	5.5	3.55	97.98	5950	SN 3		D	6.1	9.6	16.0			5.0						9-105	
								G	5.7	9.6	13.0	12.5		4.5						9-106	
								K			11.9	5.8									

TABLE VII-3 (cont.)

P _c psi _a	MR	L', in.	w _T , lb/sec	ERE, %	T _o , °R	Injector	Peripheral Station:	Axial Station										Test No.																																																																																																																																																																																																																																																																																																																																																																																																																																																																																																																																																																																																																																																																																																																																																																																																																																																																																																																																																																																																																																																																																																																																																																																																																																																																																																									
								Supersonic		Throat	Subsonic		15 L*		25 L*		40 L*																																																																																																																																																																																																																																																																																																																																																																																																																																																																																																																																																																																																																																																																																																																																																																																																																																																																																																																																																																																																																																																																																																																																																																																																																																																																																																										
								Inches from Throat:																																																																																																																																																																																																																																																																																																																																																																																																																																																																																																																																																																																																																																																																																																																																																																																																																																																																																																																																																																																																																																																																																																																																																																																																																																																																																																																			
								Diameter, in.:																																																																																																																																																																																																																																																																																																																																																																																																																																																																																																																																																																																																																																																																																																																																																																																																																																																																																																																																																																																																																																																																																																																																																																																																																																																																																																																			

TABLE VII-3 (cont.)

P _C , psia	MR	L', in.	W _T , lb/sec	ERE, %	Injector	Axial Station						Test No.				
						Supersonic	Throat	Subsonic	15 L*	25 L*	40 L*					
Inches from Throat:							2.18	1.10	0.00	1.4	3.00	4.38	7.18	10.06	11.44	
Diameter, in.:							3.04	2.50	1.92	2.80	3.64	3.64	3.64	3.64	3.64	
Low Pressure Tests (Flux to 300°F Wall)																
99	4.01	8.3	1.16	96.6	CA SN 1	Peripheral Station:	A	2.5	4.0	2.4	2.3	2.3	4.6	8-110		
							D		5.0				4.3			
							G		3.1							
99	4.92	8.3	1.19	98.8	CA SN 1		A	1.8	4.0	4.2		3.0	4.2	8-112		
							D		7.0			3.0	5.0			
									3.5							
Cold Oxidizer																
284	4.65	7.5	3.39	96.2	CA SN 1B		A	10.4	16.8	9.7	5.6	7.0		8-182		
							D		17.8		6.2					
							G	12.3	20.8	9.3		7.0				
							K		16.4							
278	5.65	7.5	3.44		CA SN 1B		A	10.5		9.7	5.91	6.5		8-183		
							D		17.0	9.2	6.5					
							G	13.0				6.5				
							K		15.4							

TABLE VII-4

SUMMARY OF HEAT FLUX DATA WITH FILM COOLING

P _c , psia	MR Core L', in.	MR TCA in.	% Fuel w _T	ERE, %	Injector	Film Cooling		Inches from Throat: Diameter, in.	Supersonic			Throat			Axial Station			Test No.								
						Area	Length		2.18	1.10	0.00	1.4	3.00	4.38	7.18	10.06	40 L*									
																			RPR	0	2.50	1.92	2.80	3.64	3.64	3.64
345	5.25	5.5	29.3	97.5	SN 3	M	0	Peripheral Station:	A	5.1	2.5*	5.1	7.1	10.06	11.44	8-122										
	3.62		3.94					K	D	7.3		7.3														
			0.25																							
333	5.20	5.5	18.7		SN 3	M	0	A	7.5	11.0	3.4*	11.0	3.4*			8-123										
	4.10		3.82					D	7.6	14.8		10.1														
			0.14					K	6.1	10.0																
337	5.21	5.5	29.0	96.8	SN 3	M	2.5	A	4.5	6.0	2.4*	3.5	1.5**			8-124										
	3.59		3.93					D	5.1		3.4	3.4														
			0.25					G	3.9	5.1	3.2															
335	5.47	5.5	30.0		SN 3	M	2.5	A	4.8	6.5	2.7*	3.7	1.4**			8-125										
	3.77		3.92					D	5.3		4.3	6.0														
			0.24					K	4.4	5.3	3.4															
								G																		
352	5.31	5.5	19.0		SN 3	M	2.5	A	6.5	10.7	6.0*	6.2	1.0**			8-126										
	4.18		3.83					D	5.3	7.5	6.0	6.0														
			0.14					K			6.0															
								G																		
337	5.25	8.3	30.0		SN 3	M	2.5	A	3.7	4.5#	5.0	3.6	2.2***			8-132										
	3.63		3.89					D			5.3	3.9	2.1***			#Flux @ 400°F										
			0.25					G								wall +										
330	5.122	8.3	20.0		SN 3	M	2.5	A	5.3	7.5	9.2	6.8	5.8	3.0		8-133										
	4.00		3.78					D			10.8		3.0***													
			0.15					G																		
346	5.19	8.3	30.0		CA SN 1A	M	0	A	5.2#	6.9	10.6	8.2#	4.6#			8-138										
	3.67		3.90					D			10.9	7.4				# = 400°F wall										
			0.25					G				7.3														
338	5.13	8.3	19.0		CA SN 1A	M	0	A	5.8	8.3	13.8	11.4	6.2			8-139										
	4.14		3.81					D			12.9	10.0														
			0.14					G				9.6														
344	5.08	8.3	29.5		CA SN 1A	M	2.5	A	4.5#	5.6	7.3	5.0	2.9*			8-140										
	3.59		3.88					D			8.0	5.5				# = 400°F wall										
			0.25					G				5.0														
311	5.16	8.3	19.0		CA SN 1A	M	2.5	A	6.0	8.3	3.1	9.0	3.6*			8-141										
	4.16		3.79					D			8.9	7.5														
			0.14					G																		

+ Except as otherwise noted.

* @ 2500F

** @ 1500F

*** @ 2000F

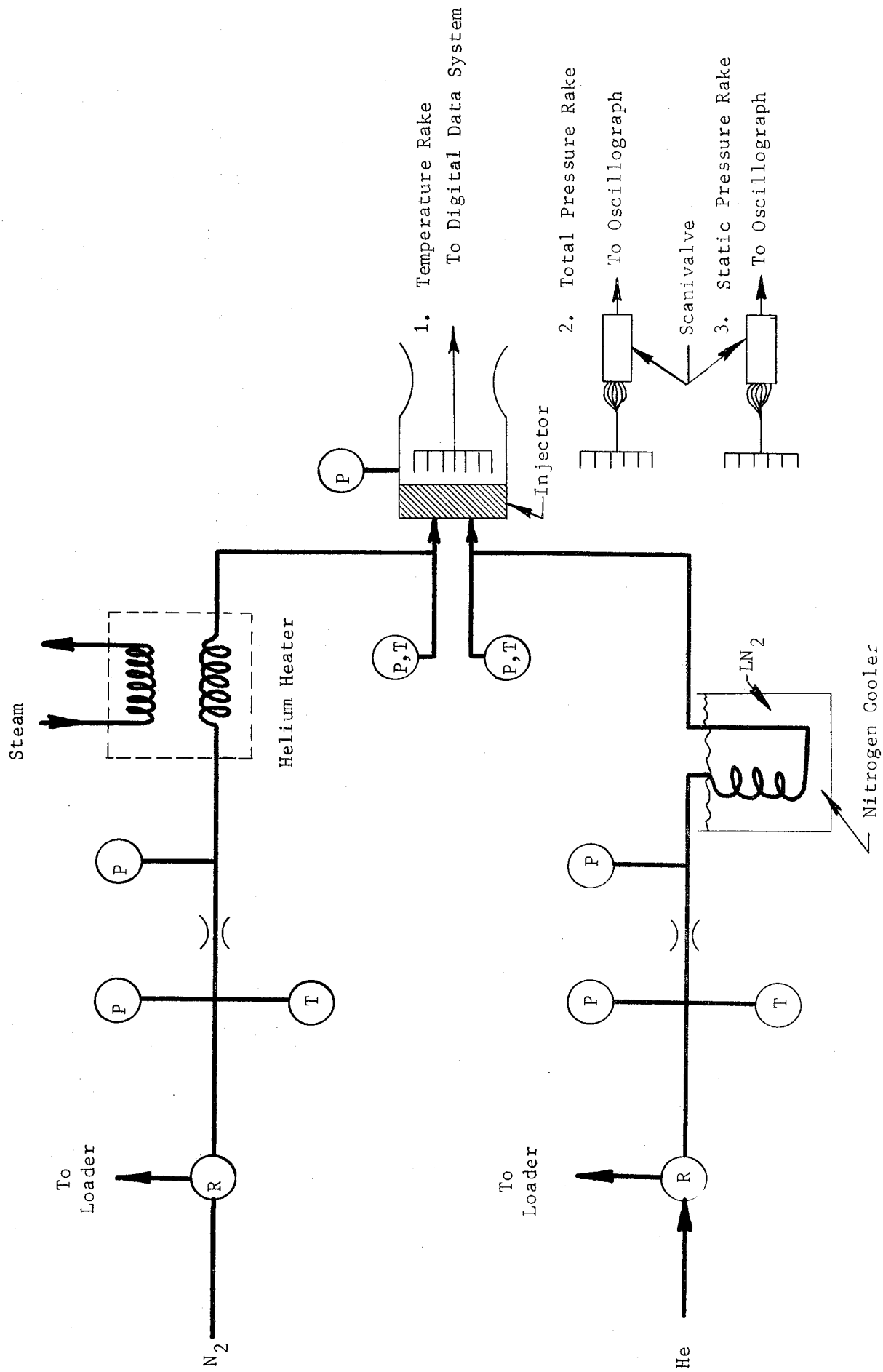


Figure VII-1. Typical Uni-Element Cold Flow Test Setup

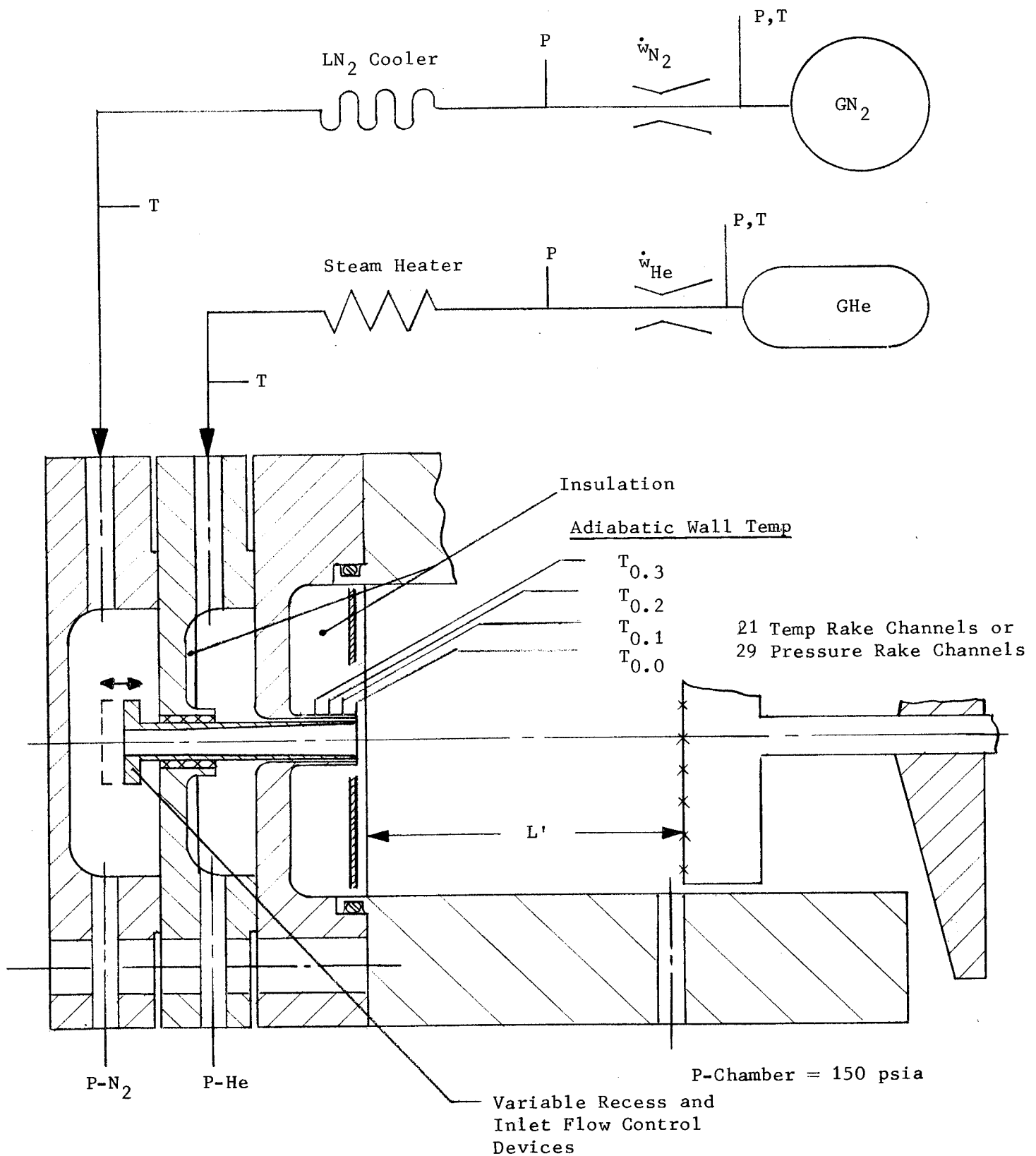
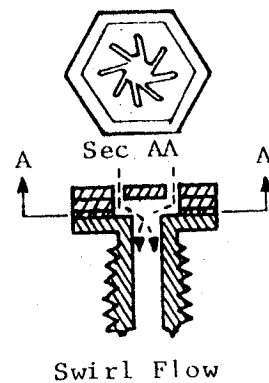
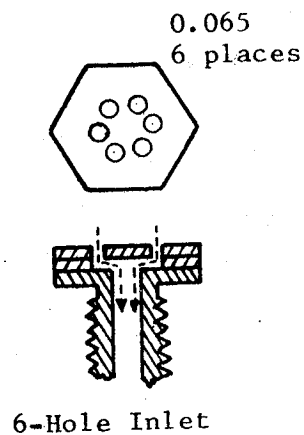
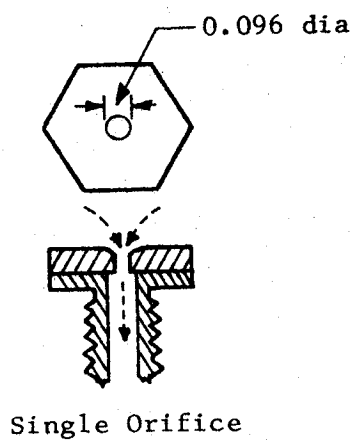
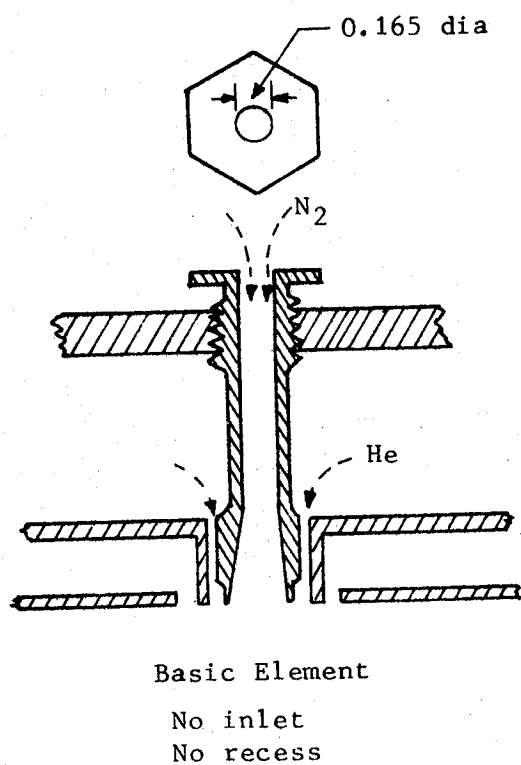


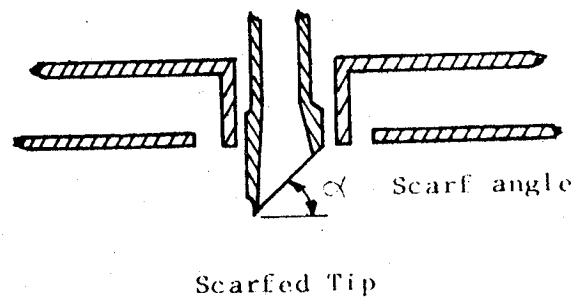
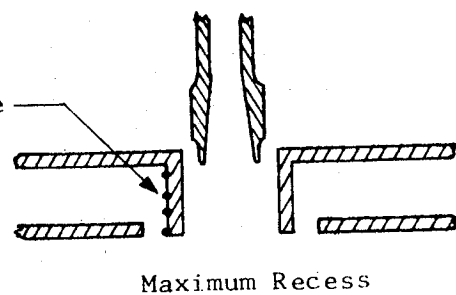
Figure VII-2. Schematic Drawing of Coaxial Element Cold Flow Test Apparatus



Oxidizer Inlet Caps



4 recessed
thermocouple
locations



Tip Configurations

Figure VII-3. Coaxial Elements Employed in Cold Flow Testing

Axial dist from injection
plane* = 0.315 in.

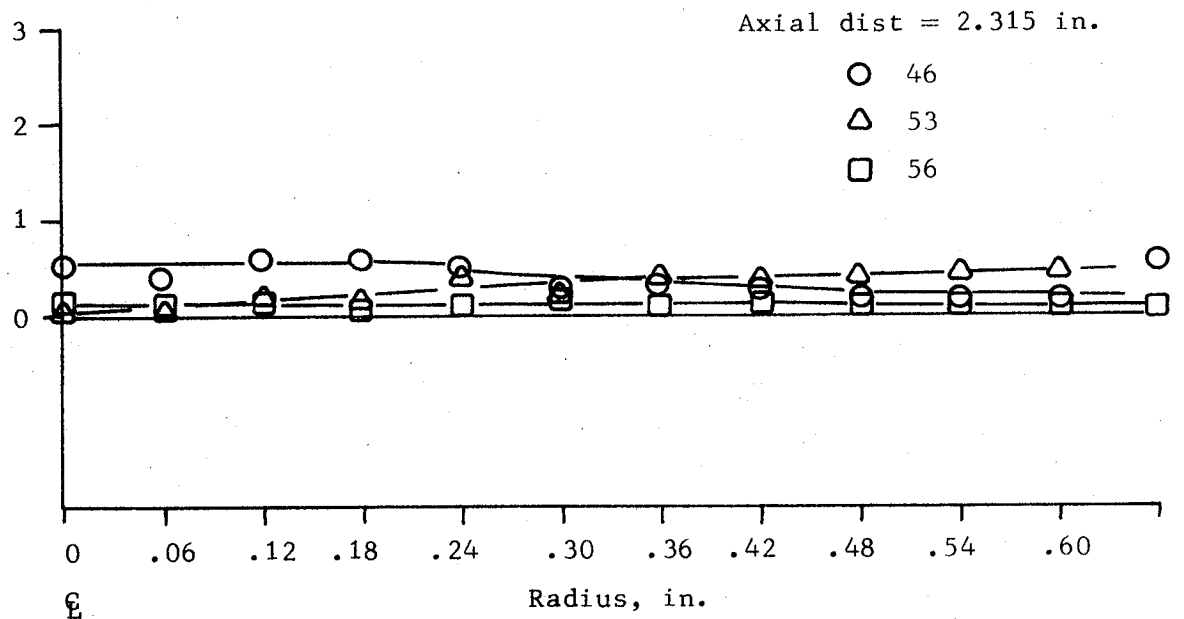
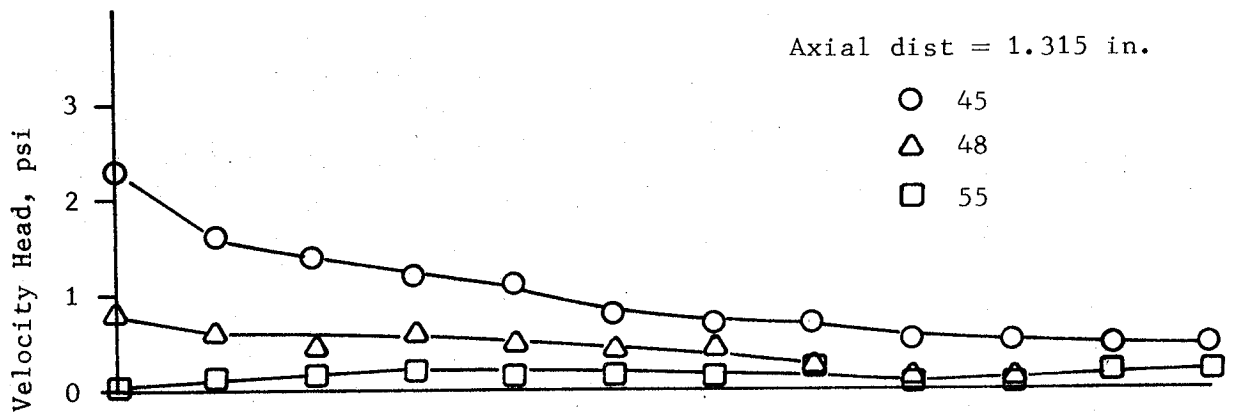
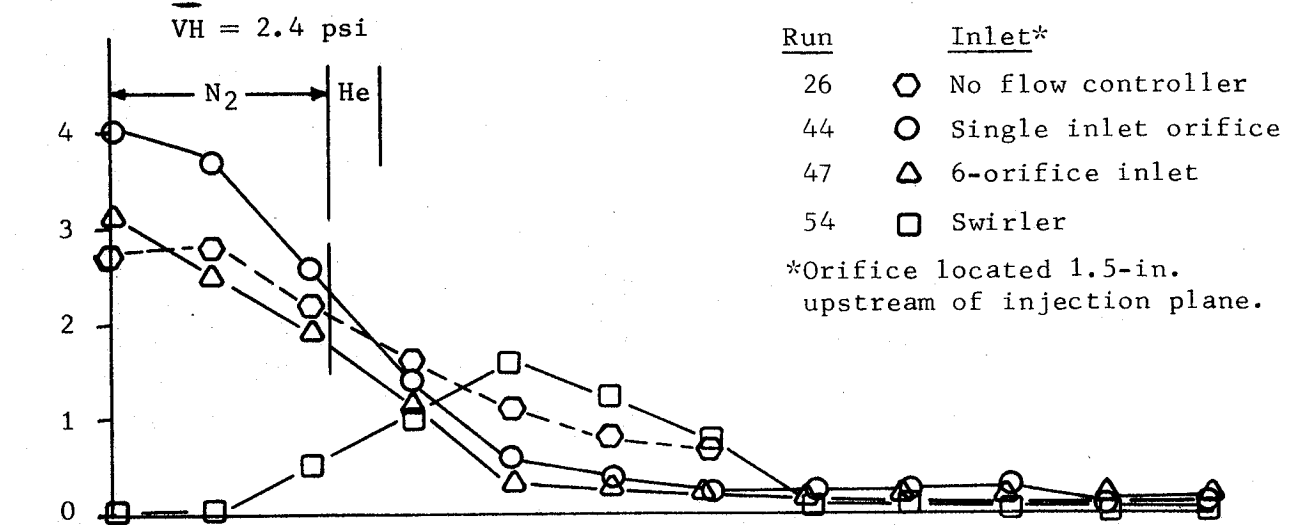


Figure VII-4. Cold Flow Profiles, Oxidizer Only

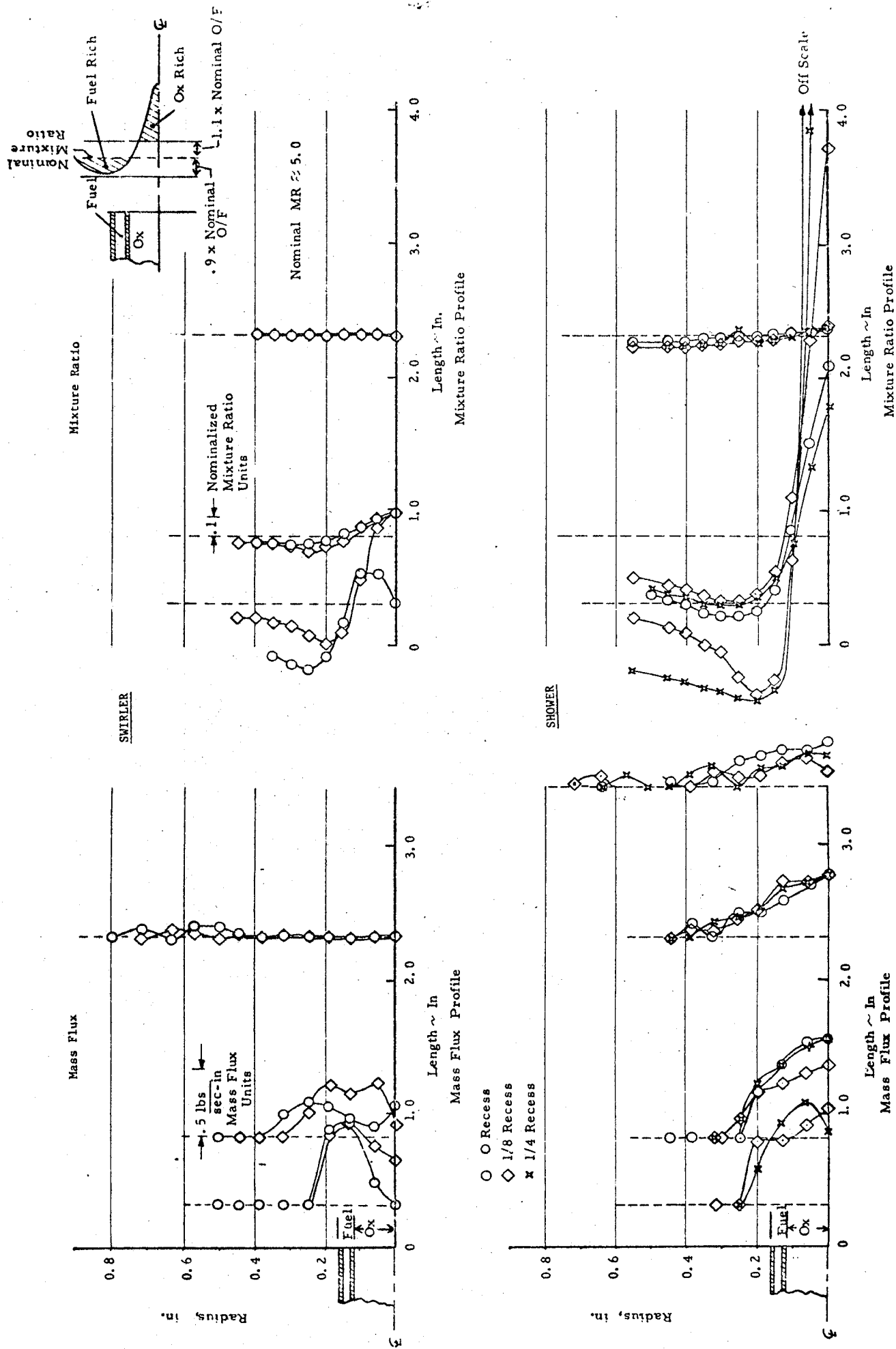


Figure VII-5. Coaxial Jet Element, Mass and Mixture Ratio Profiles

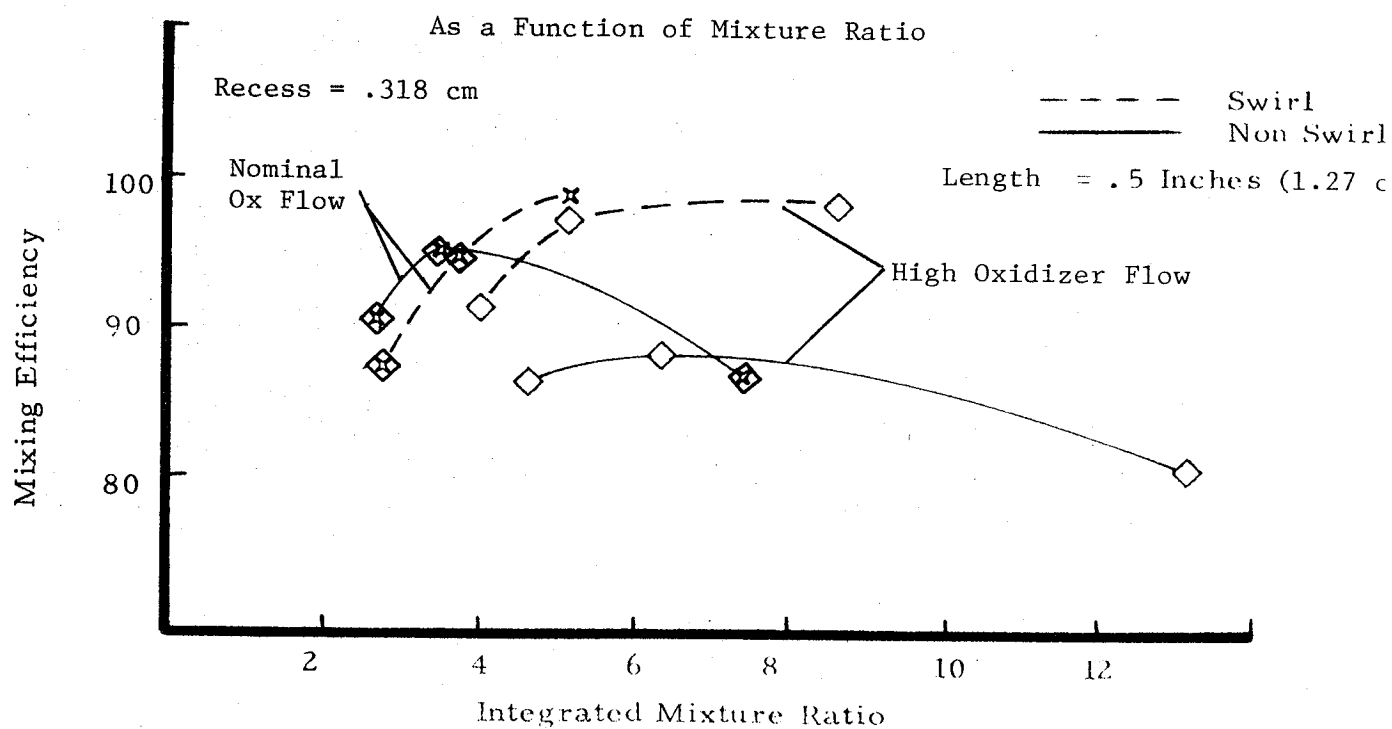
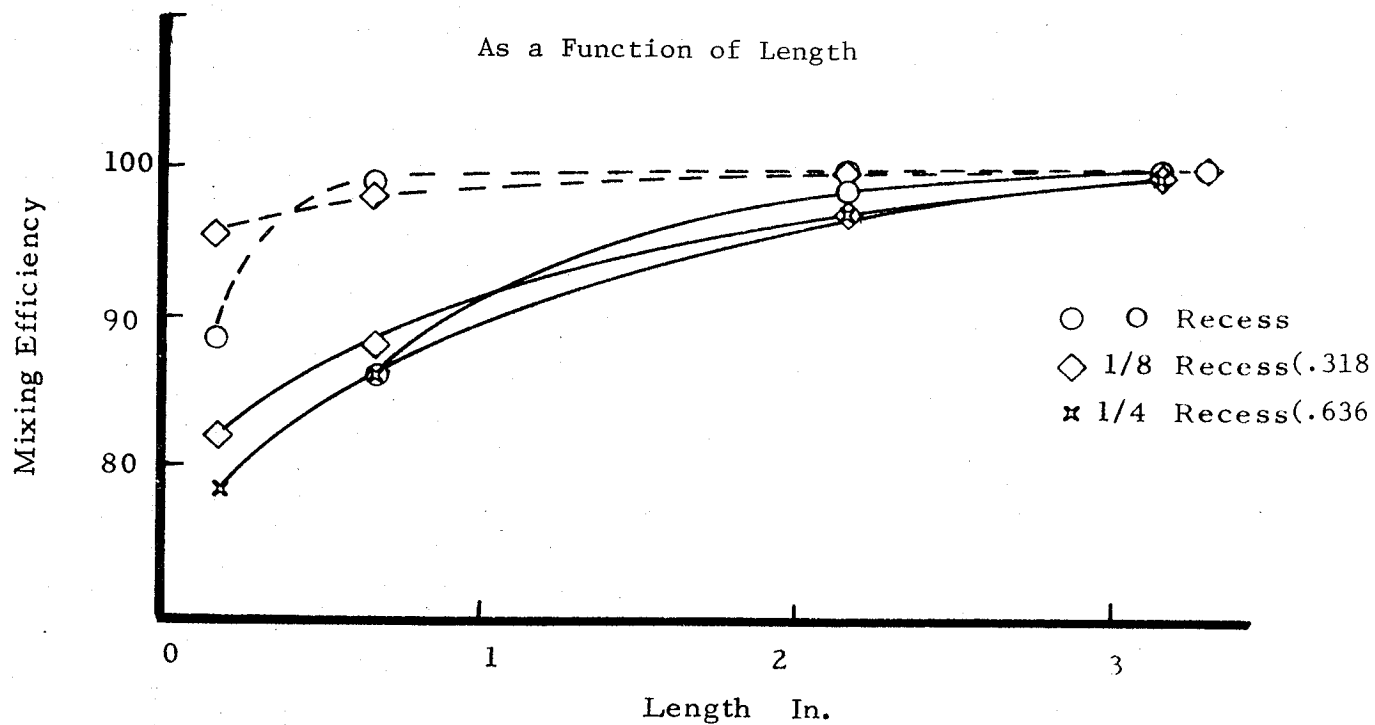


Figure VII-6. Coaxial Jet Element Mixing Efficiency

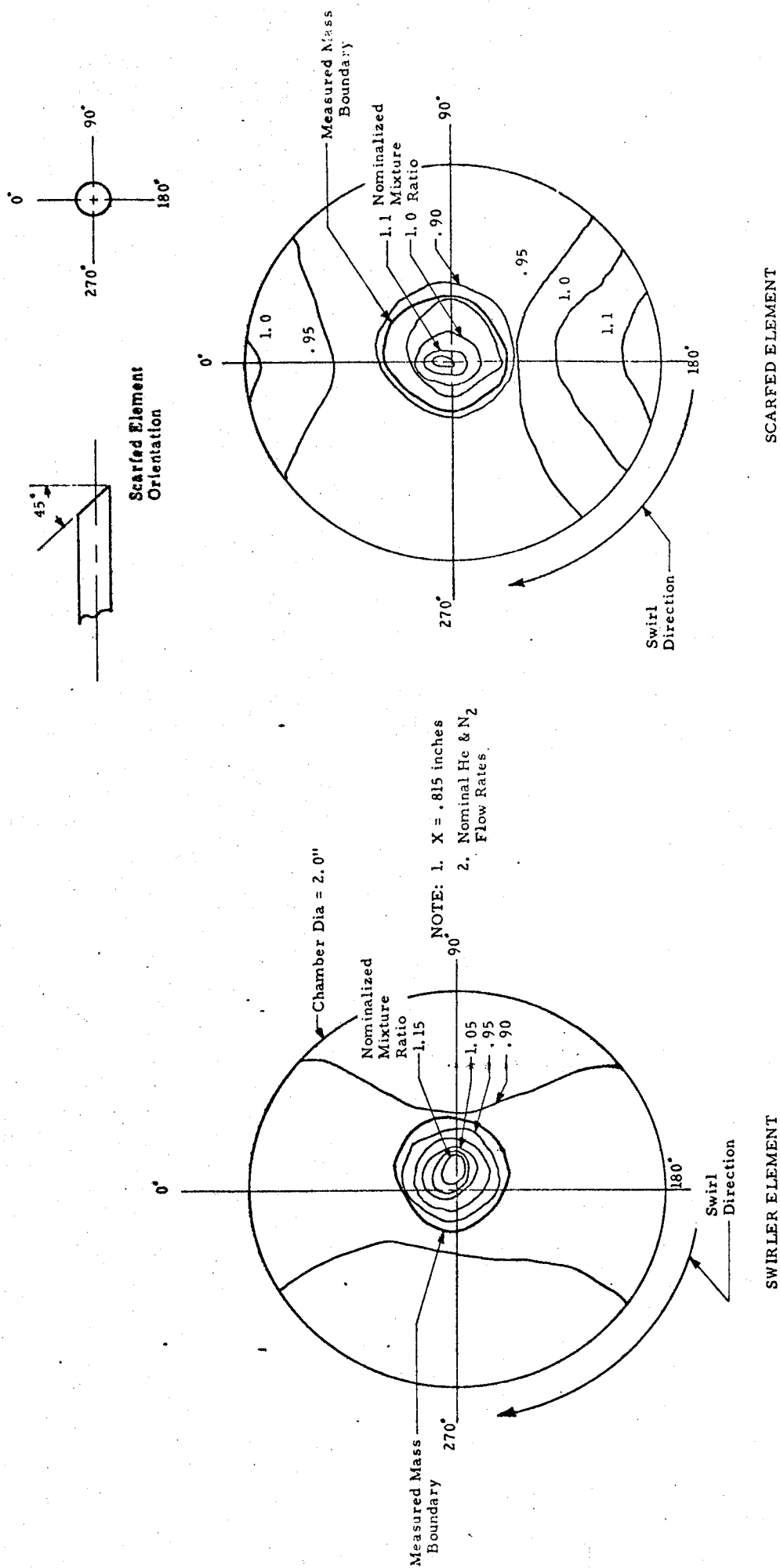


Figure VII-7. Mixture Ratio Profiles for Scarfed and Nonscarfed Swirler Elements

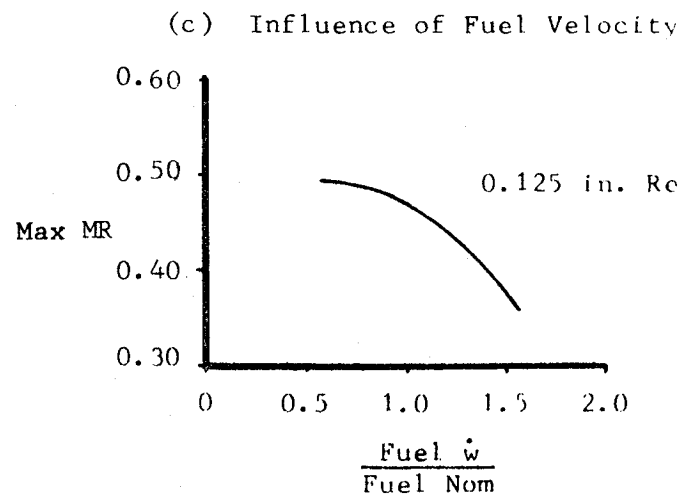
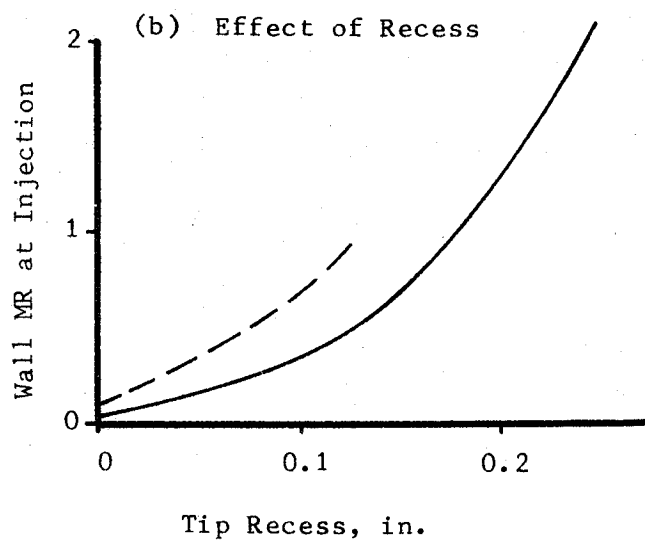
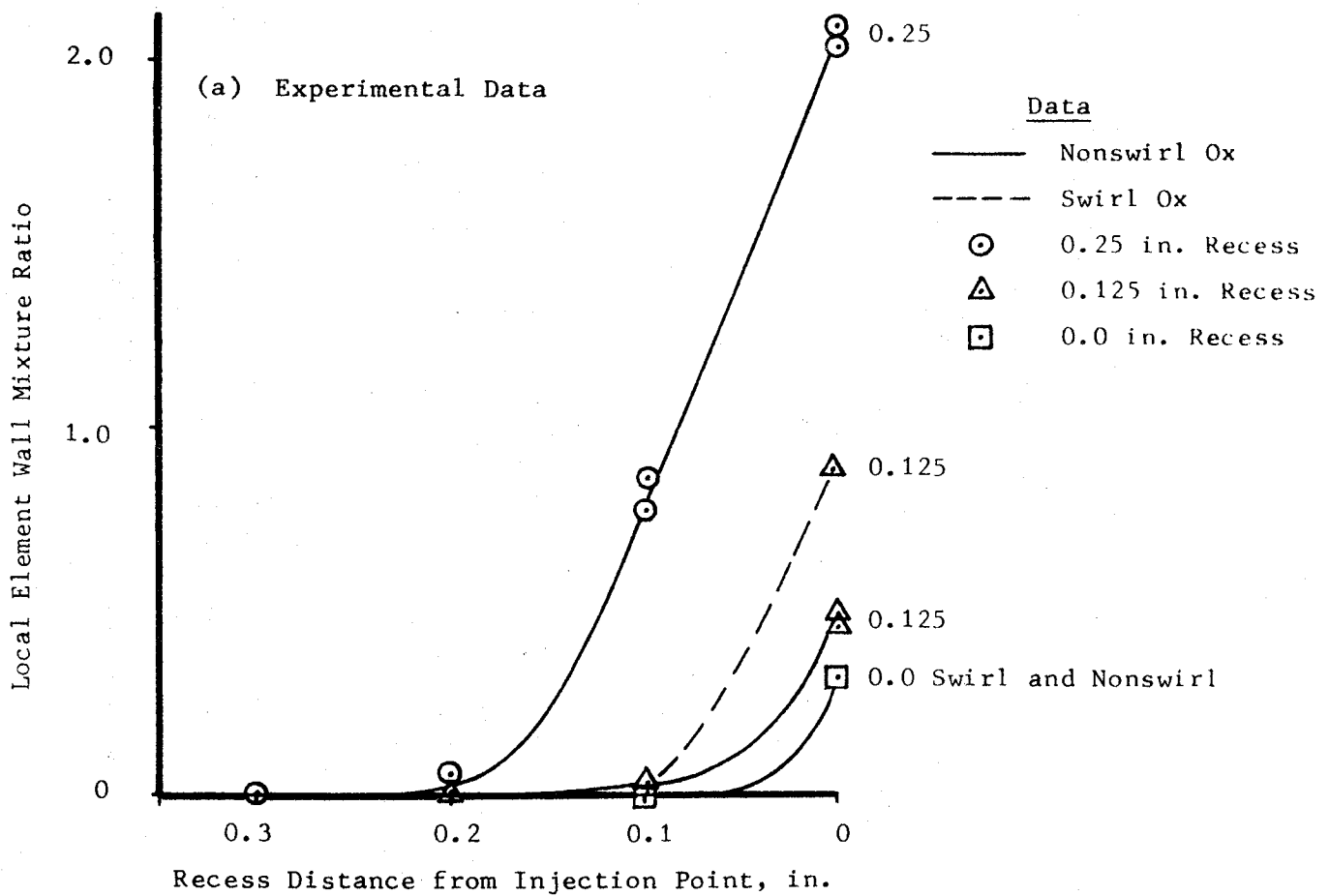


Figure VII-8. Orifice Wall Mixture Ratio vs Oxidizer Tube Recess

PREMIX ELEMENT COLD FLOW MIXING EFFICIENCY

NOTE: $R_w = O_x \text{ Dia}/\text{Fuel Slot Width}$

NOTE: All data recorded one inch from injector face

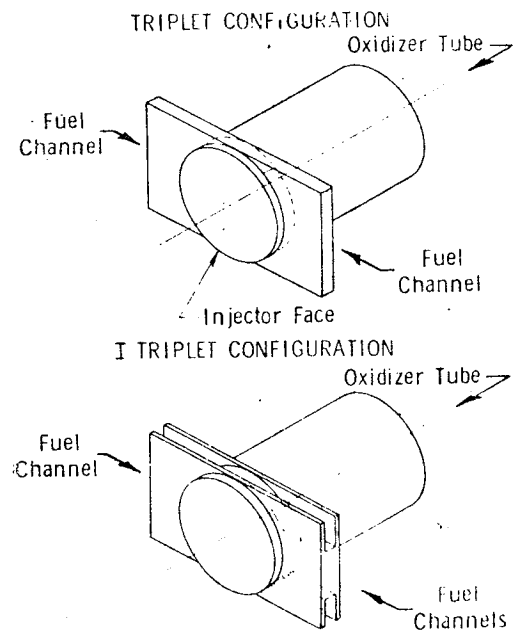
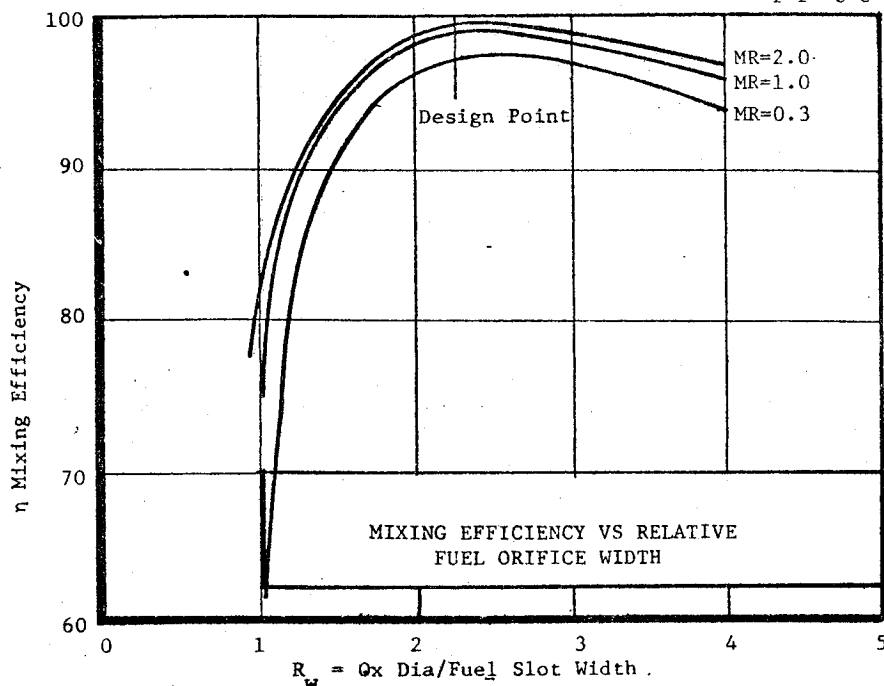
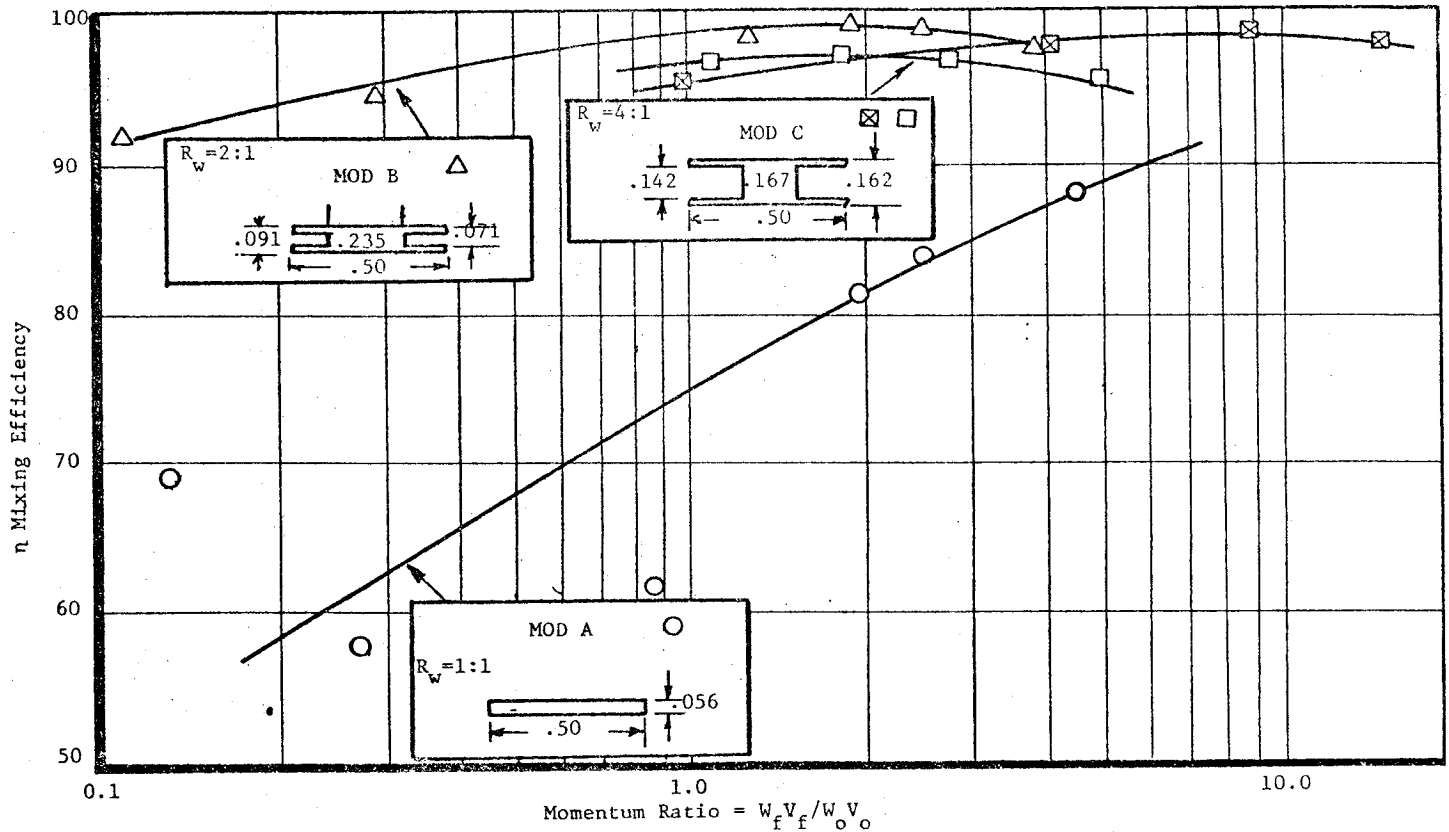
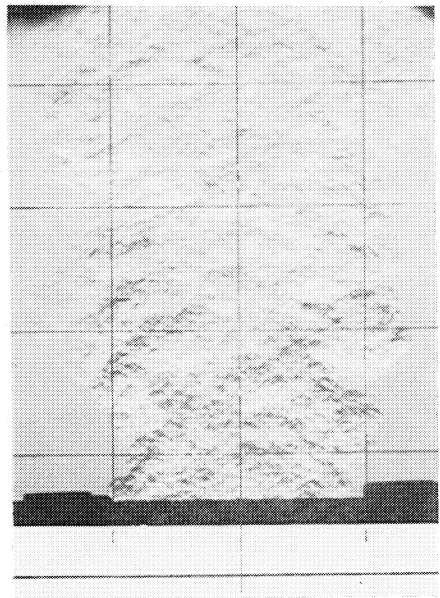
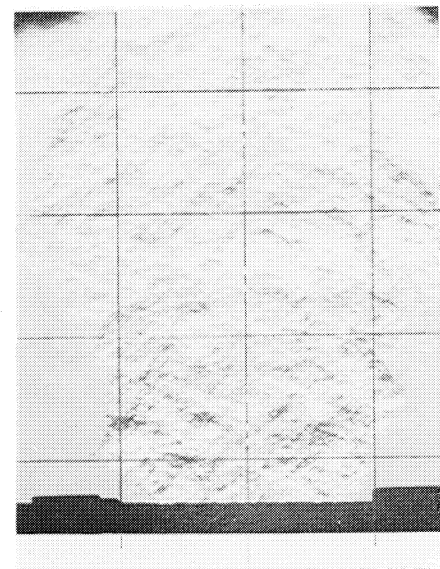


Figure VII-9. Premix Element Cold Flow Mixing Efficiency

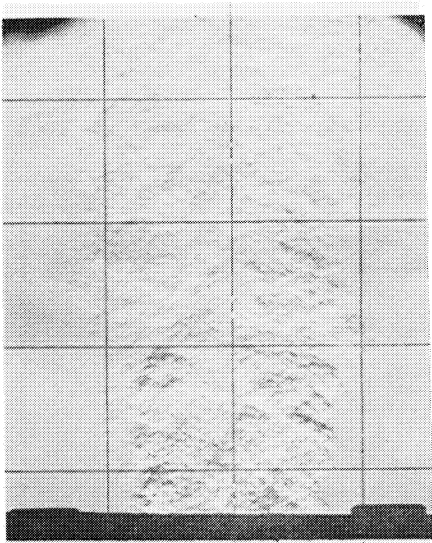
PERPENDICULAR TO FAN MAJOR AXES

$$\frac{W_f V_f}{W_o V_o} = 0.06$$

0.24



0.54



PARALLEL TO FAN MAJOR AXES

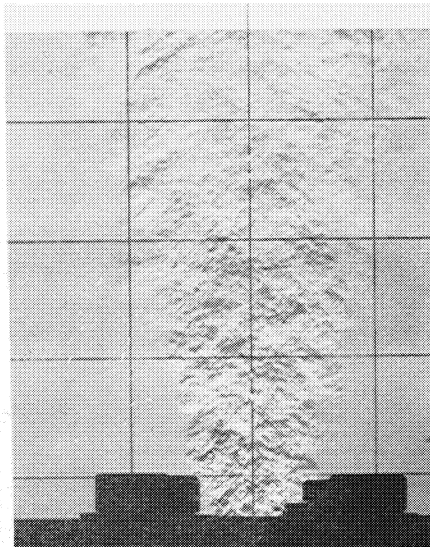
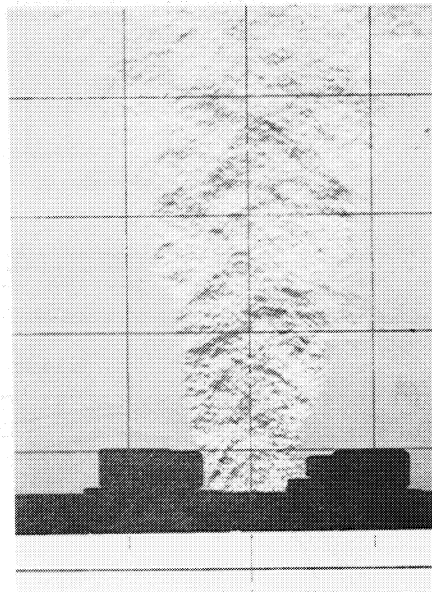
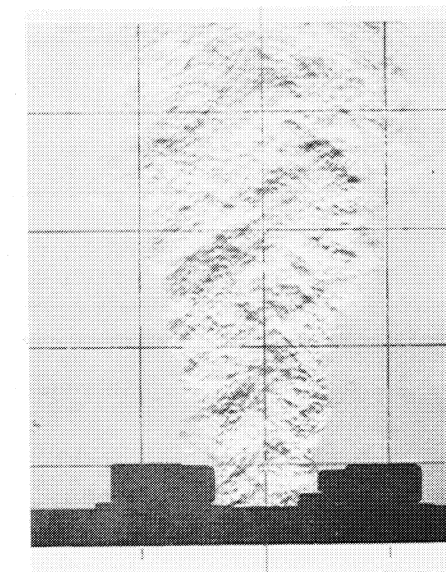


Figure VII-10. Premix Element Schlieren Photographs

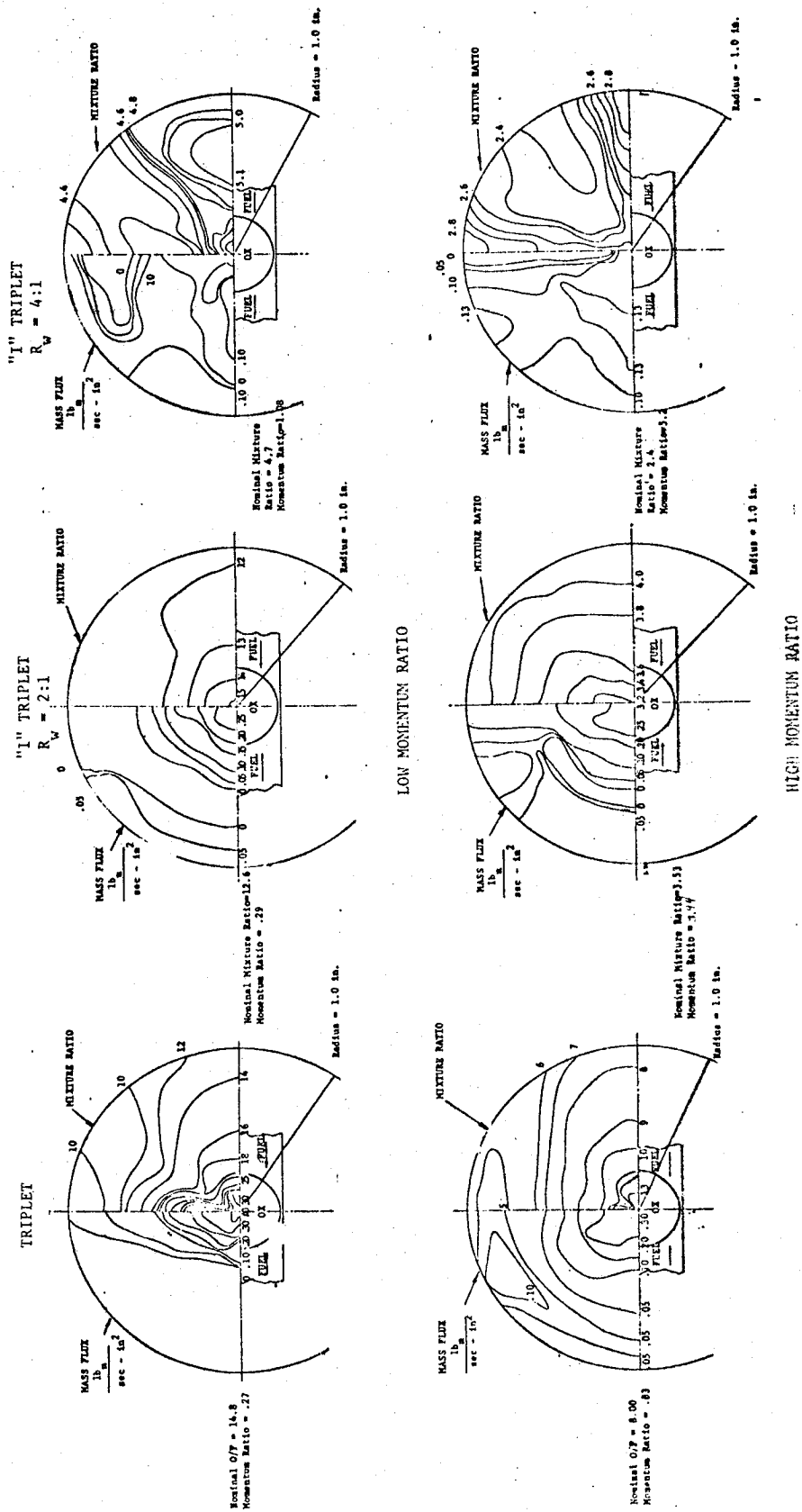
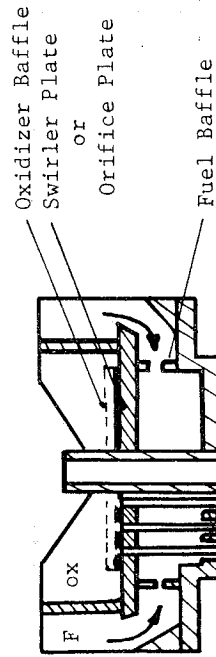
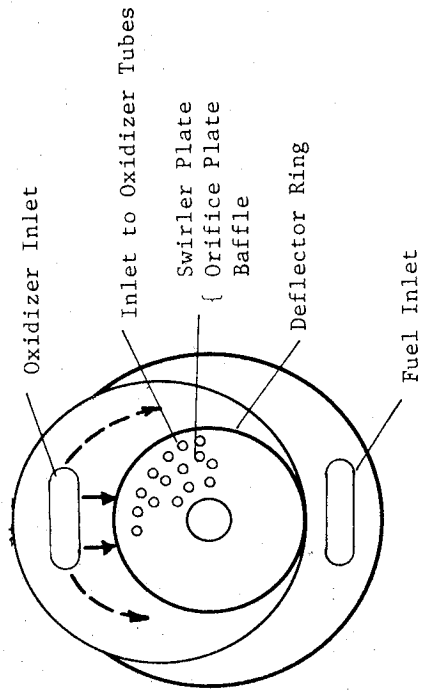
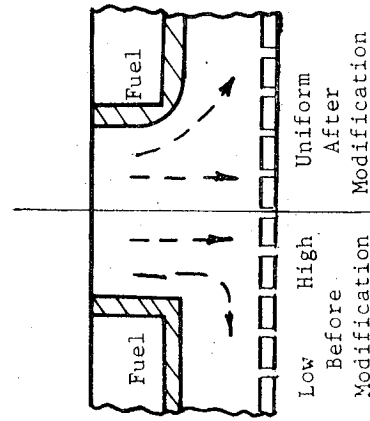
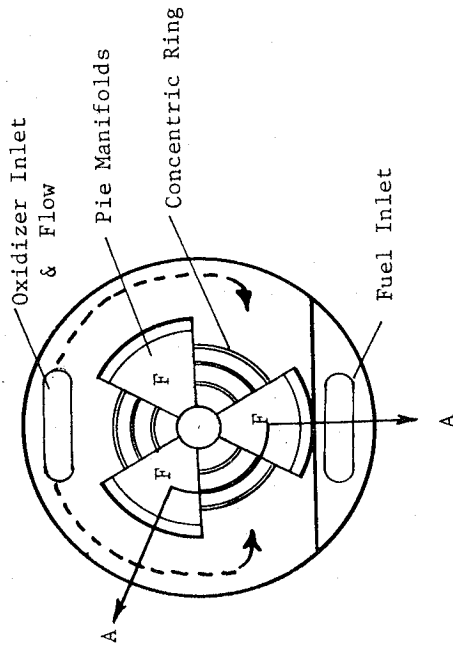


Figure VII-11. Premix Element Mass and Mixture Ratio Profiles



Flooded Back and Cross Flow
Manifolding
42-Element Injector



Pie and Concentric Ring
Manifolding
72-Element Injector

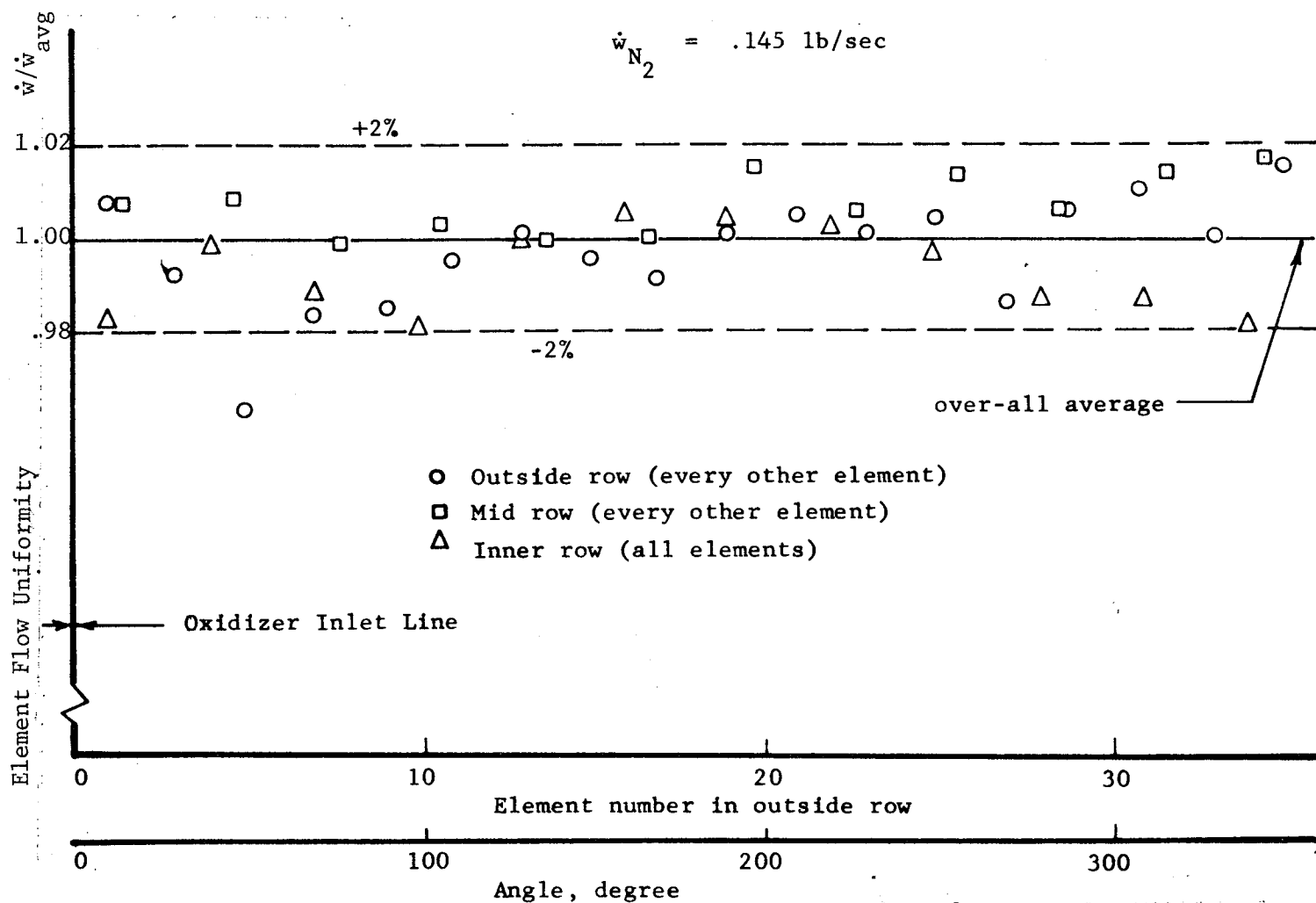
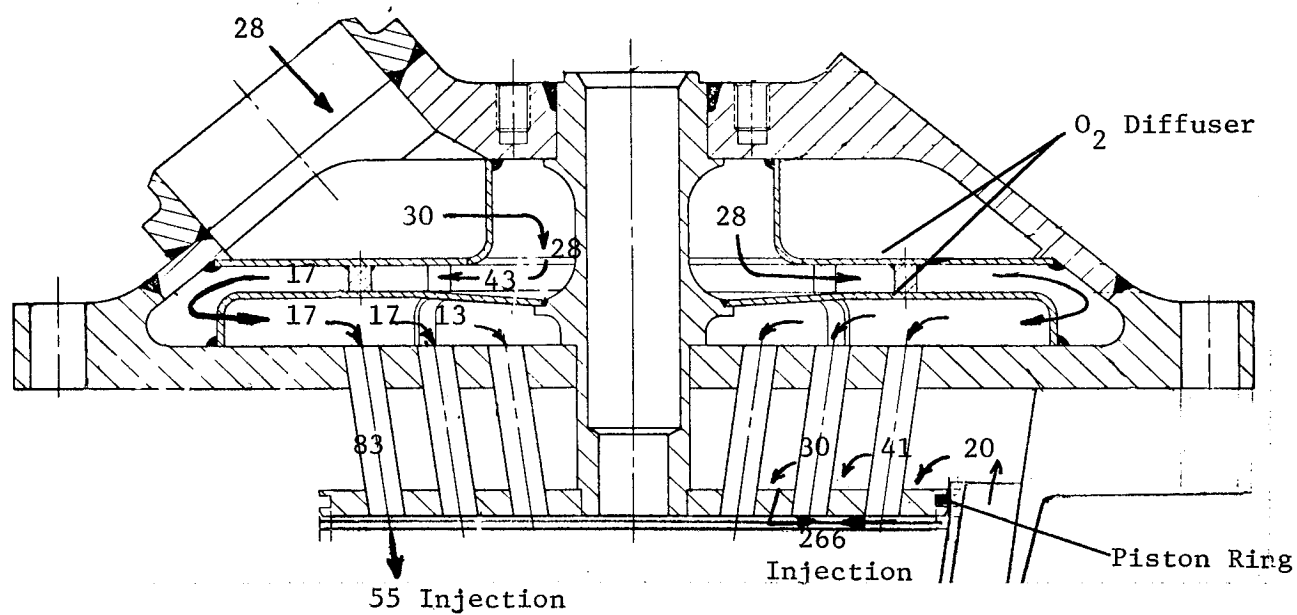


Figure VII-13. Phase II Premix Injector Manifold and Cold Flow Results

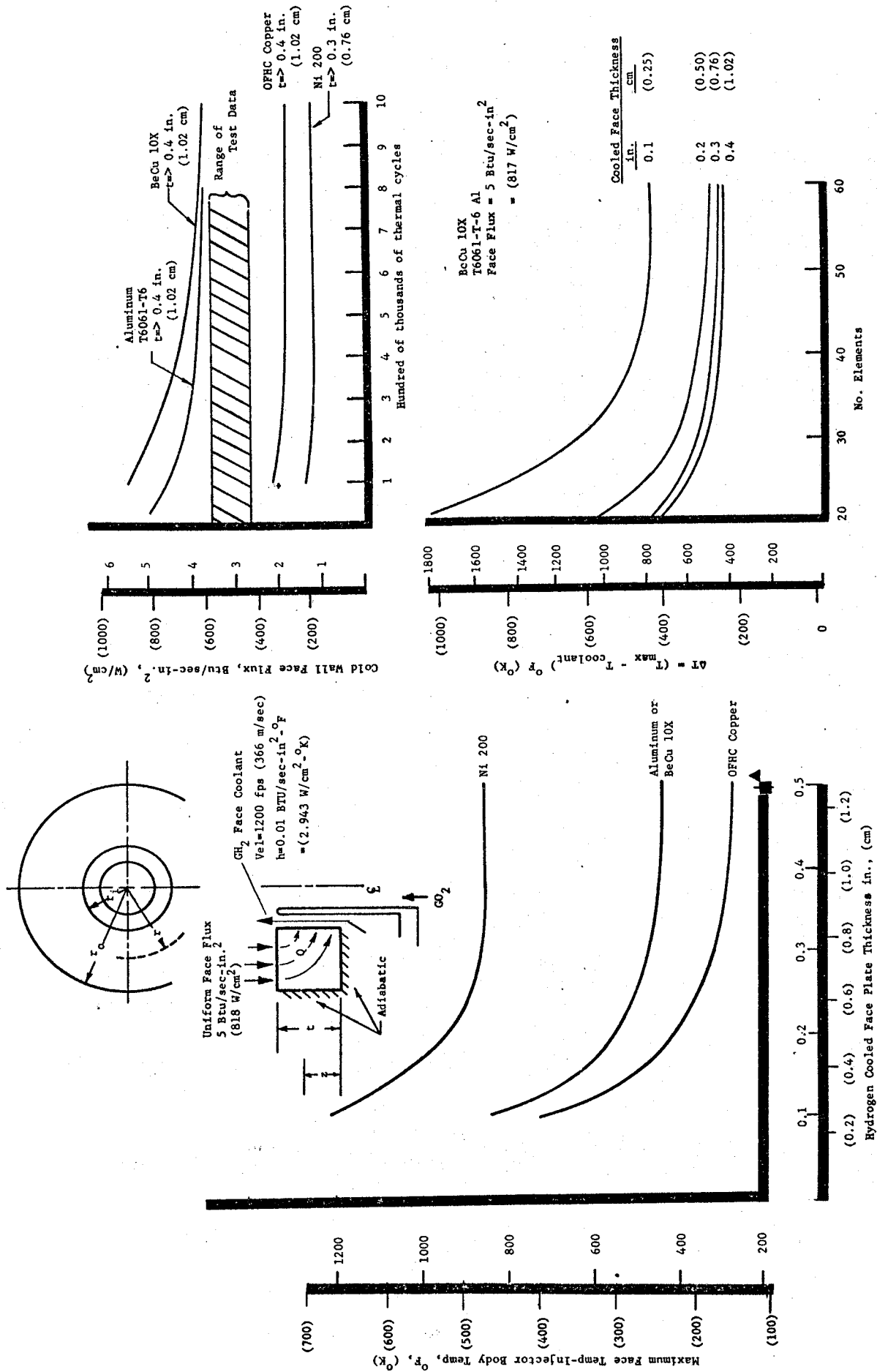
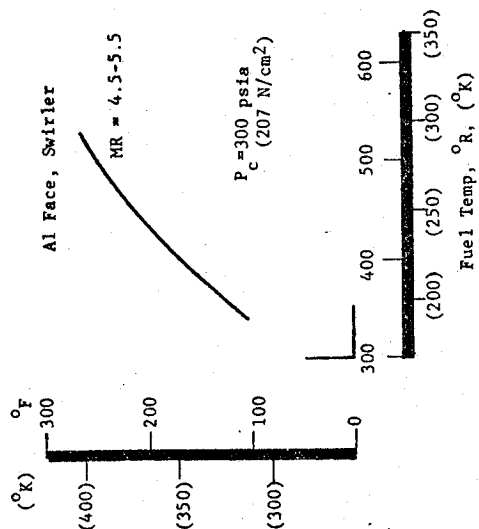
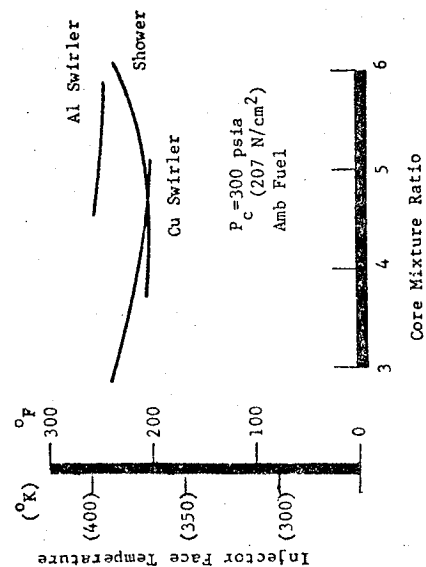


Figure VII-14. Coaxial Injector Face Cooling Optimization Analysis

STEADY STATE



TRANSIENT

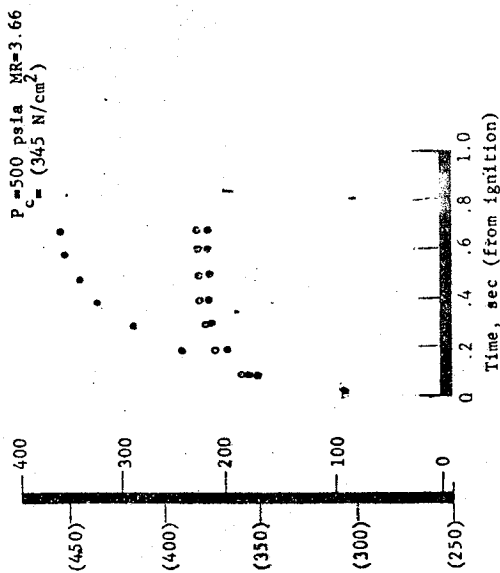
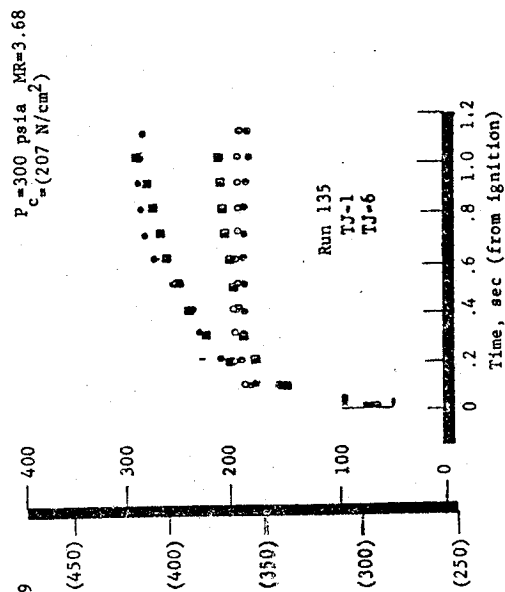
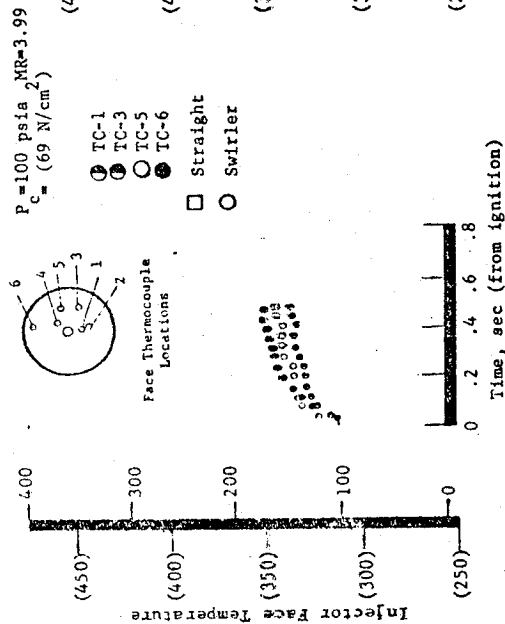
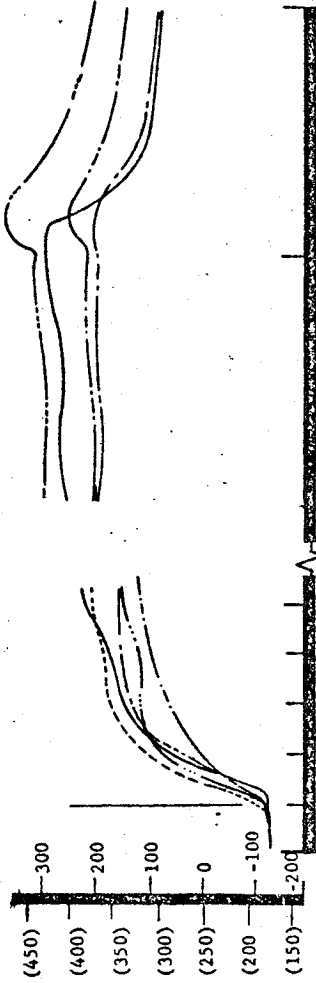


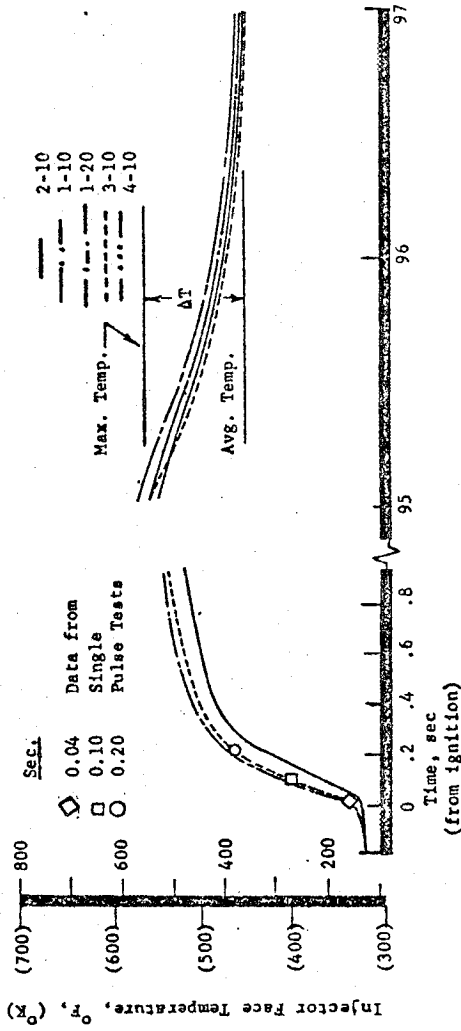
Figure VII-15. Coaxial Injector Experimental Face Temperatures.

Test Conditions

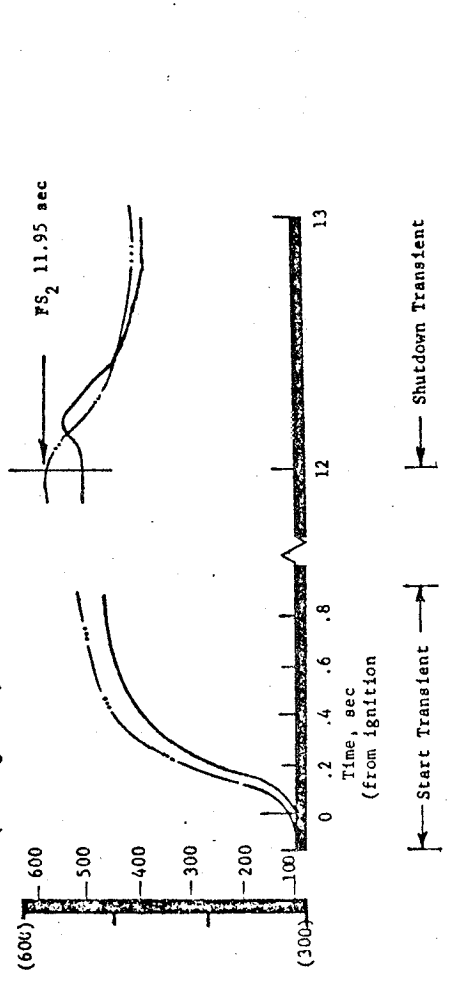
Nominal conditions
Cold propellants (4-011)
300 psia



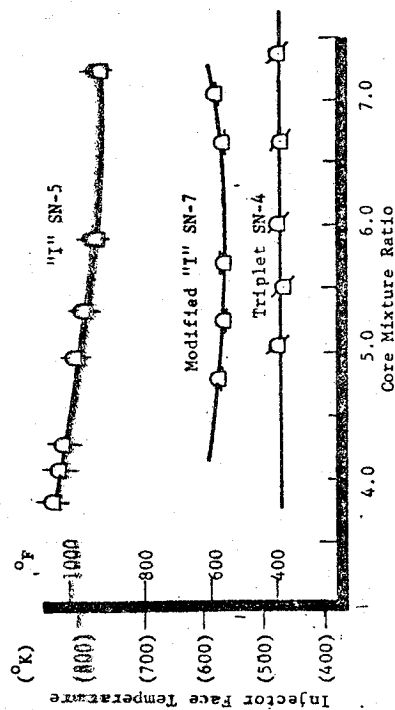
Maximum propellant temp 590°R (326°C)
300 psia (Test 04-012)



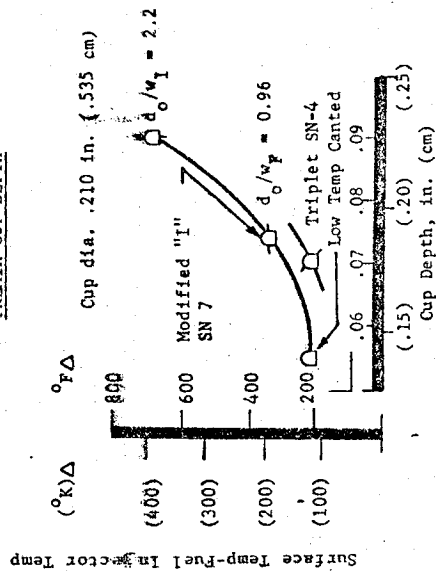
Maximum pressure 450 psia
Maximum propellant temp 560°R (311°C)
Test 04-013



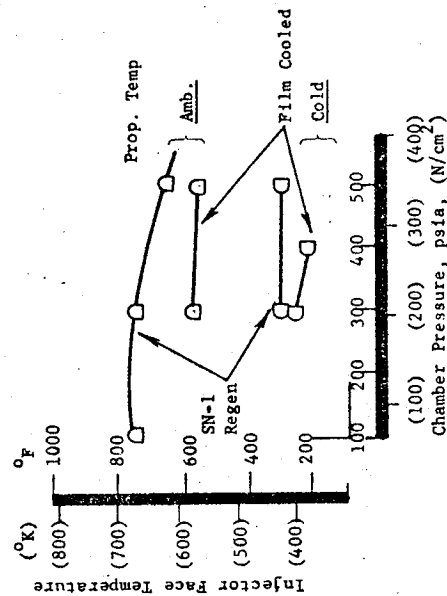
MIXTURE RATIO EFFECTS



PREMIX CUP DEPTH



CHAMBER PRESSURE EFFECTS



PROPELLANT INLET TEMP EFFECTS

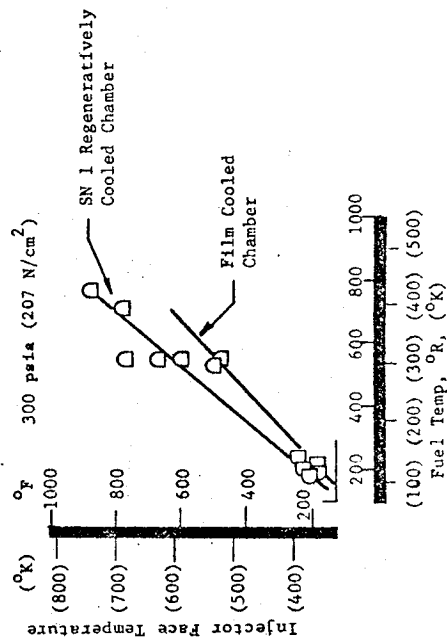
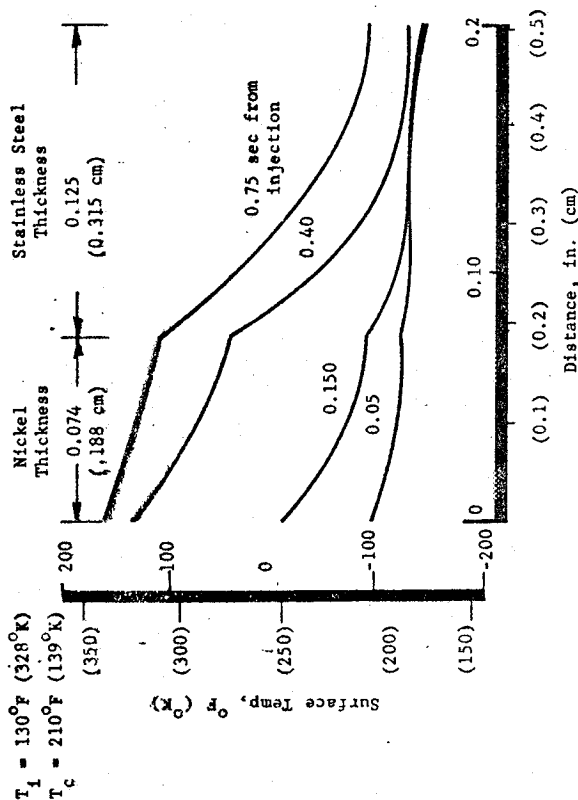
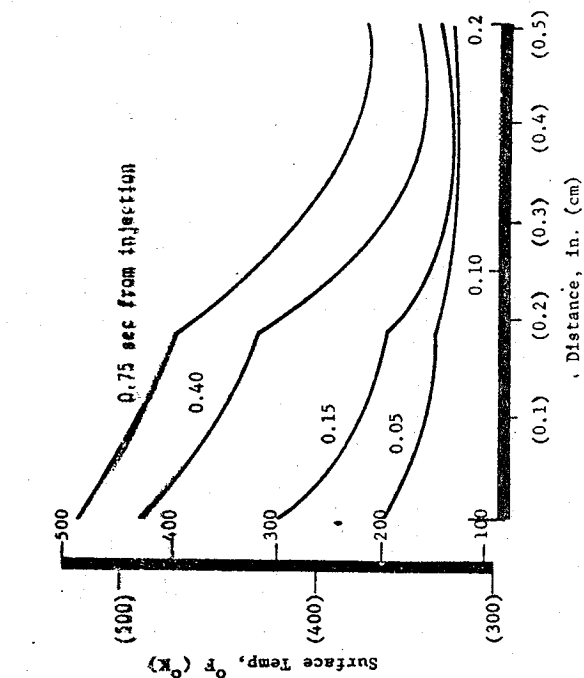


Figure VII-17. Premix Injector Steady-State Face Temperatures

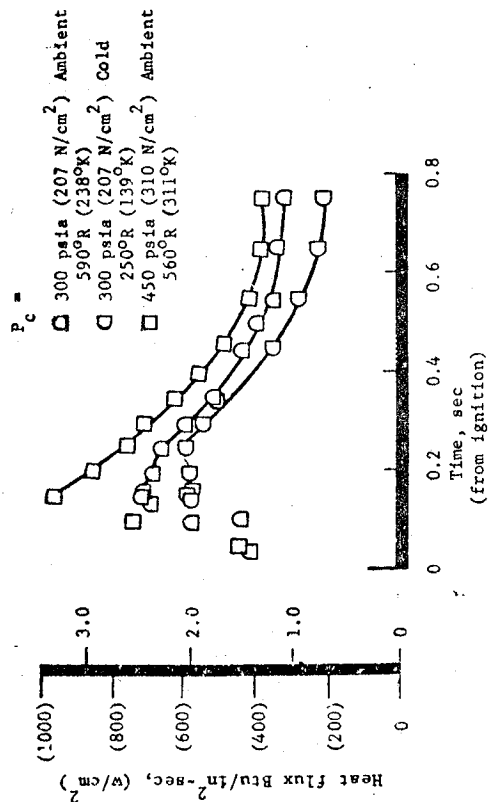
TEST #04-018 COLD PROPELLANTS



TEST #04-012 WARM PROPELLANTS



FACE HEAT FLUX



EFFECTIVE TEMPERATURE GRADIENT

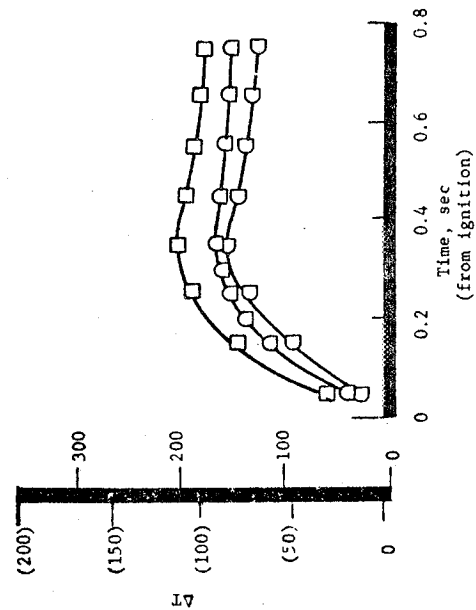
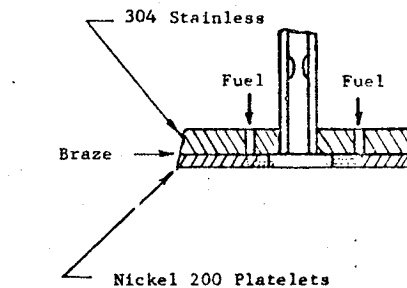
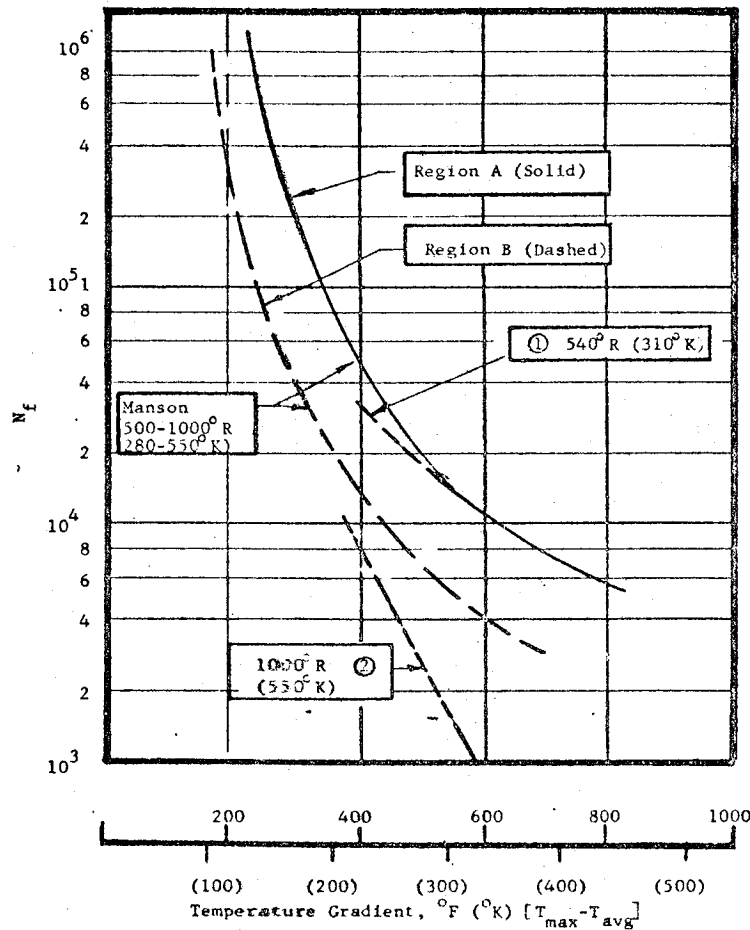
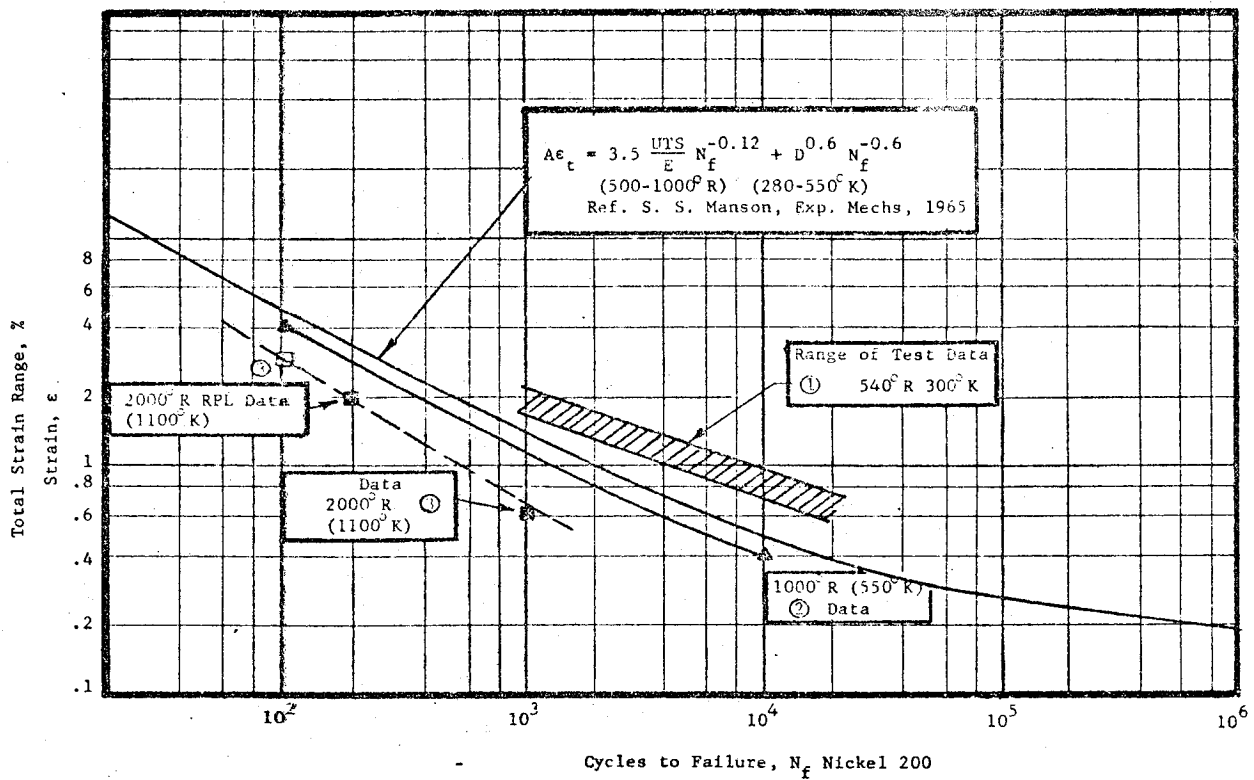
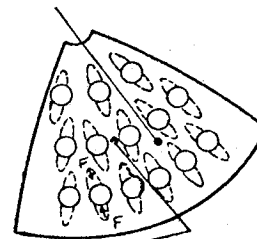


Figure VII-18. Modified "I" Premix, Face Thermal Profiles and Heat Flux



Region B
 between rows of elements



Region A
 between elements

References

- ① Coffin, Jr., L.F., "Experimental Support for Generalized Equation Predicting Low Cycle Fatigue," J. Basic Engr., ASME Trans., Dec. 1962.
- ② Majors, Jr., H., "Thermal and Mechanical Fatigue of Nickel and Titanium," Trans. ASM, Vol. 51, 1958.
- ③ Anon., "Test Report on Fatigue-Testing of Nickel-200 Panels Hypersonic Research Engine, NASA CR-66842, Jan. 1969

Figure VII-19. Premix Injector Thermal Strain vs Fatigue Life

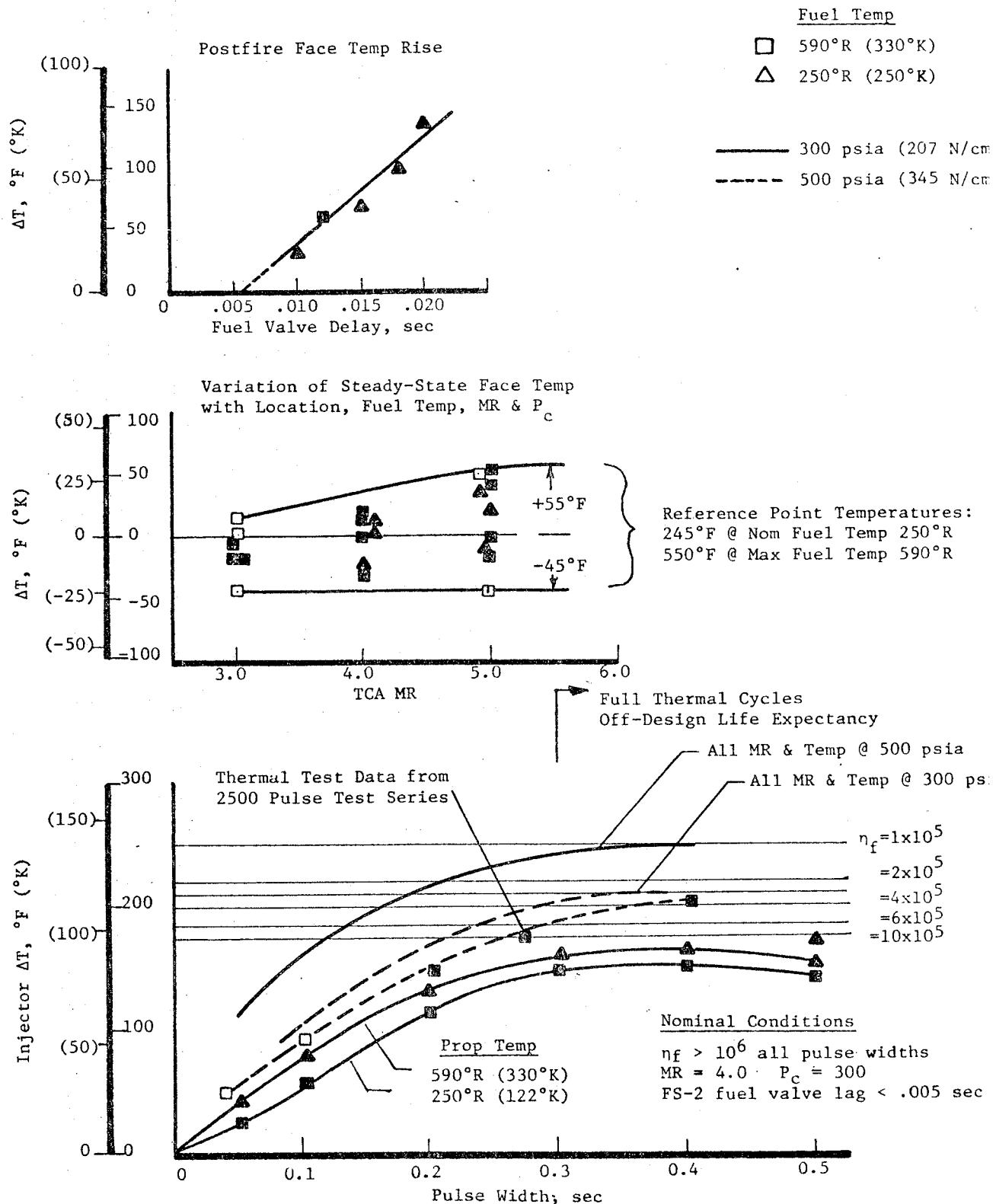


Figure VII-20. Predicted Life of Modified Premix "I" Injector

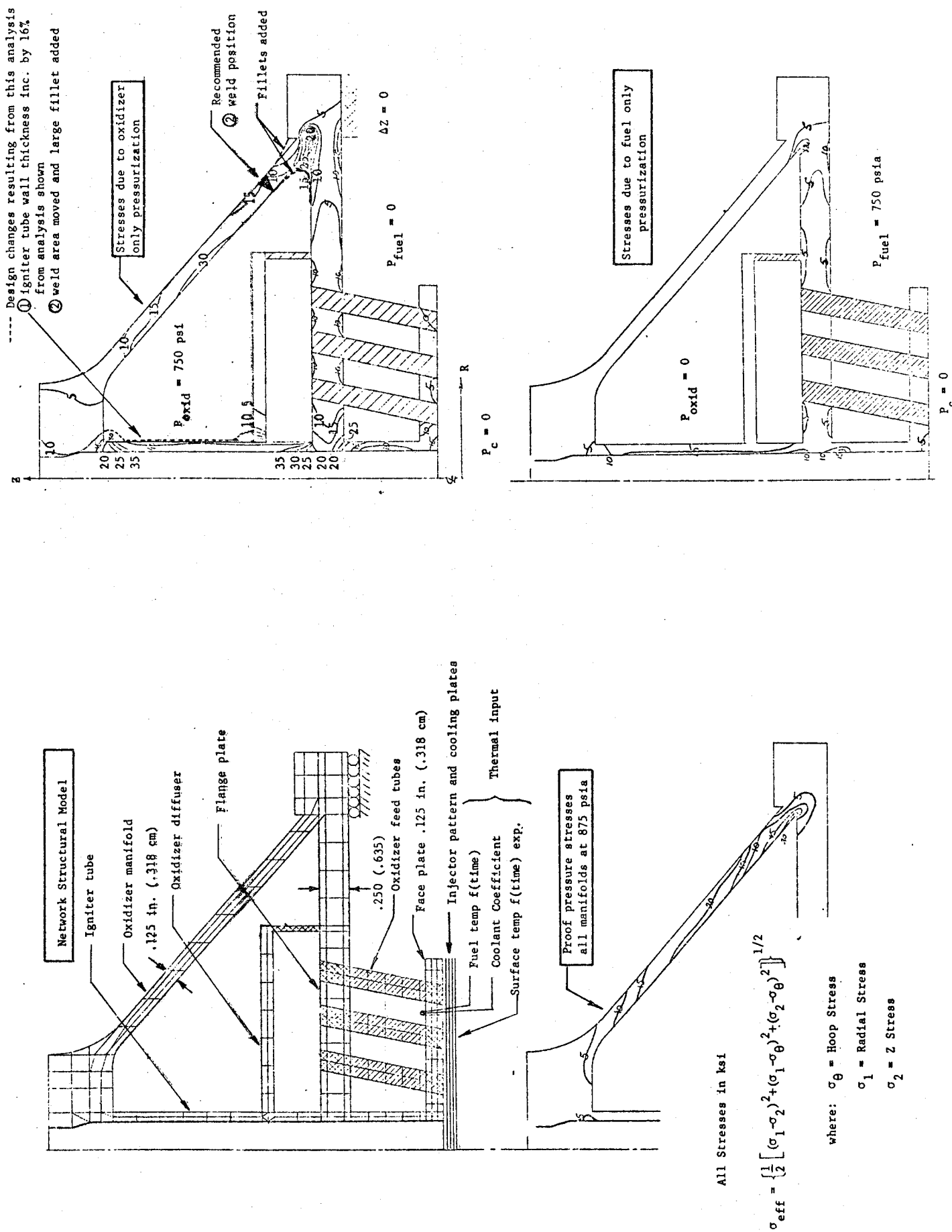


Figure VII-21. Premix Injector Structural Analysis

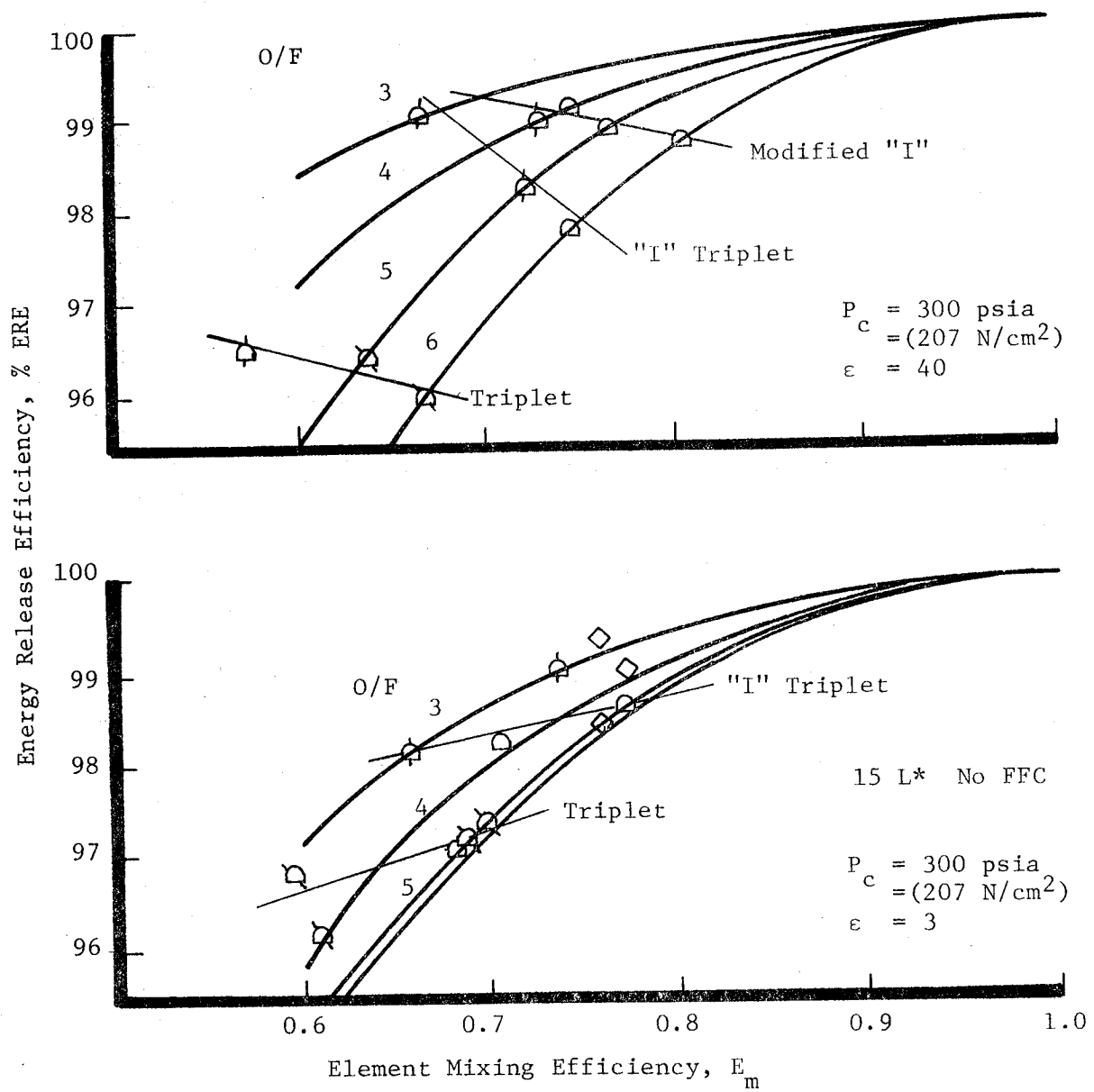
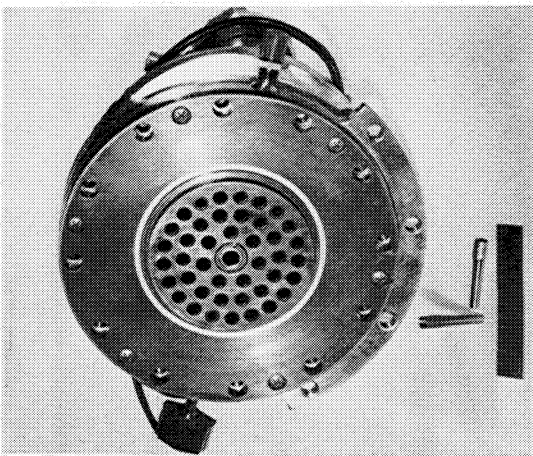
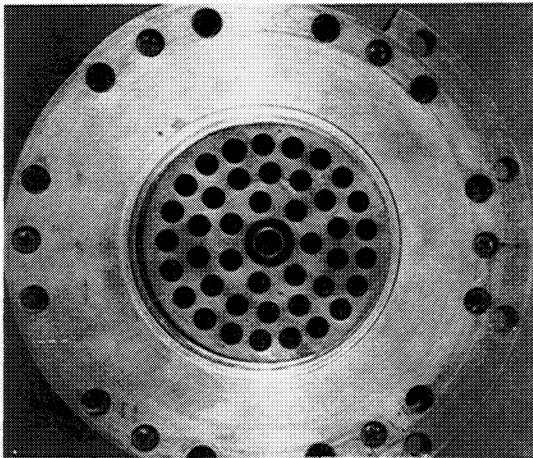


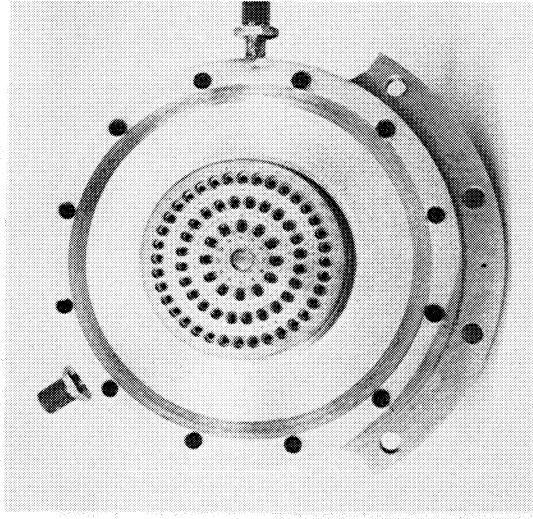
Figure VII-22. Effect of Element Mixing Efficiency on ERE



Swirler Coaxial Element
No Film Cooling



Swirler Coaxial Element
10% FFC, Reduced Swirl



Premix Triplet
No Film Cooling

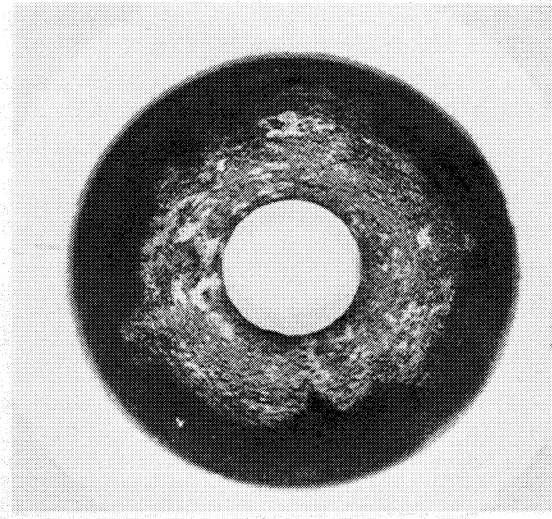
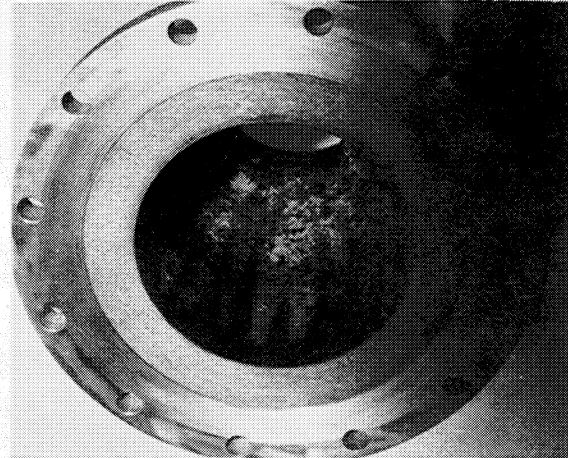
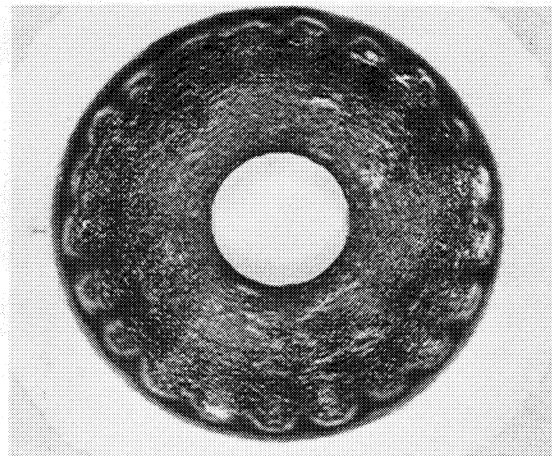
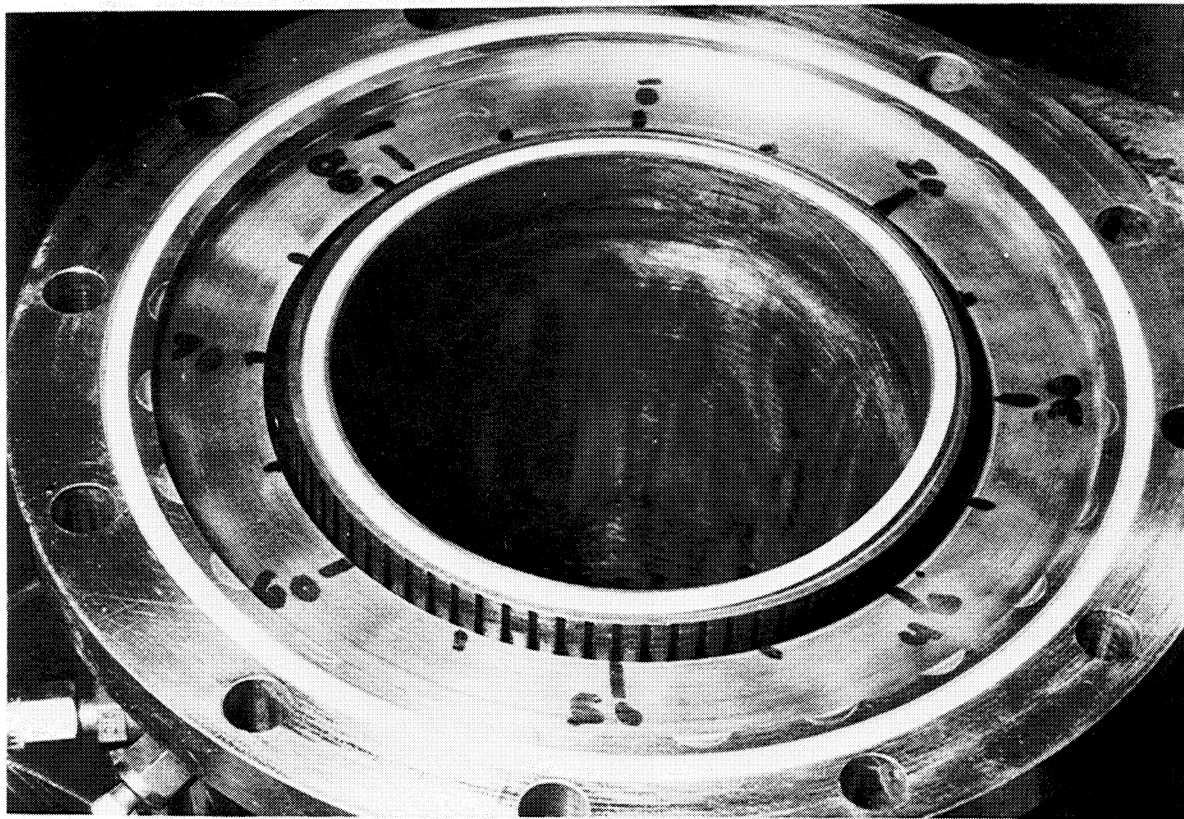
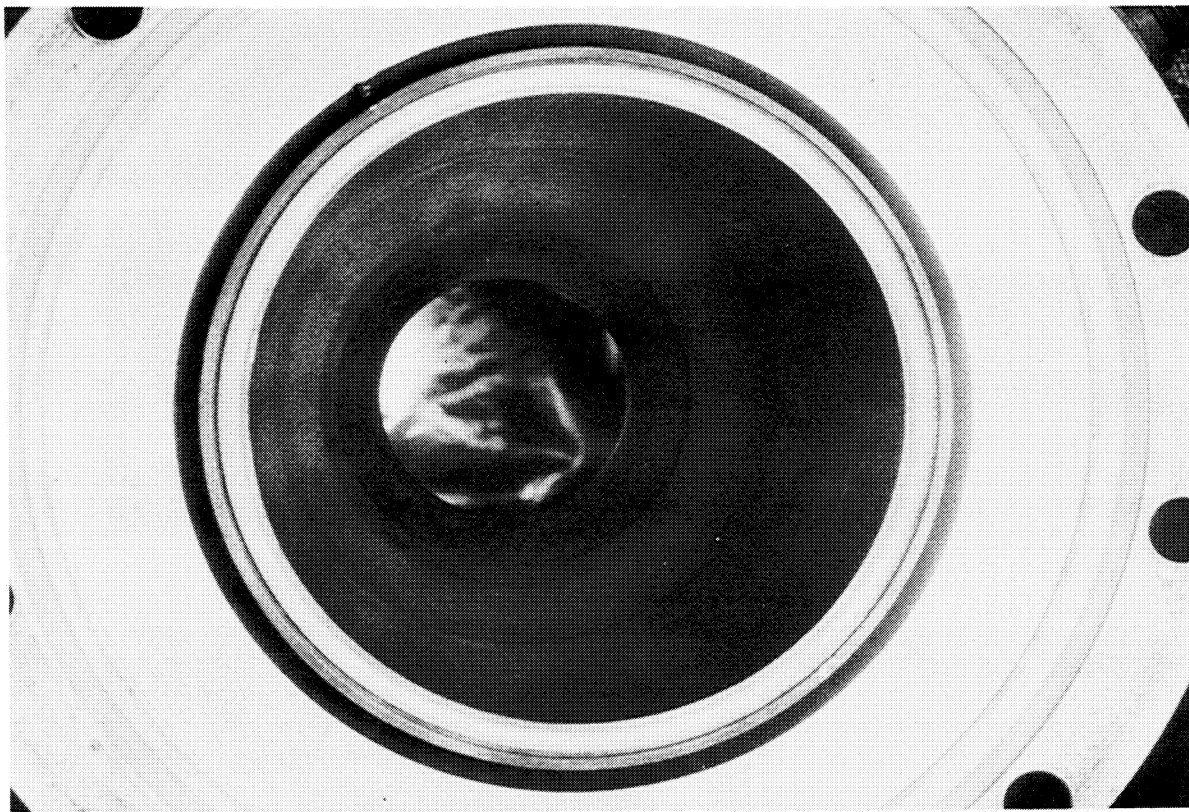


Figure VII-23. Streak Chamber Compatibility

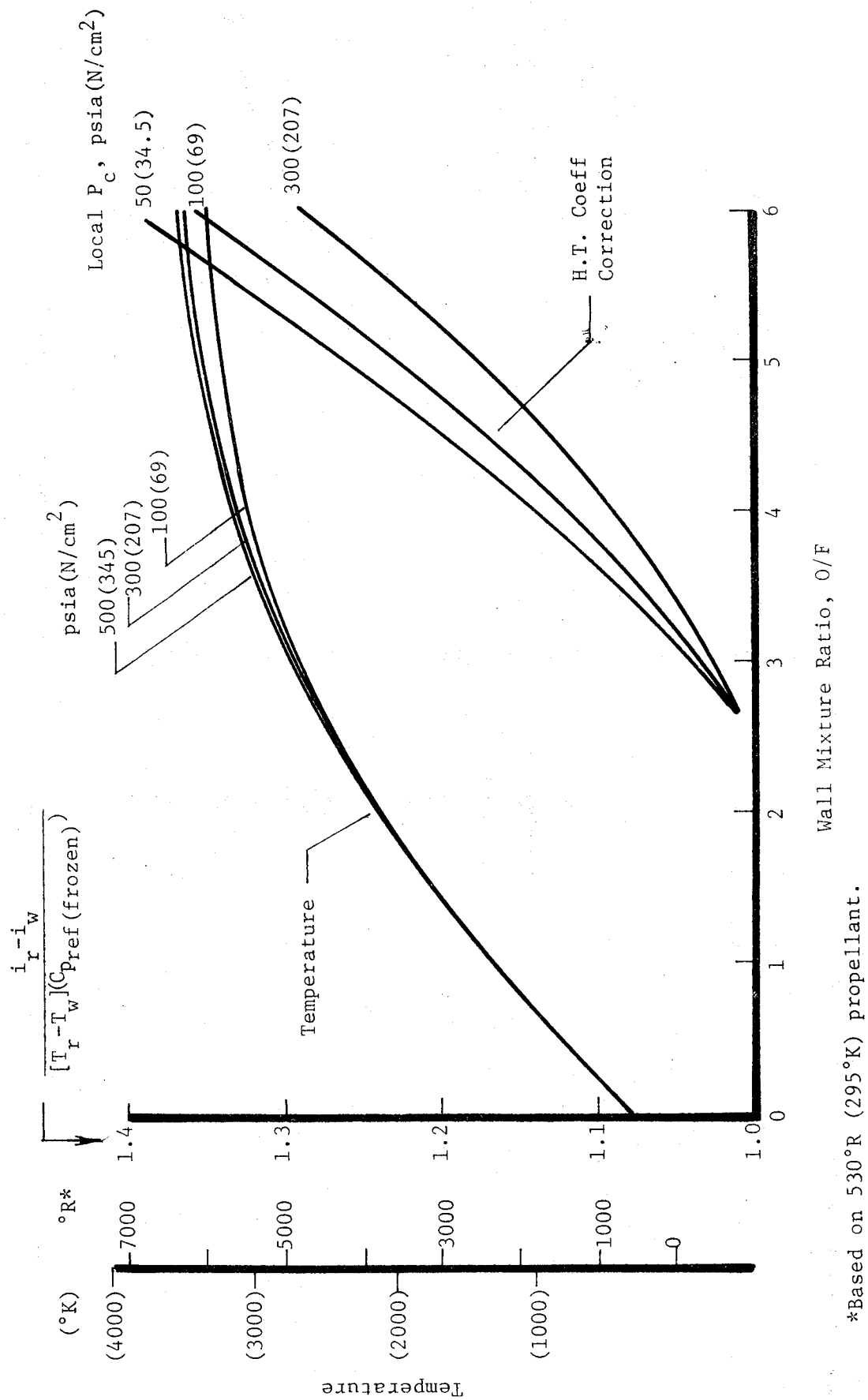


40:1 Film-Cooled Chamber with SN 4 Triplet Injector
After Test 03-023



40:1 Film-Cooled Chamber with SN 7 Modified "I" Premix
Injector After Test 05-038

Figure VII-24. Cooled Chamber Compatibility



*Based on 530°R (295°K) propellant.

Figure VII-25. Combustion Temperature and Enthalpy Heat Transfer Coefficient Correction for Oxygen/Hydrogen

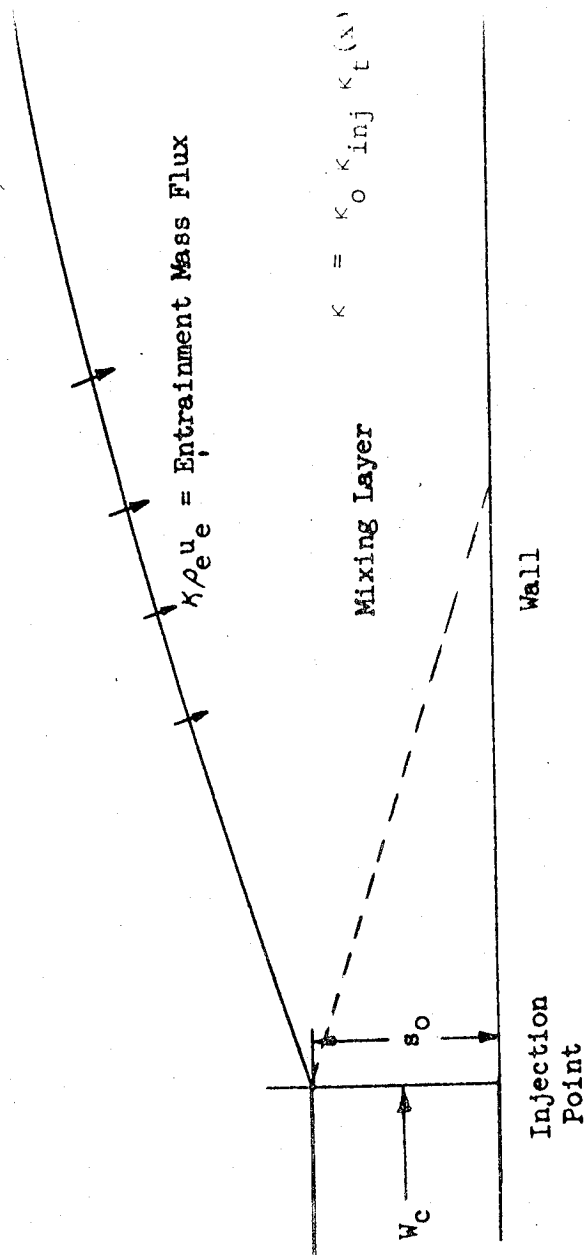
enthalpy

$$\eta = \frac{H_e - H_{aw}}{H_e - H_{in}}$$

Main Stream



$\rho_e u_e = \text{Mass Velocity}$



In which κ_0 is the entrainment fraction with laboratory conditions and acceleration; κ_{inj} accounts for increased free-stream turbulence and acceleration with liquid rocket injectors; and $\kappa_t(x)$ represents the turning of start of convergence. The bracketed term accounts for flow acceleration.

Figure VII-26. Film Cooling Mixing Model

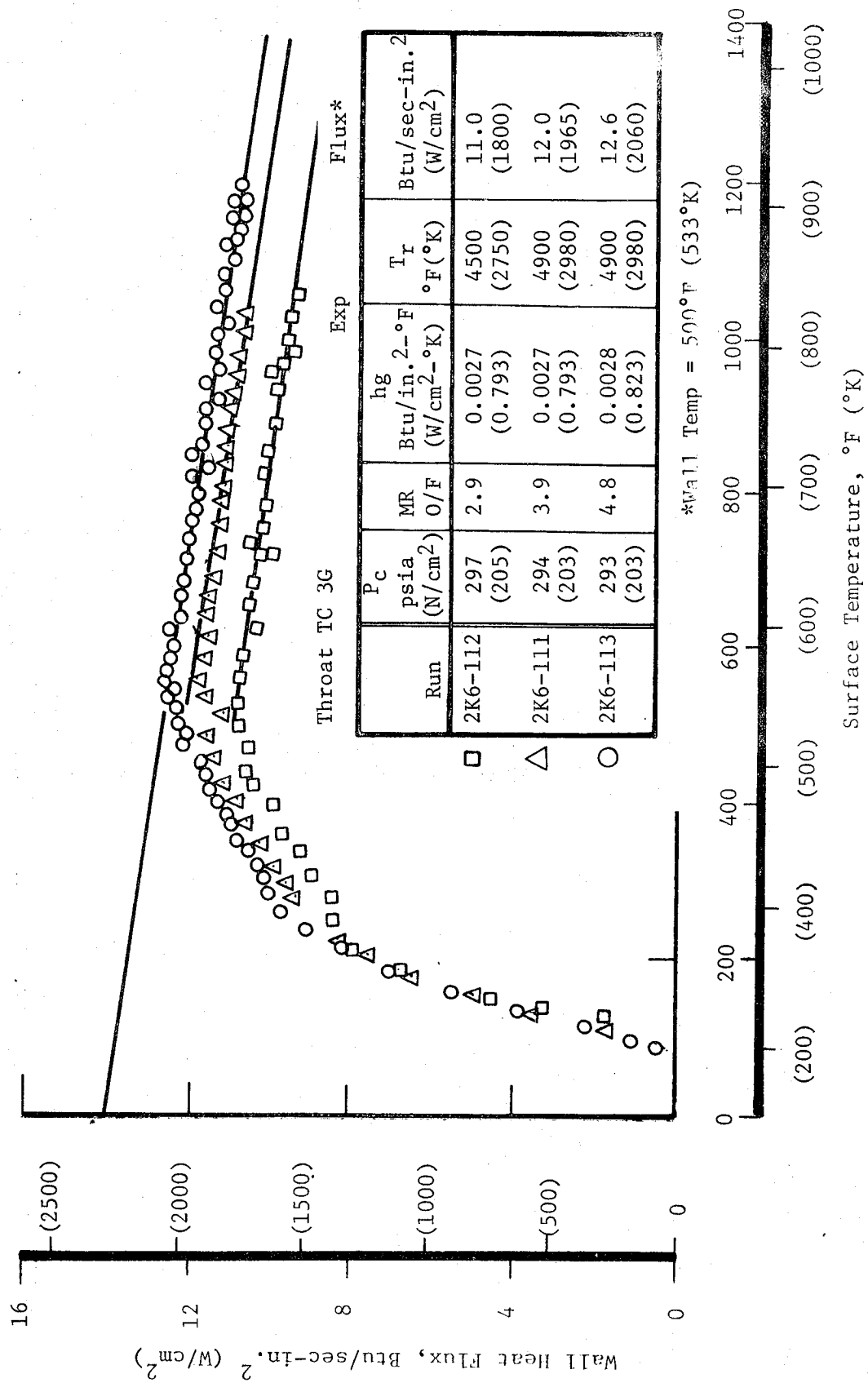
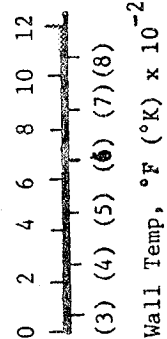
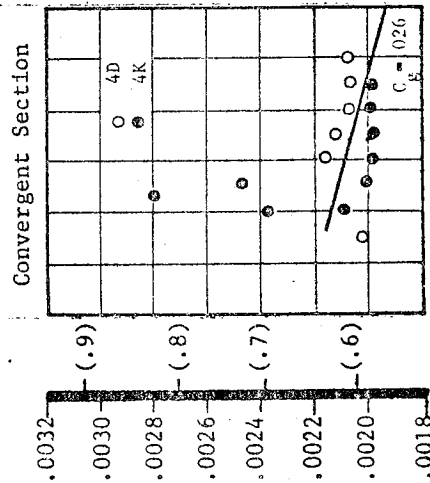
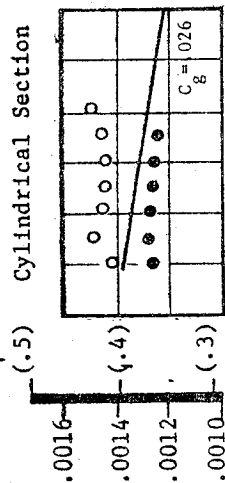


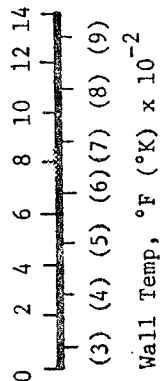
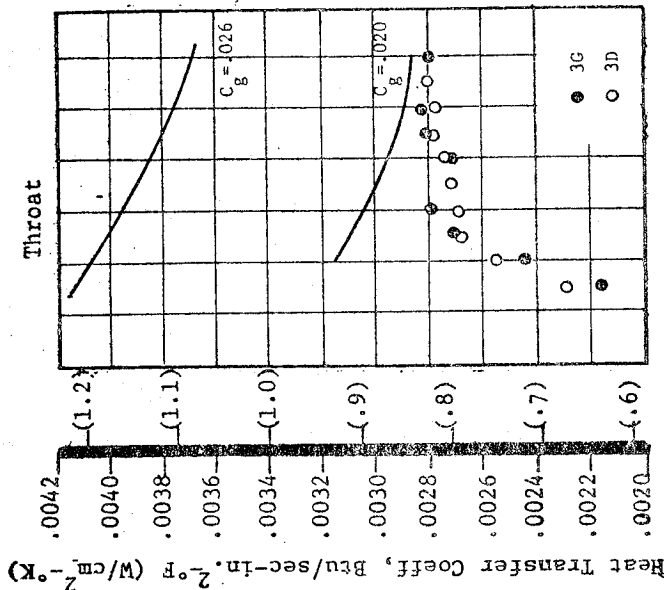
Figure VII-27. Throat Heat Flux vs Wall Temperature

$$\text{Exp } h_g = \frac{Q/A}{\eta^2 (T_o - T_{\text{wall}})}$$

$$\text{Theo } h_g = C \frac{\dot{W}}{g A} C_{pf} \left(\frac{\dot{W} D}{A \mu_f} \right)^{-0.2} (P_{Rf})^{-0.67} \left(\frac{T_{FS}}{T_f} \right)^{0.8}$$

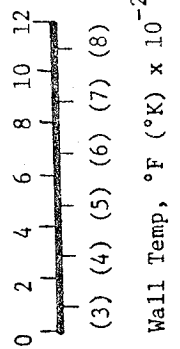
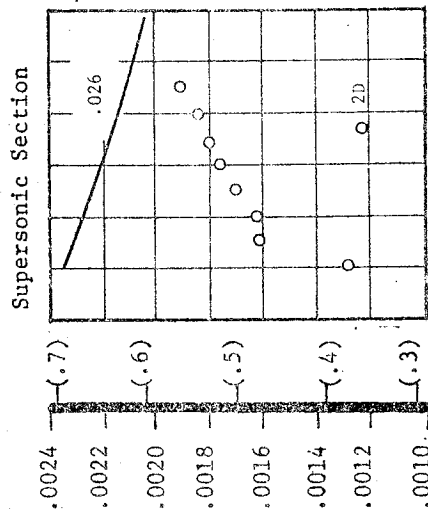


Wall Temp, °F (°K) x 10⁻²



Wall Temp, °F (°K) x 10⁻²

Injector
Premix Triplet
Test 2K6-113
MR=4.86, P_c=293(202)
L*=15, T_r=5500°R(3050°K)
No Film Cooling



Wall Temp, °F (°K) x 10⁻²

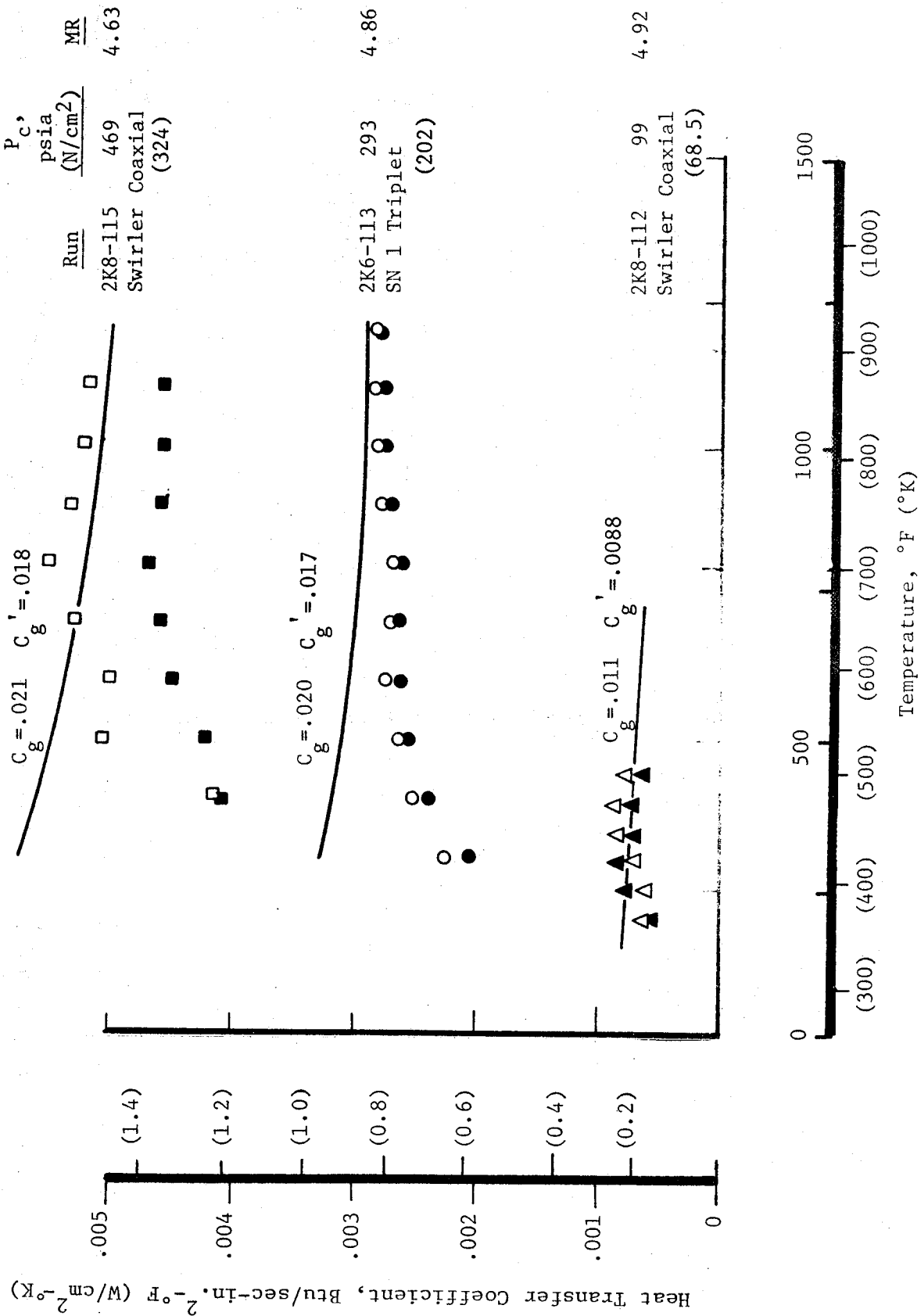


Figure VII-29. Throat Heat Transfer Coefficients with Chamber Pressure as a Parameter

5K-8 Series
APS Injector

Run	MR	P _c , psia (N/cm ²)	Thrust, lb (N)	Injector
115	4.63	469 (423)	2500 (11,130)	Swirler
113	3.64	480 (431)	2500 (11,130)	
109	4.97	316 (218)	1500 (6690)	
107	3.68	302 (208)	1500 (6690)	
110	4.01	99 (69)	500 (2220)	
112	4.92	99 (69)	500 (2220)	Nonswirl
136	4.95	319 (220)	1500 (6690)	
137	6.05	316 (218)	1500 (6690)	

72-Nonswirl Element
Recess = .25 ox tube dia
Rigimesh Face - 5% Cooling
Contraction Ratio = 2.48

5K-2 Series
OMS Injector

MR	P _c , psia (N/cm ²)	Thrust, lb (N)
5.9	450 (310)	5000 (22,200)
7.1	491 (339)	5000 (22,200)
6.0	505 (348)	5000 (22,200)
5.1	525 (362)	5000 (22,200)
6.7	294 (203)	3000 (13,380)
5.9	302 (208)	3000 (13,380)
4.9	309 (213)	3000 (13,380)
3.7	294 (203)	3000 (13,380)

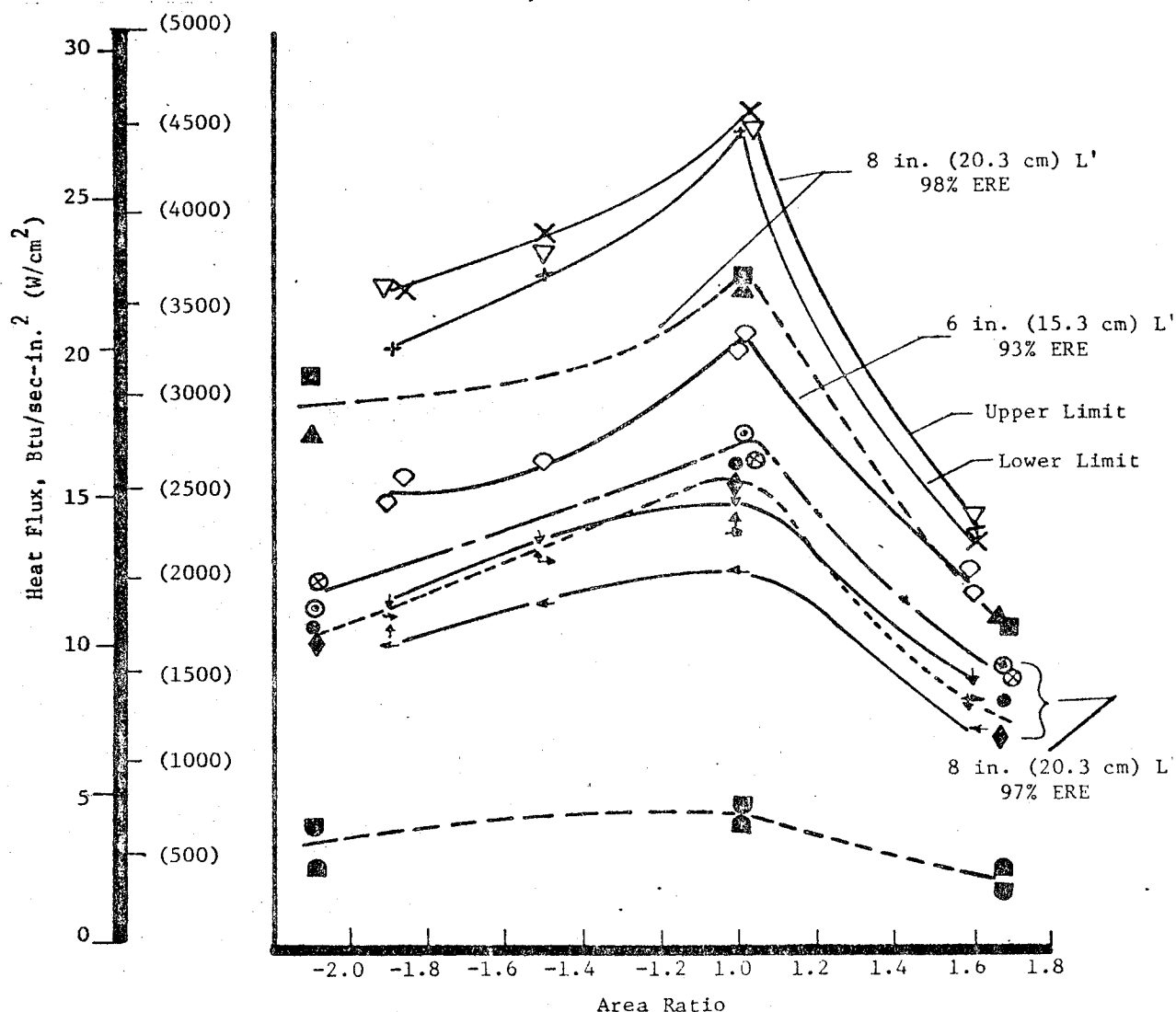


Figure VII-30. Throat Region Heat Flux Profiles for Coaxial Element Injectors

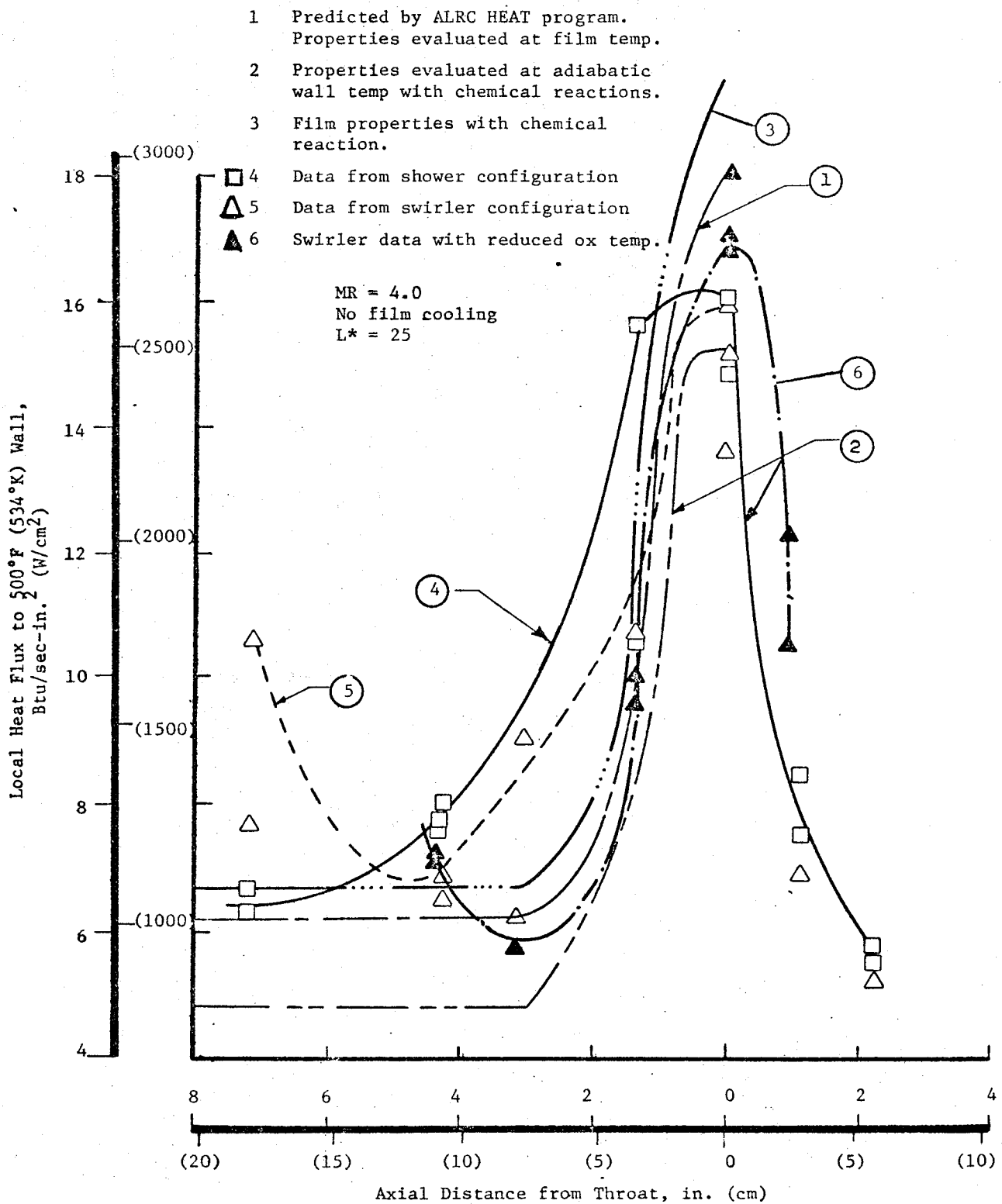
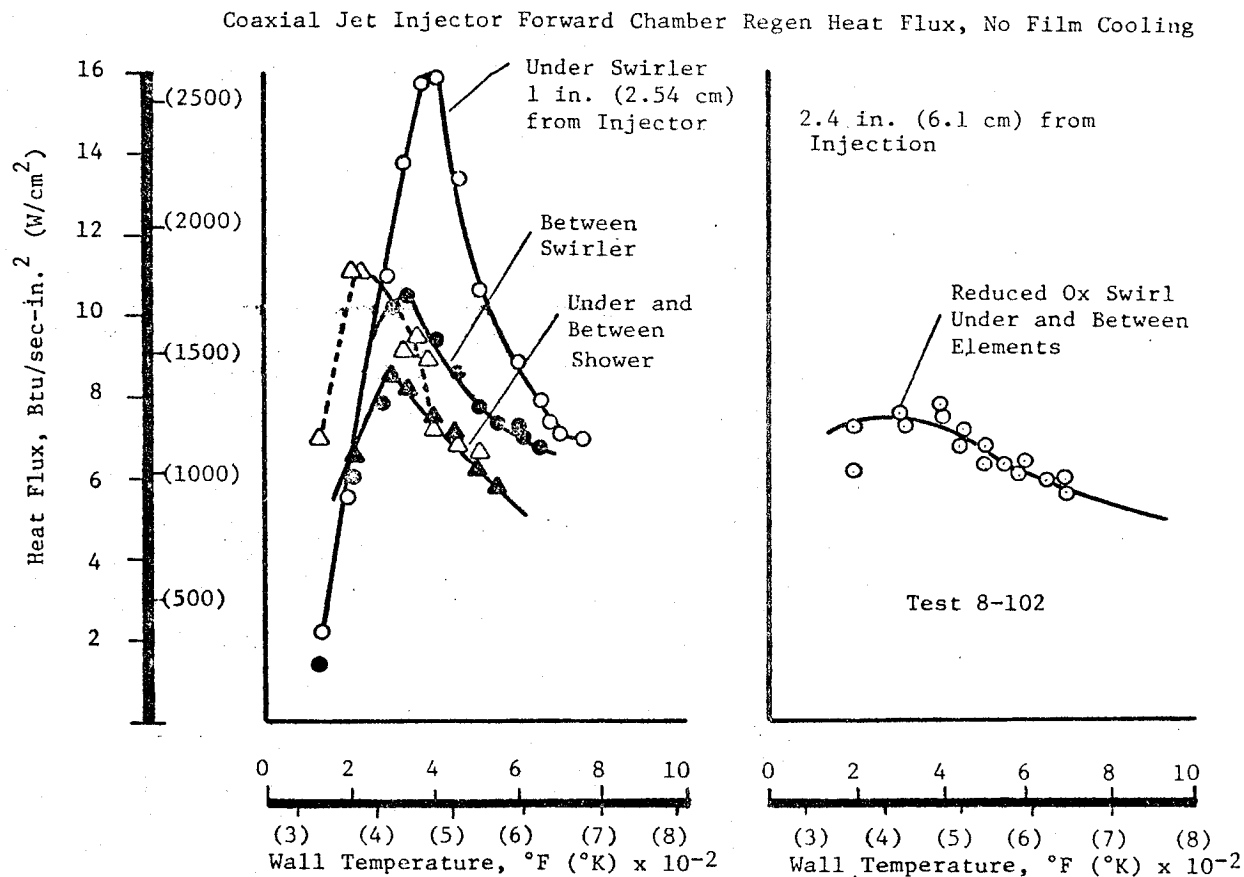


Figure VII-31. Chamber Heat Flux Profiles with Coaxial Element Injector



Axial Profile Comparisons

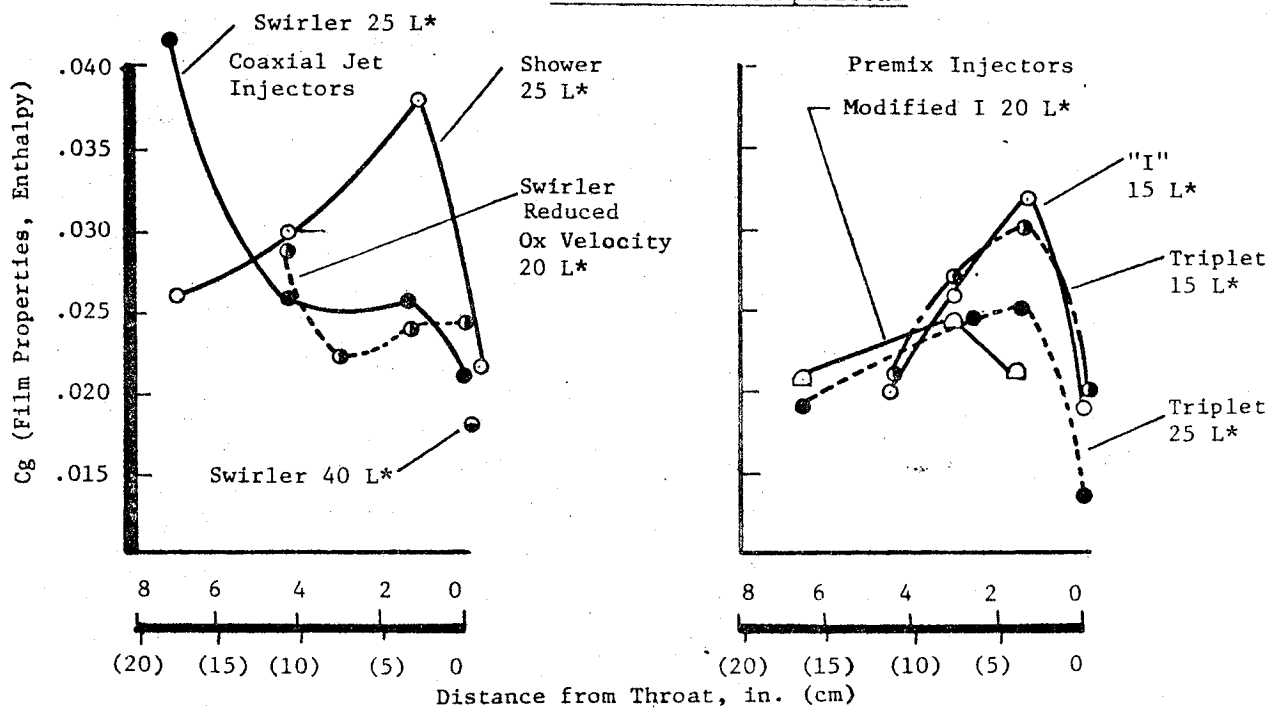


Figure VII-32. Chamber Heat Flux Profiles Injector Design Dependency

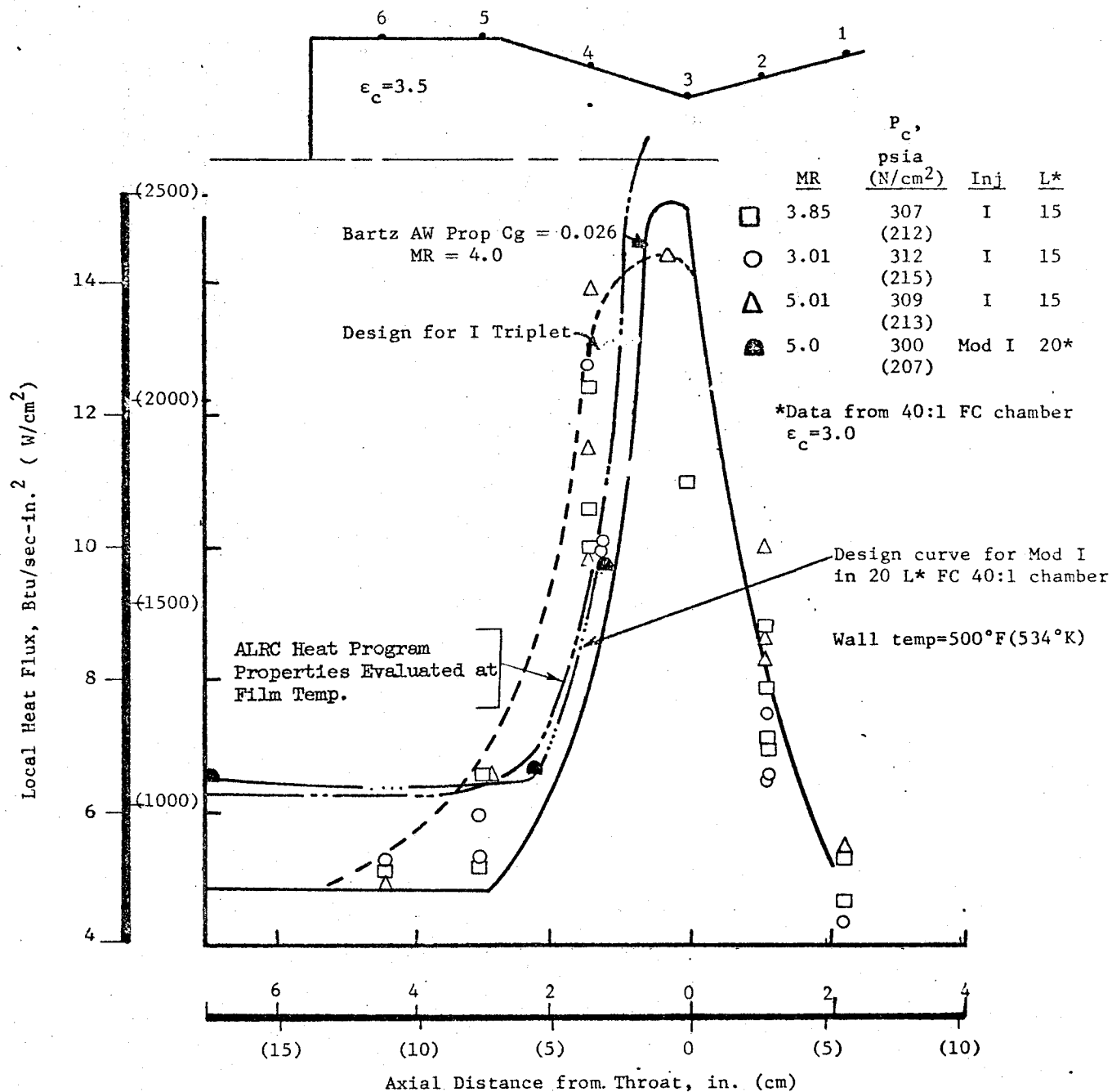


Figure VII-33. Chamber Heat Flux Profiles with Premix "I" Triplet Injector

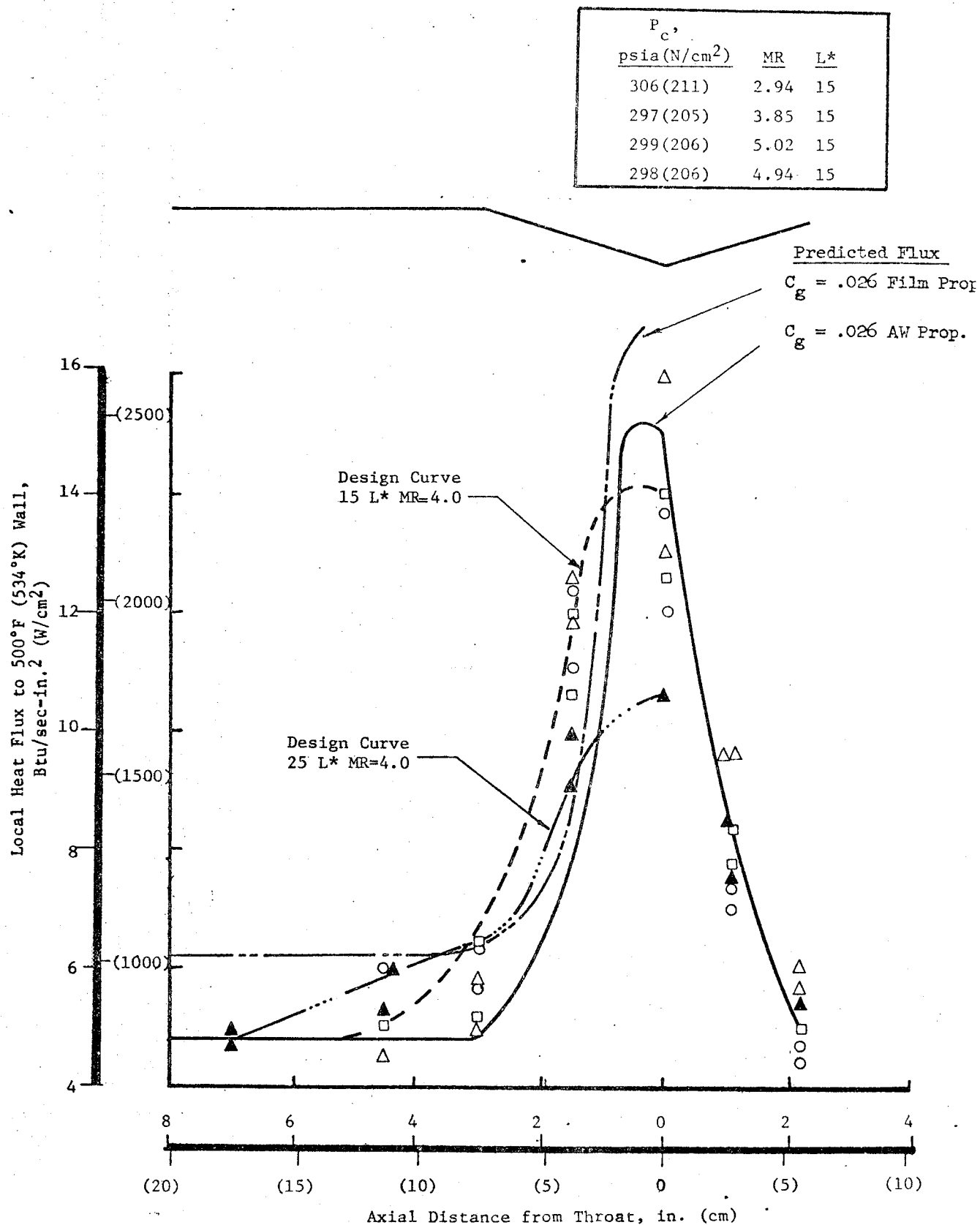


Figure VII-34. Chamber Heat Flux Profiles with Premix Triplet Injector

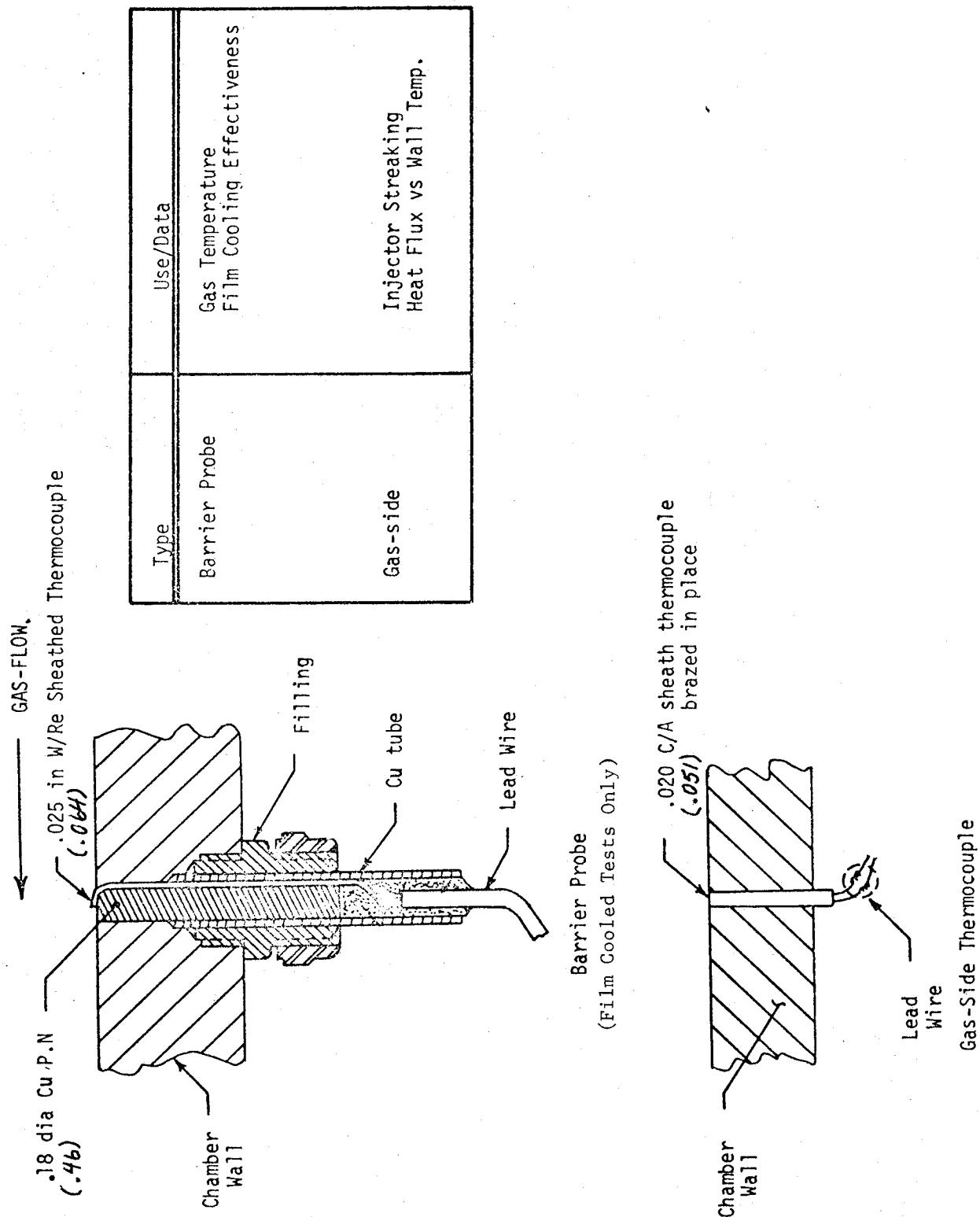


Figure VII-35. Heat Sink Chamber Thermal Instrumentation

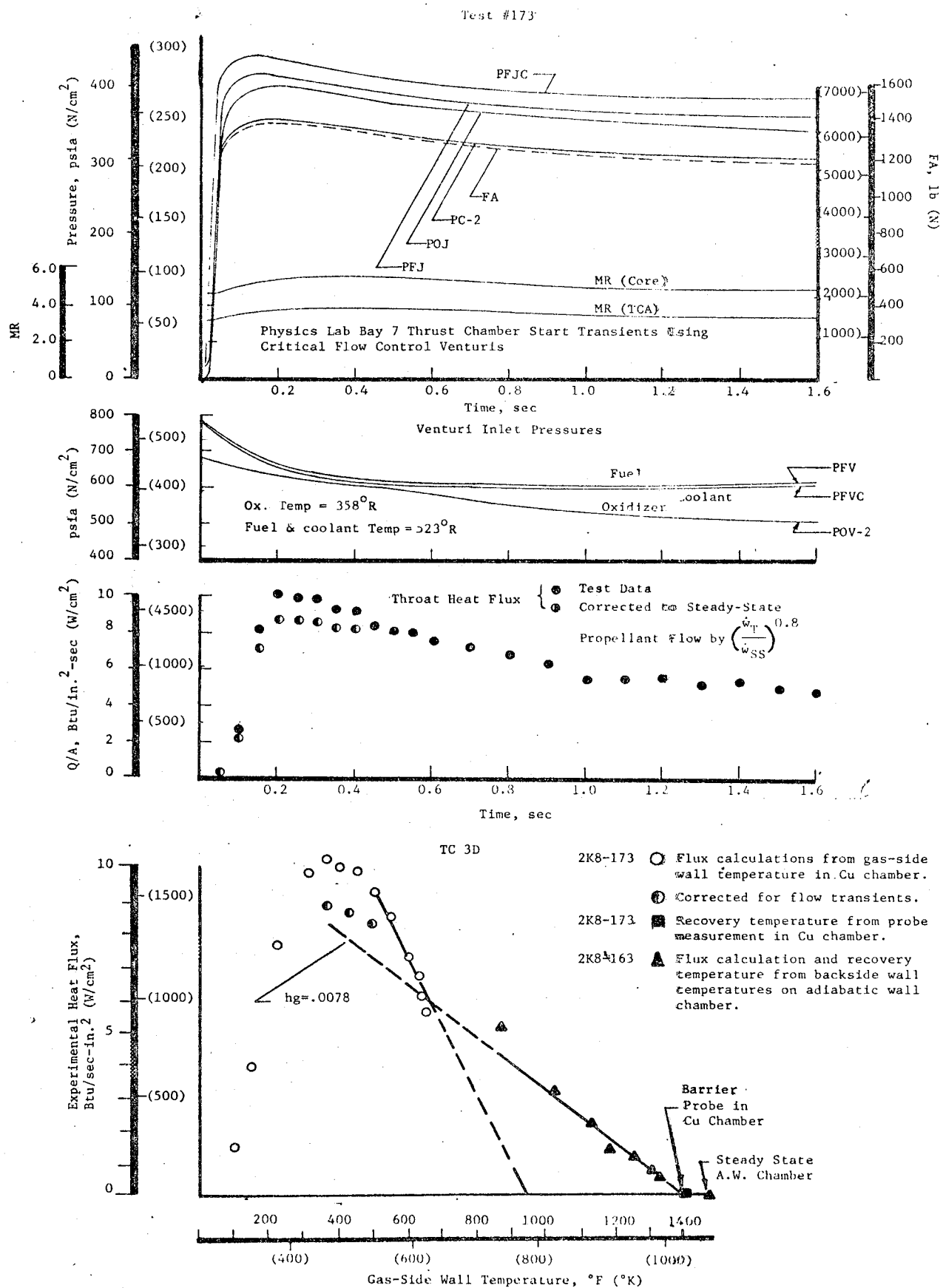


Figure VII-36. Error Analysis and Comparison of Various Experimental Techniques

HIGH P. TEST DATA
THIN-WALL STAINLESS STEEL CHAMBER AND
THICK-WALL COPPER CHAMBER

LOW P. TEST DATA
THIN-WALL MILD STEEL CHAMBER

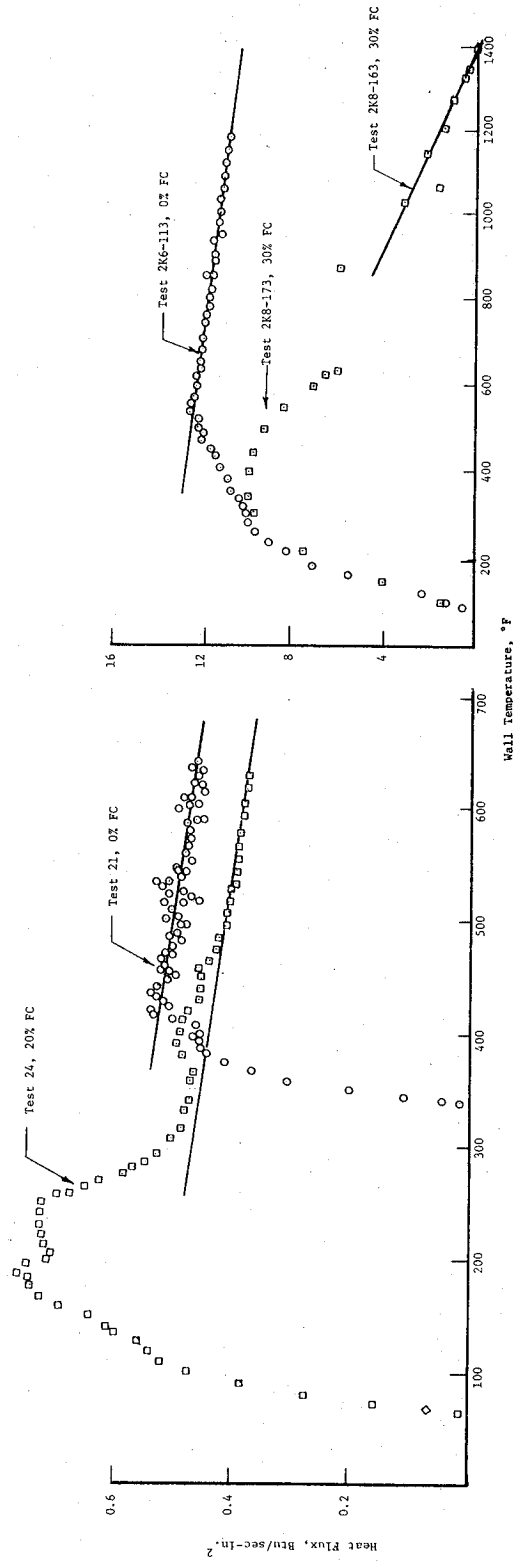


Figure VII-37. Comparison of Throat Flux vs Wall Temperature
With and Without Film Cooling

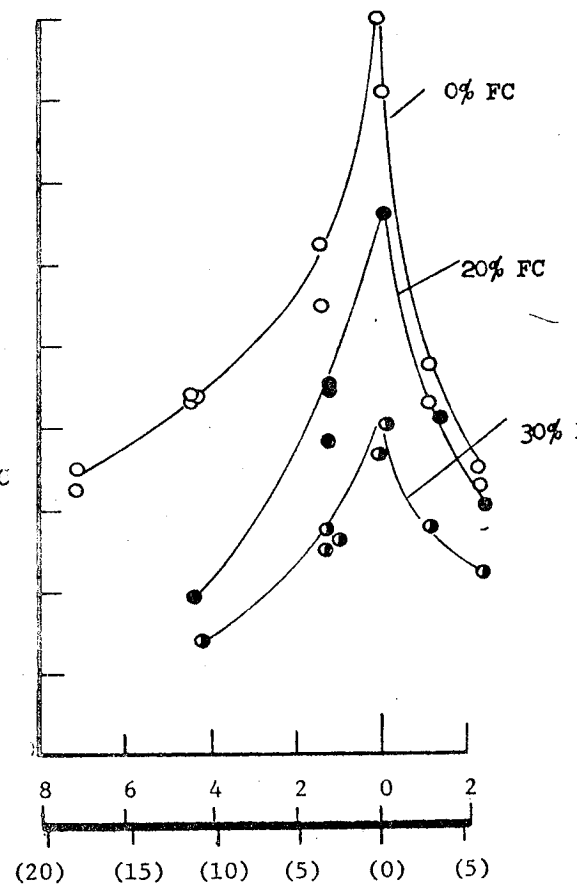
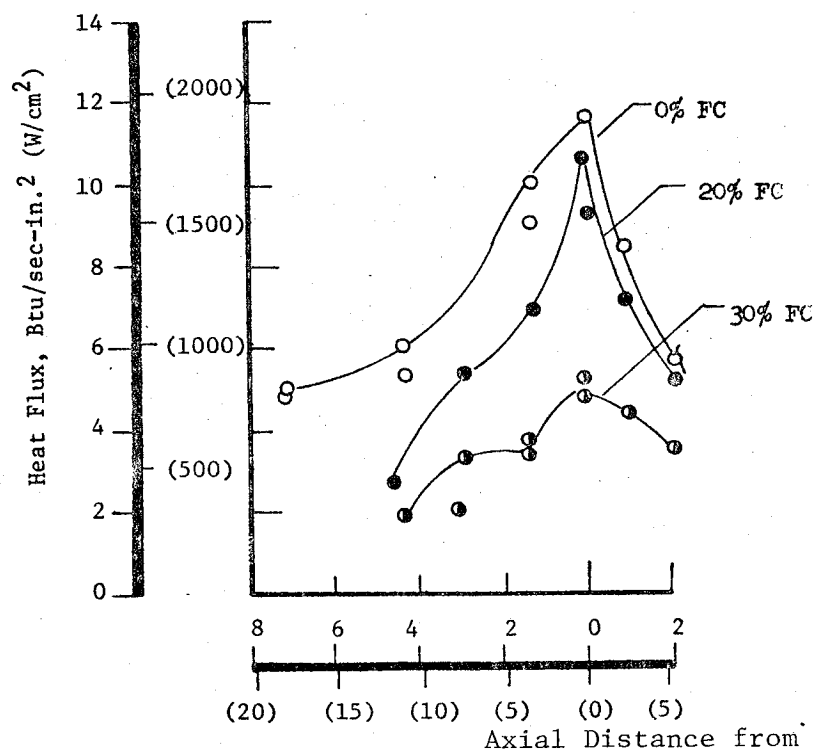
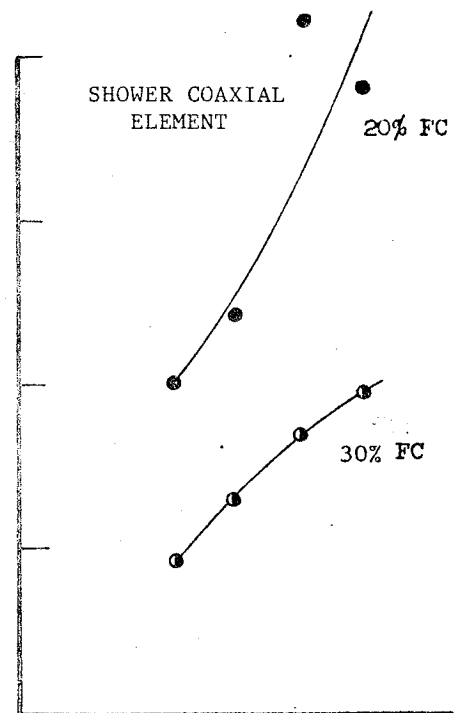
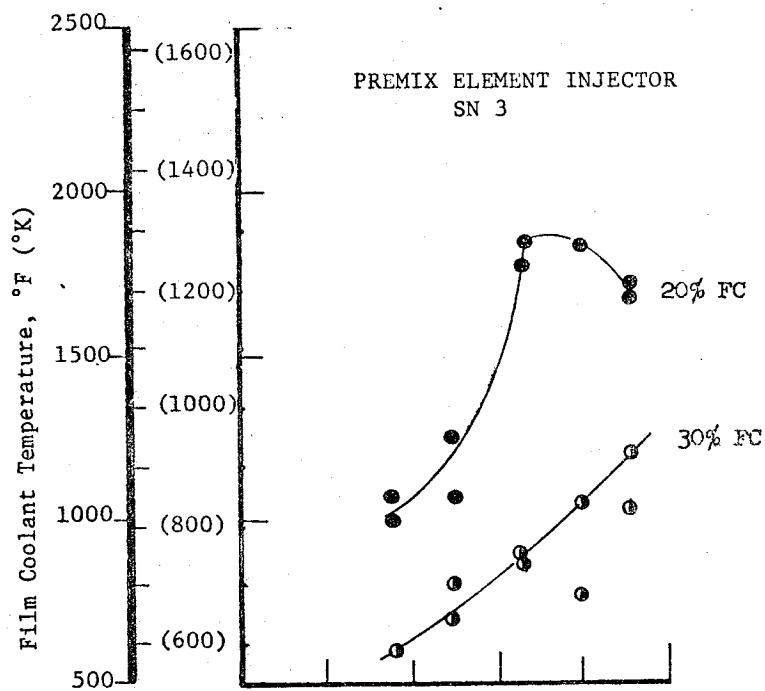


Figure VII-38. Experimental Thermal Data at 25 L* with Film Cooling

Premix Triplet, $L^* = 15$ in. (38 cm)

FILM COOLING RING = 2.5 in. (6.25 cm)

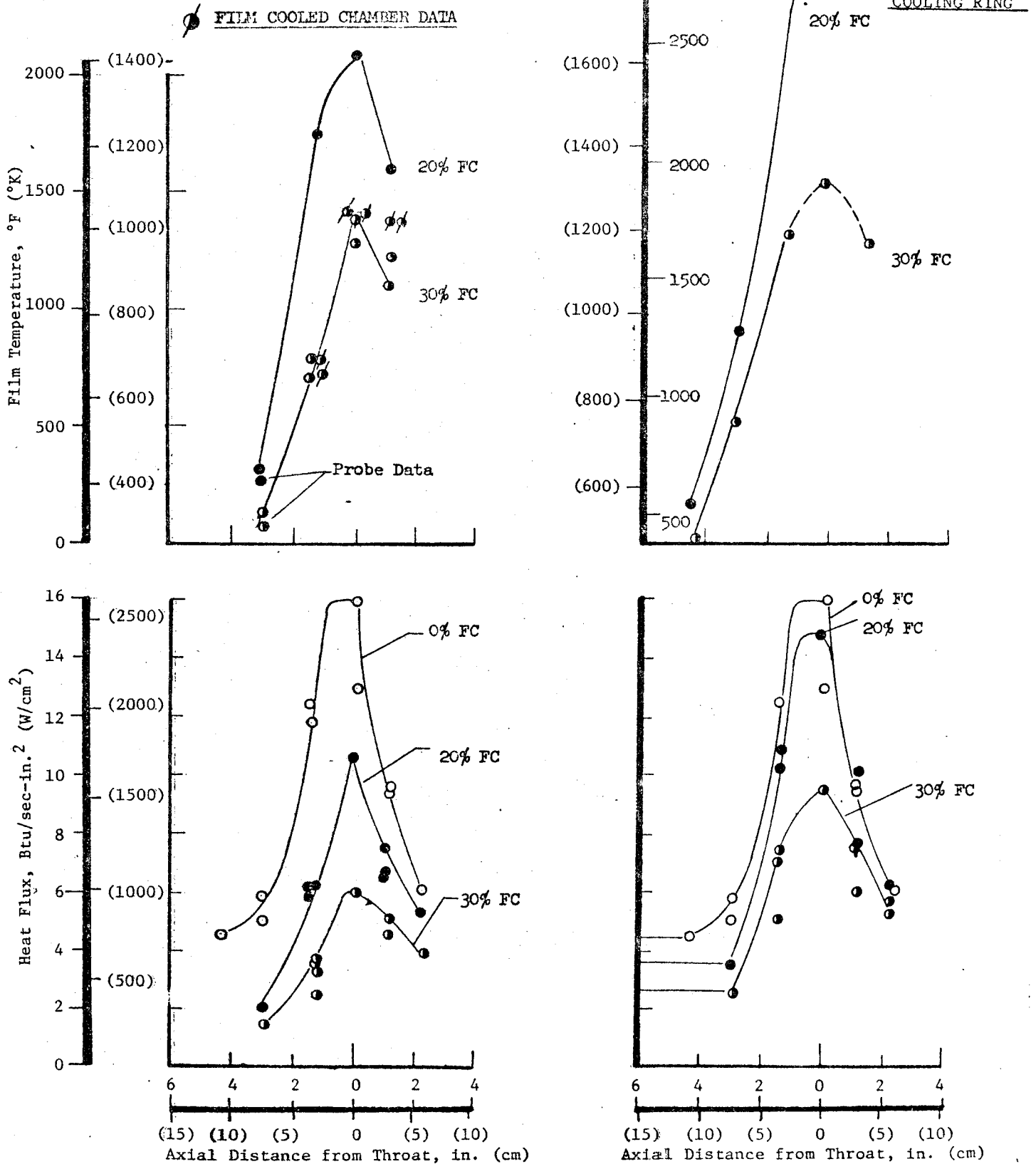


Figure VII-39. Effect of Film Cooling Ring Length on Heat Flux

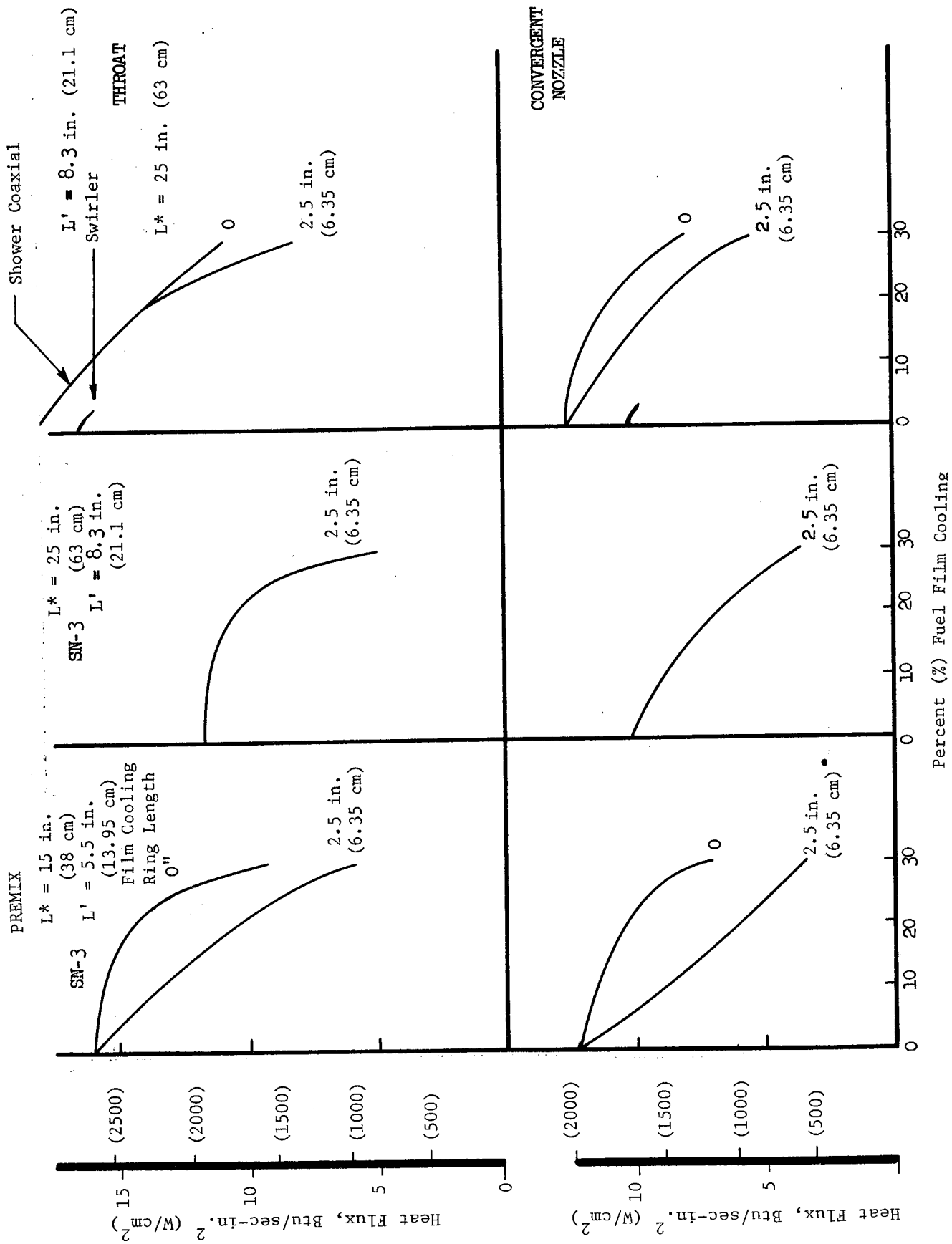


Figure VII-40. Throat Region Heat Flux Dependency on Injector Coolant Length and Coolant Flow

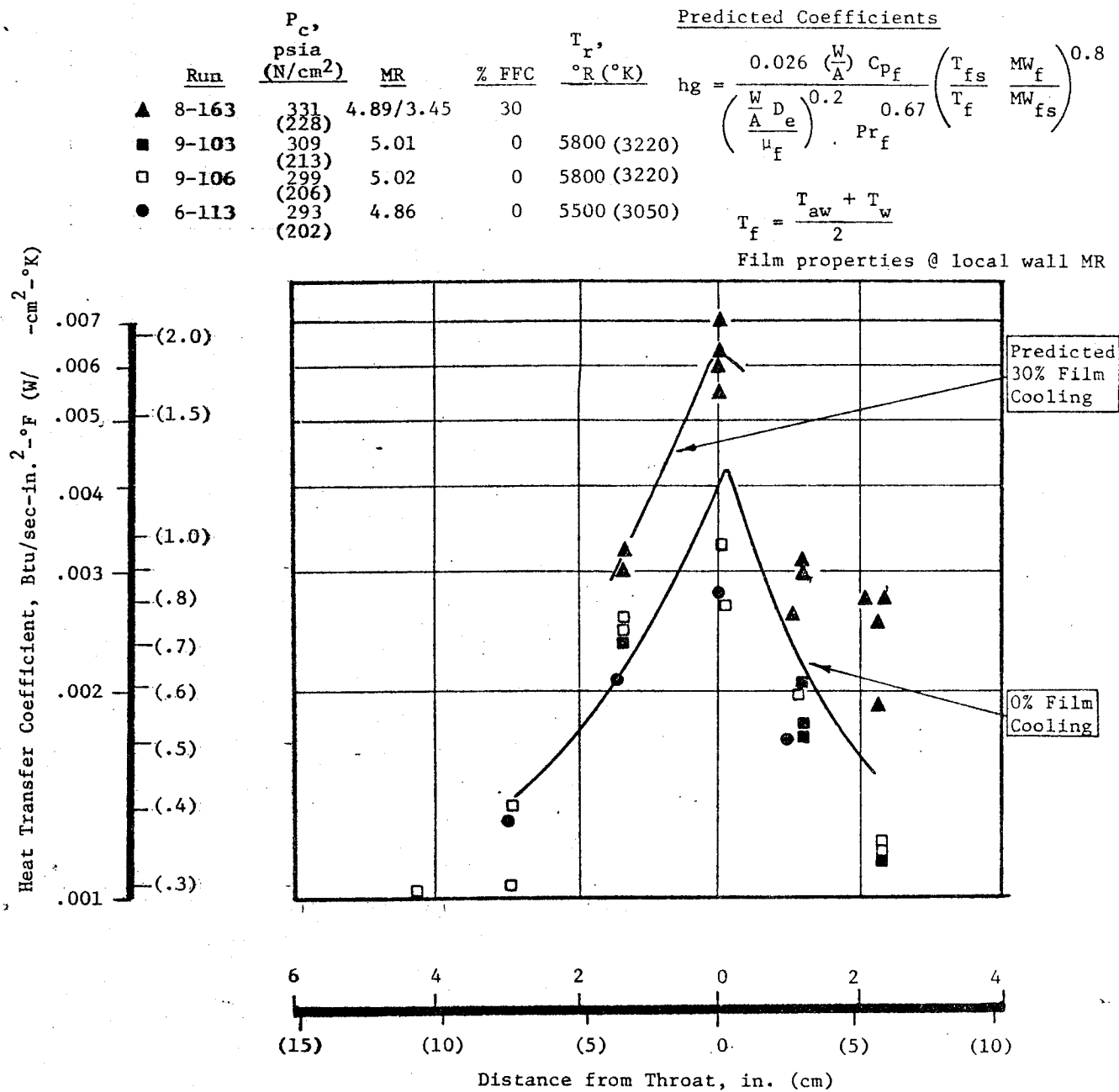


Figure VII-41. Influence of Film Cooling on Gas-Side Heat Transfer Coefficient (Sea Level Tests)

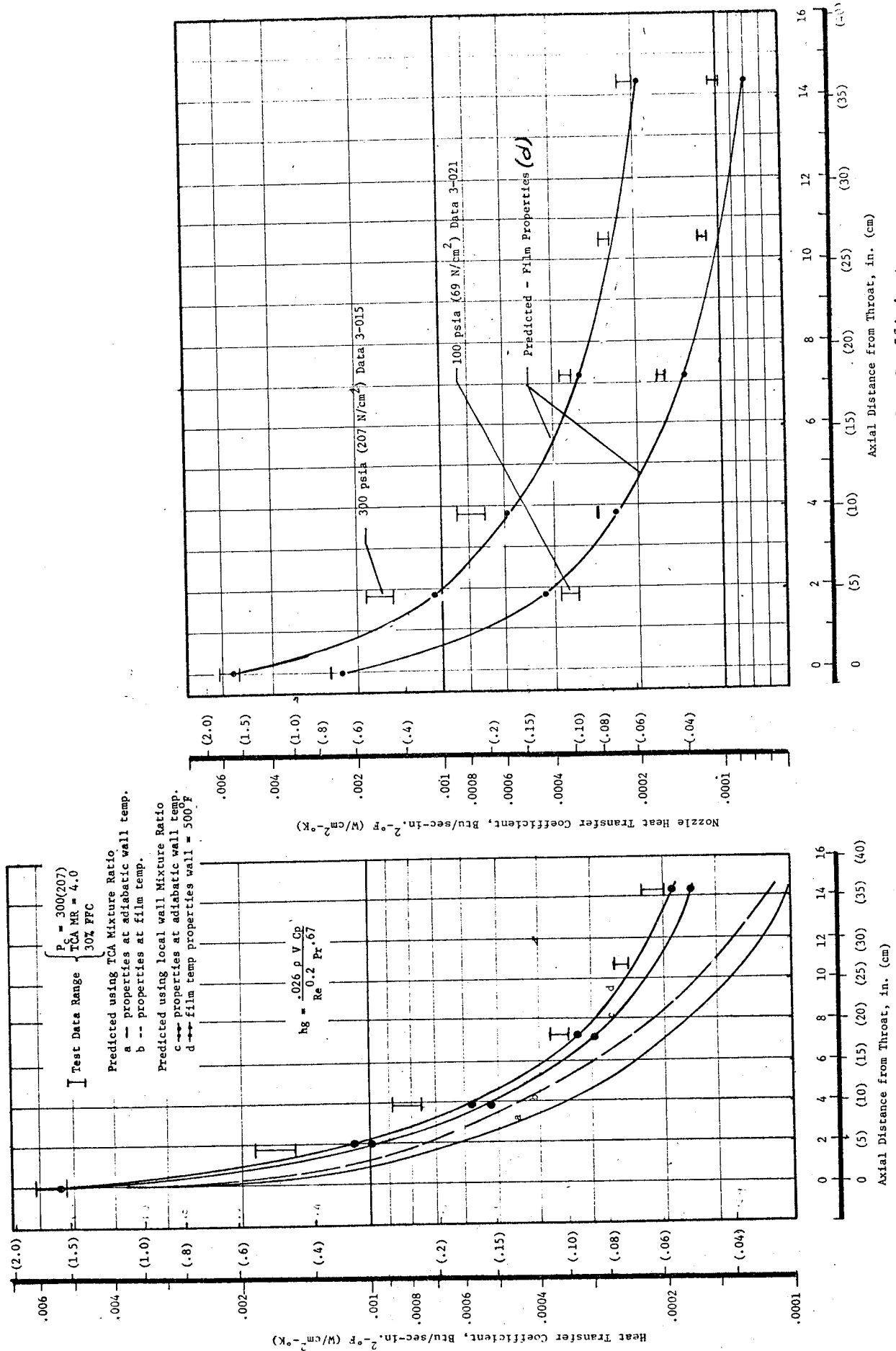


Figure VII-42. Influence of Film Cooling on Gas-Side Heat Transfer Coefficients
(Altitude Tests, 40:1 Nozzle)

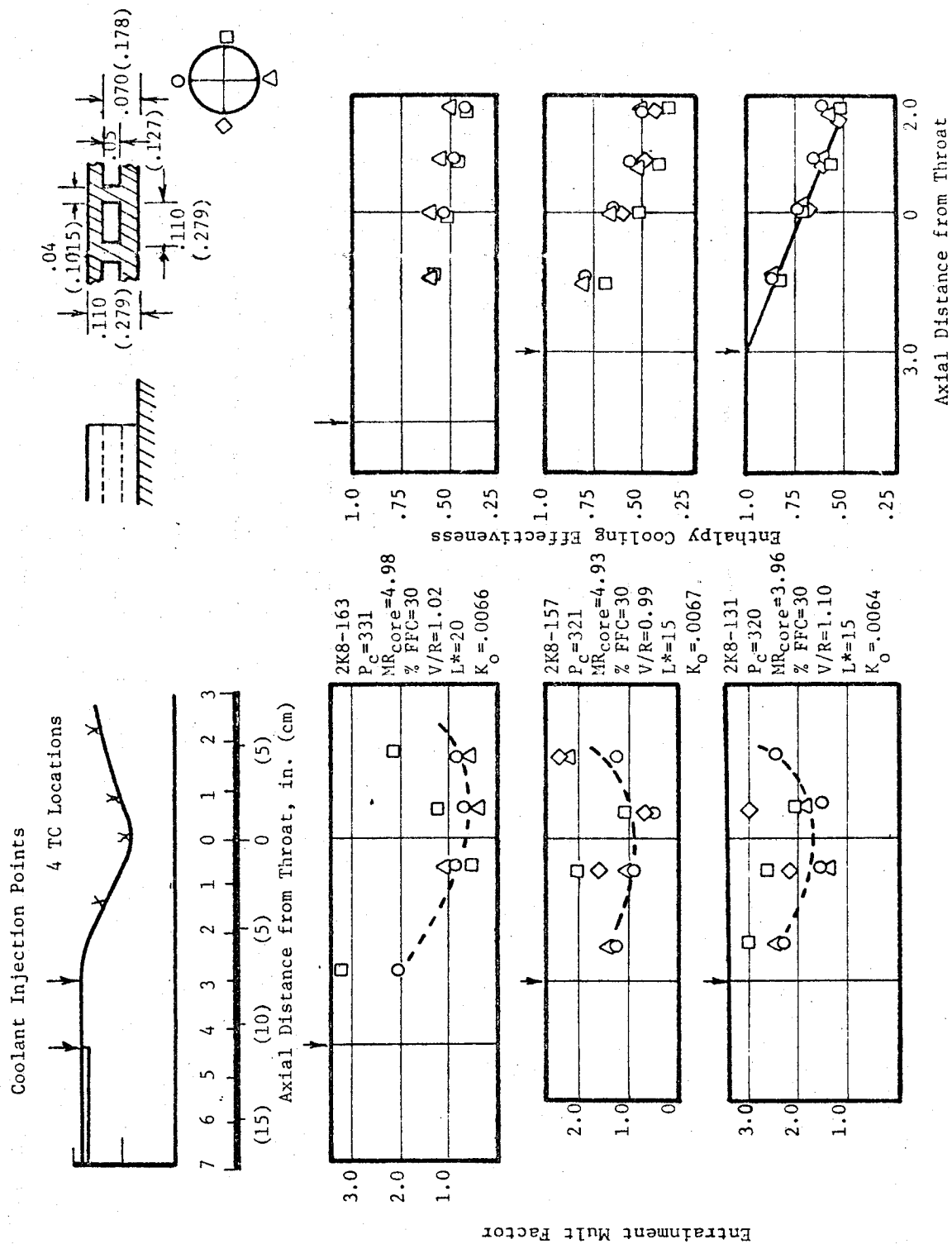


Figure VII-43. Film Cooling Entrainment Multiplying Factor and Effectiveness

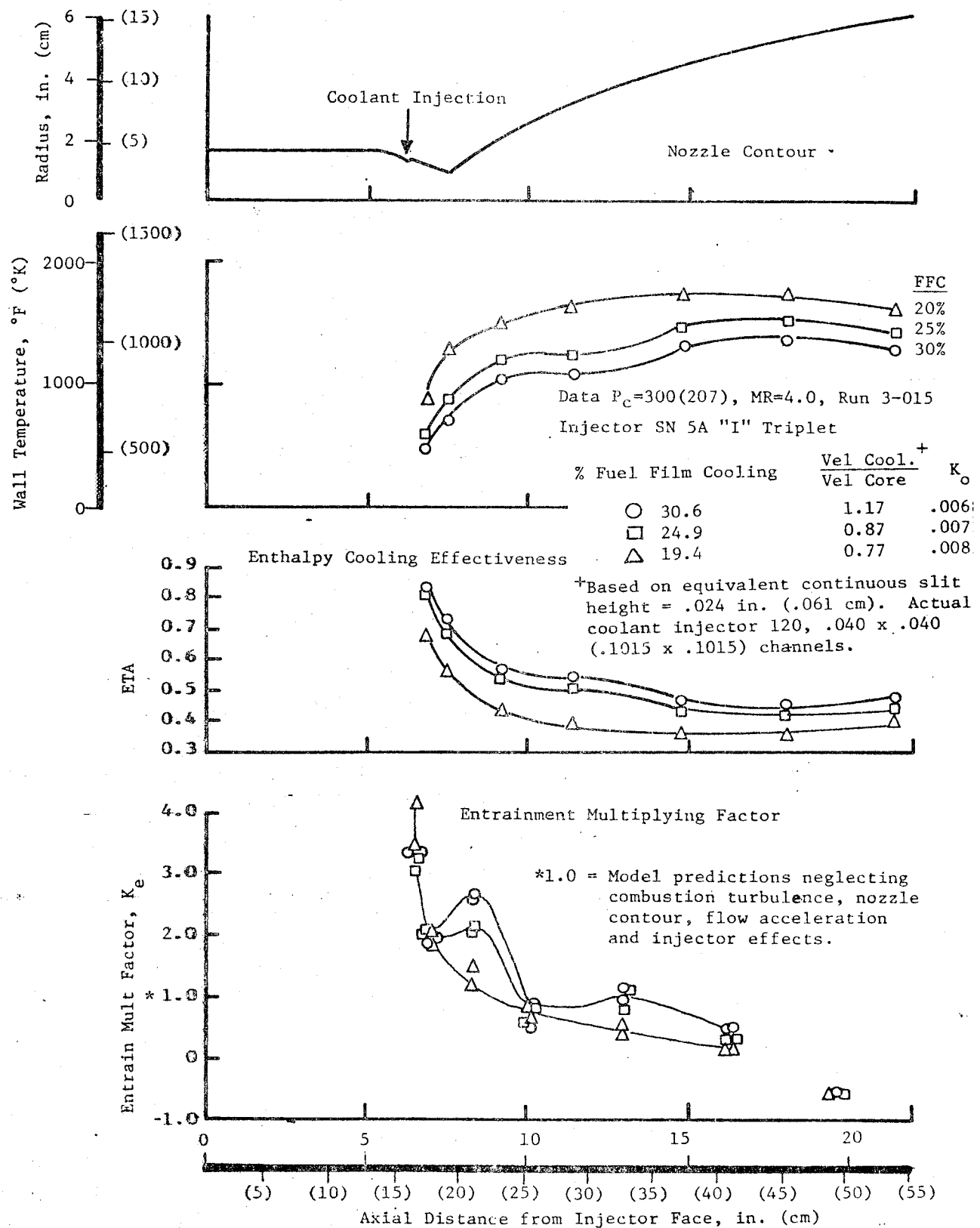


Figure VII-44. Film Cooling Characteristics, Premix "I" Injector, Ambient Temperature Propellants

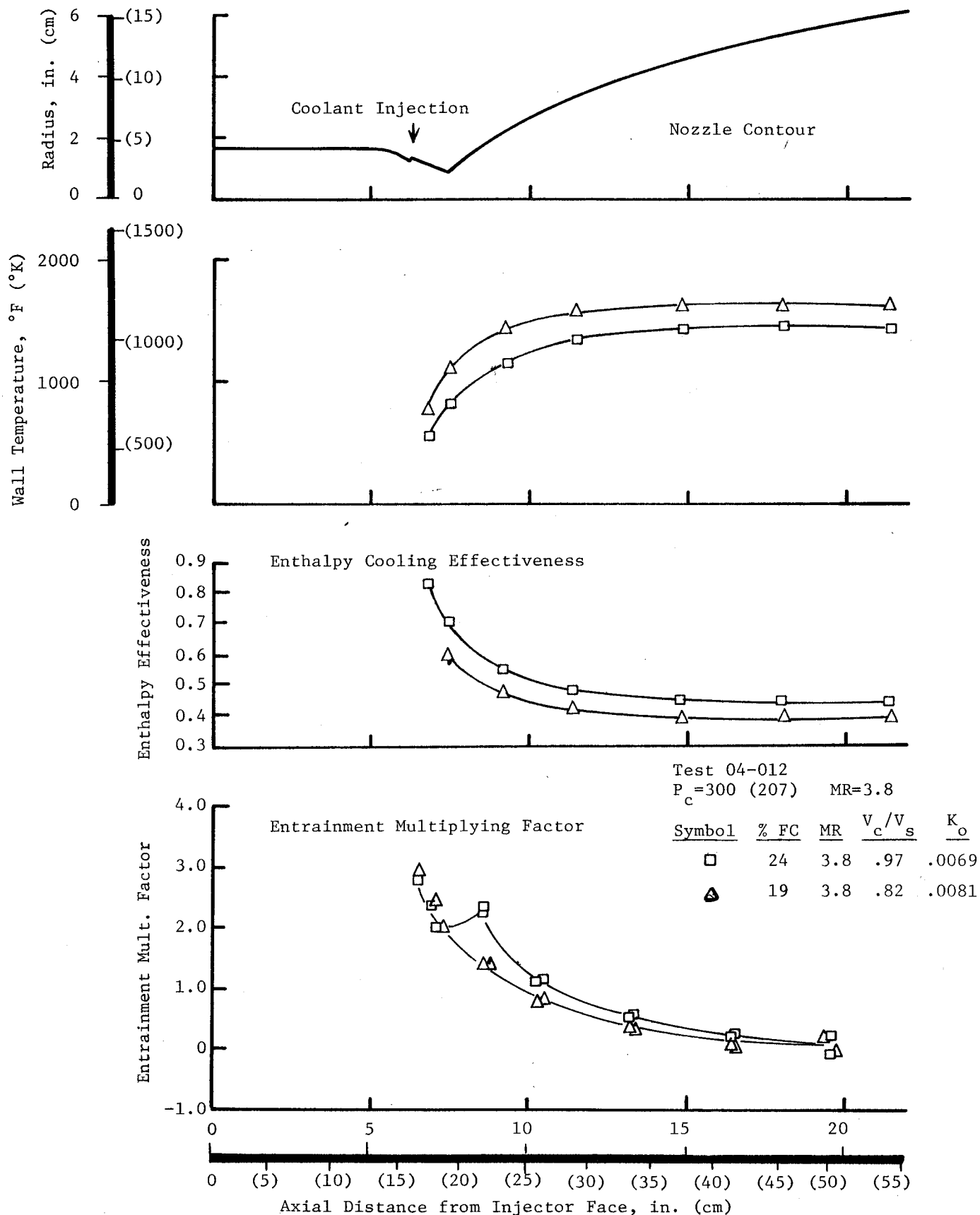


Figure VII-45. Film cooling Characteristics, Modified "I" Premix Injector, Ambient Temperature Propellants

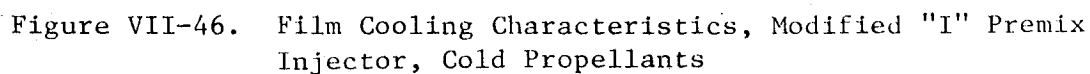


Figure VII-46. Film Cooling Characteristics, Modified "I" Premix Injector, Cold Propellants

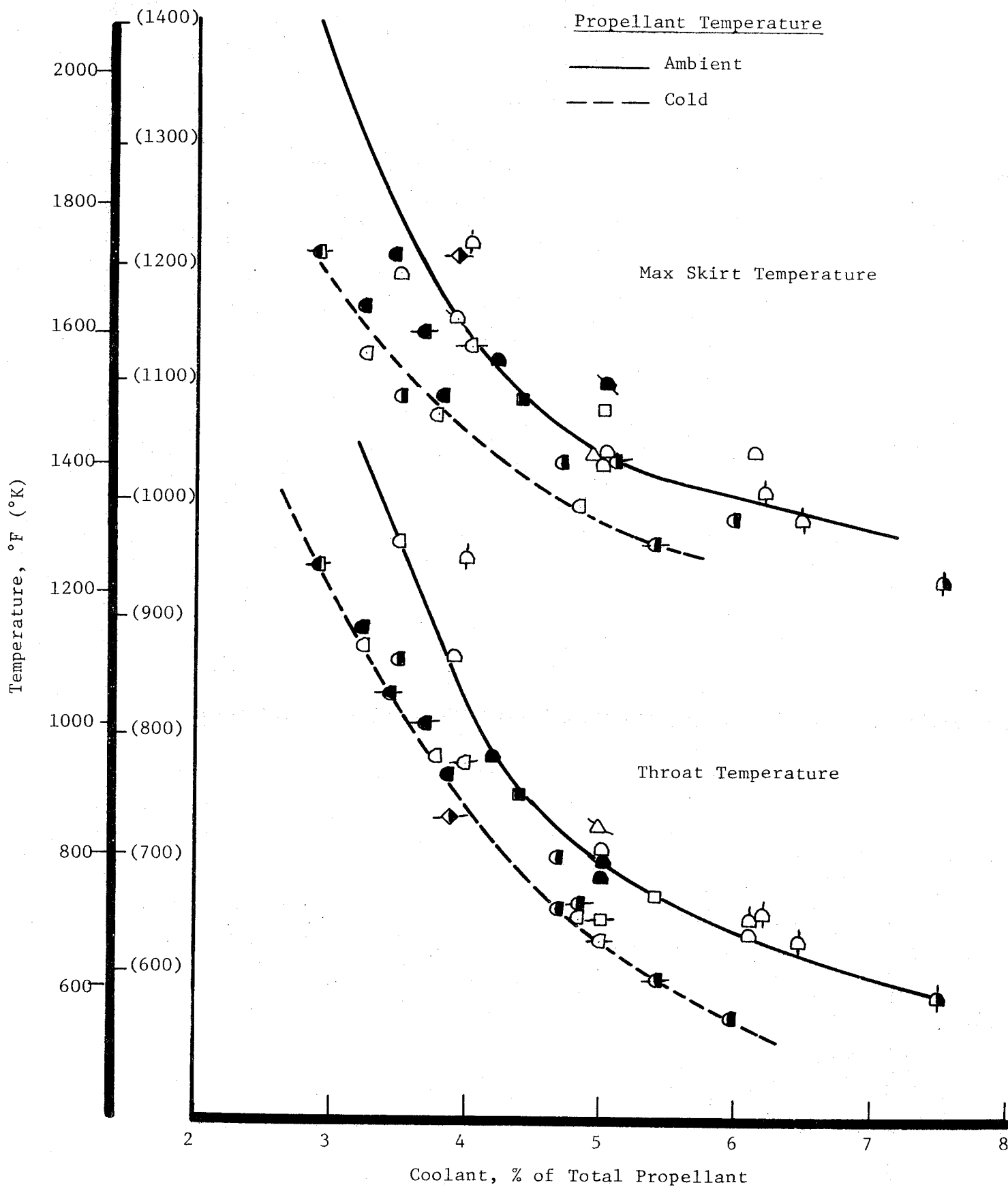
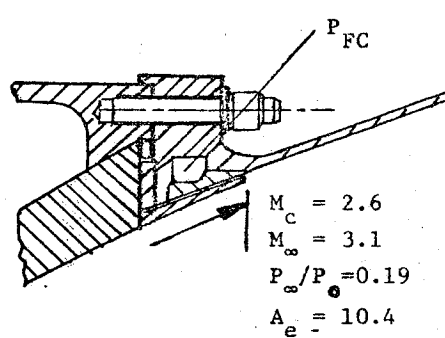
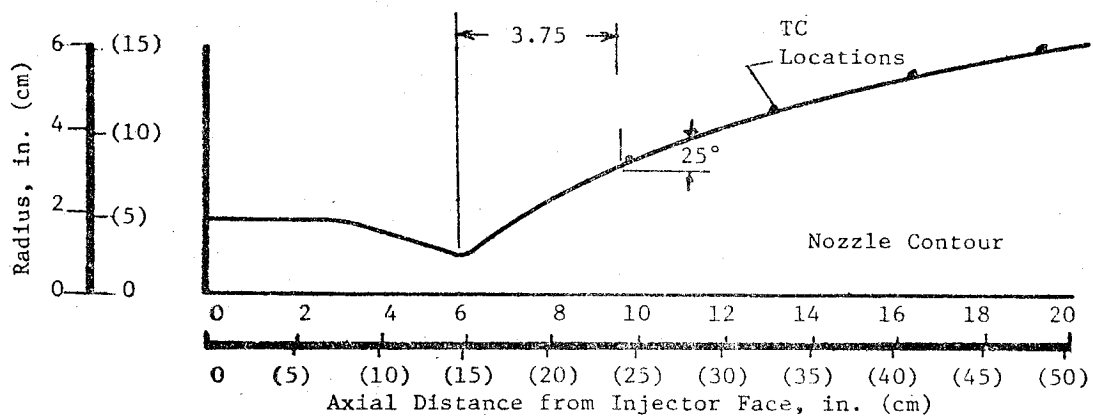


Figure VII-47. Maximum Skirt and Throat Temperatures vs Coolant Flow
(All 40:1 Film Cooled Chamber Tests)



Film Coolant Injector

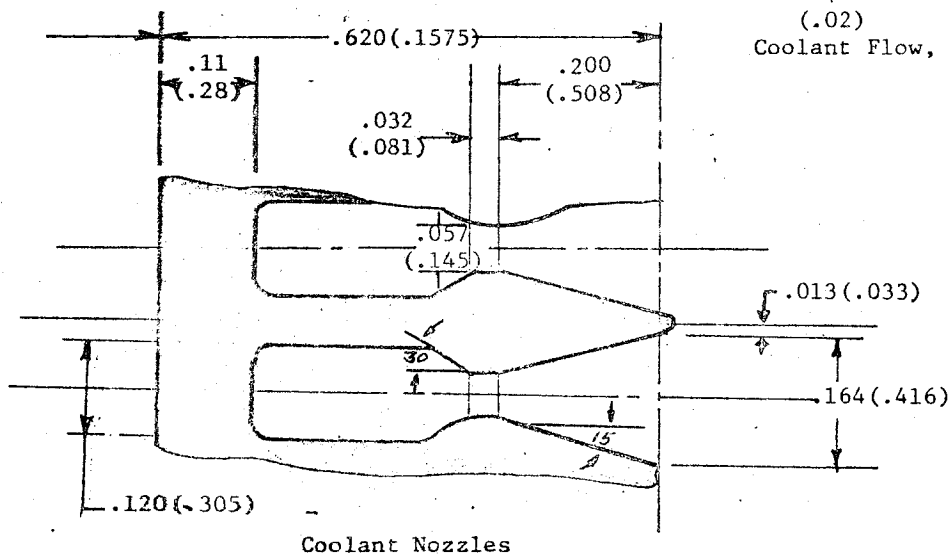
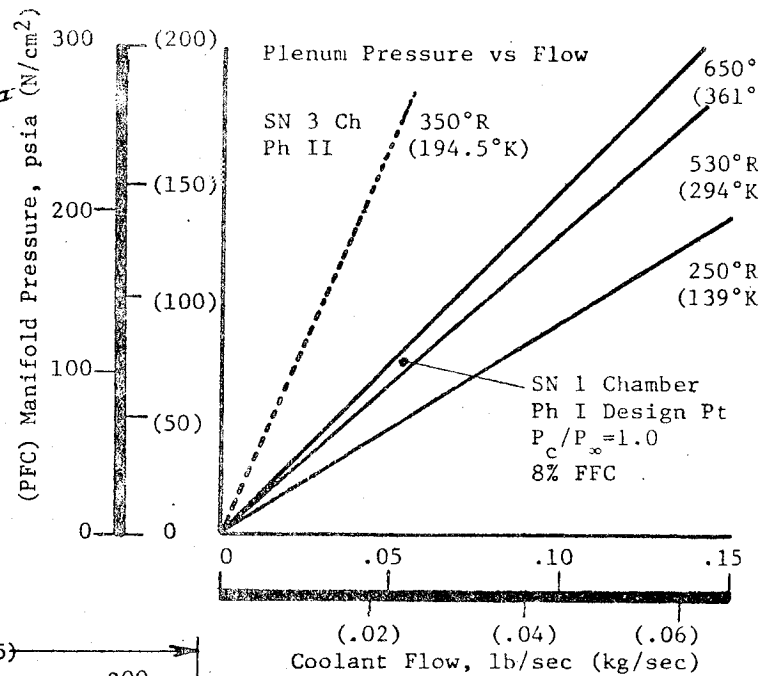


Figure VII-48. Supersonic Film Cooling Injector Design Details.

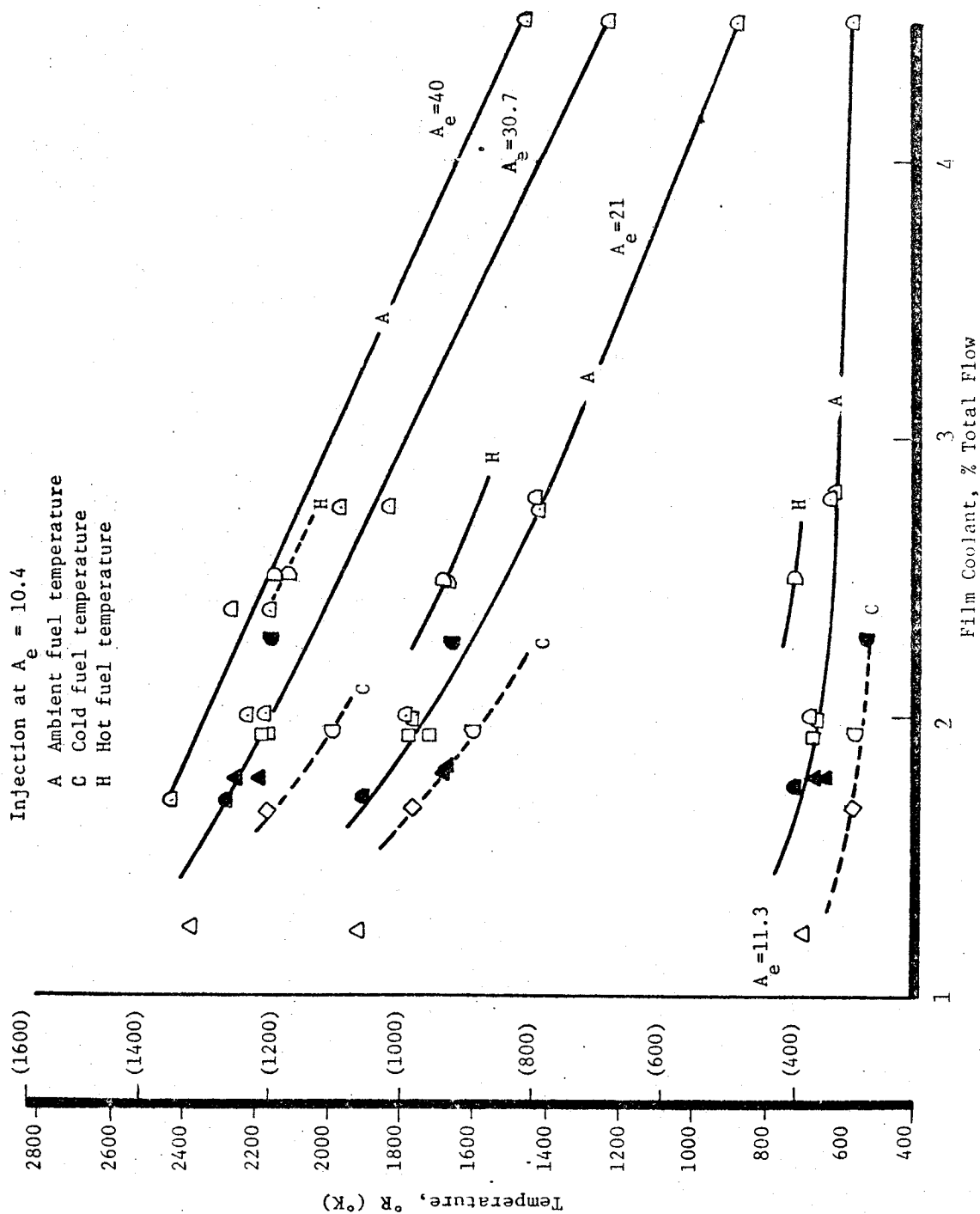
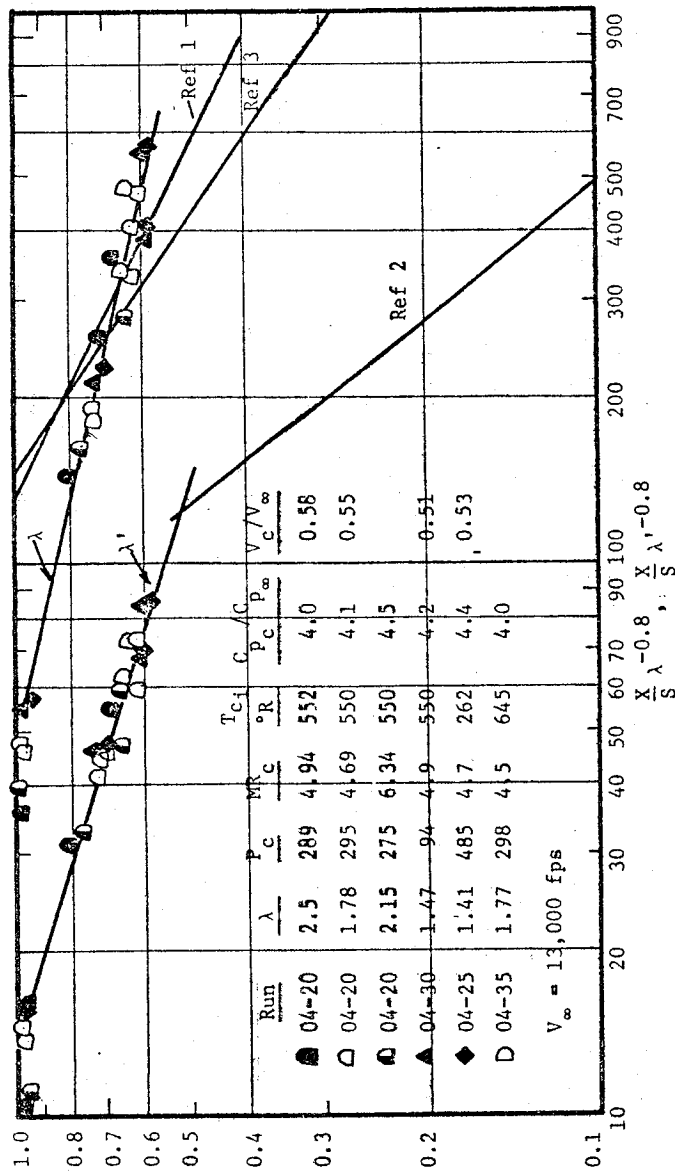


Figure VII-49. Measured Skirt Temperatures for Supersonic Film Cooling Injection



$$\lambda = \frac{(\rho_c V_c) i}{\rho_{i_\infty} V_{i_\infty}} \quad \lambda' = \frac{(C_{p_c} \rho_c V_c) i}{C_p \left[\frac{(PV)_{i_\infty}}{2} + (PV)_{x_\infty} \right]}$$

NOMENCLATURE:

C_p = specific heat

ρ = density

V = velocity

X = distance from injection

S = slot height

T = temperature

Subscripts

c = coolant at injection point static pressure, total temp

∞ = hot gas conditions at edge of boundary layer, including two-dimensional gas dynamic effects

i = at coolant injection station

x = at location x from injection

r = recovery, no film cooling

aw = measured adiabatic wall

Ref 1. V. Zakkay, L. Sakell, and K. Parthasarathy, "An Experimental Investigation of Supersonic Slot Cooling," from *Proceedings of the 1970 Heat Transfer and Fluid Mechanics Institute*, Naval Postgrad School, Monterey, Calif, June 1970, ed. by Turgut Sarpkaya, Stanford University Press.

Ref 2. R. Goldstein, E. Eckert, F. Taou, and A. Haji-Sheikh, "Film Cooling with Air and Helium Injection Through a Rearward-Facing Slot into a Supersonic Air Flow," *University of Minnesota, Heat Transfer Laboratory*, HTL TR No. 60, February 1965.

Ref 3. K. Parthasarathy and V. Zakkay, "Turbulent Slot Injection Studies at Mach 6," ARL 69-0066, April 1969.

Chamber	Test	MR	P_c	% FFC	Wt	K_o	T_{H_2}	$\frac{u_c}{u_e}$	
Film Cooled	04-12	3.8	298	24.2	3.6	.0069	550	.97	○
	04-18	4.1	260	24.6	3.2	.00795	198	.54	□
Regen	04-20	4.1	284	14.5	3.5	.0090	530	.58	□
	04-20	4.1	295	10.38	3.5	.011	530	.55	□
	04-30	4.5	94	9.75	1.15	.0096	530	.51	△
	04-21	4.1	485	10.1	5.7	.0148	--	.53	□

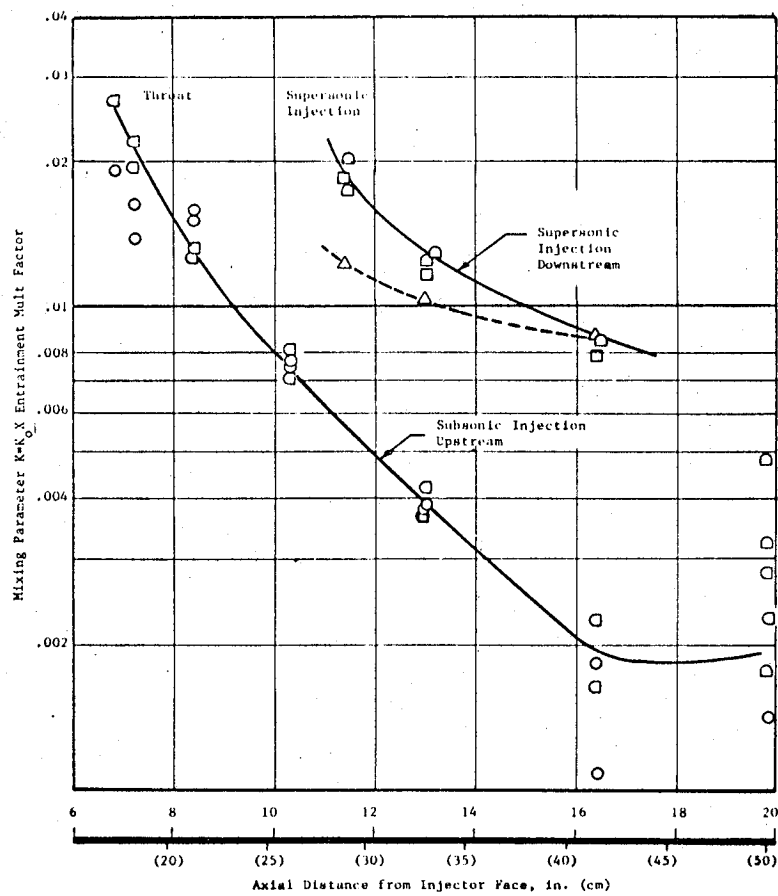


Figure VII-51. Mixing Parameters for Supersonic Film Cooling Injection

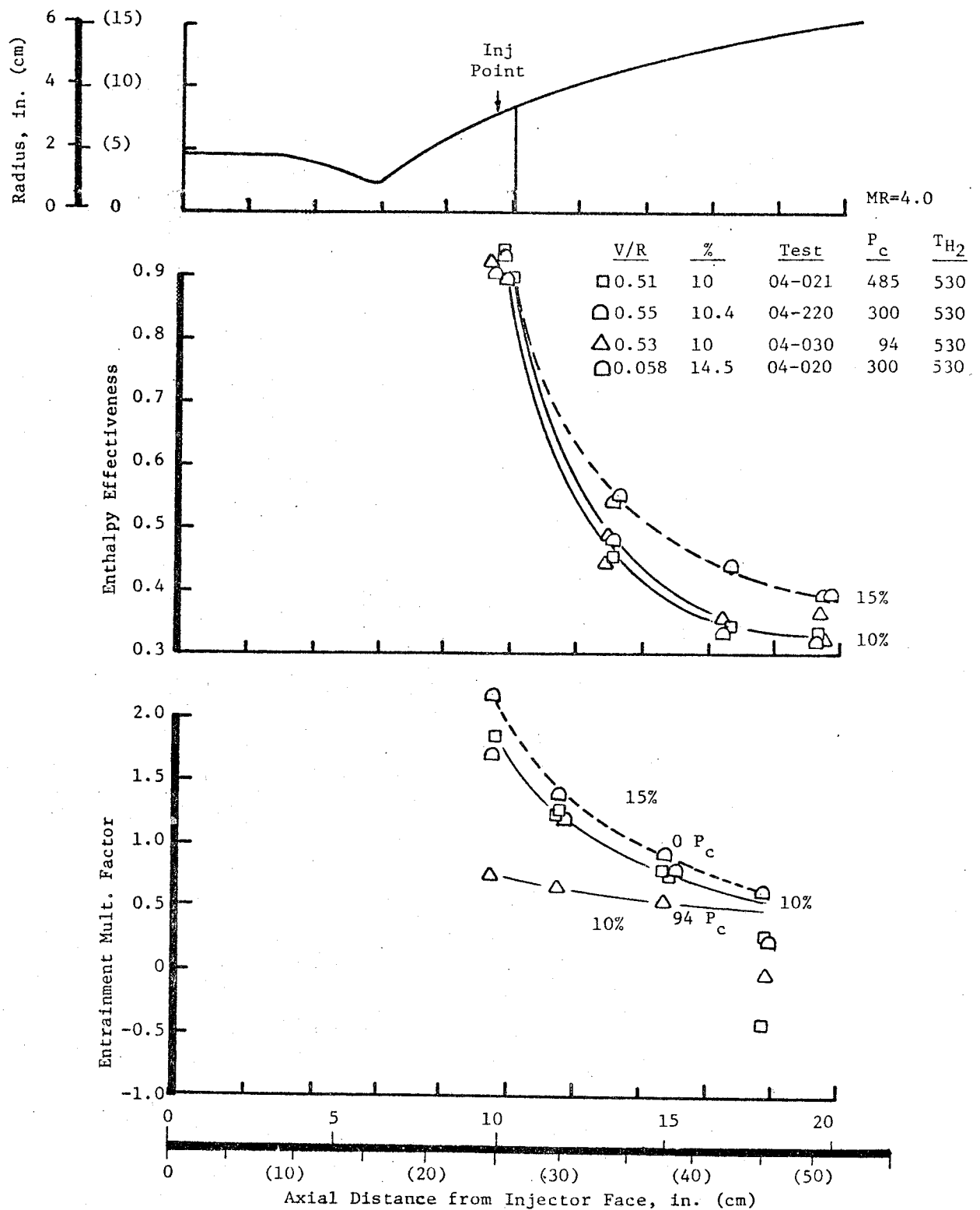


Figure VII-52. Supersonic Film Cooling Injection Enthalpy Effectiveness and Correlating Factors

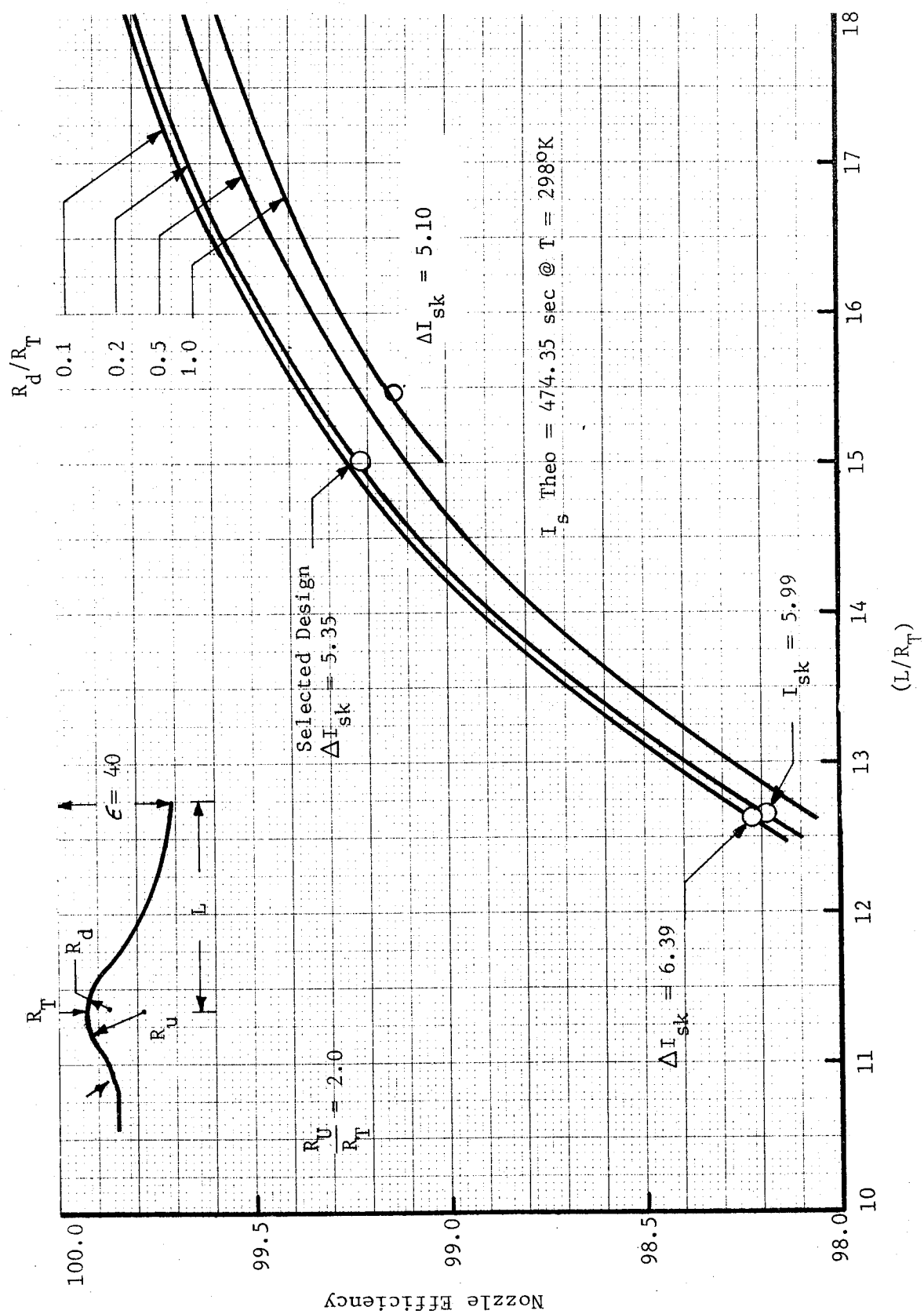
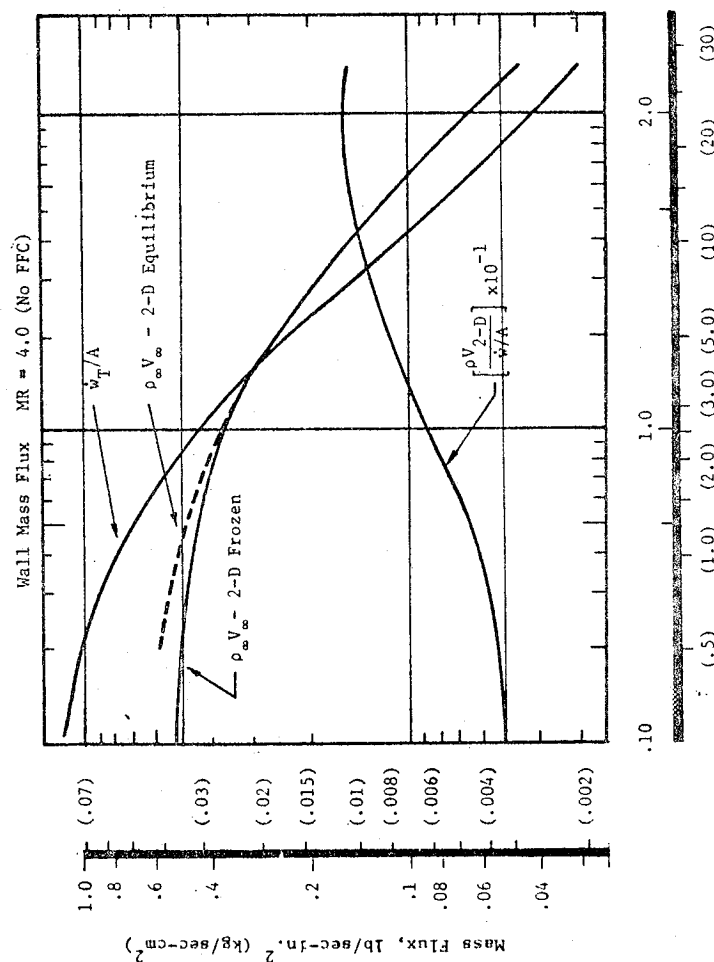
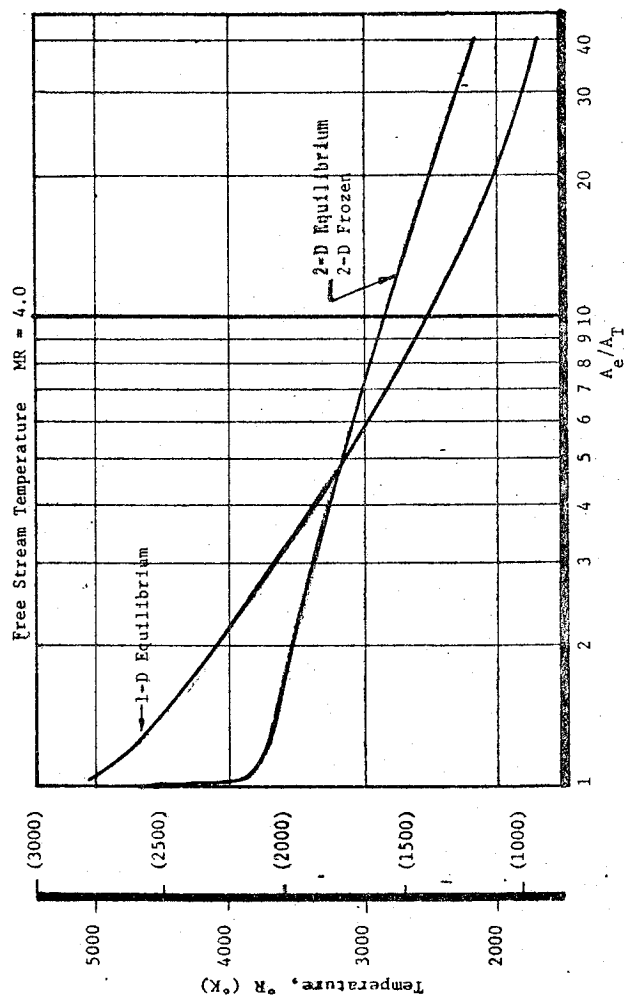
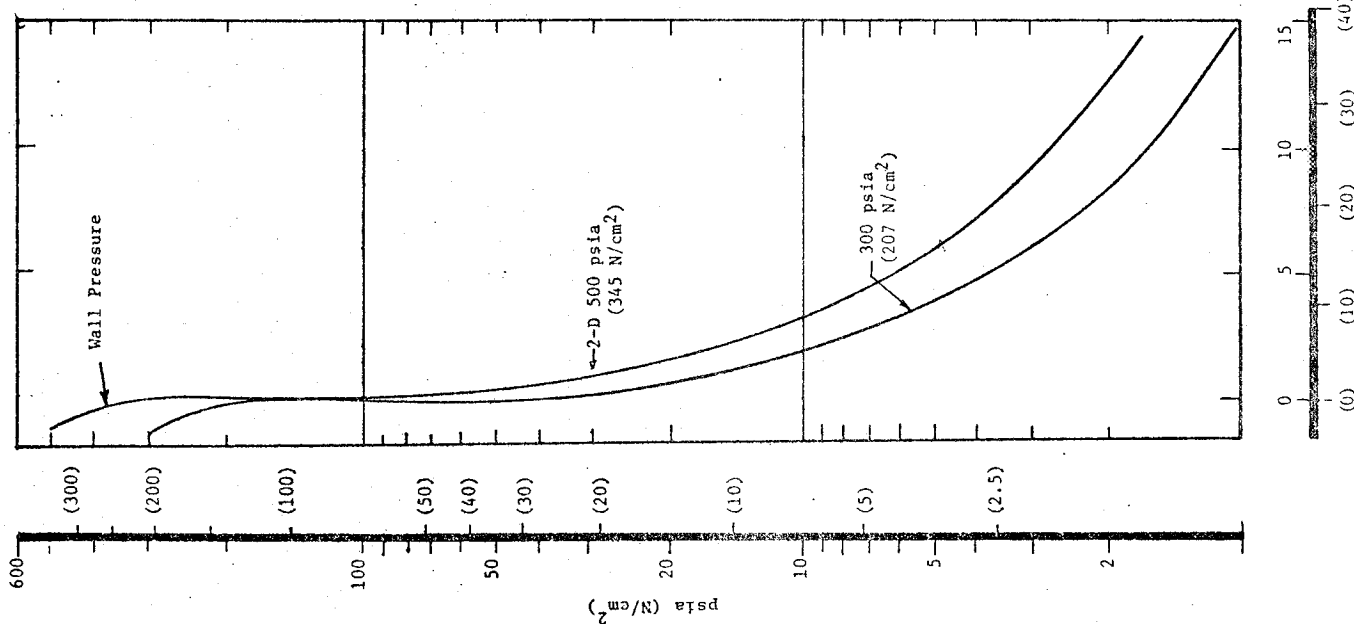


Figure VII-53. Optimization of the Rao Nozzle Contour



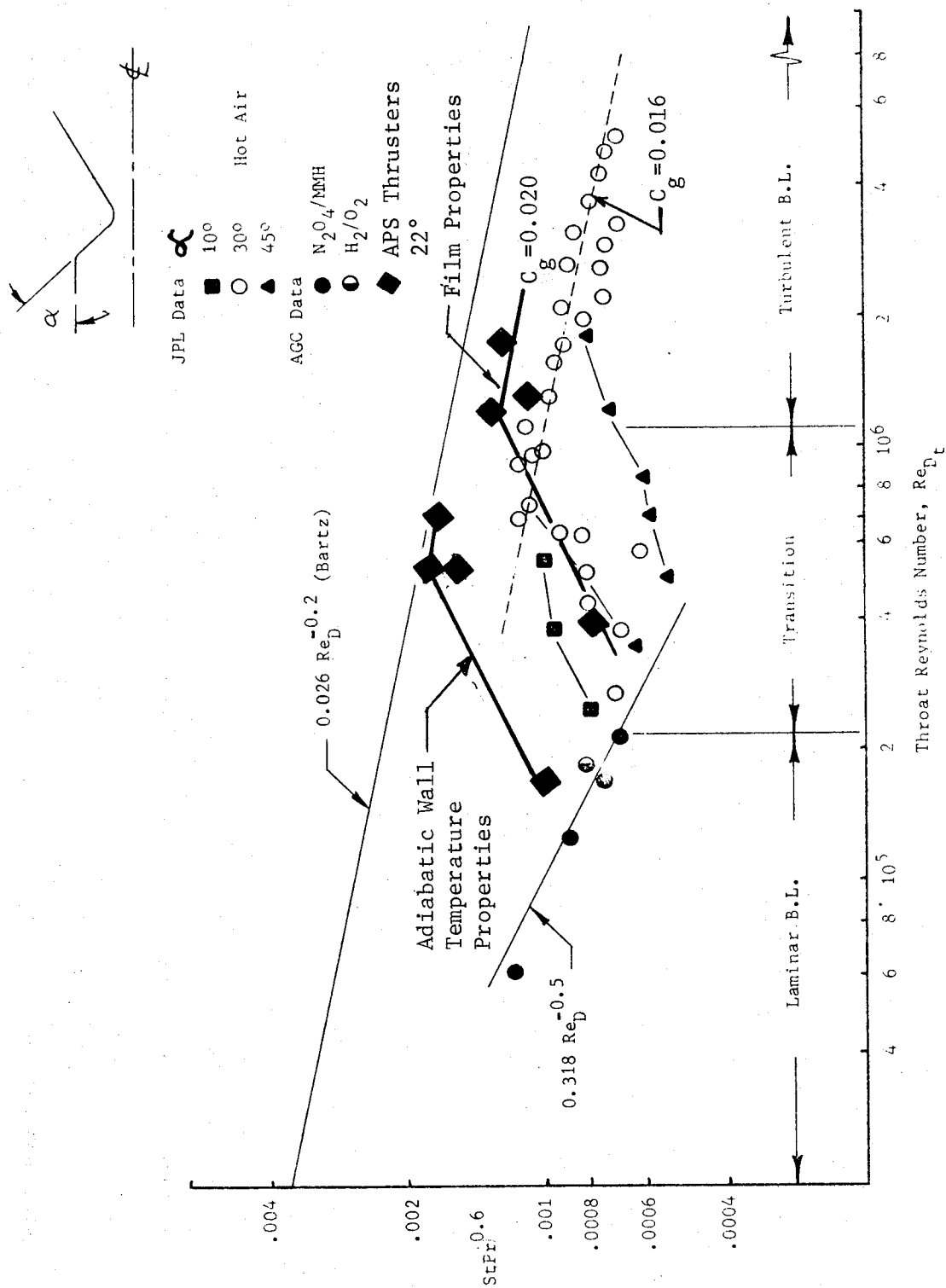


Figure VII-55. Nozzle Throat Heat Transfer Characteristics

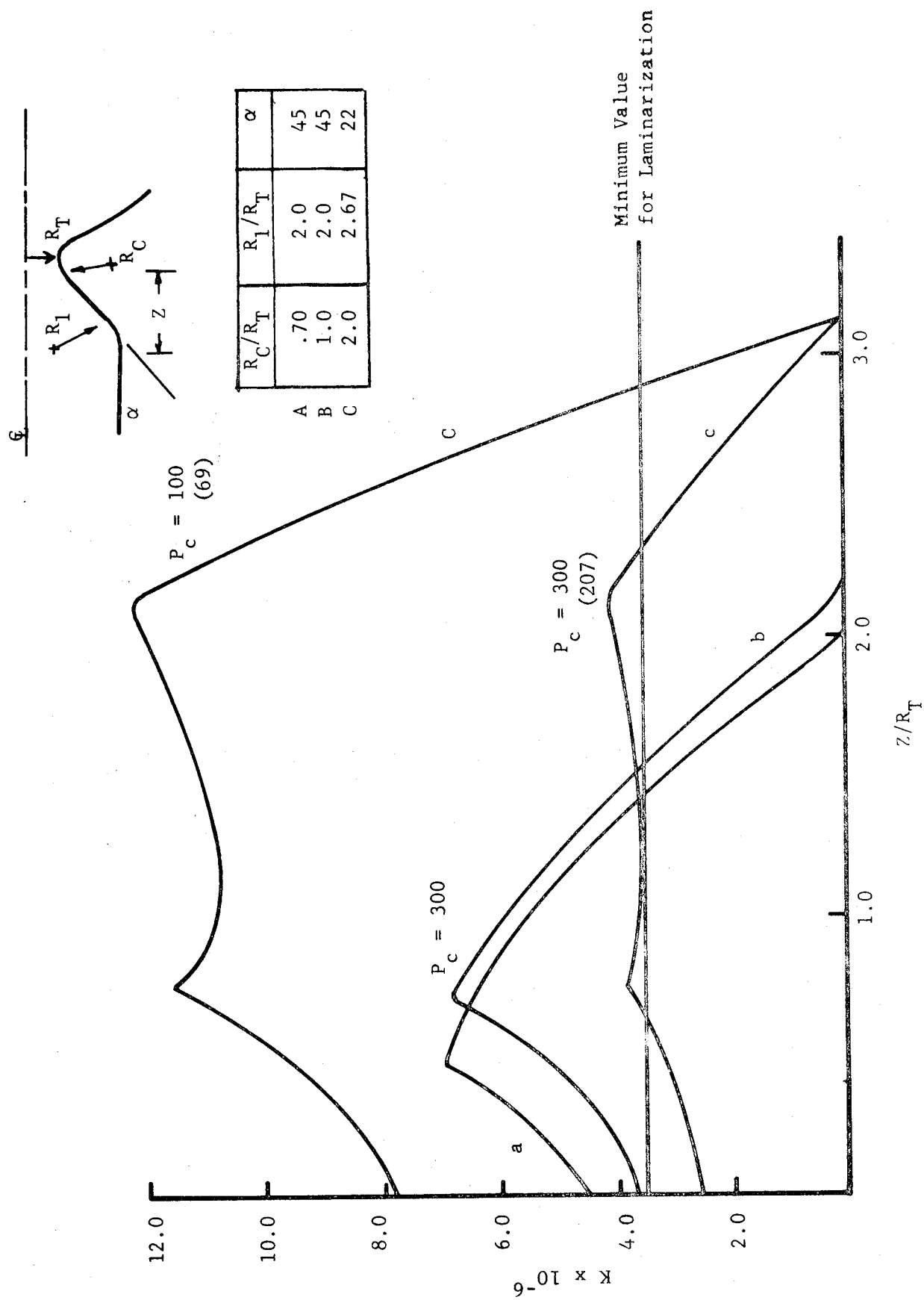


Figure VII-56. Criteria for Laminarization of the Regeneratively Cooled Chamber

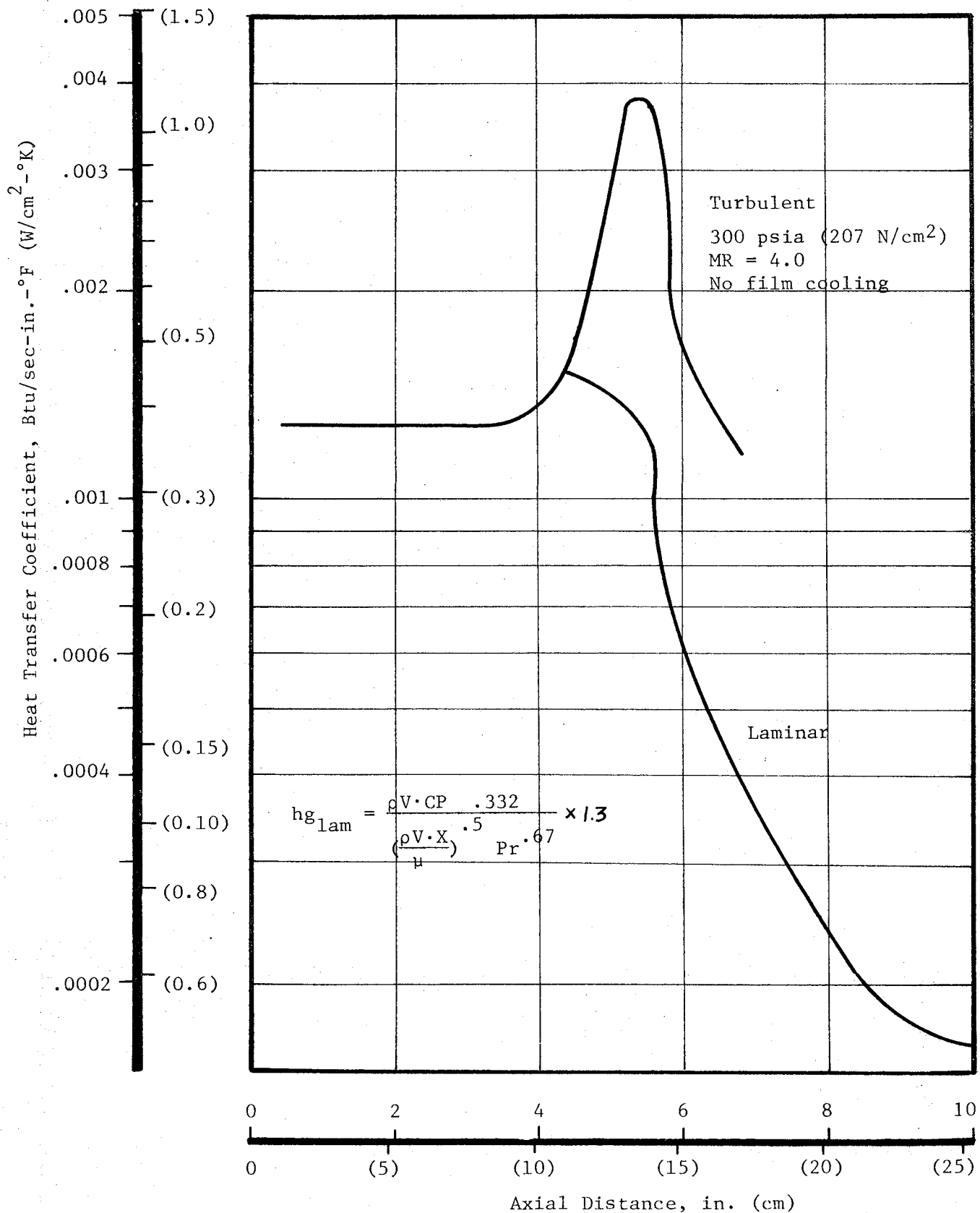


Figure VII-57. Predicted Laminar and Turbulent Heat Transfer Coefficients for Phase II Regeneratively Cooled Chamber

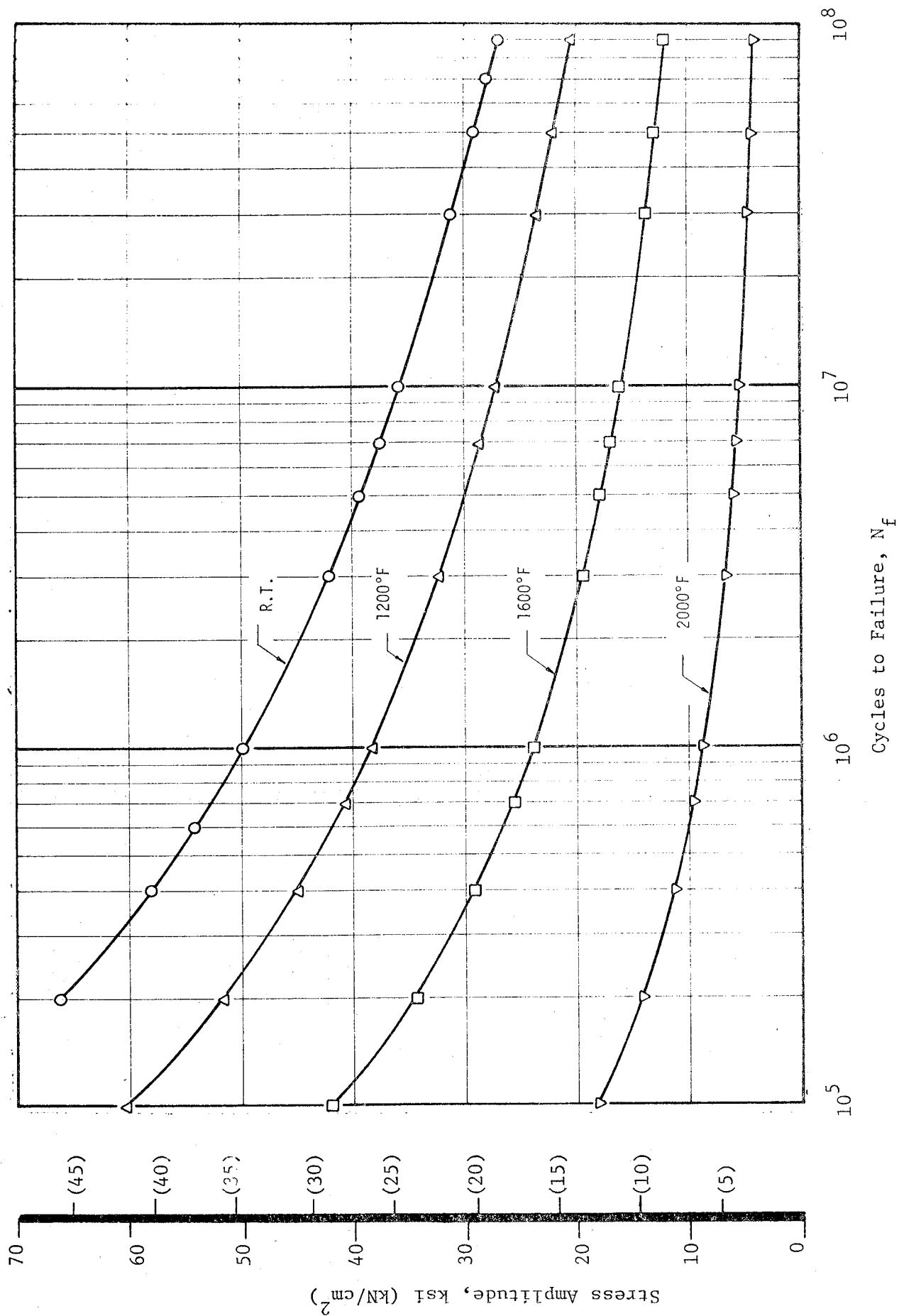


FIGURE VII-58 STRESS vs Fatigue Life (N_f). Haynes Alloy 188

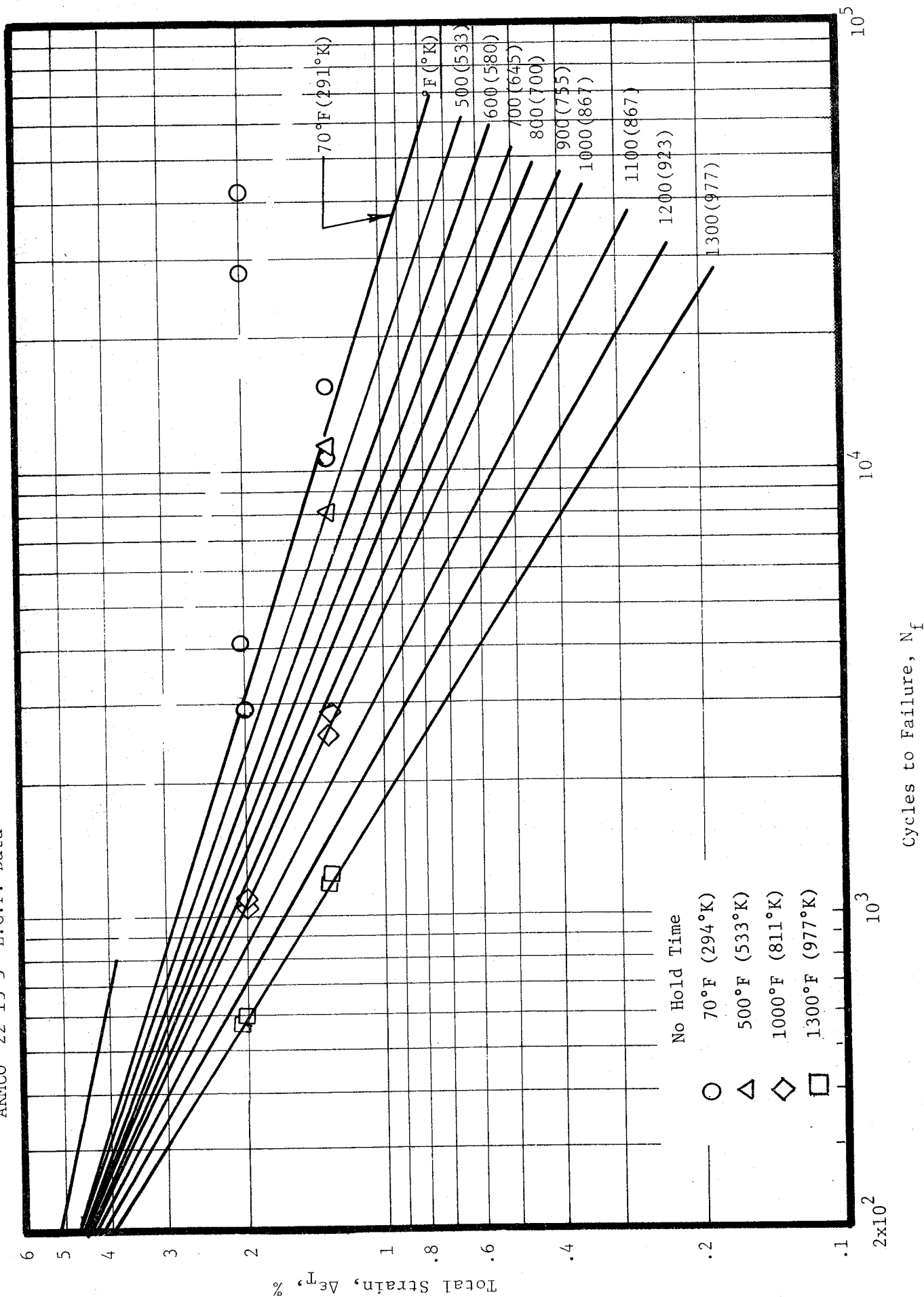
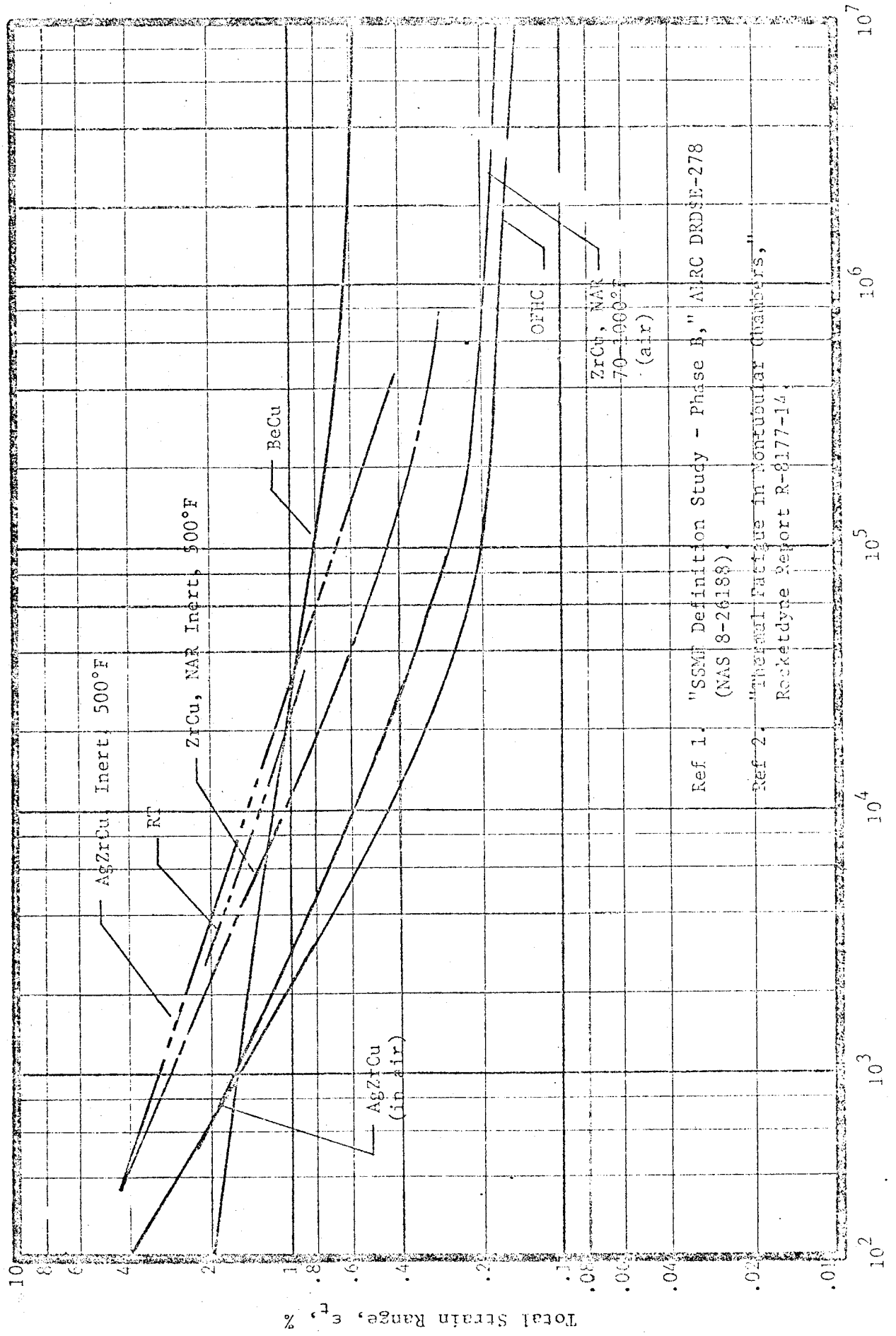


Figure VII-59. Total Strain vs Fatigue Life (N_f),
ARMCO 22-13-5



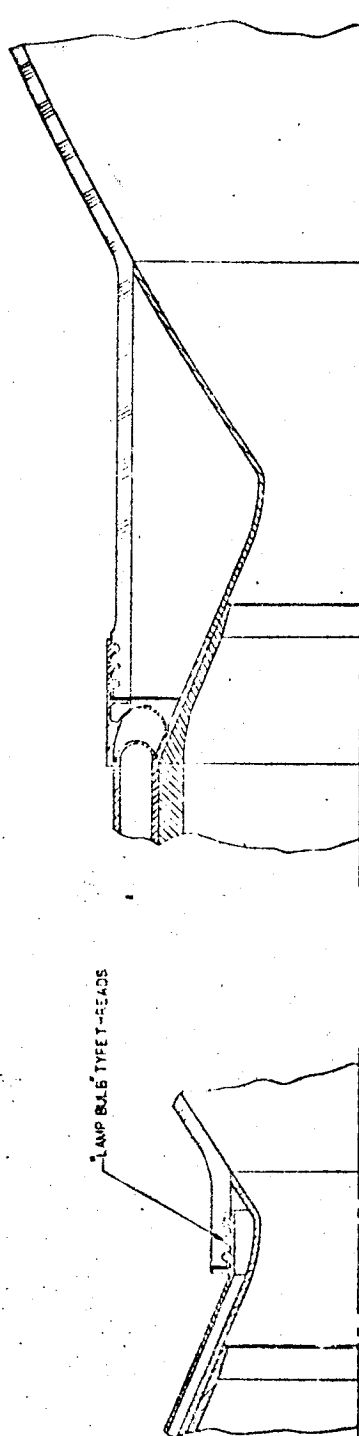
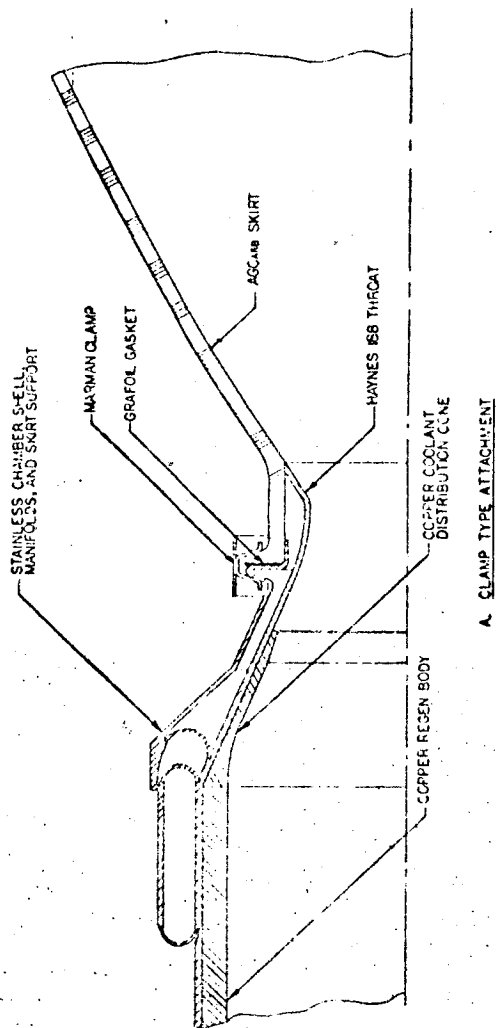


Figure VII-61. Attachment Methods for Removable or Refractory Skirts

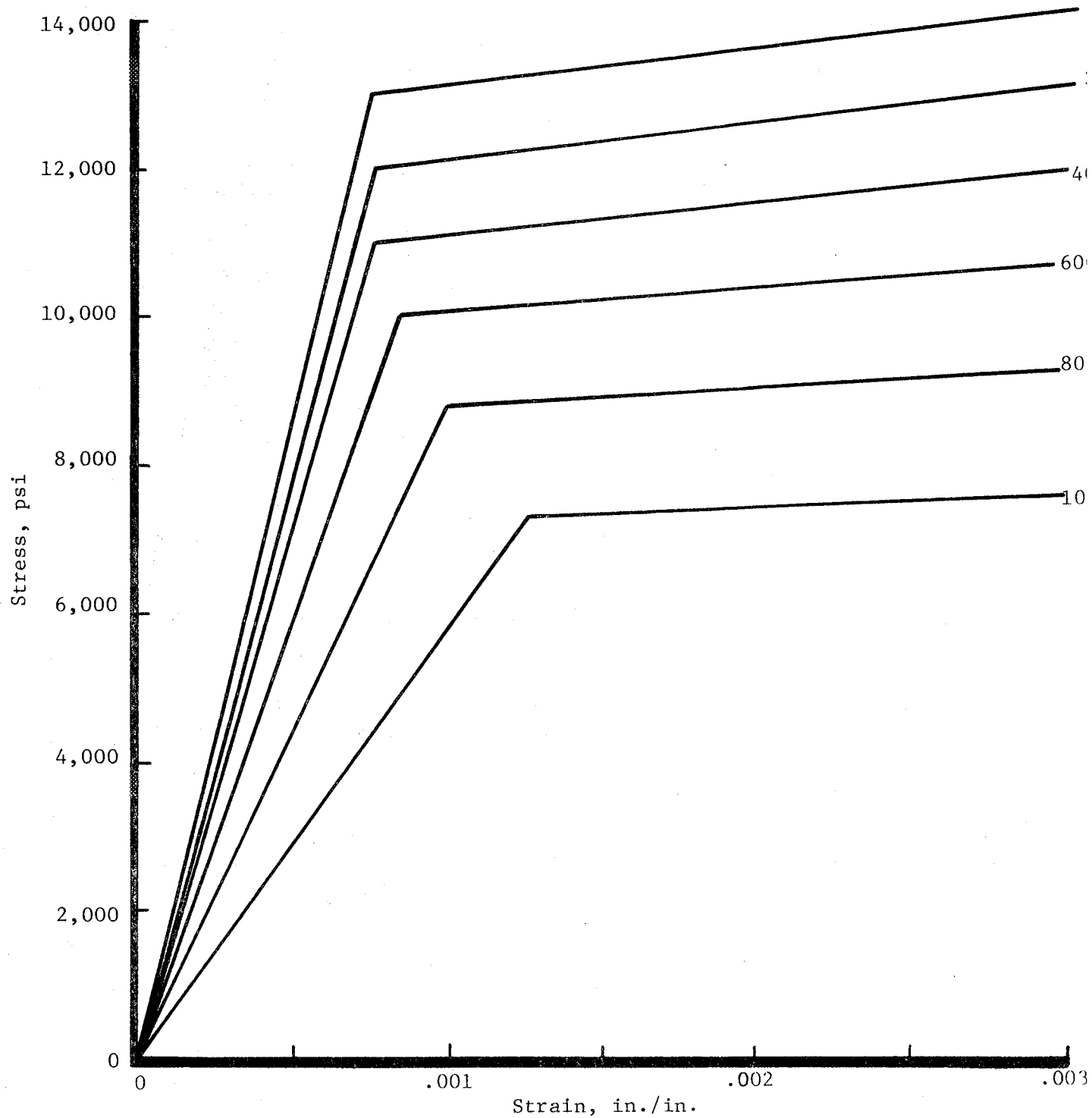


Figure VII-62. Secant Modulus Stress-Strain for Zirconium Copper

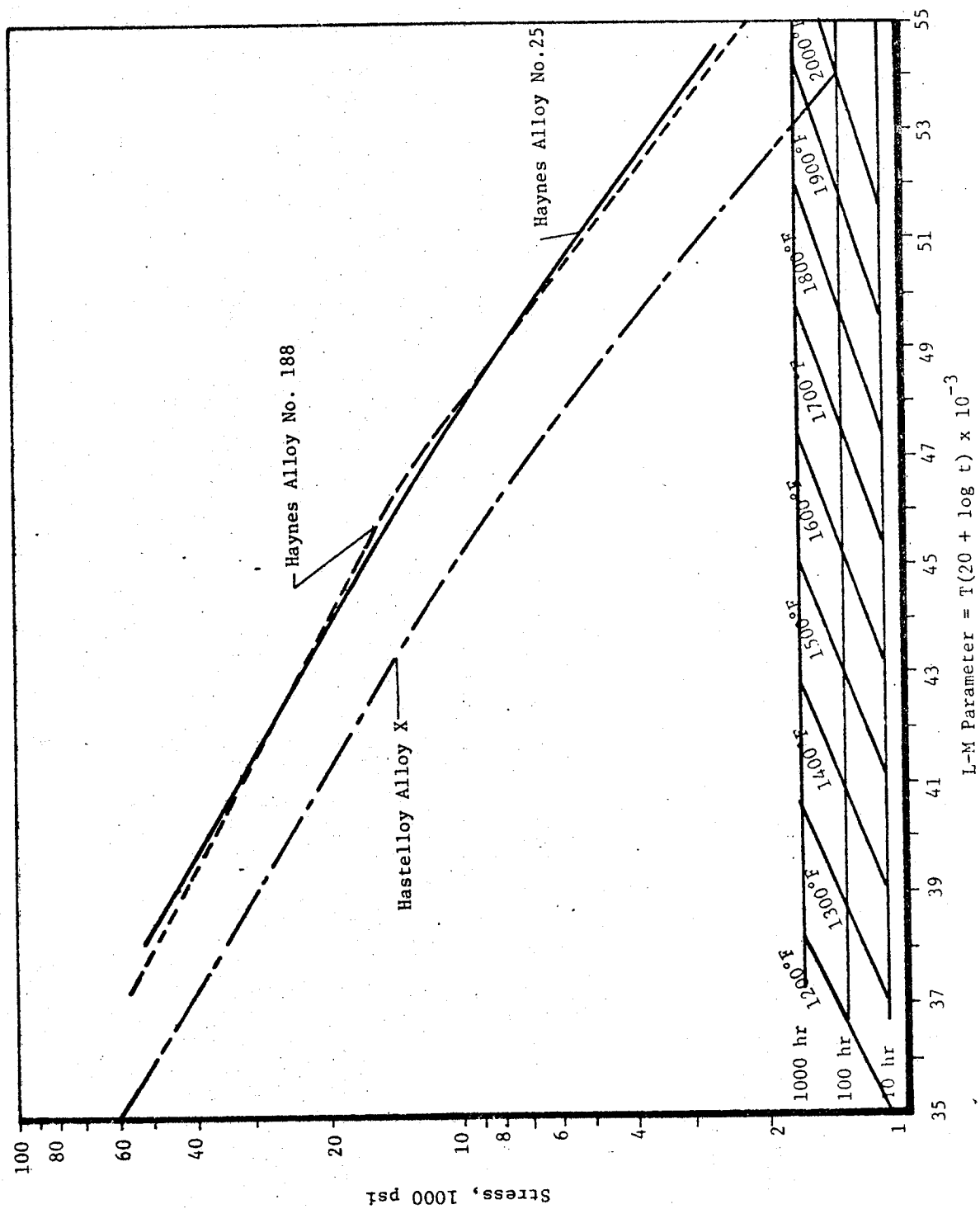


Figure VII-63. Haynes Alloy 188 Sheet Stress Rupture Strength (Larsen Miller)

VIII. LIFE ANALYSIS AND PREDICTIONS FOR 40:1 COOLED THRUST CHAMBERS

A. FILM COOLED CHAMBERS

1. Phase I Designs

Five conditions were considered to be critical in the life analyses of the Phase I film-cooled design:

(1) The local strains developed in the copper regenerative and dump cooled sections of the combustion chamber during the heating transient.

(2) The local hot and cold surface strains developed at the throat station during the heating transient due to radial temperature gradients.

(3) The strains developed between the film cooling injection plane and the throat at steady state due to the large axial temperature gradient.

(4) The creep limit life of the entire structure at steady-state operating conditions.

(5) The upper temperature limits of the skirt based on loss of material strength and chemical corrosion resistance at high temperatures.

a. Film Cooled Throat and Skirt Region

The cyclic and creep rupture life of the mono wall throat and skirt was computed based on the experimental temperatures and transient heating rates measured on SN 1 film-cooled chamber in Test 03-015. This analysis begins at the film coolant injection station, extends through the Haynes 188 throat and 304 stainless steel skirt to an area ratio of 40:1.

VIII, A, Film Cooled Chambers (cont.)

Figure VIII-1 shows the effective stress in the throat region between 0.05 and 0.10 sec when the thruster is started cold and where the Haynes 188 alloy is employed. The major component of this stress is due to the radial gradient through the wall. These stresses are actually reduced as the wall is made thinner. A nominal 0.045 in. (1.14 cm) wall thickness results in an effective stress of 72 ksi ($50,000 \text{ N/cm}^2$) (strain = 0.27%). A nominal 0.33 in. (.084 cm) wall thickness results in a 56 ksi ($39,000 \text{ N/cm}^2$) stress (strain = 0.21%). Strains of 0.27% and 0.22% convert to cycle lives of 4.6×10^5 and 1×10^6 , respectively. The region starting (.4 in.) (1 cm) away from the throat, upstream and downstream, operates in the elastic region and has a much greater life.

The radial temperature gradient decreases as the thruster continues to fire. At steady-state firing conditions (after about 1.0 sec), the remaining structural loads on the nozzle are due to thrust, internal pressure, axial temperature gradients, and whatever side loads or vibrational forces are generated by the system. These result in the effective steady-state stress profile shown in Figure VIII-2. The throat stress drops from the transient 72 ksi ($50,000 \text{ N/cm}^2$) down to a 5 ksi ($3,400 \text{ N/cm}^2$) steady-state value. The 5 ksi ($3,400 \text{ N/cm}^2$) compares favorably to an allowable, at temperature, 50-hr creep rupture stress of 40 ksi ($27,600 \text{ N/cm}^2$).

Figure VIII-2 further shows the actual steady-state stresses to be considerably below the 50-hr creep rupture limits of the selected materials throughout the length of the monowall portion of the chamber. The discontinuity in allowable stress at the 10-in. (25 cm) location is a result of the Haynes 188/304 stainless steel weld joint.

b. Regenerative Copper Lined Chamber Region

Figure VIII-3 identifies the life capabilities of the

VIII, A, Film Cooled Chambers (cont.)

convectively cooled copper lined region of the film-cooled chamber design exclusive of the manifold region for short pulses at nominal Phase I operating conditions. The predicted life is computed from experimentally measured gas and back side wall temperatures in the combustion chamber region for pulse widths based on electrical signals to the valves. The relationship between valve signal pulse width and bit impulse (BI) is also shown in this figure as measured from the pulse testing discussed in Section VI. The conclusions to be drawn from the figure are:

- (1) The chamber is capable of providing in excess of 10^6 firings of 230 lbf-sec (1020 N sec) impulse or less with either OFHC copper or zirconium copper using the most conservative material properties. This corresponds to a valve pulse width of 0.150 sec.
- (2) Chamber life drops rapidly as impulse requirements increase beyond this threshold of infinite chamber life.
- (3) The improved life provided by zirconium copper relative to OFHC becomes more significant as the pulse widths increase.
- (4) Operational modes can be selected to maximize life from this type of plot. For example, an impulse of, say, 300 lbf-sec (1335 N sec) ($N_f = 85,000$) can be achieved with less impact on chamber life by executing two 0.100-sec pulses ($N_f \gg 10^6$) rather than one 0.195-sec burn.

2. Life Expectations of Phase II Film-Cooled Chamber Design in Pulse Mode and Off-Nominal Operation

Five regions are identified as critical to chamber life:

- (1) Regenerative chamber section

VIII, A, Film Cooled Chambers (cont.)

- (2) Tip of film cooling ring
- (3) Throat
- (4) Skirt
- (5) Manifold region

A comparison of the difference between Phase I and Phase II film cooled chambers is presented in Table IV-4 while Table VIII-1 provides a summary of the analyses and life projections for the two designs. At nominal Phase II operating conditions, the life at the throat and at the tip of the coolant injector is limited by thermal transients, while the chamber and skirt achieve their life limiting condition at thermal steady state. A life vs burn time, different for each point in the chamber, therefore exists. In addition, all burns may not occur at the nominal design conditions and the extent of off-design operation will impact each of the critical locations in a different manner. In order to reduce the number of combinations of variables and provide working curves which relate life to operating conditions, those variables which were experimentally shown to have second-order effects were eliminated from consideration as indicated in the following discussion.

Figure VIII-4 shows the relationship between bit impulse, valve electrical signal, and life in the region of the combustion chamber in which the hydrogen convectively cooled slotted copper liner is employed. Two locations are shown: the critical locations in the regenerative section and the tip of the film coolant injector. Life for ZrCu and OFHC copper are provided using the minimum value properties defined in Section VII. This curve is based on nominal Phase II operating conditions defined in Table IV-1. The life in this region is not significantly influenced by mixture ratio shifts or the amount of film cooling employed. Changes in chamber pressure will result in a proportional shift in bit impulse for a given valve pulse width; however, life vs impulse is influenced to a much less extent since the more adverse thermal loadings for

VIII, A, Film Cooled Chambers (cont.)

the higher pressures will be offset by the fact that a given impulse is achieved with a proportionally shorter burn. An assumption made in the preparation of Figure VIII-4 is that the initial hardware temperature is at 530°R (295°K) and that the fuel temperature is 250°R (139°K). If the thruster is warmer than the nominal value because it had just been fired, the life expectancy is greater; if it is colder, life will be less.

An example of the use of Figure VIII-4 is as follows:

The desired impulse is 75 lb-sec (333 N-sec). What is the valve signal required as defined in Section VI and how many pulses of this width can be accumulated before there is a probability of a crack of engineering significance?

An answer is obtained by entering the left side of figure at the desired impulse and reading right to the bit impulse curve and down to 65 milli-sec valve electrical pulse width. Life is obtained by reading up to material and location curves and then right again for N_f ; i.e., 10^6 cycles on ZrCu at tip of the film cooling injector and 10^7 in the chamber region. For OFHC copper, the injector tip N_f is 10^5 .

It is noted that life decreases rapidly as pulse width increases up to about 150 millisec and that burns longer than 150 millisec produce almost no additional reduction in component life.

Figure VIII-5 is applied to the steady-state operation of the throat and skirt and provides parametric information relating mixture ratio, percent fuel film cooling, and propellant supply temperatures. Changes in chamber pressure do not measurably alter the results shown. The recommended design point for Phase II conditions is nominally 20% fuel film cooling for which the throat temperature is 870°F (740°K) and the peak skirt temperature is 1450°F (1060°K). The shaded area in Figure VIII-5 shows the safe operational

VIII, A, Film Cooled Chambers (cont.)

envelope for this balance point. Essentially, this thruster could operate at steady state up to a mixture ratio of 6.0 at chamber pressures from 100 to 500 psia (69 to 345 N/cm^2) for any propellant supply temperature defined in the Phase II envelope. Operation at mixture ratios up to 7.0 can be accommodated for periods up to 15 sec, which is the time required to achieve the skirt temperatures shown. Smaller operating envelopes would require a lesser amount of film cooling, thus improved performance, while larger variations can be accommodated by the use of higher film cooling flows as shown. The performance quoted in Section VI was based on MR excursions to 5.5 and 18% film cooling.

In contrast to skirt life, which is limited by the maximum material capabilities at elevated temperatures, the throat is limited by thermal strain which occurs early in the firing when the wall is cold. In addition, the material employed in the throat region cannot rely on protective coatings due to the thermal shock conditions which exist. Figure VIII-6 relates mixture ratio, percent film cooling, throat wall thickness, and chamber pressure to throat N_f for Haynes 188 wall material. Since maximum throat strains occur very early in a firing, every firing is assumed to be a thermal cycle in order to eliminate time as a parameter. The throat life at the nominal design point is obtained by entering at the engine design MR of 4.0, reading down to 20% fuel film cooling, right to the 0.040 in. (1.02 mm) wall thickness, and down to a life of $N_f = 1.3 \times 10^6$. Thinner walls result in greater life due to the reduced gradient, while increased chamber pressure reduces life due to combined higher heating rate and larger hoop pressure loading on the thin walls. It can be seen from Figure VIII-6 that increasing the chamber pressure to 500 psia (345 N/cm^2) results in an order of magnitude life reduction; however, this can be restored to 1.3×10^6 by simply employing 25% film cooling and a 0.030 in. (0.76 mm) wall thickness. The relationship between mixture ratio, life and film cooling can be similarly evaluated.

VIII, A, Film Cooled Chambers (cont.)

Hot starts and variations in propellant temperatures are not considered in this figure. A hot start does not constitute a thermal cycle and is less severe than the cases shown. The injection of coolant which is at a temperature greater than the design value will reduce chamber life. If all starts were to be made with 600°R (334°K) fuel, a wall thickness of 0.030 in. (0.76 mm) and 20% cooling would be required to provide the $N_f = 10^6$ capabilities at 300 psia (207 N/cm^2), $MR = 4.0$.

a. Supporting Design Analyses for Phase II Film Cooled Chamber Designs

Transient and steady-state two-dimensional heat conduction analyses were conducted on all chamber components with the exception of the manifold for which a three-dimensional network was prepared and evaluated at steady-state thermal conditions. The thermal boundary conditions employed were the recovery temperatures, gas and coolant side heat transfer coefficients derived from both sea level heat sink and 40:1 instrumented cooled chamber tests. The gas-side boundary conditions inferred from the heat sink and cooled chamber tests were in agreement. Theoretical coolant side coefficients include adjustment factors for entrance effects and roughness of the small channels such that the predicted and measured wall temperatures are in good agreement.

(1) Transient Thermal Conditions

Figure VIII-7 shows the results of the transient analysis in the copper-lined chamber region which includes a short, regeneratively cooled section (top) feeding the injector and the short, conical, convectively cooled film cooling injector (bottom). The purpose of these analyses is to establish the temperature profiles for the thermal fatigue analysis and to determine the physical location and point in time at which maximum thermal strain occurs. Temperature-time plots for three axial chamber positions and

VIII, A, Film Cooled Chambers (cont.)

four film coolant ring positions are shown. These are obtained from two-dimensional models representing the wall cross section.

Several general conclusions were drawn regarding the time of maximum thermal strain from these analyses. The time of maximum strain depends upon (1) the initial chamber temperature relative to the propellant temperature, (2) the wall thickness and nature of cooling channels, and (3) the wall material. The worst thermal condition will be at steady-state if the wall is relatively thick (large channel depth) and the initial chamber temperature is higher than the propellant temperature. [530 to 560°R (294 to 311 °K) soak temperature with 200 to 300°R (111 to 167°K) fuel coolant temperature]. In this case, firing the thruster results in cooling the backside while the gas side is heated. Such is the situation in the chamber region at nominal Phase II operating conditions.

The worst thermal strain will be found during the transient when both the gas and backside are heated when the thruster is fired, either because the coolant and initial structure are at the same temperature or because the wall thickness, material and coolant channel configuration allow penetration of a significant amount of heat to the exterior surface, causing its temperature to rise. This latter condition exists at the discharge end of the film cooling injection channels, $L/L_T = 1$.

Examples of these results are shown in Figure VIII-7 for nominal initial temperature conditions. In the chamber region, maximum thermal strain is found in the mid-region at steady state, while in the thinner conical film cooling region, maximum thermal strain occurs at the tip of the coolant injector at 0.18 sec into the firing.

VIII, A, Film Cooled Chambers (cont.)

(2) Chamber-Manifold Region Approaches - Steady-State Analyses

Figure VIII-8 shows the results of the three-dimensional steady-state thermal analysis of the more highly stressed chamber and throat region including the supply manifold. Axial heat conduction as well as heat flow through the wall and peripherally around the cooling channels are accounted for. In this activity, emphasis was placed on providing an accurate description of the temperature gradients around the inlet manifolds. Since the exterior of the manifold will always cool down when the engine is fired, the worst thermal strain at steady state rule applies. Three manifold configurations were investigated in this phase of the program. One was a single wall unitized design in which the manifold is made compliant such that it can accommodate the expansion of the heated copper liner. A second approach, shown in Figure VIII-9, had two rigid, concentric manifolds, one each for main and coolant flow, which allowed internal flow balancing. This approach accommodated biaxial thermal expansion via an axial expansion joint and radial, liner-to-jacket gap (noncontacting liner and jacket). A third approach was considered when the structural analysis, showed several highly strained regions due to the large temperature gradients between the cold manifolds and the points where they attach to the chamber. The modified design incorporates a double compliant wall manifold such that the cold H_2 flowing within the manifold contacts and cools only the inner wall, while the outer wall is attached rigidly to the structure. The outer manifold is the pressure structure and also supports the inner liner through a series of standoffs and local welds similar to the principle employed in most thermally isolated containers.

Figure VIII-9 provides the detailed three-dimensional thermal map at steady-state conditions for the monowall manifold design. This figure shows the axial, radial, and circumferential temperature profiles from the injector attachment point to approximately 2 in. (5-cm) downstream of the

VIII, A, Film Cooled Chambers (cont.)

throat, beyond which the temperature gradients are small. Thermal sections A through D provide cross sections of the chamber wall in the region of the chamber where coolant channels are machined into the copper. Each insert shows the materials involved, the wall and channel dimensions at the local stations, the radial and peripheral temperature profiles around the rectangular coolant channels, and the coolant temperature at the station involved. These maps are essential in prediction of the chamber life since it is the difference between the maximum surface temperature and a weighted average mass temperature which produces the thermal strains which can lead to fatigue failures. In these profiles, wall temperatures are lowest at the coolant manifold and increase moving in both a forward and aft direction. The temperature increase in the forward direction is due mainly to the bulk temperature rise of the fuel. The increase in the aft direction is due to combined coolant temperature rise and increasing heat flux as the flow approaches the throat. The nominal gas to backside gradients are 150 to 160°F (87°K) throughout the entire chamber, exclusive of the manifolding region, however. The radial gradient in Section D is smaller than Sections A through C even though the heat flux is higher because of the reduced channel depths and wall cross section at Section D. The peripheral variation (i.e., temperature over the cooling channel vs between channels) is seen to be very small (several degrees). This is due to the close channel spacing and high thermal conductivity of the gas-side material. The peripheral variation in the outer steel jacket is noted to be considerably larger, especially in the region directly behind the coolant channel. This is a result of the heat flow path through this low conductivity material. It is shown in the next section that the high gradients in the steel do not represent a limiting structural condition.

Section E provides the temperature distributions in the manifold and manifold attachment region. The entrance region effects of the coolant are noted to reduce the copper temperature over the coolant inlet. The slightly higher copper temperatures immediately aft are due to the trans-

VIII, A, Film Cooled Chambers (cont.)

ition from deep to shallow slots in the film cooling circuit which is supplied from the regenerative chamber circuit. Some additional design optimization may allow this situation to be improved. The major item of structural concern is the larger gas side to backside temperature differences resulting from attachment of the cold manifold, which is noted to drop the external temperature. The maximum gradients in the manifold wall also occur at the attachment point while the bulk of the manifold is at the coolant supply temperature.

The axial temperatures shown in Section F are those at the tip of the film cooling ring and film-cooled nozzle through the throat. Gas-side, backside, and two intermediate temperatures are shown for 20% of the fuel flow through the coolant injector. Large axial gradients are noted to occur between the tip of the coolant ring and the throat. The rapid drop in wall temperature immediately following termination of the copper wall and discharge of the coolant from the slots was confirmed experimentally. The drop in temperature is due to the fact that the exterior wall is now completely shielded from the combustion products by the coolant (i.e., the wall is no longer being heated by conduction through the copper). The rapid rise which follows is due to mixing of the film coolant with the core flow in the short distance between injection and the throat.

Figure VIII-10 provides comparable data for a dual wall manifold. The major difference in thermal profiles occurs in Section E where the temperatures at the manifold attachment point are much closer to what the wall temperatures would be if no manifold existed at all. In addition, the variation in temperature along the thin manifold from the backside at the attachment point to the coolant supply temperature is much more gradual. Both of these favorable effects are a result of providing a stagnation zone between the outer pressure manifold and the inner manifold containing the high velocity hydrogen supply.

VIII, A, Film Cooled Chambers (cont.)

The finite element grids and the results of plastic structural analyses are shown in Figure VIII-11 for the dual wall manifold. Manifold region grid and structural analyses are shown based on nominal operating conditions using the steady-state thermal maps shown in previous figures. Separate computer runs with the same grid provided proof pressure only data.

Several structural grids are shown in the figure. The upper left provides the detail for the dual wall manifolding, its attachment to the chamber, the chamber region, and the transition from the channeled to monowall construction at the tip of the film cooling injector. The result of this structural analysis is shown in the upper right, including total deflection in inches, resulting from pressure, thrust and thermal loads and effective stresses (ksi) from combined loads. In regions where maximum stresses are less than yield value for the material, a safety factor (defined as $s_{\text{yield}}/s_{\text{max}}$) is provided. Section AA in the lower left shows the grid, local stress, and strain profiles for the most severe loading in the regenerative chamber region, while the models at the mid and lower right were used to define the most severe environment between the coolant injection and throat stations.

The conclusions to be drawn are:

(1) The entire 22-13-5 outer structure and manifolding operate within the yield range with a minimum factor of safety based on combined stresses of 1.06 at the aft manifold attachment point. The minimum factor of safety for a pressure only load condition occurs at the flat outboard end of the 0.020 in. (0.051 cm) thick manifold and is (SF = 1.35) based on an 875 psia (604 N/cm^2) proof condition.

(2) Only the internal copper components are stressed beyond their yield point and all such loading is thermally induced. The minimum

VIII, A, Film Cooled Chambers (cont.)

life is based on the tip of the film cooling ring for which the earliest predicted crack is $N_f = 50,000$. Since the copper does not carry any structural load, however, a failure at this point has no significance.

(3) The highest strain levels of significance occur in the chamber region in the copper wall directly above (inboard of) the coolant channel. $\epsilon = 0.25\%$ corresponds to a N_f of 100,000 based on steady-state thermal conditions.

(4) The higher local stresses outboard of the slotted channel are caused by the peripheral temperature gradients around the back of the channel. These are quite acceptable since they are completely within the high strength 22-13-5 material and provide a safety factor of 1.6 during steady-state operation.

(5) The throat region cyclic life is dictated by the start transient and is nearly an order of magnitude greater than the remainder of the chamber. Slight reductions in the throat wall thickness can provide even greater life.

Comparison of the dual and monowall manifolding structural analyses using the appropriate thermal profiles and the same finite element grid provided the following results:

(1) An uninsulated (monowall) manifold causes larger bending stresses at the aft attachment point than the dual wall design. Local stresses move from elastic to inelastic operation with a resulting strain level of 0.55%. The inelastic manifold design provides a thermal life capability of 1.5×10^5 , and pressure cycle capability exceeding 10^6 compare to a thermal life exceeding 10^6 for the dual wall design.

VIII, A, Film Cooled Chambers (cont.)

(2) Copper life inboard of the manifolding decreases due to additional restraint of the cold monowall manifold. Strain increases from 0.25 to 0.34% and life decreases from 100,000 to 45,000.

(3) Stresses in elements in the structural jacket at the inlet to the coolant channels start to approach the endurance limit:

	<u>Stress Level</u>
Dual wall	39 ksi
Monowall	50 ksi
Endurance limit	60 ksi
22-13-5	

The third configuration investigated (shown in Figure VIII-9) employed expansion gaps as discussed earlier. This design was found to be less desirable because of anticipated fabrication problems in the expansion joint and generally higher stresses in both the copper and steel jacket. The initial analysis was conducted for a 304 manifold and jacket, for which the manifold life N_f was found to be limited to 30,000. A re-analysis using 22-13-5 material showed a considerable improvement, to $N_f = 10^5$, however, still marginal for the APS requirements.

The support of the copper film coolant injector rigidly at one end and by the expansion joint at the other rather than continuously as in the previous designs was found to result in high bending stresses near the aft rigid attachment point due to the relative radial growth at the restrained and unrestrained ends. The stresses resulting in the omega-type seal were also found to be structurally unacceptable for long life. Another reason for not selecting this design is that the nonbonded liner cannot withstand the over pressure which could result if there was a combustible mixture in the channels. A flashback such as described in Section V of the pulse testing is possible in the fuel manifold if an oxidizer lead is employed.

VIII, Life Analysis and Predictions for 40:1 Cooled Thrust Chambers (cont.)

B. REGENERATIVELY COOLED CHAMBERS

1. Phase I Designs

The life projections for the Phase I regeneratively cooled chambers are based on the experimental results reported in Sections V and VI. The life limiting location of this design has been experimentally identified as being just up stream of the throat for all operating modes corresponding to a turbulent boundary layer. At reduced pressures corresponding to throat laminarization the critical stress location moves to the chamber region.

a. Steady State Thermal and Life Characteristics

Figure VIII-12 provides a summary of the measured steady-state gas-side wall temperatures and wall ΔT (difference between measured gas-side and measured backside) at a station 0.6 in. (1.52 cm) upstream of the throat for various test conditions. These temperature measurements were used to calculate chamber life and identify the maximum wall temperatures for long-term creep damage analysis. The N_f values shown on the right are the ZrCu minimum values neglecting the long term creep effects. The first set of plots (left side) show the influence of variable film cooling introduced at the injector plane. Film coolant flows greater than 10% are required to provide a significant reduction in wall temperature and temperature gradients, and upstream coolant flows in excess of 30% are required to achieve the goal of 10^5 full thermal cycles.

The center plot shows the influence of chamber pressure on these parameters. Mixture ratio is a parameter of secondary importance. Increasing chamber pressure has a very significant role in increasing the temperature gradients and reducing chamber life. The plot on the right shows the influence of coolant inlet temperature at 300 and 500 psia (207 and 345 N/cm²). Lower propellant temperatures produce lower maximum wall temperatures but result in slightly higher temperature gradients.

VIII, B, Regeneratively Cooled Chambers (cont.)

The conclusions are that the regeneratively cooled chamber is not sensitive to mixture ratio or propellant temperature, life is adversely influenced by higher chamber pressures and is helped only slightly by film cooling from the injector.

b. Transient Characteristics

The data presented in Figure VIII-13 related to the transient operation of the Phase I regeneratively cooled chamber design. The upper portion of the figure shows the measured heating rate at the critical gas-side location 0.6 in. (1.52 cm) upstream of the throat for six starting conditions:

- (1) Nominal chamber pressure with cold, ambient, and heated propellants.
- (2) Maximum pressure (500 psia) (345 N/cm^2) with cold and ambient propellants.
- (3) Minimum pressure (100 psia) (69 N/cm^2) with ambient propellants.

The initial hardware temperature in the tests shown varied from 330°R to 710°R (183° to 394°K). The heated propellant tests and high pressure tests produced the most severe thermal environment.

The lower portion provides the measured gas side to back-side temperature gradient for the same six start conditions. These data fall into three major groupings with pressure as the primary operating variable and propellant temperature as a second-order effect. The gradients after several seconds of firing are slightly lower than the value shown because the exterior continues to rise after the gas-side has steadied out.

VIII, B, Regeneratively Cooled Chambers (cont.)

The most significant aspect of the gradient vs time plot is that maximum strains are not achieved until approximately 0.4 to 0.5 sec from 90% of full thrust; therefore, pulses shorter than this constitute a less damaging or partial thermal cycle. The second set of lines provides an estimated pulse width vs life for this design with ambient propellants at three chamber pressures. These curves are read from the log scale on the right which provides N_f based on minimum experimental S-N value properties for ZrCu. A single life vs pulse width line is shown from 300 and 500 psia (207 and 345 N/cm²) operation at pulse widths of 0.4 sec or less. This is apparently due to the fact that the higher pressure data correspond to a warm chamber start which made the transient conditions slightly less severe. The 100 psia (69 N/cm²) line is only of comparative interest since, at low pressures, life is controlled by the chamber region and not the throat region condition.

In summary, the 10^6 pulse capabilities is possible with the Phase I design for nominal pulse widths of 135 lb-sec or less. Life then decreases very rapidly as pulse widths become longer than this critical value. Pulses of 0.5 sec represent the most severe condition.

2. Phase II Regeneratively Cooled Chambers

The Phase II regeneratively cooled chamber was designed to provide extended life without the use of head end film cooling by providing a contour which reduced the throat heat flux. The thermal data presented in Section VI suggested that the predicted flux reduction was realized but the results were not conclusive. The following table identifies the projected life of the Phase II design based on the more optimistic experimental data.

VIII, B, Regeneratively Cooled Chambers (cont.)

P_c		Chamber				Throat			
		ΔT^*		%	N_f^{**}	ΔT^*		Strain	N_f^{**}
psia	N/cm ²	°F	°K						
100	(69)	120	(66)	.195	10^6	170	(94)	.277	2×10^5
200	(138)	230	(128)	.375	3×10^4	220	(122)	.358	3.5×10^4
300	(207)	310	(172)	.505	1.5×10^4	280	(156)	.456	2.0×10^4
400	(276)	370	(206)	.605	10^4	320	(178)	.520	1.5×10^4
500	(345)	400	(222)	.650	7.5×10^3	380	(211)	.620	9.5×10^3

* ΔT from Figure VI-23

**Min prop. ZrCu cold propellants from Figure VII-60

At nominal operating conditions, a crack of engineering significance could become probable in the chamber region after 15,000 full thermal cycles based on minimum data and in the throat region after 20,000 full thermal cycles assuming the throat has laminarized. Use of the fatigue life properties in an inert environment of Reference 2 of Figure VII-60 results in an order of magnitude higher life predictions. Additional evaluation of the fatigue life of copper in the 0.2 to 0.5% strain range in a hydrogen, H_2O atmosphere is warranted.

TABLE VIII-1

SUMMARY OF FILM COOLED CHAMBER DESIGN ANALYSES
(Nominal Operating Conditions)

<u>Location</u>	<u>Analyses</u>	<u>Results</u>
Chamber	Thermal - 2-dimensional transient and steady state, several channel geometries	Worst thermal condition at steady state; max. wall temp 320°F, max. ΔT 162°F 80 channels, .050 wide .150 deep .035 wall
	Structural - 2-dimensional finite element plastic at worst thermal conditions.	Max. strain .25 % steady state. Thermal $\eta_f = 100,000$
Film Coolant Injection Section	Thermal - 2-dimensional transient and steady state, several channel geometries	Worst thermal conditions .18 sec Trans. ΔT max = 200°F, SST max = 480°F
	Structural - 2-dimensional finite element plastic at .18 sec and thermal steady state	Max. strain .32% at .18 sec, η_f Therm = 50,000 Steady state strain .26%, η_f thermal = 90,000
Throat Region	Thermal parametric analyses of % FFC and wall thickness based on test data	Max. Temp at steady state < 1200°F Max Temp gradient at 0.05 to 0.1sec
	Structural 1 and 2-D plastic analyses transient and steady state (parametric results presented graphically)	⁶ 10 thermal cycles 19% FFC .04 wall. Transient worst condition.
Skirt	Thermal analysis transient and steady state	Steady state worst thermal condition based on max temp 20% FFC 1500°F
	One and 2-D plastic structural analysis	Life not limited by high temp creep > 1000 hrs at 1800°F with stainless steel
Manifold	3-D thermal analysis of three designs. 2-D plastic analysis of two designs 2-D elastic analysis of one design	Results discussed in separate section. One design found superior in structural life. Manifold is not a limiting factor in life. Worst condition at steady state.

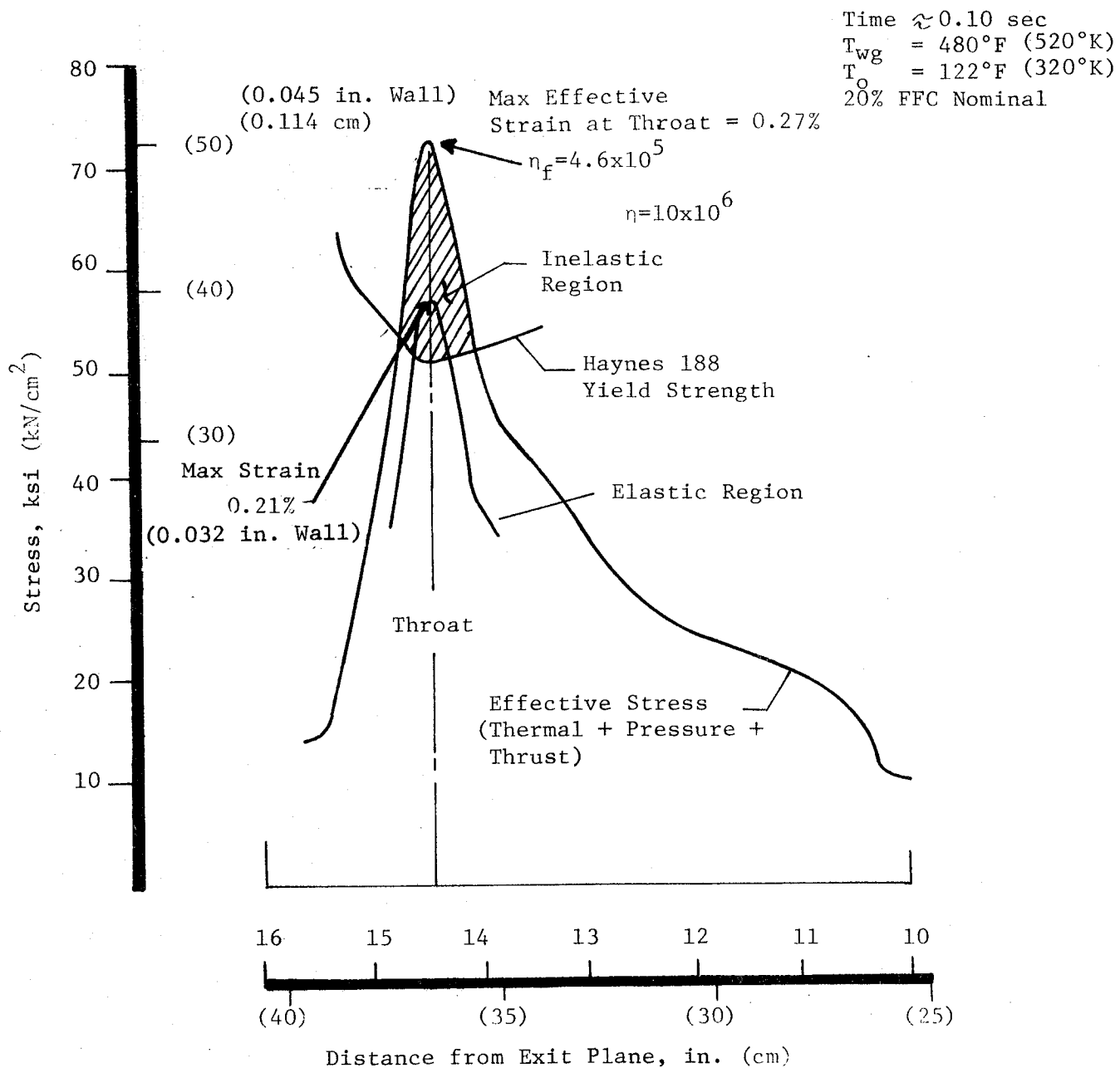


Figure VIII-1. Film Cooled Chamber, Haynes 188, Maximum Combined Stress Profile at Throat Station During Thermal Transient (300 psia [$207 \text{ N}/\text{cm}^2$])

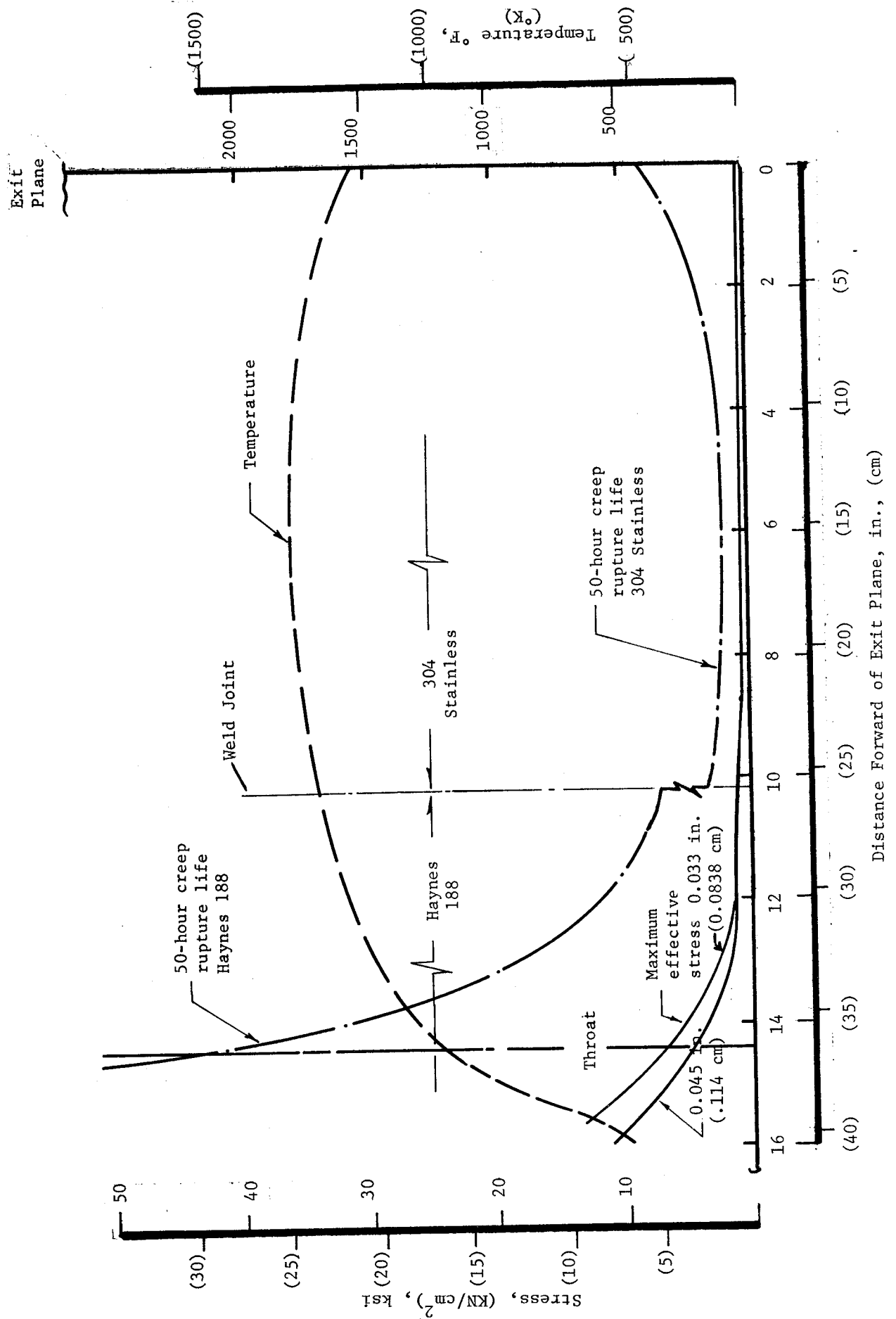


Figure VIII-2. Film Cooled Chamber Steady State Nozzle Stress Profiles

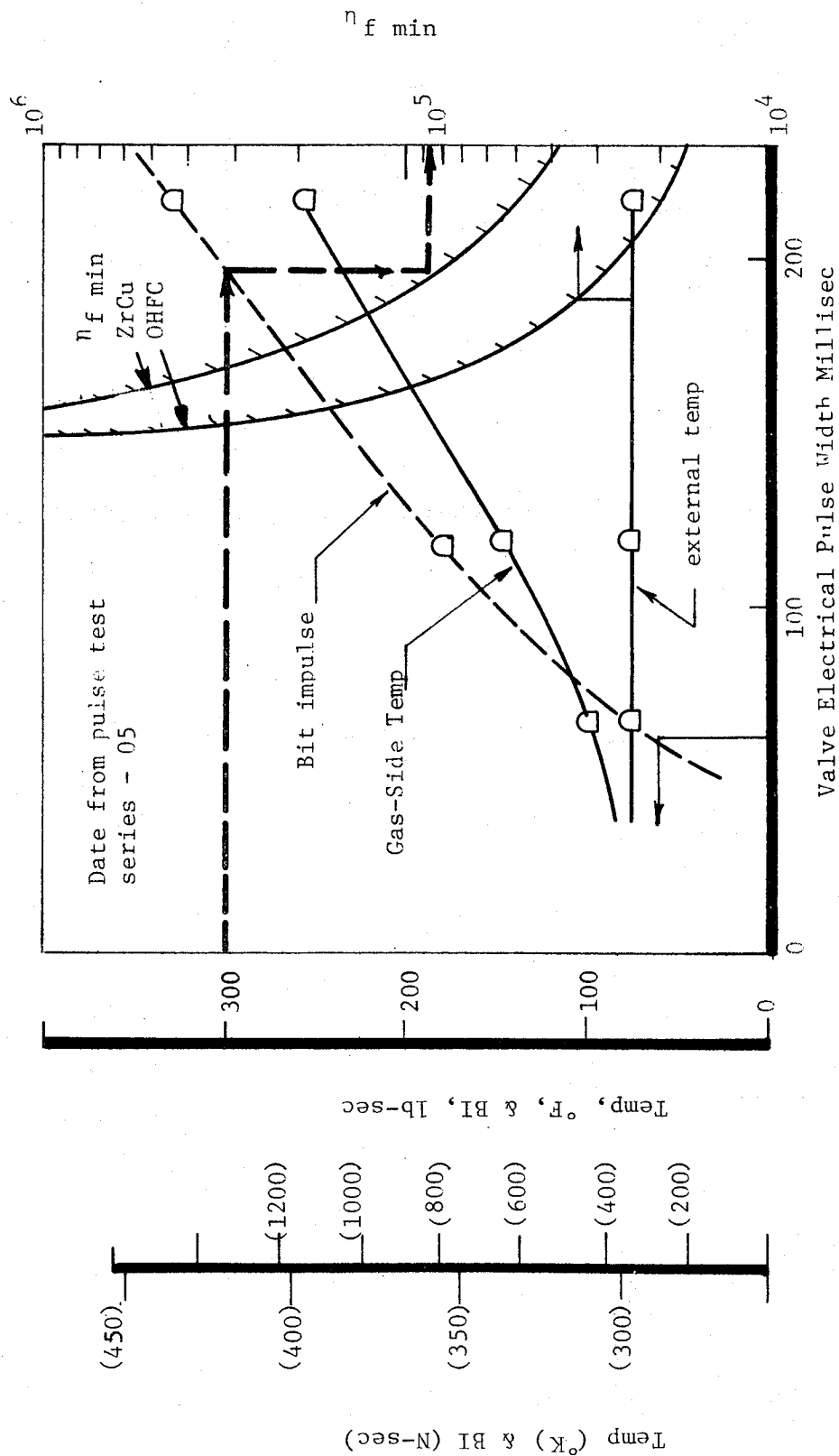


Figure VIII-3. Bit Impulse and Cycle Life of Phase I Film Cooled Chamber at Nominal Operating Conditions

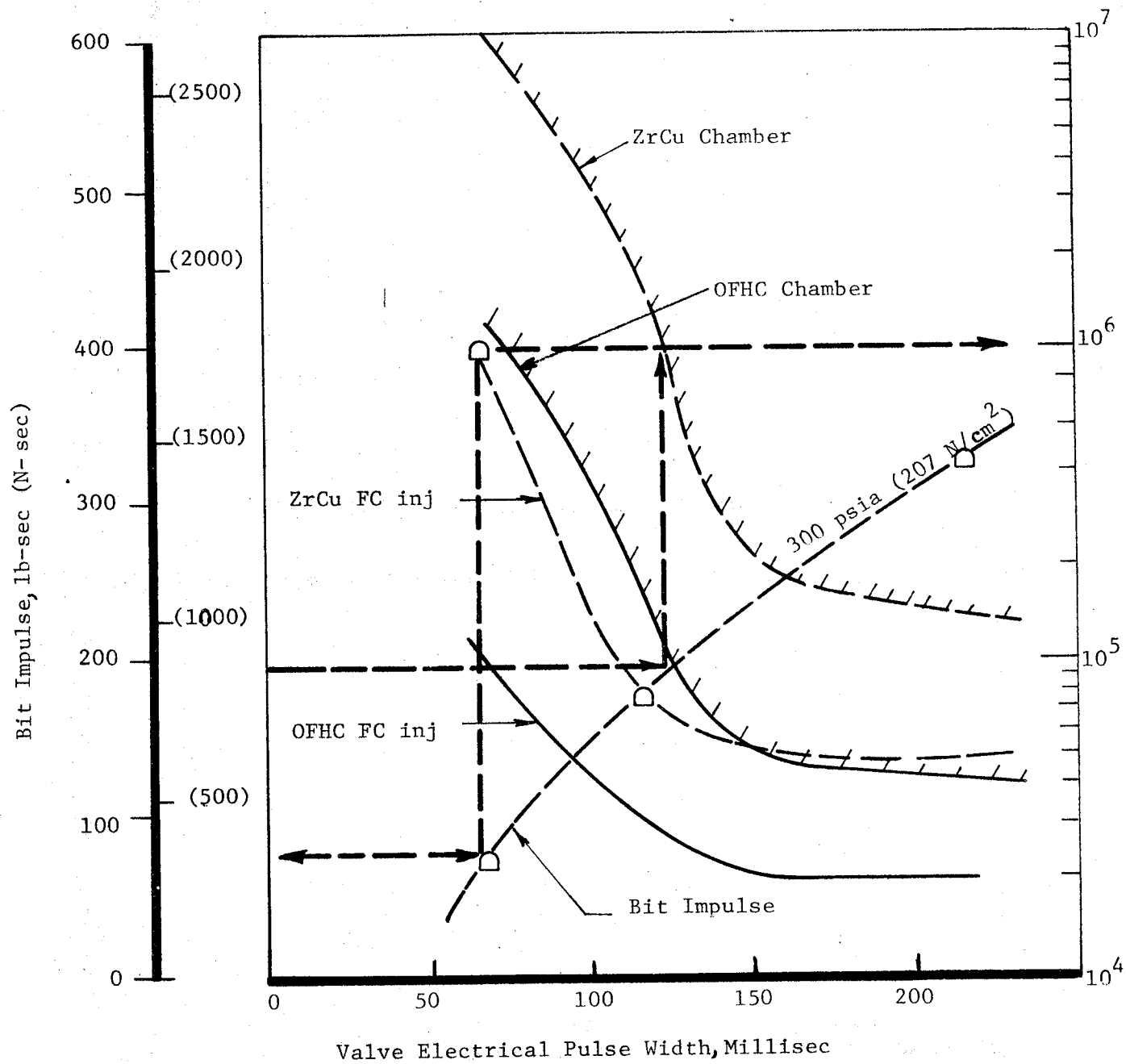


Figure VIII-4. Bit impulse and Cycle Life for Phase II Film Cooled Chamber at Nominal Operating Conditions

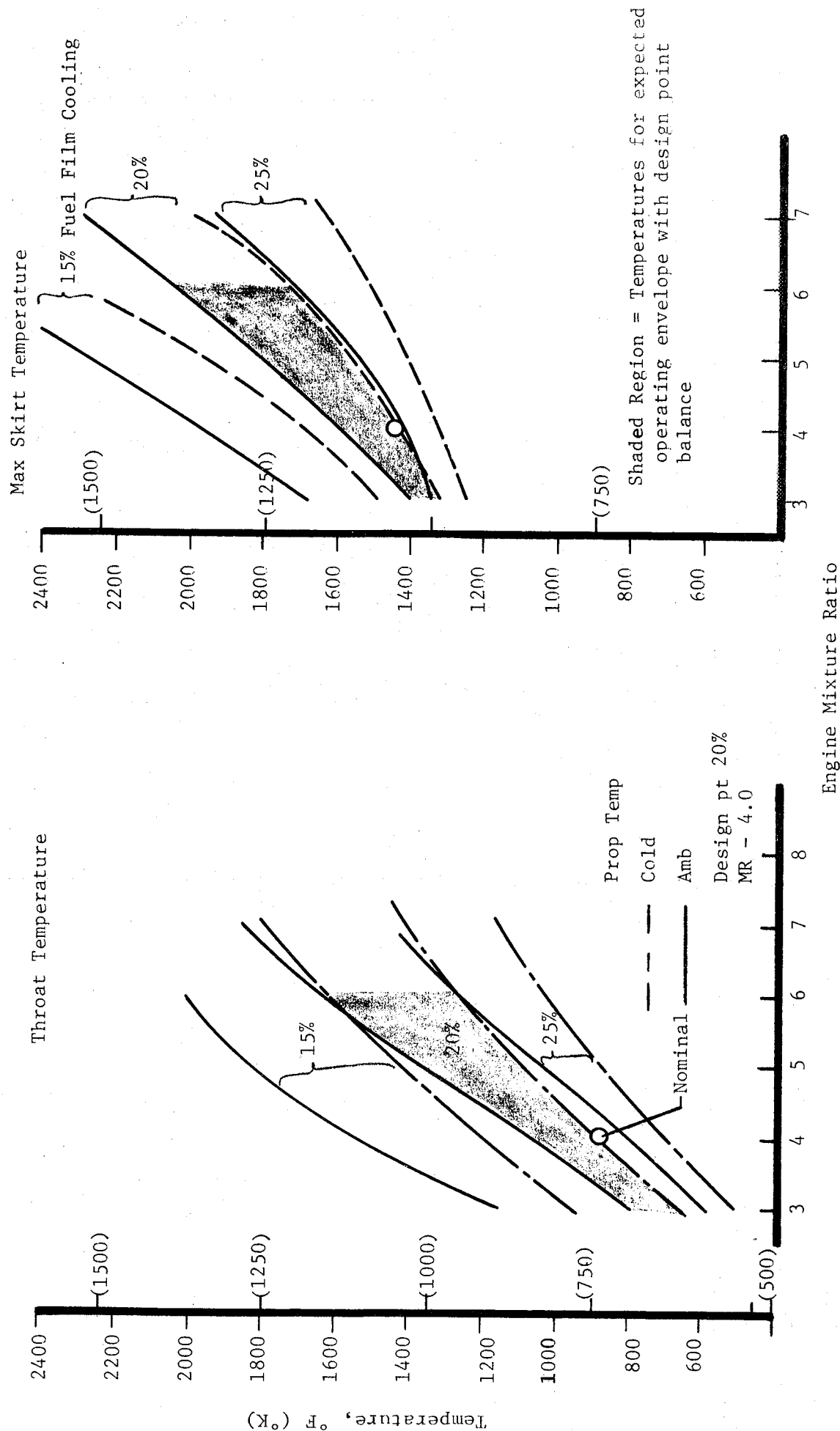
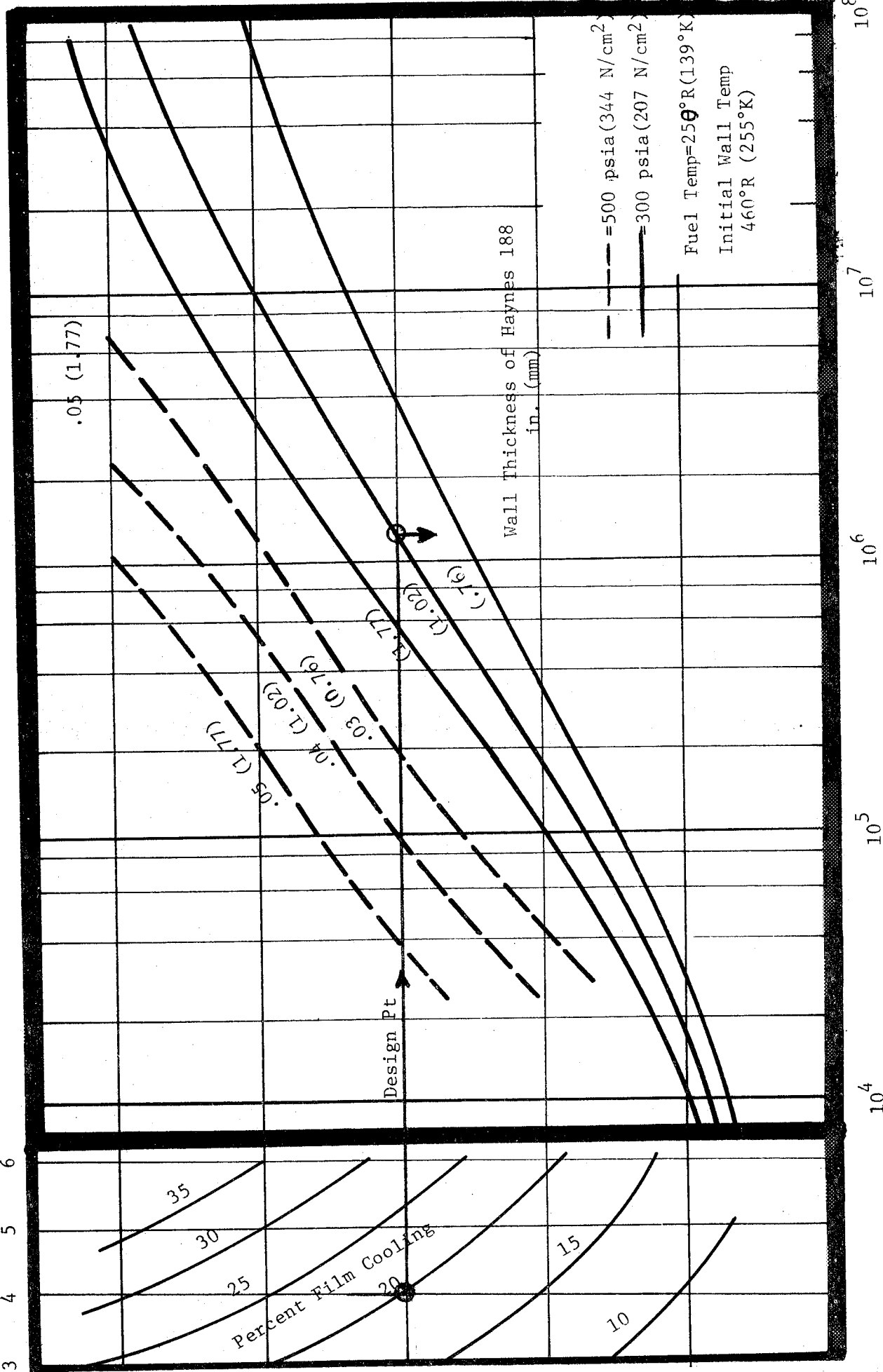


Figure VIII-5. Phase II Film Cooled Chamber Steady State Throat and Skirt Temperatures vs Engine MR, % Film Cooling and Propellant Supply Temperature

Engine Mixture Ratio

3 4 5 6



Cycles to Failure - η_f

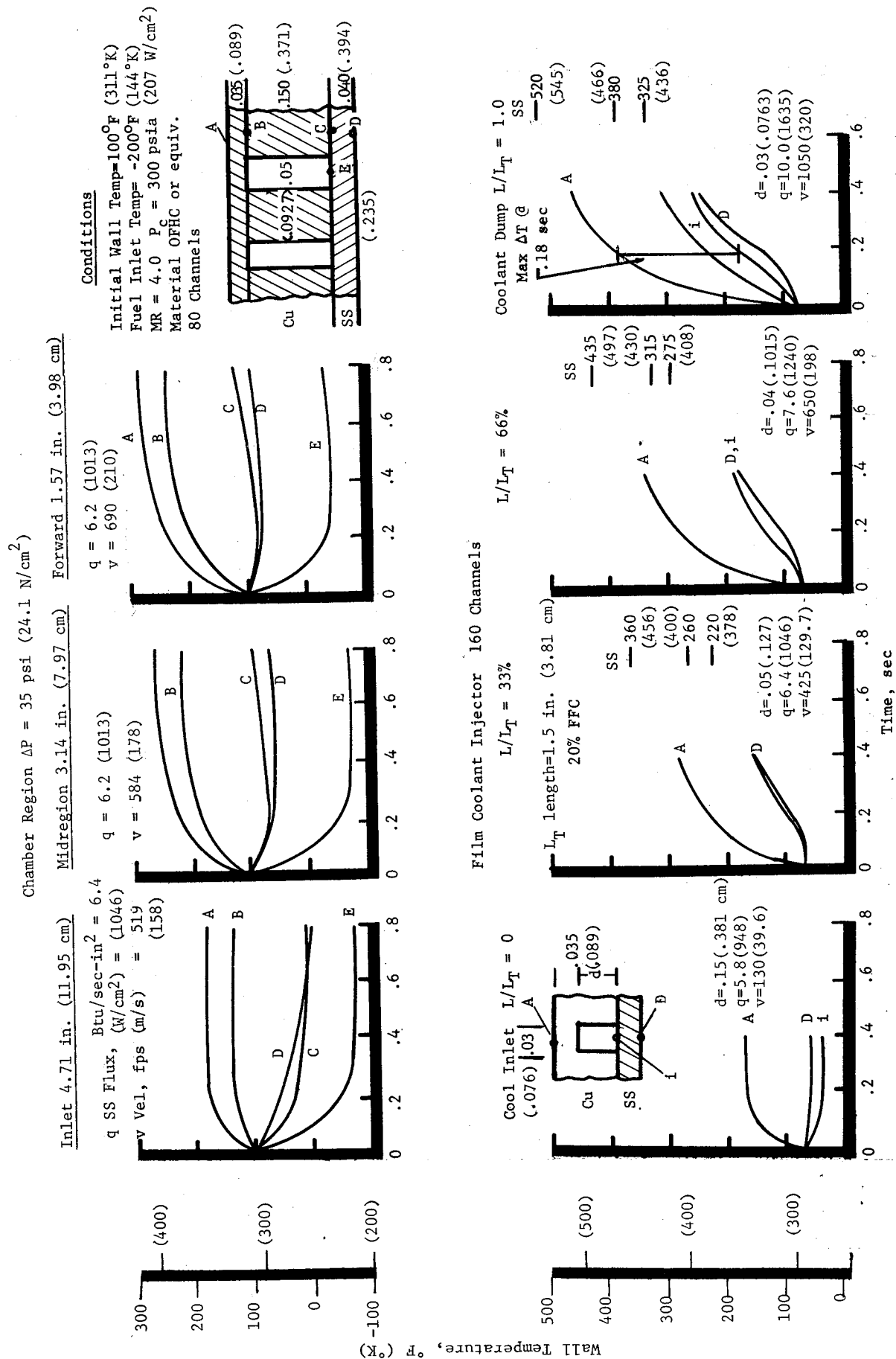


Figure VIII-7. Film Cooled Chamber Copper Lined Region Thermal Transient at Nominal Phase II Operating Conditions

NO. NO. OF COOLANT CHANNELS

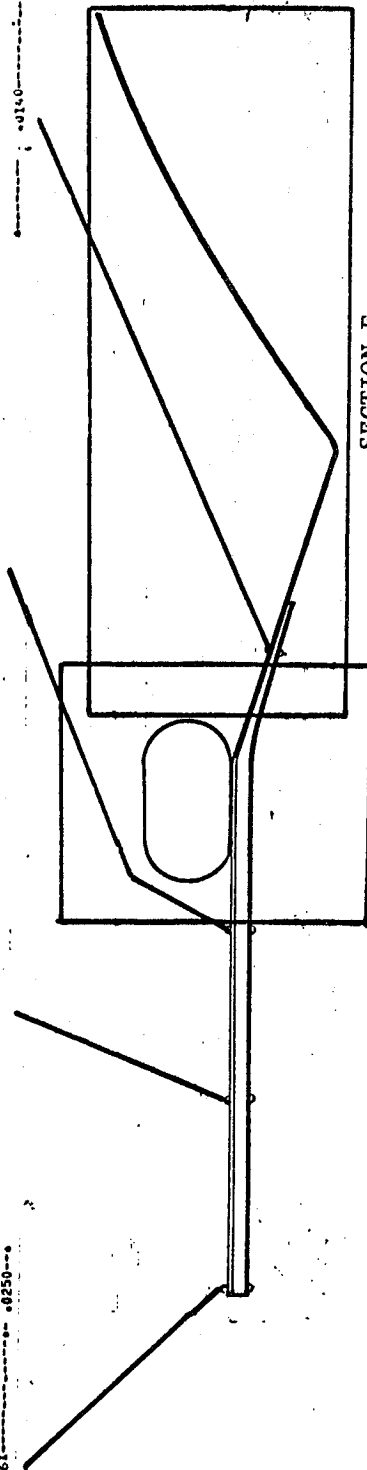
0062-

..... STEEL STEEL
149.5	140.1
152.0	143.0
159.2.....	151.0.....
171.5	165.5
204.9	199.1
253.6	252.0
273.7	273.5
294.0	294.5
..... CONFL CONFL
316.8	316.8
326.7	326.7
327.0.....	327.0.....
347.4	347.4
383.3	383.3
428.9	428.9
468.3	468.3
500.6	500.6
540.0	540.0

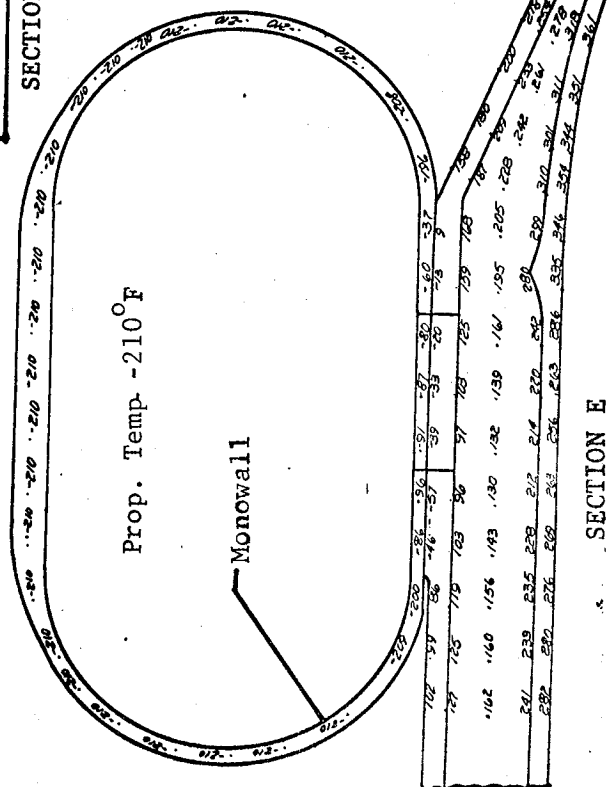
[illegible]

164. P.O. OF COOLANT CHANNELS

STELL	TEMP-DEG-F
294.2	294.0
295.6	294.8
308.1	307.2
310.2	316.7
330.8	335.0
361.6	361.7
367.0	368.0
413.4	413.5
415.0	415.0

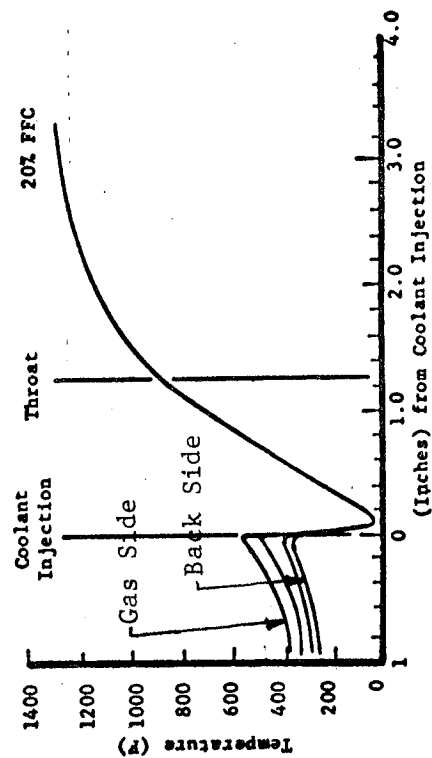


SECTION F



SECTION E

SECTION F



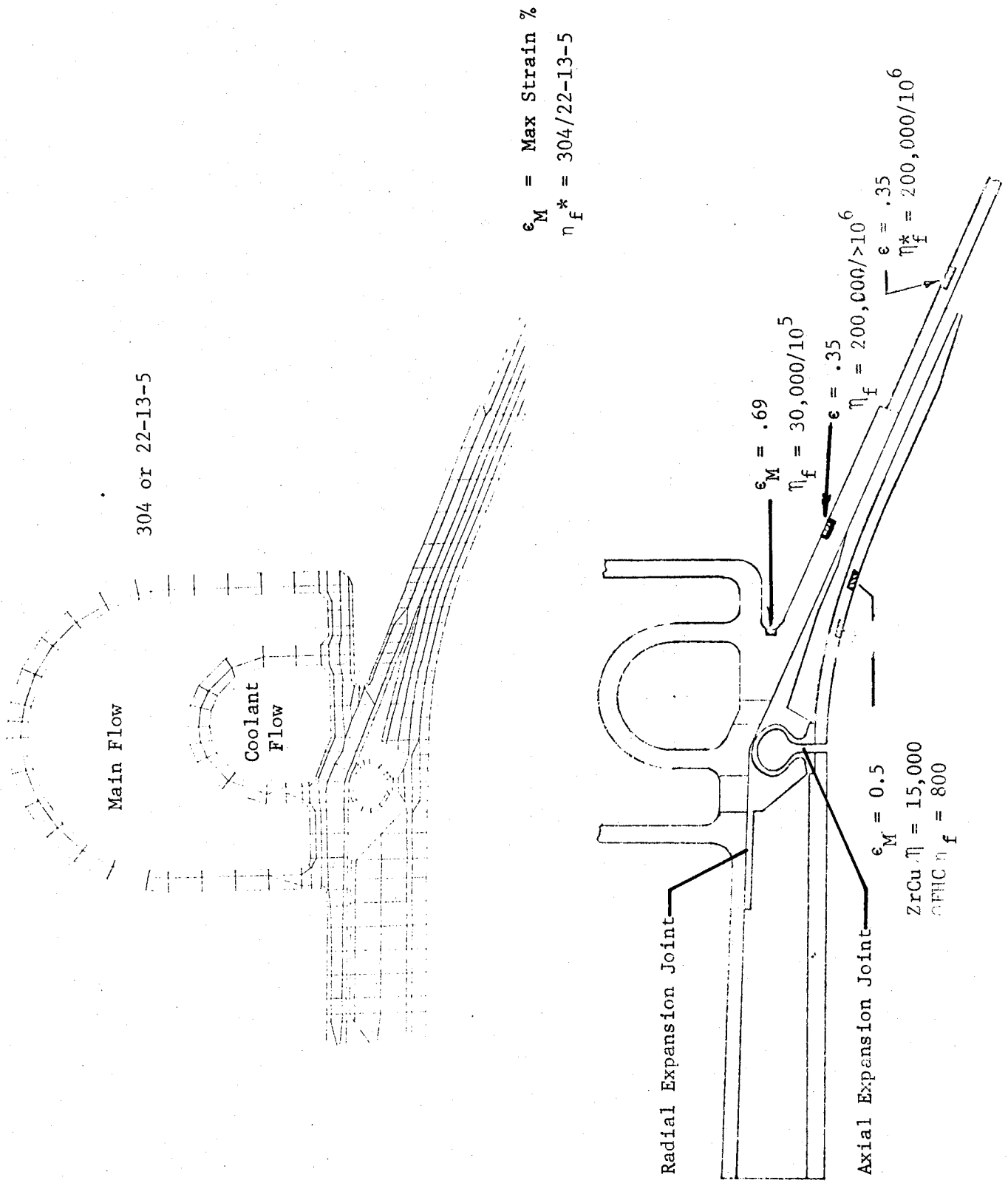


Figure VIII-9. Film Cooled Chamber Noncontacting Manifold and Liner

SECTION A

SECTION B

SECTION C

SECTION D

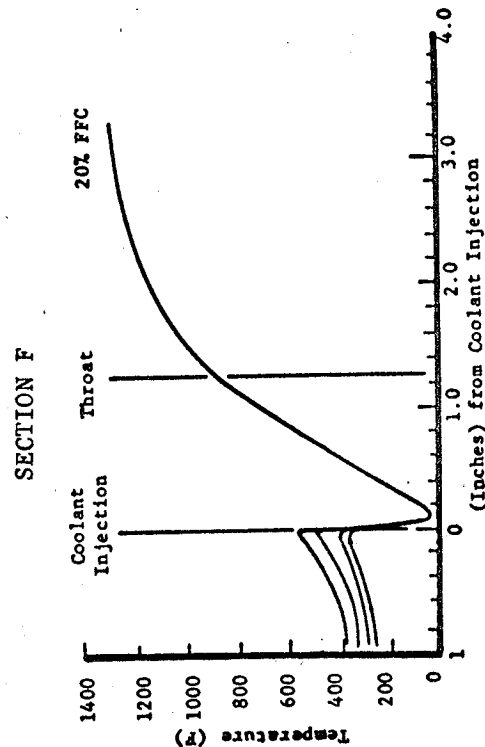
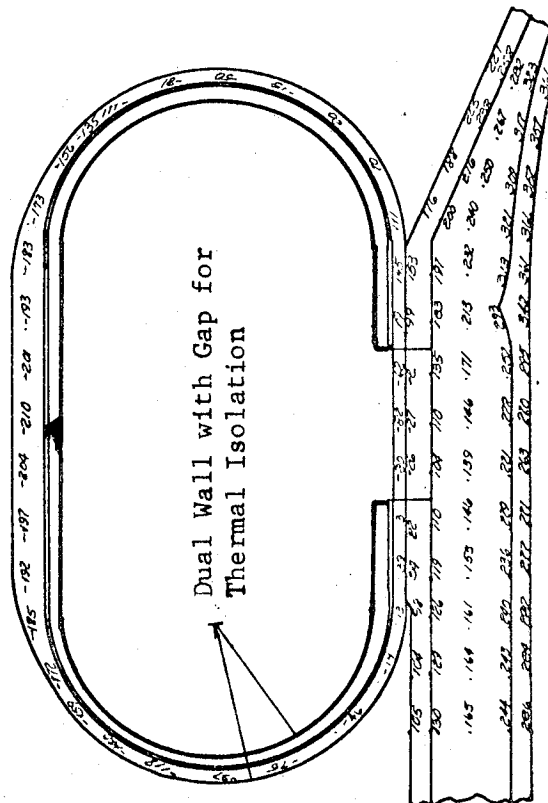
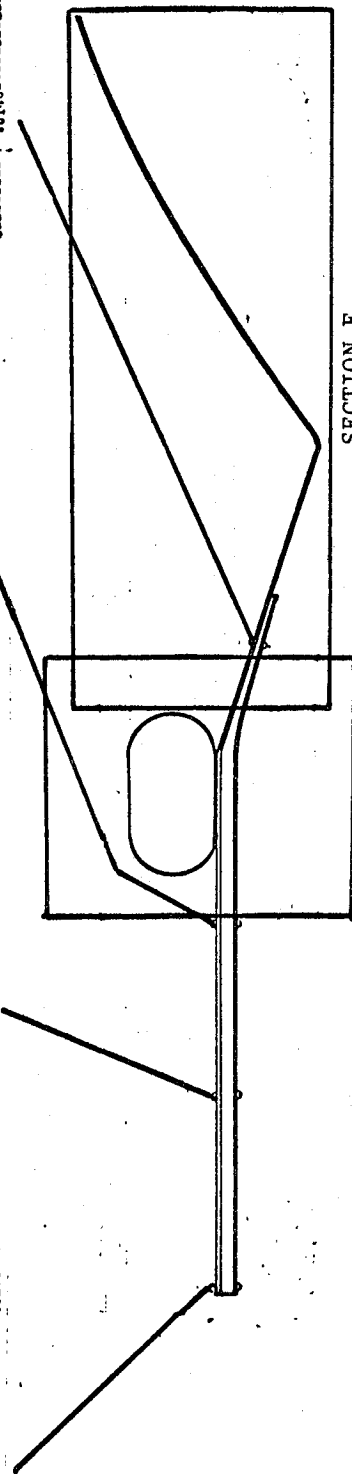
80. NO. OF COOLANT CHANNELS

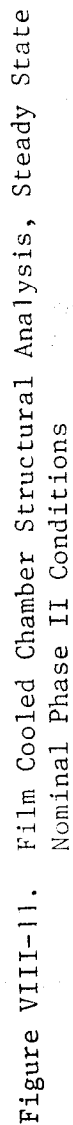
..... STEEL STEEL STEEL STEEL
163.9	161.2	153.8	142.0
160.7	163.8	154.8	133.1
175.5	173.3	166.8	80.4
190.2	168.7	184.2	
224.9	223.5	214.1	-82.9
279.7	279.8	280.1	287.6
300.3	300.6	301.3	303.1
320.6	321.4	321.8	321.6
..... COPPER COPPER COPPER COPPER
..... 8461 8461 8461 8461

..... STEEL STEEL STEEL STEEL
199.5	160.1	168.0	41.6
152.0	143.8	111.8	26.7
159.2	151.8	127.9	-26.8
171.5	165.5	147.4	-128.9
203.9	199.1	183.3	
253.8	252.8	251.1	268.3
273.7	273.5	273.7	280.8
294.0	294.5	294.9	296.4
..... COPPER COPPER COPPER COPPER
..... 8461 8461 8461 8461

..... STEEL STEEL STEEL STEEL
130.5	120.5	86.2	12.7
133.1	123.6	90.5	-3.2
143.6	133.0	104.6	-60.4
153.2	147.0	128.7	-175.4
166.1	181.3	165.4	
230.6	235.7	234.2	251.7
256.6	256.6	256.9	264.1
277.0	277.7	278.2	279.7
..... COPPER COPPER COPPER COPPER
..... 8461 8461 8461 8461

..... STEEL STEEL STEEL STEEL
294.2	294.1	294.0	293.5
295.4	295.1	294.4	291.2
306.1	307.2	304.3	299.6
316.2	317.8	316.7	
330.4	330.1	335.0	-108.9
361.4	361.7	362.4	365.5
387.0	387.9	388.0	388.3
413.4	413.5	413.5	413.6
..... COPPER COPPER COPPER COPPER
..... 8461 8461 8461 8461





Nominal Phase II Conditions

Maximum Temperature 0.6 in. Upstream of Throat

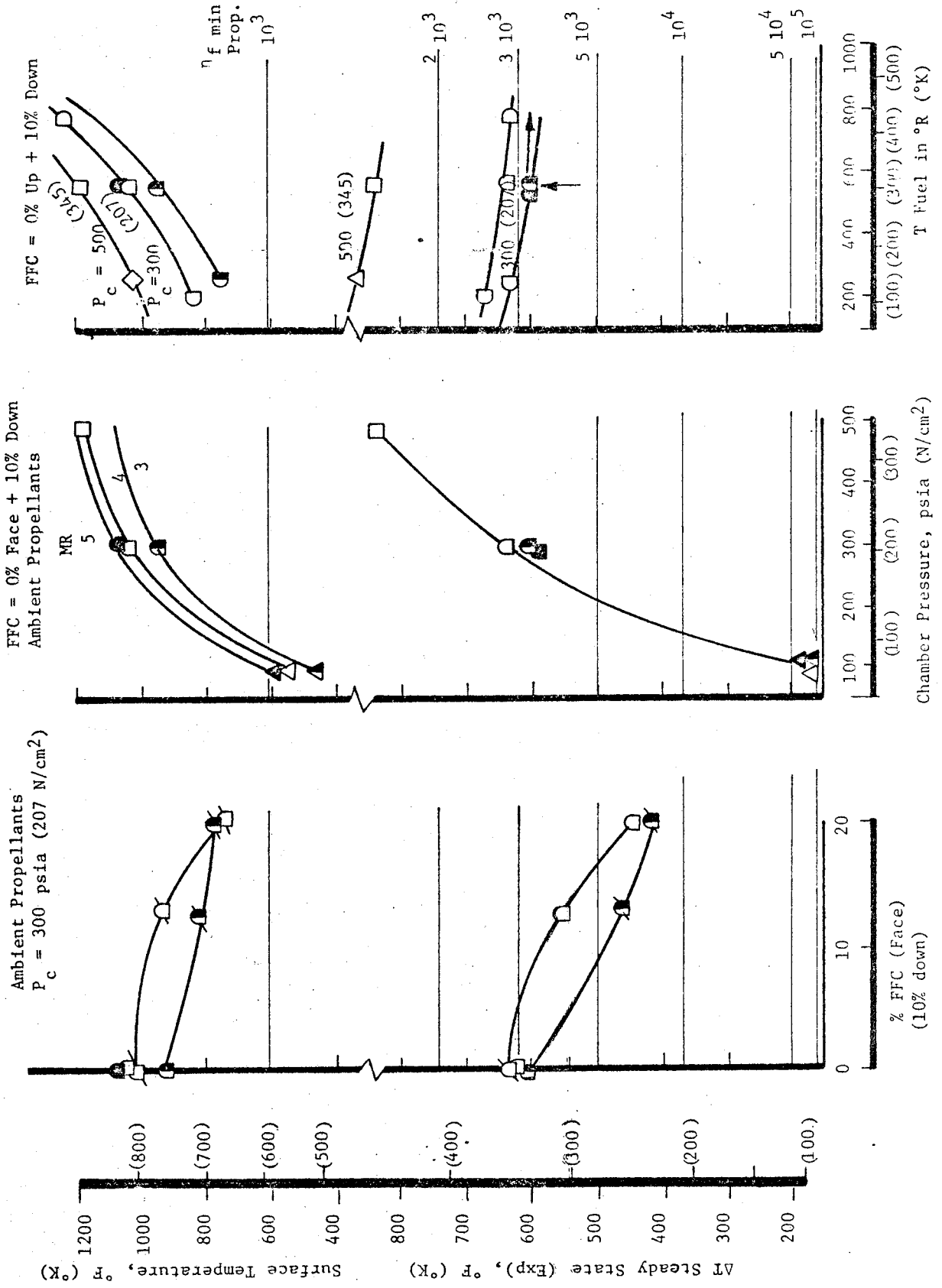


Figure VIII-12. Phase I Regeneratively Cooled Chamber Experimental Temperatures

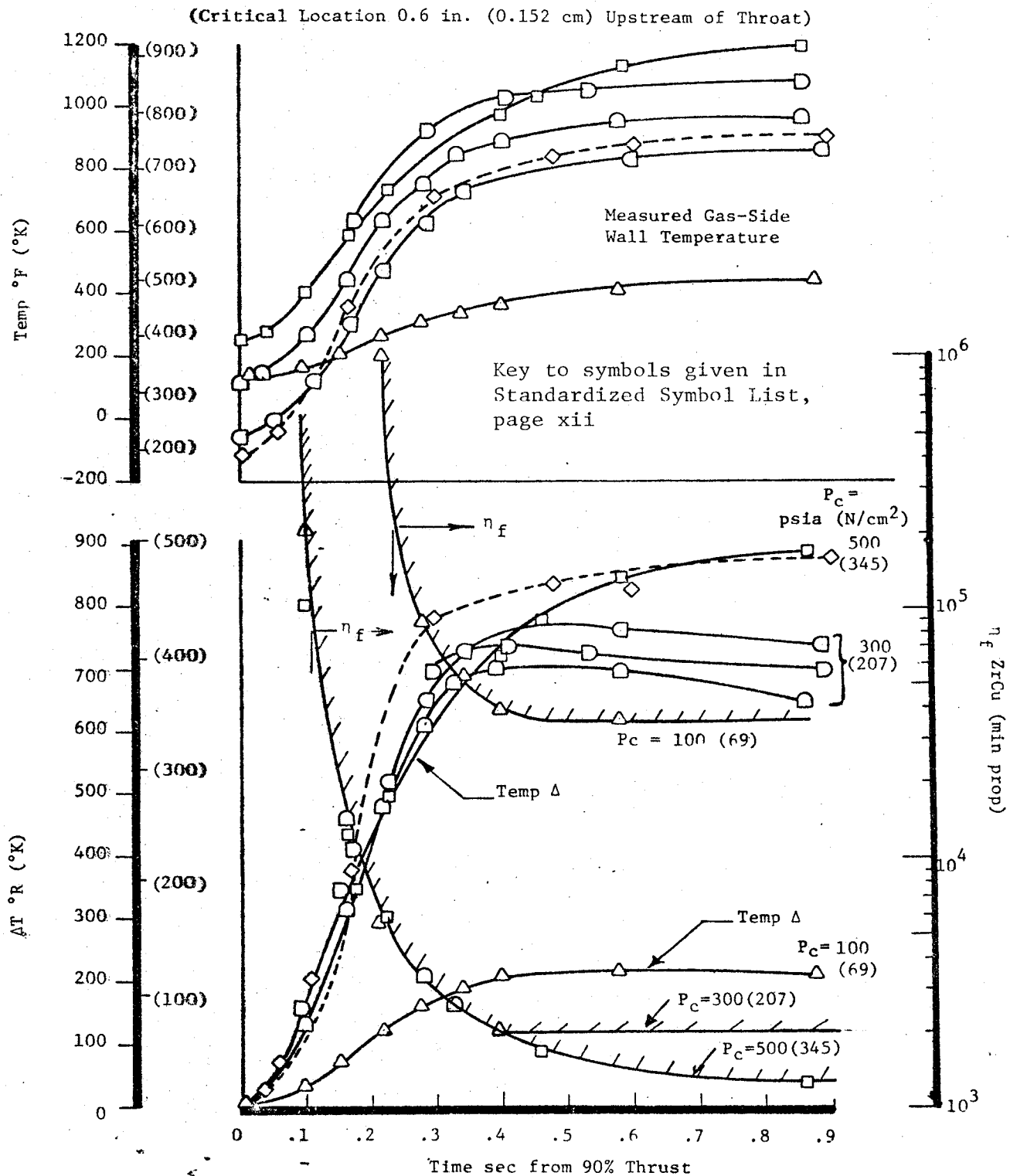


Figure VIII-13. Phase I Regeneratively Cooled Chamber Experimental Temperatures and Life Predictions in Pulse Mode Operation

REFERENCES

1. Ignition System for Space Shuttle APS, Contract NAS 3-14348, Final Report.
2. Johnson, R. C., Real Gas Effects in Critical-Flow-Through Nozzles and Tabulated Thermodynamic Properties, NASA Technical Note NASA TN D-2526, January 1965.
3. Hall, W. J., McCarty, R. D., Roder, H. M., Computer Programs for Thermodynamic and Transport Properties of Hydrogen, N.B.S. Technical Note 9288, August 1967.
4. Gregory, J. W., "FLOX/Methane Pump-Fed Engine Technology Review," AIAA Paper 70-718, presented San Diego, California, June 1970.
5. Kors, D. L. and Calhoon, D. F., "Gaseous Oxygen/Gaseous Hydrogen Injector Element Modeling," AIAA/SAE 7th Propulsion Joint Specialists Conference, Paper 71-674, 14 June 1971.
6. Pieper, J. L., ICRPG Liquid Propellant Thrust Chamber Performance Evaluation Manual, Chemical Propulsion Information Agency, Report 178, September 1968.
7. McBride, B and Gordon, S., "ICRPG One-Dimensional Equilibrium Reference Program," NASA LeRC, May 1969.
8. "One-Dimensional Kinetic Nozzle Analysis Computer Program," ICRPG Performance Standardization Working Group, 30 July 1968 (available through CPIA), AD 841201.
9. "Two-Dimensional Kinetic Nozzle Analysis Computer Program," ICRPG Performance Standardization Working Group, 30 July 1968 (available through CPIA), AD 841200.
10. Cherry, S. S., Phase II Final Report - Screening of Reaction Rates, TRW Report No. 08832-6002-T000, 6 December 1967, AD 828795.
11. Kliegel, J. R. and Quan, V., Convergent-Divergent Nozzle Flows, TRW Systems Report 02874-6002-R000, December 1966.
12. "Turbulent Boundary Layer Nozzle Analysis Computer Program," ICRPG Performance Standardization Working Group (available through CPIA), AD 841202.
13. Combs, L. P., Chadwick, W. D., and Campbell, D. T., Liquid Rocket Performance Computer Model with Distributed Energy Release, Interim Final Report R-8298, Rocketdyne, September 1970.

REFERENCES (cont.)

14. Investigation of $\text{GH}_2\text{-GO}_2$ Combustion, Contract NAS 3-14379, Final Report (to be published).
15. Bartz, D. R., "Turbulent Boundary-Layer Heat Transfer from Rapidly Accelerating Flow of Rocket Combustion Gases and of Heated Air," Advances in Heat Transfer, edited by T. F. Irvine, Jr. and J. P. Hartnett, Academic Press Inc., New York, 2, 1965.
16. Hydrogen Film Conductive Cooling, Contract NAS 3-14343, Final Report, 29 October 1971.
17. Schacht, R. L., Quentmeyer, R. J., Jones, W. L., Experimental Investigation of Hot Gas-Side Heat Transfer Rates for a Hydrogen-Oxygen Rocket, NASA Technical Note D-2832, June 1965.
18. Schoenman, L. and Block, P., "Laminar Boundary Layer Heat Transfer in Low Thrust Rocket Nozzles," J. of Spacecraft, Vol. 4, No. 9, 1968.
19. Moretti, P. M. and Kays, W. M., "Heat Transfer to a Turbulent Boundary Layer with Varying Free Stream Velocity and Surface Temperature," Int. J. Heat and Mass Trans., Vol. 8, 1965.
20. ALRC experimental data obtained in support of SSME.
21. Manson, S. S., Thermal Stress and Low "Cycle Fatigue", McGraw-Hill, 1966.
22. Back, L. H., et al., "Flow Phenomena and Convective Heat Transfer in a Conical Supersonic Nozzle," J. Spacecraft, Vol. 4, No. 8, 1967.

APPENDIX A

DISTRIBUTION LIST

Report
Copies
R D

Recipient

Designee

	National Aeronautics & Space Administration	
	Lewis Research Center	
	21000 Brookpart Road	
	Cleveland, Ohio 44135	
1	Atten: Contracting Officer, MS 500-313	
5	E. A. Bourke, MS 500-205	
1	Technical Report Control Office, MS 505	
1	Technology Utilization Office, MS 3-16	
2	AFSC Liaison Office, 501-3	
2	Library	
1	Office of Reliability & Quality Assurance, MS 500-111	
3	J. W. Gregory Chief, Propulsion Systems Branch	
	MS 500-203	
1	P. N. Herr MS 500-203	
	MS 500-203	
1	W. A. Tomazic MS 500-203	
1	L. H. Gordon MS 500-203	
1	Director, Shuttle Technology Office, RS	
	Office of Aeronautics & Space Technology	
	NASA Headquarters	
	Washington, D.C. 20546	
2	Director Space Prop. and Power, RP	
	Office of Aeronautics & Space Technology	
	NASA Headquarters	
	Washington, D.C. 20546	
1	Director, Launch Vehicles & Propulsion, SV	
	Office of Space Science	
	NASA Headquarters	
	Washington, D.C. 20546	
1	Director, Materials & Structures Div., RW	
	Office of Aeronautics & Space Technology	
	NASA Headquarters	
	Washington, D.C. 20546	

Report Copies		Recipient	Designee
R	D		
1		Director, Advanced Manned Missions, MT Office of Manned Space Flight NASA Headquarters Washington, D.C. 20546	
37		National Technical Information Service Springfield, Virginia 22151	
1	1	National Aeronautics & Space Administration Ames Research Center Moffett Field, California 94035 Attn: Library	Hans M. Mark Mission Analysis Division
1		National Aeronautics & Space Administration Flight Research Center P.O. Box 273 Edwards, California 93523	
1		Director, Technology Utilization Division Office of Technology Utilization NASA Headquarters Washington, D.C. 25046	
1		Office of the Director of Defense Research & Engineering Washington, D.C. 20301 Attn: Office of Asst. Dir. (Chem Technology)	
2		NASA Scientific and Technical Information Facility P.O. Box 33 College Park, Maryland 20740 Attn: NASA Representative	
1	1	National Aeronautics & Space Administration Goddard Space Flight Center Greenbelt, Maryland 20771 Attn: Library	Merland L. Moseson, Code 620
1	1	National Aeronautics & Space Administration John F. Kennedy Space Center Cocoa Beach, Florida 32931 Attn: Library	Dr. Kurt H. Debus

Report Copies		Recipient	Designee
R	D		
1	1	National Aeronautics & Space Administration Langley Research Center Langley Station Hampton, Virginia 23365 Attn: Library	E. Cortwright Director
1	1	National Aeronautics & Space Administration Manned Spacecraft Center Houston, Texas 77001 Attn: Library	J.G. Thiobodaux, Jr. Chief, Propulsion & Power Division C.A. Vaughan
1	1	National Aeronautics & Space Administration George C. Marshall Space Flight Center Huntsville, Alabama 35912 Attn: Library	Hans G. Paul Keith Coates
1	1	Jet Propulsion Laboratory 4800 Oak Grove Drive Pasadena, California 91103 Attn: Library	Henry Burlage, Jr. Duane Dipprey
1		Defense Documentation Center Cameron Station Building 5 5010 Duke Street Alexandria, Virginia 22314 Attn: TISIA	
1		Arnold Engineering Development Center Air Force Systems Command Tullahoma, Tennessee 37389 Attn: Library	Dr. H.K. Doetsch
1		Aeronautical Systems Division Air Force Systems Command Wright-Patterson Air Force Base Dayton, Ohio Attn: Library	D.L. Schmidt Code ARSCNC-2
1		Air Force Missile Test Center Patrick Air Force Base, Florida Attn: Library	L.J. Ullian

Report Copies		Recipient	Designee
R	D		
1		Air Force Systems Command Andrews Air Force Base Washington, D.C. 20332 Attn: Library	Capt. S.W. Bowen SCLT
1	1 1	Air Force Rocket Propulsion Laboratory (LKDS) Edwards, California 93523 Attn: Library	R.L. Wiswell W. Lawrence
1		Air Force Rocket Propulsion Laboratory (RPM) Edwards, California 93523 Attn: Library	
1		Air Force FTC (FTAT-2) Edwards Air Force Base, California 93523 Attn: Library	Donald Ross
1		Air Force Office of Scientific Research Washington, D.C. 20333 Attn: Library	SREP, Dr. J.F. Mas
1		Space & Missile Systems Organization Air Force Unit Post Office Los Angeles, California 90045 Attn: Technical Data Center	
1		Office of Research Analyses (OAR) Holloman Air Force Base, New Mexico 88330 Attn: Library RRRD	
1		U. S. Air Force Washington, D.C. Attn: Library	Col. C.K. Stambaugh Code AFRST
1		Commanding Officer U. S. Army Research Office (Durham) Box CM, Duke Station Durham, North Carolina 27706 Attn: Library	
1		U. S. Army Missile Command Redstone Scientific Information Center Redstone Arsenal, Alabama 35808 Attn: Document Section	Dr. W. Wharton

Report
Copies
R D

Recipient

Designee

1	Bureau of Naval Weapons Department of the Navy Washington, D.C. Attn: Library	J. Kay, Code RTMS-41
1	Commander U. S. Naval Missile Center Point Mugu, California 93041 Attn: Technical Library	
1	Commander U. S. Naval Weapons Center China Lake, California 93557 Attn: Library	
1	Commanding Officer Naval Research Branch Office 1030 E. Green Street Pasadena, California 91101 Attn: Library	
1	Director (Code 6180) U. S. Naval Research Laboratory Washington, D.C. 20390 Attn: Library	H.W. Carhart J.M. Krafft
1 1	Picatinny Arsenal Dover, New Jersey 07801 Attn: Library	I. Forsten
1	Air Force Aero Propulsion Laboratory Research & Technology Division Air Force Systems Command United States Air Force Wright-Patterson AFB, Ohio 45433 Attn: APRP (Library)	R. Quigley C.M. Donaldson
1	Space Division Aerojet-General Corporation 9200 East Flair Drive El Monte, California 91734 Attn: Library	S. Machlawski
1	Aeronutronic Division of Philco Ford Corp. Ford Road Newport Beach, California 92663 Attn: Technical Information Department	Dr. L.H. Linder

Report
Copies
R D

Recipient

Designee

1		Aerospace Corporation 2400 E. El Segundo Blvd. Los Angeles, California 90045 Attn: Library-Documents	J.G. Wilder
1		Astropower Laboratory McDonnell-Douglas Aircraft Company 2121 Paularino Newport Beach, California 92163 Attn: Library	
1		ARO, Incorporated Arnold Engineering Development Center Arnold AF Station, Tennessee 37389 Attn: Library	
1		Susquehanna Corporation Atlantic Research Division Shirley Highway & Edsall Road Alexandria, Virginia 22314 Attn: Library	
1		Beech Aircraft Corporation Boulder Facility Box 631 Boulder, Colorado Attn: Library	Douglas Pope
1	1 1 1	Bell Aerosystems, Inc. Box 1 Buffalo, New York 14240 Attn: Library	T. Reinhardt W. M. Smith J. Flanagan
1		Instruments & Life Support Division Bendix Corporation P.O. Box 4508 Davenport, Iowa 52808 Attention: Library	W. M. Carlson
1		Boeing Company Space Division P.O. Box 868 Seattle, Washington 98124 Attn: Library	J.D. Alexander C.F. Tiffany

Report
Copies
R D

Recipient

Designee

1	Boeing Company P.O. Box 1680 Huntsville, Alabama 35801	Ted Snow
1	Chemical Propulsion Information Agency Applied Physics Laboratory 8621 Georgia Avenue Silver Spring, Maryland 20910	Tom Reedy
1	Chrysler Corporation Missile Division P.O. Box 2628 Detroit, Michigan Attn: Library	John Gates
1	Chrysler Corporation Space Division P.O. Box 29209 New Orleans, Louisiana 70129 Attn: Librarian	
1	Curtiss-Wright Corporation Wright Aeronautical Division Woodridge, New Jersey Attn: Library	G. Kelley
1	Fairchild Stratos Corporation Aircraft Missiles Division Hagerstown, Maryland Attn: Library	
1	Research Center Fairchild Hiller Corporation Germantown, Maryland Attn: Library	Ralph Hall
1	Republic Aviation Fairchild Hiller Corporation Farmington, Long Island New York	
1	General Dynamics/Convair P.O. Box 1128 San Diego, California 92112 Attn: Library	Frank Dore

Report
Copies
R D

Recipient

Designee

1	Missiles and Space Systems Center General Electric Company Valley Forge Space Technology Center P.O. Box 8555 Philadelphia, Pa. 19101 Attn: Library	A. Cohen G.E. DeSalle
1	General Electric Company Flight Propulsion Lab. Department Cincinnati, Ohio Attn: Library	D. Suichu Leroy Smith
1	Grumman Aircraft Engineering Corporation Bethpage, Long Island, New York Attn: Library	Joseph Gavin
1	Honeywell Inc. Aerospace Division 2600 Ridgeway Road Minneapolis, Minnesota Attn: Library	
1	IIT Research Institute Technology Center Chicago, Illinois 60616 Attn: Library	C.K. Hersh
1	Kidde Aerospace Division Walter Kidde & Company, Inc. 476 Main Street Belleville, New Jersey	R.J. Hanville
1	Ling-Temco-Vought Corporation P.O. Box 5907 Dallas, Texas 75222 Attn: Library	
1	Lockheed Missiles and Space Company P.O. Box 504 Sunnyvale, California 94087 Attn: Library	
1	Lockheed Propulsion Company P.O. Box 111 Redlands, California 92374 Attn: Library, Thackwell	H.L. Thackwell

Report
Copies
R D

Recipient

Designee

1		Marquardt Corporation 16555 Saticoy Street Box 2013 - South Annex Van Nuys, California 91409	Tom Hudson
1		Martin-Marietta Corporation (Baltimore Division) Baltimore, Maryland 21203 Attn: Library	
1		Denver Division Martin-Marietta Corporation P.O. Box 179 Denver, Colorado 80201 Attn: Library	Dr. Morganthaler F.R. Schwartzberg
1	1	Western Division McDonnell Douglas Astronautics 5301 Bolsa Avenue Huntington Beach, California 92647 Attn: Library	R.W. Hallet G.W. Burge P. Klevatt
1	1	McDonnell Douglas Aircraft Corporation P.O. Box 516 Lambert Field, Missouri 63166 Attn: Library	R.A. Herzmark
1	1	Rocketdyne Division North American Rockwell Inc. 6633 Canoga Avenue Canoga Park, California 91304 Attn: Library, Department 596-306	Dr. R.J. Thompson S.F. Iacobellis
1	1	Space & Information Systems Division North American Rockwell 12214 Lakewood Blvd. Downey, California Attn: Library	R.E. Field
1		Northrop Space Laboratories 3401 West Broadway Hawthorne, California Attn: Library	Dr. William Howard

Report Copies		Recipient	Designee
R	D		
1		Radio Corporation of America Astro-Electronics Products Princeton, New Jersey Attn: Library	
1		Rocket Research Corporation Willow Road at 116th Street Redmond, Washington 98052 Attn: Library	F. McCullough, Jr.
1		Thiokol Chemical Corporation Redstone Division Huntsville, Alabama Attn: Library	John Goodloe
1	1 1	TRW Systems Inc. 1 Space Park Redondo Beach, California 90278 Attn: Tech. Lib. Doc. Acquisitions	D.H. Lee H. Burge
1		United Aircraft Corporation Corporation Library 400 Main Street East Hartford, Connecticut 06108 Attn: Library	Dr. David Rix
1		United Aircraft Corporation Pratt & Whitney Division Florida Research & Development Center P.O. Box 2691 West Palm Beach, Florida 33402 Attn: Library	R. J. Coar Dr. Schmitke
1		B. F. Goodrich Company Aerospace & Defense Products 500 South Main Street Akron, Ohio 44311	
1	1	Goodyear Aerospace Corporation 1210 Massillon Road Akron, Ohio 44306	D. Romick
1		Vought Astronautics Box 5907 Dallas, Texas Attn: Library	